


1-2012

# Investigating the Bond of Prestressing Strands in Lightweight Self-Consolidating Concrete

Royce Woodrow Floyd  
*University of Arkansas, Fayetteville*

Follow this and additional works at: <http://scholarworks.uark.edu/etd>

 Part of the [Civil Engineering Commons](#), and the [Construction Engineering and Management Commons](#)

---

## Recommended Citation

Floyd, Royce Woodrow, "Investigating the Bond of Prestressing Strands in Lightweight Self-Consolidating Concrete" (2012). *Theses and Dissertations*. 457.  
<http://scholarworks.uark.edu/etd/457>

This Dissertation is brought to you for free and open access by ScholarWorks@UARK. It has been accepted for inclusion in Theses and Dissertations by an authorized administrator of ScholarWorks@UARK. For more information, please contact [scholar@uark.edu](mailto:scholar@uark.edu), [ccmiddle@uark.edu](mailto:ccmiddle@uark.edu).



INVESTIGATING THE BOND OF PRESTRESSING STRANDS IN LIGHTWEIGHT SELF-  
CONSOLIDATING CONCRETE

INVESTIGATING THE BOND OF PRESTRESSING STRANDS IN LIGHTWEIGHT SELF-  
CONSOLIDATING CONCRETE

A dissertation submitted in partial fulfillment  
of the requirements for the degree of  
Doctor of Philosophy in Engineering

By

Royce Woodrow Floyd  
University of Arkansas  
Bachelor of Science in Civil Engineering, 2008

August 2012  
University of Arkansas

## Abstract

Lightweight self-consolidating concrete (LWSCC) is a relatively recent advancement in concrete technology. The reduced dead load from lightweight concrete is beneficial for precast elements and for elements where dead load is a significant portion of the total load, such as prestressed bridge girders. Self-consolidating concrete (SCC) is a specially proportioned concrete mixture that consolidates under its own weight without the need for vibration. The combination of lightweight concrete and self-consolidating behavior provides the benefits of both. Bond of prestressing steel has been a much debated topic since the 1950s. Limited data are available on the transfer and development length of strands cast in SCC and even less for strands cast in LWSCC. The differences in material properties resulting from the lightweight coarse aggregate and mix proportioning used for LWSCC have potential to lead to longer transfer and development lengths than those for conventional concrete, which can be detrimental to shear and flexural performance. The transfer and development length equations provided in the ACI Building Code Requirements for Structural Concrete and AASHTO Bridge Design specifications are based on studies performed using conventional concrete. This research project examined the transfer and development length of LWSCC specimens using 0.6 in. (15.2 mm) Grade 270 prestressing strand. Four specimens were cast from each mixture consisting of a combination of expanded clay, expanded shale, or limestone aggregate and a compressive strength of 4000 psi or 6000 psi (28 MPa or 41 MPa) at prestress release. Results were compared between the mixtures, to the code equations, and to previous research. The bond performance of LWSCC with a release strength of 6000 psi (41 MPa) was very similar to normal weight SCC, the transfer lengths for both strength levels were accurately predicted by the code equations, and the measured development lengths were significantly less than those predicted.

This dissertation is approved for recommendation  
to the Graduate Council.

Dissertation Director:

---

Dr. W. Micah Hale

Dissertation Committee

---

Dr. Ernie Heymsfield

---

Dr. Larry G. Pleimann

---

Dr. William T. Springer

## Dissertation Duplication Release

I hereby authorize the University of Arkansas Libraries to duplicate this dissertation when needed for research and/or scholarship.

Agreed

\_\_\_\_\_  
Royce Woodrow Floyd

Refused

\_\_\_\_\_  
Royce Woodrow Floyd

## **Acknowledgements**

My time spent in pursuit of a Ph.D. has been an exciting and rewarding experience. I first thank God and my Lord and Savior Jesus Christ for the breath I breathe every day and for the ability to reach this point in my life. I am extremely grateful to Dr. Micah Hale for the multitude of opportunities that he has given me. Without his guidance and encouragement I would not be where, nor who I am today. It is difficult to express the gratitude he deserves.

I would like to thank my mother, the rest of my family, and my friends for their constant support, encouragement, and belief in my abilities throughout my time in graduate school. I would also like to thank Carrie Forrester for her continual support. Despite hard times and issues along the way, she helped me get through some of the most difficult times.

This dissertation is the culmination of my work on this research project, and the completion of this research would not have been possible without the assistance of a number of individuals in the University of Arkansas Civil Engineering Department. They endured two very hot summers, a very cold winter, and numerous early mornings right along with me. I would like to thank each of these individuals who are: Michael Howland, Jared Bymaster, Brendan Ho, Richard Deschenes, Daniel Goad, Emerson John, Casey Jones, Jonathan Kerby, Cameron Murray, Garrison Smith, and Andy Tackett. I would also like to thank Dr. Rick Coffman, Mark Kuss, David Peachee, and Clint Wood for their assistance in more technical matters and for the use of various pieces of their equipment.

Finally I would like to thank AHTD and MBTC for sponsoring this research project and for all of the entities who contributed materials and resources to the project. These include: Big River Industries, Inc., Buildex, Inc., HW Headwaters, Inc., Insteel Industries, Inc., W.R. Grace & Co., and The University of Oklahoma.



## **Dedication**

*I dedicate this dissertation to my father, who always believed in me more than I deserved.*

## Table of Contents

<b>Chapter 1: Introduction .....</b>	<b>1</b>
1.1 Prestressed Bond in Lightweight Self-Consolidating Concrete .....	1
1.2 Lightweight Concrete .....	1
1.3 Self-Consolidating Concrete.....	2
1.4 Prestressed Concrete.....	2
1.5 Transfer Length.....	3
1.6 Development Length.....	5
1.7 Objectives .....	6
1.8 Testing Program.....	7
<b>Chapter 2: Background.....</b>	<b>8</b>
2.1 Bond of Prestressing Strand.....	8
2.1.1 Bond Mechanisms.....	8
2.1.2 Previous Research.....	9
2.1.3 Summary .....	45
2.2 Structural Lightweight Concrete.....	47
2.2.1 General Information.....	47
2.2.2 Previous Research on Lightweight Concrete.....	53
2.2.3 Previous Research in Bond of Prestressing Steel in Lightweight Concrete (LWC)....	59
2.3 Self-Consolidating Concrete.....	73
2.3.1 Benefits of SCC .....	73
2.3.2 Mix Designs.....	74
2.3.3 Properties of SCC .....	74
2.3.4 Previous Research on Bond of Prestressing Strand in SCC .....	76
2.4 Lightweight Self-Consolidating Concrete .....	93
2.4.1 Description and Benefits.....	93
2.4.2 Previous Research in Bond of Prestressing Strand in LWSCC .....	95
2.4.3 Discussion .....	98
2.5 Conclusion .....	98
<b>Chapter 3: Experimental Program .....</b>	<b>100</b>
3.1 Introduction.....	100
3.2 Aggregate Properties.....	100
3.2.1 Overview .....	100

3.2.2 Lightweight Aggregate Specific Gravity .....	101
3.2.3. Lightweight Aggregate Absorption .....	103
3.2.4 Particle Size Distribution .....	104
3.2.5 Properties of Other Aggregates.....	105
3.3 Other Materials .....	105
3.3.1 Cementitious Materials .....	105
3.3.2 Superplasticizer.....	106
3.3.3 Prestressing Strand.....	107
3.3.4 Mild Steel Reinforcement .....	107
3.4 Lightweight Aggregate Preparation.....	107
3.5 Concrete Property Tests.....	111
3.5.1 Slump Flow .....	111
3.5.2 $T_{20}$ .....	112
3.5.3 Visual Stability Index .....	113
3.5.4 J-Ring.....	114
3.5.5 Unit Weight.....	115
3.5.6 Compressive Strength .....	115
3.6 Mixture Design .....	115
3.6.1 Overview .....	115
3.6.2 Mixture Specifications .....	116
3.6.3 Trial Batching .....	116
3.7 Strand Qualification.....	117
3.8 Beam Specimen Testing .....	119
3.8.1 Overview .....	119
3.8.2 Beam Construction.....	120
3.8.3 Transfer Length Measurements .....	128
3.8.4 Development Length Measurements .....	131
3.9 Modulus of Elasticity Testing.....	135
3.9.1 Static Testing .....	136
3.9.2 Dynamic Testing.....	137
<b>Chapter 4: Concrete Mixtures.....</b>	<b>141</b>
4.1 Introduction.....	141
4.2 Normal Strength (NS) Series Mixtures ( $f'_{ci}$ of 4000 psi (28 MPa)) .....	142
4.2.1 Normal Strength Clay (NSC) Mixtures .....	142

4.2.2 Normal Strength Shale (NSS) Mixtures .....	147
4.2.3 Normal Strength Limestone (NSL) Mixtures .....	152
4.2.4 Summary .....	153
4.3 High Strength (HS) Series Mixtures ( $f'_{ci}$ of 6000 psi (41 MPa)).....	154
4.3.1 High Strength Clay (HSC) Mixtures.....	155
4.3.2 High Strength Shale (HSS) Mixtures.....	167
4.3.3 High Strength Limestone (HSL) Mixtures .....	170
4.3.4 Summary .....	171
4.4 Beam Batches .....	172
4.4.1 Test Beam .....	172
4.4.2 Normal Strength Clay (NSC) Beams.....	173
4.4.3 Normal Strength Shale (NSS) Beams .....	174
4.4.4 Normal Strength Limestone (NSL) Beams.....	175
4.4.5 High Strength Clay (HSC) Beams .....	176
4.4.6 High Strength Shale (HSS) Beams .....	177
4.4.7 High Strength Limestone (NSL) Beams .....	178
4.4.8 Modulus of Elasticity.....	179
4.4.9 Summary .....	182
<b>Chapter 5: Transfer Length Results .....</b>	<b>184</b>
5.1 Introduction.....	184
5.2 DEMEC Transfer Lengths .....	184
5.2.1 Normal Strength Clay (NSC) Beams.....	185
5.2.2 Normal Strength Shale (NSS) Beams .....	193
5.2.3 Normal Strength Limestone (NSL) Beams.....	201
5.2.4 High Strength Clay (HSC) Beams .....	207
5.2.5 High Strength Shale (HSS) Beams .....	214
5.2.6 High Strength Limestone (HSL) Beams .....	221
5.2.7 Summary of DEMEC Transfer Lengths .....	227
5.3 End Slip Transfer Lengths .....	233
5.3.1 Normal Strength Clay (NSC) Specimens .....	234
5.3.2 Normal Strength Shale (NSS) Specimens.....	234
5.3.3 Normal Strength Limestone (NSL) Specimens .....	235
5.3.4 High Strength Clay (HSC) Specimens.....	236
5.3.5 High Strength Shale (HSS) Specimens.....	237

5.3.6 High Strength Limestone (HSL) Specimens.....	238
5.3.7 Summary of End Slip Transfer Lengths .....	240
5.4 Comparison of DEMEC and End Slip Transfer Lengths .....	240
5.5 Conclusion .....	244
<b>Chapter 6: Development Length Results.....</b>	<b>246</b>
6.1 Introduction.....	246
6.2 Standard Test for Strand Bond (STSB) .....	246
6.3 Normal Strength Clay (NSC) Development Length.....	247
6.3.1 NSC-1 .....	247
6.3.2 NSC-2 .....	251
6.3.3 NSC-3 .....	253
6.3.4 NSC-4 .....	257
6.3.5 Summary and Discussion.....	259
6.4 Normal Strength Shale (NSS) Development Length.....	262
6.4.1 NSS-1.....	262
6.4.2 NSS-2.....	265
6.4.3 NSS-3.....	269
6.4.4 NSS-4.....	271
6.4.5 NSS-5.....	275
6.4.6 Summary and Discussion.....	278
6.5 Normal Strength Limestone (NSL) Development Length.....	280
6.5.1 NSL-1.....	280
6.5.2 NSL-2.....	283
6.5.3 NSL-3.....	285
6.5.4 NSL-4.....	289
6.5.5 Summary and Discussion.....	293
6.6 High Strength Clay (HSC) Development Length.....	295
6.6.1 HSC-1 .....	295
6.6.2 HSC-2 .....	297
6.6.3 HSC-3 .....	301
6.6.4 HSC-4 .....	303
6.6.5 Summary and Discussion.....	308
6.7 High Strength Shale (HSS) Development Length .....	309
6.7.1 HSS-1.....	309

6.7.2 HSS-2.....	311
6.7.3 HSS-3.....	316
6.7.4 HSS-4.....	319
6.7.5 Summary and Discussion.....	323
6.8 High Strength Limestone (HSL) Development Length.....	324
6.8.1 HSL-1.....	324
6.8.2 HSL-2.....	328
6.8.3 HSL-3.....	331
6.8.4 HSL-4.....	333
6.8.5 Summary and Discussion.....	338
6.9 Conclusion .....	339
<b>Chapter 7: Conclusions .....</b>	<b>342</b>
7.1 Introduction.....	342
7.2 Mix Design Phase .....	342
7.3 Transfer Length.....	345
7.3.1 DEMEC Measurements .....	345
7.3.2 End Slip Measurements .....	349
7.4 Development Length.....	349
7.5 Recommendations.....	351
7.6 Contribution to the Body of Knowledge.....	352
<b>References .....</b>	<b>353</b>
<b>Appendix A: Testing Procedures.....</b>	<b>360</b>
A.1 Strand Tensioning .....	360
A.2 Standard Test for Strand Bond (STSB) .....	361
A.3 Flexural Testing .....	362
<b>Appendix B: Beam Analysis Calculations .....</b>	<b>364</b>
B.1 Cross-Section Properties .....	364
B.2 Moment Capacity Using Strain Compatibility.....	366
B.3 Shear Capacity .....	369
B.4 Prestress Losses.....	374
B.4.1 Elastic Shortening .....	374
B.4.2 Shrinkage.....	376

B.4.3 Creep .....	377
B.4.4 Relaxation.....	378
B.5 Concrete Elastic Moduli at Seven Days.....	380
<b>Appendix C: Moisture Content Errors.....</b>	<b>381</b>
C.1 Normal Strength Clay (NSC) Trial Batches.....	381
C.2 Normal Strength Shale (NSS) Trial Batches.....	382
C.3 High Strength Clay (HSC) Trial Batches.....	383
C.4 High Strength Shale (HSS) Trial Batches .....	388
<b>Appendix D: Transfer Length Data .....</b>	<b>390</b>
D.1 DEMEC Strain Plots .....	390
D.1.1 NSC-1.....	390
D.1.2 NSC-2.....	393
D.1.3 NSC-3.....	395
D.1.4 NSC-4.....	397
D.1.5 NSS-1 .....	399
D.1.6 NSS-2 .....	402
D.1.7 NSS-3 .....	404
D.1.8 NSS-4.....	407
D.1.9 NSS-5 .....	409
D.1.10 NSL-1 .....	412
D.1.11 NSL-2.....	414
D.1.12 NSL-3.....	417
D.1.13 NSL-4.....	419
D.1.14 HSC-1.....	422
D.1.15 HSC-2.....	424
D.1.16 HSC-3.....	427
D.1.17 HSC-4.....	429
D.1.18 HSS-1 .....	432
D.1.19 HSS-2 .....	434
D.1.20 HSS-3 .....	437
D.1.21 HSS-4 .....	439
D.1.22 HSL-1 .....	442
D.1.23 HSL-2.....	444

D.1.24 HSL-3 .....	447
D.1.25 HSL-4 .....	449
D.2 DEMEC Transfer Length Statistics .....	452
D.2.1 Sample Statistical Parameters .....	452
D.2.2 95% Confidence Intervals Using a <i>t</i> Distribution .....	454
D.2.3 Hypothesis Testing.....	456
D.3 End Slip Data .....	460
D.4 End Slip Transfer Lengths .....	462
D.5 Comparisons of Average End Slip and DEMEC Transfer Lengths .....	465
<b>Appendix E: Development Length Data .....</b>	<b>468</b>
E.1 Normal Strength Clay (NSC) Specimens .....	468
E.2 Normal Strength Shale (NSS) Specimens .....	469
E.3 Normal Strength Limestone (NSL) Specimens .....	470
E.4 High Strength Clay (HSC) Specimens .....	471
E.5 High Strength Shale (HSS) Specimens .....	472
E.6 High Strength Limestone (NSL) Specimens .....	473
<b>Appendix F: STSB Curves .....</b>	<b>474</b>
F.1 Batch 1 .....	474
F.2 Batch 2 .....	475



## List of Figures

### Chapter 1: Introduction

Figure 1.1: Idealized steel stress distribution illustrating transfer and development length..... 4

### Chapter 2: Background

### Chapter 3: Experimental Program

Figure 3.1: Lightweight aggregate specific gravity using the pycnometer method.....	102
Figure 3.2: Variation of moisture content with centrifuge time .....	104
Figure 3.3: Gradation of expanded clay aggregate .....	105
Figure 3.4: Gradation of expanded shale aggregate.....	106
Figure 3.5: Aggregate preparation using tarp and perforated bucket lid .....	109
Figure 3.6: Aggregate preparation using steel drum and tractor loader .....	110
Figure 3.7: Performance of aggregate unit weight.....	110
Figure 3.8: Final expanded clay moisture-density relationship .....	111
Figure 3.9: Final expanded shale moisture-density relationship .....	112
Figure 3.10: Adequate slump flow.....	113
Figure 3.11: Measurement of J-Ring flow .....	114
Figure 3.12: Setup for Standard Test for Strand Bond .....	118
Figure 3.13: Beam specimen details .....	120
Figure 3.14: Strand tensioning apparatus with stopper blocks in place.....	123
Figure 3.15: Concrete placement directly from the mixer.....	126
Figure 3.16: Placement of DEMEC points using epoxy.....	127
Figure 3.17: Placement of block clamps used to measure end slip .....	128
Figure 3.18: DEMEC Measurements.....	129
Figure 3.19: Measurement of strand end slip.....	130
Figure 3.20: Beam supports with roller constrained (left) and unconstrained (right) .....	132
Figure 3.21: Flexural test specimen setup.....	133
Figure 3.22: Application of point load for flexural testing.....	134
Figure 3.23: Placement of LVDTs to measure strand slip during flexural testing .....	134
Figure 3.24: Static modulus of elasticity setup using MTS (left) and Forney (right).....	137
Figure 3.25: Longitudinal fundamental frequency measurement setup.....	138
Figure 3.26: Transverse fundamental frequency measurement setup.....	139

## Chapter 4: Concrete Mixtures

Figure 4.1: Slump flow of NSC mixture used to cast beams.....	146
Figure 4.2: Effect of aggregate moisture content error on NSC $f'_{ci}$ .....	147
Figure 4.3: Effect of aggregate moisture content error on NSC $f'_c$ .....	148
Figure 4.4: Slump flow of final NSS mixture.....	151
Figure 4.5: Effect of aggregate moisture content error on NSS $f'_{ci}$ .....	151
Figure 4.6: Effect of aggregate moisture content error on NSS $f'_c$ .....	152
Figure 4.7: Effect of aggregate moisture content error on Type I cement HSC $f'_{ci}$ .....	157
Figure 4.8: Effect of aggregate moisture content error on silica fume HSC $f'_{ci}$ .....	161
Figure 4.9: Effect of aggregate moisture content error on partial limestone HSC $f'_{ci}$ .....	163
Figure 4.10: Slump flow of final HSC mixture.....	166
Figure 4.11: Effect of aggregate moisture content error on Type III cement HSC $f'_{ci}$ .....	167
Figure 4.12: Effect of aggregate moisture content error on Type III cement HSC $f'_c$ .....	168
Figure 4.13: Slump flow of final HSS mixture.....	169
Figure 4.14: Effect of aggregate moisture content error on Type III cement HSS $f'_{ci}$ .....	170
Figure 4.15 Effect of moisture content error on $f'_{ci}$ of beam batches.....	183
Figure 4.16 Effect of moisture content error on $f'_c$ of beam batches.....	183

## Chapter 5: Transfer Length Results

Figure 5.1: 28-Day strain profile with 95% AMS for specimen NSC-1.....	186
Figure 5.2: 28-Day strain profile with 95% AMS for specimen NSC-2.....	188
Figure 5.3: 28-Day strain profile with 95% AMS for specimen NSC-3.....	190
Figure 5.4: 28-Day strain profile with 95% AMS for specimen NSC-4.....	191
Figure 5.5: 28-Day strain profile with 95% AMS for specimen NSS-1.....	194
Figure 5.6: 28-Day strain profile with 95% AMS for specimen NSS-2.....	196
Figure 5.7: 28-Day strain profile with 95% AMS for specimen NSS-3.....	197
Figure 5.8: 28-Day strain profile with 95% AMS for specimen NSS-4.....	199
Figure 5.9: 28-Day strain profile with 95% AMS for specimen NSS-5.....	200
Figure 5.10: 28-Day strain profile with 95% AMS for specimen NSL-1.....	202
Figure 5.11: 28-Day strain profile with 95% AMS for specimen NSL-2.....	204
Figure 5.12: 28-Day strain profile with 95% AMS for specimen NSL-3.....	205
Figure 5.13: 28-Day strain profile with 95% AMS for specimen NSL-4.....	206
Figure 5.14: 28-Day strain profile with 95% AMS for specimen HSC-1.....	209
Figure 5.15: 28-Day strain profile with 95% AMS for specimen HSC-2.....	211
Figure 5.16: 28-Day strain profile with 95% AMS for specimen HSC-3.....	212

Figure 5.17: 28-Day strain profile with 95% AMS for specimen HSC-4 .....	213
Figure 5.18: 28-Day strain profile with 95% AMS for specimen HSS-1 .....	215
Figure 5.19: 28-Day strain profile with 95% AMS for specimen HSS-2 .....	217
Figure 5.20: 28-Day strain profile with 95% AMS for specimen HSS-3 .....	219
Figure 5.21: 28-Day strain profile with 95% AMS for specimen HSS-4 .....	220
Figure 5.22: 28-Day strain profile with 95% AMS for specimen HSL-1 .....	222
Figure 5.23: 28-Day strain profile with 95% AMS for specimen HSL-2 .....	224
Figure 5.24: 28-Day strain profile with 95% AMS for specimen HSL-3 .....	225
Figure 5.25: 28-Day strain profile with 95% AMS for specimen HSL-4 .....	226
Figure 5.26: Average DEMEC transfer length measurements .....	230
Figure 5.27: Average NSC transfer length measurements .....	235
Figure 5.28: Average NSS transfer length measurements .....	236
Figure 5.29: Average NSL transfer length measurements .....	237
Figure 5.30: Average HSC transfer length measurements .....	238
Figure 5.31: Average HSS transfer length measurements .....	239
Figure 5.32: Average HSL transfer length measurements .....	240
Figure 5.33: Comparison of DEMEC transfer lengths and measured end slip .....	242
Figure 5.34: Average DEMEC and end slip ( $\alpha = 2$ ) transfer lengths at 28 days .....	243
Figure 5.35: Average DEMEC and end slip ( $\alpha = 3$ ) transfer lengths at 28 days .....	244
Figure 5.36: Average DEMEC and end slip ( $\alpha = 2.85$ ) transfer lengths at 28 days .....	245

## Chapter 6: Development Length

Figure 6.1: Cracking pattern of specimen NSC-1D .....	248
Figure 6.2: Plot of moment vs. deflection for specimen NSC-1D .....	249
Figure 6.3: Shear cracking and poor consolidation of specimen NSC-1L .....	250
Figure 6.4: Plot of moment vs. deflection for specimen NSC-1L .....	250
Figure 6.5: Plot of moment vs. deflection for specimen NSC-2D .....	251
Figure 6.6: Failure of specimen NSC-2D .....	252
Figure 6.7: Cracking pattern of specimen NSC-2L .....	253
Figure 6.8: Plot of moment vs. deflection for specimen NSC-2L .....	254
Figure 6.9: Shear cracking of specimen NSC-3D .....	255
Figure 6.10: Plot of moment vs. deflection for specimen NSC-3D .....	255
Figure 6.11: Shear cracking of specimen NSC-3L .....	256
Figure 6.12: Plot of moment vs. deflection for specimen NSC-3L .....	257
Figure 6.13: Cracking behavior of specimen NSC-4D .....	258

Figure 6.14: Plot of moment vs. deflection for specimen NSC-4D.....	259
Figure 6.15: Cracking behavior of specimen NSC-4L .....	260
Figure 6.16: Plot of moment vs. deflection for specimen NSC-4L .....	260
Figure 6.17: Plot of moment vs. deflection for specimen NSS-1D .....	263
Figure 6.18: Cracking behavior and failure of specimen NSS-1D .....	263
Figure 6.19: Plot of moment vs. deflection for specimen NSS-1L.....	264
Figure 6.20: Cracking behavior and failure of specimen NSS-1L.....	265
Figure 6.21: Cracking behavior and beginning of failure of specimen NSS-2D.....	266
Figure 6.22: Plot of moment vs. deflection for specimen NSS-2D .....	267
Figure 6.23: Shear failure of specimen NSS-2L.....	268
Figure 6.24: Plot of moment vs. deflection for specimen NSS-2L.....	268
Figure 6.25: Shear failure of specimen NSS-3D .....	269
Figure 6.26: Plot of moment vs. deflection for specimen NSS-3D .....	270
Figure 6.27: Plot of moment vs. deflection for specimen NSS-3L.....	271
Figure 6.28: Failure of specimen NSS-3L .....	272
Figure 6.29: Plot of moment vs. deflection for specimen NSS-4D .....	273
Figure 6.30: Failure of specimen NSS-4D.....	273
Figure 6.31: Plot of moment vs. deflection for specimen NSS-4L.....	274
Figure 6.32: South side shear cracking of specimen NSS-4L .....	275
Figure 6.33: Flexural cracking with beginning of concrete crushing for NSS-5D.....	276
Figure 6.34: Plot of moment vs. deflection for specimen NSS-5D .....	276
Figure 6.35: Shear cracking of specimen NSS-5L.....	277
Figure 6.36: Plot of moment vs. deflection for specimen NSS-5L.....	278
Figure 6.37: Shear cracking of specimen NSL-1D.....	281
Figure 6.38: Plot of moment vs. deflection for specimen NSL-1D.....	281
Figure 6.39: Cracking of specimen NSL-1L.....	282
Figure 6.40: Plot of moment vs. deflection for specimen NSL-1L .....	283
Figure 6.41: Plot of moment vs. deflection for specimen NSL-2D .....	284
Figure 6.42: Spalling at support of specimen NSL-2D.....	285
Figure 6.43: Cracking of specimen NSL-2L.....	286
Figure 6.44: Plot of moment vs. deflection for specimen NSL-2L .....	286
Figure 6.45: Shear cracking of specimen NSL-3D.....	287
Figure 6.46: Plot of moment vs. deflection for specimen NSL-3D.....	288
Figure 6.47: Plot of moment vs. deflection for specimen NSL-3L .....	289

Figure 6.48: Cracking and failure of specimen NSL-3L .....	290
Figure 6.49: Plot of moment vs. deflection for specimen NSL-4D .....	291
Figure 6.50: Shear cracking and failure of specimen NSL-4D.....	291
Figure 6.51: Cracking and failure of specimen NSL-4L .....	292
Figure 6.52: Plot of moment vs. deflection for specimen NSL-4L .....	293
Figure 6.53: Cracking and failure of specimen HSC-1D.....	295
Figure 6.54: Plot of moment vs. deflection for specimen HSC-1D.....	296
Figure 6.55: Cracking of specimen HSC-1L .....	297
Figure 6.56: Plot of moment vs. deflection for specimen HSC-1L .....	298
Figure 6.57: Plot of moment vs. deflection for specimen HSC-2D.....	299
Figure 6.58: Cracking and failure of specimen HSC-2D.....	299
Figure 6.59: Cracking and failure of specimen HSC-2L .....	300
Figure 6.60: Plot of moment vs. deflection for specimen HSC-2L .....	301
Figure 6.61: Cracking and failure of specimen HSC-3D.....	302
Figure 6.62: Plot of moment vs. deflection for specimen HSC-3D.....	303
Figure 6.63: Shear failure of specimen HSC-3L .....	304
Figure 6.64: Plot of moment vs. deflection for specimen HSC-3L .....	304
Figure 6.65: Shear failure of specimen HSC-4D .....	305
Figure 6.66: Plot of moment vs. deflection for specimen HSC-4D.....	306
Figure 6.67: Cracking and failure of specimen HSC-4L .....	307
Figure 6.68: Plot of moment vs. deflection for specimen HSC-4L .....	307
Figure 6.69: Shear cracking of specimen HSS-1D .....	310
Figure 6.70: Plot of moment vs. deflection for specimen HSS-1D .....	311
Figure 6.71: Plot of moment vs. deflection for specimen HSS-1L.....	312
Figure 6.72: Cracking and failure of specimen HSS-1L.....	312
Figure 6.73: Cracking and failure of specimen HSS-2D .....	313
Figure 6.74: Plot of moment vs. deflection for specimen HSS-2D .....	314
Figure 6.75: Cracking and failure of specimen HSS-2L showing crack width .....	315
Figure 6.76: Plot of moment vs. deflection for specimen HSS-2L.....	315
Figure 6.77: Cracking and failure of specimen HSS-3D showing crack width.....	316
Figure 6.78: Plot of moment vs. deflection for specimen HSS-3D .....	317
Figure 6.79: Cracking and failure of specimen HSS-3L.....	318
Figure 6.80: Plot of moment vs. deflection for specimen HSS-3L.....	319
Figure 6.81: Cracking and failure of specimen HSS-4D .....	320

Figure 6.82: Plot of moment vs. deflection for specimen HSS-4D .....	320
Figure 6.83: Cracking and failure of specimen HSS-4L.....	321
Figure 6.84: Plot of moment vs. deflection for specimen HSS-4L.....	322
Figure 6.85: Plot of moment vs. deflection for specimen HSL-1D .....	325
Figure 6.86: Cracking and failure of specimen HSL-1D .....	326
Figure 6.87: Plot of moment vs. deflection for specimen HSL-1L .....	327
Figure 6.88: Cracking and failure of specimen HSL-1L .....	327
Figure 6.89: Plot of moment vs. deflection for specimen HSL-2D .....	328
Figure 6.90: Cracking and failure of specimen HSL-2D .....	329
Figure 6.91: Cracking and failure of specimen HSL-2L .....	330
Figure 6.92: Plot of moment vs. deflection for specimen HSL-2L .....	331
Figure 6.93: Plot of moment vs. deflection for specimen HSL-3D .....	332
Figure 6.94: Cracking and failure of specimen HSL-3D .....	333
Figure 6.95: Plot of moment vs. deflection for specimen HSL-3L .....	334
Figure 6.96: Strand fracture at failure of specimen HSL-3L.....	334
Figure 6.97: Cracking and failure of specimen HSL-4D.....	335
Figure 6.98: Plot of moment vs. deflection for specimen HSL-4D.....	336
Figure 6.99: Cracking and failure of specimen HSL-4L .....	337
Figure 6.100: Plot of moment vs. deflection for specimen HSL-4L .....	337

## Chapter 7: Conclusions

### References

#### Appendix A: Testing Procedures

#### Appendix B: Beam Analysis Calculations

Figure B.1: Beam support conditions and free body diagram for initial shear calculations.....	370
Figure B.2: Beam support conditions and free body diagram for initial shear calculations.....	370

#### Appendix C: Moisture Content Errors

Figure C.1: Effect of aggregate moisture content error on NSC $f'_{ci}$ by cement content.....	381
Figure C.2: Effect of aggregate moisture content error on NSC $f'_c$ by cement content .....	381
Figure C.3: Effect of aggregate moisture content error on NSS $f'_{ci}$ by cement content .....	382
Figure C.4: Effect of aggregate moisture content error on NSS $f'_c$ by cement content.....	382
Figure C.5: Effect of aggregate moisture content error on Type I cement HSC $f'_c$ .....	383

Figure C.6: Effect of aggregate moisture content error on Type I cement HSC $f'_{ci}$ by cement content.....	383
Figure C.7: Effect of aggregate moisture content error on Type I cement HSC $f'_c$ by cement content.....	384
Figure C.8: Effect of aggregate moisture content error on $f'_c$ of silica fume HSC.....	384
Figure C.9: Effect of aggregate moisture content error on silica fume HSC $f'_{ci}$ by percent silica fume .....	385
Figure C.10: Effect of aggregate moisture content error on silica fume HSC $f'_c$ by percent silica fume .....	385
Figure C.11: Effect of aggregate moisture content error on $f'_c$ of HSC with limestone.....	386
Figure C.12: Effect of aggregate moisture content error on $f'_{ci}$ of HSC with limestone by cement content.....	386
Figure C.13: Effect of aggregate moisture content error on $f'_c$ of HSC with limestone by cement content.....	387
Figure C.14: Effect of aggregate moisture content error on $f'_{ci}$ of Type III cement HSC by cementitious material content .....	387
Figure C.15: Effect of aggregate moisture content error on $f'_c$ of Type III cement HSC by cementitious material content .....	388
Figure C.16: Effect of aggregate moisture content error on HSS $f'_c$ .....	388
Figure C.17: Effect of aggregate moisture content error on HSS $f'_{ci}$ by cementitious material content.....	389
Figure C.18: Effect of aggregate moisture content error on HSS $f'_c$ by cementitious material content.....	389

#### **Appendix D: Transfer Length Data**

Figure D.1: Release strain profile with 95% AMS for specimen NSC-1 .....	390
Figure D.2: 3-Day strain profile with 95% AMS for specimen NSC-1.....	391
Figure D.3: 5-Day strain profile with 95% AMS for specimen NSC-1.....	391
Figure D.4: 7-Day strain profile with 95% AMS for specimen NSC-1.....	392
Figure D.5: 14-Day strain profile with 95% AMS for specimen NSC-1.....	392
Figure D.6: Release strain profile with 95% AMS for specimen NSC-2 .....	393
Figure D.7: 3-Day strain profile with 95% AMS for specimen NSC-2.....	393
Figure D.8: 5-Day strain profile with 95% AMS for specimen NSC-2.....	394
Figure D.9: 7-Day strain profile with 95% AMS for specimen NSC-2.....	394
Figure D.10: 14-Day strain profile with 95% AMS for specimen NSC-2.....	395
Figure D.11: Release strain profile with 95% AMS for specimen NSC-3 .....	395
Figure D.12: 5-Day strain profile with 95% AMS for specimen NSC-3.....	396

Figure D.13: 7-Day strain profile with 95% AMS for specimen NSC-3.....	396
Figure D.14: 14-Day strain profile with 95% AMS for specimen NSC-3.....	397
Figure D.15: Release strain profile with 95% AMS for specimen NSC-4.....	397
Figure D.16: 5-Day strain profile with 95% AMS for specimen NSC-4.....	398
Figure D.17: 7-Day strain profile with 95% AMS for specimen NSC-4.....	398
Figure D.18: 14-Day strain profile with 95% AMS for specimen NSC-4.....	399
Figure D.19: Release strain profile with 95% AMS for specimen NSS-1.....	399
Figure D.20: 3-Day strain profile with 95% AMS for specimen NSS-1.....	400
Figure D.21: 5-Day strain profile with 95% AMS for specimen NSS-1.....	400
Figure D.22: 7-Day strain profile with 95% AMS for specimen NSS-1.....	401
Figure D.23: 14-Day strain profile with 95% AMS for specimen NSS-1.....	401
Figure D.24: Release strain profile with 95% AMS for specimen NSS-2.....	402
Figure D.25: 3-Day strain profile with 95% AMS for specimen NSS-2.....	402
Figure D.26: 5-Day strain profile with 95% AMS for specimen NSS-2.....	403
Figure D.27: 7-Day strain profile with 95% AMS for specimen NSS-2.....	403
Figure D.28: 14-Day strain profile with 95% AMS for specimen NSS-2.....	404
Figure D.29: Release strain profile with 95% AMS for specimen NSS-3.....	404
Figure D.30: 3-Day strain profile with 95% AMS for specimen NSS-3.....	405
Figure D.31: 5-Day strain profile with 95% AMS for specimen NSS-3.....	405
Figure D.32: 7-Day strain profile with 95% AMS for specimen NSS-3.....	406
Figure D.33: 14-Day strain profile with 95% AMS for specimen NSS-3.....	406
Figure D.34: Release strain profile with 95% AMS for specimen NSS-4.....	407
Figure D.35: 3-Day strain profile with 95% AMS for specimen NSS-4.....	407
Figure D.36: 5-Day strain profile with 95% AMS for specimen NSS-4.....	408
Figure D.37: 7-Day strain profile with 95% AMS for specimen NSS-4.....	408
Figure D.38: 14-Day strain profile with 95% AMS for specimen NSS-4.....	409
Figure D.39: Release strain profile with 95% AMS for specimen NSS-5.....	409
Figure D.40: 3-Day strain profile with 95% AMS for specimen NSS-5.....	410
Figure D.41: 5-Day strain profile with 95% AMS for specimen NSS-5.....	410
Figure D.42: 7-Day strain profile with 95% AMS for specimen NSS-5.....	411
Figure D.43: 14-Day strain profile with 95% AMS for specimen NSS-5.....	411
Figure D.44: Release strain profile with 95% AMS for specimen NSL-1.....	412
Figure D.45: 3-Day strain profile with 95% AMS for specimen NSL-1.....	412
Figure D.46: 5-Day strain profile with 95% AMS for specimen NSL-1.....	413



Figure D.47: 7-Day strain profile with 95% AMS for specimen NSL-1 .....	413
Figure D.48: 14-Day strain profile with 95% AMS for specimen NSL-1 .....	414
Figure D.49: Release strain profile with 95% AMS for specimen NSL-2 .....	414
Figure D.50: 3-Day strain profile with 95% AMS for specimen NSL-2.....	415
Figure D.51: 5-Day strain profile with 95% AMS for specimen NSL-2.....	415
Figure D.52: 7-Day strain profile with 95% AMS for specimen NSL-2.....	416
Figure D.53: 14-Day strain profile with 95% AMS for specimen NSL-2.....	416
Figure D.54: Release strain profile with 95% AMS for specimen NSL-3 .....	417
Figure D.55: 3-Day strain profile with 95% AMS for specimen NSL-3.....	417
Figure D.56: 5-Day strain profile with 95% AMS for specimen NSL-3.....	418
Figure D.57: 7-Day strain profile with 95% AMS for specimen NSL-3.....	418
Figure D.58: 14-Day strain profile with 95% AMS for specimen NSL-3.....	419
Figure D.59: Release strain profile with 95% AMS for specimen NSL-4 .....	419
Figure D.60: 3-Day strain profile with 95% AMS for specimen NSL-4.....	420
Figure D.61: 5-Day strain profile with 95% AMS for specimen NSL-4.....	420
Figure D.62: 7-Day strain profile with 95% AMS for specimen NSL-4.....	421
Figure D.63: 14-Day strain profile with 95% AMS for specimen NSL-4.....	421
Figure D.64: Release strain profile with 95% AMS for specimen HSC-1 .....	422
Figure D.65: 3-Day strain profile with 95% AMS for specimen HSC-1.....	422
Figure D.66: 5-Day strain profile with 95% AMS for specimen HSC-1.....	423
Figure D.67: 7-Day strain profile with 95% AMS for specimen HSC-1.....	423
Figure D.68: 14-Day strain profile with 95% AMS for specimen HSC-1.....	424
Figure D.69: Release strain profile with 95% AMS for specimen HSC-2 .....	424
Figure D.70: 3-Day strain profile with 95% AMS for specimen HSC-2.....	425
Figure D.71: 5-Day strain profile with 95% AMS for specimen HSC-2.....	425
Figure D.72: 7-Day strain profile with 95% AMS for specimen HSC-2.....	426
Figure D.73: 14-Day strain profile with 95% AMS for specimen HSC-2.....	426
Figure D.74: Release strain profile with 95% AMS for specimen HSC-3 .....	427
Figure D.75: 3-Day strain profile with 95% AMS for specimen HSC-3.....	427
Figure D.76: 5-Day strain profile with 95% AMS for specimen HSC-3.....	428
Figure D.77: 7-Day strain profile with 95% AMS for specimen HSC-3.....	428
Figure D.78: 14-Day strain profile with 95% AMS for specimen HSC-3.....	429
Figure D.79: Release strain profile with 95% AMS for specimen HSC-4 .....	429
Figure D.80: 3-Day strain profile with 95% AMS for specimen HSC-4.....	430

Figure D.81: 5-Day strain profile with 95% AMS for specimen HSC-4.....	430
Figure D.82: 7-Day strain profile with 95% AMS for specimen HSC-4.....	431
Figure D.83: 14-Day strain profile with 95% AMS for specimen HSC-4.....	431
Figure D.84: Release strain profile with 95% AMS for specimen HSS-1.....	432
Figure D.85: 3-Day strain profile with 95% AMS for specimen HSS-1 .....	432
Figure D.86: 5-Day strain profile with 95% AMS for specimen HSS-1 .....	433
Figure D.87: 7-Day strain profile with 95% AMS for specimen HSS-1 .....	433
Figure D.88: 14-Day strain profile with 95% AMS for specimen HSS-1 .....	434
Figure D.89: Release strain profile with 95% AMS for specimen HSS-2.....	434
Figure D.90: 3-Day strain profile with 95% AMS for specimen HSS-2.....	435
Figure D.91: 5-Day strain profile with 95% AMS for specimen HSS-2.....	435
Figure D.92: 7-Day strain profile with 95% AMS for specimen HSS-2.....	436
Figure D.93: 14-Day strain profile with 95% AMS for specimen HSS-2.....	436
Figure D.94: Release strain profile with 95% AMS for specimen HSS-3.....	437
Figure D.95: 3-Day strain profile with 95% AMS for specimen HSS-3.....	437
Figure D.96: 5-Day strain profile with 95% AMS for specimen HSS-3.....	438
Figure D.97: 7-Day strain profile with 95% AMS for specimen HSS-3.....	438
Figure D.98: 14-Day strain profile with 95% AMS for specimen HSS-3.....	439
Figure D.99: Release strain profile with 95% AMS for specimen HSS-4.....	439
Figure D.100: 3-Day strain profile with 95% AMS for specimen HSS-4.....	440
Figure D.101: 5-Day strain profile with 95% AMS for specimen HSS-4.....	440
Figure D.102: 7-Day strain profile with 95% AMS for specimen HSS-4.....	441
Figure D.103: 14-Day strain profile with 95% AMS for specimen HSS-4.....	441
Figure D.104: Release strain profile with 95% AMS for specimen HSL-1 .....	442
Figure D.105: 3-Day strain profile with 95% AMS for specimen HSL-1.....	442
Figure D.106: 5-Day strain profile with 95% AMS for specimen HSL-1.....	443
Figure D.107: 7-Day strain profile with 95% AMS for specimen HSL-1.....	443
Figure D.108: 14-Day strain profile with 95% AMS for specimen HSL-1.....	444
Figure D.109: Release strain profile with 95% AMS for specimen HSL-2 .....	444
Figure D.110: 3-Day strain profile with 95% AMS for specimen HSL-2.....	445
Figure D.111: 5-Day strain profile with 95% AMS for specimen HSL-2.....	445
Figure D.112: 7-Day strain profile with 95% AMS for specimen HSL-2.....	446
Figure D.113: 14-Day strain profile with 95% AMS for specimen HSL-2.....	446
Figure D.114: Release strain profile with 95% AMS for specimen HSL-3 .....	447

Figure D.115: 3-Day strain profile with 95% AMS for specimen HSL-3.....	447
Figure D.116: 5-Day strain profile with 95% AMS for specimen HSL-3.....	448
Figure D.117: 7-Day strain profile with 95% AMS for specimen HSL-3.....	448
Figure D.118: 14-Day strain profile with 95% AMS for specimen HSL-3.....	449
Figure D.119: Release strain profile with 95% AMS for specimen HSL-4 .....	449
Figure D.120: 3-Day strain profile with 95% AMS for specimen HSL-4.....	450
Figure D.121: 5-Day strain profile with 95% AMS for specimen HSL-4.....	450
Figure D.122: 7-Day strain profile with 95% AMS for specimen HSL-4.....	451
Figure D.123: 14-Day strain profile with 95% AMS for specimen HSL-4.....	451
Figure D.124: Live end DEMEC and end slip ( $\alpha = 2$ ) transfer lengths at 28 days.....	465
Figure D.125: Dead end DEMEC and end slip ( $\alpha = 2$ ) transfer lengths at 28 days.....	465
Figure D.126: Live end DEMEC and end slip ( $\alpha = 3$ ) transfer lengths at 28 days.....	466
Figure D.127: Dead end DEMEC and end slip ( $\alpha = 3$ ) transfer lengths at 28 days.....	466
Figure D.128: Live end DEMEC and end slip ( $\alpha = 2.85$ ) transfer lengths at 28 days.....	467
Figure D.129: Dead end DEMEC and end slip ( $\alpha = 2.85$ ) transfer lengths at 28 days.....	467

## Appendix E: Development Length Data

### Appendix F: STSB Curves

Figure F.1: Load vs. dead end slip and ram travel for strand specimen 1 .....	474
Figure F.2: Load vs. dead end slip and ram travel for strand specimen 2 .....	474
Figure F.3: Load vs. dead end slip and ram travel for strand specimen 3 .....	475
Figure F.4: Load vs. dead end slip and ram travel for strand specimen 4 .....	475
Figure F.5: Load vs. dead end slip and ram travel for strand specimen 5 .....	476
Figure F.6: Load vs. dead end slip and ram travel for strand specimen 6 .....	476

## List of Tables

### Chapter 1: Introduction

### Chapter 2: Background

Table 2.1: Transfer Length Equations .....	46
Table 2.2: Development Length Equations .....	47
Table 2.3: Thatcher's Comparison of Transfer Length Methods .....	63
Table 2.4: Summary of LWC Transfer Length Data .....	71
Table 2.5: Summary of LWC Development Length Data .....	71
Table 2.6: Summary of Ward's Transfer and Development Length Data .....	98

### Chapter 3: Experimental Program

Table 3.1: Aggregate Properties .....	103
---------------------------------------	-----

### Chapter 4: Concrete Mixtures

Table 4.1: NSC Trial Batches .....	143
Table 4.2: Concrete Properties of NSC Batches .....	144
Table 4.3: NSS Trial Batches .....	148
Table 4.4: Concrete Properties of NSS Batches .....	149
Table 4.5: NSL Trial Batches .....	153
Table 4.6: Concrete Properties of NSL Batches .....	153
Table 4.7: Final NS Mix Designs .....	154
Table 4.8: HSC Trial Batches Using Only Type I Cement .....	155
Table 4.9: Concrete Properties of HSC Batches Using Only Type I Cement .....	156
Table 4.10: HSC Trial Batches Using Silica Fume .....	158
Table 4.11: Concrete Properties of HSC Batches Using Silica Fume .....	159
Table 4.12: HSC Trial Batches With Limestone .....	162
Table 4.13: Concrete Properties of HSC Batches With Limestone .....	162
Table 4.14: HSC Trial Batches Using Type III Cement .....	164
Table 4.15: Concrete Properties of HSC Batches Using Type III Cement .....	165
Table 4.16: HSS Trial Batches .....	168
Table 4.17: Concrete Properties of HSS Batches .....	168
Table 4.18: HSL Trial Batches .....	171
Table 4.19: Concrete Properties of HSL Batches .....	171
Table 4.20: Final HS Mix Designs .....	172

Table 4.21: Concrete Properties of NSC Beam Batches.....	173
Table 4.22: Mix Design for Beam NSS-1.....	174
Table 4.23: Concrete Properties of NSS Beam Batches.....	174
Table 4.24: Concrete Properties of NSL Beam Batches.....	176
Table 4.25: Concrete Properties of HSC Beam Batches.....	177
Table 4.26: Concrete Properties of HSS Beam Batches.....	178
Table 4.27: Concrete Properties of HSL Beam Batches.....	179
Table 4.28: Concrete Properties of Companion Batches for Modulus of Elasticity.....	180
Table 4.29: Measured Modulus of Elasticity at One Day of Age.....	181
Table 4.30: Measured Modulus of Elasticity at 28 Days of Age.....	181

## **Chapter 5: Transfer Length Results**

Table 5.1: NSC Transfer Length Measurements Over Time.....	187
Table 5.2: Comparison of NSC Transfer Length Predictions at 28 Days.....	187
Table 5.3: NSS Transfer Length Measurements Over Time.....	195
Table 5.4: Comparison of NSS Transfer Length Predictions.....	195
Table 5.5: NSL Transfer Length Measurements Over Time.....	202
Table 5.6: Comparison of NSL Transfer Length Predictions.....	203
Table 5.7: HSC Transfer Length Measurements Over Time.....	209
Table 5.8: Comparison of HSC Transfer Length Predictions.....	210
Table 5.9: HSS Transfer Length Measurements Over Time.....	216
Table 5.10: Comparison of HSS Transfer Length Predictions.....	216
Table 5.11: HSL Transfer Length Measurements Over Time.....	222
Table 5.12: Comparison of HSL Transfer Length Predictions.....	223
Table 5.13: 95% Upper-Confidence Bound for the Mean of Using a t Distribution.....	232
Table 5.14: 95% Upper-Confidence Bound for the Mean Using a t Distribution.....	232
Table 5.15: 95% Upper-Confidence Bound for the Mean Using a t Distribution.....	233

## **Chapter 6: Development Length Results**

Table 6.1: STSB Results for the Strand Used to Construct Beam Specimens.....	247
Table 6.2: Summary of NSC Flexural Test Data.....	261
Table 6.3: Development Length Predictions for the NSC Specimens.....	261
Table 6.4: Summary of NSS Flexural Test Data.....	279
Table 6.5: Development Length Predictions for the NSS Specimens.....	279
Table 6.6: Summary of NSL Flexural Test Data.....	294

Table 6.7: Development Length Predictions for NSL Specimens .....	294
Table 6.8: Summary of HSC Flexural Test Data .....	308
Table 6.9: Development Length Predictions for the HSC Specimens .....	309
Table 6.10: Summary of HSS Flexural Test Data .....	323
Table 6.11: Development Length Predictions for the HSS Specimens .....	324
Table 6.12: Summary of HSL Flexural Test Data .....	338
Table 6.13: Development Length Predictions for the HSL Specimens .....	339
Table 6.14: Summary of Measured Development Length .....	340

## **Chapter 7: Conclusions**

### **References**

### **Appendix A: Testing Procedures**

### **Appendix B: Beam Analysis Calculations**

Table B.1: Beam Gross-Section Properties .....	365
Table B.2: Normal Strength (NS) Beam Transformed-Section Properties .....	366
Table B.3: High Strength (HS) Beam Transformed-Section Properties .....	366
Table B.4: Moment Capacity Calculations .....	368
Table B.5: Initial Shear Capacity Parameters .....	373
Table B.6: Initial Shear Capacity Parameters .....	374
Table B.7: Elastic Shortening Parameters .....	375
Table B.8: Concrete Shrinkage Loss Parameters .....	378
Table B.9: Concrete Creep, Relaxation, and Total Losses .....	379
Table B.10: Measured Modulus of Elasticity at Seven Days of Age .....	380

### **Appendix C: Moisture Content Errors**

### **Appendix D: Transfer Length Data**

Table D.1: NSC Series Statistical Parameters .....	452
Table D.2: NSS Series Statistical Parameters .....	452
Table D.3: NSL Series Statistical Parameters .....	452
Table D.4: HSC Series Statistical Parameters .....	453
Table D.5: HSS Series Statistical Parameters .....	453
Table D.6: HSL Series Statistical Parameters .....	453
Table D.7: NSC Series 95% Confidence Intervals .....	454

Table D.8: NSS Series 95% Confidence Intervals.....	454
Table D.9: NSL Series 95% Confidence Intervals .....	454
Table D.10: HSC Series 95% Confidence Intervals .....	454
Table D.11: HSS Series 95% Confidence Intervals.....	455
Table D.12: HSL Series 95% Confidence Intervals .....	455
Table D.13: Test for Difference in the Means of the NSC and NSS Series .....	457
Table D.14: Test for Difference in the Means of the NSC and NSL Series .....	457
Table D.15: Test for Difference in the Means of the NSS and NSL Series .....	457
Table D.16: Test for Difference in the Means of the HSC and HSS Series .....	458
Table D.17: Test for Difference in the Means of the HSC and HSL Series .....	458
Table D.18: Test for Difference in the Means of the HSS and HSL Series .....	458
Table D.19: Test for Difference in the Means of the NSC and HSC Series.....	459
Table D.20: Test for Difference in the Means of the NSS and HSS Series.....	459
Table D.21: Test for Difference in the Means of the NSL and HSL Series .....	459
Table D.22: NSC End Slip Over Time .....	460
Table D.23: NSS End Slip Over Time.....	460
Table D.24: NSL End Slip Over Time.....	460
Table D.25: HSC End Slip Over Time .....	461
Table D.26: HSS End Slip Over Time.....	461
Table D.27: HSL End Slip Over Time.....	461
Table D.28: NSC End Slip Transfer Lengths Over Time.....	462
Table D.29: NSS End Slip Transfer Lengths Over Time .....	462
Table D.30: NSL End Slip Transfer Lengths Over Time .....	463
Table D.31: HSC End Slip Transfer Lengths Over Time.....	463
Table D.32: HSS End Slip Transfer Lengths Over Time .....	464
Table D.33: HSL End Slip Transfer Lengths Over Time .....	464

## **Appendix E: Development Length Data**

Table E.1: Results of Flexural Tests on NSC Specimens.....	468
Table E.2: NSC Embedment Lengths Divided by Predicted Development Lengths .....	468
Table E.3: Results of Flexural Tests on NSS Specimens .....	469
Table E.4: NSS Embedment Lengths Divided by Predicted Development Lengths.....	469
Table E.5: Results of Flexural Tests on NSL Specimens .....	470
Table E.6: NSL Embedment Lengths Divided by Predicted Development Lengths.....	470
Table E.7: Results of Flexural Tests on HSC Specimens.....	471

Table E.8: HSC Embedment Lengths Divided by Predicted Development Lengths .....	471
Table E.9: Results of Flexural Tests on HSS Specimens .....	472
Table E.10: HSS Embedment Lengths Divided by Predicted Development Lengths .....	472
Table E.11: Results of Flexural Tests on HSL Specimens .....	473
Table E.12: HSL Embedment Lengths Divided by Predicted Development Lengths .....	473

## **Appendix F: STSB Curves**



## Chapter 1: Introduction

### 1.1 Prestressed Bond in Lightweight Self-Consolidating Concrete

Lightweight structural concrete has been used in many applications due to the possibility of reduced dead loads. In the precast/prestressed industry these reduced dead loads also lead to lower transportation and handling costs. The absorptive, porous, and even pozzolanic nature of lightweight aggregates provides a stronger interfacial transition zone and internal curing that can even lead to improved durability for lightweight concrete over conventional concrete. It is only logical to combine these benefits with the reduced labor costs and energy usage of self-consolidating concrete. Numerous studies have been conducted on the bond of prestressing strand to normal weight concrete since the first research by Jack R. Janney in the 1950s, but information on the bond of prestressing strand used along with lightweight self-consolidating concrete (LWSCC) is somewhat lacking. As bond failures tend to be sudden and catastrophic, more research is needed to ensure the safety of using members cast with LWSCC.

### 1.2 Lightweight Concrete

Concrete made using lightweight aggregates dates back to as early as the Roman Empire, but was not widely used until the rotary kiln process for expanding shale, clay, and slate was patented in the early twentieth century. Lightweight structural concrete (LWC) is defined as “concrete having a minimum 28-day compressive strength in excess of 2500 psi (17 MPa), an equilibrium density between 70 and 120 lb/ft<sup>3</sup> (1120 to 1920 kg/m<sup>3</sup>), and consists entirely of lightweight aggregate or a combination of lightweight and normal-density aggregate.” (ACI 2003). Unit weights are typically between 105 lb/ft<sup>3</sup> and 120 lb/ft<sup>3</sup> (1680 kg/m<sup>3</sup> to 1920 kg/m<sup>3</sup>). Aggregates used for lightweight structural concrete typically include processed aggregates satisfying ASTM C330. These include rotary kiln expanded shales, clays, and slates; sintered

shales, clays, or slags; and pelletized or sintered fly ash. Concrete can be “all-lightweight” where both the coarse and fine aggregates are replaced with lightweight aggregates or “sand lightweight” where only the coarse aggregate is lightweight and natural sand is used for the fine aggregate (ACI 2003).

### **1.3 Self-Consolidating Concrete**

Self-consolidating concrete (SCC), sometimes known as self-compacting concrete, is concrete specially proportioned such that it exhibits high deformability in the fresh state, but with a high segregation resistance. This segregation resistance should be in spite of flow distance and vertical drop. SCC flows and compacts under its own weight without the need for vibratory consolidation and is able to flow through congested reinforcement and confined spaces without losing flow characteristics. It was developed in Japan in the late 1980s in response to durability problems caused by a shortage of skilled workers needed for concrete placement (Okamura 2003, Bonen and Shah 2005).

### **1.4 Prestressed Concrete**

Pretensioned, prestressed concrete utilizes reinforcement that is tensioned between fixed abutments before the concrete is placed around it. Once the concrete reaches an acceptable strength, the tension force is transferred to the concrete as an axial compressive force. This compressive prestress mitigates some of the tension forces resulting from the applied loads, and the tensile strength of the reinforcement is utilized once the beam is loaded past cracking. In order to utilize the benefits of this concept, the pretension force must be effectively transferred to the concrete to provide the compression. This is typically done entirely by bond between the concrete and steel. The end of a specimen nearest the tensioning apparatus is termed the live end while that opposite the tensioning apparatus is termed the dead end of the specimen. The

reinforcement used for prestressed concrete is typically a seven wire strand with six wires wrapped around a center wire in a helical pattern. Prestressing strand typically has a tensile strength greater than 270 ksi (1862 MPa) and nominal diameters of 0.5 in. and 0.6 in. (12.7 mm and 15.2 mm) are commonly used for larger members such as bridge girders.

### **1.5 Transfer Length**

The length of steel to concrete bond that is required to develop the full prestressing force in the steel is known as the transfer length. The stress in the strand varies from zero at the free end of the strand up to the full initial prestress at the opposite end of the transfer length. This variation is typically assumed to be linear (AASHTO 2007, ACI 2011), as shown in Figure 1.1. Other models have been suggested (FIP 1982, Thatcher et al. 2002) and the true variation is unknown. There are three factors with potential to contribute to bond in the transfer zone. These include adhesion, friction, and mechanical resistance between the concrete and the reinforcement. Friction is considered to be the main factor influencing bond in the transfer zone with mechanical resistance due to the helical shape of strand providing some contribution. Adhesion does not contribute since there is relative movement between concrete and steel at prestress transfer. When the tension force is released from the reinforcement the diameter increases causing an outward pressure that increases the friction force along with providing wedging action. This is known as the Hoyer Effect (Hanson 1959). Steel stress becomes basically constant at the end of the transfer length, and due to the stress/strain relationship of steel, can be determined by measuring the strains in the steel (Russell 1996). Some researchers have used end slip at prestress transfer as a correlation to transfer length as well (Logan 1997). The current codes do not specify a required transfer length, but transfer length prediction can be

pulled from the development length equation of both ACI 318-11 *Building Code Requirements for Structural Concrete* and AASHTO LRFD *Bridge Design Specifications* in the form of

$$L_t = \frac{f_{se}}{3} d_b.$$

In this expression  $f_{se}$  is the effective prestress in the strand after all losses are accounted for (ksi) and  $d_b$  is the nominal diameter of the prestressing strand (in.) (Russell 1996, ACI 2011, AASHTO 2007). The ACI 318 code also gives a provision of  $50d_b$  (ACI 2011) and the AASHTO LRFD Specifications  $60d_b$  (AASHTO 2007) for use in determining shear strength. Transfer lengths as predicted by these equations are typically less than 36 in. (915 mm) for commonly used strand diameters.

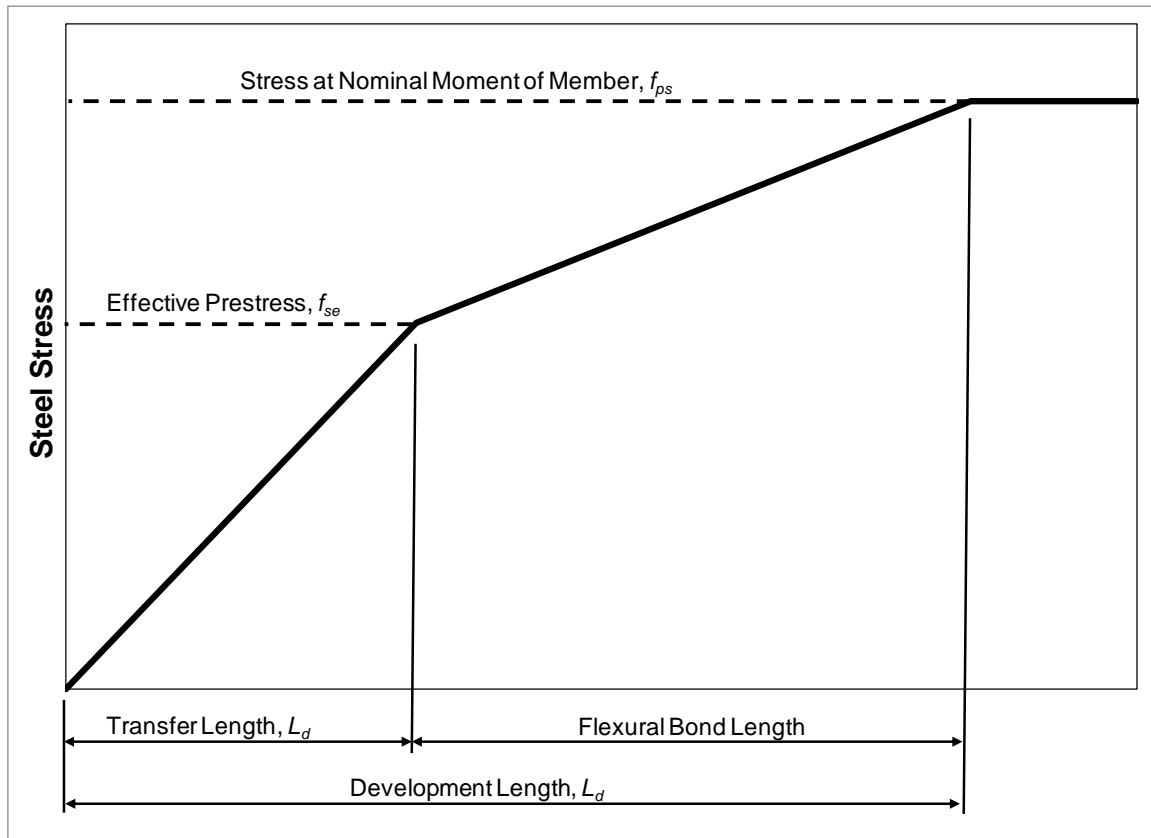


Figure 1.1: Idealized steel stress distribution illustrating transfer and development length

## 1.6 Development Length

The length of bonding required to resist a given load will increase as the load increases to a maximum at beam failure. The distance from the free end of the prestressing steel required to fully bond the strand to the concrete such that the design strength of the strand may be utilized is termed the development length (ACI 2011). This is taken to mean that the development length is equal to the distance from the end of bonding to the section where the nominal moment can be resisted, as shown in Figure 1.1. This length is measured from the beam end for fully bonded strands and from the end of debonding for debonded strands.

Development length is the sum of both the transfer length and the flexural bond length. Flexural bond length is the length required between the end of the transfer length and the point of maximum moment to develop the additional stress difference between the initial prestress and the strength of the strand. Flexural bond is only present after the member has been loaded to cracking. When the beam cracks, the bond stress near the cracks increases to a limiting value, local slip occurs and the bond stress returns to a lower value. This effect continues away from the cracks toward the beam ends, and if it reaches the transfer zone, can cause general strand slip. Flexural bond in a prestressed member behaves in a manner similar to beams with deformed reinforcement (Janney 1954, Hanson and Kaar 1959). The steel stress within the flexural bond length varies with a smaller slope than that in the transfer length do to the lack of the Hoyer effect as a bond mechanism.

ACI 318-11 uses the equation,

$$L_d = \left(\frac{f_{se}}{3}\right) d_b + (f_{ps} - f_{se}) d_b$$

to predict development length where  $f_{se}$  is the effective prestress in the strand after all losses are accounted for (ksi),  $f_{ps}$  is the stress in the steel at nominal flexural strength (ksi), and  $d_b$  is the

nominal diameter of the prestressing strand (in.) (ACI 2011). Development lengths calculated using this expression are typically less than 100 in. (2540 mm) for commonly used strand diameters. This same equation is used in a slightly different form in the AASHTO LRFD Specifications. The AASHTO version includes a multiplier of 1.6 for members having a depth greater than 24 in. (AASHTO 2007).

## 1.7 Objectives

Lightweight self-consolidating concrete (LWSCC) has recently begun to come into more widespread use as a structural construction material. Little research has been conducted on the bond behavior of LWSCC, especially in prestressed applications. This project focused on the bond behavior of members cast using LWSCC made with expanded clay and shale aggregates, with limestone aggregate SCC as control. The main objective of this project was to determine if the current code provisions for transfer and development length produced an accurate prediction for 0.6 in. (15.2 mm) strands in members cast with LWSCC. Numerous factors are involved in the bond behavior of prestressed concrete members. The effects of aggregate type and concrete compressive strength were the main factors considered in this project. Strand with a diameter of 0.6 in. (15.2 mm) was examined as it is commonly used in bridge girders due to its ability to carry a similar force with fewer strands. It was also the focus of a ban by FHWA in the 1990s. Other objectives included comparing the bond behavior of LWSCC to that of normal weight SCC, determining whether surface strain or end slip measurements were most effective for measuring transfer length, and what factors, if any, should be added to the existing equations.

## 1.8 Testing Program

The testing program included a number of activities. Numerous LWSCC mixtures were examined in order to obtain the desired fresh and hardened concrete properties using the different aggregates. Six concrete mixtures were developed meeting the compressive strength requirements of 4000 psi and 6000 psi (28 MPa and 41 MPa) at one day of age and using the expanded clay, expanded shale, and limestone aggregates. Prestressing strand was qualified using the methods developed by previous researchers to ensure that the strand used for the project indeed had good bonding characteristics. Transfer and development length were measured for 25 small-scale beam specimens measuring 6.5 in. by 12 in. by 18 ft long (165 mm by 305 mm by 5.5 m). These dimensions were based on those used for previous research (Logan 1997, Rose and Russell 1997, Peterman et al 2000, Larson et al. 2007, Ramirez and Russell 2008, Staton et al. 2009, Ward et al. 2009, and Floyd et al. 2011) in order to produce comparable data. Four specimens were constructed with each of the six different concrete mixtures, and an extra specimen was cast using an earlier version of one of the mixtures for a total of 25 specimens. The measured transfer and development lengths were compared between the different concrete types and to the equations from the established design codes and previous research.

## Chapter 2: Background

### 2.1 Bond of Prestressing Strand

In order to utilize the benefits of prestressed concrete, the prestressing force must be adequately transferred to the concrete member and the member must be able to utilize the tensile strength of the reinforcement to reach full moment capacity. These two functions are typically fully accomplished through bond between the concrete and the steel. Bond stresses in the transfer zone transfer the initial pretension force in the reinforcement to a compression force in the member. The length of the member that is required to produce bond forces adequate to transfer the prestress to the beam is termed the transfer length, which is described in Chapter 1. Bond stresses between the concrete and steel transfer the tension forces from the concrete to the steel after cracking has occurred in the beam. The portion of the beam required to provide the bond force necessary to resist this tension force is termed the flexural bond length. The summation of these two factors is the length of the beam required to provide the bond force needed to develop the full strength of the strand reinforcement and is termed the development length.

#### 2.1.1 Bond Mechanisms

Several mechanisms are used to transfer the force between the concrete and the steel. The three main factors that contribute to bond between steel and concrete are adhesion, friction, and mechanical resistance. Adhesion resistance is typically small and does not contribute once relative movement between strand and concrete has occurred. Friction forces are considered to be the main factor in transfer of prestress to a pretensioned member. When the prestressing strand is tensioned, a reduction in diameter occurs as per Poisson's ratio. Once the tension force is released the strand diameter increases, which causes outward pressure on the concrete as well



as a wedging action. This increased outward pressure increases the frictional resistance between the steel and the concrete. The helical shape of the typically used seven wire prestressing strand provides substantial mechanical resistance as the concrete that fills the gaps between the individual wires resists the direct pull-out of the strand (Hanson 1959).

### **2.1.2 Previous Research**

Numerous research programs concerned with bond between prestressing steel and normal weight concrete have been conducted beginning with Janney in the 1950's. As larger diameter strands, high-performance concrete, self-consolidating concrete, and lightweight concrete have come into wider usage, these materials have increasingly been studied as well. These other forms of concrete have shown properties dissimilar to conventional concrete, and their bond performance has also been questioned at times. The use of 0.6 in. (15.2 mm) strand was questioned to the point that it was banned by the FHWA between 1988 and 1996 (Kose 2005 ACI). An adequate knowledge of the behavior of materials used in prestressed concrete construction is necessary for safe design and construction of structures.

#### **2.1.2.1 Janney**

Some of the first work on the nature of bond in prestressed members was published by Jack Janney in the 1950s. He investigated the influence of wire diameter, surface condition, and concrete strength on the transfer of prestressing force, flexural bond, and the interaction between transfer bond and flexural bond. Testing was broken into two series, one to investigate each of the two bond actions. The first series involved small prestressed concrete prisms consisting of four wire diameters and one strand diameter, three steel surface conditions, and two concrete strengths to examine the effects on transfer bond. The second series consisted of short beam specimens loaded at midspan in order to examine flexural bond stresses. Three wire diameters

and one strand, two surface conditions, and several degrees of pretension were used in this second series (Janney 1954).

Prisms used in the first series of tests measured 2 in. x 2 in. (50 mm x 50 mm) in cross-section, had a length of either 72 in. or 96 in. (1.83 m or 2.44 m), and contained a single wire or strand. Wire diameters and surface conditions included 0.162 in. (4.1 mm) wire tested clean, lubricated, and rusted and 0.100 in. (2.5 mm) wire, 0.197 in. (5.0 mm) wire, 0.276 in. (7.0 mm) wire, and 5/16 in. (7.9 mm) strand all tested both clean and lubricated. Reinforcement was stressed to 120,000 psi (827 MPa) and specimens were cast using a concrete mixture with a strength of 4500 psi (31 MPa) except for one 0.162 in. (4.1 mm) clean wire specimen using 6500 psi (45 MPa) concrete (Janney 1954).

Concrete surface strains were measured using SR-4 strain gauges and these were used to determine the strain and therefore stress in the steel. Compatibility of strains was considered to be adequate except at the very end regions of the specimens. At the ends of the specimens concrete strain was zero and the corresponding steel strain was at a maximum. The difference between steel and concrete strains decreased up to a point where the strains became equal and constant. In the region of strain gradient between the end of the specimen and the location of constant strain slip must have occurred, therefore no adhesion was considered for transfer of prestress. Mechanical resistance was also discounted due to the use of smooth wire and therefore friction was the main mechanism of transfer. This frictional resistance was aided by the increase in wire diameter after prestress release. Little difference was found in the bonding ability of the different wire diameters, but the length of embedment required for transfer increased with wire diameter. The larger diameter wires placed a larger force on the concrete specimens which caused a greater shortening of the specimens and a corresponding loss of tension stress in the

steel. Since transfer bond was considered to be mostly due to friction, increased concrete strength was determined to have little effect on the coefficient of friction, but it was suspected to help sustain the radial pressure utilized in the Hoyer effect. Rusted wires were found to develop transfer of prestress more quickly than clean wire while lubricated wires did not transfer stress as quickly, most likely due to a reduced coefficient of friction (Janney 1954).

Beam specimens used in the second series of tests had a cross-section measuring 6 in. x 10 in. (152 mm x 254 mm) and were 78 in. (1.98 m) in length. Wire or strand reinforcement was placed 1.25 in. (32 mm) from the bottom of the specimens and each beam was loaded at the midpoint of a 6 ft span. (1.83 m) Reinforcement ratios between 0.137 and 0.199 were used in conjunction with the three wire sizes and one strand size. Several different values of prestress were used for reinforcement in both clean and rusted conditions. Concrete used to cast the beam specimens had a compressive strength at release of 4000 psi (28 MPa) and a strength of 4500 psi (31 MPa) at the time of testing. Beams were loaded to failure over the course of a few minutes. Strains were measured continuously and deflection measurements were taken at intervals during loading. All beams containing clean wire failed due to bond while all beams reinforced with rusted wire failed due to fracture of the wire. Ultimate flexural bond stresses were determined to be substantially higher for rusted wires as opposed to those for clean wires on the order of 500 psi to 800 psi (3.4 MPa to 5.5 MPa) and 160 psi to 220 psi (1.1 to 1.5 MPa) respectively. The author indicated that the bond performance of rusted wire is far superior to that of clean wire, but also that corrosion to the point of a reduced cross-section is unacceptable (Janney 1954).

When flexural cracking occurred in beams reinforced with unstressed wire, it was observed that the local bond stress near the flexural cracks increased to some limiting value followed by local slip of the reinforcement. As load increased past this point, the bond stress

concentration moved toward the ends of the beam as a wave until the maximum bond stress reached the end of the beam at bond failure. It was suspected that this action occurred smoothly. The rusted wire specimens did not exhibit bond failure as the higher bond stresses allowed for a larger load that caused fracture of the wires. In specimens reinforced with pretensioned wire, a bond failure occurred when the wave of limiting bond stress met the end of the transfer bond region. This was due to the fact that the increased tension force in the wire reduced the diameter in the transfer zone which is detrimental to the bonding characteristics, explained earlier, in this region. Therefore, it was concluded that the effective length available for flexural bond action is the length from the end of the beam to the critical section minus the prestress transfer length (Janney 1954).

This research conducted by Janney was some of the first investigative work done concerning the bond behavior of pretensioned reinforcement. Despite the fact that his work consisted mostly of specimens constructed using wire reinforcement, not the seven wire strand typically used in modern prestressing, his foundation has been used in the research of many other investigators in the many years that have followed. The conclusions drawn from this research concerning bond behavior and mechanisms are still used to explain the behavior of bond in prestressed members today.

#### 2.1.2.2 Thorsen

This research examined the use of larger prestressing strands instead of many smaller wires. As this was very early in the development of prestressed concrete, 7/16 in. (11.1 mm) and 1/2 in. (12.7 mm) strands were only used on a very limited basis. The benefits of using larger tendons were indicated to include simplified design and construction since less reinforcement could be used to get the same prestressing force. Steel stress curves for both transfer of prestress

and maximum flexural stress were developed and indicated as being different phenomena. The transfer of prestress causes the strands to expand outward near the ends thus producing an outward normal force and increasing the friction force with the surrounding concrete. Therefore, the prestress transfer curve developed bond forces faster than the rest of the strand. This was very similar to the description of bond forces given by Janney. Transfer length measurement methods included using both strain gauges placed on the outer concrete surface as well as measuring end slip at prestress release. Flexural bond/development length measurement methods included flexural tests using point loads at various distances from the supports and simple pull-out tests. These different test methods were then used to draw the bond strength curves for both transfer bond and flexural bond (Thorsen 1956).

Concrete compressive strengths of less than 3500 psi (24 MPa) were found to result in a wide scatter of bond values. Therefore, 3500 psi (24 MPa) was recommended as the minimum strength of concrete at prestress release for small tendons and 4000 psi (28 MPa) was recommended for 7/16 in. (11.1 mm) and 1/2 in. (12.7 mm) strands. Conservative values of transfer length were recommended for use until more accurate predictions could be developed. These values included 3 ft (0.91 m) for 0.196 in. (5.0 mm) wire and 2 ft (0.61 m) for 0.276 in. (7.0 mm) wire and strands 3/8 in. (9.5 mm) or less in diameter. It was indicated that 5 ft (1.52 m) would be adequate for development length of strands up to 3/8 in. (9.5 mm) in diameter. Concentrated forces at the end zone of the strands were indicated to be a problem for cracking. Therefore, minimum spacings, minimum cover, and a triangular strand distribution were recommended. Debonding of strands at the ends of members or using curved tendons were also suggested as possibilities for reducing concentrated forces at the strand end regions (Thorsen 1956).

### 2.1.2.3 Nordby and Venuti

This research program was one of the first investigating bond in both normal weight concrete (NWC) and lightweight concrete (LWC). It was mainly concerned with fatigue behavior of prestressed members, but some bond information was collected as well. Four rectangular beam cross-sections were examined using 5/16 in. (7.9 mm) and 3/8 in. (9.5 mm) seven-wire stress-relieved strands. Concrete mixtures consisted of either expanded shale or conventional stone aggregate and had similar strengths at 28 days (5500 psi to 6500 psi (38 MPa to 45 MPa)). Overnight steam curing was used for all concrete to reach the desired strength of 4000 psi (28 MPa) at release. Modulus of elasticity and modulus of rupture were less for the expanded shale aggregate concrete, but drying shrinkage measured over two months was comparable for both mixtures. Four beam cross-sections were cast. Three of the sections measured 6 in. (152 mm) wide by 4.5 in. (114 mm) deep. One had three 5/16 in. (7.9 mm) strands placed 1.25 in. (32 mm) from the bottom, one had two 3/8 in. (9.5 mm) strands placed 1.25 in. (32 mm) from the bottom, and the third had two 3/8 in. (9.5 mm) strands 1 in. (25 mm) from the bottom. The fourth cross-section measured 5 in. (127 mm) wide by 10 in. (254 mm) deep and had two rows of two 3/8 in. (9.5 mm) strands 1.5 in. and 3.5 in. (38 mm and 89 mm) from the bottom. Each beam had two No. 3 (No. 10) reinforcing bars in the compression zone (Nordby 1957).

In the first phase, conventional concrete beams were cast in identical pairs and one of each pair was subjected to fatigue loading. If the beam did not fail under this loading, both it and its partner would be tested under static load to failure. The second phase compared LWC and NWC beams in both fatigue and static testing. In the third phase the largest cross-section beams made of both LWC and NWC were tested only under static load. Fatigue tests were performed

using a special fatigue machine that applied the specified load at a rate of 90 cycles per minute. Static load tests consisted of a 12 ft (3.66 m) simple span with two concentrated loads placed either 6 in. or 18 in. (152 mm or 457 mm) apart at the center of the beam or at the quarter points. Deflection was measured at the center of the span, dial gauges monitored strand slip, and electric strain gauges were attached to the strands and to the concrete surface (Nordby 1957).

No bond failures resulted from fatigue testing, but nine beams in phase 2 and 3 failed in bond. These failures typically resulted in a shear failure due to a reduction in prestress after a slip of 0.01 in. (0.25 mm). Embedment length was determined to be a more important factor than bond stress. An embedment of 6 ft (1.83 m) resulted in strand rupture for the 3/8 in. (9.5 mm) strand in the 6000 psi (41 MPa) NWC and an embedment of 3 ft (0.91 m) was recommended for the 5/16 in. (7.9 mm) strand under the same conditions. Larger values were recommended for the expanded shale concrete. General observations of the tests confirmed the wave of bond stress theory proposed by Janney (Nordby 1957).

#### 2.1.2.4 Hanson and Kaar

Hanson and Kaar studied the bond behavior of 7 wire prestressing strands. Their work was concerned with the development of theory to predict bond strength as well as the influence of various factors on bond performance. These factors included primarily embedment length and strand diameter, but also reinforcement ratio and concrete strength. Influence of strand surface condition and embedded end anchorages were also given some consideration. The nature of transfer and flexural bond were described in a manner very similar to the description given by Janney with the addition of mechanical resistance of the strand having a substantial effect in the transfer zone. This extra resistance can increase capacity once the flexural bond stress wave has reached the transfer zone (Hanson 1959).

The research program consisted of 47 beam tests utilizing various combinations of the variables mentioned previously. Beam specimens had widths between 4 in. and 8 in. (102 mm and 203 mm), effective depths between 5.50 in. and 11.47 in. (140 mm and 291 mm), and contained between 1 and 6 strands depending on the variable being tested. The beams were divided into four series examining strand diameter and embedment, concrete strength, variation of reinforcement ratio, and strand surface condition. All beams used the same conventional concrete mixture having a 2 in. (51 mm) slump that was placed using internal vibration. Concrete strengths at release were 4500 psi (31 MPa) for most beams and 3500 psi (24 MPa) for lower strength concretes. Concrete strengths at the time of flexural testing varied from 3700 psi (26 MPa) to 7800 psi (54 MPa) depending on the variables being tested. Strand diameters used included ¼ in. (6.4 mm), 3/8 in. (9.5 mm), and ½ in. (12.7 mm). The beam tests used a continuously increasing load on a simple shear span having various lengths. Strains were monitored using continuously recording SR-4 strain gauges mounted to the strands; deflection and strand slip were measured using dial gauges that were read without interruption of loading (Hanson 1959).

Moment at general bond slip was compared to the ultimate moment capacity predicted using strain compatibility. Shorter embedment lengths resulted in general strand slip at lower moments, but some resistance was developed after slip due to mechanical interlock of the strands. It was determined that a critical embedment length to achieve strand fracture existed for each strand size, but that this might not be necessary if the beam failed by concrete crushing. Increasing the percentage of steel was found to reduce the average bond stress at flexural failure for a given embedment length. Reduced concrete strengths led to failure in flexure without slip as the concrete crushed before high steel stresses were reached. Rusted strand was found to



perform better than clean strand and embedded end anchors were found to have little effect (Hanson 1959).

A relationship between strand size, embedment length, and the average bond stress at general bond slip was determined and is shown here as

$$u_a = \frac{f_{sb} A_s}{l_u \Sigma o}$$

In this expression  $u_a$  is average bond stress,  $f_{sb}$  is maximum steel stress at the time of general bond slip,  $A_s$  is area of reinforcement,  $l_u$  is embedment length, and  $\Sigma o$  is total circumferential area per inch of beam. This relationship was used to produce design criteria relating steel stress at general bond slip to embedment length for ¼, 3/8, and ½ in. (6.4, 9.5, and 12.7 mm) prestressing strand. Results of the tests supported the flexural bond wave theory of Janney and confirmed that a general bond slip occurs in a pretensioned beam when the flexural bond stress wave reaches the prestress transfer zone. It was also confirmed that reinforcement having a rusted surface performed better than clean reinforcement. Seven wire strand was found to have superior performance when compared to smooth wires due to the increased bond capacity provided by mechanical interlock (Hanson 1959).

#### 2.1.2.5 Hanson

This research program examined the effects of strand surface roughness on transfer length of 7/16 in. (11.1 mm) prestressing strands. Fourteen prestressed concrete prisms were constructed using as received, partially rusted, and rusted strands. Specially deformed (dimpled) strand was also examined. Transfer lengths were measured using the prisms and flexural strength was examined with the prisms loaded in such a way as to produce large moments in the transfer zone. A 30% reduction in transfer length was found for rusted strand and a similar improvement for dimpled strand over as received strand. High moments could also be resisted

by prisms with rusted or deformed strand. The use of controlled surface roughness was indicated to be a potential method for improving bond in short members (Hanson 1969).

#### 2.1.2.6 Zia and Mostafa

This research consisted of an extensive examination of literature in order to examine the adequacy of the ACI equation for transfer and development length of prestressing strands. It was indicated that previous theories of transfer length underestimate actual values as they predicted unrealistically high localized concrete stresses in the transfer zone. It was also agreed that transfer length varies directly with strand size and is also affected by steel stress and concrete strength. Transfer length was found to generally be longer for larger strand sizes, higher prestress levels, and lower concrete strengths. Sudden prestress release also leads to longer transfer lengths but can be mitigated by heating the strands before cutting. Using data from previous experiments, the authors proposed the expression

$$L_t = 1.5 \frac{f_{si}}{f'_{ci}} d_b - 4.6$$

for transfer length where  $f_{si}$  is the initial prestress (ksi),  $f'_{ci}$  is the concrete strength at prestress release (ksi), and  $d_b$  is the nominal strand diameter (in.). This equation is more conservative than the ACI expression and is applicable to concrete strengths at release of 2000 psi to 8000 psi (14 MPa to 55 MPa) (Zia 1977).

Using the development length data from Hanson and Kaar (Hanson 1959) the authors proposed that the required embedment for each strand size was shorter than that reported. The average flexural bond stress was then calculated from these actual embedment lengths and was found to be 233 psi (1.6 MPa), which was less than the 250 psi (1.7 MPa) used in the ACI equation. The authors therefore proposed a value of 200 psi (1.4 MPa) be used for the flexural bond portion of the design equation and proposed the expression

$$L_d = 1.5 \frac{f_{si}}{f'_{ci}} d_b - 4.6 + 1.25(f_{su} - f_{se})d_b,$$

for development length. In this expression  $f_{su}$  is the stress in the strand at ultimate strength (ksi),  $f_{se}$  is the effective stress in the steel after all losses (ksi), and the other variables are as defined previously (Zia 1977).

#### 2.1.2.7 Fédération Internationale de la Précontrainte (FIP)

This report by the International Federation for Prestressing presented a mathematical model for what was termed “transmission length” as well as a standard test for measuring an experimental value useful for comparing various prestressing steels. “Transmission length” was defined as the length of concrete embedment from the end of the specimen to the point after which the stress in the prestressing steel is constant, which corresponds to the term transfer length described in Chapter 1. The mathematical model was formulated based on the different deformations that occur during transfer of prestress to the concrete. These include a small zone of unabated strand slip at the end of the member, relative displacement between the strand and concrete that varies in magnitude along the transfer length, and differences in concrete compressive strain between that immediately adjacent to the strand and across the rest of the cross-section. The small unabated end slip was deemed insignificant and other modifications due to the difference in concrete compressive strain were determined to be unnecessary by experimental study. The resulting simplified equation is

$$L_t = \beta \delta \frac{E_p}{\sigma_{po}}$$

where  $L_t$  is the transfer length,  $\beta$  is a shape factor for the stress distribution in the prestressing steel,  $\delta$  is the strand draw-in.,  $E_p$  is the modulus of elasticity of the prestressing steel, and  $\sigma_{po}$  is the stress in the steel after release, outside the transfer length. The value of  $\beta$  depends on the

assumed steel stress distribution, 2 for a linear variation, 3 for a parabolic distribution, and 4 if the steel stress rapidly increases from the point of zero stress. The value of 3 was recommended based on experimental results that determined  $\beta = 2.86$  (FIP 1982).

Several factors were described as affecting differences in theoretical transmission length and that in actual structures. A test method was presented that was intended to include the effects of these parameters including: initial prestress, time of release in relation to tensioning, spacing between tendons, concrete cover, concrete stress at release, concrete composition, concrete modulus of elasticity, tendon surface condition, release type, and type of loading. The experimental test consisted of prestressing strands cast in a rectangular prismatic section with the dimensions of the specimen based on the strand diameter, strand spacing, and concrete cover with a length equal to twice an assumed transmission length plus 1 m (3.3 ft). Strands were tensioned 24 hours prior to concrete placement and tension was adjusted to ensure that the stress in the steel was 75 percent of the tensile strength of the steel immediately after release. Concrete compressive strength varied between 3600 psi (25 MPa) and 7250 psi (50 MPa) at release of prestress depending on prestressing steel type. Three specimens were tested for each set of experimental conditions providing a minimum of six points for an average value of transfer length. Strand slip at release was measured using dial gauges or similar devices accurate to 0.0004 in. (0.01 mm) attached to the prestressing strands. Measurements were taken at 1 hour, 6 hours, 24 hours, and 7 days after release. The mathematical relationship was used to determine transfer length from these end slip measurements. Longitudinal concrete strains were measured with mechanical dial gauges having gage lengths placed in such a way as to provide five readings within the expected transmission length. Measurements were taken at the same accuracy and time increments as the strand draw-in measurements. Transfer length was then

determined as the point where the longitudinal concrete strain became constant along the length of the specimen. Values resulting from this test were described as standard for a specific prestressing steel and could be different than those on actual structural elements (FIP 1982).

#### 2.1.2.8 Cousins et al.

This research was conducted in response to the 1988 FHWA restrictions on development length. The goal was to develop a simple test that could be correlated to transfer and development length. This test attempted to reproduce the actual mechanisms of transfer bond in prestressed members. The adhesion and mechanical interlock can be modeled by a simple pullout test while the Hoyer effect and associated friction cannot. In order to account for the Hoyer effect, the strand was first pretensioned and a block of concrete was cast around it. The block was then forced off of the tensioned strand with a hydraulic actuator. The force in the strand versus the strand slip was measured to determine the force at which failure occurred. As the force applied to the block was increased, the stress in the strand on the side of the block opposite the applied force would decrease while the stress on the side with the hydraulic actuator would increase. The difference in stress from one side of the block to the other would cause a swelling effect in the strand on the side with the reduced stress which replicated the Hoyer effect in an actual member. While this was a reproduction of transfer bond, it could still be used to examine development length (Cousins 1992).

Results from these tests indicated higher bond stress at initial slip when compared to the direct pullout tests. This behavior is to be expected due to the swelling effect in the strand. Strand surface condition had a large impact on test results as well. Standard deviations were similar between the two methods, but were high enough to indicate that several tests would be required to obtain an average for a particular lot of strand. This test was found to be easy to

perform and repeat, but adequate research was not done in this study for comparison to transfer length results by other researchers (Cousins 1992).

#### 2.1.2.9 Shahawy et al.

This experimental and analytical investigation examined the transfer length of 0.5 in. and 0.6 in. (12.7 mm and 15.2 mm) prestressing strands in 41 ft (12.5 m) long AASHTO Type II girders. As debonded strands are often used to reduce stresses at the beam ends, different amounts of debonding were examined in addition to strand size and amount of shear reinforcement. Strands were spaced at 2 in. (50 mm), which was the code minimum for 0.5 in. (12.7 mm) strands and less than the minimum of 2.4 in. (61 mm) for 0.6 in. (15.2 mm) strands. Beams were cast end to end using strand that was generally shiny with small rust spots tensioned to 75 percent of  $f_{pu}$ . Prestress transfer was done using flame cutting, one strand at a time, 48 hours after casting. Electrical Resistance Strain Gauges (ERSGs) mounted to the concrete surface were used to measure concrete strains at the level of the prestressing steel. Measurements were monitored during release and recorded every two hours for two days after release (Shahawy et al. 1992).

The point of tangency between the line of constant slope and the line of constant strain on the strain plot from the ERSGs was taken as the transfer length of the beams. This method was used since the ERSGs produced well defined smooth curves. Average transfer length for 0.5 in. (12.7 mm) fully bonded strands was 30 in. (76 mm) and was 34 in. (86 mm) for the 0.6 in. (15.2 mm) strands. The behavior of the 0.6 in. (15.2 mm) strands spaced at 2 in. (50 mm) was similar to that of the 0.5 in. (12.7 mm) strands. This spacing was concluded to be adequate for 0.6 in. (15.2 mm) strands. These transfer lengths were greater than those calculated using the ACI equation and the expression

$$L_t = \frac{f_{si}}{3} d_b$$

where the variables are as defined previously, was recommended instead. The authors also recommended that the transfer length for debonded strands should be equal to the length of debonding plus the value calculated using this equation (Shahawy et al 1992).

#### 2.1.2.10 Lutz et al.

This study examined the development length of fully bonded concrete beams containing 0.5 in. (12.7 mm) and 0.6 in. (15.2 mm) prestressing strands. Nine I-shaped members resembling AASHTO sections with a composite deck were cast. The beam cross-section had an overall depth of 22 in. (559 mm), a flange width of 16 in. (406 mm), flange thickness of 5 in. (127 mm), and a web thickness of 4.5 in (114 mm). Four specimens contained five 0.5 in. (12.7 mm) strands and five specimens contained four 0.6 in. (15.2 mm) strands. All strand was seven-wire Grade 270 low-relaxation strand. The concrete used for the beams had a compressive strength of 4500 psi (31 MPa) at prestress release and a design strength of 6000 psi (41 MPa) at 28 days. The concrete was placed in two lifts and was consolidated using internal and form vibration. Prestress release was accomplished at 48 hours using flame cutting for all but one strand, which was gradually detensioned to prevent excessive movement of the beams (Lutz et al. 1992).

Development length was examined for these specimens using static load tests with varied embedment lengths on each end of the specimens. One specimen with 0.5 in. (12.7 mm) strands was tested three times, but it was not clearly explained how the third test was conducted. This resulted in a total of 19 development length tests. Load was applied using a simply supported arrangement with two point loads applied 24 in. (610 mm) apart using a single hydraulic ram and a spreader beam. Load increments of 5 kips (22 kN) were used until flexural cracking was

observed and increments of 2.5 kips (11 kN) were used after that. Measurements of load, strand strain, end slip, deflection, and compressive strain were recorded after each load increment. Each beam was loaded to failure and the failure type was examined to determine the relation of the embedment length to the development length. Applied load was measured using both a pressure transducer and load cells. Deflection and strand slip were measured using linear variable differential transformers (LVDTs) and extreme compression fiber strain was measured using the Detachable Mechanical Strain Measurement (DEMEC) system. These were monitored using a data acquisition system during each test to determine failure type. Development length was defined as “the embedment length required for the strand to develop the stress required for the beam to fail in flexure” (Lutz et al. 1992).

It was determined from these tests that development length for 0.5 in. and 0.6 in. (12.7 mm and 15.2 mm) strands was adequately predicted using the code equations. Measured development lengths were 72 in. (1830 mm) for the 0.5 in. (12.7 mm) strand and 84 in. (2130 mm) for the 0.6 in. (15.2 mm) strand. These are approximately 90 percent of the code prediction. Some slip was detected at these embedment lengths, but the specimens were able to achieve the predicted moment capacity. Required embedment lengths would be longer if no slip is allowed. Beams that failed due to bond reached moment capacities on the order of 90 percent of the predicted moment capacity but failed in a much more sudden and unpredictable manner. Web shear cracking was also discovered to be closely tied to bond failure behavior. Loss of prestress due to bond slip reduces shear and flexural capacity. It was determined that the beam cross section had a significant effect on the development length which could explain the disparity of conclusions by different researchers concerning this topic (Lutz et al. 1992).



#### 2.1.2.11 Deatherage et al.

This research program was conducted to produce data for comparison to the 1988 FHWA restrictions on prestressing strand. Twenty full-scale AASHTO Type I girders were constructed for testing using Grade 270 low relaxation 7-wire strand. Strand diameters examined included ½ in. (12.7 mm), ½ in. special (13.3 mm), 9/16 in. (14.3 mm), and 0.6 in (15.2 mm). Practices considered to have an influence on transfer and development length were used in construction. These included flame cutting at release and protection of the strand from weathering. Each 31 ft (9.45 m) long beam was cast using concrete with a design strength of 5000 psi (34 MPa) at 28 days around strands pretensioned to 203 ksi (1400 MPa), 75 percent of the specified ultimate strength. Prestress transfer was done when the concrete reached 4000 psi (28 MPa) except for two beams that were 3350 psi (23 MPa) and 3750 psi (26 MPa). Both ends were flame cut simultaneously. Electrical resistance strain gauges were bonded to the outer strands at the estimated development length and mechanical gauge points were attached to both sides of the beams at the neutral axis and center of gravity of the steel to measure strain (Deatherage et al. 1994).

Transfer lengths were determined using the slope intercept method and strains measured from the mechanical gauge points. Development length tests were performed using a single point loading configuration consisting of two steel tubes filled with concrete as supports and a hydraulic actuator as a single point load. An LVDT was used to measure displacement at the load point, which was then used to control the movement of the hydraulic ram. Applied load was measured using a load cell and strand slip was monitored using dial gauges placed on the bottom strands. An iterative procedure was used for determination of development length beginning with the calculated development length and then examining the failure type to

determine the relationship of that embedment length to the development length. This information was then used to locate the next load (Deatherage et al. 1994).

It was concluded from this research that the adhesion force and friction force on a prestressing strand are affected by strand diameter and that mechanical resistance is significant for larger strands due to larger gaps between individual wires. Minor weathering was also found to improve strand bonding capabilities. The ACI/AASHTO equations were found to be somewhat unconservative and modifications were proposed. It was proposed that the transfer length equation be modified by using the initial prestress,  $f_{si}$ , in ksi instead of the effective stress after losses,  $f_{se}$ , resulting in the form

$$L_t = \frac{f_{si}}{3} d_b$$

for strands smaller than 0.6 in. (15.2 mm) and that more research was required for transfer length of 0.6 in. (15.2 mm) strands. The author recommended that 0.6 in. (15.2 mm) strands should not be prohibited as results were comparable to other strand sizes. A multiplier of 1.5 was proposed for the flexural bond portion of the development length resulting in the equation

$$L_d = \frac{f_{si}}{3} d_b + 1.5(f_{ps} - f_{se})d_b$$

where  $f_{ps}$  is the stress in the strand at nominal strength (ksi) and the other variables are as defined previously. This equation provides an increase in the development length of about 35 percent. Finally, it was determined that a reduction of strand spacing from  $4d_b$  to 1.75 in. (44.5 mm) for 0.5 in. (12.7 mm) strands resulted in no detrimental effects and, therefore it was recommended that the spacing requirement could be reduced to  $3.5d_b$  (Deatherage et al. 1994).

#### 2.1.2.12 Buckner

Buckner noted that while strand bond rarely governs design in pretensioned members, the original design equation taken from Hanson and Kaar's data was not a conservative estimate. Since several bond failures had occurred since the equations were put into use, some research indicated development lengths longer than the code prediction, and since strand strength had increased to 270 ksi from the 250 ksi used by Hanson and Kaar (Hanson 1959), the FHWA restricted the use of prestressing strand in 1988. These restrictions included a ban of 0.6 in. (15.2 mm) strand, minimum strand spacing of four times the strand diameter, development length for strand sizes up to 9/16 in. (14.3 mm) 1.6 times the equation value, and a double requirement for debonded strands. Numerous research projects were conducted in response to these restrictions. These projects often had conflicting results and recommendations for transfer and development length and, therefore, the FHWA conducted an independent review of the results of these projects. Buckner summarized this study that attempted to conduct a literature review concerning transfer and development length, analyze data from previous studies and try to understand discrepancies in conclusions, and recommend transfer and development length equations based on the total knowledge obtained. This study focused on uncoated, seven-wire, low-relaxation strands in normal weight concrete (Buckner 1995).

Buckner indicated that the ACI/AASHTO equations were based on inappropriate data for current conditions at the time of this study. It was indicated that the equations underestimated mean transfer length under contemporary conditions. Recommended changes based on the use of Grade 270, seven wire, low-relaxation, uncoated strands cast in normal weight concrete with a strength of 3500 psi (24 MPa) at release and 5000 psi (34 MPa) at 28 days were therefore provided. The equation

$$L_t = \frac{f_{si}d_b}{3}$$

based on research by the Florida Department of Transportation was recommended for transfer length where the variables are as defined previously. This value would be multiplied by a factor of 1.3 for strands that end in the top 1/3 of the member depth and have more than 12 in. (305 mm) of concrete below them. It was also recommended from this research that the provision of  $50d_b$  be increased to  $60d_b$  (Buckner 1995).

The discussion on development length was somewhat more complicated. Wide ranges of development length values for design were recommended by the numerous studies, with most recommended expressions similar to the ACI/AASHTO equations with modifications to the transfer and flexural bond components. One study even recommended the abandonment of the development length concept and embracing crack prevention criteria in the transfer zone. However, this approach was considered generally unconservative and unproven along with being more complicated to implement. The author therefore recommended that the concept of a two part equation for development length be retained with modifications to both parts. While bond failure conditions are not generally encountered, the possibility of a sudden failure warrants a conservative equation. The expression

$$L_d = \frac{f_{si}d_b}{3} + \lambda(f_{ps} - f_{se})d_b$$

where the variables are as defined previously was recommended. The value of  $\lambda$  is taken to be

$$(0.6 + 0.40\varepsilon_{ps})$$

where  $\varepsilon_{ps}$  is the strain corresponding to  $f_{ps}$ , for general applications and

$$\left(0.72 + 0.102 \frac{\beta_1}{\omega_p}\right)$$

where  $\beta_I$  is found in ACI 318,  $\omega_p$  is equal to  $\rho_p f_{ps} / f'_c$ , and  $\rho_p$  is the prestressed reinforcement ratio, for applications where design stress is approximated by the ACI code equation. The 1.3 multiplier mentioned for the transfer length applies here as well (Buckner 1995).

#### 2.1.2.13 Russell and Burns

This experimental program examined the effects of strand spacing, debonding, confining reinforcement, number of strands per specimen, and size and shape of the cross section on transfer lengths for 0.5 in. (12.7 mm) and 0.6 in. (15.2 mm) prestressing strand. Thirty-two of the specimens were rectangular prisms with concentric prestressing and twelve were constructed as scale model AASHTO-type beam specimens for a total of forty-four specimens. Strands were tensioned to 75 percent of  $f_{pu}$  and strand release was accomplished using flame cutting. Concrete surface strains were measured using DEMEC points and a DEMEC gauge. Measurements were taken before and after release by two persons on two sides of the member to produce four independent readings. Electrical Resistance Strain Gauges (ERSGs) were also attached to the strand wires but were mostly ineffective due to a number of issues. Strand end slips were measured at release using a tape mark on the strand and a steel rule accurate to 1/32 in. as dial gauges were damaged by the violent strand release (Russell 1996).

Transfer lengths were determined using the concrete surface strain data. Strain profiles were smoothed by taking the average of each three adjacent points and then the 95% Average Maximum Strain method was used to determine the transfer length. This method consists of plotting the strain profile with a horizontal line at 95 percent of the average of all strains in the strain plateau. Transfer length is then taken as the point where this line intersects the strain profile. Results were found to have a somewhat normal distribution around an average value with strand diameter being the only significant variable. Average transfer length was 29.5 in.

(750 mm) with a standard deviation of 6.9 in. (175 mm) for 0.5 in. (12.7 mm) strand and 40.0 in. (1016 mm) with a standard deviation of 6.8 in. (173 mm) for 0.6 in. (15.2 mm) strand. Larger cross-sections were found to have a shorter transfer length and 0.6 in. (15.2 mm) strand adequately bonded at a 2 in. (50 mm) spacing (Russell 1996).

Transfer length is important to determining the shear strength of a member and there has been wide variability in measured results. Therefore, the authors recommended the conservative expression

$$L_t = \frac{f_{se}}{2} d_b$$

for design, where variables are as defined previously, or  $80d_b$ . This equation exceeded most of the transfer lengths measured in this study and uses the same variables as the ACI equation. A correlation between transfer length and strand end slip was also suggested with a linear best fit relationship of

$$L_t = 294.9L_{es}$$

which is almost identical to the theoretical relationship

$$L_t = 2L_{es} \left( \frac{E_{ps}}{f_{si}} \right) = 290L_{es}$$

where  $L_{es}$  is the measured end slip (in.),  $f_{si}$  is the initial prestress (ksi), and  $E_{ps}$  is the modulus of elasticity of the prestressing steel (ksi) (Russell 1996).

#### 2.1.2.14 Logan

This research program examined the effects of strand quality on transfer and development length as previous researchers had not considered this possibility. The author had previously noted substantial variability between strand manufacturers, however. Six samples of 0.5 in. (12.7 mm) Grade 270 prestressing strand obtained from different regions of the country were

examined using the Moustafa pullout test to ascertain strand quality. Pullout test specimens were 34 in. (864 mm) long and were embedded 18 in. (457 mm) into concrete having a one day strength of 4350 psi (30 MPa). Strand specimens were visually inspected, given a towel-wipe test, and straightened to limit curvature of the specimen before the concrete was cast. Beam specimens measured 6.5 in. by 12 in. (165 mm by 305 mm) and contained a single strand placed 2 in. (50 mm) from the bottom of the beam on center. Beams were cast in 90 ft (27.4 m) lengths using concrete with a one day strength of 4250 psi (29 MPa). Prestress release was accomplished using simultaneous flame cutting of both ends of the strands and then the beams were saw-cut into 5, 18 ft (5.5 m) sections for each strand sample. This resulted in a total of 30 beam specimens. No lifting hooks were used in order to limit disturbance in the transfer and development zones. Vacuum lifters were instead used to move the beams (Logan 1997).

Transfer length was determined for the beams indirectly by measuring the end slip of the strand immediately after prestress release and at subsequent weekly intervals. Measurements were made using a mark scribed on the strand 1 in. (25 mm) from the concrete surface on the flame cut ends and using a depth gauge to measure the indentation made at the saw cut ends. Transfer lengths were found to increase over time for some of the strand types. Flexural tests to examine development length were performed on each end of the beam specimens using the following embedment lengths: the calculated development length for a simply supported or cantilever condition, 6.08 ft (1.85 m), the calculated transfer length for the cantilever condition, 2.42 ft (0.74 m), and 80 percent of the calculated simple span development length, 4.83 ft (1.47 m).

The author discovered that the simple pullout tests gave a reliable prediction of the differences in transfer and development length behavior, that light rust is not necessary for good

bond, and that surface color or residue are not adequate indicators of strand performance. Specimens requiring a pullout force greater than 36 kips (160 kN) led to transfer lengths that were shorter than the ACI Code requirement and flexural failures at the ACI required development length. Specimens requiring a pullout force of 12 kips (53 kN) or less led to initial transfer lengths equal to the ACI requirement that also increased over time. These beams also failed in bond at an embedment length equal to the ACI development length. Logan recommended a pullout test requirement of 36 kips (160 kN) for 0.5 in. (12.7 mm) strand and also specifically recommended an examination of lightweight concrete (Logan 1997).

#### 2.1.2.15 Rose and Russell

This research program studied the potential of three different tests to predict bond performance of Grade 270 low-relaxation prestressing strands. Possible differences in strand production and the resulting differences in surface condition were cited as possible causes of poor bond behavior, and the need for a standardized method of predicting bond quality was expressed. The examined tests included simple pullout tests, tensioned pullout tests, and measured end slips, and the results of each were compared to transfer length measurements. Strand from three different manufacturers was tested in its “as received” condition, while specimens from one manufacturer were also tested using cleaned, silane treated, and weathered surfaces (Rose 1997).

Transfer length specimens measured 6 in. by 12 in. by 17 ft long (152 mm by 305 mm by 5.2 m) except for those used for silane treated strands, which were 24 ft (7.3 m) long. Two 0.5 in. (12.7 mm) strands were placed in the tension region, two No. 6 (No.19) reinforcing bars in the compression region, and 0.25 in. (6.4 mm) closed stirrups were used as shear reinforcement. The concrete used for all specimens had a strength of 4000 psi (28 MPa) at release and 6000 psi



(41 MPa) at 28 days. Strand was pretensioned to 75 percent of  $f_{pu}$  and flame cutting was used for prestress release. Transfer lengths were determined using strain measurements between DEMEC points and the 95% Average Maximum Strain method (Russell 1996). End slip was also measured for the transfer length specimens by placing metal clamps on the exposed end of the strand and measuring the distance to the concrete face before and after release. Simple pullout tests using the Moustafa method were performed using specimens that measured 2 ft by 3 ft by 4 ft (0.61 m by 0.91 by 1.22 m) and contained 12 strands spaced 9 in. (229 mm) apart on a 4 x 3 grid with an 18 in. (457 mm) embedment. Six strands in each block had the same surface condition of an accompanying transfer length specimen and the other six had the cleaned, silane treated, or weathered conditions. Tensioned pullout specimens had a 5.5 in. by 5.5 in. (140 mm by 140 mm) square cross-section and a fully bonded 12 in. (305 mm) length (Rose 1997).

The authors discovered that simple pullout tests do not strongly correlate to bond performance, but also that standardized procedures were necessary for a good evaluation. The tensioned pullout test was found to be impractical for consistent evaluation of bond performance. The authors concluded that measured strand end slips provided the most reliable and repeatable prediction of transfer length when compared to simple pullout tests and tensioned pullout tests. They proposed the equation

$$L_t = 2L_{es} \left[ \frac{E_{ps}}{f_{si}} \right]$$

where variables are as defined previously, to predict transfer length. While the authors indicated that surface condition and flame cutting can influence transfer length they believe that end slip measurements provide a prediction that is independent of these factors (Rose 1997).

#### 2.1.2.16 Lane

This research was part of a large study conducted by the Federal Highway Administration (FHWA) in response to the 1988 memorandum banning 0.6 in. (15.2 mm) prestressing strands along with restricting spacings and increasing required development length of prestressing strands. The project was divided into two phases, the first examining 50 rectangular prestressed concrete specimens and the second involving 32 AASHTO Type II girders and 32 prestressed concrete sub-deck panels. Half of the members were cast with uncoated strands and half with epoxy coated strands (Lane 1998). The results of this study were used to examine the AASHTO equation for development length (AASHTO 2007) as well as that proposed by Buckner (Buckner 1995). Only portions of the total project will be discussed here.

Phase I of this study consisted of 24 rectangular specimens that were concentrically prestressed, 24 that were eccentrically prestressed, and 2 that were used to monitor shrinkage of the concrete. The concentric specimens contained one or four uncoated or epoxy-coated strands, ranged in size from 4 in. by 4 in. (102 mm by 102 mm) to 9 in. by 9 in. (229 mm to 229 mm), and were 12 ft (3.66 m) long. The specimen length was chosen to accommodate at least twice the anticipated transfer length so both ends could be used for measurements. All prestressing strand was Grade 270 low relaxation seven wire prestressing strand. The concrete was designed for a 28-day compressive strength of between 5000 psi and 6500 psi (34.4 MPa and 44.8 MPa) and a strength at release of 4000 psi (27.6 MPa) (Lane 1992).

Mechanical gauge points were attached to the concrete at 1.97 in. (50 mm) increments for measurement of concrete surface strains. Measurements were taken immediately before and after prestress release as well as at 1 day after detensioning, and 7, 14, 28, 56, 90, 180, 270, and 365 days of concrete age. Transfer lengths were determined at each of these ages as the distance

to the point on the curve equal to the average value of the strain plateau. Average transfer lengths for single uncoated strands were 26.9 in. (683 mm) for 3/8 in. (9.5 mm) strand, 33.0 in. (838 mm) for 0.5 in. (12.7 mm) strand, and 43.2 in. (1097 mm) for 0.6 in. (15.2 mm) strand. Four strand specimens had average transfer lengths of 33.7 in. (856 mm), for 3/8 in. (9.5 mm) strand, 40.0 in. (1016 mm) for 0.5 in. (12.7 mm) strand, and >72.0 in. (1829 mm) for 0.6 in. (15.2 mm) strand. These transfer lengths were measured at an age of 365 days. Transfer lengths of the epoxy coated strands were shorter than these values for all cases. Transfer length increased along with strand diameter and the four strand specimens had longer transfer lengths than the single strand specimens. The measured transfer lengths for uncoated strands were in all cases longer than the AASHTO predictions. Single strand epoxy coated specimens and those containing four 0.6 in. (15.2 mm) epoxy coated strands were the only specimens that were adequately predicted using the AASHTO equations (Lane 1992).

Sixteen AASHTO Type II girders were cast using uncoated strands in Phase II of the project. Three different strand patterns were used for these beams. Pattern A consisted of eight 0.5 in. (12.7 mm) strands spaced at 2 in. (50 mm) in the bottom flange. Pattern B used nine 0.5 in. (12.7 mm) strands spaced at 1.75 in. (44 mm) in the bottom flange. Pattern C consisted of eight 0.6 in. (15.2 mm) strands spaced at 2 in. (50 mm) in the bottom flange. All bottom strands were placed in a single row for each beam and each beam also contained two strands of the same diameter as the bottom strands in the top flange. All beams were 31 ft (9.46 m) long and contained single leg stirrups spaced at 3 in. (76 mm) for shear reinforcement. Six of the beams were equipped with a cast-in-place composite deck while the other ten were tested without a deck. Prestressing strands were all Grade 270 low-relaxation strand and had occasional surface rust. Twelve of the beams were cast with a normal strength concrete mixture having a design

compressive strength of 4000 psi (27.6 MPa) at release and 5000 psi to 6500 psi (34.4 MPa to 44.8 MPa) at 28 days. Four beams were cast using a high strength concrete having a design compressive strength of 7000 psi (48.2 MPa) at release and 10,000 psi to 13,000 psi (68.9 MPa to 89.6 MPa) at 28 days (Lane 1998).

Mechanical gauge points were attached to the beam flanges for monitoring of concrete strains. Measurements were taken before and after release, at 7, 14, and 28 days of age, before and after casting of the composite decks, and immediately before development length testing. Strand end slip readings were also taken at the same time as readings from the gauge points. Transfer lengths were determined using the concrete surface strain data taken at 28 days along with the 95% Average Maximum Strain Method. Development length testing was performed using each end of each girder and an iterative approach. A single point load was applied at a specified embedment length and the failure type was examined to determine what subsequent embedment length would be used. Strand slip was monitored using LVDTs, electrical resistance strain gauges were used to monitor the outer fiber compressive stress, load was monitored using a load cell, and deflection was monitored using linear potentiometers. Bond failure was defined as strand slip greater than 0.01 in. (0.25 mm) and flexural failures were marked by crushing of the top compression fiber (Lane 1998).

Measured transfer lengths for the normal strength specimens were between 31.1 in. (790 mm) and 63.0 in. (1600 mm) and between 12.4 in. (315 mm) and 26.9 in. (683 mm) for the high strength specimens. Transfer length values grew an average of 30 percent from time of transfer until 28 days and an additional 7 percent between 28 days and the time of development length testing (185 days). Measured transfer lengths for the normal strength concrete were all greater than the predictions given by the AASHTO equation and the Buckner equation (Buckner 1995).

Transfer lengths for the high strength concrete were all shorter than the predicted values and consistently shorter than the normal strength concrete for the same strand size. Development length results for the normal strength concrete were greater than the AASHTO prediction, and the Buckner equation provided predictions that were sometimes longer and sometimes shorter than measured values. The development lengths measured in the high strength concrete were consistently shorter than the predictions of both equations and were shorter than those for the normal strength concrete for a given strand size (Lane 1998).

Since the results of this study indicated that the existing prediction equations for both transfer and development length were inadequate, these results were used to develop new prediction equations. Data from previous research were then used to correlate the result and ensure that the equation represented all available data. The recommended transfer length equation was

$$L_t = \frac{4f_{pt}D}{f'_c} - 5$$

where  $f_{pt}$  is the stress in the strand prior to transfer of prestress (psi),  $D$  is the strand diameter (in.), and  $f'_c$  is the concrete compressive strength at 28 days (psi). This expression was then combined with the recommended flexural bond portion to form the development length equation

$$L_d = \left[ \frac{4f_{pt}D}{f'_c} - 5 \right] + \left[ \frac{6.4(f_{su}^* - f_{se})D}{f'_c} + 15 \right]$$

where  $f_{su}^*$  is the stress in the prestressing strand at the ultimate strength of the member (psi) and  $f_{se}$  is the effective prestress after all losses (psi). The concrete compressive strength was also limited to a maximum value of 10,000 psi and values of the constants in the expression would change with conversion to SI units (Lane 1998). It should be noted that no tests of the bonding quality of the strand were mentioned as part of this research program. The inconsistencies in

bond behavior of these strands are similar to those mentioned by Logan (Logan 1997) as for strands possibly having poor bonding characteristics. The quality of this strand has also been questioned by other research (Osborn 2008).

#### 2.1.2.17 Kose and Burkett

This research examined the effects of concrete strength and strand surface condition on transfer and development length of 0.6 in. (15.2 mm) strands in AASHTO Type I girders. It also compared results to the ACI and AASHTO requirements as well as equations proposed by Buckner (Buckner 1995) and Lane (Lane 1998). Six beams were constructed using concrete having a compressive strength between 5000 psi and 7000 psi (34.5 MPa and 48.2 MPa) and 0.6 in. (15.2 mm) diameter strands with a rusty surface condition. Each of the three beam pairs had either fully bonded, 50 percent debonded, or 60 percent debonded strands. A composite deck measuring 6.5 in. (165 mm) thick and 60 in. (1524 mm) wide was provided for each beam. The composite slabs provided the compression resistance necessary to develop a strain of 0.035 in the prestressing strands during flexural testing. Each end of the beams was tested for both transfer and development length resulting in a total of 12 tests (Kose 2005 ACI).

Transfer lengths were determined for each end of the girders by using measured concrete surface strains at the level of the prestressing steel. Surface strains were measured using DEMEC points attached with epoxy. Measurements were taken immediately before and after prestress release as well as at 4 to 6 weeks after release. Strain profiles were smoothed using a three point average and the 95% Average Maximum Strain method was used to determine the transfer length. Transfer lengths were found to increase with time and with level of debonding. Average short term transfer lengths ranged from 15 in. to 21.5 in. (381 mm to 546 mm) and long-term values ranged from 16.5 in. to 24.0 in. (419 mm to 610 mm). Only one short-term

transfer length measurement (30.5 in. (775 mm)) exceeded the ACI requirement of  $50d_b$  (30 in. (762 mm)) and no short or long-term transfer length exceeded the AASHTO requirement of  $60d_b$ . No measured transfer lengths exceeded the predictions of Buckner (Buckner 1995) or Lane (Lane 1998) and the Lane equation was very conservative (Kose 2005 ACI).

Flexural load tests were used for examination of development length. A simply supported beam span was used with a single load applied to the beam through a spreader beam and two point loads placed at a specified embedment length. Applied load, beam deflection at the center of load, concrete strain in the top fiber of the deck, and strand end slip were monitored during each test. Load was applied incrementally and data were recorded after each increment. Embedment lengths were incrementally shortened between tests and failure modes were examined in order to bracket the development length. The shortest embedment that resulted in a flexural failure was taken as the development length resulting in values of 54 in., 96 in., and 114 in. (1372 mm, 2438 mm, and 2896 mm) for the fully bonded, 50 percent debonded, and 60 percent debonded specimens respectively. All three equations predicted conservative results for fully bonded beams and the FHWA factor of 1.6 for the code equation was concluded to be unnecessary. The Buckner (Buckner 1995) and Lane (Lane 1998) equations were overly conservative for fully bonded strands and provided conservative results for the beams with some debonded strands. The code requirement of double the fully bonded prediction for debonded strands was found to be overly conservative when compared to the measured values (Kose 2005 ACI).

These authors also published a study that endeavored to produce a development length prediction equation with data from previous tests based on certain qualifications. Specimens made with normal weight concrete, uncoated 0.5 in. or 0.6 in. (12.7 mm or 15.2 mm) Grade 270

low relaxation strands, full size AASHTO standard or state specific I-girders, rectangular beams or T-beams, and that utilized flame cutting for strand release were included. Transfer lengths must have used measured strain profiles and the 95% Average Maximum Strain (AMS) method, and were multiplied by 0.9 if the 100% AMS method was used and original data were not available. Development length tests must have included end slip measurements, classified failure as flexure, hybrid, or bond failure, and used one or two point loading. Both transfer and development length testing must have been done for a research program to be included (Kose 2005 PCI).

Numerous parameters were examined statistically for inclusion in the transfer length portion of the equation and several trends were observed from the data. Increased strand diameter was shown to decrease transfer length due to the larger strand perimeter to contribute resisting forces. Increased concrete strength showed a decrease in transfer length while increased effective prestress force showed an increase in transfer length. A simple regression model was determined from these data and then modified for ease of use and to meet the 95 percent confidence interval. This resulted in the expression

$$L_t = 95 \frac{f_{pi}(1 - d_b)^2}{\sqrt{f'_c}}$$

for transfer length where  $f_{pi}$  is the stress in the strands prior to release and  $f'_c$  is the 28-day compressive strength of the concrete. This equation is applicable to 0.5 in. and 0.6 in. (12.7 mm and 15.2 mm) strands, concrete strengths of 4000 psi to 14,000 psi (28 MPa to 97 MPa), and an initial prestress of 202.5 ksi (1400 MPa) (Kose 2005 PCI).

The same general procedure was followed for the development length. It was observed that the increase in strand diameter from 0.5 in. to 0.6 in. (12.7 mm to 15.2 mm) decreased the flexural bond length. This was again explained by the increased resisting forces provided by the



larger strand perimeter in spite of the larger force. Concrete strength was found to have no significant effect on flexural bond length and an increase in the difference between stress in the strand at ultimate load and stress in the strand after all losses ( $f_{ps} - f_{se}$ ) yielded a slight decrease in flexural bond length. A simple regression equation was then developed for flexural bond length which was in turn modified for ease of use and to produce a conservative estimate. This flexural bond length equation was based on the same conditions as the transfer length equation. Both expressions were then combined to obtain the equation

$$L_d = \left[ 95 \frac{f_{pi}(1 - d_b)^2}{\sqrt{f'_c}} \right] + \left[ 8 + 400 \frac{(f_{pu} - f_{pi})(1 - d_b)^2}{\sqrt{f'_c}} \right]$$

for development length where  $f_{pu}$  is the ultimate tensile strength of the strand and the other variables are as defined previously. This equation covers a range of 71 in. (1803 mm) to 191 in. (4851 mm) over the range of applicable conditions and a multiplier of 2.0 was recommended for partially debonded strands (Kose 2005 PCI).

#### 2.1.2.18 Ramirez and Russell

This research program examined transfer and development length of prestressing strand and development and splice length of mild steel reinforcement in normal weight concrete with compressive strengths up to 15,000 psi (103.4 MPa). The results of the research were used to develop recommendations for revisions for the AASHTO *LRFD Bridge Design Specifications* (AASHTO 2007). Another focus of the research was to develop a standardized test method for bond of prestressing strands. An extensive literature review was conducted on the topics targeted in the research. Transfer length measurements were made on both rectangular and I-shaped beams and development length tests were also conducted on these beams. The North American Strand Producers (NASP) bond test and modified versions of this test were used for all bond testing (Ramirez 2008).

A total of 43 rectangular beams and 8 I-shaped beams were fabricated for transfer and development length testing. These were cast using concrete having one day strengths of 4000 psi, 6000 psi, 8000 psi, or 10,000 psi (27.6 MPa, 41.4 MPa, 55.2 MPa, or 68.9 MPa) and either 0.5 in. (12.7 mm) or 0.6 in. (15.2 mm) prestressing strands. The 0.5 in. (12.7 mm) strands were taken from three different sources and the 0.6 in. (15.2 mm) strands were taken from a single source. The rectangular beam sections measured 6.5 in. (165 mm) wide by 12 in. (305 mm) deep and were 17 ft (5.18 m) in length. These beams contained either two strands placed 2 in. (50 mm) from the bottom of the section or two strands 2 in. (50 mm) from the bottom of the section and two strands 2 in. (50 mm) from the top of the section. All rectangular beams contained two No. 6 (No. 19) bars in the compression block to ensure ductile failures and No. 3 (No. 10) shear stirrups spaced 6 in. (150 mm) on center. The I-shaped beams were all 24 ft (7.32 m) in length and the cross-section had a total depth of 24 in. (610 mm). Each beam contained No. 3 (No. 10) shear stirrups at 7 in. (178 mm) on center. Those cast using 0.5 in. (12.7 mm) strands contained four strands in the bottom bulb and one strand 2 in. (50 mm) from the top of the cross-section. Those cast using 0.6 in. (15.2 mm) strand contained three strands in the bottom bulb and one strand 2 in. (50 mm) from the top of the cross-section. Strands were tensioned to 75 percent of the guaranteed strength of the strand (Ramirez 2008).

Transfer lengths were determined for all strands using end slips measured after prestress release with a micrometer and specially made clamps. Some specimens also were instrumented with DEMEC points for measurement of concrete surface strains. Transfer lengths were then determined from these strain measurements using the 95% Average Maximum Strain method. These transfer length measurements were used to determine the effects of concrete strength on

transfer length as well as whether the NASP Bond Test is an indicator of transfer length.

Transfer length was observed to decrease with increasing concrete strength (Ramirez 2008).

Development length testing was conducted using flexural testing on the two strand rectangular beams and the I-shaped beams. The beams were designed for testing on both ends, but not all ends were tested. A total of 50 flexural tests were performed on the rectangular beams and 14 flexural tests on the I-shaped beams. The flexural tests consisted of a simply supported beam arrangement with two point loads spaced at 24 in. (610 mm) placed at the desired embedment length. Embedment lengths varied between tests depending on the results of the previous test. Load, hydraulic pressure, beam deflection, and strand end slip were recorded at regular intervals for each test using a data acquisition system. Applied load was measured with a load cell, hydraulic pressure with a pressure transducer, deflection with wire transducers, and strand slip was measured using LVDTs. If the beam failed due to bond, the embedment length was considered to be shorter than the development length. If the beam failed in flexure, the embedment length was considered to be longer than the development length. As with transfer length, shorter development lengths were observed with increased concrete strength (Ramirez 2008).

The results of this research program indicated that the AASHTO code provisions for transfer and development length are adequate for normal strength concrete having a compressive strength of 4000 psi (27.6 MPa) at release and 6000 psi (41.4 MPa) at 28 days. Variation of concrete strength was shown to affect both transfer and development length. Expressions relating transfer and development length to the square root of the concrete compressive strength were developed using this information and the relationships developed using the modified NASP tests mentioned below. The recommended transfer length expression is

$$L_t = \frac{120}{\sqrt{f'_{ci}}} d_b \geq 40d_b$$

where  $f'_{ci}$  is the concrete compressive strength at release (ksi) and  $d_b$  is the strand diameter (in.).

The recommended development length equation is

$$L_d = \left[ \frac{120}{\sqrt{f'_{ci}}} + \frac{225}{\sqrt{f'_c}} \right] d_b \geq 100d_b$$

where all variables are as defined previously. These expressions return transfer and development lengths corresponding to the AASHTO requirements for the normal strength concrete. The limiting values of these equations are based on a maximum compressive strength at release of 9000 psi (62.0 MPa) and a maximum strength of 14,000 psi (96.5 MPa) at 28 days (Ramirez 2008).

The North American Strand Producers (NASP) Bond Test was used for the bond testing portion of the research program. The NASP test is performed by casting a single strand in sand-cement mortar inside a cylindrical steel casing. The steel casing has an outer diameter of 5 in. (127 mm) and a bonded length of 16 in. (406 mm). The mortar is designed to produce a compressive strength of 4500 psi to 5000 psi (31.0 MPa to 34.5 MPa) at 24 hours of age and to have a flow of 100 to 125 as measured by ASTM C 1437. The strand is then pulled from the mortar at a rate of 0.10 in./min (2.5 mm/min) at 24 hours of age. The pullout force that corresponds to a free end strand slip of 0.10 in. is recorded and an average of six specimens is the “NASP Bond Test Value” (Ramirez 2008).

NASP tests were conducted in a series of trials at both Oklahoma State University and Purdue University using both sand-cement mortar and concrete of varying compressive strengths. The modified NASP test using concrete was conducted in the same manner as that using mortar except that the concrete had a slump of 2 in. to 3 in. (50 mm to 75 mm) instead of a

specified flow. The compressive strengths that were tested included 4000 psi, 6000 psi, 8000 psi, and 10,000 psi (27.6 MPa, 41.4 MPa, 55.2 MPa, or 68.9 MPa) at one day. These were the same strengths as those used for the subsequent beam testing and the same strands were utilized as well. From these NASP tests it was determined that higher concrete strengths resulted in higher NASP pull-out values for a given strand. When normalized with the NASP Bond Test Values in mortar, the results of the NASP test in concrete were found to vary with the square root of the concrete compressive strength. This result then formed part of the basis for the variation with concrete strength that was incorporated into the proposed transfer and development length equations (Ramirez 2008).

The NASP Bond Test, renamed the “Standard Test Method for Bond of Prestressing Strands” (STSB), was recommended for inclusion in the AASHTO Specifications. Recommended values for 0.5 in. (12.7 mm) prestressing strands include a minimum average pullout value of 10,500 lb (46.7 kN) for a set of six specimens with no single test falling below 9000 lb (40.0 kN). Corresponding minimum values for 0.6 in. (15.2 mm) strands are an average pullout value of 12,600 lb (56.0 kN) with no single test falling below 10,800 lb (48.0 kN). These minimum values are an indication that the strand possesses adequate bonding characteristics (Ramirez 2008).

### **2.1.3 Summary**

As shown in section 2.1.2, a significant volume of research has been conducted concerning the bond of prestressing strand in conventional concrete. While the adequacy of the AASHTO/ACI equations for transfer and development length has been questioned, most research has confirmed that these equations are applicable and they are still used in current practice. Some of the research indicating very poor agreement with the prediction equations may

have been influenced by poor quality prestressing strand as well. Several modifications to the AASHTO/ACI equations have been proposed as a result of previous research. These typically have taken a similar form to the existing equations. A summary of the different proposed transfer length equations is shown in Table 2.1.

Table 2.1: Transfer Length Equations

AASHTO LRFD/ACI 318-11	$L_t = \frac{f_{se}}{3} d_b$
AASHTO LRFD	$L_t = 60d_b$
ACI 318-08	$L_t = 50d_b$
Zia and Mostafa	$L_t = 1.5 \frac{f_{si}}{f'_{ci}} d_b - 4.6$
Shahawy, Deatherage et al., Buckner	$L_t = \frac{f_{si}}{3} d_b$
Russell and Burns	$L_t = \frac{f_{se}}{2} d_b$ $L_t = 80d_b$
Lane	$L_t = \frac{4f_{pt}D}{f'_c} - 5$
Kose and Burkett	$L_t = 95 \frac{f_{pi}(1 - d_b)^2}{\sqrt{f'_c}}$
Ramirez and Russell	$L_t = \frac{120}{\sqrt{f'_{ci}}} d_b \geq 40d_b$

It can be seen from Table 2.1 that several researchers have favored the expression

$$L_t = \frac{f_{si}}{3} d_b$$

for predicting transfer length or another more conservative version of the code expression. A summary of the different proposed development length equations is shown in Table 2.2. It can be seen that all the equations are broken into a transfer length and flexural bond length portion.

All variables used in the equations shown in Tables 2.1 and 2.2 have been defined in section 2.1.2 of the text. While the code equations have been shown adequate for conventional concrete, more research is still needed to confirm these results in other types of concrete.

Table 2.2: Development Length Equations

AASHTO LRFD/ACI 318-11	$L_d = \left(\frac{f_{se}}{3}\right) d_b + (f_{ps} - f_{se})d_b$
Zia and Mostafa	$L_d = 1.5 \frac{f_{si}}{f'_{ci}} d_b - 4.6 + 1.25(f_{su} - f_{se})d_b,$
Deatherage et al.	$L_d = \frac{f_{si}}{3} d_b + 1.5(f_{ps} - f_{se})d_b$
Buckner	$L_d = \frac{f_{si}d_b}{3} + \lambda(f_{ps} - f_{se})d_b$
Lane	$L_d = \left[ \frac{4f_{pt}D}{f'_c} - 5 \right] + \left[ \frac{6.4(f_{su}^* - f_{se})D}{f'_c} + 15 \right]$
Kose and Burkett	$L_d = \left[ 95 \frac{f_{pi}(1 - d_b)^2}{\sqrt{f'_c}} \right] + \left[ 8 + 400 \frac{(f_{pu} - f_{pi})(1 - d_b)^2}{\sqrt{f'_c}} \right]$
Ramirez and Russell	$L_d = \left[ \frac{120}{\sqrt{f'_{ci}}} + \frac{225}{\sqrt{f'_c}} \right] d_b \geq 100d_b$

## 2.2 Structural Lightweight Concrete

### 2.2.1 General Information

Lightweight concrete (LWC) has been in use for at least the last 2000 years. Before the 20<sup>th</sup> century, however, its use was mostly limited to the Roman Empire. Numerous Roman structures utilized LWC including the Port of Cosa, the Pantheon Dome, and the Coliseum. These are all very famous structures and the Pantheon is still in use today. Naturally occurring volcanic aggregates were utilized in these concretes. Lightweight concrete did not find

widespread use until the rotary kiln method for expanding shale, clay, or slate was patented in 1918. Since then LWC has found a wide variety of uses, including bridges and other prestressed applications, high-rise buildings, and offshore oil platforms (ACI 2003)

#### 2.2.1.1 Definition

Lightweight structural concrete is defined by ACI 213 *Guide for Structural Lightweight Aggregate Concrete* as “concrete having a minimum 28-day compressive strength of 2500 psi (17 MPa), an equilibrium density between 70 lb/ft<sup>3</sup> and 120 lb/ft<sup>3</sup> (1120 kg/m<sup>3</sup> to 1920 kg/m<sup>3</sup>), and consists entirely of lightweight aggregate or a combination of lightweight and normal-density aggregate.” (ACI 2003) The International Federation for Prestressing (FIP) defined it as “concrete containing expanded or porous aggregates having a unit weight of 85 lb/ft<sup>3</sup> to 120 lb/ft<sup>3</sup> (1400 kg/m<sup>3</sup> to 2000 kg/m<sup>3</sup>) and capable of developing compressive strengths generally ranging from 4000 psi to 7000 psi (28 MPa to 48 MPa)” (FIP 1967). Concrete can be “all-lightweight” where both the coarse and fine aggregates are replaced with lightweight aggregates or “sand lightweight” where only the coarse aggregate is lightweight and natural sand is used for the fine aggregate (ACI 2003). Lightweight concrete is typically considered as a material entirely separate from normal weight concrete (NWC) due to the fact that, while similar, its properties are different from NWC (FIP 1967).

#### 2.2.1.2 Aggregates

Aggregates typically used for lightweight structural concrete include processed aggregates satisfying ASTM C330. These include expanded shales, clays, and slates; sintered shales, clays, or slag; and pelletized or sintered fly ash (ACI 2003). Expanded clays, shales, and slates manufactured using the rotary kiln method are most commonly used and are highly suitable for use in lightweight structural concrete. Natural aggregates are not typically suitable



for use due to poor quality and inconsistency. High quality lightweight aggregates are necessary for high quality LWC. However, since the aggregates are typically manufactured, good quality control is possible. Lightweight aggregate is more expensive than normal aggregates and can cost up to twice as much. The demand is therefore driven by the benefits of LWC (FIP 1967).

Lightweight aggregates typically have an absorption capacity substantially higher than that of normal weight aggregates. Therefore, lightweight aggregates must be pre-wetted to prevent a loss of mixing water to absorption by the aggregate. The excess water that is contained in the aggregate from this pre-wetting becomes available later during the curing of the concrete and can provide an internal curing effect. Internal curing can be very helpful in concrete with a very low permeability (Castrodale 2008).

Bleed water in concrete with normal weight aggregates becomes trapped on the outer surface of the aggregate particles after concrete placement. This effect increases the  $w/c$  in the interface area and prevents good bond between the paste and aggregate particles. Therefore, the contact zone between the cement paste and normal weight aggregates is usually a zone of weakness within the hardened concrete. However, the porous nature of lightweight aggregate allows some of the bleed water and even some of the actual cement paste to be absorbed by the aggregate particles. This absorption combined with a pozzolanic reaction of the aggregate and the cement paste produces a stronger transition zone between the aggregate and the paste. Decreased microcracking results from this stronger transition zone which leads to decreased permeability, and as a result, increased durability of the concrete (Castrodale 2008). The bond between the aggregate particles and paste typically exceeds the strength of the aggregate particles (Nichols 1970, Castrodale 2008). This effect can also lead to failures of the concrete that pass through the aggregate particles instead of failing within the transition zone.

### 2.2.1.3 Concrete Properties

Lightweight concrete behaves in a manner similar to that of NWC, but it does have differing properties. Unit weight can be 60 percent to 80 percent of NWC depending on the definition of LWC that is used. Even greater benefits relating to weight are observed when the concrete is used in submerged applications. Compressive strengths are comparable to NWC possibly with the addition of additional cement for a particular strength level (FIP 1967). Compressive strengths up to 12 ksi (83 MPa) have been reported (Meyer 2002). The ultimate shear strength for LWC is typically between 65 percent and 100 percent of that for NWC. Splitting tensile strength varies with the aggregate used from less to more than NWC in the partially dry condition. They are about the same in the wet condition. Modulus of rupture is similar in the wet condition and slightly less in the partially dry condition. Modulus of elasticity ranges from 2000 ksi to 3000 ksi (14 MPa to 21 MPa) which is  $\frac{1}{2}$  to  $\frac{2}{3}$  the value for NWC.

Creep behavior is considered to be similar to that of NWC while shrinkage is typically larger, with the amount depending on the quality of the concrete (FIP 1967). Lopez et al discovered that high-performance LWC had less creep but more shrinkage than comparable NWC (Lopez et al 2004). Prestress losses are therefore typically 10 to 20 percent larger than NWC. Thermal insulation properties of LWC are much greater than NWC due to a thermal conductivity 40 percent that of NWC. This yields 20 to 50 percent better fire resistance, better response to steam curing, and better winter concreting. Permeability is similar to NWC due to this being a paste property. Water absorption is almost twice that of NWC. Abrasion resistance is typically less than NWC, but LWC should perform well if placed well. Freeze/thaw resistance of air entrained LWC is similar to high quality air entrained NWC. Corrosion protection is basically the same as NWC for similar mixes (FIP 1967).

Large portions of the research done on the structural behavior of high strength LWC were performed in studies pertaining to the construction of particular structures. Many of these structures were offshore oil platforms. Therefore, much of the information found from these analyses is proprietary between various research institutions and oil companies (Mitchell 2007).

#### 2.2.1.4 Benefits of Lightweight Concrete

Structural LWC has many benefits over conventional NWC, especially in precast construction. The lighter dead loads caused by LWC can reduce the required size of foundations and therefore the cost of the structure. A savings of 20 percent to 25 percent of the weight of the structure can be realized through the use of LWC (Makarichev 1964). This savings of weight has an even greater impact when LWC is used in submerged or floating operations (FIP 1967). The reduction of weight was exemplified in the construction of the One Shell Plaza building in Houston, Texas, around 1970. The building was constructed entirely using LWC, including the floating mat foundation. This allowed for the building to be increased from 35 to 52 stories in height without changing the foundation depth (Khan 1971). The reduced weight can also be very beneficial in retrofit operations since the lighter loads may not require a foundation retrofit when using NWC would (Shi 2005).

Great savings can also be made through the fact that LWC construction elements can be made larger and still be transported and erected easily. This reduces the total number of elements required to construct a structure which in turn reduces construction time and labor costs (Bender 1980). The use of high strength LWC can increase the maximum length of some standard AASHTO girder sections as well (Ferhadi 2010, Meyer 2002). The reduced weight for a given length girder or the same weight for a longer girder using LWC when compared to NWC can also help avoid overload permits for transportation in some states (Meyer 2002). While

LWC may have a reduced modulus of elasticity (MOE), this is helpful in resisting dynamic shock and seismic loads which are also reduced due to the lower weight of the structure. LWC also gives a better fire rating and thermal insulation than NWC due to the reduced thermal conductivity (FIP 1967).

#### 2.2.1.5 Drawbacks of Lightweight Concrete

As in any relationship, there are some drawbacks to using LWC as well. Concrete costs depend heavily on the availability and cost of lightweight aggregates. Currently, high quality lightweight aggregates are not readily available everywhere without substantial shipping costs. Lightweight aggregate is also considerably more expensive than conventional aggregate. Over-vibration can bring aggregate to the concrete surface and care must be taken while finishing to not scrape aggregate out of the concrete mass (FIP 1967). Increased amounts of prestressing steel may be required due to higher losses from creep and shrinkage. Individual precast segment construction costs may be higher due to increased segment size. Variations in aggregate properties among aggregates from different manufacturers can affect concrete properties as well and must be considered in design (Bender 1980). Difficulties arise in determining MOE values for use in design as the prediction equations have been shown to be inadequate for LWC. Designing structures using LWC can also be more challenging simply due to the fact that it is more difficult to determine the proper reduction factors required for LWC in the ACI 318 Code (ACI 2011) (Meyer 2010).

Difficulties may also arrive in gaining approval for use of lightweight aggregates by state departments of transportation (DOTs). Each state may have different guidelines for technician certification and aggregate approval that may further increase the cost of using LWC. The variable density of lightweight aggregate particles can be problematic in relation to aggregate

gradation requirements as well. Since particle density increases as the particle size decreases, a larger percentage of weight may pass a certain sieve size than the actual volume that passed. This must be accounted for to compare effectively with normal weight aggregate gradations (Wall 2010).

## **2.2.2 Previous Research on Lightweight Concrete**

### **2.2.2.1 Makarichev**

Makarichev reported on the use of lightweight concrete (LWC) in Russia in 1964. He stated that LWC having strengths of 3000 psi to 4600 psi (21 MPa to 32 MPa) and unit weights of 106 lb/ft<sup>3</sup> to 112 lb/ft<sup>3</sup> (1698 kg/m<sup>3</sup> to 1794 kg/m<sup>3</sup>) was useful where a combination of structural and insulating functions were necessary. While he stated that a 20 percent to 25 percent savings in structure weight could be realized, he also found that the lower compressive strengths of LWC caused problems in anchorage of prestressing steel as well as larger prestress losses. Ribs of normal weight concrete (NWC) in the tension section of members were suggested as a solution to this problem (Makarichev 1964).

### **2.2.2.2 Fédération Internationale de la Précontrainte (FIP) Commission Report**

The 1967 *Report of the FIP (International Federation for Prestressing) Commission on Prestressed Lightweight Concrete* discusses 4000 psi to 7000 psi (28 MPa to 48 MPa) LWC made with expanded clays, shales, and slates. Their study focused on concrete made with high-quality aggregates and having high strengths for use in prestressed applications. Though the commission found that properties of LWC were similar to those of NWC, it was recommended that LWC be treated as a material separate from NWC due to its differing properties. While unit weight values were 60 percent to 80 percent of NWC (approximately 90 lb/ft<sup>3</sup> to 115 lb/ft<sup>3</sup>), similar compressive strengths were still easily attainable (FIP 1967).

Satisfactory values of creep and shrinkage were measured along with improved fire resistance and thermal insulation properties over conventional concrete. The modulus of elasticity (MOE) was determined to be about half that of NWC. Ultimate shear strength was between 65 percent and 100 percent of NWC and the splitting tensile strength ranged from less to more than that for NWC. Modulus of rupture values were the same or slightly less than NWC. Pullout tests showed ultimate bond strengths similar to but slightly less than those for NWC. Transfer lengths were similar, but slightly greater than those for NWC, due to a lower MOE. The similarity was explained as transfer length being primarily a paste property. Prestress losses were approximately 110 percent to 115 percent of NWC prestress losses under normal curing and 124 percent under steam curing. Permeability values were similar to NWC. This similarity was attributed to permeability being a paste property. Corrosion resistance was essentially the same. Abrasion resistance was less than for NWC, but well placed and cured samples still performed well. Freeze/thaw resistance of air entrained LWC was equal to good quality air entrained NWC. Fatigue behavior was also very similar. Greater camber was experienced due to the reduced dead loads and lower MOE. Most problems in the LWC examined were due to poor workmanship, and most LWC performed well even when overloaded (FIP 1967).

The authors stated that manufacture of LWC was very similar to that of NWC and that it could be used in many of the same applications as NWC. They recommended the use of normal weight sand in most cases, water reducers, strength accelerating admixtures, air entrainment, and careful selection of aggregates. Steam curing was found to improve the concrete properties, and gradual release of prestress was found to be advantageous due to possibly shorter transfer lengths than flame cutting. The FIP report listed numerous direct and indirect advantages of LWC. These were found to outweigh the increased aggregate cost in most applications (FIP 1967).

### 2.2.2.3 Khan et al.

Khan et al. studied the construction of the One Shell Plaza building in Houston, Texas, around 1970 (Khan et al. 1971). The authors examined many aspects of the use of lightweight concrete in the construction of such high-rise buildings. All concrete used in the construction of the building had a compressive strength of either 4500 psi or 6000 psi (31 MPa to 41 MPa). They determined that careful selection of quality lightweight aggregates was necessary to achieve a viable LWC mixture for such a high-performance application. Very tight quality control was also deemed necessary to attain the required consistency between concrete batches. They provided a checklist of quality control items that was recommended for careful monitoring of such construction. Tests were performed to measure the creep properties of the LWC used since the columns would be under very large loads. These tests included both 6 in. x 6 in. x 36 in. (152 mm x 152 mm x 915 mm) specimens tested at the Portland Cement Association laboratory as well as monitoring creep in some of the columns of the actual constructed building. Specimen testing was done by loading the columns with 2 percent of the total load per week for 50 weeks. The slow loading rate was used to mimic the actual loads on a column during the progress of construction. These tests indicated little difference between LWC and NWC (Khan et al. 1971). Since the prestress load is applied instantly in prestressed applications these creep conclusions may not apply directly to creep in prestressed members.

### 2.2.2.4 Bender

Bender conducted a study based on the cost estimate of a segmental post-tensioned precast box girder bridge. He found that use of LWC allowed for the use of larger bridge segments which reduced the erection time from 260 to 199 days. Some increase in fabrication time may be necessary for larger segments, but even a substantial increase still does not reduce

the benefits. The author acknowledged questions about concrete durability but was confident that technological advances would solve these issues (Bender 1980).

#### 2.2.2.5 Slate et al.

Slate et al. examined the mechanical properties of high-strength LWC (Slate et al. 1986). The authors compared both the internal behavior of the concrete and the mechanical properties to NWC. The authors considered high strength LWC to have a compressive strength greater than 6000 psi (41 MPa) and high strength NWC to have a compressive strength greater than 8000 psi (55 MPa). The LWC tested utilized expanded shale aggregate and had a unit weight between 90 lb/ft<sup>3</sup> and 103 lb/ft<sup>3</sup> (1442 kg/m<sup>3</sup> and 1650 kg/m<sup>3</sup>). Only conventional techniques and commercially available products were used in the concrete production (Slate et al. 1986).

The authors determined, among other things, that the ACI equation overestimated MOE for LWC having a compressive strength greater than 5000 psi (34 MPa). The authors therefore proposed the relationship

$$E_c = (40,000 \sqrt{f'_c} + 1,000,000) \left( \frac{w_c}{145} \right)^{1.5}$$

where  $f'_c$  is the 28 day concrete compressive strength (psi) and  $w_c$  is the concrete unit weight (lb/ft<sup>3</sup>). This equation applies for concrete having a unit weight between 90 lb/ft<sup>3</sup> and 145 lb/ft<sup>3</sup> (1442 kg/m<sup>3</sup> and 2323 kg/m<sup>3</sup>) and compressive strength between 3000 psi and 9000 psi (21 MPa and 62 MPa). The authors measured a Poisson's ratio of 0.2 regardless of strength, curing, or age. They discovered no correlation between the square root of  $f'_c$  and the modulus of rupture for dry cured LWC. For wet cured specimens a value of  $6.5\sqrt{f'_c}$  was recommended based on a measured range between  $6.5\sqrt{f'_c}$  and  $10\sqrt{f'_c}$ . The value of  $5\sqrt{f'_c}$  was recommended to estimate splitting cylinder strength for both wet and dry cured lightweight concretes with compressive strength between 3000 psi and 9000 psi (21 MPa and 62 MPa). This was due to a



measured range of  $5\sqrt{f'_c}$  to  $7.5\sqrt{f'_c}$  for moist cured specimens and a range of  $4\sqrt{f'_c}$  to  $7\sqrt{f'_c}$  for dry cured specimens (Slate 1986).

#### 2.2.2.6 Zhang and Gjrv

This research studied the mechanical properties of nine different high-strength LWC mixtures using five different lightweight aggregates. Aggregates included four different expanded clay aggregates and one sintered fly ash. Lightweight coarse aggregate was used exclusively in all mixes while lightweight fine aggregate was used in five of the mixes and four of the mixes had a 40 percent replacement of lightweight fine aggregate with normal weight sand. Water-cementitious material ratios ( $w/cm$ ) varied between 0.28 and 0.44 with cement contents between 675 lb/yd<sup>3</sup> and 1011 lb/yd<sup>3</sup> (400 kg/m<sup>3</sup> and 600 kg/m<sup>3</sup>). Nine percent silica fume by weight was used as cement replacement (Zhang 1991).

Lightweight aggregates were dried to constant weight before use and were premixed with half of the total mixing water for 10 minutes. The other materials were then added and mixed for 5 more minutes. Slump varied between 9.25 in. and 10.75 in. (235 mm and 275 mm), concrete unit weights varied from 100 lb/ft<sup>3</sup> to 117 lb/ft<sup>3</sup> (1595 kg/m<sup>3</sup> to 1880 kg/m<sup>3</sup>), and 28-day compressive strengths were between 8310 psi and 14,850 psi (57.3 MPa and 102.4 MPa). All test specimens were moist cured until time of testing. Increasing density showed an increase in concrete compressive strength. However, strength of the lightweight aggregate was determined to be the controlling factor for compressive strength of the concrete mixes as strengths would reach a plateau before 28 days or soon after. Failure planes were found to pass through the aggregate particles. Measured 28-day MOE ranged between 1450 ksi and 2900 ksi (10 GPa and 20 GPa) as compared to 5000 ksi to 13,800 ksi (35 GPa to 95 GPa) for limestone aggregate

concrete. The authors found the Norwegian code equation to be a fairly adequate estimation of MOE and the ACI 318 equation to overestimate MOE. The authors proposed the relationship

$$E_c = 1.19^3 \sqrt{f_{ck}^2}$$

where  $E_c$  is modulus of elasticity (GPa) and  $f_{ck}$  is compressive strength (MPa) (Zhang 1991).

#### 2.2.2.7 Meyer and Kahn

Meyer and Kahn performed an analytical investigation studying the possibility of using high strength LWC in standard AASHTO bridge girders in order to increase the lengths of such girders as well as to reduce the weight and avoid Georgia “superload” permits. Expanded slate lightweight aggregate concrete with strengths of 8 ksi, 10 ksi, and 12 ksi (55 MPa, 69 MPa, and 83 MPa) was used. Concrete unit weights were somewhat higher than the 115 lb/ft<sup>3</sup> (1842 kg/m<sup>3</sup>) limit for LWC given by ACI (ACI 2003) with averages varying from 119 lb/ft<sup>3</sup> (1906 kg/m<sup>3</sup>) for the 8 ksi (55 MPa) mix, 124 pcf (1986 kg/m<sup>3</sup>) for the 10 ksi (69 MPa) mix, to 128 pcf (2050 kg/m<sup>3</sup>) for the 12 ksi (83 MPa) mix (Meyer 2002).

AASHTO Type II to Type V I-girders were examined along with AASHTO-PCI bulb-tee sections BT-54, BT-63, and BT-72 (both standard and modified). The AASHTO Standard Specifications for Highway Bridges were used for design of the girders along with the Georgia DOT computer program with modification for the use of high strength LWC. Prestress losses were assumed to be the same as those for normal strength concrete since conventional and lightweight HPC has been shown to have lower prestress losses than normal strength concrete. The authors found that the use of high strength LWC allows an increase in length of 3 percent for AASHTO I-girders and 4 percent for AASHTO-PCI bulb-tee sections. For spans between 125 ft and 155 ft (38.1 m and 47.2 m) the use of high strength LWC allowed the transport load to be under the 150 kip (667 kN) limit requiring Georgia “superload” permits. While the use of high

strength LWC showed general benefits, it did not show any significant benefit for AASHTO Type II and III girders (Meyer 2002).

### **2.2.3 Previous Research in Bond of Prestressing Steel in Lightweight Concrete (LWC)**

The *Guide for Structural Lightweight Aggregate Concrete (ACI 213R-03)* published by the American Concrete Institute bases its discussion of strand bond in lightweight concrete (LWC) on the research of Meyer and Kahn (Meyer 2004), Thatcher et al (Thatcher et al. 2002), and Nassar (Nassar 2002), all discussed in the following sections. These research programs along with others have stated differing results on the adequacy of bond in LWC. Some research has determined that the current code equations for transfer and development length are adequate while other research has indicated that these equations are only marginally acceptable or in need of modification. The ACI 213 guidelines indicate that a conservative design approach or project specific testing program should be considered in the case of special structures, use of large diameter strands, or use of high strength LWC in highly reinforced thin members. This recommendation is based on the higher splitting forces that can be caused by large diameter strands or close spacing. The need for more research is also mentioned (ACI 2003). The following discussions summarize much of the research that has been conducted concerning transfer and development length in members utilizing LWC.

#### **2.2.3.1 Nordby and Venuti**

This research program was mostly concerned with fatigue behavior of prestressed concrete beams but was one of the first research programs to study bond of prestressing strand in LWC. It was determined from this research that expanded shale aggregates could be used to produce acceptable concrete for prestressed applications and the LWC beams performed comparably with the normal weight concrete (NWC) beams. Details of the research were

mentioned previously, but it was concluded that longer embedment lengths were required for the expanded shale concrete (Nordby 1957).

#### 2.2.3.2 Peterman et al.

This study involved 25 development length tests conducted on rectangular and T-shaped semi-lightweight prestressed concrete beams. Concrete mixtures utilized a partial replacement of coarse aggregate with expanded shale lightweight aggregate and had a unit weight of approximately 130 lb/ft<sup>3</sup> (2080 kg/m<sup>3</sup>). Two different mix designs were used in conjunction with two different diameters of prestressing strand. A 7000 psi (48 MPa) mixture was used with ½ in. special (13.3 mm) prestressing strand, and a 10,000 psi (69 MPa) mixture was used with 0.6 in. (15.2 mm) prestressing strand. Nine single strand rectangular beams and seven multiple strand T-beams were constructed for testing. The rectangular beams had a cross-section measuring 8 in. x 12 in. (200 mm x 305 mm) with the single strand located at a depth of 10 in (255 mm). Flexural testing of these beams for development length consisted of a single point load applied at the development length calculated using the AASHTO equation on a 15 ft 3 in. (4.65 m) or 16 ft 3 in. (4.95 m) span. Each beam was tested on both ends for a total of 18 data points. The T-beam cross-section had a total depth of 21 in. (535 mm) and a compression flange measuring 36 in. (915 mm) by 6.5 in. (165 mm). Each T-beam contained 5 strands placed at a depth of 19 in. (483 mm) spaced 2 in. (50 mm) on center. The beams had a length equal to twice the calculated development length and were tested using a single point load at mid-span. Analysis of the failure mode was used to determine the adequacy of the embedment length for both single and multiple strand beams (Peterman et al. 2000).

The author concluded from the 18 single strand beam tests that the AASHTO development length equation is adequate for a single strand in this semi-lightweight concrete.

However, the formation of flexure-shear cracks in the multiple strand T-beams led to bond failures in a portion of the specimens. More beams were cast using increased shear reinforcement which corrected the cracking problem and resulted in a flexural failure. The author indicated that without the problems caused by this flexure-shear cracking, the AASHTO development length equation was conservative for these semi-lightweight concretes (Peterman et al. 2000). Therefore, the author recommended that “the current requirements for strand development length should be enforced at a critical section that is located a distance  $d_p$  from the point of maximum moment toward the free end of the strand, where  $d_p$  is the distance from the extreme compression fiber to the centroid of the prestressed reinforcement” (Peterman et al. 2000).

#### 2.2.3.3 Thatcher et al.

This study centered on the application of high performance lightweight concrete using materials local to Texas in pretensioned girders and deck panels (Thatcher et al. 2002). Design concrete compressive strengths were 6000 psi (41 MPa) and 8000 psi (55 MPa). Six 40 ft (12.2 m) long and two 20 ft (6.1 m) long AASHTO Type I girders were used in this research. Two of the six 40 ft (12.2 m) girders were cast using the 6000 psi (41 MPa) LWC, two using the 8000 psi (55 MPa) LWC, one using 6000 psi (41 MPa) NWC, and one using 8000 psi (55 MPa) NWC. Each beam contained twelve 0.5 in. (12.7 mm) Grade 270 prestressing strands arranged with ten in the tension region and two in the compression region. Adequate shear reinforcement to prevent failure at ultimate load was utilized for all of the beams. A 78 in. (1980 mm) wide by 8 in. (200 mm) thick composite deck was added to each of the beams. Both NWC and LWC decks were used in the project. The two 20 ft (6.1 m) beams were not part of the original study and were constructed just to ensure that the precaster could work with the LWC mixtures. One each

was cast with the 6000 psi (41 MPa) and 8000 psi (55 MPa) mixtures. The most congested section typically encountered was used to test production of these girders using this type of concrete (Thatcher et al. 2002).

For the six beams tested, concrete surface strains were measured using the Detachable Mechanical Strain Measurement (DEMEC) system and transfer lengths were calculated from these measurements using the 95% Average Maximum Strain (AMS) method. All data for similar beams were then averaged due to scatter in the individual data. Measurements of strand draw-in after prestress release were also used to determine transfer length using the expression

$$L_t = \frac{\alpha \Delta_d}{\varepsilon_{si}}$$

In this expression  $\Delta_d$  is the measured strand draw-in,  $\varepsilon_{si}$  is the initial strain in the strand due to prestress,  $\alpha = 2$  is used for a bilinear strand strain profile, and  $\alpha = 3$  is used for a parabolic strain profile. End slip measurements were taken by measuring the change in distance between an aluminum U-channel attached to the free end of the strand and a glass slide glued to the concrete surface. These two methods of transfer length measurement yielded distinctly different results as can be seen in Table 2.3. Development length was determined using flexural tests of each end of the six 40 ft (12.2 m) beams. The embedment length for the tests was varied between the code prediction of development length and 60 in (1524 mm). Strand slip was monitored during testing using linear potentiometers and the failure type was examined to determine the relationship of the embedment length to the development length (Thatcher et al. 2002).

Transfer lengths for the beams cast using LWC were determined to be longer than those for the beams cast with NWC. The authors suggest that the ACI and AASHTO provisions for transfer length are conservative for beams cast with NWC, but underestimate transfer length in beams cast with LWC. It is therefore indicated that the models used are not conservative

Table 2.3: Thatcher's Comparison of Transfer Length Methods

Concrete Type	Individual Strain Profiles, (in.)	Average Strain Profiles, (in.)	Draw-in ( $\alpha = 2$ ), (in.)	Draw-in ( $\alpha = 3$ ), (in.)
NWC 6000 psi	18.3	18.2	15.6	23.5
LWC 6000 psi	22.1	35.8	15.4	23.0
LWC 8000 psi	29.7	34.4	13.1	19.6

Note: 1 in. = 25.4 mm

because they do not accurately model the behavior of LWC since they were developed for NWC.

The reduced MOE for LWC may be a large factor in the difference. In contrast, the authors

concluded that the development length was similar for both LWC and NWC and that the

ACI/AASHTO equation is conservative for both cases (Thatcher et al. 2002).

#### 2.2.3.4 Nassar et al.

This study considered the feasibility of high strength LWC for bridges in Virginia. Three AASHTO Type II girders and two AASHTO Type IV girders were constructed for use in this research. The Type IV girders were identical to a bridge actually constructed in Virginia. All beams were cast using a single LWC mixture except for one of the Type II girders that was cast using normal weight high-performance concrete. The LWC mixture consisted of expanded slate coarse aggregate and natural sand. Concrete density was approximately 114 lb/ft<sup>3</sup> (1830 kg/m<sup>3</sup>) and the 28-day compressive strength was 6375 psi (44.0 MPa). A normal-weight composite deck measuring 48 in. (1220 mm) by 8 in. (200 mm) was placed on each of the Type II girders. These girders were 36 ft (11.0 m) in length and were prestressed using six straight strands and two strands harped (draped) 14 ft (4.3 m) from each end. The Type IV girders were 84 ft (25.6 m) in length and were prestressed with 30 straight strands and 8 strands harped 32 ft 8 in. (10.0 m) from each end of the beam. All strands were 0.5 in. (12.7 mm) Grade 270 low relaxation strand. Tests were performed for transfer length, development length, flexural strength, and prestress loss (Nassar 2002).

A Whittemore strain measurement device was used to measure concrete surface strains for transfer length determination on the Type IV girders only. Transfer lengths were then determined from these measurements by the 95% Average Maximum Strain (AMS) method. The Type II girders were used for development length testing accomplished by flexural testing utilizing a single point load applied at varied embedment lengths. Strand slip was monitored using linear variable differential transformers (LVDTs) and the failure mode was analyzed to determine the relationship of the embedment length to the development length. A 24 ft (7.3 m) long span was used in the tests so that two flexural tests could be performed for each beam. This resulted in a total of six tests for development length (Nassar 2002).

Measured transfer lengths were less than the ACI and AASHTO predictions. However, the author recommended increasing all code requirements for transfer length to the value of  $60d_b$  recommended by AASHTO LRFD or the expression  $f_{st}d_b/3$  recommended by others (Shahawy 1992, Buckner 1995). These recommendations were to ensure a conservative estimate of transfer length for all cases. The author stated that the development length results were not conclusive. He did indicate, however, that the AASHTO/ACI development length equation was conservative for beams using this high strength LWC to reach nominal moment capacity. He indicated that this may be true for the actual moment capacity and recommended a modification factor of 1/0.85 for use until more testing could be completed. Additional development length testing with varied girder type, prestressing force, and high strength LWC type was recommended (Nassar 2002).

#### 2.2.3.5 Meyer and Kahn

Meyer and Kahn used six pretensioned AASHTO Type II girders to study transfer and development length (Meyer 2004). These girders were cast using expanded slate LWC having



design compressive strengths of 8000 psi (55 MPa) and 10,000 psi (69 MPa). The actual compressive strengths of the concrete mixtures were between 8,790 psi (60.6 MPa) and 11,010 psi (76 MPa). Ten 0.6 in. (15.2 mm) diameter Grade 270 low relaxation strands were used for each girder with an applied prestress of 75 percent of the ultimate strength of the strand. The strand arrangement consisted of eight strands in the bottom of each beam and two in the top. Three girders were cast with each of the two different strength concrete mixtures. Girder lengths of 39 ft (11.9 m) and 43 ft (13.1 m) were used to allow for development length tests at both ends of the girders as well as tests for shear and flexure in the center section. A composite normal weight deck 19 in. (483 mm) wide and 11.5 in. (292 mm) thick was placed on each beam. These dimensions were used to simulate the moment arm caused by a normal deck 8 in. (203 mm) thick with an effective width of 93 in. (2.36 m). Shear reinforcement was placed in accordance with the AASHTO and ACI requirements. The required shear reinforcement was doubled in some of the beams to study the effects of shear reinforcement on development length (Meyer 2004).

Measured transfer lengths were determined using concrete surface strain measurements and the 95% AMS method. Strain measurements were taken immediately before and after prestress release, and then at 1, 2, 3, 7, and 14 days after release. For the 8000 psi (55 MPa) and 10,000 psi (69 MPa) concrete mixtures, average transfer lengths were 21.9 in. (556 mm) and 15.6 in. (396 mm) respectively. Longer transfer lengths were measured for the lower strength concrete which supports an effect of compressive strength on transfer length. The prediction equations overestimated transfer length by an average of 37 percent for the AASHTO equation (AASHTO 2007) and 41 percent for the ACI equation (ACI 2011). The prediction equations did not underestimate transfer length for any specimen. The authors therefore suggested that no

modification of the equations was necessary for the concrete mixtures tested in these experiments (Meyer 2004).

Specimens measuring 24 in. x 36 in. x 24 in. (610 mm x 914 mm x 610 mm) and containing four strands were cast from each mix during girder placement and were used for pull-out tests. Strand segments were 48 in. (1.22 m) in length, had a minimum spacing of 8 in. (203 mm) and had a total embedment of 18 in. (457 mm). Pull-out tests were performed in agreement with the work of Logan (Logan 1997). The required minimum pull-out force of 43.2 kips (192 kN) used in this research for 0.6 in. (15.2 mm) strand was extrapolated from the average bond stress resulting from Logan's required 36 kips (160 kN) for 0.5 in. (12.7 mm) strand. Only one test was slightly below this value of 43.2 kips indicating that the strand had adequate condition for reliable results (Meyer 2004).

Both ends of each girder were tested in flexure at embedment lengths between 70 percent and 100 percent of the estimated development length in order to bracket the actual development length. Strain in the strand and end slip were monitored during flexural testing and slip greater than 0.01 in. (0.25 mm) was considered to be a bond failure. The actual development length was considered to be the point where flexural and bond failures occurred at the same time. Therefore, if the failure was purely flexure, the embedment length was greater than the development length and if the failure was purely bond, the embedment length was less than the development length. Actual development lengths for the 8000 psi (55 MPa) mix were determined to be 91 in. (2311 mm) using single density stirrups and 81 in. (2057 mm) for double density stirrups. Development length for the 10,000 psi (69 MPa) mix was 67 in. (1702 mm) for both cases of shear reinforcement. Shear cracking in the transfer zone resulted in increased strand slip but doubled stirrup density reduced this effect. The results also indicated that the

silica fume used in the 10,000 psi (69 MPa) mix may have helped improve bond. The authors stated that the equations overestimated the measured development lengths by 19 percent and therefore that the equations were conservative and no modifications were necessary for 0.6 in. (15.2 mm) strands in this type of high strength LWC (Meyer 2004).

#### 2.2.3.6 Mitchell and Marzouk

This experimental program reported on bond strength characteristics of high strength LWC and consisted of 72 pull-out and push in specimens using No. 8 and No. 11 (No. 25 and No. 36), 58 ksi (400 MPa), deformed bars embedded in high strength LWC with a compressive strength of 11.6 ksi (80 MPa). These tests may not be directly applicable to bond with prestressing strand, but they do show some of the bond characteristics of LWC. This work was a direct comparison to previous work by Marzouk on high strength NWC using the same procedures. The authors conducted the push in and pull out tests under both static and cyclic loading. The concrete had a  $w/c$  ratio of 0.30, 810 lb/yd<sup>3</sup> to 826 lb/yd<sup>3</sup> (480 to 490 kg/m<sup>3</sup>) of cement, and 12 percent by weight of cement of silica fume. The coarse aggregate was lightweight aggregate from North Carolina with a specific gravity of 1.45, maximum size of  $\frac{3}{4}$  in. (19 mm), and dry density of 60 lb/ft<sup>3</sup> (960 kg/m<sup>3</sup>). Fine aggregate was simply fine sand (Mitchell 2007).

Thirty-six specimens were tested for both the No. 8 and No. 11 (No. 25 and No. 36) bars for a total of 72 tested specimens. The concrete specimens were 10 in. (250 mm) in height, 15 times the bar diameter in length, and 5 to 7 times the bar diameter in width. The bond length was contained at the center of the specimen with pvc pipe used to break the bond at the ends of each specimen. The load was measured using a load cell in the hydraulic actuator used to apply the load. This actuator also contained an LVDT used to measure the movement of the loaded end of

the bar. A linear potential differential transducer (LPDT) was used to monitor movement at the other end. Specimens were tested in both tension and compression under static loading. The load rate was also varied for these as well as the cyclic loading tests. Results showed that high strength LWC behavior is very similar to that of high strength NWC. The maximum bond stress for the high strength LWC using No. 8 (25 mm) bars was within 10 percent of the value for the high strength NWC while the maximum bond stress was greater for the high strength LWC using No. 11 (35 mm) bars. The high strength LWC exhibited more brittle behavior, however, and a larger decrease from maximum bond stress to that at failure. The larger decrease was attributed to weak aggregate interlock. The shape of the stress-displacement curve for the two concretes was very similar. The authors concluded that increased development length requirements for deformed bars cast in high strength LWC are unnecessary as high strength LWC behaves in a manner very similar to high strength NWC. The authors disputed the 30 percent increase in development length for LWC specified by ACI 318-05 when using high strength LWC (Mitchell 2007).

#### 2.2.3.7 Greene and Graybeal

This research project examined development length of AASHTO Type II girders cast with specified density concrete; concrete mixtures containing both lightweight and normal weight aggregate. Four different girder designs were used in combination with three different lightweight aggregates for a total of twelve 45 ft (13.7 m) long specimens. Three of the girder designs utilized 0.5 in. (12.7 mm) strands and the fourth had 0.6 in. (15.2 mm) strands. Number of strands and amount of shear reinforcement were varied between the girder designs. An 8 in. by 36 in. (200 mm by 915 mm) NWC deck was cast on each beam after delivery from the prestress yard. The lightweight aggregates used included Haydite, an expanded shale from Ohio,

Utelite, an expanded shale from Utah, and Stalite, an expanded slate from North Carolina. Concrete compressive strengths for the three mixes ranged from 7.4 ksi to 10.5 ksi (51 MPa to 72 MPa) and unit weights ranged from 126.1 lb/ft<sup>3</sup> to 130.6 lb/ft<sup>3</sup> (2020 kg/m<sup>3</sup> to 2092 kg/m<sup>3</sup>) (Greene 2010).

An iterative procedure was used to bracket development length results for each of the girder and mix design combinations. One end of each girder was subjected to a flexural test at 90 percent to 100 percent of the calculated development length. The other end was then loaded at either a longer or shorter embedment depending on the failure mode of the first test. A simply supported beam arrangement was used and load was applied through the support opposite the end being tested. This induced a reaction against a load frame and spreader beam located near the end being tested that transferred the load to the beam at the proper embedment length. All but one of the 20 tests that had been completed at the time this paper was published failed in flexure using embedment lengths between 60 percent and 100 percent of the development length calculated using the AASHTO/ACI equation (AASHTO 2007, ACI 2011). The other test ended with a shear failure in one end of the only girder tested with the most highly reinforced design. Negligible slip was also measured in this failure. From this preliminary testing, the authors concluded that the AASHTO/ACI development length equation calculated conservative results for 0.5 in. and 0.6 in. (12.7 mm and 15.2 mm) strands in these specified density concrete mixtures (Greene 2010).

#### 2.2.3.8 Mor

This study considered how high strength LWC properties were affected by condensed silica fume (CSF) (Mor 1992). Concrete mixtures having a compressive strength of 10,000 psi (69 MPa) were used for both expanded shale lightweight aggregate and normal weight aggregate.

Bond performance was examined using pullout tests on specimens of 24 in. (610 mm) long deformed No. 6 (No. 19) reinforcing bars cast in 6 in. x 6 in. x 6 in. (152 mm x 152 mm x 152 mm) concrete cubes. Bond behavior was found to be similar up to a slip of 0.01 in. (0.25 mm) and the addition of CSF was found to double the bond strength of the LWC over both NWC and LWC not containing CSF. Since LWC has a lower splitting tensile strength and fails in splitting sooner, it had a lower bond stress at large strains. This was due to the fact that in this strain range the bond mechanism shifts to friction and mechanical interlock, which causes a splitting failure in LWC sooner than NWC. It was also suggested that the compatibility of paste and aggregate in LWC reduces the effect of cracking due to differential strains under stress. This allows a more full utilization of the adhesion between concrete and steel and, therefore, higher bond strength at small strains (Mor 1992).

#### 2.2.3.9 Discussion

As can be seen from the previous discussion, most research has shown that, for the most part, bond behavior of LWC is very similar to bond behavior of NWC. The code equations for transfer and development length were determined to be conservative for prestressed LWC beams as well. Summaries of the transfer and development length data from these research programs are shown in Tables 2.4 and 2.5.

Meyer and Kahn's (Meyer 2004), Thatcher's (Thatcher et al. 2002), and Nassar's (Nassar 2002) research should be comparable as they used similar full size specimens. Meyer and Kahn concluded conservatism of the code equations for both transfer and development length.

Thatcher questioned the conservatism of the transfer length provision, but concluded similar behavior to NWC and a conservative estimate by code equations when considering development length. Nassar measured transfer lengths that were less than the current code provision, but also

Table 2.4: Summary of LWC Transfer Length Data

Ref.	Agg. Type	Dia. (in.)	Specimen Type	$f'_c$ (psi)	$f'_{ci}$ (psi)	$L_t$ Strain (in.)	$L_t$ Slip (in.)	$f_{se}d_b/3$ (in.)	$50d_b$ (in.)	$60d_b$ (in.)
Meyer and Kahn	Slate	0.6	AASHTO Type II	8000	6000	21.9	NA	30.8	30	36
				10000	7500	15.6		34.2		
Thatcher	Hard Rock	0.5	AASHTO Type I	6000	3490	18.2	19.6	32.1	25	30
	Clay				4900	35.8	19.2	30.7		
				8000	5560	34.4	16.4	30.5		
Nassar	Slate	0.5	AASHTO Type IV	6380	4775	17.2	NA	--	25	30

Note: 1000 psi = 1 ksi = 6.9 MPa, 1 in. = 25.4 mm

Table 2.5: Summary of LWC Development Length Data

Ref.	Agg. type	Dia. (in.)	Specimen Type	$f'_c$ (psi)	Embedment Length $L_e$ (in.)	ACI/AASHTO $L_d$ (in.)	Estimated Actual $L_d$ (in.)
Meyer and Kahn	Slate	0.6	AASHTO Type II	8000	67 - 96	96.7 - 107.8	91
				10000	67 - 91	96.3 - 103.3	67
Thatcher	Hard Rock	0.5	AASHTO Type I	6000	60 - 80	82	<60
	Clay			6000	60 - 80	86	<60
				8000	60 - 80	86	<60
Nassar	Slate	0.5	AASHTO Type II	6380	60 - 96	75 - 76	72
Peterman	Shale	1/2 in. Special A	Rect.	7000	73.5	73.5	<73.5
		1/2 in. Special B			73.5	73.5	<73.5
		0.6 A	10000	85.5	85.5	<85.5	
		1/2 in. Special	T-Beam	7000	73.5	73.5	73.5
		0.6	T-Beam	10000	85.5	85.5	<85.5
Ward	Clay	0.5	Rect.	6700	25 - 45	74.5 - 77.0	<27.5

Note: 1000 psi = 1 ksi = 6.9 MPa, 1 in. = 25.4 mm

recommended increasing these provisions to ensure conservatism. It was concluded that the development length provision was adequate, but also recommended to increase the requirements with the goal of ensuring conservatism.

Meyer and Kahn studied 0.6 in. (15.2 mm) strand while Thatcher and Nassar examined 0.5 in (12.7 mm) strand. Concrete strengths varied somewhat as Meyer and Kahn utilized 8000 psi and 10,000 psi (55 MPa and 69 MPa) concrete, Thatcher examined 6000 psi and 8000 psi (41 MPa and 55 MPa) concrete, and Nassar used approximately 6000 psi (41 MPa) concrete. Meyer and Kahn and Nassar both used expanded slate aggregate, possibly from the same source, while Thatcher utilized an unspecified lightweight aggregate from Texas. Again the differences in variables make the results more applicable to the particular research than as a general application.

Due to the differences between the research projects in so many of the variables studied along with the differing opinions on the conservatism of the code equations, more research is necessary. The high strengths of all the concretes tested in previous research may have as much or more to do with the bond behavior of the concrete than anything else. Other factors to consider include the effects of internal curing and the improved transition zone between paste and aggregate as well as the compatibility between the elastic moduli of the lightweight aggregate and the cement paste. Different aggregates should be tested in direct comparison with equal compressive strength. Different diameters of prestressing strand should be examined with all other variables held constant. The effect of strand surface condition should be considered as well and all prestressing strand should be subject to strand qualification.



## **2.3 Self-Consolidating Concrete**

Self-consolidating concrete (SCC), sometimes known as self-compacting concrete, was developed in Japan in the late 1980s. Its invention was the result of a lack of skilled labor for concrete placement and consolidation that was resulting in poor concrete durability (Okamura 2003). SCC can fill formwork and achieve complete compaction without the need for vibratory consolidation. This property is produced through a low yield stress resulting in high deformability in the fresh state combined with a moderate to high viscosity and resistance to segregation (Okamura 2003).

### **2.3.1 Benefits of SCC**

Numerous benefits are realized from the self-compacting behavior of SCC. Typical concrete placement practices require skilled labor for vibratory concrete consolidation. Poor vibratory consolidation can lead to entrapped air and other voids especially around reinforcing bars. Excessive vibration can lead to segregation, bleeding, and interference with entrained air (Bonen 2005). SCC eliminates these concerns and reduces the cost of concrete placement by reducing the required amount of skilled labor. An improved concrete surface finish is also a typical result of using SCC. The reduction in surface imperfections and bug holes can lead to cost savings in the form of reduced patching and surface repair. Construction time is also reduced due to the elimination of vibratory consolidation. The concrete is simply placed in the forms and allowed to consolidate under the force of gravity. Elimination of vibration greatly reduces the noise level of the construction site or precast plant which makes for a substantially improved work environment. Finally, SCC can be used to cast complicated shapes and heavily congested elements that would be very difficult to construct otherwise (Bonen 2005).

### 2.3.2 Mix Designs

There are two methods that are typically used for the design of SCC mixtures: powder-type SCC and VMA-type SCC. Powder-type SCC utilizes a low  $w/c$ , a relatively high dosage of superplasticizer or high range water reducer (HRWR), and a low aggregate to binder ratio. A high cementitious material content is required along with the low  $w/cm$  in order to obtain the required high plastic viscosity and segregation resistance (Bonen 2005). Numerous filler materials can also be used to increase viscosity in SCC including fly ash, slag cement, glass powder, limestone powder, silica fume, and quartzite filler, which is basically fine sand (Persson 2001). The powder-type method was originally used by the investigators in Japan (Okamura 2003). The mixture proportions are very similar to other forms of high performance or high strength concrete and therefore, many of the same properties are expected from this type of SCC. These include high strength, low permeability, and good freeze-thaw durability among others. VMA-type SCC is based on the addition of superplasticizer to reduce the yield stress of the mixtures and viscosity modifying agents (VMA) to control the plastic viscosity and segregation resistance. The addition of VMA controls the viscosity to the point that a reduction in water content is unnecessary. The interaction between superplasticizer and VMA should be carefully considered. It should be noted that both types of SCC have a larger fine-to coarse aggregate ratio than conventional concrete (Bonen 2005).

### 2.3.3 Properties of SCC

Fresh concrete properties for SCC are significantly different from those of normal concrete and are measured using different test methods. The main requirements for SCC are related to deformability/flow ability, passing ability, and segregation resistance. There are several test methods that are currently used to assess these properties (Bonen 2005, Khayat

2009). The most common tests for filling ability include slump flow,  $T_{20}$  ( $T_{50}$ ), V-Funnel, and filling vessel. The first two give a good measure of deformability and are covered by ASTM C1611 which also includes the methods for visual stability index (VSI). The others are not standardized. Methods to assess segregation resistance of SCC include VSI, surface settlement and rate of settlement, and column segregation. The column segregation test is covered by ASTM C1610 and the others are not standardized. Typical tests for passing ability include the J-Ring (ASTM C1621), U-box, and L-box. There is very little standardization of the last two and many device dimensions can be used (Khayat 2009, Bonen 2005). In order to get an adequate representation of the rheological properties of SCC, it is recommended to use a combination of slump flow and J-Ring or slump flow and L-box along with VSI or column segregation (Khayat 2009).

There has been some debate as to differences in hardened properties between SCC and conventional concrete. Compressive strengths are usually similar or higher due to increased binder contents and a lower  $w/cm$  for SCC. Lower and higher MOE values have been measured for SCC. This is typically attributed to the increased paste content in SCC mixtures. Increased creep and shrinkage have been observed in some cases again due to the increased paste content. Permeability properties have also been reported in a wide range with both good and poor performance being documented.

Bonen and Shah indicated higher shrinkage for SCC but MOE values that were in reasonable agreement with code predictions (Bonen 2005). Persson found that creep, shrinkage, and MOE were very similar to conventional concrete for the same strength (Persson 2001). Zhu and Bartos measured lower water permeability for SCC mixtures when compared to similar strength conventional concrete mixtures. They also discovered that chloride ion diffusivity

depended on the type of additional powder used and that equal strength SCC mixtures were similar to conventional mixtures. They indicated that VMA type SCC had higher permeability than powder type SCC as well (Zhu 2003).

### **2.3.4 Previous Research on Bond of Prestressing Strand in SCC**

#### 2.3.4.1 Hamilton et al.

This research was conducted on six precast, pretensioned AASHTO Type II girders. Three girders were cast using an SCC mixture and three using a conventional concrete mixture. The SCC had a compressive strength at testing of over 9000 psi (62 MPa), two of the conventional concrete girders were 7500 psi (52 MPa) and one was 10,000 psi (69 MPa). Prestressed reinforcement consisted of twelve 0.5 in. (12.7 mm) Grade 270 strands in each girder. Shear reinforcement was designed such as to promote diagonal cracking and strand slip in order to discern changes in behavior caused by use of SCC. Two beams from each series of three were outfitted with a composite section used to simulate the action of a bridge deck while the third was tested without a composite section. Prestress transfer was accomplished by simultaneously flame cutting both strand ends at 15 days due to scheduling conflicts and low early strength of the SCC mixture. Strain gauges were installed along the bottom flange of one each of the SCC and conventional concrete beams before prestress release in order to measure transfer length (Hamilton 2005).

Structural tests were performed using a simply supported beam arrangement and a single point load placed near the end of the beam being tested. Two beams were tested for shear behavior, two for combined shear and flexure, and two for strand slip failure. The different failure modes were used to evaluate the behavior of SCC girders in relation to those cast with conventional concrete. At early ages compressive strength of the SCC specimens was lower than

that of the conventional concrete, whereas at the time of beam tests, the SCC specimens had a higher compressive strength. No substantial differences were discovered in flexural capacity, shear capacity, or web cracking between the SCC and conventional concrete beams. It was noted that the sudden prestress release may have had a larger contribution than concrete type in the case of strand slip failures (Hamilton 2005).

#### 2.3.4.2 Burgueño and Haq

In this study small scale T-beams were used to evaluate the effects of SCC on transfer and development length of 0.5 in. (12.7 mm) seven wire prestressing strand. Three different SCC mixtures were utilized in order to represent the different approaches used to achieve SCC as well as a conventional mixture for comparison. All four mixtures had a design compressive strength of 7000 psi (48 MPa) and an entrained air content of 6 percent. Tests similar to the Moustafa pullout test (Logan 1997) were used to provide a baseline comparison of the bonding characteristics of the mixes. Large test blocks containing 6 unstressed strands embedded 18 in. (457 mm) into the concrete were used for the tests. Strands projected from both top and bottom of the block so that slip could be monitored at both live and dead ends. Displacement transducers were used to measure slip as load was applied using a hollow core jack and monitored using a load cell (Burgueno 2005).

The beams used for testing had a total depth and flange width of 15 in. (380 mm) a flange thickness of 3 in. (75 mm) and were 38 ft (11.58 m) long. Each contained two strands located 2 in. (50 mm) from the bottom of the beam and two No. 4 (No 13) reinforcing bars in the top flange along with 0.25 in. (6.4 mm) shear stirrups spaced at 12 in. (305 mm). Each mix design was utilized in the construction of two beams. Strands were tensioned to 75 percent of the ultimate tensile strength. Prestress release was accomplished by annealing the strands to reduce

tension and then flame cutting. Measured concrete surface strains at the level of the prestressing steel were used to determine transfer length as were measurements of strand slip at transfer. Flexural load tests were performed using a single concentrated load applied at the estimated development length from one end. A servo-controlled hydraulic actuator was used to apply the load. An iterative approach was then used to determine flexural bond length by testing embedment lengths that led to both the flexural and bond-slip failure modes. These values were then used to bracket the location of the development length. Two flexural tests were conducted for each beam in order to determine development length. This provided four tests for each mix design (Burgueno 2005).

Peak pullout forces in the Moustafa pull-out tests were much lower for the SCC mixtures than for the conventional concrete mixture indicating lower bond strength. Transfer lengths were determined to be within the bounds of the ACI/AASHTO equation, however. SCC mixtures using a moderate  $w/c$  and moderate amounts of admixtures had performance closer to that of conventional concrete than did those with large amounts of fines or coarse aggregate. These mixtures had lower bond strengths and longer transfer lengths than did the conventional concrete. Development length testing was not complete at the time of this publication (Burgueno 2005).

#### 2.3.4.3 Girgis and Tuan

This research program utilized Moustafa pullout tests and measured transfer lengths on pretensioned bridge girders to examine the bond behavior of SCC mixtures. Large blocks for the Moustafa pullout tests measured 24 in. by 24 in. by 80 in. (610 mm by 610 mm by 2030 mm) and contained two rows of 0.6 in. (15.2 mm) strand specimens. Strands were spaced at 8 in. (200 mm) within a row and the rows were 12 in. (305 mm) apart. Forty-one specimens of both

deformed bars and 0.6 in. (15.2 mm) prestressing strand cast in both SCC and conventional concrete were used for small block pullout tests. Specimens measured 6 in. by 6 in. by 8 in. (150 mm by 150 mm by 200 mm). Two different SCC mixtures were used along with the conventional concrete that was identical to one of the SCC mixes without the admixtures. Three Nebraska DOT type bridge girders were cast from these concrete mixtures for measurement of transfer length (Girgis 2005).

The Moustafa pullout tests were conducted using an 18 in. (457 mm) embedment and a 2 in. (50 mm) bond breaker at the block surface. A center hole hydraulic actuator braced on a steel frame was used to apply the load. Applied load was measured using a load cell. Of the forty-one small test specimens, thirty-two were cast using one of the SCC mixtures and nine were cast using the conventional concrete. Eleven specimens contained No. 4 (No. 13) deformed bars, ten specimens contained No.6 (No. 19) bars, nine specimens contained No. 9 (No. 29) bars, and thirty specimens contained 0.6 in. (15.2 mm) prestressing strand. Embedment lengths varied from 1.5 in. to 3.5 in. (38 mm to 89 mm) and each specimen had a 1 in. (25 mm) bond breaker at the concrete surface. Two methods were used for applying the pullout force. The first utilized a pullout force applied to the bar being tested while the block was held by two embedded No. 8 (No. 25) bars on the other side of the specimen. The other method used bearing on the concrete to brace against the pullout force. A load rate of 1 kip (4.4 kN) per minute was used for all specimens and the load at bond failure was recorded. Transfer length was determined for the three beam specimens using concrete surface strains measured using DEMEC points and the 95% Average Maximum Strain method (Girgis 2005).

The researchers concluded from this study that bond strength for deformed bars cast in SCC was adequate. It was also concluded, however, that viscosity modifying admixtures (VMA)

in SCC may reduce early age compressive strengths. The consequence of this reduction could be a reduction in bond strength with the prestressing strands at release and longer transfer lengths. Transfer lengths were 30 in. (762 mm) and 36 in. (914 mm) for the two SCC mixtures and 20 in. (508 mm) for the conventional concrete mixture. Transfer length was found to be more than 50 percent longer for SCC members in these tests indicating this lower early bond strength. The pullout tests did not make this difference apparent, possibly due to different stresses being present in the tests and the actual members. At 28 days, however, SCC had higher bond strength possibly indicating shorter development length than conventional concrete. All pullout tests also showed that smaller bar diameters had higher bond strengths (Girgis 2005).

#### 2.3.4.4 Naito et al.

This research program examined transfer length and bond characteristics of prestressing strands cast in SCC and conventional high early strength concrete. Both concrete mixtures were designed for a compressive strength of 6800 psi (46.9 MPa) at 24 hours and 8000 psi (55.2 MPa) at 28 days and used both Type III cement and slag cement. The strand utilized was ½ in. special (13.3 mm) Grade 270 seven wire prestressing strand. Strand was prequalified using the methods of Logan (Logan 1997) and all specimens failed in pullout at a capacity less than the extrapolated minimum value of 37.4 kips (166 kN) for ½ in. special (13.3 mm) strand. However, strand was considered adequate since the maximum embedment required for strand fracture was computed to be less than that required development length (Naito et al. 2005).

Four bulb tee specimens were cast for a variety of nondestructive and destructive testing. These sections measured 45 in. (1140 mm) deep, contained 24 strands in the 32 in. (810 mm) bottom bulb, and 2 strands 41.25 in. (1048 mm) from the bottom in the 47 in. (1195 mm) wide top flange. The beams measured 35 ft (10.7 m) in length. Two each were cast using high early



strength concrete and SCC. One of each type was modified by removing local concrete cover and flame cutting the bottom row of 14 strands at the load point to produce a tension failure. Strands were detensioned gradually and simultaneously. Strain gauges were placed at one end of each beam and measured strains were used to calculate transfer length. Similar transfer lengths were found for both the high early strength and SCC beams, and both were shorter than the ACI and AASHTO recommendations. Flexural load tests consisted of a single point load placed at an embedment length equal to or less than the calculated development length. Strand slip was observed in the full section tests but was typically minimal and could be attributed to the formation of shear cracks. No slip occurred in the tests using the reduced cross-section. The author therefore concluded that both the SCC and high early strength produced adequate bond at the specified development length (Naito et al. 2005).

#### 2.3.4.5 Hegger et al

This study examined the bond strength and shear capacity of SCC members to provide a better understanding of these behaviors and validate other research that had shown no effect on flexural capacity. Bond in prestressed members was described by the researchers as being a combination of adhesion, the Hoyer effect, and mechanical interlocking due to the helical shape of prestressing strand, the accepted mechanisms of bond. Modified pullout tests were performed that kept the strand prestressed with at least half of the expected bond strength as opposed to the unstressed specimens in normal pullout tests. In a normal pullout test the tensile force used reduces the strand diameter and does not represent the radial pressure and friction that define the Hoyer effect. The modified pullout tests used in this research utilized a shearing of the concrete over the strand instead of tension force being applied to the strand. This action led to the term push-pullout test. Cubic specimens measuring 5.9 in. (150 mm) on each side and containing 0.5

in. (12.7 mm) prestressing strand were used in these tests with a 2 in. (50 mm) portion of each specimen kept at an almost constant bond strength. The rest of the length was debonded using PVC pipe. Several different values of stress were used to imitate different points along the transfer length. The results of these push-pullout tests on SCC specimens were compared to similar tests on normal-strength and high-strength concrete (Hegger 2007).

Based on the observation of the Hoyer effect only, no substantial difference was found between the strand bond strength for SCC and conventional concrete mixtures. Correlations to bond strength were discovered relating to compressive strength and concrete age. Both of these were actually related to a higher bond strength for a higher concrete strength. Type of concrete was also determined to affect bond strength. The effect of particle shape was discovered to be substantial, as SCC mixtures containing fly ash showed reduced bond strengths while SCC mixtures containing limestone powder showed bond strengths similar to conventional mixtures. This was explained by the spherical nature of fly ash particles and the angular shape of limestone powder particles (Hegger 2007).

Transfer length tests were conducted using rectangular specimens measuring 6.6 ft (2.0 m) long. These specimens were constructed using 0.5 in. (12.7 mm) seven wire prestressing strand. A prestress of 185 ksi (1275 MPa) with a gradual release was used for the specimens and concrete surface strains were measured using DEMEC points attached to the concrete surface. The researchers found that concrete type had some effect on transfer length with some increase due to reduced bond strength. It was concluded that the current transfer length equations contained adequate safety margins to cover the differences (Hegger 2007).

#### 2.3.4.6 Larson et al.

This research for the Kansas Department of Transportation (KDOT) examined the material and bond characteristics of prestressed bridge girders cast with SCC. Large block pullout tests using SCC and 0.5 in. (12.7 mm) prestressing strand indicated that SCC specimens had smaller values for ultimate load and first slip than did conventional concrete which indicated that development length tests were necessary. Therefore, beam specimens were constructed. Fresh concrete properties were examined using inverted cone slump flow, visual stability index, J-ring, and L-box tests. Concrete compressive strength and modulus of elasticity were measured at prestress release and at the time of flexural load tests (Larson 2007).

Twelve single strand beam specimens were constructed from two cross-sections for development length testing, but only eleven of these were tested. The first cross-section measured 8 in. by 12 in. (200 mm by 305 mm) with the strand located at a depth of 10 in. (255 mm). The second cross-section also had a width of 8 in. (200 mm) but the depth was increased to 24 in. (610 mm) and the strand located 22 in. (560 mm) from the bottom. These specimens were used to simulate the case where there is more than 12 in. (305 mm) of concrete below the reinforcement, also called the “top bar effect.” The larger beams had their total depth reduced to 12 in. (305 mm) at mid span so that results would be compatible between the two cross-sections. All single strand beam sections contained no shear reinforcement. In order to evaluate development length of multiple strands at close spacing, multiple strand T-beams with a total height of 21 in. (530 mm) and a 36 in. (915 mm) wide, 6.5 in. (165mm) thick compression flange were constructed. The T-beams had 5 strands located at a depth of 19 in. (480 mm) and shear reinforcement in the form of No. 4 (No. 13) stirrups spaced 6 in. (150 mm) (Larson 2007).

Transfer length was examined using measured strand draw-in and the methods outlined by Logan (Logan 1997). Flexural testing consisted of an initial test using the calculated development length for that situation as the embedment length. Embedment lengths for subsequent tests were based on the failure mode of this initial test. If the initial test resulted in a flexural failure, the next embedment length tested was 80 percent of the calculated development length. If the initial test resulted in a bond failure, the following test used an embedment length 120 percent of the calculated development length. Strand slip was monitored during testing using LVDTs so that bond failures could be detected. Three different loadings were used in the testing. The first loaded the beams at 100 lb/min (0.44 kN/min) until cracking and then to failure at 10 lb/min (0.04 kN/min). The second loaded the beam to 76.5 percent of the calculated nominal moment capacity,  $M_n$ , at 100 lb/min (0.44 kN/min). This load was then maintained for 24 hours after which the beam was loaded to failure at 10 lb/min (0.04 kN/min) if it had not failed under the sustained load. The final loading was like the second except it used 100 percent of  $M_n$ . Servo-controlled actuators with a spreader beam on rollers were used to apply the load. The two point loads were placed directly over crack formers placed at the desired embedment length during beam casting. These crack formers ensured that the first cracks were due to bending and occurred at the desired embedment length (Larson 2007).

All beams failed in flexure with strands rupturing at both the 100 percent and 80 percent values of the ACI/AASHTO prediction for development length. Average 21-day implied transfer lengths were 21 in. (530 mm) for the single strand beams, 30 in. (760 mm) for the top strand beams, and 29 in. (740 mm) for the multiple strand T-beams. These were also determined to be within the requirements of the AASHTO and ACI provisions. It was concluded that the

current equations for development length were therefore adequate for this SCC mixture and these beam geometries (Larson 2007).

#### 2.3.4.7 Peterman

This study examined transfer and development length characteristics, the top strand effect and development of a simple, standard bond test for SCC members. The first portion of the testing used six SCC mixtures that were currently in use made with admixtures from major U. S. suppliers. Identically sized specimens were cast at five different plants across the country using the same prequalified strand. Six specimens were cast for each SCC mixture along with two extra specimens with the same dimensions using lower bond quality strand for one mixture. Five of each set of six specimens contained a single strand and measured 10 in. wide by 15 in. deep (254 mm by 380 mm). Three of these five had the strand located 2 in. (50 mm) from the bottom and the other two located 2 in. (50 mm) from the top. All were loaded at an embedment length equal to either the calculated development length or 80 percent of that value. The sixth specimen in each group measured 8 in. wide by 6 in. deep (200 mm by 150 mm) and was loaded at the 80 percent embedment length only. All strand was 0.5 in. (12.7 mm) Grade 270 prestressing strand and all beams contained no shear reinforcement. Transfer length was determined indirectly using measured values of strand end slip (Peterman 2007).

Transfer lengths for all bottom strand specimens using the prequalified strand were within the bounds of the ACI Code, but the specimens using strand with a lower bond quality showed transfer lengths over 40 percent longer than the ACI Code guidelines. It was also concluded that the position of the strands vertically in the cross-section did influence transfer length as top strand specimens showed transfer lengths substantially in excess of the ACI Code

equations. Despite longer transfer lengths in the top strand and poor strand specimens, all specimens reached their calculated moment capacity when tested in flexure (Peterman 2007).

After the first round of testing, more specimens were cast to examine the effects of various amounts of concrete above and below the strands. These specimens were 4 in. (100 mm) wide by either 28 in. or 16 in. (710 mm or 405 mm) deep and contained either three or five ½ in. special (13.3 mm) diameter prestressing strands. This strand was also qualified using Logan's recommendations (Logan 1997). These sections were used to compare strands with the same amount of concrete above but not below and below but not above. From these tests it was discovered that top strand effect is most influenced by the nearness of the strands to the top of the member (as cast), but the amount of concrete below the strands does still play a role. Finally, testing was performed on standard rectangular beams, L-beams, and panels both 4 in. and 6 in. (100 mm and 150 mm) thick produced at the precast plants. These were cast using flowable concrete and again the strand used was qualified. This last set of tests showed the same trends as the others. While this research project indicated that increasing concrete fluidity led to a reduction in bond capacity, no particular rheological property showed good correlation with bond capacity. The authors indicated that measured end slips are a reliable predictor of transfer length and recommend this approach for precasters when bond is an issue. Transfer length can be estimated from the measured end slips using the relationship

$$L_t = \frac{2\Delta E_{ps}}{f_{si}}$$

where  $\Delta$  is the measured end slip,  $E_{ps}$  is the elastic modulus of the prestressing steel, and  $f_{si}$  is the initial stress in the strand immediately after release (Peterman 2007).

#### 2.3.4.8 Trent

This research program examined effects of SCC on transfer and development lengths and flexural strength of prestressed members when compared to conventional concrete, and examined prestress losses. Three transfer length specimens were fabricated using two SCC mixtures and one conventional concrete mixture. These specimens had a 6 in. by 6 in. (150 mm by 150 mm) square cross-section and contained a single 9/16 in. (14.3 mm) diameter strand 2 in. (50 mm) from the bottom of the cross-section. These specimens were intended to mimic the stem of the stub tee sections used for development length testing. Development length specimens also contained a single 9/16 in. (14.3 mm) strand 2 in. (50 mm) from the bottom of the cross-section which had a stem measuring 6.5 in. (165 mm) at the bottom and 7.5 in. (190 mm) at the top. The flange of the section had a width of 12 in. (305 mm) and a thickness of 4 in. (100 mm). The total section height was 14 in. (355 mm) and the beams contained adequate mild steel shear reinforcement. All prestressing steel was Grade 270 low relaxation strand. Two SCC mixtures and one conventional concrete mixture were utilized in this study. All three concrete mixtures were designed for a compressive strength of 3500 psi (24 MPa) at 12 hours and 6000 psi (41 MPa) at 28 days. The SCC mixtures only differed in the type of fine aggregate used. Strands were released gradually for the transfer length specimens and using bolt cutters, flame cutting, or saw cutting for the development length specimens (Trent 2007).

The transfer length specimens were instrumented with DEMEC points utilized to measure concrete surface strains for transfer length determination. Measurements were taken immediately before and after prestress release, 7 days after release and 28 days after release. Measured strain values from each side of the member were smoothed using a moving average and then the two profiles were averaged. The 95% Average Maximum Strain method was used to

determine the transfer length from the smoothed profiles. The transfer lengths from each end were averaged and the transfer length from the average of the four profiles was also calculated. These measured values were then compared to the predictions given by the ACI, AASHTO, and Buckner (ACI 2011, AASHTO 2007, Buckner 1995) recommendations. All transfer lengths were less than the AASHTO and Buckner predictions, however one of the SCC values was greater than the ACI code prediction. Since the ACI prediction is an average value and differences may have had other causes, the author concluded that the use of SCC did not adversely affect the transfer length (Trent 2007).

Development length was examined using iterative load testing on both ends of the 12 stub tee specimens for a total of 24 tests. Beams were tested over a six week period and increases in compressive strength were accounted for in calculation of theoretical beam capacities. Deflection and strand slip were monitored as load was applied in 1 kip (4.4 kN) increments for each flexural test performed. Embedment length was varied using 6 in. (150 mm) increments between tests. If the beam failed due to strand slip the subsequent embedment length was increased, and if it failed in flexure the embedment length was decreased. A strand slip failure was characterized by slip greater than 0.01 in. (0.25 mm). A flexural failure was characterized by concrete crushing near the applied load and plastic behavior. Development length was not determined for the conventional concrete specimens due to non-repeating results that may have been caused by poor strand bonding quality in one of the strands. These results consisted of bond failures at three different embedment lengths and then flexural failures when the same embedment lengths were tested a second time. The development lengths for the SCC specimens were substantially shorter than the ACI/AASHTO predicted values. This could be due to a



shorter flexural bond length since transfer lengths were close to code predictions even with gradual release, while the development length specimens used sudden release (Trent 2007).

#### 2.3.4.9 Andrawes et al.

This study involved the review and combination of literature information involving the transfer and development length of prestressing strands cast in SCC. Its basic goals were to look at the effects of SCC on transfer and development length and determine whether SCC should and could be used in AASHTO bridge girders in Illinois. Research undertaken at seven different universities was included in the study (Andrawes et al. 2009). The work of Larson, sponsored by the Kansas Department of Transportation, included pullout testing as well as transfer and development length tests on rectangular and T-beams for both conventional concrete and SCC (Larson et al. 2007). Trent examined transfer and development length also using rectangular and T-beams with both SCC and conventional concrete at Virginia Tech (Trent 2007). The work of Haq at Michigan State included pullout testing as well as transfer and development length tests using T-beams and both conventional concrete and SCC (Burgueno 2005). Girgis and Tuan examined bond strength with SCC using pullout tests and transfer length using full size Nebraska girder sections (Girgis 2005). Hamilton and Labonte examined structural performance and transfer length of AASHTO Type II girders cast with both conventional concrete and SCC (Hamilton et al. 2005). Naito et al. conducted pullout tests along with structural performance and transfer length tests on full-scale bulb tee girders at Lehigh University using both conventional concrete and SCC (Naito et al. 2005). Ruiz et al. examined transfer lengths of prestressing strands in rectangular beams cast with high strength SCC and conventional concrete (Ruiz et al. 2006). Most of these previous studies are detailed earlier in this paper.

From the previous research examined in the Illinois DOT report, the authors were able to make various conclusions concerning the use of SCC in prestressed bridge girders. Compressive strength had a minor effect on transfer and development length for all types of concrete. Strand location and spacing impacted transfer length to a greater extent than development length. Three of the studies showed lower bond strength for SCC and transfer lengths that exceeded the ACI/AASHTO design recommendations. One of the three studies that conducted development length testing showed development lengths that were longer than the ACI/AASHTO prediction. Overall, it was concluded that the complexity of SCC mixtures could cause differences in transfer and development lengths between producers and that cross-section geometry could have the same effects. More research was recommended using the mixtures specific to Illinois (Andrawes 2009).

#### 2.3.4.10 Staton et al.

This research program was concerned with the transfer lengths of members cast with two different high strength SCC mixtures and one conventional high strength concrete (HSC). Twenty fully bonded prestressed concrete beams were cast from these three concretes mixtures. Each beam had a 6.5 in. by 12 in. (165 mm by 300 mm) cross section and measured 18 ft (5.5 m) in length. Two 0.6 in. (15 mm) Grade 270, low-relaxation, seven wire prestressing strands were placed at a distance of 10 in. (250 mm) from the top of each beam. Two No. 6 (No. 19) reinforcing bars were placed in the compression block of the beams and ¼ in. (6.4 mm) smooth shear stirrups were spaced at 6 in. (150 mm) along the entire length of each beam. Six beams were cast with one SCC mixture, eight with the other, and six were cast with the HSC mixture. All concrete had a target strength of 7000 psi (48 MPa) at release and 12,000 psi (83 MPa) at 28 days. Strands were stressed to 75 percent of the tensile strength, 202.5 ksi (1400 MPa), and

concrete was placed in the formwork in two lifts. Prestress release was performed gradually at approximately one day (Staton et al. 2009).

The North American Strand Producers (NASP) strand bond test was used to examine the quality of the prestressing strand used. Strand specimens measuring 32 in. (810 mm) long were cast in a block of mortar contained in a 5 in. (127 mm) diameter by 18 in. tall (130 mm by 460 mm) thin walled steel cylinder with 2 in. (50 mm) of strand exposed at the top and a 2 in. (50 mm) bond breaker at the other end. Specimens were tested when the mortar reached a strength near 4500 psi (31 MPa). End slip was monitored using an LVDT while the specimens were loaded at 0.100 in./min (2.54 mm/min). Loads associated with 0.010 in. (0.254 mm) and 0.100 in. (2.54 mm) of slip were recorded (Staton 2009).

Transfer lengths were determined from measured concrete surface strains. The beams were instrumented with DEMEC points on each side at the center of gravity of the prestressing steel at a spacing of 4 in. (100 mm). Readings were taken immediately before and after prestress release and then at 3, 5, 7, 14, and 28 days of age. The concrete surface strains were calculated from the change in distance between the points. Average measured transfer lengths were 21.8 in. (554 mm) with a standard deviation of 3.8 in. (97 mm) for the live end of the beams made with SCC containing only Type I cement and 21.1 in. (536 mm) with a standard deviation of 3.8 in. (97 mm) for the dead end. The SCC made with Type III cement and fly ash yielded transfer lengths of 19.6 in. (498 mm) with a standard deviation of 3.6 in. (91 mm) for the live end and 19.8 in. (503 mm) for the dead end. The conventional HSC beams had live and dead end transfer lengths of 24.0 in. (610 mm) and 23.5 in. (597 mm) with standard deviations of 2.9 in. (74 mm) and 4.4 in. (110 mm) respectively. All measured transfer lengths were shorter than the requirements of ACI 318-05 and AASHTO LRFD specifications (Staton et al. 2009).

The two strand reels had NASP pullout loads of 22.2 kips (98.8 kN) and 19.8 kips (88.1 kN), which exceeded the minimum requirement of 12.6 kips (86.9 MPa) and indicates adequate bonding characteristics. The SCC beams had lower compressive strengths at early ages but shorter transfer lengths than the HSC beams, which is opposite of expected behavior in relation to compressive strength. The average transfer lengths for the Type I cement SCC beams and the HSC beams were found to be statistically equal, while the Type III cement SCC beams had slightly shorter transfer lengths. The authors concluded that the transfer length equations deemed adequate for conventional HSC should be adequate for high-strength SCC beams (Staton et al. 2009).

#### 2.3.4.11 Floyd et al.

This research program utilized the same specimens tested for transfer length by Staton et al. An iterative process of flexural testing similar to that used by many previous researchers was utilized to examine development length. One end of each beam specimen was tested using simple supports and a single point load placed at a specified embedment length. Strand slip was continuously monitored using LVDTs and a data acquisition system. The failure mode was examined to determine the relationship of the embedment length to the development length. If no strand slip was recorded before the nominal moment was reached, the subsequent test would be at a shorter embedment length. If strand slip was recorded, a longer embedment length would be used. This process was repeated until the actual development length could be approximated. Load was applied at 5 kip (22.2 kN) increments until cracking was observed and then at 2.5 kip (11.1 kN) increments until failure. Deflection was measured after each increment and the beam was examined for new cracks (Floyd et al. 2011).

Flexural tests were performed on 19 of the 20 beams with all six of the HSC beams being tested along with 13 of the SCC beams. At least one beam from each of the three concrete mixtures exhibited strand slip before the nominal moment was reached. Shear failures at the short embedment lengths required for the Type III cement SCC beams made determination of the development length somewhat difficult, however. Measured development length for the HSC specimens was between 30 in. and 35 in. (760 mm and 890 mm) which is much shorter than the 86.3 in. to 88.4 in. (2192 mm to 2245 mm) predicted by the ACI/AASHTO equation. The Type I cement SCC beams had a development length between 35 in. and 37.5 in. (890 mm and 950 mm) as compared to a prediction of 86.1 in. to 88.3 in. (2187 mm to 2243 mm). Measured development length for the Type III cement SCC specimens was between 30 in. and 32.5 in. (760 mm and 825 mm) compared to a prediction of 89.2 in. to 88.3 in. (2266 mm to 2243 mm). It was concluded from these results that these high strength SCC mixtures performed very similarly to the conventional HSC. It was also noted that the ACI/AASHTO prediction overestimated the development length by more than 60 percent for all specimens. This may have been due to the high strengths used along with the gradual release of prestress and small specimen size (Floyd et al. 2011).

## **2.4 Lightweight Self-Consolidating Concrete**

### **2.4.1 Description and Benefits**

Lightweight self-consolidating concrete (LWSCC) has come into more widespread use in recent years. As its name suggests, this type of concrete combines the properties and benefits of both lightweight concrete (LWC) and self-consolidating concrete (SCC). The potential is available for savings in both the loads on the structure as well as for concrete placement. It is possible to obtain self-consolidating behavior using the same materials as LWC and methods

similar to those used for normal weight SCC. Concrete density tends to be slightly higher for LWSCC when compared to LWC due to the increased paste content required for SCC as well as the need to limit the coarse aggregate content for stability (Wall 2010). Less research has been done in this area than for LWC or normal weight SCC and therefore future research, such as the research program described in this dissertation, is necessary.

It is possible to obtain good quality SCC using lightweight aggregates, as demonstrated by several researchers (Kaszynska 2010, Wall 2010, Ward 2009, Shi 2005). As is the case for normal weight SCC, it is necessary to pay careful attention to the constituents of LWSCC. Aggregate size and gradation are important factors to consider for SCC. The combination of lightweight and normal weight aggregates can also have a substantial impact on the properties of LWSCC (Kaszynska 1010). The density differences between large and small lightweight aggregate particles can increase the segregation potential of LWSCC. Therefore, maximum size and percentage of large particles should be limited. Combinations of both lightweight coarse and fine aggregates along with normal weight aggregates can be used to achieve the specified density, segregation resistance, and finish. Lightweight fine aggregates have been shown to be detrimental to some hardened concrete properties, such as creep and shrinkage, but can greatly improve finishing characteristics and segregation resistance (Wall 2010).

It is important to be aware of other aspects of LWSCC just as is the case for normal weight SCC. Proper moisture conditioning of the lightweight aggregates is necessary along with proper determination of free water content in order to have control over the water content of the concrete mixtures. Adequate viscosity very similar to normal weight SCC is necessary to control flow and stability. Flow characteristics should be suited to the particular application to limit the possibility of segregation. Air entrainment improves the workability and durability of the

mixture while also helping reduce the density of the paste to something more similar to the aggregate, which helps with stability (Wall 2010).

As is the case with normal LWC and NWC, mix proportioning of LWSCC is different than that for normal SCC. The volume of paste necessary to produce the desired flow characteristics is based on many of the aggregate characteristics including gradation, particle shape, surface texture and ratio of fine to coarse aggregate. Supplementary cementitious materials and other fillers have been used successfully in LWSCC to obtain the extra paste required for flowability. These include fly ash, slag cement, and waste glass powders. Shi and Wu documented successful use of waste glass powder without deleterious expansion of the concrete due to alkali-aggregate reaction (Shi 2005). This may be a result of the porous nature of the aggregates accommodating the reaction products. In addition to high paste, relatively large amounts of VMA have been required to increase stability (Colleparidi 2004). As a lightweight aggregate producer, Wall suggested a  $w/c$  for LWSCC of 0.30 to 0.40 with total binder between 700 lb/yd<sup>3</sup> and 850 lb/yd<sup>3</sup> (415 kg/m<sup>3</sup> and 504 kg/m<sup>3</sup>). He recommended a slump flow between 22 in. and 26 in. (560 mm and 660 mm), air content between 4.5 percent and 7.5 percent, and a maximum lightweight coarse aggregate volume of 32 percent with a maximum size of 0.5 in. (12.7mm) (Wall 2010).

## **2.4.2 Previous Research in Bond of Prestressing Strand in LWSCC**

### **2.4.2.1 Lachemi et al**

This research program consisted of twenty-four pullout tests of deformed reinforcing bars cast in three lightweight self-consolidating concrete (LWSCC) mixtures and one normal weight SCC. The effects of blast furnace slag aggregate and expanded shale aggregate with a nominal size of 3/8 in. (10 mm) were examined along 4 in. (100 mm) and 8 in. (200 mm) embedment

lengths. Compressive strengths of all concrete mixtures were between 5250 psi and 6320 psi (36.2 MPa and 43.6 MPa) at 28 days. Reinforcing bars used in the test specimens had a nominal diameter of 0.6 in. (15 mm) and a yield strength of 58 ksi (400 MPa) and were cleaned with a wire brush immediately before specimens were cast. Concrete specimens measured 8 in. by 8 in. (200 mm by 200 mm) by either 4 in. or 8 in. (100 mm or 200 mm) (Lachemi 2009).

Concrete was cast vertically around a horizontal reinforcing bar placed at mid-depth and 2.4 in. (60 mm) from one edge. Direct pullout tests were then performed using a hydraulic ram, load cell, and LVDT to measure bond slip. All specimens failed due to splitting of the concrete with no pullout failures, and it was observed that longer embedments produced larger pullout loads. Normal weight SCC had the highest pullout force followed by expanded shale and then blast furnace slag. This indicates that expanded shale aggregate produces better bond strengths than blast furnace slag aggregate possibly due to a better interfacial transition zone at the aggregate. While LWSCC was shown to have lower bond strength than normal weight SCC, it appears that type of lightweight aggregate can have a substantial effect on the bond strength of lightweight SCC (Lachemi 2009).

#### 2.4.2.2 Ward et al.

Previous research at the University of Arkansas consisted of a study on the bond properties of 0.5 in. (12.7 mm) prestressing strand cast in LWSCC (Ward et al. 2009). The concrete utilized an expanded clay lightweight aggregate and had an average compressive strength of 4530 psi (31.2 MPa) at prestress release and 6700 psi (46.2 MPa) at 28 days. The concrete had an average unit weight of 119 lb/ft<sup>3</sup> (1910 kg/m<sup>3</sup>). Six rectangular beams with a 6.5 in. (165 mm) by 12 in. (305 mm) cross-section and a length of 18 ft (5.5 m) were cast. Each beam was prestressed using two 0.5 in. (12.7 mm) Grade 270 low relaxation prestressing strands



placed at a depth of 10 in. (255 mm) in each specimen. Shear reinforcement in the form of closed 0.25 in. (6.4 mm) stirrups was used to avoid shear failures. No mechanical vibration was utilized when placing the concrete. Concrete surface strain measurements for determination of transfer length were taken immediately before and after prestress release, and then at 5, 7, 14, and 28 days after placement of the concrete using the DEMEC system. Transfer lengths were determined from these measurements using the 95% Average Maximum Strain method. Development length was evaluated for the beam specimens using iterative flexural tests accomplished through a simply supported span and single point load placed at varied embedment lengths. Strand slip was monitored using LVDTs and the relationship of the embedment length to the development length was determined by examining the failure type (Ward et al. 2009).

The results of Ward's work are summarized in Table 2.6. Average measured transfer lengths of between 17.5 in. (445 mm) and 22.3 in. (566 mm) were substantially less than the predicted values of 27.9 in. (709 mm) to 29.3 in. (744 mm) (Ward et al. 2009). Estimated transfer lengths were calculated using the expression

$$l_t = \frac{f_{se}}{3} d_b$$

taken from the ACI/AASHTO equation that was used to estimate development length as well (ACI 2011, AASHTO 2007). Tested embedment lengths between 27.5 in. (700 mm) and 45 in. (1145 mm) resulted in no strand slip before achievement of the calculated nominal moment. The 45 in. (1145 mm) embedment length resulted in fracture of the strand with no slip. A bond failure occurred before the nominal moment was reached at a tested embedment length of 25 in. (635 mm). These values were compared to the ACI/AASHTO predictions of 74.5 in. (1890 mm) to 77 in. (1955 mm). Therefore, the authors concluded that the ACI and AASHTO equations overestimated both transfer and development lengths for this LWSCC (Ward et al. 2009).

Table 2.6: Summary of Ward's Transfer and Development Length Data

$f'_c$ (psi)	$f'_{ci}$ (psi)	$L_t$ Strain (in.)	$f_{se}d_b/3$ (in.)	$50d_b$ (in.)	$60d_b$ (in.)	Embedment Length $L_e$ (in.)	ACI/ AASHTO $L_d$ (in.)	Estimated Actual $L_d$ (in.)
6700	4530	20.1	28.7	25	30	25 - 45	74.5 - 77.0	<27.5

Note: 1000 psi = 1 ksi = 6.9 MPa, 1 in. = 25.4 mm

### 2.4.3 Discussion

The previous two sections illustrate the limited quantity of research concerning prestressing strand bond in LWSCC. The similarity of the specimen size allows for a good comparison of results between Ward's (Ward et al. 2009) results and those described by Peterman for conventional LWC in Section 2.2.3.2 (Peterman et al. 2000). Both researchers determined that the code equations were conservative for development length and that shear cracking could cause bond issues. Ward also found the transfer length provisions to be conservative. The concrete used in these two experimental programs utilized different aggregates and had different unit weights, but similar compressive strengths. The extra variable of self-consolidating behavior was also considered in Ward's research. Different strand diameters were also tested by the two researchers. While these two research programs yielded similar conclusions about the bond of LWC, these conclusions are really only applicable to the specific research and not as a generality. More research is needed comparing the performance of the same size strands cast in LWSCC, and with conventional LWC and NWC having similar compressive strengths.

### 2.5 Conclusion

Substantial research has been performed on the bond behavior of prestressing strands cast in conventional concrete since the first research was performed in the 1950s. While there has

been some debate over the years between then and now, the equations developed for conventional concrete have been determined to be adequate and are used in current practice. Since SCC is a more recent development in concrete technology, less research has been performed on its bond characteristics with prestressing strand. However, most research has shown that SCC behavior is typically similar to and even better than conventional concrete in some cases.

Lightweight concrete has been in use for a very long time, but it is not as common as conventional concrete and, therefore, not as much research has been conducted in this area. LWC has much different properties than NWC in many aspects. However, it has also been shown to perform in a similar manner to conventional concrete in relation to bond with prestressing strand. There are several very beneficial characteristics of LWC that may aid in its bond behavior. Limited research has been performed in the area of LWSCC. A similar project to that described in this dissertation was performed by Ward at the University of Arkansas (Ward et al. 2009), but his project examined only 0.5 in. (12.7 mm) prestressing strand cast in one LWSCC mixture. As this material is becoming increasingly common, more research is needed in this area to ensure that this material can be used safely in prestressed applications. The research described in the following chapters examined 0.6 in. (15.2 mm) prestressing strand and had a more inclusive scope.

## Chapter 3: Experimental Program

### 3.1 Introduction

The experimental program described herein consisted of developing lightweight self-consolidating concrete (LWSCC) mixtures suitable for use in pretensioned, prestressed bridge girders along with normal weight self-consolidating concrete (NWSCC) mixtures used as control. Eighty-one LWSCC mix proportions were tested using both expanded clay and expanded shale coarse aggregates and eight were tested using conventional limestone coarse aggregate. Fresh and hardened concrete properties were measured for each of these mixtures. A total of six mixtures were chosen from these to meet the required variable combinations of aggregate type and compressive strength. Each mixture was required to meet fresh concrete property specifications as well. Four pretensioned prestressed beam specimens were cast using each of the six final concrete mixtures, and an extra specimen was cast using an earlier version of one of the mixtures, for a total of 25 specimens. These specimens were used to examine transfer and development length of 0.6 in. (15.2 mm) prestressing strands. The number of specimens was chosen based on the number of data points, considerations of cost, laboratory setup for construction, and previous research. Four specimens allowed for transfer length measurements and a flexural test on each end of the specimen for a total of eight data points for each mixture. This was still a limited number of data points but was similar to previous research and was the maximum amount feasible based on cost and construction restraints.

### 3.2 Aggregate Properties

#### 3.2.1 Overview

The properties of lightweight aggregates differ significantly from those of conventional coarse aggregates and require special procedures for their determination. Lightweight aggregate

absorbs water over a considerably longer period of time than conventional aggregates. Concrete mix designs are typically based on aggregates at the saturated surface dry (SSD) condition, which is difficult to obtain for lightweight aggregates with a high absorption capacity. Henceforth, in reference to lightweight aggregate, the SSD condition shall refer to aggregate having been soaked for 24 hours and excess surface moisture removed by means of a towel or centrifuge. Specific gravity factors (S) and absorption capacities (AC) were determined for each of the lightweight aggregates using the procedures described in the appendix of the Standard Practice for Selecting Proportions for Structural Lightweight Concrete (ACI 1998). Specific gravity and absorption capacity were determined on samples obtained by splitting 2 ft<sup>3</sup> to 3 ft<sup>3</sup> (0.057 m<sup>3</sup> to 0.085 m<sup>3</sup>) samples to the desired size and then submerged in water for 24 hours. Two different shipments of expanded shale aggregate from the same supplier were used in the project and these two shipments had slightly different properties due to variation in the aggregate source material.

### **3.2.2 Lightweight Aggregate Specific Gravity**

Specific gravity was determined using both the pycnometer method and the procedures of ASTM C127 (ASTM 2007), which ACI 211.2 refers to as “wholly equivalent” (ACI 1998). The pycnometer method utilizes a measure with known volume that is calibrated by filling with water, agitating to remove entrapped air, and weighing at the required volume. The Mason jar type pycnometer described in ACI 211.2 was not available, so the test was performed using a typical pycnometer used for fine aggregate specific gravity. Aggregate specimens were prepared by washing dust and other coatings from the aggregate as prescribed in ASTM C127 (ASTM 2007) and were soaked for approximately 24 hours before testing. One aggregate sample was towel dried as described in ASTM C127, weighed, and then introduced into the empty

pycnometer along with approximately three quarters of the volume of water. Entrapped air was removed by rolling and shaking the pycnometer. The water level was then adjusted to capacity and the weight recorded at 5, 10, 20, and 30 minutes, with agitating and topping off before each weight was recorded. The pycnometer filled with aggregate is shown in Figure 3.1. The specific gravity factor,  $S$ , was calculated at each time increment using

$$S = \frac{C}{C + B - A}$$

where  $A$  is the weight of the pycnometer charged with aggregate and filled with water (g),  $B$  is the weight of the pycnometer filled with water only (g), and  $C$  is the weight of the aggregate sample (g). A second specimen was also towel dried in a manner similar to ASTM C127 (ASTM 2007) and was used to determine the moisture content of the aggregate tested and the specific gravity according to those methods (ACI 1998). The procedures of ASTM C127 (ASTM 2007) involved weighing the aggregate in air and submerged in water at an SSD



Figure 3.1: Lightweight aggregate specific gravity using the pycnometer method

condition. The SSD condition was obtained by blotting an aggregate sample that had been washed and soaked for 24 hours with a towel until it was no longer shiny in appearance. A piece of geosynthetic material was attached to the top of the basket used to weigh the aggregate sample submerged in water in order to prevent loss of floating particles. The specific gravity factor,  $S$ , was then calculated using

$$S = \frac{C}{C - E}$$

where  $C$  is the weight of the aggregate sample in air (g) and  $E$  is the weight of the aggregate sample under water (g) (ACI 1998). The specific gravity factors determined using both methods are presented in Table 3.1. The results of these tests show very good agreement between the two methods.

Table 3.1: Aggregate Properties

Aggregate Type	Limestone	Clay	Shale 1	Shale 2
Nom. Max. Size (in.)	3/8	1/2	3/4	3/4
S (ASTM C127)	2.68	1.24	1.41	1.40
S (ACI 211.2)	NA	1.25	1.41	1.41
AC (ASTM C127) (%)	0.38	16.3	9.9	15.0
AC (ACI 211.2) (%)	NA	15.0	9.3	12.9

Note: 1 in. = 25.4 mm

### 3.2.3. Lightweight Aggregate Absorption

Aggregate absorption was determined using the procedures of ASTM C127 (ASTM 2007) and the centrifuge method described in ACI 211.2 (ACI 1998). The procedures of ASTM C127 consisted of taking the SSD sample mentioned previously and drying to constant weight after weighing the sample submerged in water. The difference between the SSD and dry weights was then taken as the absorption capacity. The centrifuge method of ACI 211.2 consisted of spinning small samples of aggregate that had been presoaked for 24 hours in a centrifuge at 500 rpm for 20 minutes to obtain an SSD condition. The centrifuge was stopped at 5, 10, and 20

minutes to obtain the weights of the samples. The samples were then dried to constant weight and the difference between the wet and dry weights was taken as the moisture content at those time increments (ACI 1998). The variation of moisture content with centrifuge time is shown in Figure 3.2. The moisture content after 20 minutes of centrifuge time was taken as the absorption capacity. The results from both test methods are shown in Table 3.1 and some difference between the two methods was evident. The absorption capacity determined from the centrifuge method was used for moisture content adjustments during batching.

### 3.2.4 Particle Size Distribution

The particle size distribution for each lightweight aggregate was determined using the methods of ASTM C136 (ASTM 2006). The particle size distributions are shown in Figures 3.3 and 3.4 and the nominal maximum sizes are presented in Table 3.1. It was later determined that

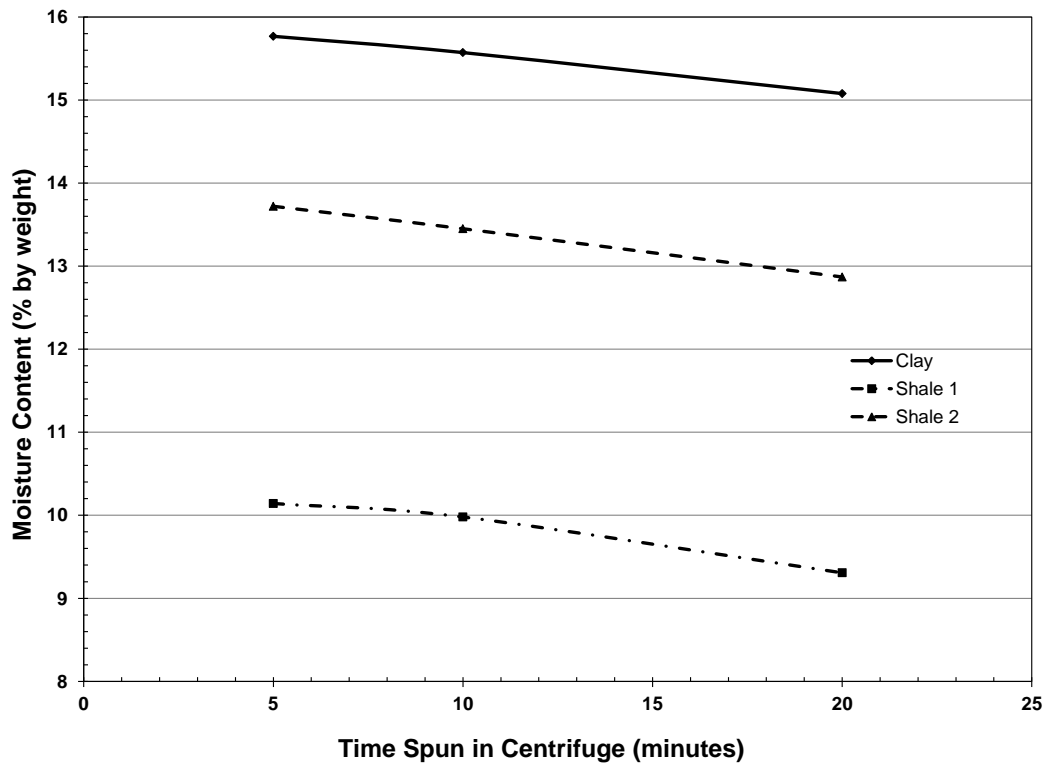


Figure 3.2: Variation of moisture content with centrifuge time



the large expanded shale aggregate particles were causing problems for both slump flow and compressive strength. Particles larger than ½ in. (12.7 mm) were removed using a ½ in. (12.7 mm) sieve for all subsequent expanded shale aggregate.

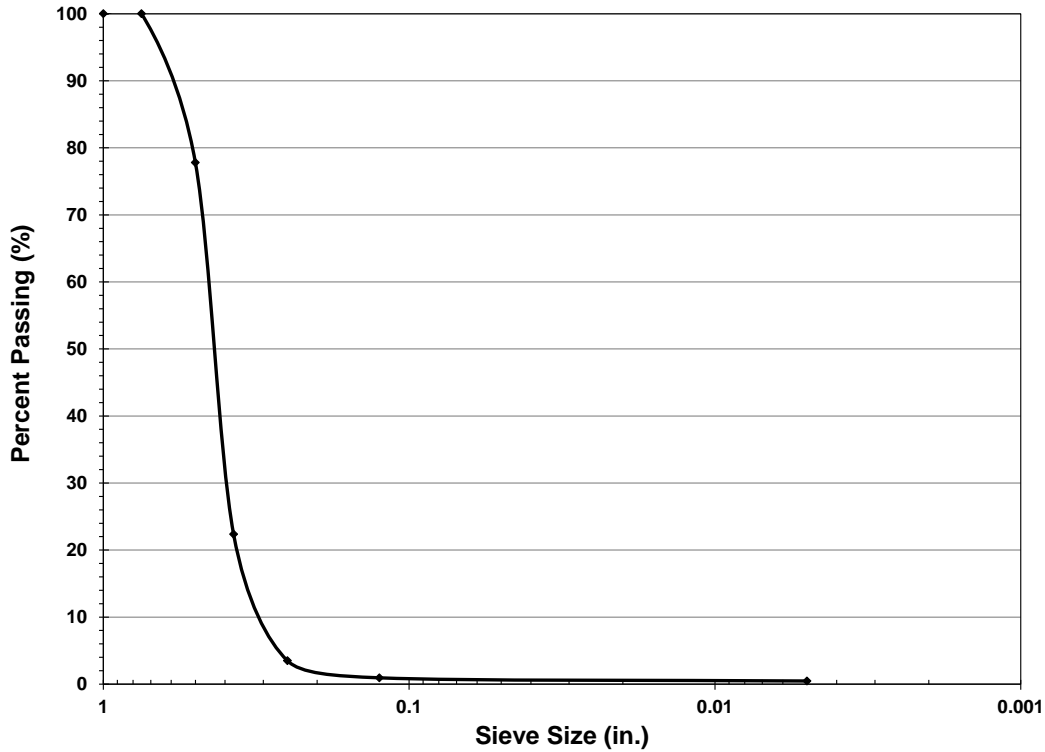


Figure 3.3: Gradation of expanded clay aggregate

### 3.2.5 Properties of Other Aggregates

The properties of the limestone control aggregate, as determined from previous research, are also presented in Table 3.1. Locally available river sand with a specific gravity of 2.6 and absorption capacity of 0.48 percent was used for each concrete mixture.

## 3.3 Other Materials

### 3.3.1 Cementitious Materials

Several different cementitious materials were used throughout the project. Type I portland cement manufactured by Larfarge North America was used for all early mixtures. Type

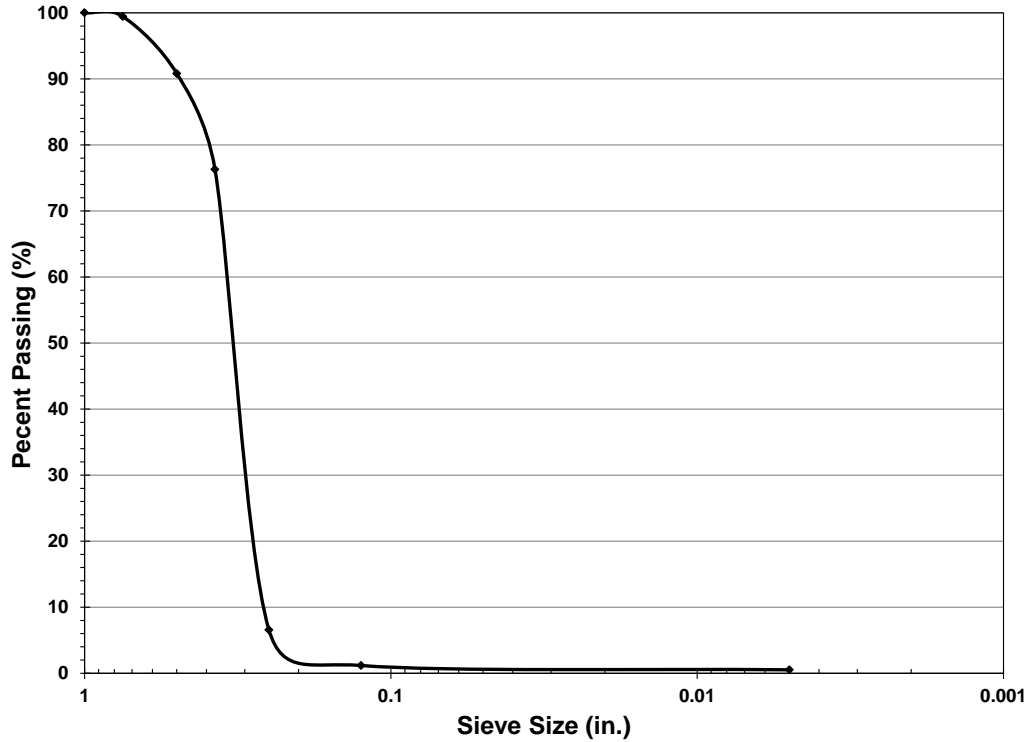


Figure 3.4: Gradation of expanded shale aggregate

III and Type I/II cement manufactured by Ash Grove were used for the higher strength concretes produced later in the project. Class C fly ash obtained from Headwaters Resources was used in conjunction with the Type III cement. Force 10,000 D condensed silica fume (CSF) supplied by W.R. Grace was used in test batching, but was not utilized for any beam specimens. The material cost for Type III cement was somewhat higher and for silica fume substantially higher than that of Type I cement, while fly ash was considerably cheaper.

### 3.3.2 Superplasticizer

The superplasticizer used throughout the project was the W. R. Grace product ADVA Cast 575. This is a polycarboxylate-based high range water reducer (HRWR) that meets ASTM C494 as a Type A and F, and ASTM C1017 Type I plasticizing. It is specifically designed for mixtures with a low  $w/c$  and is used in self-consolidating concrete for the precast/prestressed

industry. The recommended dosage for most applications is 3 oz/cwt to 6 oz/cwt (200 mL/100 kg to 390 mL/100 kg), where cwt represents 100 lb (45 kg) of cementitious material, with a maximum recommended dosage of 10 oz/cwt (650 mL/100 kg).

### **3.3.3 Prestressing Strand**

All prestressing strand was Grade 270 seven wire strand provided by Insteel Industries, Inc. with a guaranteed ultimate strength of 270 ksi (1862 MPa) and a modulus of elasticity of 28,500 ksi (196,500 MPa). Strand was kept inside the Engineering Research Center building in order to reduce the possibility of corrosion or surface damage. No preparation or cleaning was performed on the strand before use.

### **3.3.4 Mild Steel Reinforcement**

Mild steel reinforcing bars used for compression reinforcement were Grade 60 deformed bars. Some rust was present on many of the bars that were used. Shear reinforcement consisted of 0.25 in. (6.35 mm) diameter smooth bars. Shear stirrups were bent into the proper shape by hand using a lever and jig prepared specifically for that purpose.

### **3.4 Lightweight Aggregate Preparation**

The absorption capacity of lightweight aggregates is typically much higher than that of conventional aggregate and care must be exercised to ensure that the excess moisture is properly accounted for in mix proportioning and batching of lightweight concrete (Castrodale 2008). In order to maintain a consistent aggregate moisture content, a quantity of lightweight aggregate was presoaked for between 12 and 24 hours prior to each trial batch or beam batch. Several methods of presoaking and preparation for both small scale test batches and large beam batches were examined before the most effective methods were determined.

The first method utilized for soaking and draining the aggregate consisted of a 55 gallon (208 L) steel drum with a perforated PVC pipe drain at the bottom. This pipe was covered in geosynthetic material to reduce the loss of fines during draining of the aggregate and had a plastic cap on the end that allowed for filling of the drum and then draining as desired. The drum was filled with aggregate and water and allowed to soak overnight. When the desired soaking time had been achieved or preparation for a test batch had been completed, the drum would be drained and left undisturbed for at least fifteen minutes to allow excess water to drain off of the aggregate particles. It was very difficult to maintain an adequate seal around the perforated pipe drain in the aggregate drum to hold water for the desired presoaking period. This issue led to soaking the aggregate in 5 gallon (19 L) buckets and then draining the aggregate in the drain equipped barrel. This method was abbreviated to using a piece of geosynthetic material to drain the buckets and then pouring the aggregate onto a tarp to remove the excess water. Preparation of aggregate using the buckets and tarp is shown in Figure 3.5.

Finally, numerous small holes were drilled in a plastic bucket lid and this lid was used to drain the individual 5 gallon (19 L) buckets. This process is shown in Figure 3.5. While each of these methods produced aggregate with a consistent moisture content, presoaking in buckets and using the perforated lid to drain the buckets was determined to be the most effective method for preparing the aggregate for small-scale test batches. For the first round of large beam batches using expanded clay, a sprinkler was placed on the aggregate pile for the desired presoaking time. The sprinkler was removed and the aggregate allowed to drain for approximately 15 minutes before the portion required for the batches was obtained from the top of the pile. The aggregate was presoaked in 55 gallon (208 L) drums for the remainder of the beam batches using both expanded clay and expanded shale. Numerous holes were drilled on one side of the lids of



Figure 3.5: Aggregate preparation using tarp and perforated bucket lid

these barrels and they were drained using the front end loader of a tractor. This procedure is shown in Figure 3.6.

Despite the method of presoaking and draining, the same method was used for estimation of the aggregate moisture content for each batch. A method similar to that used for aggregate bulk density specified by ASTM C29 (ASTM 2009) was used to determine the unit weight of the presoaked aggregate. A  $0.25 \text{ ft}^3$  ( $.0071 \text{ m}^3$ ) measure was filled with presoaked aggregate in three layers. Each layer was rodded 25 times with a  $5/8 \text{ in.}$  (16 mm) hemispherical tipped steel tamping rod and the top surface was smoothed with the tamping rod. It was difficult to obtain a uniform surface due to the irregular shape of the aggregate, but results were consistent for a single operator. Performance of the unit weight test is shown in Figure 3.7. A moisture content sample was then taken from the contents of the unit weight measure. The resulting moisture contents were plotted against the corresponding unit weight values and a second order



Figure 3.6: Aggregate preparation using steel drum and tractor loader



Figure 3.7: Performance of aggregate unit weight

polynomial was used to fit the data. A plot was created for each lightweight aggregate and the values were continually updated with each batch. More and more data were included in the prediction as the project went on. As experience with the aggregates increased, it was possible to make a reasonable estimate of the moisture content from the measured unit weight using this method. The final moisture-density plot used for the expanded clay aggregate is shown in Figure 3.8 and that for the expanded shale aggregate in Figure 3.9.

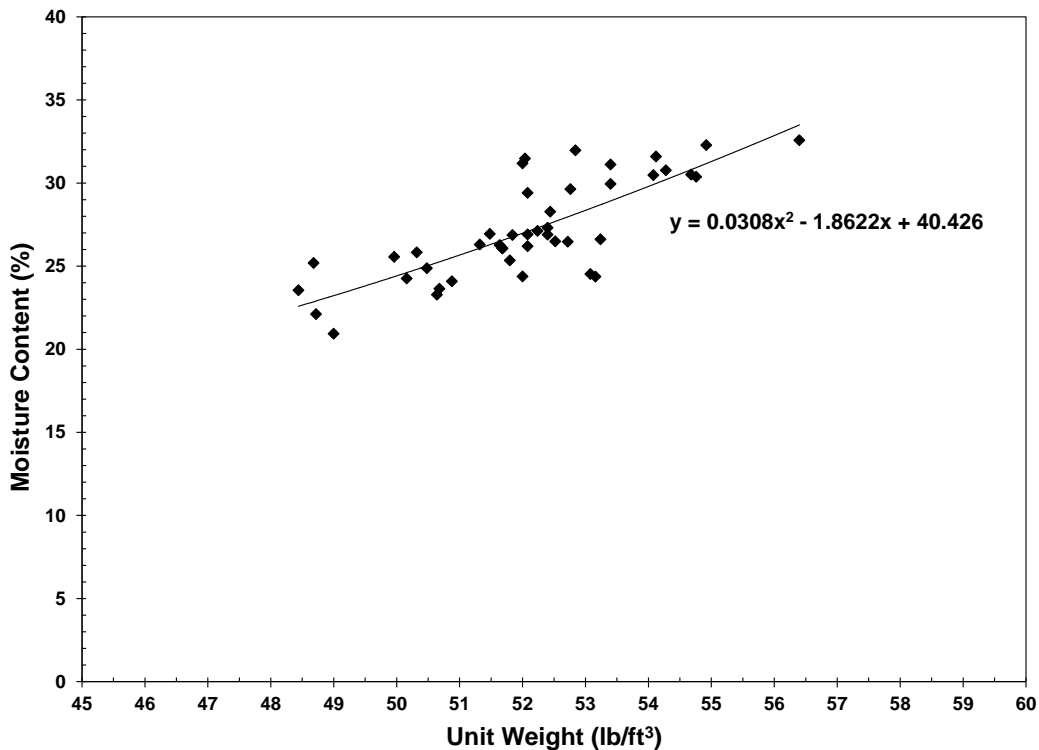


Figure 3.8: Final expanded clay moisture-density relationship

### 3.5 Concrete Property Tests

#### 3.5.1 Slump Flow

Slump flow tests were run in accordance to ASTM C1611 (ASTM 2009). The slump flow test consists of filling an inverted slump cone in one layer, removing the cone in a controlled manner, and measuring the diameter of the resulting spread. Two perpendicular

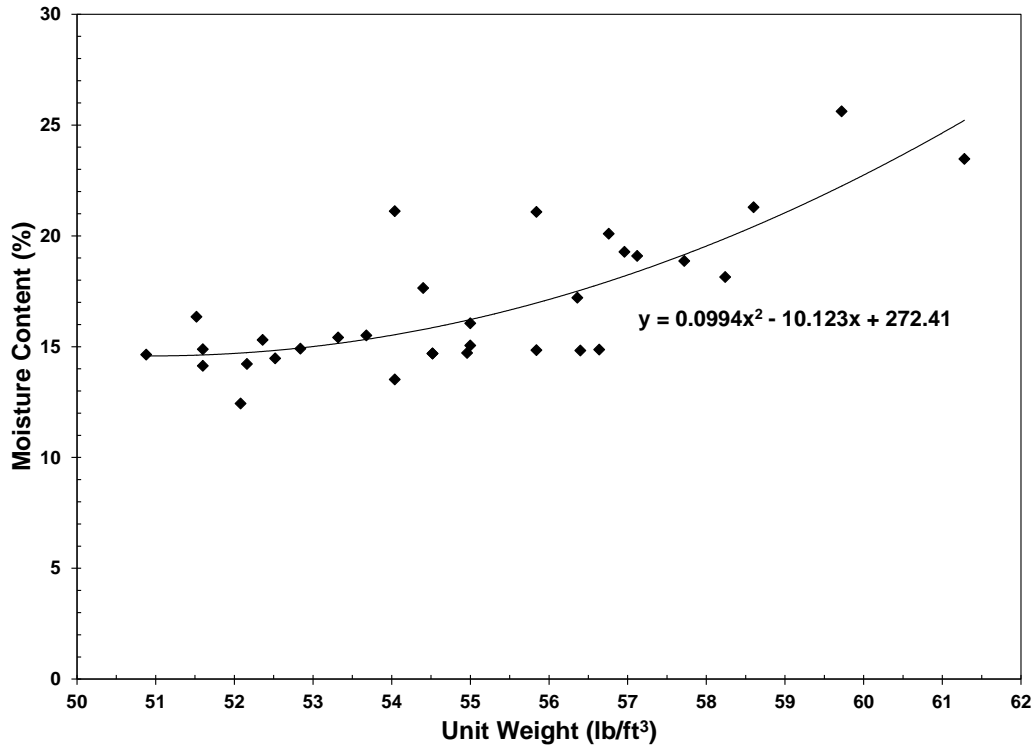


Figure 3.9: Final expanded shale moisture-density relationship

diameters are taken, one of which is measured at the widest portion of the slump flow patty.

These two diameters are then averaged to determine the value for the mixture, which is taken to the nearest half inch. An adequate slump flow result is shown in Figure 3.10. This test measures the consistency and flowability of the mixture and is somewhat analogous to slump for conventional concrete.

### 3.5.2 $T_{20}$

The time required for the slump flow to reach a diameter of 20 in. (50 mm), referred to as  $T_{20}$  or  $T_{50}$ , gives an indication of the viscosity of the concrete mixture. This value is typically measured by an observer. The time is measured from the initial lifting of the slump cone until the outer edge of the concrete mass reaches the 20 in. (50 mm) circle inscribed on the slump flow base plate. This test is also included in the specifications of ASTM C1611 (ASTM 2009).





Figure 3.10: Adequate slump flow

### 3.5.3 Visual Stability Index

An indication of the segregation resistance of the mixture is determined based on the appearance of the slump flow mass. A visual stability index (VSI), consisting of a number between 0 and 3 in increments of 0.5, is assigned to the mixture based on the requirements of ASTM C1611 (ASTM 2009). A VSI value of 0 describes a homogeneous concrete mass with no evidence of bleeding, a value of 1 describes slight bleeding shown by a sheen on the concrete surface, a value of 2 describes a concrete mass with a mortar halo and water sheen, and a value of 3 indicates a concentration of coarse aggregate at the center and a mortar halo. The segregation potential of the concrete is smallest with a VSI of 0 and increases with increasing values of VSI. A slump flow mass with a VSI of 0 is shown in Figure 3.10.

### 3.5.4 J-Ring

In addition to measuring the free flow potential of the concrete, some indication of the passing ability of the concrete is also necessary. The J-Ring test is outlined by ASTM C1621 (ASTM 2009) and consists of placing the inverted slump cone inside of a 12 in. (300 mm) diameter ring of 5/8 in. (16 mm) vertical bars used to simulate reinforcement. The diameter of the resulting flow is measured and compared to the slump flow. The difference in height ( $\Delta h$ ) of the concrete mass between the inside and outside of the ring was also measured in this research project by placing a tamping rod across the top of the J-Ring apparatus and measuring from the tamping rod down to the center of the concrete mass as well as directly outside the ring. Measurement of this height difference is not included in ASTM C1621, but was also used as an indicator of blockage in the same way as previous research at the University of Arkansas (Do 2007). Measurement of J-Ring flow is shown in Figure 3.11.

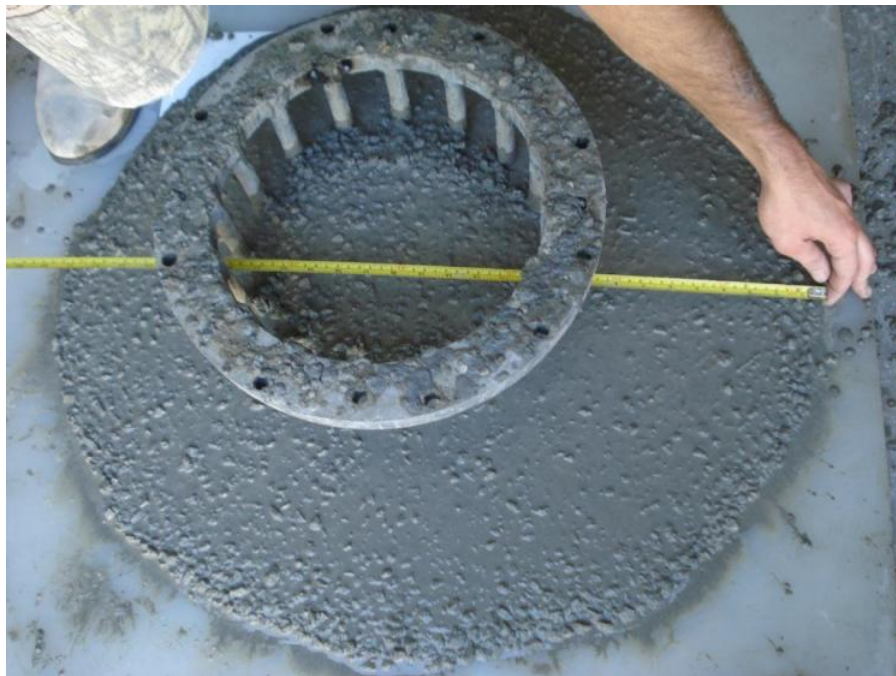


Figure 3.11: Measurement of J-Ring flow

### 3.5.5 Unit Weight

The fresh concrete unit weight was measured using a modified version of ASTM C138 (ASTM 2010). A 0.25 ft<sup>3</sup> (.0071 m<sup>3</sup>) measure was filled in three equal layers but without the use of a tamping rod. Only blows from a rubber mallet were used to consolidate the concrete. The top of the measure was finished using a strike-off plate as prescribed by ASTM C138.

### 3.5.6 Compressive Strength

Compressive strength was measured using 4 in. by 8 in. (100 mm by 200 mm) cylinders cast from each batch of concrete. Tests were run at a minimum of one ( $f'_{ci}$ ) and 28 days ( $f'_c$ ) of age depending on the batch. Additional tests were performed at seven days of age and at the time of development length testing for beam batches. Compressive strength tests were performed according to the requirements of ASTM C39 (ASTM 2011). Unbonded neoprene caps were used in accordance with ASTM C1231 (ASTM 2010) to meet the planeness requirements of ASTM C39. Saw cutting or end grinding was required for the majority of the LWSCC cylinders in addition to unbonded neoprene caps due to aggregate particles floating to the surface of the cylinders.

## 3.6 Mixture Design

### 3.6.1 Overview

Lightweight self-consolidating concrete (LWSCC) is not a commonly used material; therefore development of concrete mix designs was included in the research project. It was necessary to develop LWSCC mixtures using each of the aggregates and meeting the required specifications for compressive strength and fresh concrete properties. A series of trial batches with adjustments between batches was used to determine the optimum mix design for each combination of material property specifications. The variables adjusted during mixture

development included cement content, supplementary cementitious material type and content, total water content, water-cementitious materials ratio ( $w/cm$ ), coarse aggregate content, and ratio of fine aggregate (sand) volume to total aggregate volume ( $s/agg$ ). Superplasticizer dosage was adjusted between batches to account for differences in cementitious materials, ambient temperature, and moisture content error.

### 3.6.2 Mixture Specifications

The first set of mixtures that were developed had a targeted compressive strength of 4000 psi (28 MPa) at one day of age ( $f'_{ci}$ ) and 6000 psi (48 MPa) at 28 days ( $f'_c$ ). The second set of mixtures had a targeted  $f'_{ci}$  of 6000 psi (48 MPa) and  $f'_c$  of 8000 psi (55 MPa). A mixture meeting each of these strength requirements was developed using expanded clay, expanded shale, and conventional limestone aggregates for a total of six mixtures used to cast beam specimens. A slump flow between 25 in. and 30 in. (635 mm and 760 mm),  $T_{20}$  between 2 and 5 seconds, VSI of 1.0 or less, and a J-Ring  $\Delta h$  less than 1.5 in. (38 mm) were targeted for each of these concrete mixtures.

### 3.6.3 Trial Batching

Each trial batch had a volume of 1.5 ft<sup>3</sup> (0.043 m<sup>3</sup>) and was mixed in a 12.5 ft<sup>3</sup> (0.35 m<sup>3</sup>) rotating drum concrete mixer at the University of Arkansas Engineering Research Center. All materials were weighed out in 5 gallon (19 L) buckets using a floor scale with 100 lb (45 kg) capacity. The mixing procedure consisted of adding all of the coarse aggregate and all of the mixing water with the mixer at rest, then the sand and finally the cementitious materials with the mixer turning. An initial dosage of superplasticizer, based on the manufacturer's recommendations, was added to the mixing water before the water was added to the mixer. Additional increments of superplasticizer were then added during mixing until the concrete

reached the desired consistency. Mixing times varied slightly since the additional dosage of superplasticizer varied based on the mix design and ambient temperature. However, the average mixing time was approximately 15 minutes.

Fresh concrete property tests were performed for each trial batch. These tests included slump flow,  $T_{20}$  ( $T_{50}$ ), visual stability index (VSI), J-Ring flow, J-Ring  $\Delta h$ , and unit weight. The combination of the slump flow and J-Ring flow give a full indication of filling ability, passing ability, and filling capacity without the need for more complicated testing (Khayat 2009). Therefore, these relatively simple tests were used to give a full indication of the self-consolidating properties of the concrete. Six, 4 in. by 8 in. (100 mm by 200 mm) cylinders were cast for each trial batch so that three cylinders could be used for compressive strength testing at both one ( $f'_{ci}$ ) and 28 days ( $f'_c$ ) of age.

### 3.7 Strand Qualification

The Standard Test for Strand Bond (STSB) was used to examine the bonding quality of the prestressing strand (Ramirez 2008). These tests were similar to tests performed in past research at the University of Arkansas (Sobin 2005). A detailed testing procedure is presented in Appendix A. Pullout loads were compared to the minimum values required by the test for 0.6 in. (15.2 mm) prestressing strands. Steel confinement casings were constructed by welding a 6 in. by 6 in. (152 mm by 152 mm) piece of  $\frac{1}{4}$  in. (6.35 mm) steel plate to the bottom of an 18 in. (457 mm) piece of steel pipe with 5 in. (127 mm) outside diameter and  $\frac{1}{4}$  in. (6.35 mm) wall thickness. Strand specimens 32 in. (810 mm) in length were cast inside these casings using a sand/cement mortar with approximately 2 in. (51 mm) of strand exposed at the dead end. The mortar was introduced in two lifts with vibration applied after approximately half the mortar was placed and after 90 percent of the mortar was placed. A 1 in. (25 mm) diameter by 2 in. (51 mm)

long bond breaker made from pipe insulation was used to eliminate stress concentrations at the live end of the specimen. Care was taken to ensure that the strand was centered within the casing using a wooden strand centering device and the specimens were allowed to cure in an environmentally controlled environment. The targeted compressive strength of the mortar was between 4500 psi and 5000 psi (31 MPa and 34.5 MPa) during testing performed at 24 hours  $\pm$  2 hours of age. Six specimens were cast with the strand used for building the beams. Two batches of mortar were used to cast the specimens so that the time lapse between the first and last test would not affect the mortar strength.

Tests were performed using a 100 kip (445 kN) MTS testing machine and the apparatus shown in Figure 3.12. Tensile load was applied to the strand by displacement at a rate of 0.100 in./min  $\pm$  0.005 in./min (2.5 mm/min  $\pm$  0.13 mm/min) and displacement was monitored using a



Figure 3.12: Setup for Standard Test for Strand Bond

DCT1000A linear variable displacement transducer (LVDT) and bridge apparatus across the dead end of the strand. Load and deflection were continuously recorded using the MTS data acquisition system and the load corresponding to a strand slip 0.10 in. (0.25 mm and 2.54 mm) for each specimen was compared to the minimum of 10,800 lb (48 kN) required by the test. The average of these values for the six specimens was then compared to the test requirement of 12,600 lb (56 kN) for a six specimen set (Ramirez 2008).

### **3.8 Beam Specimen Testing**

#### **3.8.1 Overview**

Beam specimens were fabricated using each of the combinations of aggregate and compressive strength. These specimens measured 6.5 in. by 12 in. by 18 ft long (165 mm by 305 mm by 5.5 m). These dimensions were based on those used for previous research (Logan 1997, Rose and Russell 1997, Peterman et al 2000, Larson et al. 2007, Ramirez and Russell 2008, Staton et al. 2009, Ward et al. 2009, and Floyd et al. 2011) in order to produce comparable data. Two 0.6 in. (15.2 mm) prestressing strands tensioned to 75 percent of the guaranteed tensile strength were located a distance of 10 in. (250 mm) from the top of each beam. Due to the large available tension force carried by the prestressing strands and due to high tensile stresses at release, two No. 6 (No. 19) deformed reinforcing bars were placed at a distance of 2.5 in. (65 mm) from the top. The nominal flexural strength was calculated for each specimen using the procedures of strain compatibility described in the PCI Design Handbook (PCI 2010) and presented in Appendix B. Prestress losses were calculated using the AASHTO refined method described in the AASHTO LRFD Specifications (AASHTO 2007) and shown in Appendix B. The calculated moduli of elasticity determined from the relationship presented in the ACI Code (ACI 2011) were used in these calculations. Shear reinforcement was designed to ensure a

tension failure during flexural testing of the beam specimens using the procedures of the ACI Code for prestressed elements (ACI 2011) as shown in Appendix B. The reinforcement consisted of ¼ in. (6.4 mm) smooth bar closed stirrups. These stirrups were spaced at 3 in. (75 mm) on center for the first 4 ft (1.2 m) from each end of each beam and 5 in. (125 mm) for the remainder of the beam for the first two sets of beams. The 3 in. (75 mm) spacing was extended to 5 ft (1.5 m) from each end of each beam for the remainder of the beams. A diagram of the beam cross-section and elevation view is shown in Figure 3.13. Each specimen was instrumented with detachable mechanical (DEMEC) gage points on each side of the specimen for measurement of concrete surface strain, and in turn, transfer length. Each end of each beam was also tested in flexure in order to determine development length. A smaller 8 ft (2.4 m) long beam specimen was cast using the first expanded clay mixture to test the production methods and concrete consolidation. This specimen was constructed with wooden dowels instead of prestressing strand and rebar in order to reduce the cost.

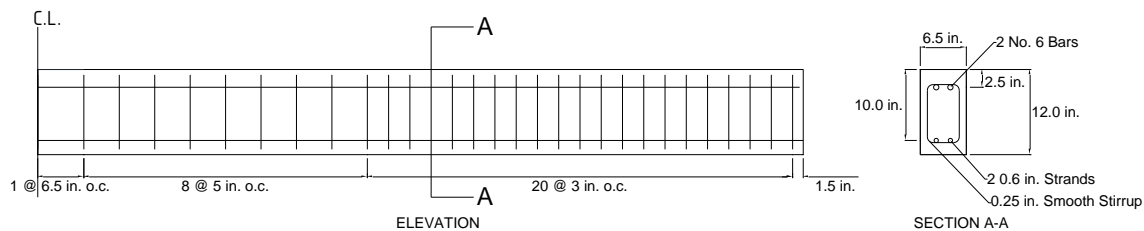


Figure 3.13: Beam specimen details

### 3.8.2 Beam Construction

#### 3.8.2.1 Overview

All beam construction was conducted at the University of Arkansas Engineering Research Center in Fayetteville, Arkansas, using a 50 ft (15.2 m) prestressing bed. Four specimens were cast using each LWSCC mixture and each NWSCC control mixture. Two



beams were cast at one time placed end to end with approximately 10 ft (3 m) clear between the ends of the two sets of forms. Formwork was placed on a wooden platform between the prestressing abutments that was adjusted to place the formwork at the proper elevation to ensure the proper strand location of 10 in. (250 mm) from the top of the each beam. Strands were tensioned using two 100 ton (890 kN) jacks the morning beams were cast. Concrete was placed approximately two hours after completion of pretensioning. Forms were removed at approximately 18 hours of concrete age and the beams were instrumented with DEMEC points before strand tension was released at an age of approximately 24 hours. Beams were then moved to storage in the yard of the Engineering Research Center.

### 3.8.2.2 Formwork

Plywood formwork was constructed with provisions for continuous strand reinforcement along with sides that folded down to facilitate the placement of the DEMEC points before prestress release. Since any alteration of the steel surface could interfere with the bond of the prestressing strands, no release agents were used. Three methods were used instead. The first method consisted of lining the inside of the forms with a water resistant paneling. This material was significantly damaged after the first set of beams was cast and was removed after the first three sets of beams were completed. After the lining was removed, the plywood formwork was used with no surface treatment. This made the forms difficult to remove and the plywood absorbed water from the concrete mixture which resulted in a poor surface finish. Finally, thin plastic sheeting was used to line the inside of the formwork in order to facilitate easy removal of the forms and also to hold in moisture as the concrete cured in the forms. This worked very well and the concrete surface was drastically improved. The forms were lined with new plastic after each set of beams was cast.

### 3.8.2.3 Reinforcement

The compression and shear reinforcement was tied together to form rebar cages in advance of casting days. These cages were then placed in the formwork and the prestressing strands were run through the prestressing abutments, the formwork, and the rebar cages. The prestressing strand was kept on a roll inside a room with access to the outside of the Engineering Research Center as near as possible to the prestressing bed. This location allowed for easy access to the strand while keeping the possibility of strand corrosion to a minimum. Plastic sheeting was placed on the ground between the building and the prestressing bed to ensure that strand contamination was minimal during transportation to the prestressing bed. After the strands were tensioned, the forms were adjusted to ensure that the prestressing strands were located at the correct distance from the top of the beams. The compression reinforcement was also adjusted to the proper location and was suspended in place from the top of the forms using heavy-duty tie wire. A final check was done for every beam to ensure that the shear stirrups were as close to the proper spacing as possible and oriented properly.

### 3.8.2.4 Strand Tensioning

The strand tensioning apparatus consisted of two 100 ton (890 kN) hydraulic rams arranged to push a 3.5 in. by 3.5 in. (90 mm by 90 mm) steel bar against the strand chucks on the live end of the prestressing bed. This apparatus is shown in Figure 3.14. The ends of the hydraulic rams were positioned 1.125 in. (28.6 mm) from the face of each cylinder so that an extension of the rams of 4.875 in. (124.8 mm) would produce the desired initial prestress of 202.5 ksi (1396 MPa) corresponding to  $0.75f_{pu}$  in each strand and allow for placement of 6 in. (152 mm) steel blocks to hold the tension. The ram movement included provisions for chuck seating, strand sag, and an actual required strand elongation of 4.5 in. (115 mm). Once the



Figure 3.14: Strand tensioning apparatus with stopper blocks in place

strands were threaded through both prestressing abutments, chucks were placed against the dead end of the prestressing bed, the strands were pulled as tight as possible by hand, and chucks were placed on the live end of the strand. Pressure was applied to the hydraulic rams using a hand pump. Progress was monitored using a steel rule to measure movement of the hydraulic rams along with monitoring the pressure in the hydraulic system to ensure that it did not exceed that required to reach the 43.7 kips (194.4 kN) needed to achieve the proper prestress for each strand. Once the proper elongation was achieved, steel blocks having a width of exactly 6 in. (152 mm) were placed between the hydraulic rams and the bar reacting against the strand chucks. The placement of these blocks is shown in Figure 3.14. The pressure was released from the hydraulic system and these blocks held the entire prestress until the concrete reached the desired age.

#### 3.8.2.5 Concrete Placement

All materials were prepared the day prior to beam casting. For the first set of beams the expanded clay aggregate was placed under a sprinkler for approximately 12-18 hours prior to

removing the sprinkler and weighing the material. For all remaining lightweight beams, the aggregate was placed in 55 gallon (208 L) steel drums with perforated lids which were in turn filled with water. The aggregate was allowed to soak for approximately 24 hours before draining. Sand and cement were weighed in increments placed in 5 gallon (19 L) plastic buckets the day before beams were cast. Moisture content samples taken from the sand and the lightweight aggregate moisture density relationship described in Section 3.4 were used to adjust the final mixing water quantities. A portion of the required superplasticizer was added to the mixing water before placement in the mixer, with the remainder withheld until the concrete was partially mixed to ensure that the concrete was not overdosed.

For the first fifteen LWSCC beams and first four NWSCC beams, the concrete was divided into two  $7.0 \text{ ft}^3$  to  $7.5 \text{ ft}^3$  ( $0.20 \text{ m}^3$  to  $0.21 \text{ m}^3$ ) batches for each beam due to the limited capacity of the laboratory mixer. Mixing a larger quantity of concrete in the  $12.5 \text{ ft}^3$  ( $0.35 \text{ m}^3$ ) would not allow for proper mixing, and even a full mixer would not produce a single batch large enough to cast an entire beam. Concrete was mixed following the same procedure used for the trial batches. All of the coarse aggregate was placed in the mixer along with all of the mixing water. The sand and lastly the cement were then added with the mixer turning. After mixing for approximately 10 minutes, an examination of the concrete was made and additional superplasticizer was added if the concrete did not have the desired consistency. The typical mixing time was approximately 15 minutes, at which time the concrete was transported to the forms using wheelbarrows or the loader bucket of a tractor. The concrete was placed in the beams in a manner to fill the entire beam to a level above both of the prestressing strands to ensure that the concrete in the immediate influence area of the strands would have the same properties. The second batch was begun immediately after the first batch was placed leading to

typical time delay of approximately 30 to 45 minutes between lifts for each beam. After the second layer was placed, the concrete was screeded and floated with a magnesium float, lifting hooks were put into place, and the beams were covered with plastic sheeting.

A sample was taken from the middle of each batch for fresh concrete tests and for molding strength test specimens. Slump flow,  $T_{20}$ , VSI, J-Ring flow, J-Ring  $\Delta h$ , and unit weight were measured and recorded for each batch. A volumetric air content was run in accordance with ASTM C173 (ASTM 2010) on the very last batch of each day for LWSCC mixtures and a pressure method air content was run in accordance with ASTM C231 (ASTM 2010) on the last batch of each day for the normal weight mixtures. Nine 4 in. by 8 in. (100 mm by 200 mm) cylinders were cast for each batch. These cylinders were used for compressive strength testing at 1, 7, and 28 days for the first batch for each beam and at 1 and 28 days for the second batch for each beam. The final three cylinders were tested at the time of flexural testing for each beam.

The last two high strength expanded shale beams and all of the high strength limestone beams were cast using a 1.5 yd<sup>3</sup> (1.2 m<sup>3</sup>) rotating drum mixture that allowed for two beams to be cast from a single batch of concrete. The same quality control methods were used to adjust the mixing water for the moisture content of the aggregates. The materials were weighed out in four batches and each batch was adjusted as previously discussed in order to maintain consistent results. All materials were then added to the mixer in one batch using a procedure very similar to that used with the smaller mixer. The only difference was that approximately 25 percent of the mixing water was held until the end in order to wash down material stuck to the sides of the mixer. The concrete was then transported inside the mixer to the beam forms. Concrete placement directly from the mixer is shown in Figure 3.15. A sample was taken from the middle of the portion used to cast each beam for fresh concrete property testing and for molding strength



Figure 3.15: Concrete placement directly from the mixer

testing specimens. Twelve 4 in. by 8 in. (100 mm by 200 mm) specimens were cast for each beam for testing at 1, 7, and 28 days and at the time of flexural testing.

#### 3.8.2.6 Instrumentation

The forms were removed at approximately 18 to 20 hours of concrete age to facilitate the placement of the DEMEC points used for transfer length measurements. These gage points were placed at the level of the prestressing steel beginning 1 in. (25 mm) from each end of the beam and then at 4 in. (100 mm) increments for the first 60 in. (1525 mm) from each end. This allowed for overlapping 8 in. (200 mm) gage lengths in the area of prestress transfer. Points were also placed at the centerline of the beam and two 4 in. (100 mm) increments on each side of the beam centerline. DEMEC point placement is shown in Figure 3.16. The points were held in place using a two-part, fast setting epoxy. It was difficult to maintain a consistent mix of epoxy so every point was rechecked after all were placed and any problems were corrected.



Figure 3.16: Placement of DEMEC points using epoxy

Steel block clamps were placed on each strand at a distance from the beam end that allowed for the stroke of a depth micrometer used to determine the change in proximity of the block from the beam before and after release of the prestress. The placement of these clamps is shown in Figure 3.17. After difficulties experienced with the concrete surface at the beam ends for the first set of beams, rectangular pieces of Plexiglas were placed on the beam ends directly above the protruding prestressing strands using epoxy. These plates provided a consistent surface for measurements using the depth micrometer.

#### 3.8.2.7 Beam Storage

Beams were removed from the prestressing bed immediately after post-release measurements were completed and were stored outside on wood supports. The first two sets of beams were supported at approximately the third points, but supports were placed at the ends of later beams in order to reproduce the condition immediately after prestress release. Compressive



Figure 3.17: Placement of block clamps used to measure end slip

strength specimens were stored alongside the beams so that they would be exposed to similar curing conditions.

### 3.8.3 Transfer Length Measurements

Measurements were taken for each 8 in. (200 mm) gage length using a DEMEC gage immediately before and after prestress release and at 3, 5, 7, 14, and 28 days. The DEMEC gage is shown in Figure 3.18. The difference in these measurements from the initial values allowed for the calculation of the strain at the concrete surface over each gage length. These values were then used along with the 95% Average Maximum Strain method (Russell 1996) to determine the transfer length for each specimen. This method consists of smoothing the data for each side of the specimen using a three point moving average. The strain values over three consecutive gage lengths are averaged, and this average is assumed to act at the center point of those three gage lengths. The results from the two sides of the beam are then averaged to produce a strain profile for each end of the beam. The strain values are plotted versus length along the beam, the values





Figure 3.18: DEMEC Measurements

making up the strain plateau are averaged, and 95 percent of this average is calculated. The point where the strain curve first reaches this 95 percent value is taken as the transfer length. The strain profiles were plotted using the metric spacing for the individual points since the spacer bar used to space the points placed them at an exactly 400 mm spacing. The transfer length values were then converted to inches in order to easily compare to the predicted values.

End slip measurements were taken at the same intervals as the DEMEC measurements. These were taken using a depth micrometer placed through a hole in the steel block clamp attached to each strand. Performance of these measurements is shown in Figure 3.19. The difference between the initial measurement and the subsequent measurements was taken as the slip for each strand after accounting for the elastic shortening of the free portion of the strand between the beam end and the block clamp. Transfer length was determined for each strand using these strand slip measurements along with the theoretical relationship



Figure 3.19: Measurement of strand end slip

$$L_t = \alpha L_{es} \left( \frac{E_{ps}}{f_{si}} \right)$$

(FIP 1982, Balazs 1993, Russell 1996, Rose 1997, Marti-Vargas 2006) where  $L_{es}$  is the end slip (in.),  $E_{ps}$  is the modulus of elasticity of the prestressing steel (ksi),  $f_{si}$  is the stress in the strand immediately after prestress release (ksi), and  $\alpha$  is a factor dependent on the bond stress distribution. This relationship was developed by assuming a bond stress distribution and integrating the difference between steel and concrete strains along the transfer length. A constant bond stress distribution with a resulting linear variation of strain in the prestressing strand has been accepted by many researchers and yields a value of 2.0 for  $\alpha$  (FIP 1982, Balazs 1993, Marti-Vargas 2006, Russell 1996, Rose 1997). A linear variation of bond stress with a quadratic prestressing steel strain distribution resulting in an  $\alpha$  value of 3.0 has also been accepted in many cases along with several  $\alpha$  values between these two extremes (FIP 1982, Balazs 1993, Marti-Vargas 2006, Rose 1997). The values of transfer length determined for each

of the two strands were averaged to determine transfer length for each end of a particular specimen. The transfer lengths resulting from various values of  $\alpha$  were compared to those determined using the traditional surface strain measurements in order to determine the best correlation between the two methods.

### **3.8.4 Development Length Measurements**

All beams were tested in flexure after reaching 28 days of age in order to examine the development length. Testing procedures were very similar to those used in previous research at the University of Arkansas (Floyd 2011). Various embedment lengths were examined for each set of specimens beginning with approximately half of the development length calculated using the ACI/AASHTO equation (ACI 2011, AASHTO 2007).

#### **3.8.4.1 Specimen Setup**

The arrangement for each flexural test consisted of a 9 ft (2.74 m) simple span with a single point load which allowed for the examination of multiple embedment lengths. The beam was supported 3 in. to 9 in. (75 mm to 230 mm) from the end being tested and near the beam centerline. This left a 99 in. to 105 in. (2.51 m to 2.67 m) overhang subjected to only its weight, which allowed for flexural testing of both ends of each beam. The supports consisted of two hollow steel rollers, one of which was held stationary by rods welded to the base plate, and the other had some freedom to move horizontally. The support details and span configuration are shown in Figures 3.20 and 3.21. The load was applied through a steel roller held stationary between two rods welded to a 1 in. (25 mm) thick steel plate using a 100 ton (890 kN) hydraulic actuator and a hand pump. The first few tests were performed using a hollow steel roller similar to those used for the supports. The high loads resulting from a short embedment length caused

some distortion of this roller and it was replaced with a solid steel cylinder. The load application configuration is shown in Figure 3.22.

#### 3.8.4.2 Instrumentation

Load was monitored throughout each flexural test using a Sensotec TJE/743-11 pressure transducer connected to the hydraulic system. The measured pressure was multiplied by the area of the hydraulic piston to determine the applied load. Strand slip was monitored using Trans-TEK 350-0000 linear variable differential transformers (LVDTs) placed on each strand end protruding from the beam, as shown in Figure 3.23. The LVDTs were placed such that they touched the end of the beam and would move in the direction of the beam as the strands slipped. Deflection was monitored with a Red Lion LES1500S linear cable encoder attached to the hydraulic actuator and the top plate of the load application roller. Deflection measurements were also taken after each load increment using a steel rule and measuring from the load application



Figure 3.20: Beam supports with roller constrained (left) and unconstrained (right)

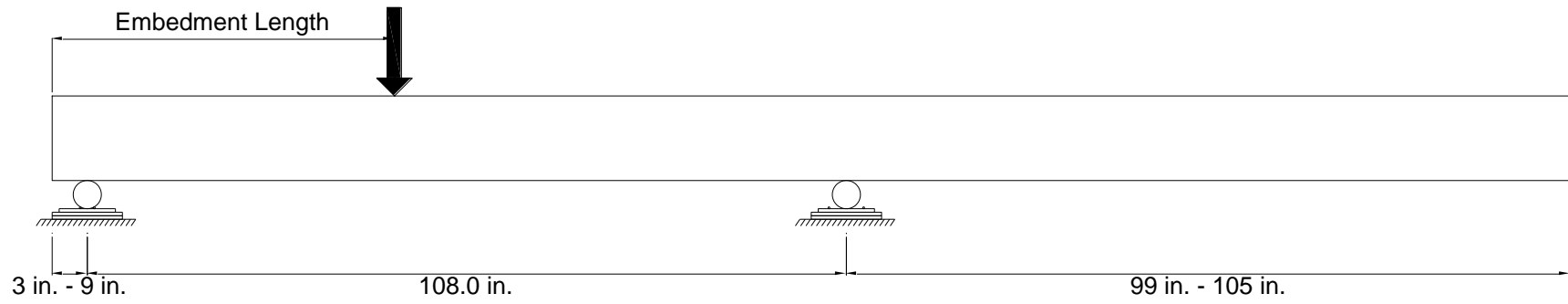


Figure 3.21: Flexural test specimen setup



Figure 3.22: Application of point load for flexural testing



Figure 3.23: Placement of LVDTs to measure strand slip during flexural testing

plate to the strong floor. All instruments were monitored continuously throughout each test with measurements recorded every second using a data acquisition system.

### 3.8.4.3 Flexural Tests

Each flexural test was based on a particular embedment length measured from the end of the beam being tested. Load was applied at this location in approximately 5000 lb (22 kN) increments until cracking was observed and 2500 lb (11 kN) increments from observed cracking until failure. The beam was examined for cracking and manual deflection measurements were made after each load increment. The continuous deflection measurements recorded with the data acquisition system were used to create a load/deflection plot that was later examined to confirm the actual cracking moment and failure type. The cracking load was determined by pinpointing the location on the curve where the slope changed due to the difference in moment of inertia from an uncracked to cracked section.

The beam was loaded until it could no longer sustain additional load or until strand fracture, concrete crushing, shear failure, or excessive strand slip occurred. The failure type was examined to determine the relationship of the tested embedment length to the development length. If strand slip in excess of 0.10 in. (0.25 mm) was measured before flexural failure occurred, the embedment length was increased for the subsequent test. If the beam failed in flexure before this level of strand slip occurred, the embedment length was reduced for the subsequent test. This iterative process was used to bracket the development length for that particular beam set.

## 3.9 Modulus of Elasticity Testing

An additional batch of each concrete mixture used to construct beams was mixed to fabricate specimens used for modulus of elasticity testing. Nine 4 in. by 8 in. (100 mm by 200 mm) cylinders and three 4 in. by 4 in. by 16 in. (100 mm by 100 mm by 405 mm) rectangular prismatic specimens were cast for each modulus of elasticity batch. Three cylindrical specimens

were tested at 1, 7, and 28 days using the static method of ASTM C469 (ASTM 2010) and the three rectangular specimens were tested using the dynamic methods of ASTM C215 (ASTM 2008). A comparison was made between the two methods to determine the feasibility of using a dynamic test to determine modulus of elasticity and in turn estimate transfer length.

### **3.9.1 Static Testing**

The static tests were performed using either a 100 kip (445 kN) MTS testing machine for the lower strength clay and limestone mixtures or a 400 kip (1789 kN) capacity Forney compression testing machine for the remaining mixtures along with a compressometer. The area at mid-height of each specimen was calculated using the average of two perpendicular diameters measured with steel calipers. The ends of the specimens were ground to the planeness requirements of ASTM C469 (ASTM 2010). Each specimen was loaded to 40 percent of its compressive strength using the loading rate required by the specifications. Each loading was repeated three times and the results of the final two loadings were used to calculate modulus of elasticity. Disregarding the results of the first loading eliminated the influence of instrument seating and non-recoverable deformation during the first loading.

The compressometer used along with the MTS machine was equipped with an LVDT for measurement of the change in length of the specimen. This test setup is shown in Figure 3.24. Measurements of load and displacement were continuously recorded using the MTS data acquisition system. These values were converted to stress and strain using the area of the specimen at mid-height and the geometry of the compressometer. The ASTM required stress/strain points corresponding to a strain of 50 millionths and 40 percent of the concrete compressive strength were then picked from the resulting data. The compressometer used along with the Forney testing machine was equipped with a dial gage that measured the change in



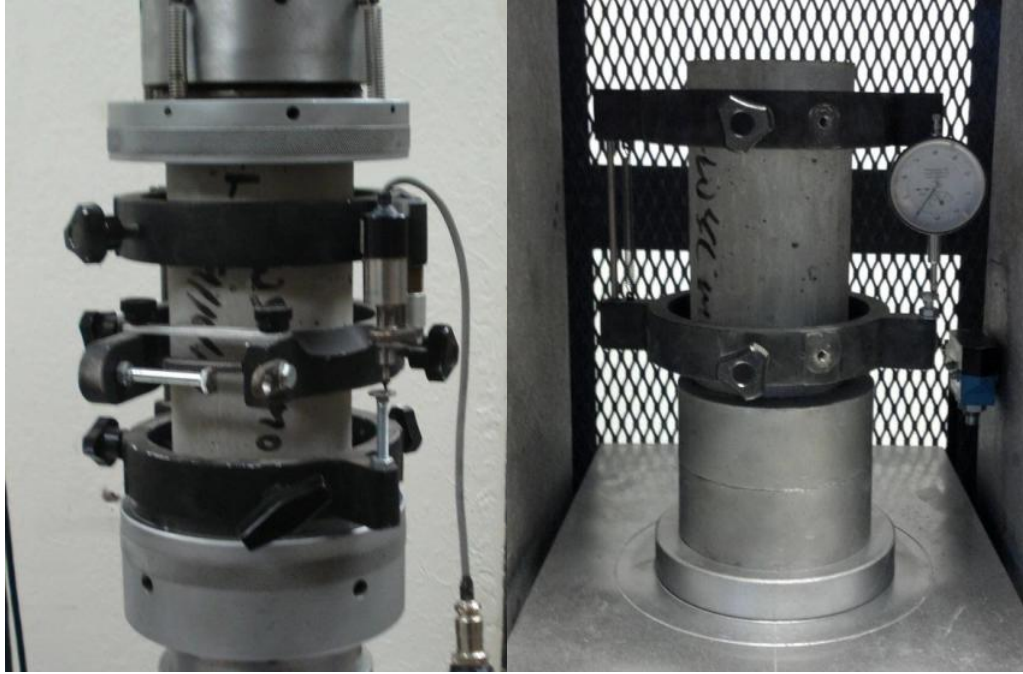


Figure 3.24: Static modulus of elasticity setup using MTS (left) and Forney (right)

length of the specimen. This setup is shown in Figure 3.24. The change in length required for a strain of 50 millionths was calculated along with 40 percent of the compressive strength. The load and deflection corresponding to these values were then read from the machine and dial gage respectively, while the test was running. The measured points were then converted to stress and strain using the area of the specimen and the geometry of the compressometer. The chord modulus of elasticity was calculated for each set of stress/strain measurements and the average of the three specimens was then taken as the modulus of elasticity.

### 3.9.2 Dynamic Testing

The fundamental longitudinal and transverse frequencies of the prismatic concrete specimens were used to calculate modulus of elasticity based on the methods presented in ASTM C215 (ASTM 2008). The cross-sectional dimensions of each specimen were measured using steel calipers and the length with a steel tape prior to each test. The specimens were examined using a James Instruments, Inc., Non-Destructive Testing System. For longitudinal testing, the

dynamic source was placed at the center of one end face of the specimen and an accelerometer was placed at the center of the other end face, as shown in Figure 3.25. The specimen was supported on a single point at the midpoint of the specimen. For transverse testing, the specimen was supported at  $0.224L$ , 3.58 in. (91 mm), from each end. The dynamic source was placed at the top of the specimen at the specimen midpoint and the accelerometer was placed at the top of the specimen at one extreme edge as shown in Figure 3.26.

Input frequencies for each test were cycled between 0 and 10,000 hertz and the response was monitored with the E-Meter. The lowest frequency with a significant response was recorded as the fundamental frequency. These frequencies were then used along with the equations provided by ASTM C215 to calculate the modulus of elasticity. The equation used along with the transverse frequency is

$$E = CMn^2$$

where  $M$  is the mass of the specimen (kg), and  $n$  is the fundamental transverse frequency (Hz).

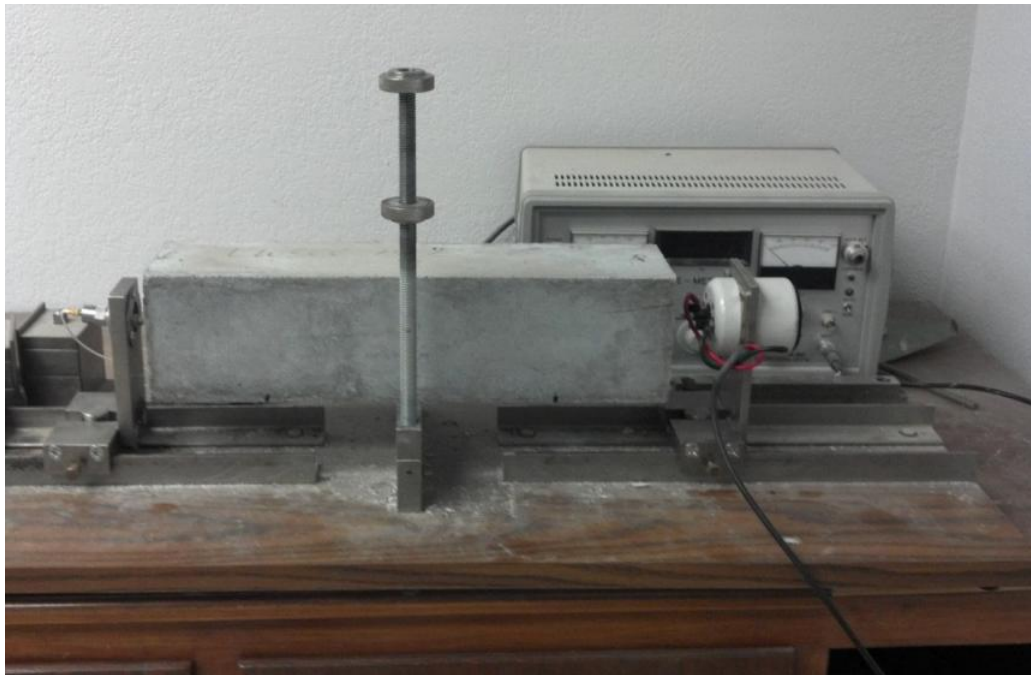


Figure 3.25: Longitudinal fundamental frequency measurement setup

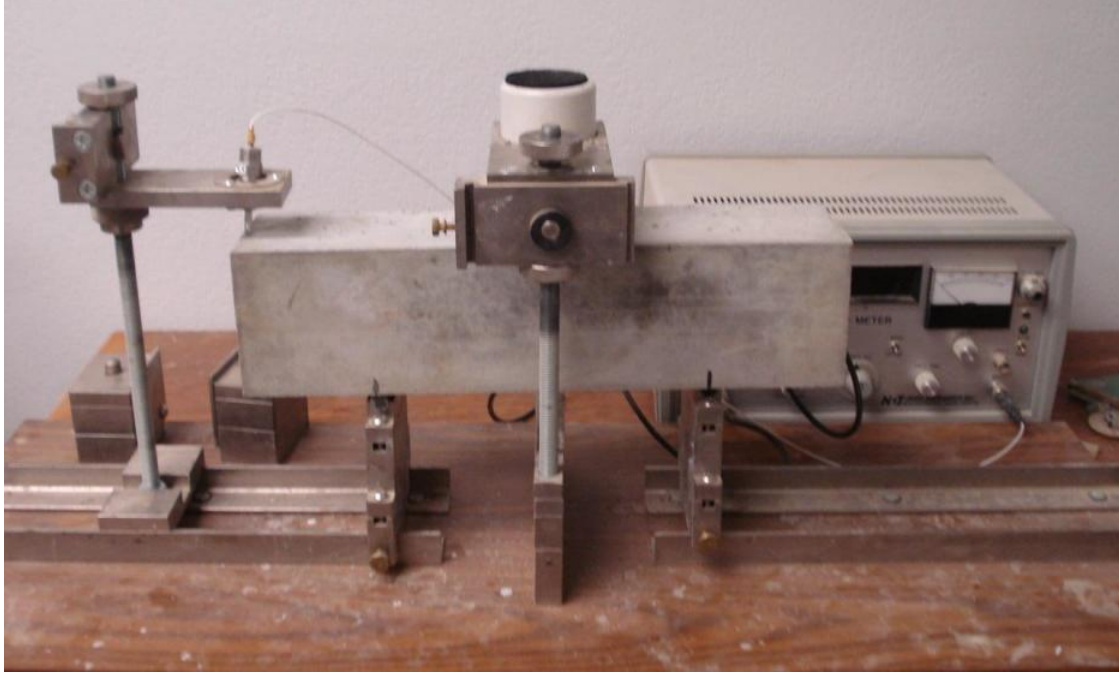


Figure 3.26: Transverse fundamental frequency measurement setup

The value of  $C$  is given by

$$C = 1.6067 \left( \frac{L^3 T}{d^4} \right)$$

for cylindrical specimens ( $\text{N}\cdot\text{s}^2\cdot\text{kg}\cdot\text{m}^2$ ) or

$$C = 0.9464 \left( \frac{L^3 T}{bt^3} \right)$$

for prismatic sections ( $\text{N}\cdot\text{s}^2\cdot\text{kg}\cdot\text{m}^2$ ), where  $L$  is the length of the specimen (m),  $d$  is the diameter of the cylinder (m),  $t$  is the cross-sectional dimension of the prism in the direction excitation is applied (m),  $b$  is the dimension of the prism in the direction transverse to the direction excitation is applied, and  $T$  is a correction factor dependent on the radius of gyration of the specimen and Poisson's ratio. A Poisson's ratio of 0.17 was used for choosing the correction factor  $T$ . The equation used along with the longitudinal frequency is

$$E = DM(n')^2$$

where  $n'$  is the fundamental longitudinal frequency (Hz),  $D$  is taken as

$$D = 5.093 \frac{L}{d^2}$$

for cylindrical specimens ( $\text{N}\cdot\text{s}^2\cdot\text{kg}\cdot\text{m}^2$ ) or

$$D = 4 \frac{L}{bt}$$

for prismatic specimens ( $\text{N}\cdot\text{s}^2\cdot\text{kg}\cdot\text{m}^2$ ) and the other symbols are as defined previously. The average of the three specimens was taken as the dynamic modulus of elasticity for that particular mixture.

## Chapter 4: Concrete Mixtures

### 4.1 Introduction

Lightweight self-consolidating concrete (LWSCC) is not a routinely used material. It was therefore necessary to develop LWSCC mixtures using each of the desired aggregates and meeting the required specifications for compressive strength and fresh concrete properties. The first phase of mixtures had a targeted compressive strength of 4000 psi (28 MPa) at one day of age ( $f'_{ci}$ ) and 6000 psi (48 MPa) at 28 days ( $f'_c$ ). These are designated with the prefix NS for “normal strength”. The second phase of mixtures had a targeted  $f'_{ci}$  of 6000 psi (41 MPa) and  $f'_c$  of 8000 psi (55 MPa) and are designated with the prefix HS for “high strength”. A mixture meeting each of these strength requirements was developed using expanded clay, expanded shale, and conventional limestone aggregates for a total of six mix designs used to cast beam specimens. The letters C, S, and L were added to each mixture designation for the expanded clay, expanded shale, and limestone respectively.

A slump flow between 25 in. and 30 in. (635 mm and 760 mm),  $T_{20}$  between 2 and 5 seconds, VSI of 1.0 or less, and a J-Ring  $\Delta h$  less than 1.5 in. (38 mm) were targeted for each of these concrete mixtures. A series of trial batches with adjustments between batches was used to determine the optimum mix design for each combination of material property specifications. The variables that were adjusted between batches included: cement content, supplementary cementitious material type and content, total water content, water-cementitious materials ratio ( $w/cm$ ), coarse aggregate content and ratio of sand volume to total aggregate volume ( $s/agg$ ). Superplasticizer dosage was adjusted between batches to account for differences in cementitious materials, ambient temperature and aggregate moisture content error.

## 4.2 Normal Strength (NS) Series Mixtures ( $f'_{ci}$ of 4000 psi (28 MPa))

The baseline LWSCC mixture used for development of those used in this research project was based on previous work at the University of Arkansas by Ward (Ward 2009). His research focused on LWSCC containing expanded clay aggregate. Two variations of mixtures used in Ward's research were examined and then adjusted to account for differences in the lightweight aggregate between the expanded clay aggregate used in Ward's research and the expanded clay and shale aggregates used in this research. The specific gravity factors and absorption capacities of these aggregates varied from those used in Ward's research.

Several variables were manipulated to produce LWSCC with the particular set of fresh properties and compressive strength required for the NS phase. These variables included cement content, water-cement ratio ( $w/c$ ), total water content, ratio of sand to total aggregate by volume ( $s/agg$ ), and superplasticizer dosage. Due to the relatively high strength requirements at one day and the inherent weakness of lightweight aggregate compared to normal weight aggregate, only the powder-type method of developing SCC was utilized. No supplementary cementitious materials or other filler materials were incorporated in these mixtures due to their detrimental effects on either early age strength or workability, as in the case of fly ash and silica fume, respectively.

### 4.2.1 Normal Strength Clay (NSC) Mixtures

Mixtures using expanded clay aggregate were examined first. The different mix proportions that were tested are presented in Table 4.1 and the properties of these concrete mixtures are presented in Table 4.2. The properties of the expanded clay aggregate were not adequately known when trial batching commenced, so the specific gravity factor from Ward's research was used along with an assumption of an SSD condition after soaking of the aggregate

Table 4.1: NSC Trial Batches

Batch	Cement (lb/yd <sup>3</sup> )	Coarse Agg. (lb/yd <sup>3</sup> )	Fine Agg. (lb/yd <sup>3</sup> )	Water (lb/yd <sup>3</sup> )	HRWR (oz/cwt)	w/c	s/agg
1	795	715	1218	390	5.0	0.49	0.46
2	795	668	1218	390	4.6	0.49	0.48
3	795	743	1365	302	4.0	0.38	0.48
4	795	743	1365	302	3.0	0.38	0.48
5	795	743	1365	302	4.0	0.38	0.48
6	795	700	1451	302	4.0	0.38	0.51
7	795	684	1483	302	3.0	0.38	0.52
8	795	684	1483	302	4.0	0.38	0.52
9	795	700	1451	302	2.5	0.38	0.51
10	850	675	1402	302	4.0	0.36	0.50
11	795	700	1451	302	4.0	0.38	0.51
12	795	648	1462	318	4.5	0.40	0.52
13	850	675	1402	302	7.0	0.36	0.50
14	825	649	1407	329	6.5	0.40	0.51
15	825	642	1450	318	8.5	0.39	0.52
16	825	636	1434	329	6.0	0.40	0.52
17	795	659	1491	298	13.0	0.37	0.52
18	825	636	1434	329	8.0	0.40	0.52
19	825	649	1407	329	8.0	0.40	0.51
20	825	662	1380	329	7.5	0.40	0.50
21	825	676	1350	329	7.5	0.40	0.49
22	825	662	1380	329	7.0	0.40	0.50

Note: 1 lb = 0.454 kg, 1 oz = 29.57 mL, 1 yd<sup>3</sup> = 0.765 m<sup>3</sup>

for the first nine trial batches. Since the absorption capacity was not known at the time these batches were made, the moisture density relationship described in Section 3.4 was not usable until batch 10 when an approximate absorption capacity was determined using the methods of ASTM C127 (ASTM 2007). This absorption capacity of 17 percent was used for batches 10 through 13 until the absorption capacity was determined using the centrifuge method described in Section 3.2.3. This absorption capacity of 15 percent was utilized for the remaining batches.

The *w/c* and total water content were too high for the first two batches, as indicated by the significant segregation of these mixtures with the recommended superplasticizer dosage. The lack of knowledge of the aggregate properties most likely contributed to these difficulties. The

Table 4.2: Concrete Properties of NSC Batches

Batch	Slump Flow (in.)	$T_{20}$ (sec)	VSI	J-Ring Flow (in.)	J-Ring $\Delta$ (in.)	J-Ring $\Delta h$ (in.)	Unit Weight (lb/ft <sup>3</sup> )	$f'_{ci}$ (psi)	$f'_c$ (psi)
1	--	--	--	--	--	--	--	--	--
2	--	--	--	--	--	--	--	--	--
3	27.0	7.4	3.0	19.5	7.5	4.00	109.7	2860	4450
4	15.0	--	--	12.0	3.0	--	113.5	3330	5280
5	24.5	6.2	1.5	16.0	8.5	3.50	111.1	3380	5720
6	29.5	3.2	1.5	26.0	3.5	2.00	113.4	2590	4970
7	16.5	--	--	12.0	4.5	--	115.0	3020	5170
8	28.5	2.6	1.5	22.0	6.5	3.00	114.1	2750	4850
9	22.5	3.4	0.5	16.5	6.0	2.25	116.0	2930	5370
10	26.0	6.2	0.5	21.0	5.0	2.25	113.7	3640	5680
11	24.0	6.4	0.0	21.5	2.5	2.00	114.2	3760	5970
12	23.5	6.2	0.0	20.0	3.5	2.00	115.2	3650	5730
13	26.0	8.4	0.5	22.5	3.5	2.25	117.3	4780	6320
14	28.0	5.2	1.5	25.0	3.0	2.25	113.7	3520	5540
15	21.5	12.2	0.0	16.5	5.0	2.75	118.1	4510	6000
16	20.5	5.4	0.0	15.5	5.0	2.50	118.9	3740	6810
17	27.5	8.6	1.5	24.0	3.5	2.75	119.2	3770	5580
18	22.5	6.8	0.0	16.0	6.5	3.25	119.1	4400	7000
19	26.0	5.4	0.0	20.5	5.5	2.25	116.3	3630	6020
20	27.0	6.0	0.5	23.5	3.5	2.00	118.1	4250	6630
21	28.5	5.0	1.0	24.0	4.5	2.50	118.4	3640	5580
22	28.5	4.4	1.0	24.5	4.0	2.50	117.3	3990	5120

Note: 1 in. = 25.4 mm, 1 psi = 0.006895 MPa, 1 lb = 0.454 kg, 1 ft<sup>3</sup> = 0.0283 m<sup>3</sup>, -- indicates no measurements were taken

water content was then reduced in order to change the  $w/c$  from 0.49 to 0.38 for batch 3. Trial batches 3 through 9 and 11 used this 0.38  $w/c$  with a constant cement content of 795 lb/yd<sup>3</sup> (276 kg/m<sup>3</sup>). Superplasticizer dosage or  $s/agg$  was varied for these mixtures to examine effects on flowability and stability. Mixtures with  $s/agg$  between 0.48 and 0.52 produced acceptable slump flow,  $T_{20}$ , and VSI values, but the J-Ring test showed the potential for significant blockage. Increasing  $s/agg$  from 0.48 resulted in an increase in slump flow, and a  $s/agg$  of 0.51 produced the best combination of deformability and viscosity. None of these first mixtures reached the required minimum compressive strength of 4000 psi (28 MPa) at 24 hours of age.



Since compressive strength of lightweight concrete is considered to be more closely related to cement content than to water content when the exact moisture adjustment parameters are unknown (ACI 1998), the cement content for batches 10 and 13 was increased to 850 lb/yd<sup>3</sup> (295 kg/m<sup>3</sup>) without changing the water content, which reduced the *w/c* to 0.36. This increase in the volume of fine particles with no more available water increased the viscosity of the mixture and required a larger dose of superplasticizer. The cement content of the remaining trial batches, 14-22, was then reduced to 825 lb/yd<sup>3</sup> (490 kg/m<sup>3</sup>); except for batch 17, which was produced to simply fill in data missing from the 795 lb/yd<sup>3</sup> (472 kg/m<sup>3</sup>) mixtures. The water content was increased to produce a *w/c* of 0.40 for batches 14, 16, and 18-22 and 0.39 for batch 15. The proportions resulting from these mix design modifications are shown in Table 4.1. The reduction in cement content and increase in water content allowed for a better slump flow for these mixtures as can be seen in Table 4.2. The *s/agg* was varied from 0.49 to 0.52 and the superplasticizer dosage was adjusted between these mixtures until a mixture was developed that exhibited acceptable values for each fresh concrete property.

As only four of the trial batches met the required minimum for one-day compressive strength, a mixture with an acceptable combination of flow properties and unit weight, and a compressive strength greater than 3500 psi (24 MPa) was chosen for casting the first set of beam specimens. This mix design corresponded to that used for batches 14 and 19 presented in Table 4.1 with a superplasticizer dosage that varied with ambient temperature. A slump flow of the final NSC mixture design is shown in Figure 4.1. In determining the final expanded clay mix design it was very important to keep a high cement content and relatively low *w/c* in order to fulfill both the workability and compressive strength requirements. It was also necessary to have



Figure 4.1: Slump flow of NSC mixture used to cast beams

a coarse aggregate content of at least  $650 \text{ lb/yd}^3$  ( $385 \text{ kg/m}^3$ ) to keep the unit weight under the  $120 \text{ lb/ft}^3$  ( $1922 \text{ kg/m}^3$ ) requirement.

Errors were observed between the predicted moisture content used for adjusting the mixing water for each batch and the actual moisture content measured from the unit weight sample. These errors were due to the fact that moisture content could not be measured in the traditional manner before each batch was mixed. The relationship between this moisture content error and  $f'_{ci}$  for each  $w/c$  is plotted in Figure 4.2. The values are the difference in the predicted percent of moisture by weight and the actual measurement. A positive error indicates that there was more water in the mix than anticipated, whereas a negative error implies less water in the mix than anticipated. No statistical analyses were performed due to the small sample size, but the plot indicates that small errors (less than 3 percent) in moisture content did not appear to have a large effect on  $f'_{ci}$  for a given  $w/c$ . There is also some scatter in the results for the closely spaced data points from mixtures with a 0.40  $w/c$ . This scatter is even more evident in the plot of

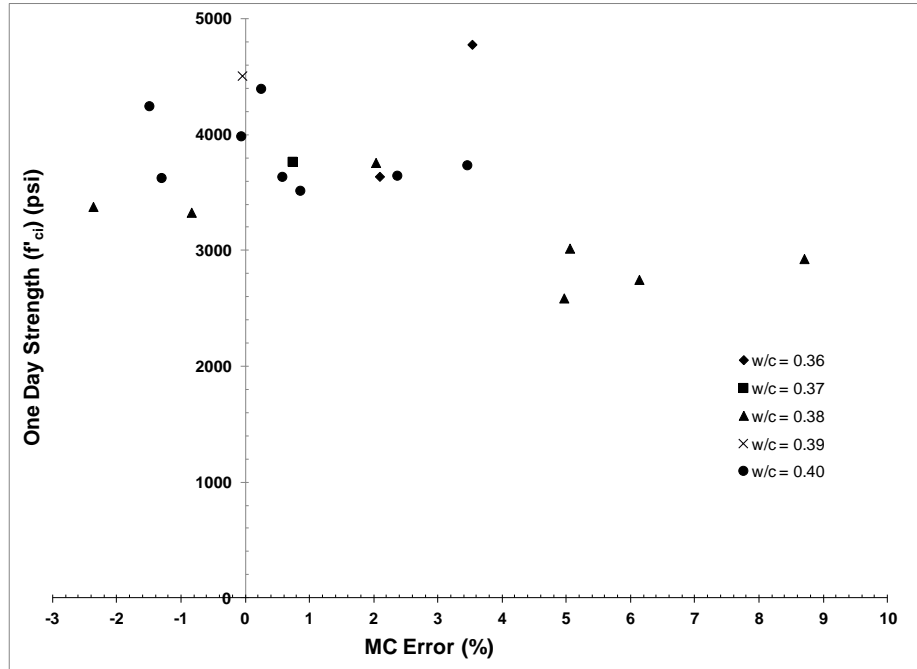


Figure 4.2: Effect of aggregate moisture content error on NSC  $f'_{ci}$

moisture content error with  $f'_c$  for each  $w/c$  shown in Figure 4.3. Small errors (less than 3 percent) in moisture content do not appear to have a large effect on  $f'_c$  for these mixtures either.

Plots displaying the effect of moisture content error on compressive strength for each cement content are presented in Appendix C. These plots also do not imply a relationship between small errors in aggregate moisture content predictions and compressive strength.

#### 4.2.2 Normal Strength Shale (NSS) Mixtures

The major issues in proportioning LWSCC including basic water content, cement content, and superplasticizer dosage, were resolved during testing of the expanded clay mixtures; therefore refining the NSS mixtures was substantially less involved than was the case for the normal strength clay (NSC) mixtures. The different mixture proportions tested and their resulting concrete properties are presented in Tables 4.3 and 4.4 respectively. The first mixture, batch 23, using expanded shale aggregate was again based on the mixtures utilized by Ward (Ward 2009), but had a larger volume of coarse aggregate to keep the unit weight at a reasonable

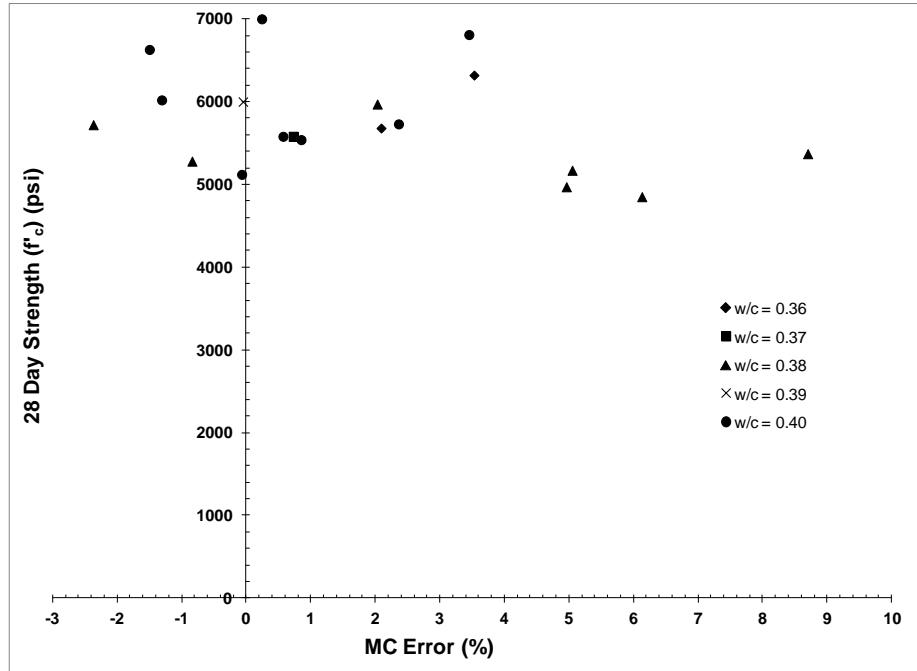


Figure 4.3: Effect of aggregate moisture content error on NSC  $f'_c$

value. This first mixture was very rocky and exhibited significant blockage in the J-Ring test. The  $s/agg$  and cement content were increased for the subsequent batches to provide more fine particles in the mix. The same 0.40  $w/c$  was used for batches 23-25, but low compressive strengths prompted a decrease in  $w/c$  to 0.35 and a further increase in cement content from

Table 4.3: NSS Trial Batches

Batch	Cement (lb/yd <sup>3</sup> )	Coarse Agg. (lb/yd <sup>3</sup> )	Fine Agg. (lb/yd <sup>3</sup> )	Water (lb/yd <sup>3</sup> )	HRWR (oz/cwt)	w/c	s/agg
23	800	790	1344	320	4.0	0.40	0.48
24	825	747	1376	330	6.0	0.40	0.51
25	825	717	1432	330	6.0	0.40	0.52
26	850	733	1465	298	7.5	0.35	0.52
27	850	748	1437	298	8.0	0.35	0.51
28	850	748	1437	298	11.0	0.35	0.51
29	850	764	1408	298	8.0	0.35	0.50
30	850	748	1383	319	7.0	0.38	0.50
31	900	726	1392	315	4.0	0.35	0.50
32	850	748	1437	298	6.0	0.35	0.51
33	900	726	1392	315	6.0	0.35	0.51
34	850	748	1437	298	6.0	0.35	0.51
35	900	726	1392	315	5.0	0.35	0.51

Note: 1 lb = 0.454 kg, 1 oz = 29.57 mL, 1 yd<sup>3</sup> = 0.765 m<sup>3</sup>

Table 4.4: Concrete Properties of NSS Batches

Batch	Slump Flow (in.)	$T_{20}$ (sec)	VSI	J-Ring Flow (in.)	J-Ring $\Delta$ (in.)	J-Ring $\Delta h$ (in.)	Unit Weight (lb/ft <sup>3</sup> )	$f'_{ci}$ (psi)	$f'_c$ (psi)
23	22.0	4.0	0.0	16.0	6.0	3.00	122.0	3090	5740
24	24.0	4.2	0.0	24.0	0.0	2.00	114.1	3000	5140
25	26.5	3.2	1.0	24.5	2.0	2.00	118.4	2940	5280
26	27.0	8.2	1.0	21.5	5.5	2.50	116.2	3430	5450
27	25.0	12.8	0.5	21.5	3.5	1.50	120.2	3920	6270
28	25.5	11.0	1.0	20.0	5.5	2.00	121.3	4010	5270
29	26.0	7.4	0.5	23.5	2.5	1.25	118.4	3520	5080
30	28.5	4.2	1.5	22.0	6.5	3.00	115.4	2720	4580
31	17.5	--	0.0	17.5	0.0	2.75	117.0	2880	5500
32	25.0	4.8	0.5	21.0	4.0	2.75	122.1	3690	5280
33	27.5	4.0	1.0	26.5	1.0	2.00	113.4	3900	5550
34	26.0	6.6	1.0	25.5	0.5	1.50	118.8	4080	6070
35	25.0	5.4	0.5	23.0	2.0	1.50	119.5	3860	6450

Note: 1 in. = 25.4 mm, 1 psi = 0.006895 MPa, 1 lb = 0.454 kg, 1 ft<sup>3</sup> = 0.0283 m<sup>3</sup>, -- indicates no measurements due to lack of SCC behavior

825 lb/yd<sup>3</sup> (490 kg/m<sup>3</sup>) to 850 lb/yd<sup>3</sup> (505 kg/m<sup>3</sup>). These values were then used for batches 26-29, 32, and 34. The slump flow and VSI were adequate for all but batches 23 and 31, but problems with  $T_{20}$  and J-Ring blockage persisted throughout testing. Values of  $s/agg$  between 0.50 and 0.52 were examined, and a  $s/agg$  of 0.51 was again determined to produce the best balance of flow and viscosity to reduce blockage. It was observed that a small number of large, irregularly shaped aggregate particles were contributing to the blockage problems in the J-Ring test. The aggregate used for batches 34 and 35 was therefore passed over a 1/2 in. (13 mm) sieve prior to presoaking in water. This significantly reduced the observed blockage from a  $\Delta h$  of over 2 in. (50 mm) to 1.5 in. (38 mm). It was also decided at this point in the research that a larger  $\Delta h$  was acceptable for the lightweight mixtures than for normal weight mixtures based on the NSC beam casting results. Values of  $\Delta h$  did not correlate well with J-Ring  $\Delta$  for batches 24 and 25 or 27, 29, 34, and 35. These had differences of more than 2 in. (50 mm) in  $\Delta$  for the same  $\Delta h$  or differences of more than 2 in. (100 mm) in  $\Delta h$  for the same value of  $\Delta$ .

The consistently lower compressive strengths for the NSS mixtures in spite of higher cement contents and lower  $w/c$  than the NSC mixtures were attributed to a combination of several factors. The expanded shale aggregate surface appeared to be somewhat smoother than the expanded clay, which may have combined with the lower absorption capacity to produce a weaker paste to aggregate bond. It was observed that the NSS cylinder failures passed around the aggregate particles whereas the NSC failures showed fracture of the individual aggregate particles. It is also possible that early age internal curing effects were not as pronounced in the NSS mixtures due to the smaller absorption capacity of the aggregate. Therefore, a stronger paste was needed to achieve the same  $f'_{ci}$ . The removal of aggregate particles larger than ½ in. (13 mm) also resulted in a slight increase in compressive strength between batches 32 and 34. The reduced density of these larger particles may have caused aggregate strength irregularities in the concrete that contributed to reduced compressive strength. The final NSS mix design chosen for casting beam specimens for transfer and development length testing corresponded to that used for batches 27, 28, 32, and 34. The slump flow of the final expanded clay mixture design is shown in Figure 4.4. Some bleed water is visible, and adjustment of superplasticizer for consistent stability of the mixture was challenging.

The relationship between error in estimated and actual moisture content and  $f'_{ci}$  for each  $w/c$  is shown in Figure 4.5 and that with  $f'_c$  is shown in Figure 4.6. The small number of data points again made statistical analysis difficult, but the plot indicated that, for a given  $w/c$ ,  $f'_{ci}$  was fairly consistent when the actual moisture content was less than 3 percent greater than predicted. Some scatter is visible in the data for a  $w/c$  of 0.35, especially relating to  $f'_c$ . Even the mixtures with the largest error still had an  $f'_c$  that was fairly consistent with the remainder of the data. When compared for a given cement content, as presented in Appendix C, these data still show



Figure 4.4: Slump flow of final NSS mixture

that relatively small errors in the prediction of aggregate moisture content do not have a major effect on either  $f'_{ci}$  or  $f'_c$ .

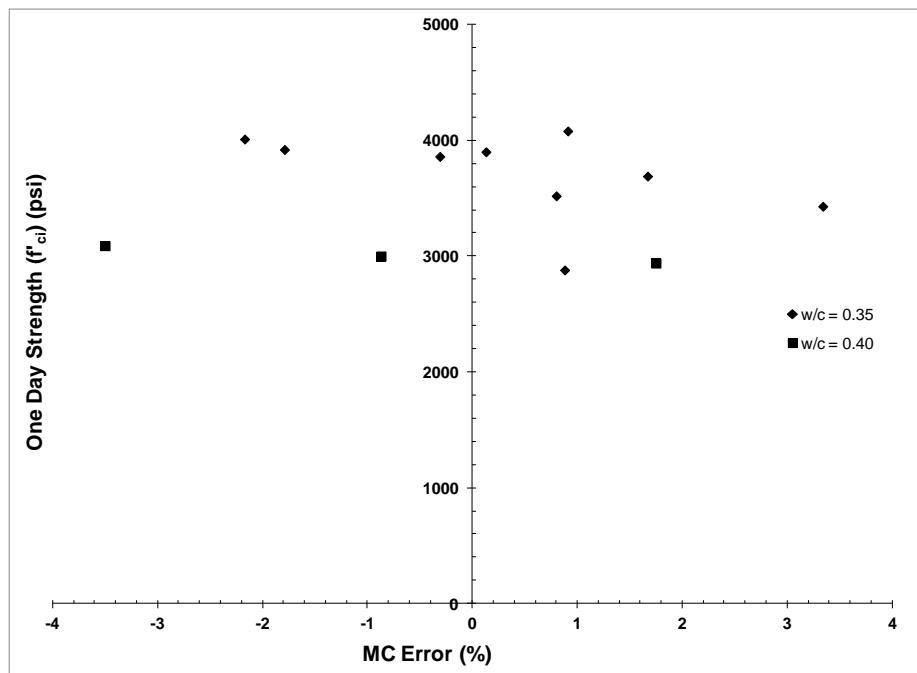


Figure 4.5: Effect of aggregate moisture content error on NSS  $f'_{ci}$

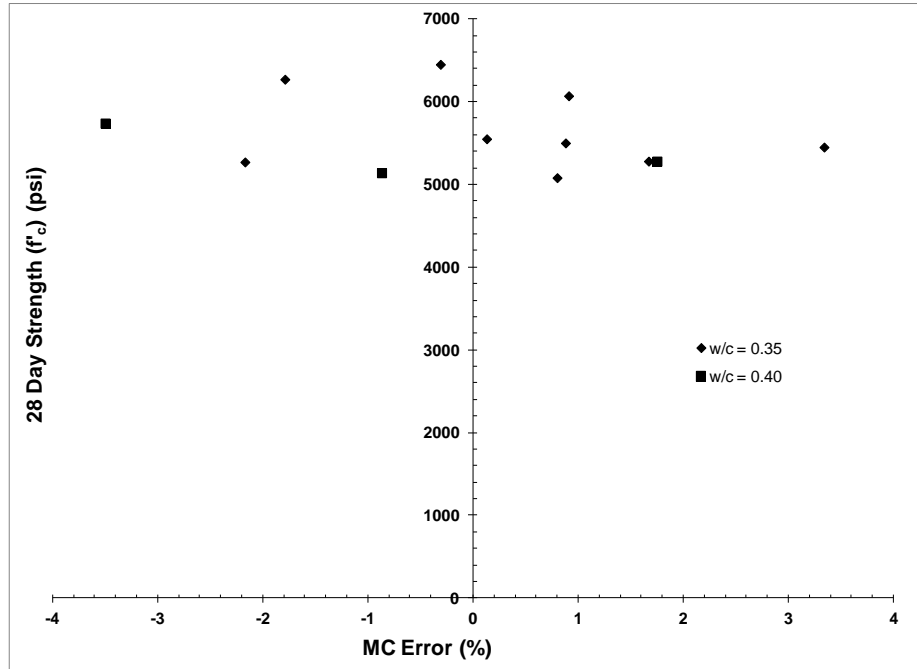


Figure 4.6: Effect of aggregate moisture content error on NSS  $f'_c$

#### 4.2.3 Normal Strength Limestone (NSL) Mixtures

A conventional SCC mixture was developed to meet the targeted fresh concrete properties and compressive strengths described in Section 4.1 by modifying a mix design produced by other research at the University of Arkansas (Smith 2011). The different batches tested are presented in Table 4.5 and the corresponding concrete properties in Table 4.6. A  $w/c$  of 0.44 was used for batches 36-38 along with slight variations in cement content and  $s/agg$ . The cement content was increased for batch 39 which led to a lower  $w/c$  and produced the best fresh concrete properties. However, the compressive strength of this mixture was higher than desired for an adequate comparison to the other mixtures. Since time did not allow for another trial batch, the cement content was reduced to  $775 \text{ lb/yd}^3$  ( $460 \text{ kg/m}^3$ ) for the mix design used to cast beams, while the  $w/c$  and  $s/agg$  were the same as used for batch 39.



Table 4.5: NSL Trial Batches

Batch	Cement (lb/yd <sup>3</sup> )	Coarse Agg. (lb/yd <sup>3</sup> )	Fine Agg. (lb/yd <sup>3</sup> )	Water (lb/yd <sup>3</sup> )	HRWR (oz/cwt)	w/c	s/agg
36	761	1380	1454	335	7.0	0.44	0.52
37	775	1367	1439	341	7.0	0.44	0.52
38	775	1425	1384	341	6.0	0.44	0.50
39	825	1362	1433	330	6.0	0.40	0.52

Note: 1 lb = 0.454 kg, 1 oz = 29.57 mL, 1 yd<sup>3</sup> = 0.765 m<sup>3</sup>

Table 4.6: Concrete Properties of NSL Batches

Batch	Slump Flow (in.)	T <sub>20</sub> (sec)	VSI	J-Ring Flow (in.)	J-Ring Δ (in.)	J-Ring Δh (in.)	Unit Weight (lb/ft <sup>3</sup> )	f <sub>ci</sub> (psi)	f <sub>c</sub> (psi)
36	19.5	7.0	0.0	15.5	4.0	3.00	147.8	4970	11,150
37	26.0	4.0	1.0	21.0	5.0	2.00	148.0	4480	9770
38	23.0	4.8	0.0	20.0	3.0	1.75	147.2	4110	9860
39	27.0	3.6	0.5	23.5	3.5	1.50	149.2	5890	12,200

Note: 1 in. = 25.4 mm, 1 psi = 0.006895 MPa, 1 lb = 0.454 kg, 1 ft<sup>3</sup> = 0.0283 m<sup>3</sup>

#### 4.2.4 Summary

A total of 35 trial batches were required to develop LWSCC mixtures meeting both the fresh property and compressive strength requirements of Section 4.1. The variables adjusted to meet these requirements included cement content, water content, w/c, s/agg, and superplasticizer dosage. Superplasticizer dosages within the range recommended by the manufacturer were adequate for these mixtures. The most difficult aspect of this phase of mixture development was finding the proper balance between fresh properties and compressive strength. Aggregate type played a significant role in the difficulties encountered while seeking this balance. The limestone coarse aggregate produced the least difficulty in achieving conformance to the required fresh concrete properties followed by the expanded clay. The expanded shale aggregate was the most difficult to work with and required the most effort in achieving the proper balance of strength and workability. The mixtures used to cast the normal strength (NS) series of beams are presented in Table 4.7 along with the ranges of concrete properties measured during beam construction. The variation in these properties is due to the variations in ambient temperature of

Table 4.7: Final NS Mix Designs

Material	NSC	NSS	NSL
Cement (lb/yd <sup>3</sup> )	825	850	775
Coarse Agg. (lb/yd <sup>3</sup> )	649	748	1408
Fine Agg. (lb/yd <sup>3</sup> )	1407	1437	1481
Water (lb/yd <sup>3</sup> )	329	298	310
HRWR (oz/cwt)	6.0-6.5	5.0-6.0	4.5-7.0
w/c	0.40	0.35	0.40
s/agg	0.51	0.51	0.52
Slump Flow (in.)	25.0 – 28.0	26.0 – 29.5	19.0 – 27.0
$T_{20}$ (sec)	3.4 – 5.4	2.0 – 6.4	2.0 – 3.2
J-Ring $\Delta h$ (in.)	1.25 – 2.25	1.25 – 2.25	1.0 – 2.25
$f'_{ci}$ (psi)	3800 – 5600	3700 – 4500	4000 – 5600
$f'_c$ (psi)	4900 – 7200	5800 – 7100	6700 – 8000

Note: 1 lb = 0.454 kg, 1 oz = 29.57 mL, 1 yd<sup>3</sup> = 0.765 m<sup>3</sup>, 1 in. = 25.4 mm, 1 psi = 0.006895 MPa, 1 lb = 0.454 kg, 1 ft<sup>3</sup> = 0.0283 m<sup>3</sup>

up to 30° F between casting days. Superplasticizer dosage was adjusted to mitigate these differences, but they persisted in many cases.

### 4.3 High Strength (HS) Series Mixtures ( $f'_{ci}$ of 6000 psi (41 MPa))

Difficulty was encountered in regards to achieving the targeted 4000 psi (28 MPa)  $f'_{ci}$  for the first set of concrete mixtures. Therefore the powder-type SCC method was again utilized to produce the high strength (HS) LWSCC mixtures. The first mixture was based on high strength normal weight SCC produced by previous research at the University of Arkansas (Do 2007). Several methods were used in an attempt to obtain the required combination of compressive strength and concrete workability. These included using a very high cement content, replacing a percentage of the cement with silica fume, incorporating a portion of normal weight limestone aggregate, and finally, using Type III cement. The variables examined were very similar to those adjusted for the normal strength (NS) mixtures. In addition to cementitious material type and content, these included  $w/cm$ ,  $s/agg$ , water content, and total volume of sand and cementitious materials.

### 4.3.1 High Strength Clay (HSC) Mixtures

#### 4.3.1.1 Type I Portland Cement Mixtures

Mixtures using expanded clay were examined first since a much larger quantity of this material was available and thus the major issues could be resolved with these mixtures before getting to the more limited expanded shale aggregate. The first method used in pursuit of the targeted concrete properties involved only Type I portland cement. The different mix proportions examined using these parameters are presented in Table 4.8. The previously used high strength normal weight SCC mixture (Do 2007) was adjusted for lightweight aggregate by replacing the coarse aggregate with the approximate volume of coarse aggregate required to achieve the desired unit weight of 120 lb/ft<sup>3</sup> (1920 kg/m<sup>3</sup>) and then making minor adjustments to the *w/c* to keep the total water content fairly high and the *s/agg* at 0.50. This mix design was used for batch 40 and batch 41 was mixed using the same proportions to determine if the 2.5 percent error in the moisture content of the coarse aggregate used for batch 40 had a significant effect of *f'ci*. The fresh properties for both of these mixtures were within the required specifications, but *f'ci* did not reach the required 6000 psi (41 MPa). The fresh concrete properties and compressive strengths for this set of trial batches are presented in Table 4.9.

Table 4.8: HSC Trial Batches Using Only Type I Cement

Batch	Cement (lb/yd <sup>3</sup> )	Coarse Agg. (lb/yd <sup>3</sup> )	Fine Agg. (lb/yd <sup>3</sup> )	Water (lb/yd <sup>3</sup> )	HRWR (oz/cwt)	<i>w/c</i>	<i>s/agg</i>
40	950	649	1368	304	6.0	0.32	0.50
41	950	649	1368	304	7.5	0.32	0.50
42	825	649	1576	264	13.0	0.32	0.54
43	950	649	1303	329	6.0	0.35	0.49
44	825	649	1576	264	14.0	0.32	0.54
45	825	660	1490	288	9.0	0.35	0.52
46	950	649	1303	329	7.0	0.35	0.49
47	902	649	1286	329	7.0	0.36	0.49
48	1000	649	1338	300	10.0	0.30	0.50

Note: 1 lb = 0.454 kg, 1 oz = 29.57 mL, 1 yd<sup>3</sup> = 0.765 m<sup>3</sup>

Table 4.9: Concrete Properties of HSC Batches Using Only Type I Cement

Batch	Slump Flow (in.)	$T_{20}$ (sec)	VSI	J-Ring Flow (in.)	J-Ring $\Delta$ (in.)	J-Ring $\Delta h$ (in.)	Unit Weight (lb/ft <sup>3</sup> )	$f'_{ci}$ (psi)	$f'_c$ (psi)
40	27.5	5.0	0.0	27.0	0.5	1.00	117.8	3610	6480
41	25.5	--	1.0	--	--	--	120.6	3910	5990
42	25.5	11.2	1.0	--	--	--	124.5	2460	4730
43	30.0	6.0	0.5	26.5	3.5	1.25	117.4	2460	6180
44	18.0	--	0.0	--	--	--	125.0	3790	6460
45	24.0	14.8	1.0	18.5	5.5	2.50	123.4	3210	5720
46	28.0	6.4	0.5	27.0	1.0	1.50	121.3	3500	6200
47	29.0	6.2	1.0	22.0	7.0	1.75	119.3	3650	6190
48	29.0	17.6	0.5	24.5	4.5	1.75	125.5	5620	6670

Note: 1 in. = 25.4 mm, 1 psi = 0.006895 MPa, 1 lb = 0.454 kg, 1 ft<sup>3</sup> = 0.0283 m<sup>3</sup>, -- indicates no measurements were taken

Batches 43 and 46 had the same water content as the mixture used for the NSC beams with the cement content increased to 950 lb/yd<sup>3</sup> (565 kg/m<sup>3</sup>) and the resulting reduction in sand volume changed the  $s/agg$  to 0.49. This mixture again produced adequate fresh concrete properties, but  $f'_{ci}$  was inadequate. This was in spite of an aggregate moisture content less than estimated, and thus a water content less than expected, for both mixtures.

In contrast to increasing cement content, the cement and coarse aggregate contents from the mix design used for the NSC beams were used with the  $w/c$  reduced to 0.32 for batches 42 and 44. This reduction in water volume required an increase in sand that adjusted the  $s/agg$  to 0.54. The low water content and high sand content resulted in a very cohesive mixture requiring a very high dosage of superplasticizer, which resulted in some bleeding and segregation. The  $w/c$  was increased to 0.35 for batch 45 in order to increase the flowability of the mixture.

Compressive strength was not adequate for these three mixtures either. Batch 47 was intended to have silica fume in addition to the portland cement, but the silica fume was erroneously not added to the mixer. This mixture had significant blockage as shown by the J-Ring test and did not meet the compressive strength requirement. The final portland cement mixture, batch 48,

had the highest cement content and lowest  $w/c$  deemed practical. This mixture was very cohesive, exhibited blockage in the J-Ring test, had a high unit weight, and while it produced the highest compressive strength up to that point, still did not meet the targeted compressive strength. Discrepancies were observed between J-Ring  $\Delta$  and  $\Delta h$  for batches 45-48 similar to those observed for the NSS mixtures.

The effect of moisture content error on  $f'_{ci}$  of these mixtures for each  $w/c$  is illustrated in Figure 4.7. There does not appear to be a correlation between the difficulties experienced in obtaining the proper compressive strength for these mixtures and the error in moisture content estimation. One data point shows that the mixture with the highest  $w/c$  and highest error still had a compressive strength very similar to that of the other mixtures. A plot of the effect of moisture content error on  $f'_c$  is shown in Appendix C along with similar plots separating the data by cement content. None of these plots imply a major effect of moisture content error on compressive strength.

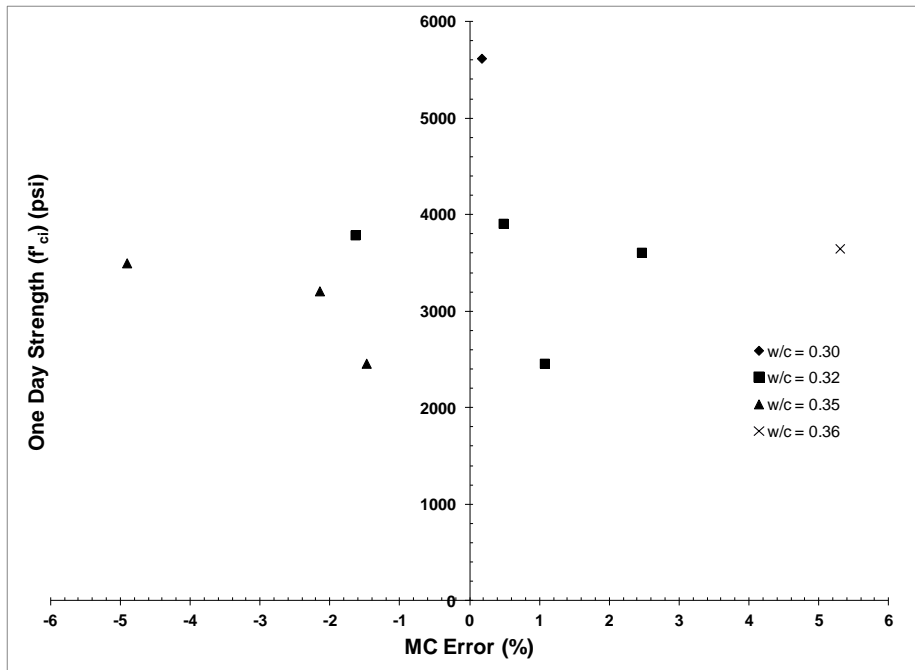


Figure 4.7: Effect of aggregate moisture content error on Type I cement HSC  $f'_{ci}$

#### 4.3.1.2 Silica Fume Mixtures

The second method used to pursue a high strength LWSCC mixture with the desired properties consisted of incorporating silica fume as a percentage replacement of portland cement by weight. This finely divided material has a significant impact on early age strength of concrete, but also has substantial negative effects on workability. The different mixture proportions examined including silica fume are presented in Table 4.10 and the corresponding concrete properties in Table 4.11. The first batch that incorporated silica fume, batch 49, had the same water and coarse aggregate contents as the mixture used for the NSC beams with the total cementitious material content increased to the same 950 lb/yd<sup>3</sup> (565 kg/m<sup>3</sup>) used for the portland cement only mixtures described in Section 4.3.1.1. Silica fume was incorporated at a replacement rate of 5 percent by weight of cement. This mixture was very viscous, had a very high  $T_{20}$ , and exhibited blockage in the J-Ring test. In order to decrease the viscosity of the mixture, the coarse aggregate content for batch 50 was increased to reduce the  $s/agg$  to 0.48.

Table 4.10: HSC Trial Batches Using Silica Fume

Batch	Cement (lb/yd <sup>3</sup> )	Silica Fume (lb/yd <sup>3</sup> )	Coarse Agg. (lb/yd <sup>3</sup> )	Fine Agg. (lb/yd <sup>3</sup> )	Water (lb/yd <sup>3</sup> )	HRWR (oz/cwt)	w/c	s/agg
49	902	48	649	1286	329	8.5	0.35	0.49
50	902	48	659	1266	329	7.5	0.35	0.48
51	902	48	659	1331	304	10.0	0.32	0.49
52	855	95	649	1270	329	9.0	0.35	0.48
53	784	41	649	1392	329	7.0	0.40	0.51
54	902	48	649	1286	329	8.5	0.35	0.49
55	902	48	649	1286	329	10.0	0.35	0.49
56	855	95	649	1270	329	12.0	0.35	0.48
57	742	83	649	1377	329	10.0	0.40	0.50
58	902	48	649	1286	329	9.5	0.35	0.49
59	855	95	649	1270	329	9.0	0.35	0.48
60	950	50	649	1244	329	10.0	0.33	0.48
61	902	48	649	1286	329	9.0	0.35	0.49
62	950	50	649	1244	329	10.0	0.33	0.48
63	950	50	649	1200	346	10.0	0.35	0.47

Note: 1 lb = 0.454 kg, 1 oz = 29.57 mL, 1 yd<sup>3</sup> = 0.765 m<sup>3</sup>

Table 4.11: Concrete Properties of HSC Batches Using Silica Fume

Batch	Slump Flow (in.)	$T_{20}$ (sec)	VSI	J-Ring Flow (in.)	J-Ring $\Delta$ (in.)	J-Ring $\Delta h$ (in.)	Unit Weight (lb/ft <sup>3</sup> )	$f'_{ci}$ (psi)	$f'_c$ (psi)
49	22.0	13.2	0.0	16.0	6.0	2.75	121.4	5040	8010
50	28.5	4.8	0.5	26.0	2.5	1.50	116.2	3960	6500
51	29.0	11.8	0.0	25.5	3.5	1.25	119.9	3880	7070
52	26.0	8.6	0.0	21.5	4.5	1.75	119.3	5130	7300
53	24.0	7.4	0.0	20.5	3.5	2.00	118.6	3260	6390
54	29.5	5.0	0.5	26.5	3.0	1.25	122.1	2940	6190
55	29.5	6.8	0.5	27.5	2.0	1.25	121.2	2950	6350
56	27.0	12.0	0.0	25.0	2.0	1.50	122.1	3580	6810
57	27.0	6.2	1.0	22.0	5.0	1.75	123.1	3130	6250
58	27.5	9.4	0.5	25.0	2.5	1.50	125.6	4610	6950
59	28.0	10.0	1.0	24.5	3.5	1.75	123.5	4070	7010
60	28.5	17.4	1.0	26.0	2.5	2.00	122.3	3710	6110
61	28.5	8.4	0.5	24.5	4.0	1.75	124.5	4450	6580
62	28.5	7.4	0.5	26.5	2.0	1.75	123.5	4850	6480
63	30.5	6.8	1.0	29.5	1.0	1.25	114.8	4120	5940

Note: 1 in. = 25.4 mm, 1 psi = 0.006895 MPa, 1 lb = 0.454 kg, 1 ft<sup>3</sup> = 0.0283 m<sup>3</sup>

This change greatly improved the fresh properties of the concrete, but  $f'_{ci}$  was still inadequate.

The  $w/c$  was reduced to 0.32 for batch 51 in an attempt to increase compressive strength. This change resulted in a slight increase in the viscosity of the concrete with no increase in compressive strength. The silica fume replacement was increased to 10 percent from the proportions of batch 49 for batch 52, which produced a slightly higher compressive strength.

This mixture was retested with batches 56 and 59 with the same basic results. It was determined that the benefits of this high silica fume replacement rate did not offset the detrimental effects on workability or the increased material cost of silica fume over that of Type I cement.

Batch 53 had the same basic mix design used for the NSC beams with an incorporation of 5 percent silica fume by weight of cement. Neither the fresh concrete properties nor  $f'_{ci}$  of this mixture met the required standards. The replacement rate was therefore increased to 10 percent for batch 57. The compressive strength was still inadequate and the 825 lb/yd<sup>3</sup> (490 kg/m<sup>3</sup>) cementitious materials content was abandoned. Batches 54, 55, 58, and 61 all had the same

proportions as the first silica fume mixture, batch 49. This was due to the aggregate moisture content error for batch 49 and to examine effects of temperature on the mixture. These batches exhibited adequate fresh concrete properties, but the compressive strength did not reach the targeted value. The maximum tested cementitious material content of 1000 lb/yd<sup>3</sup> (590 kg/m<sup>3</sup>) with a silica fume replacement rate of 5 percent was used for batches 60 and 62 with the same water content as the NSC mixture. These batches had high  $T_{20}$  times, exhibited blockage in the J-Ring test, and did not meet the compressive strength requirements. The water content was increased for batch 63 to improve the flow characteristics, which resulted in adequate fresh concrete properties, but the compressive strength was still inadequate. Discrepancies between J-Ring  $\Delta$  and  $\Delta h$  existed for these mixtures in the form of differences in  $\Delta$  of 2.5 in. (64 mm) for the same  $\Delta h$ .

The relationship between moisture content error and  $f'_{ci}$  separated by  $w/c$  for the HSC batches utilizing silica fume is shown in Figure 4.8. While there are again only a small number of data points, there is clearly scatter in the data with several points that had a larger excess moisture content having a higher compressive strength for a 0.35  $w/c$ . This is most likely due to the behavior of the silica fume in the mixture. It is less likely to be affected by variations in water due to its reactivity and the less workable mixtures may have produced poorly consolidated cylinders that exhibited lower strengths. No relationship is apparent between excess moisture (3 percent or less) in the mix and the difficulty of developing a mix design with the required  $f'_{ci}$  using silica fume. The effect of moisture content error on  $f'_c$  is presented in Appendix C. While the scatter does not appear to be as noticeable in this plot, it still does not imply that moisture content errors contributed to the difficulties experienced in achieving the



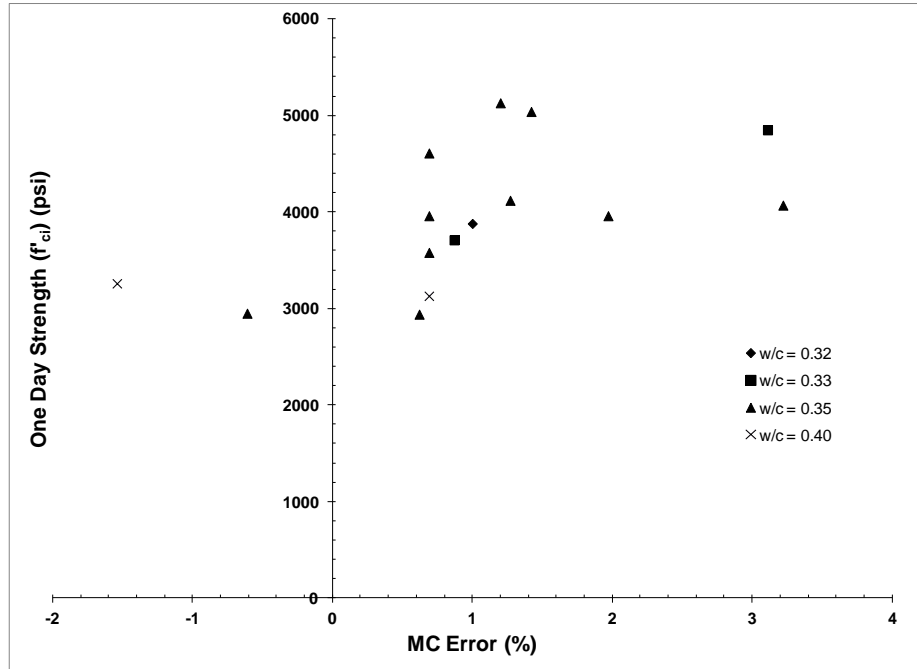


Figure 4.8: Effect of aggregate moisture content error on silica fume HSC  $f'_{ci}$

required  $f'_{ci}$ . Similar plots separated by percentage replacement of silica fume are also presented in Appendix C and do not imply a major effect of moisture content error on  $f'_{ci}$ .

#### 4.3.1.3 Expanded Clay and Limestone Mixtures

Once results clearly indicated that the incorporation of silica fume would not produce an adequate balance of workability and compressive strength, the third method for pursuing an adequate high-strength LWSCC mixture was examined. This method involved combining the lessons learned from batches with only portland cement and those incorporating silica fume with replacement of a portion of the coarse aggregate volume with normal weight, limestone aggregate. It was known that these mixtures would have a higher unit weight than the desired  $120 \text{ lb/ft}^3$  ( $1920 \text{ kg/m}^3$ ) maximum, but the need to increase the compressive strength outweighed this concern. The different mixture proportions that were examined are presented in Table 4.12 and the resulting concrete properties in Table 4.13.

Table 4.12: HSC Trial Batches With Limestone

Batch	Cement (lb/yd <sup>3</sup> )	Silica Fume (lb/yd <sup>3</sup> )	LW Agg. (lb/yd <sup>3</sup> )	NW Agg. (lb/yd <sup>3</sup> )	Fine Agg. (lb/yd <sup>3</sup> )	Water (lb/yd <sup>3</sup> )	HRWR (oz/cwt)	w/c	s/agg
64	950	0	555	200	1305	329	6.0	0.35	0.49
65	950	0	463	400	1302	329	6.5	0.35	0.49
66	950	0	325	695	1303	329	5.0	0.35	0.49
67	902	48	555	200	1288	329	7.0	0.35	0.49
68	902	48	463	400	1285	329	7.0	0.35	0.49
69	825	0	552	281	1406	302	7.5	0.37	0.50
70	784	41	455	418	1390	329	9.0	0.40	0.51
71	784	41	325	696	1391	329	7.0	0.40	0.51

Note: 1 lb = 0.454 kg, 1 oz = 29.57 mL, 1 yd<sup>3</sup> = 0.765 m<sup>3</sup>

Table 4.13: Concrete Properties of HSC Batches With Limestone

Batch	Slump Flow (in.)	T <sub>20</sub> (sec)	VSI	J-Ring Flow (in.)	J-Ring Δ (in.)	J-Ring Δh (in.)	Unit Weight (lb/ft <sup>3</sup> )	f' <sub>ci</sub> (psi)	f' <sub>c</sub> (psi)
64	30.5	5.0	1.0	29.0	1.5	1.25	123.4	4490	6530
65	29.5	4.4	0.0	26.0	3.5	1.25	127.1	4930	7160
66	29.0	4.0	0.5	27.0	2.0	1.00	130.9	4300	7470
67	24.5	8.2	0.0	24.0	0.5	1.75	123.0	3940	6500
68	27.5	5.2	0.5	26.5	1.0	1.50	121.8	4070	6860
69	27.0	11.0	1.0	23.5	3.5	1.50	123.8	3320	6490
70	26.0	8.2	1.0	21.0	5.0	2.25	130.6	3480	7150
71	25.0	6.4	0.5	21.5	3.5	2.00	134.9	3300	7380

Note: 1 in. = 25.4 mm, 1 psi = 0.006895 MPa, 1 lb = 0.454 kg, 1 ft<sup>3</sup> = 0.0283 m<sup>3</sup>

Batch 64 was produced using the same water content and aggregate volume as the mixture used for the NSC beams with the cement content increased to 950 lb/yd<sup>3</sup> (565 kg/m<sup>3</sup>) and 15 percent of the lightweight coarse aggregate volume replaced with limestone coarse aggregate. A 30 percent and 50 percent replacement of lightweight aggregate with limestone was used for batches 65 and 66 respectively. These mixtures exhibited excellent fresh concrete properties with unit weights only slightly higher than the specified 120 lb/ft<sup>3</sup> (1920 kg/m<sup>3</sup>), but f'<sub>ci</sub> still did not reach the targeted 6000 psi (41 MPa). Silica fume was used to replace 5 percent of the portland cement in batches 67 and 68 which also included 15 percent and 30 percent replacement of lightweight aggregate with limestone coarse aggregate respectively. The fresh

concrete properties of these mixtures were adequate, but the compressive strength requirement was again not met.

Batch 66 had the same proportions as the mixture used for the NSC beams, except that the  $w/c$  was reduced to 0.37 and the volume of water removed was replaced with limestone aggregate in addition to a 15 percent replacement of the lightweight coarse aggregate volume. This mixture was very viscous and did not meet the compressive strength requirement. Batches 70 and 71 were also both based on the mix design used for the NSC beams with a replacement of the lightweight coarse aggregate with 30 percent and 50 percent by volume of limestone and with an incorporation of 5 percent silica fume by weight of cement. These mixtures exhibited blockage as indicated by the J-Ring test and did not meet the compressive strength requirement. Discrepancies between J-Ring  $\Delta$  and  $\Delta h$  were also observed for these mixtures. The effect of aggregate moisture content error on  $f'_{ci}$  for each  $w/c$  is shown in Figure 4.9. The very small number of data points makes relating the two difficult, but it appears that the moisture content

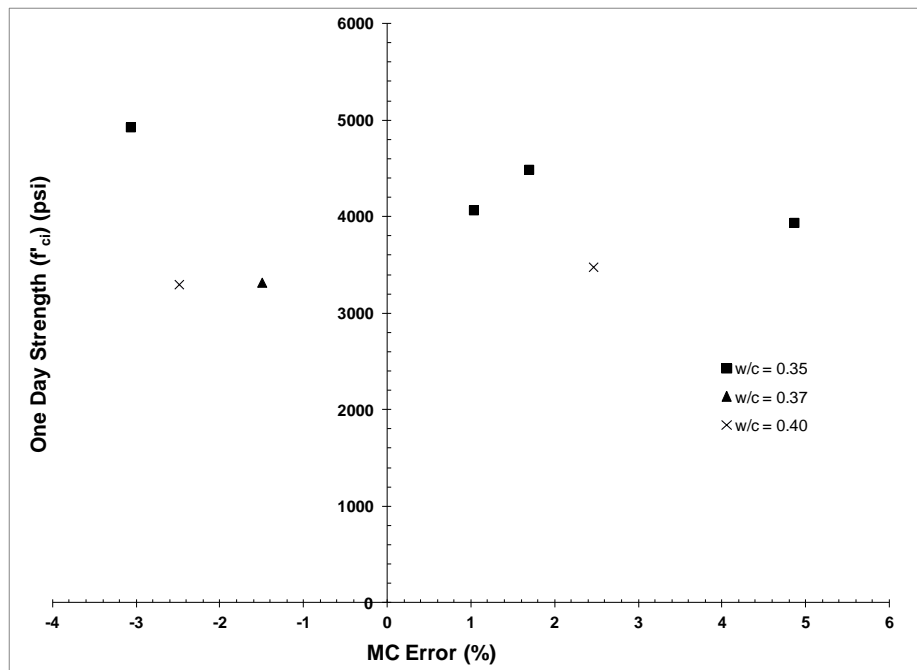


Figure 4.9: Effect of aggregate moisture content error on partial limestone HSC  $f'_{ci}$

error cannot be linked to compressive strength issues. As no mixtures were developed that met the compressive strength requirement, the use of limestone coarse aggregate as replacement of lightweight aggregate was abandoned, and the final method of obtaining high strength LWSCC was examined. A plot showing the effects of aggregate moisture content error on  $f'_c$  for the partial limestone mixtures is presented Appendix C along with plots that separate these values by cementitious material content. These plots also indicate that the moisture content errors were not the cause of difficulties in obtaining adequate compressive strength using limestone replacement of lightweight coarse aggregate.

#### 4.3.1.4 Type III Cement Mixtures

The final method examined in pursuit of the high strength LWSCC required for the project involved the use of Type III cement. This type of cement is utilized in many precast applications due to its rapid strength gain. The incorporation of Type III cement in SCC can also improve the fresh concrete properties due to the fine particles available for increased viscosity (Do 2007). The mix proportions examined in this series of trial batches are presented in Table 4.14 and the corresponding concrete properties are presented in Table 4.15.

Table 4.14: HSC Trial Batches Using Type III Cement

Batch	Type III Cement (lb/yd <sup>3</sup> )	Fly Ash (lb/yd <sup>3</sup> )	Coarse Agg. (lb/yd <sup>3</sup> )	Fine Agg. (lb/yd <sup>3</sup> )	Water (lb/yd <sup>3</sup> )	HRWR (oz/cwt)	w/c	s/agg
72	950	0	649	1303	329	11.0	0.35	0.49
73	808	142	630	1331	314	13.0	0.33	0.50
74	808	142	630	1235	351	7.0	0.37	0.49
75	825	0	649	1407	329	8.0	0.40	0.51
76	808	142	630	1235	351	9.0	0.37	0.49
77	808	142	649	1196	351	8.0	0.37	0.47
78	808	142	630	1282	333	9.0	0.35	0.49
79	808	142	649	1242	333	10.0	0.35	0.48
80	808	142	649	1242	333	9.0	0.35	0.48
81	808	142	649	1242	333	11.0	0.35	0.48

Note: 1 lb = 0.454 kg, 1 oz = 29.57 mL, 1 yd<sup>3</sup> = 0.765 m<sup>3</sup>

Table 4.15: Concrete Properties of HSC Batches Using Type III Cement

Batch	Slump Flow (in.)	$T_{20}$ (sec)	VSI	J-Ring Flow (in.)	J-Ring $\Delta$ (in.)	J-Ring $\Delta h$ (in.)	Unit Weight (lb/ft <sup>3</sup> )	$f'_{ci}$ (psi)	$f'_c$ (psi)
72	24.0	16.4	0.0	20.0	4.0	2.00	120.7	6100	7340
73	23.5	15.8	0.0	16.0	7.5	2.75	124.3	6350	7060
74	21.5	4.0	0.0	18.5	3.0	1.50	120.8	5810	7000
75	25.0	7.6	0.0	18.5	6.5	3.00	123.0	6160	6630
76	22.0	5.4	0.0	18.0	4.0	2.00	121.1	5930	7240
77	24.0	4.6	0.0	18.5	5.5	2.50	121.1	5540	6690
78	24.0	3.8	0.0	19.0	5.0	2.00	122.9	6120	7210
79	27.0	5.2	0.5	20.0	7.0	1.50	122.7	6330	7580
80	21.5	4.2	0.0	16.0	5.5	3.50	121.7	5490	6990
81	26.5	3.8	0.5	21.5	5.0	1.75	122.0	5980	7400

Note: 1 in. = 25.4 mm, 1 psi = 0.006895 MPa, 1 lb = 0.454 kg, 1 ft<sup>3</sup> = 0.0283 m<sup>3</sup>

The first mixture using Type III cement, batch 72, was again based on the coarse aggregate and water contents used for the NSC beams with the cement content increased to 950 lb/yd<sup>3</sup> (565 kg/m<sup>3</sup>). This mixture reached the required compressive strength at one day of age, but was very viscous, as shown by a very high  $T_{20}$ , and exhibited blockage in the J-Ring test. This was due to the extremely small particle size and resulting high surface area of the Type III cement. The successful use of SCC mixtures combining fly ash with Type III cement was documented by previous research (Do 2007, Khayat 2009) and fly ash was utilized at a rate of 15 percent by weight of cement for all subsequent batches except batch 75. Batch 75 was mixed to investigate whether a higher cementitious material content was actually necessary when using Type III cement. This mixture showed did meet the requirement for  $f'_{ci}$ , but exhibited significant blockage in the J-Ring test.

Batch 73 was the first to include fly ash and the  $w/c$  was reduced slightly to offset the slow strength gain of fly ash. The coarse aggregate content was also reduced from that of batch 72 to 630 lb/yd<sup>3</sup> (374 kg/m<sup>3</sup>). This mixture was also very viscous and blockage was observed in the J-Ring test, but it did have a compressive strength in excess of the required minimum. The

$w/c$  was therefore increased to 0.37 for batches 74 and 76 to improve the workability of the mixture. These batches had slump flows and compressive strengths slightly lower than desired, but the stability and viscosity indicated the potential of this mixture. The aggregate content was increased back to 649 lb/yd<sup>3</sup> (385 kg/m<sup>3</sup>) for batch 77 in an effort to reduce the unit weight of the mixture slightly and to improve the flowability. This mixture exhibited greater blockage potential and had a lower  $f'_{ci}$ . The  $w/c$  was reduced back to 0.35 for batches 78 through 81 to improve compressive strength. A coarse aggregate content of 630 lb/yd<sup>3</sup> (374 kg/m<sup>3</sup>) was used for batch 78 in order to have a  $s/agg$  of 0.49 while 649 lb/yd<sup>3</sup> (385 kg/m<sup>3</sup>) was used for batches 79-81 in consideration of the concrete unit weight. The final HSC mix design chosen for use in casting beam specimens for transfer and development length testing was that used for batches 79-81. A slump flow of this mixture is shown in Figure 4.10. A discrepancy between J-Ring  $\Delta$  and  $\Delta h$  similar to those observed previously was observed between batches 74 and 79.



Figure 4.10: Slump flow of final HSC mixture

The effect of moisture content error on  $f'_{ci}$  for the HSC mixtures incorporating Type III cement separated by  $w/c$  is shown in Figure 4.11. The limited data points again indicated that small variations (less than 2 percent in this case) in moisture content of the lightweight aggregate do not have a major effect on  $f'_{ci}$ . The extremely high reactivity of Type III cement combined with the limiting effects of the lightweight aggregate strength most likely compensated for any small effects caused by excess water in the mixture. The same is true for the effects of moisture content error on  $f'_c$  for each  $w/c$  shown in Figure 4.12 and for the plots separating the data by cementitious material content presented in Appendix C.

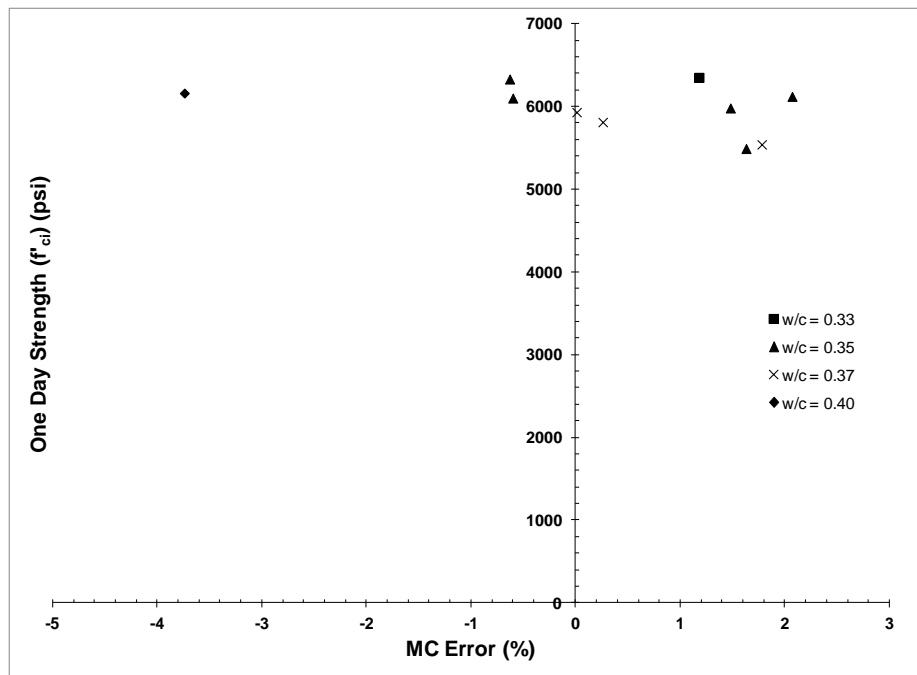


Figure 4.11: Effect of aggregate moisture content error on Type III cement HSC  $f'_{ci}$

### 4.3.2 High Strength Shale (HSS) Mixtures

The different high strength mixtures tested using expanded shale are presented in Table 4.16 and the corresponding concrete properties in Table 4.17. The first HSS mixture, batch 82, was based directly on the final high strength clay (HSC) mixture. The same proportions were used with a volume of expanded shale coarse aggregate equal to that of the expanded clay in the

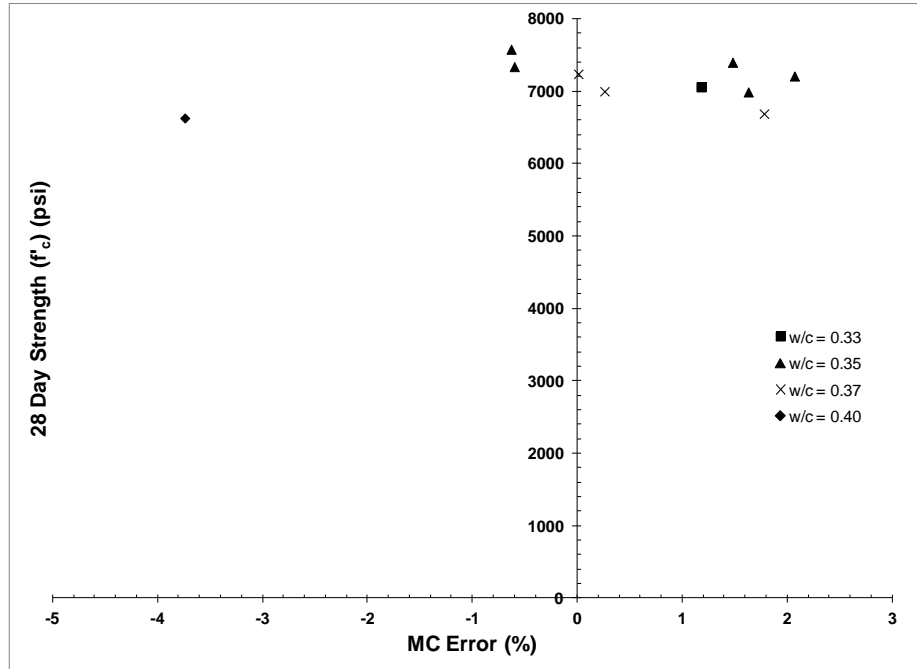


Figure 4.12: Effect of aggregate moisture content error on Type III cement HSC  $f'_c$

Table 4.16: HSS Trial Batches

Batch	Type III Cement (lb/yd <sup>3</sup> )	Fly Ash (lb/yd <sup>3</sup> )	Coarse Agg. (lb/yd <sup>3</sup> )	Fine Agg. (lb/yd <sup>3</sup> )	Water (lb/yd <sup>3</sup> )	HRWR (oz/cwt)	w/c	s/agg
82	808	142	732	1243	333	8.0	0.35	0.48
83	808	142	703	1296	333	9.0	0.35	0.50
84	808	142	703	1296	333	10.0	0.35	0.50
85	832	147	703	1270	333	13.0	0.34	0.49

Note: 1 lb = 0.454 kg, 1 oz = 29.57 mL, 1 yd<sup>3</sup> = 0.765 m<sup>3</sup>

Table 4.17: Concrete Properties of HSS Batches

Batch	Slump Flow (in.)	$T_{20}$ (sec)	VSI	J-Ring Flow (in.)	J-Ring $\Delta$ (in.)	J-Ring $\Delta h$ (in.)	Unit Weight (lb/ft <sup>3</sup> )	$f'_{ci}$ (psi)	$f'_c$ (psi)
82	22.5	4.4	0.0	19.5	3.0	2.00	119.9	5340	6790
83	22.5	6.4	0.5	21.0	1.5	2.00	121.9	5930	7370
84	24.5	5.2	0.0	22.0	2.5	1.50	122.0	5890	7640
85	25.0	4.8	0.0	22.5	2.5	1.50	124.5	6270	7730

Note: 1 in. = 25.4 mm, 1 psi = 0.006895 MPa, 1 lb = 0.454 kg, 1 ft<sup>3</sup> = 0.0283 m<sup>3</sup>

HSC mixture. This mixture had a low slump flow, the J-Ring test indicated some blockage potential, and the mixture did not reach the required  $f'_{ci}$ . The  $s/agg$  was increased to 0.50 for batches 83 and 84 in order to increase slump flow and decrease blockage, results that had been



observed in previous testing. A higher superplasticizer dosage was used for batch 84 than for 83 which resulted in adequate fresh properties. The compressive strength was still slightly less than the required 6000 psi (41 MPa), so the total cementitious material content was increased to 979 lb/yd<sup>3</sup> (581 kg/m<sup>3</sup>) with the same 15 percent replacement of cement with fly ash. This mixture produced adequate fresh concrete properties and compressive strength, and was chosen for use in casting the HSS beams. A slump flow of the final mixture is shown in Figure 4.13.

All of the HSS mix designs tested were very similar to the final HSC mixture. The corresponding relationships between moisture content error and compressive strength show very similar results to those obtained from the Type III cement HSC mixtures. The plot of the effects of moisture content error on  $f'_{ci}$  for each  $w/c$  is presented in Figure 4.14. Those for  $f'_c$  and those separated by cementitious material content are shown in Appendix C. As with the previous HS mixtures, the limited data indicated that small variations in aggregate moisture content did not have a significant effect on compressive strength at one or 28 days.



Figure 4.13: Slump flow of final HSS mixture

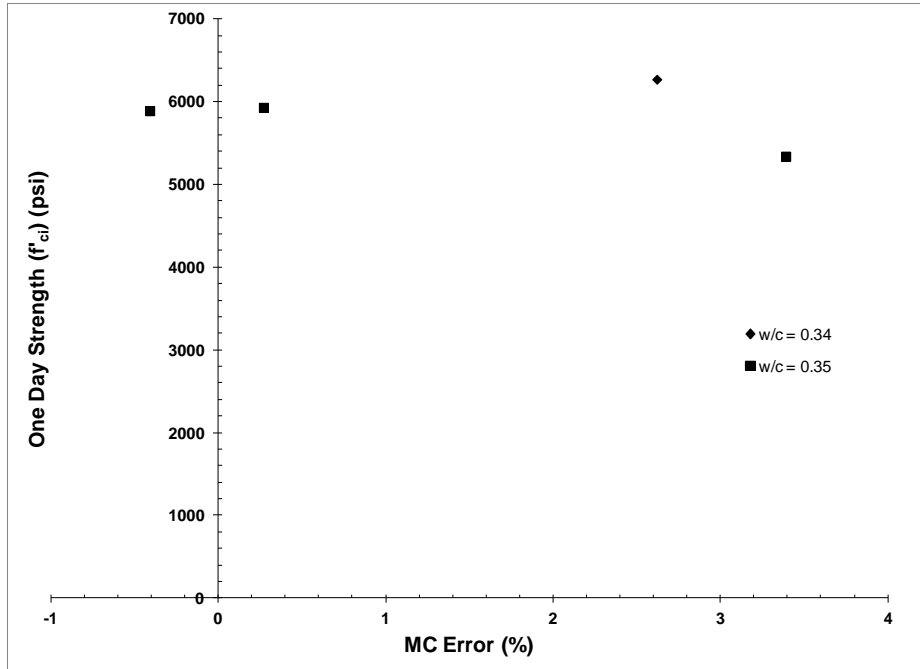


Figure 4.14: Effect of aggregate moisture content error on Type III cement HSS  $f'_{ci}$

### 4.3.3 High Strength Limestone (HSL) Mixtures

The normal weight high strength SCC mixture was proportioned using lessons learned from developing the normal strength limestone (NSL) mixture. The different proportions that were tested are presented in Table 4.18 and the corresponding concrete properties in Table 4.19. The compressive strength at 28 days was not measured for these trial batches since time was a constraint and only the strength at one day was of concern. It was known that the later age compressive strength would be more than adequate if it reached 6000 psi (41 MPa) at one day. The cement content was held constant at 825 lb/yd<sup>3</sup> (490 kg/m<sup>3</sup>) for all of the batches. The  $s/agg$  was set at 0.52 for the first batch and 0.51 for the subsequent batches based on previous observation of the effects of  $s/agg$  on stability and flow of SCC mixtures. A  $w/c$  of 0.35 was used for the first batch, 86, to ensure a high compressive strength. When  $f'_{ci}$  for this mixture significantly exceeded the 6000 psi (41 MPa) requirement, the  $w/c$  was increased to 0.40 for batch 87 and to 0.42 for batch 88. It was determined that 0.40 was the best  $w/c$  for the

Table 4.18: HSL Trial Batches

Batch	Cement (lb/yd <sup>3</sup> )	Coarse Agg. (lb/yd <sup>3</sup> )	Fine Agg. (lb/yd <sup>3</sup> )	Water (lb/yd <sup>3</sup> )	HRWR (oz/cwt)	w/c	s/agg
86	825	1415	1488	289	11.0	0.35	0.52
87	825	1392	1403	330	5.0	0.40	0.51
88	825	1369	1382	347	6.0	0.42	0.51
89	825	1392	1403	330	8.0	0.40	0.51

Note: 1 lb = 0.454 kg, 1 oz = 29.57 mL, 1 yd<sup>3</sup> = 0.765 m<sup>3</sup>

Table 4.19: Concrete Properties of HSL Batches

Batch	Slump Flow (in.)	T <sub>20</sub> (sec)	VSI	J-Ring Flow (in.)	J-Ring Δ (in.)	J-Ring Δh (in.)	Unit Weight (lb/ft <sup>3</sup> )	f <sub>ci</sub> (psi)	f <sub>c</sub> (psi)
86	26.0	2.8	0.5	23.0	3.0	1.25	149.4	7150	--
87	20.5	4.6	0.0	18.0	2.5	2.50	148.9	6360	--
88	24.5	2.6	0.5	23.0	1.5	1.75	148.2	5620	--
89	20.5	5.0	0.0	16.0	4.5	2.00	149.6	6900	--

Note: 1 in. = 25.4 mm, 1 psi = 0.006895 MPa, 1 lb = 0.454 kg, 1 ft<sup>3</sup> = 0.0283 m<sup>3</sup>, -- indicates no measurements were taken

combination of fresh concrete properties and compressive strength and so the mixture used for batches 87 and 89 was chosen for use in the normal weight SCC control beams.

#### 4.3.4 Summary

The major issue encountered in developing the high strength (HS) mixtures was achieving an adequate compressive strength at one day of age. Fresh concrete property specifications were easily met, but the high early strength requirement caused significant difficulty. The reactivity of the cementitious material was the most critical variable in obtaining the required compressive strength. The use of silica fume or Type III cement provided a substantial increase in compressive strength. The detrimental effects of these materials on the concrete workability required some adjustment of the other mixture components in order to achieve a balance of fresh concrete properties and compressive strength. It was therefore determined that the most effective method for obtaining high-strength LWSCC involved the use of Type III cement and an incorporation of fly ash into the mixture. This allowed for utilization

of the high reactivity of the Type III cement while still having the workability provided by the particle shape of the fly ash. The required superplasticizer dosage was still at, or greater than, the maximum recommended dosage for the HSC and HSS mixtures. The final mix designs chosen for casting the HS series transfer and development length specimens are presented in Table 4.20 along with the ranges of concrete properties measured during beam casting. Some of the differences in concrete properties were caused by differences in temperature of up to 17° F between casting days. The final HSC or HSS mixtures did not meet the targeted compressive strength of 8000 psi (55 MPa) at 28 days, most likely due to the strength of the lightweight aggregates, and 7000 psi was the expected value for the beams cast with these mixtures.

Table 4.20: Final HS Mix Designs

Material	HSC	HSS	HSL
Cement (lb/yd <sup>3</sup> )	808*	832*	825
Fly Ash (lb/yd <sup>3</sup> )	142	147	0
Coarse Agg. (lb/yd <sup>3</sup> )	649	703	1392
Fine Agg. (lb/yd <sup>3</sup> )	1242	1270	1403
Water (lb/yd <sup>3</sup> )	333	333	330
HRWR (oz/cwt)	10.0 – 14.0	10.0 – 11.0	6.0
w/cm	0.35	0.34	0.4
s/agg	0.48	0.49	0.51
Slump Flow (in.)	25.5 – 29.0	26.0 – 30.5	26.0 – 28.0
T <sub>20</sub> (sec)	5.0 – 11.2	1.4 – 4.8	2.0 – 2.8
J-Ring Δh (in.)	1.00 – 2.00	0.50 – 1.75	0.50 – 1.00
f' <sub>ci</sub> (psi)	5700 – 6500	4730 – 6930	6830 – 7020
f' <sub>c</sub> (psi)	6660 – 7920	5840 – 8060	8910 – 10790

Note: \*indicates Type III cement, 1 lb = 0.454 kg, 1 oz = 29.57 mL, 1 yd<sup>3</sup> = 0.765 m<sup>3</sup>, 1 in. = 25.4 mm, 1 psi = 0.006895 MPa, 1 lb = 0.454 kg, 1 ft<sup>3</sup> = 0.0283 m<sup>3</sup>

## 4.4 Beam Batches

### 4.4.1 Test Beam

A test beam was produced using the normal strength clay (NSC) mixture in order to examine the actual flow and consolidation properties of the concrete. The mixture exhibited excellent fresh concrete properties as shown in Table 4.21. This beam showed adequate

consolidation and confirmed that the mixture was ready for use in casting the remaining beam specimens. The  $f'_{ci}$  was somewhat below the required 4000 psi (28 MPa), the cause of which is unknown. The actual aggregate moisture content was 2.5 percent greater than that assumed for the mixing water adjustment, so there was more water than expected in the mix. An error of this magnitude did not typically produce a large effect on compressive strength, as was discussed in Section 4.1.2. This batch also confirmed that larger batches of LWSCC could be easily mixed using the available equipment.

#### 4.4.2 Normal Strength Clay (NSC) Beams

The properties of each of the eight batches required to cast the four NSC beams are presented in Table 4.21. The J-Ring test indicated that some blockage potential existed for the two batches used to cast beam NSC-1, but the beam exhibited adequate consolidation. The unit weight for these two batches was also below the average for this beam set, the cause of which was not determined. Batch NSC-2b had a compressive strength substantially higher than that of the rest of the beams in this set both at prestress release and at 28-days. Batches NSC-3a and NSC-4a both had a compressive strength slightly below the 4000 psi (28 MPa) requirement, and only the batches for NSC-2 and batch NSC-4b met the desired 6000 psi (41 MPa) compressive

Table 4.21: Concrete Properties of NSC Beam Batches

Beam	Slump Flow (in.)	T <sub>20</sub> (sec)	VSI	J-Ring Flow (in.)	J-Ring $\Delta$ (in.)	J-Ring $\Delta h$ (in.)	Unit Weight (lb/ft <sup>3</sup> )	$f'_{ci}$ (psi)	$f'_c$ (psi)
Test	28.0	3.8	0.5	27.0	1.0	1.50	115.7	3050	5240
NSC-1	27.0	5.4	0.0	23.0	4.0	2.25	115.2	4010	4910
	26.0	5.0	0.0	24.5	1.5	1.75	114.0	4190	5160
NSC-2	26.5	4.0	0.0	24.0	2.5	1.25	119.4	4630	6140
	27.5	4.6	0.5	23.5	4.0	1.75	119.6	5680	7250
NSC-3	28.0	3.4	0.5	25.5	2.5	1.50	116.4	3810	5200
	27.0	3.4	0.0	22.0	5.0	2.00	116.4	4230	5240
NSC-4	26.0	4.4	0.0	24.5	1.5	1.50	116.2	3960	5430
	25.0	4.4	0.0	24.5	0.5	1.25	119.9	4870	6170

Note: 1 in. = 25.4 mm, 1 psi = 0.006895 MPa, 1 lb = 0.454 kg, 1 ft<sup>3</sup> = 0.0283 m<sup>3</sup>

strength at 28 days. Overall, the fresh properties and early age compressive strength of this mix design were within the specified requirements given a few exceptions. The J-Ring test did show some potential for blockage issues, but adequate consolidation was observed for all beams.

#### 4.4.3 Normal Strength Shale (NSS) Beams

An extra beam was cast with the NSS series due to an opportunity produced during collaboration with another project. Space for casting an extra beam was available and the beam was cast to avoid wasting that portion of the prestressing strand. This beam provided an excellent test opportunity for the NSS mixture just as the test beam did for the NSC mixture. The mix design utilized in casting this beam is shown in Table 4.22 and the concrete properties for this and the remaining NSS beams are presented in Table 4.23. The test mixture had a  $T_{20}$  that was higher than desired and showed some potential for bleeding and segregation. This was

Table 4.22: Mix Design for Beam NSS-1

Beam	Cement (lb/yd <sup>3</sup> )	Coarse Agg. (lb/yd <sup>3</sup> )	Fine Agg. (lb/yd <sup>3</sup> )	Water (lb/yd <sup>3</sup> )	HRWR (oz/cwt)	w/c	s/agg
NSS-1	850	764	1408	298	6.0	0.35	0.50

Note: 1 lb = 0.454 kg, 1 oz = 29.57 mL, 1 yd<sup>3</sup> = 0.765 m<sup>3</sup>

Table 4.23: Concrete Properties of NSS Beam Batches

Beam	Slump Flow (in.)	$T_{20}$ (sec)	VSI	J-Ring Flow (in.)	J-Ring $\Delta$ (in.)	J-Ring $\Delta h$ (in.)	Unit Weight (lb/ft <sup>3</sup> )	$f'_{ci}$ (psi)	$f'_c$ (psi)
NSS-1	27.0	7.0	2.0	25.5	1.5	--	120.3	3300	4790
	24.0	8.0	0.5	22.0	2.0	1.75	118.0	3500	5200
NSS-2	27.5	4.4	0.5	24.5	3.0	2.00	116.4	4270	5760
	26	6.2	0.0	22.0	4.0	2.25	119.4	4240	6460
NSS-3	26	6.4	1.0	23.5	2.5	2.00	116.6	4350	6250
	26	6.2	1.0	25.0	1.0	2.00	116.9	4550	6220
NSS-4	26.5	3.6	0.5	22.5	4.0	1.75	122.3	4190	7110
	27	5.4	1.5	25.0	2.0	1.50	117.5	4200	6280
NSS-5	28.5	2.4	1.5	24.5	4.0	1.50	119.6	4180	6740
	29.5	2.0	1.0	27.0	2.5	1.25	120.3	3730	6350

Note: 1 in. = 25.4 mm, 1 psi = 0.006895 MPa, 1 lb = 0.454 kg, 1 ft<sup>3</sup> = 0.0283 m<sup>3</sup>, -- indicates measurement taken incorrectly

evident in the appearance of a white film on the top of the finished beam that was a direct result of excess bleed water. The compressive strength of the batches used to cast this beam was also inadequate in regards to the targeted 4000 psi (28 MPa) at release. Some of the issues with this mixture were resolved by passing all expanded shale aggregate for subsequent beams over a ½ in. (12.7 mm) sieve and by increasing the  $s/agg$  to 0.51, which produced a more cohesive mixture.

Batch NSS-2b and both batches for beam NSS-3 had  $T_{20}$  values greater than the specified 2-5 seconds, and all batches except NSS-4b and those for NSS-5 had J-Ring  $\Delta h$  values greater than the 1.5 in. maximum, but all beams exhibited adequate consolidation externally. Discrepancies between J-Ring  $\Delta$  and  $\Delta h$  were also observed in the form of differences of 2 in. (50 mm) in  $\Delta$  for the same  $\Delta h$ . After adjustment to the mixture shown in Table 4.7, all batches except NSS-5b met the 4000 psi (28 MPa) requirement for  $f'_{ci}$  without any exceeding this value by a significant amount. All batches except NSS-2a met the targeted 6000 psi (41 MPa) 28-day compressive strength with that of NSS-4a exceeding this value by a significant amount. The concrete unit weight was less the desired 120 lb/ft<sup>3</sup> (1922 kg/m<sup>3</sup>) maximum for all but batch NSS-4a. Due to the highly flowable nature of this concrete, operator error in the unit weight test is very possible. The difficulty encountered in developing an adequate LWSCC mixture using expanded shale is evident in the slightly reduced compliance to the specified properties for this set of beams. Even with these issues, the beams still appeared adequately consolidated.

#### **4.4.4 Normal Strength Limestone (NSL) Beams**

The concrete properties of the batches used to cast the NSL beams are presented in Table 4.24. The extreme August temperatures made construction of these beams very difficult, as indicated by the poor properties of batch NSL-1a. An inadequate dose of superplasticizer was

added to this batch due to a lack of experience with this particular mixture. Variation in the compressive strength of the individual batches was also attributed to the temperature variation between casting days and the time of day that the beams were cast. Beams NSL-1 and NSL-2 were cast in the morning and NSL-3 and NSL-4 were cast in the afternoon. The longer exposure to the high daytime temperatures resulted in a higher  $f'_{ci}$  for the first two beams than for the second two. All batches except NSL-3b met the required 4000 psi (28 MPa) compressive strength at release, and that of this batch was within 50 psi (0.3 MPa). The time between lifts, extreme temperatures, and low slump flow for batch NSL-4b caused very poor consolidation for the dead end of beam NSL-4. The cylinders cast for testing  $f'_c$  for batch NSL-2b were tested at 14 days due to a communication error and the final three cylinders were used to test compressive strength at the time of flexural testing.

#### 4.4.5 High Strength Clay (HSC) Beams

The concrete properties of the batches used to cast the HSC beams are presented in Table 4.25. The nature of this mixture, with its high powder content including Type III cement and fly ash, allowed for high slump flows in spite of high  $T_{20}$  values. The mixture flowed somewhat slower than desired, which typically presents an opportunity for blockage of the mixture. All  $T_{20}$

Table 4.24: Concrete Properties of NSL Beam Batches

Beam	Slump Flow (in.)	$T_{20}$ (sec)	VSI	J-Ring Flow (in.)	J-Ring $\Delta$ (in.)	J-Ring $\Delta h$ (in.)	Unit Weight (lb/ft <sup>3</sup> )	$f'_{ci}$ (psi)	$f'_c$ (psi)
NSL-1	19.0	--	0.0	16.5	2.5	2.25	144.2	5260	6670
	25.5	2.4	0.5	24.0	1.5	1.00	145.0	5010	6750
NSL-2	26.5	2.8	1.0	24.5	2.0	1.75	146.8	5600	7970
	27.0	2.0	1.0	26.0	1.0	1.00	145.6	5360	--
NSL-3	26.5	3.2	1.0	24.0	2.5	1.50	146.7	4240	7840
	25.0	2.2	0.0	22.5	2.5	1.50	145.6	3960	7840
NSL-4	25.0	2.8	0.5	22.5	2.5	1.50	145.9	4110	7780
	23.5	2.6	0.0	20.5	3.0	2.00	145.6	4420	7930

Note: 1 in. = 25.4 mm, 1 psi = 0.006895 MPa, 1 lb = 0.454 kg, 1 ft<sup>3</sup> = 0.0283 m<sup>3</sup>, -- indicates that no measurements were taken



values were outside the specified range of 2-5 seconds. All but batches HSC-1a, HSC-1b, and HSC-4a had adequate behavior measured by the J-Ring test, however. The mixture exhibited adequate flowability during placement in the formwork and all beams displayed satisfactory consolidation. Discrepancies between J-Ring  $\Delta$  and  $\Delta h$  were observed in the form of differences greater than 2 in. (50 mm) in  $\Delta$  for the same  $\Delta h$ . The unit weight measured for these batches was somewhat higher than that measured for the NSC mixtures, which was expected. The cause of the overly high unit weight of batch HSC-2b again may be attributable to operator error. All batches except HSC-1a and HSC-2b met the required 6000 psi (41 MPa)  $f'_{ci}$ , and these two batches were within 300 psi (2 MPa). Batches HSC-1a, HSC-3a, and HSC-3b did not meet the expected 7000 psi (48 MPa)  $f'_c$ , but were within 350 psi (2.4 MPa).

Table 4.25: Concrete Properties of HSC Beam Batches

Beam	Slump Flow (in.)	$T_{20}$ (sec)	VSI	J-Ring Flow (in.)	J-Ring $\Delta$ (in.)	J-Ring $\Delta h$ (in.)	Unit Weight (lb/ft <sup>3</sup> )	$f'_{ci}$ (psi)	$f'_c$ (psi)
HSC-1	27	11.2	0.5	25.0	2.0	2.00	121.6	5890	6670
	29	5.8	1.0	24.5	4.5	2.00	120.0	6500	7660
HSC-2	27	7.8	0.0	26.0	1.0	1.50	121.4	5700	7150
	28	6.4	0.5	27.5	0.5	1.00	126.4	6210	7920
HSC-3	25.5	5.8	0.0	22.5	3.0	1.50	120.7	6480	6760
	25.5	8.8	0.5	25.0	0.5	1.00	120.2	6340	6660
HSC-4	26	6.0	0.5	22.5	3.5	1.75	117.9	6480	7040
	25.5	6.8	0.5	23.5	2.0	1.50	122.4	6070	7120

Note: 1 in. = 25.4 mm, 1 psi = 0.006895 MPa, 1 lb = 0.454 kg, 1 ft<sup>3</sup> = 0.0283 m<sup>3</sup>

#### 4.4.6 High Strength Shale (HSS) Beams

Concrete properties for the batches used to cast the HSS beams are presented in Table 4.26. Beams HSS-1 and HSS-2 were cast using four 7.0 ft<sup>3</sup> (0.20 m<sup>3</sup>) batches while beams HSS-3 and HSS-4 were cast from the same 28.0 ft<sup>3</sup> (0.79 m<sup>3</sup>) batch mixed in a 1.5 yd<sup>3</sup> (1.15 m<sup>3</sup>) mixer instead of the 12.5 ft<sup>3</sup> (0.35 m<sup>3</sup>) mixer used previously. Samples were taken from the middle of the portion of the batch used for each of beams HSS-3 and HSS-4. The batches for beams HSS-

Table 4.26: Concrete Properties of HSS Beam Batches

Beam	Slump Flow (in.)	$T_{20}$ (sec)	VSI	J-Ring Flow (in.)	J-Ring $\Delta$ (in.)	J-Ring $\Delta h$ (in.)	Unit Weight (lb/ft <sup>3</sup> )	$f'_{ci}$ (psi)	$f'_c$ (psi)
HSS-1	30.5	3.6	1.0	30.5	0.0	0.50	117.6	5530	5960
	27	3.0	0.5	26.5	0.5	0.75	120.9	6610	7210
HSS-2	27	3.0	0.0	28.0	-1.0	0.75	120.0	6440	7000
	30	2.4	1.0	28.5	1.5	1.00	117.8	4730	5840
HSS-3	26	4.8	1.5	25.5	0.5	1.75	116.3	5530	8060
HSS-4	30	1.4	1.5	31.5	-1.5	0.50	123.0	6930	7000

Note: 1 in. = 25.4 mm, 1 psi = 0.006895 MPa, 1 lb = 0.454 kg, 1 ft<sup>3</sup> = 0.0283 m<sup>3</sup>

1 and HSS-2 exhibited adequate fresh concrete properties, with the J-Ring flow for HSS-2a and HSS-4 exceeding the slump flow for those samples. Batches HSS-1a and HSS-2b did not meet the requirements for  $f'_{ci}$  and  $f'_c$  in spite of the acceptable fresh concrete properties. The concrete used for both HSS-3 and HSS-4 showed some bleeding and potential for segregation. This was partially due to the fact that water was added to the mixer during batching due to inexperience with the mixer. It was thought that a large error in the moisture content of the coarse aggregate had been made and that this addition of water was necessary to produce the required fresh concrete properties. The  $w/cm$  of the mixture after this addition was 0.37 as opposed to the design 0.34. It did not appear to affect the overall compressive strength of the concrete even though  $f'_{ci}$  for HSS-3 was below the required 6000 psi (41 MPa). A discrepancy was noted between J-Ring  $\Delta$  and  $\Delta h$  in the form of a 0.75 in. (19 mm) greater  $\Delta h$  for a 1 in. (25 mm) smaller  $\Delta$ .

#### 4.4.7 High Strength Limestone (NSL) Beams

The concrete used to cast the HSL series of beams was also mixed using the 1.5 yd<sup>3</sup> (1.15 m<sup>3</sup>) concrete mixer and the properties of the samples taken from the middle of the portion used for each beam are presented in Table 4.27. The flowability and passing ability were excellent with the concrete from HSL-1 and HSL-3 having a J-Ring flow larger than the slump flow. The

Table 4.27: Concrete Properties of HSL Beam Batches

Beam	Slump Flow (in.)	$T_{20}$ (sec)	VSI	J-Ring Flow (in.)	J-Ring $\Delta$ (in.)	J-Ring $\Delta h$ (in.)	Unit Weight (lb/ft <sup>3</sup> )	$f'_{ci}$ (psi)	$f'_c$ (psi)
HSL-1	28.0	2.6	1.5	29.0	-1.0	0.50	147.0	6870	8850
HSL-2	26.0	2.0	0.5	25.0	1.0	1.00	147.2	7020	9150
HSL-3	26.5	2.8	1.0	27.5	-1.0	0.50	148.0	6920	9300
HSL-4	26.0	2.0	0.5	25.5	0.5	0.75	148.3	6830	9700

Note: 1 in. = 25.4 mm, 1 psi = 0.006895 MPa, 1 lb = 0.454 kg, 1 ft<sup>3</sup> = 0.0283 m<sup>3</sup>

first sample of concrete from each batch exhibited some bleeding, but all beams were well consolidated and had an excellent surface finish. The  $f'_{ci}$  values substantially exceeded the required 6000 psi (41 MPa) and the  $f'_{ci}$  of the lightweight mixtures. These high strengths were as expected for a normal weight concrete mixture with the high cement content required for acceptable SCC behavior. The values of  $f'_c$  were also much higher than those of the LWSCC mixtures, which was taken into consideration in the analysis of the transfer and development length test results.

#### 4.4.8 Modulus of Elasticity

The companion batches used for testing the modulus of elasticity for each concrete mixture had concrete properties that were representative of the batches used for casting each set of beam specimens. Fresh concrete properties and compressive strengths for each of the companion batches are presented in Table 4.28. A second batch was required corresponding to both the normal strength clay (NSC) and normal strength shale (NSS) specimens due to issues with the testing equipment or concrete properties. Problems with the testing equipment did not allow for static tests on the first NSC batch at one and seven days so only dynamic testing was performed on the end-ground cylinders.

The second NSC batch had a one day compressive strength substantially less than that of the batches used to cast the NSC beams. The one day compressive strength and unit weight

Table 4.28: Concrete Properties of Companion Batches for Modulus of Elasticity

Batch	Slump Flow (in.)	$T_{20}$ (sec)	VSI	J-Ring Flow (in.)	J-Ring $\Delta$ (in.)	J-Ring $\Delta h$ (in.)	Unit Weight (lb/ft <sup>3</sup> )	Air (%)	$f'_{ci}$ (psi)	$f'_c$ (psi)
NSCa	29.0	2.4	0.5	27.0	2.0	1.25	119.9	1.50	3820	5710
NSCb	25.5	4.2	0.5	24.0	1.5	1.50	119.6	--	3360	6290
NSSa	25.5	7.0	0.5	22.5	3.0	1.75	126.8	--	5860	7890
NSSb	26.0	5.8	1.0	21.0	5.0	2.00	124.4	1.25	4880	6810
NSL	23.0	4.2	0.0	21.0	2.0	2.00	150.0	--	4010	8640
HSC	24.0	5.0	0.5	18.5	5.5	2.00	122.4	2.00	6260	7290
HSS	24.0	3.6	0.0	23.5	0.5	1.75	115.8	1.50	5500	6300
HSL	23.0	3.6	0.5	22.5	0.5	1.50	148.8	1.6	7230	10830

Note: 1 in. = 25.4 mm, 1 psi = 0.006895 MPa, 1 lb = 0.454 kg, 1 ft<sup>3</sup> = 0.0283 m<sup>3</sup>

measured for the first NSS companion batch was significantly greater than that of the batches used to cast the NSS specimens. The second NSS companion batch also had a larger unit weight and compressive strength at one day, but the disparity was less pronounced. The slump flow values for the NSL, HSC, HSS, and HSL companion batches were less than those for the corresponding beam batches and did not meet the 25 in. (635 mm) target for SCC behavior. This inadequacy most likely had only slight effects on the casting of the cylinders and specimens used for modulus of elasticity testing.

The measured values for modulus of elasticity, based on an average of three specimens, at one day and 28 days of age are presented in Tables 4.29 and 4.30, respectively, along with the corresponding values calculated using the ACI equation (ACI 2011). Measurements at seven days of age are presented in Appendix A. The elastic moduli of the expanded clay and expanded shale mixtures were very similar for the same strength level and even between the NS and HS mixtures. A significant difference between limestone and lightweight mixtures was evident, with the LWSCC mixtures having a modulus approximately 30 percent less than the limestone mixtures at one day of age and approximately 30 to 40 percent less at 28 days.

Table 4.29: Measured Modulus of Elasticity at One Day of Age

Batch	Static (ksi)	Dynamic (ksi)		ACI (ksi)
		Longitudinal	Transverse	
NSCa	--	2710	--	2680
NSCb	2840	2210	2990	2500
NSSa	3440	4100	4040	3610
NSSb	3350	3990	4150	3200
NSL	4780	4830	4750	3840
HSC	3300	3950	3890	3540
HSS	3270	3940	3830	3050
HSL	4710	5790	5580	5090

Note: 1 psi = 0.006895 MPa

Table 4.30: Measured Modulus of Elasticity at 28 Days of Age

Batch	Static (ksi)	Dynamic (ksi)		ACI (ksi)
		Longitudinal	Transverse	
NSCa	3510	3500	--	3270
NSCb	3570	4000	3780	3420
NSSa	3870	4540	4110	4190
NSSb	3890	4670	4370	3780
NSL	6110	6090	5800	5640
HSC	3820	3810	3230	3820
HSS	2940	4040	3840	3260
HSL	5430	6270	5870	6230

Note: 1 psi = 0.006895 MPa

The fresh concrete unit weight was used in the calculation of modulus of elasticity since tests were run only out to 28 days of age, and equilibrium unit weight was not reached by this age. The ACI equation produced an inconsistent prediction of the static modulus of elasticity, sometimes overestimating and sometimes underestimating the measured values. Calculated moduli of elasticity for the LWSCC mixtures were within 350 ksi (2410 MPa) of the measured values at both one and 28 days. The NSL modulus differed by approximately 900 ksi (6200 MPa) at one day and 450 ksi (3100 MPa) at 28 days with the measured values having a larger magnitude. The calculated HSL modulus was 800 ksi (5520 MPa) greater than the measured value at 28 days. Due to the variation of compressive strength between the mixtures used to cast the beam specimens, the small number of tests, and the relative agreement between the ACI

equation and the measured modulus of elasticity for the LWSCC mixtures, the ACI equation values were used in all calculations requiring modulus of elasticity.

The modulus of elasticity values measured using dynamic methods typically exceeded those measured using static methods and those calculated using the ACI equation. The values measured using a longitudinal excitation also typically exceeded those measured using a transverse excitation. The two values were within 220 ksi (1520 MPa) at one day of age for all but the NSC mixture while the difference was between 220 and 600 ksi (1520 and 4140 MPa) at 28 days. Even with these disparities, the dynamic measurements exhibited potential as a fast assessment of the stiffness of these different mixtures. The limited number of collected data points did not allow for a precise correlation between the static and dynamic methods.

#### **4.4.9 Summary**

The concrete mixtures utilized to cast the 25 beam specimens used for transfer and development length testing were developed specifically for that purpose. Concrete properties of the individual batches had some variation from the desired specifications, but the concrete performed satisfactorily. The substantial effects of external factors such as temperature on the concrete properties were outside the control of the researchers. The effect of error in estimating the moisture content of each lightweight aggregate on  $f'_{ci}$  is shown in Figure 4.15 and the effect on  $f'_c$  is shown in Figure 4.16. As was indicated by the results of the trial batches, these plots provide no indication moisture content estimation errors less than 3 percent in magnitude had any significant effect on the compressive strength of the beam batches at one or 28 days.

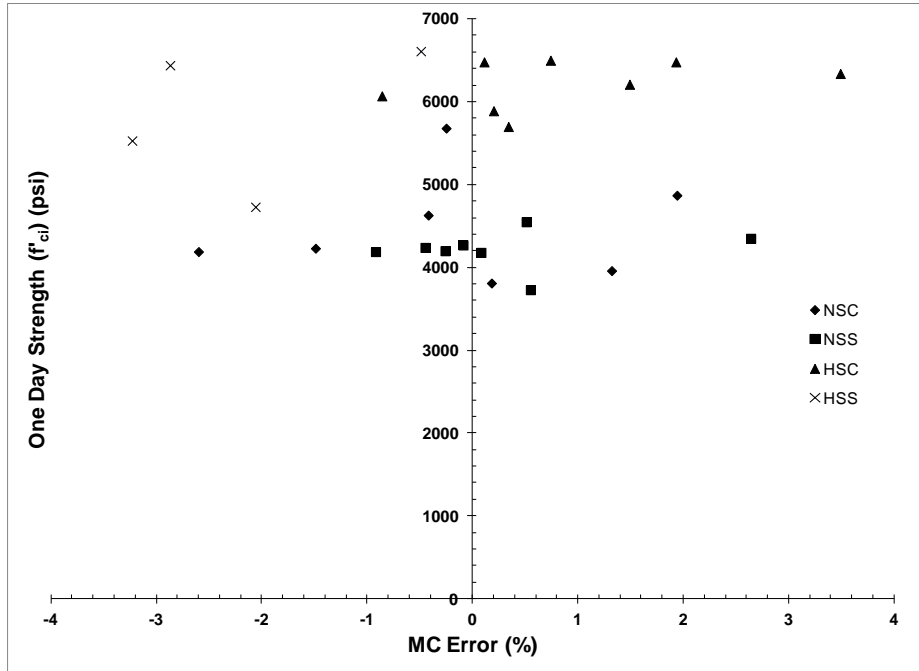


Figure 4.15 Effect of moisture content error on  $f'_{ci}$  of beam batches

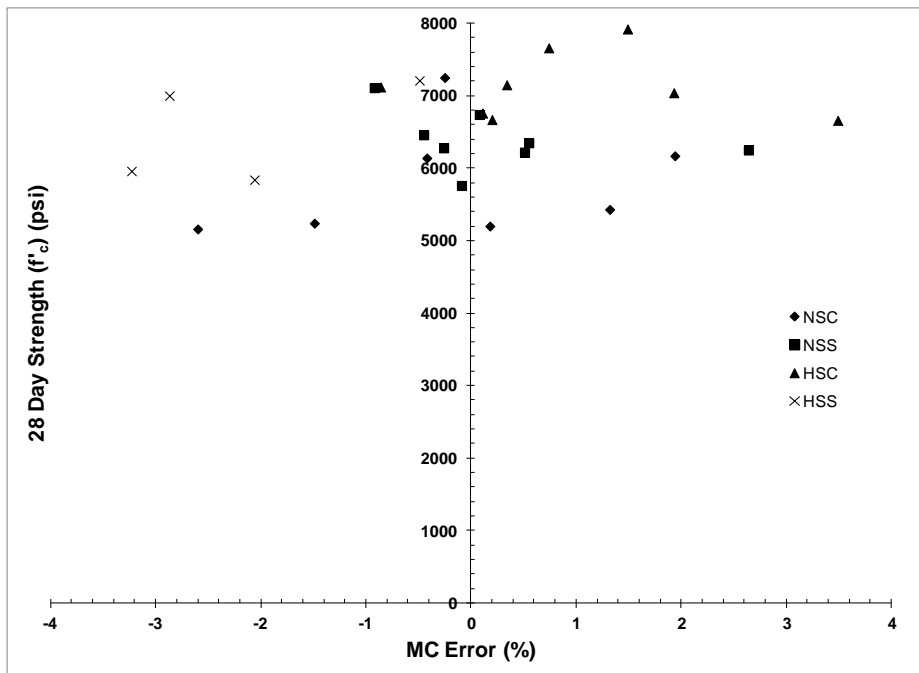


Figure 4.16 Effect of moisture content error on  $f'_c$  of beam batches

## Chapter 5: Transfer Length Results

### 5.1 Introduction

The main focus of this research project was to examine the bond behavior of 0.6 in. (15.2 mm) prestressing strand. One of the characteristics used to quantify prestress bond behavior is the transfer length. This chapter describes the results of transfer length measurements made on the 25 prestressed concrete beams described in Section 3.8 using the concrete mixtures described in Chapter 4. Transfer lengths determined using concrete surface strains measured with the DEMEC system are presented first followed by those determined using end slip measurements. These values were then compared to predictions made by the equations provided in accepted codes as well as by previous research.

### 5.2 DEMEC Transfer Lengths

Surface strain measurements were taken using the method described in Section 3.8.3. The transfer lengths determined using these measurements and the 95% Average Maximum Strain (AMS) method are discussed in this section. The surface strains from each side of a given beam were combined to produce a mean transfer length value for both the live and dead ends of each beam. The beams produced with lightweight self-consolidating concrete (LWSCC) exhibited much more erratic strain behavior than did the beams cast using normal weight self-consolidating concrete (NWSCC). This behavior was most likely due to cracking in the LWSCC members caused by a smaller tensile strength combined with high release stresses and by a smaller aggregate stiffness. Some of the earliest measurements were very difficult to resolve and interpret. The lack of a clear strain plateau for these and some of the other specimens made determination of an accurate transfer length very difficult. The strain profiles are presented in SI units since the DEMEC gage was calibrated to work in these units and the gage length basis was



exactly 200 mm (8 in.). Strain profiles at 28 days are presented in this chapter and those at other time increments are presented in Appendix D.

### 5.2.1 Normal Strength Clay (NSC) Beams

The first beams cast were those using the normal strength clay (NSC) mixture. Several difficulties were experienced in regards to using the DEMEC system and taking the concrete surface strain measurements. Problems with the epoxy used to attach the gage points combined with high ambient temperatures at the time of placement caused some of the points to detach from the beams during measurements after release and over time. Some gage points also may have been slightly loose introducing more error into the measurements and contributing to the erratic behavior that was observed. The redundant measurements from points of both sides of each specimen compensated for most of these errors in the final strain profile.

#### 5.2.1.1 NSC-1

Several DEMEC points were lost on the south side of specimen NSC-1, which had the longest exposure to direct sunlight. The loss of these points complicated determination of the transfer length. Only the north side measurements were used for the average strain profile in the areas where no measurements were available on the south side and where only a single data point was available on the south side. This led to a very erratic strain profile, as the north side strain measurements were significantly larger in magnitude. The very large magnitude of the north side live end strain measurements may have also skewed the transfer length that would have been tempered by the more moderate measurements of the south side. Strain plateaus with a slight downward trend were evident for all profiles that had adequate data to make an accurate observation. The south side live end was missing most of the DEMEC points in the area of the strain plateau whereas the south side dead end had points missing in the area of the initial slope.

The average 28-day strain profile presented in Figure 5.1 shows live end strain values that were substantially larger in magnitude than those of the other beam specimens, were significantly larger than the dead end strains for this specimen, and were larger than the strains measured at the beam midpoint. The live end profile also had an unusual peak and downward slope after a long initial slope.

The measured transfer lengths for each time increment are presented in Table 5.1. The live end transfer length remained fairly consistent over time with an increase of approximately 1 in. (25 mm) between prestress release and 28 days. The dead end transfer length had a decreasing trend over time with a net shortening of approximately 3 in. (75 mm) between prestress release and 28 days. The measured transfer lengths at 28 days compared to the values calculated using the various prediction equations described in Chapter 2 are shown in Table 5.2.

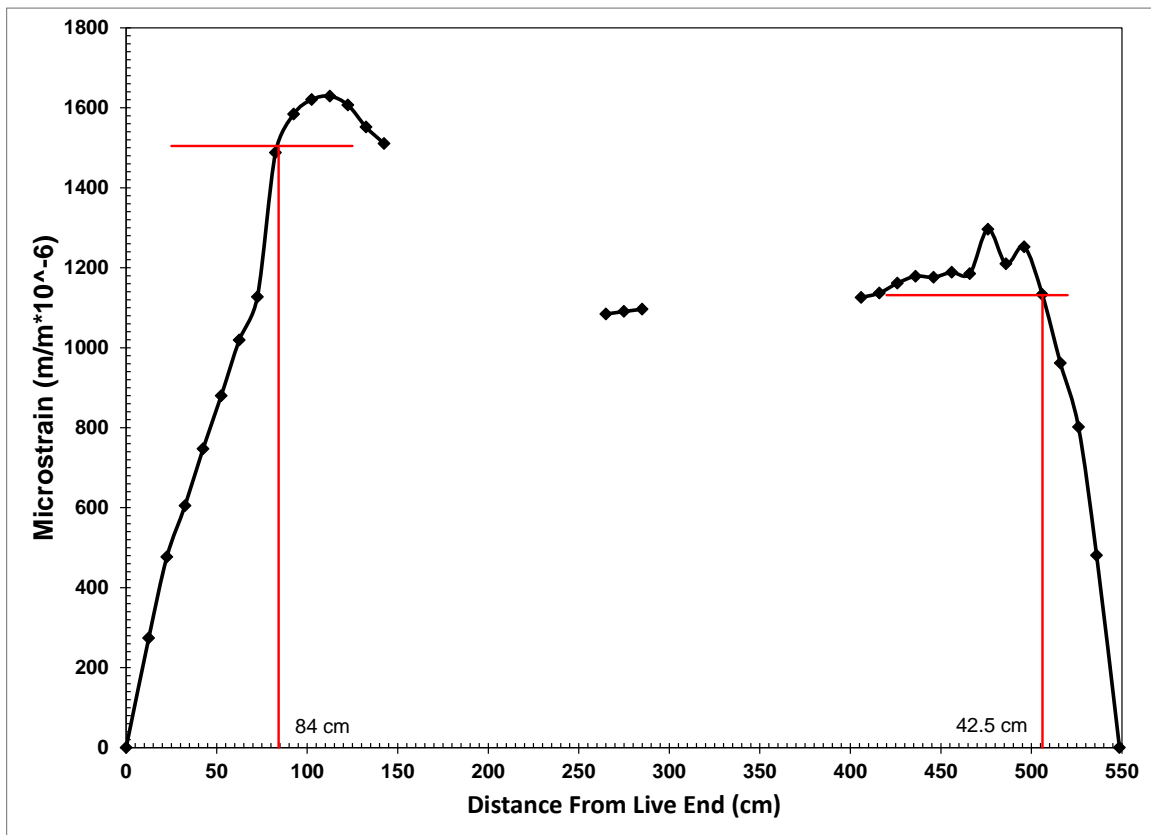


Figure 5.1: 28-Day strain profile with 95% AMS for specimen NSC-1

Table 5.1: NSC Transfer Length Measurements Over Time

End	Live (in.)				Dead (in.)			
	NSC-1	NSC-2	NSC-3	NSC-4	NSC-1	NSC-2	NSC-3	NSC-4
Release	32.1	19.7	28.3	21.3	19.5	27.2	20.5	19.5
3-Day	33.9	22.2	--	--	19.7	27.2	--	--
5-Day	33.3	22.0	31.1	22.8	18.3	26.8	21.7	29.3
7-Day	33.1	21.5	30.7	23.0	17.9	26.6	23.4	28.3
14-Day	32.7	22.0	31.5	23.0	17.3	27.0	20.3	26.8
28-Day	33.1	22.2	31.3	23.2	16.7	25.6	19.7	28.3

Note: 1 in. = 25.4 mm, -- indicates no measurement

Table 5.2: Comparison of NSC Transfer Length Predictions at 28 Days

Specimen	NSC-1	NSC-2	NSC-3	NSC-4
Measured (Live) (in.)	33.1	22.2	31.3	23.2
Measured (Dead) (in.)	16.7	25.6	19.7	28.3
ACI 318/AASHTO LRFD (in.)	30.6	32.0	30.4	31.0
ACI (50d <sub>b</sub> ) (in.)	30.0	30.0	30.0	30.0
AASHTO (60d <sub>b</sub> ) (in.)	36.0	36.0	36.0	36.0
Zia and Mostafa (in.)	35.5	30.7	37.5	36.2
Shahawy, Deatherage et al., Buckner (in.)	35.7	36.3	35.6	35.9
Russell and Burns (in.)	46.0	48.1	45.6	46.5
Russell and Burns (80d <sub>b</sub> ) (in.)	48.0	48.0	48.0	48.0
Lane (in.)	89.2	62.0	87.7	73.8
Kose and Burkett (in.)	42.8	36.1	42.5	39.2
Ramirez and Russell (in.)	36.0	33.5	36.9	36.2

Note: 1 in. = 25.4 mm

The dead end transfer length was smaller than all of the predictions. The live end transfer length was nearly double that of the dead end and was larger than the ACI/AASHTO prediction and the ACI 50d<sub>b</sub> prediction. It was less than the transfer length predicted by all of the other equations, including the AASHTO 60d<sub>b</sub> requirement.

#### 5.2.1.2 NSC-2

The strain profiles for specimen NSC-2 exhibited clear strain plateaus for all but the south side dead end at all ages. The south side dead end profile had a slight double slope before forming a clear plateau at early ages. The south side live end exhibited a peak at the initial break-over point followed by a downward slope. The north side live end profile had a very

consistent strain plateau. The north side dead end profile exhibited a slight dip after the initial break-over point followed by an increasing slope to the end of the instrumented length. Several points were lost from this end by 28 days, making for an incomplete profile. The south side measurements were used to create the final average profile at each of these gaps in data. The live end data concurred with the measurements at the beam midpoint for both north and south sides while the dead end profile was larger in magnitude than the midpoint measurements on the south side and smaller in magnitude on the north side. The 28-day average strain profile is presented in Figure 5.2. The strain plateaus were clear and the erratic behavior for the dead end was due to the missing gage points on the north side.

The measured transfer lengths over time are presented in Table 5.1. The live end transfer length was very consistent over time after an increase of approximately 2.5 in. (65 mm) between

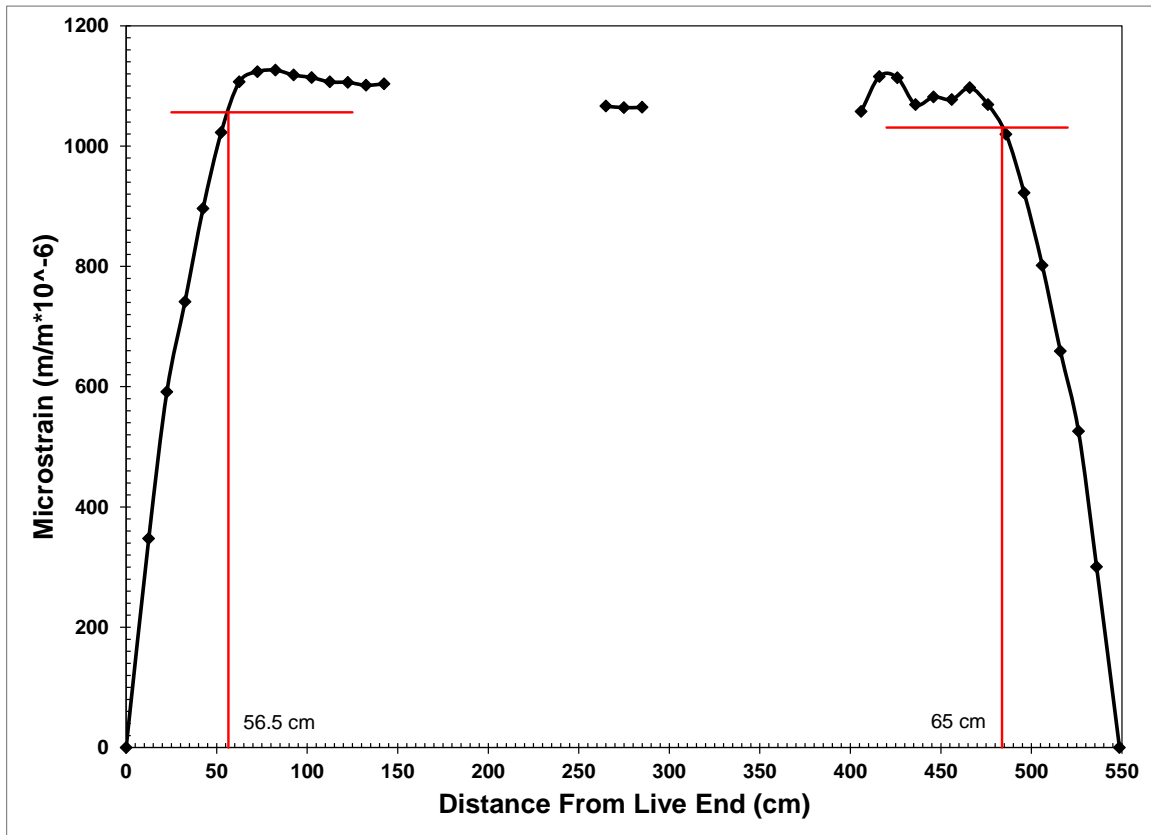


Figure 5.2: 28-Day strain profile with 95% AMS for specimen NSC-2

release and 3 days of age. The dead end transfer length was also very consistent over time except for the 28 day measurement that was most likely influenced by the missing gage points. A comparison of the 28-day transfer lengths with the values given by each of the prediction equations is shown in Table 5.2. The dead and live end transfer lengths were substantially less than those determined using each of the prediction equations.

#### 5.2.1.3 NSC-3

The strain profiles for specimen NSC-3 had very distinct strain plateaus on all ends except the south side dead end. This strain profile had a small peak after the initial break-over point followed by a sharp downward slope. It is possible that this inconsistency was caused by errors in the strain measurements. The south side live end had an upward slope after the initial break-over point and the north side live end had a downward slope after the initial break-over point. The north side dead end had a very clear strain plateau. The live end profiles for both sides of the specimen were greater in magnitude than the measurements taken at the beam midpoint whereas the dead end profiles concurred with those measurements. The average 28-day strain profile is presented in Figure 5.3. The live end strain plateau was very clear and the erratic behavior of the dead end strain profile was caused by the irregularities in the south side measurements. The live end transfer length was significantly larger than that of the dead end and was indicated on the strain plot by the longer and less steep slope of the live end profile.

The measured transfer lengths over time are presented in Table 5.1. The live end transfer length was very consistent after an initial increase of approximately 3 in. (75 mm) between prestress release and 5 days of age. A scheduling error caused the 3-day measurements to be missed for this specimen. The dead end transfer length was more erratic than the live end over time which can again be attributed to the erratic measurements of the south side dead end. There

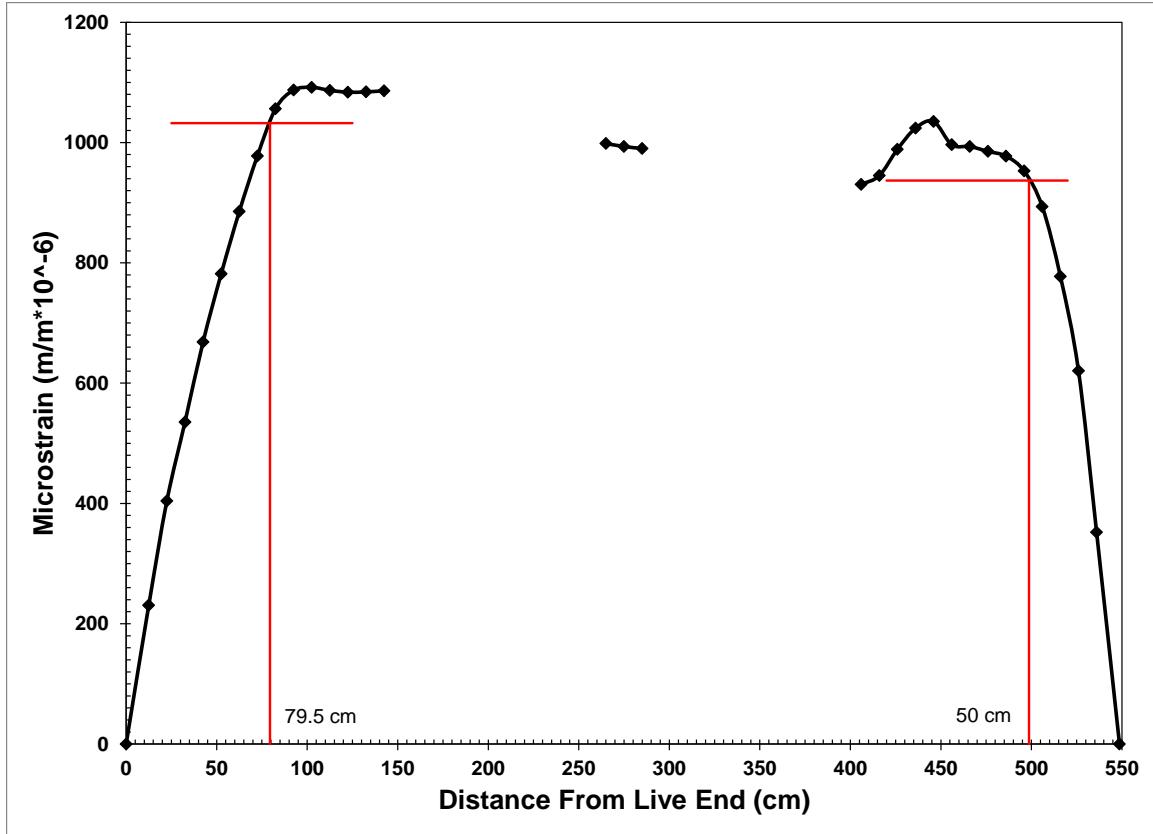


Figure 5.3: 28-Day strain profile with 95% AMS for specimen NSC-3

was a net decrease in the dead end transfer length of less than 1 in. (25 mm) over the 28 days measurements were taken, but it is difficult to quantify as a decreasing trend due to the erratic behavior of the measurements. The 28-day transfer lengths and the values given by the various prediction equations are presented in Table 5.2. The live end transfer length was greater than the predictions produced by the ACI/AASHTO equation and the ACI  $50d_b$  provisions but was less than the predictions calculated using all other equations. The dead end transfer length was significantly less than the values given by all of the prediction equations.

#### 5.2.1.4 NSC-4

The strain profiles for specimen NSC-4 were very irregular. The north side live and dead end profiles exhibited secondary slopes after the initial break-over point that both trended toward the measurements at the beam midpoint. The south side live end profile had a peak at the initial

break-over point with significantly larger magnitude than the remainder of the strain plateau, which had a downward slope. There was an error in the placement of two of the DEMEC gage points that did not allow for measurements between those two points and may have also contributed to this large peak. The south side dead end profile had a secondary slope after the initial break-over point, but did have a clear strain plateau. The profiles of both ends had a magnitude greater than that of the measurements at the beam midpoint. The average strain profile at 28 days is presented in Figure 5.4. The irregularity in the live end profile initial slope was caused by the use of only north side data to calculate the value at that point. The live end strain plateau used to calculate the average maximum strain was very clear. The dead end plateau was not nearly as clear, and the values used to calculate the average maximum strain included all those after the break-over from the initial steep slope.

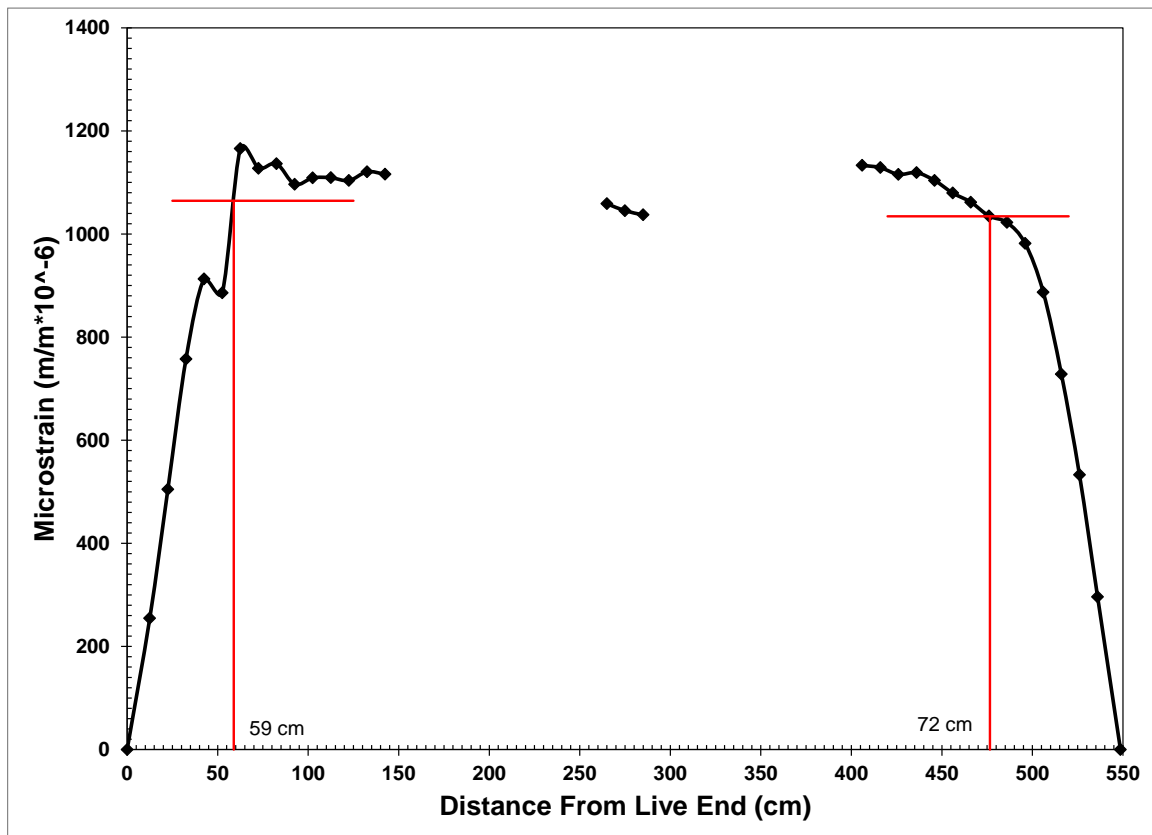


Figure 5.4: 28-Day strain profile with 95% AMS for specimen NSC-4

The measured transfer lengths over time are presented in Table 5.1. The live end transfer length was very consistent after 5 days and had a net increase of approximately 2 in. (50 mm) between prestress release and 28 days. The 3-day measurements were also missed for this specimen due to the same scheduling error as for NSC-3. The dead end transfer length exhibited some variability over time and had a net increase of approximately 9 in. (230 mm) between prestress release and 28 days. The 28-day transfer lengths along with the values calculated using the various prediction equations are presented in Table 5.2. The measured transfer lengths for both the live and dead ends were less than the predictions of each equation.

#### 5.2.1.5 Summary and Discussion

Issues with the epoxy used to place the DEMEC points for the normal strength clay (NSC) specimens caused inconsistencies in the strain measurements for these specimens. The effects of these inconsistencies were limited since measurements were taken on both sides of each specimen allowing for data when points were lost on one side of a specimen. In spite of any issues, clear determination of the transfer length was possible for each specimen using the 95% AMS method. Some of the irregularities in the strain profiles may have been caused by the placement of the beams in the yard. The NSC specimens were supported near the third points for the duration of measurements and observation. The calculated stresses caused by the overhanging portions of the beams caused only minor additional strains using the uncracked cross-section, but these effects may have been amplified by the cracking caused by the initial prestress. Differences between the measurements at release and at later ages should have been evident were this the case since the beams were supported only at the ends immediately after prestress release. These differences were not evident.



The live end transfer length measurements all had a slight increase over time while all the dead end measurements, except those for NSC-4, tended toward a slight decrease over time. The live end transfer length was greater than the dead end transfer length for specimens NSC-1 and NSC-3. The dead end transfer length was greater for specimens NSC-2 and NSC-4. These differences correlate with the placement of the beams in the prestressing bed. Specimens NSC-1 and NSC-3 were closest to the tensioning frame while specimens NSC-2 and NSC-4 were opposite the tensioning frame. In spite of the gradual release of prestress, the end closest to the tensioning frame took the brunt of the release forces. During release, the beams would not move enough to entirely relieve the stress in the strands between the dead end abutment and the beam end. Therefore, some stress was still present in this portion of the strands that was released suddenly when these strands were cut.

### **5.2.2 Normal Strength Shale (NSS) Beams**

The issues with epoxy and DEMEC point placement were mostly resolved before the normal strength shale (NSS) beams were cast, and no points were lost during measurements. Some irregularities were still observed during data reduction for specimens NSS-2 and NSS-3, however. Specimens NSS-1, NSS-4, and NSS-5 had smooth strain profiles that allowed for simple transfer length determination.

#### **5.2.2.1 NSS-1**

As this specimen was cast using a mixture that differed slightly from the other NSS specimens, its results may not compare directly with those other specimens. The mixture was very similar in composition, but had a substantially lower compressive strength, which could contribute to differences in transfer length. Other than a slight variation on the live end of the south side of the specimen, the strain profile exhibited a distinct plateau that allowed for a simple

determination of transfer length for both ends of the specimen. The plot of the 28-day strain profile showing the 95% Average Maximum Strain (AMS) values and the resulting transfer length is presented in Figure 5.5.

The measured transfer lengths over time are presented in Table 5.3. The measured live end transfer length was significantly larger than that for the dead end. The live and dead end transfer lengths increased by approximately 3 in. (75 mm) over 28 days with most of the growth occurring over the first 14 days. The 28-day transfer lengths along with the values calculated using the various prediction equations are presented in Table 5.4. The dead end transfer length was smaller than the values calculated using all of the equations. The live end transfer length measured for specimen NSS-1 slightly exceeded the predictions given by the ACI/AASHTO equation and the ACI  $50d_b$  requirement, but was within the bounds of all other predictions.

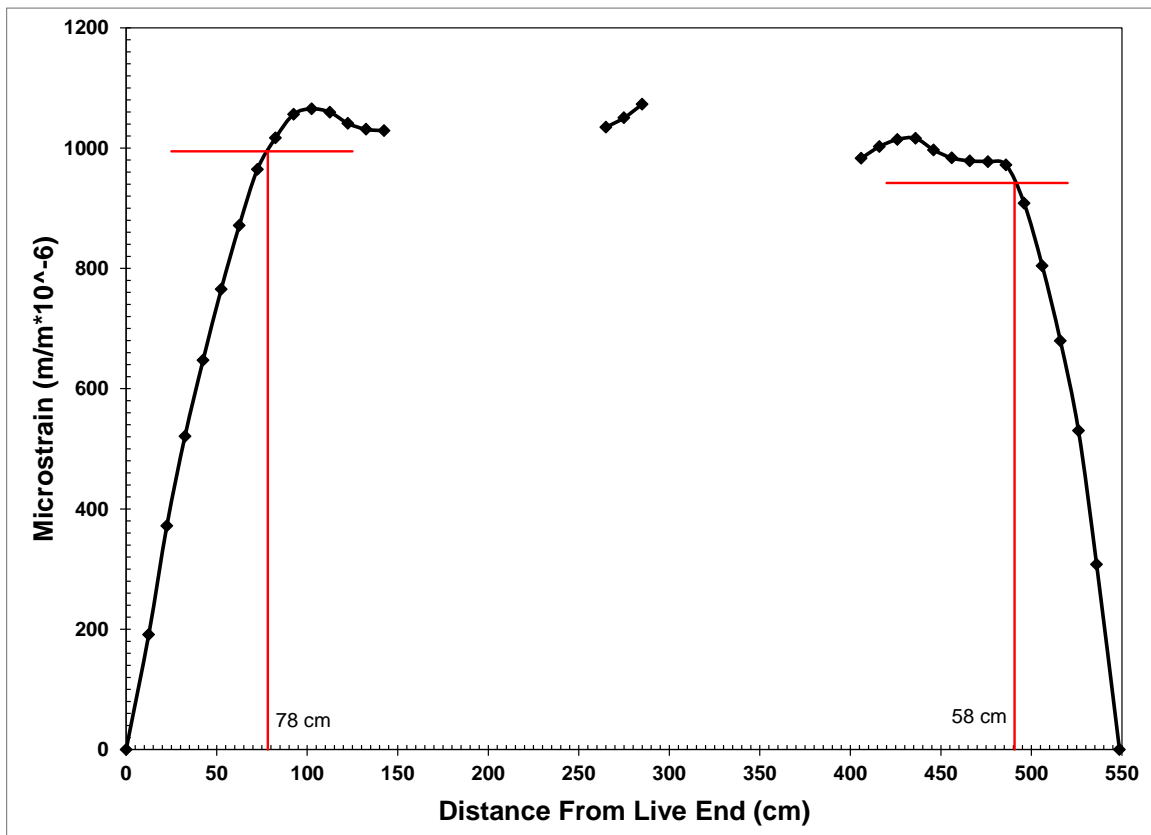


Figure 5.5: 28-Day strain profile with 95% AMS for specimen NSS-1

Table 5.3: NSS Transfer Length Measurements Over Time

End Specimen	Live (in.)					Dead (in.)				
	NSS-1	NSS-2	NSS-3	NSS-4	NSS-5	NSS-1	NSS-2	NSS-3	NSS-4	NSS-5
Release	28.0	42.9	38.4	32.5	29.9	19.9	22.0	24.4	28.0	22.4
3-Day	29.5	33.1	32.3	32.7	28.0	21.1	21.3	25.6	29.9	23.0
5-Day	30.3	42.1	28.0	32.3	27.2	21.7	24.8	34.6	32.3	24.0
7-Day	29.9	28.3	26.4	33.9	27.2	21.3	24.2	40.6	26.0	23.6
14-Day	30.3	28.0	27.2	30.3	24.2	22.4	25.0	39.4	24.4	23.4
28-Day	30.7	27.0	27.4	29.1	22.8	22.8	24.0	38.2	24.0	22.0

Note: 1 in. = 25.4 mm

Table 5.4: Comparison of NSS Transfer Length Predictions

Specimen	NSS-1	NSS-2	NSS-3	NSS-4	NSS-5
Measured (Live) (in.)	30.7	27.0	27.4	29.1	22.8
Measured (Dead) (in.)	22.8	24.0	38.2	24.0	22.0
ACI 318/AASHTO LRFD (in.)	30.2	31.5	31.6	31.5	31.2
ACI (50d <sub>b</sub> ) (in.)	30.0	30.0	30.0	30.0	30.0
AASHTO (60d <sub>b</sub> ) (in.)	36.0	36.0	36.0	36.0	36.0
Zia and Mostafa (in.)	42.6	33.4	31.9	34.1	36.3
Shahawy, Deatherage et al., Buckner (in.)	35.7	36.1	36.1	36.1	36.0
Russell and Burns (in.)	45.3	47.2	47.4	47.3	46.8
Russell and Burns (80d <sub>b</sub> ) (in.)	48.0	48.0	48.0	48.0	48.0
Lane (in.)	92.2	70.2	72.9	67.5	69.2
Kose and Burkett (in.)	43.5	38.3	39.0	37.6	38.0
Ramirez and Russell (in.)	39.0	34.8	34.1	35.1	36.2

Note: 1 in. = 25.4 mm

#### 5.2.2.2 NSS-2

The strain profiles for specimen NSS-2 exhibited substantial irregularities, as illustrated in the 28-day strain profile presented in Figure 5.6. The north side profile came to a plateau from both ends and then began to increase again at a certain point. The south side, dead end profile was also somewhat erratic, whereas the south side, live end profile had a smooth plateau. These issues led to the erratic shape of the strain profile shown in Figure 5.6. In order to determine the transfer length, all points after the first break into a plateau were included in the average maximum strain. The measurements at the beam midpoint did not concur with the increase in strain after the first plateau, but all the values in each plateau were used for consistency.

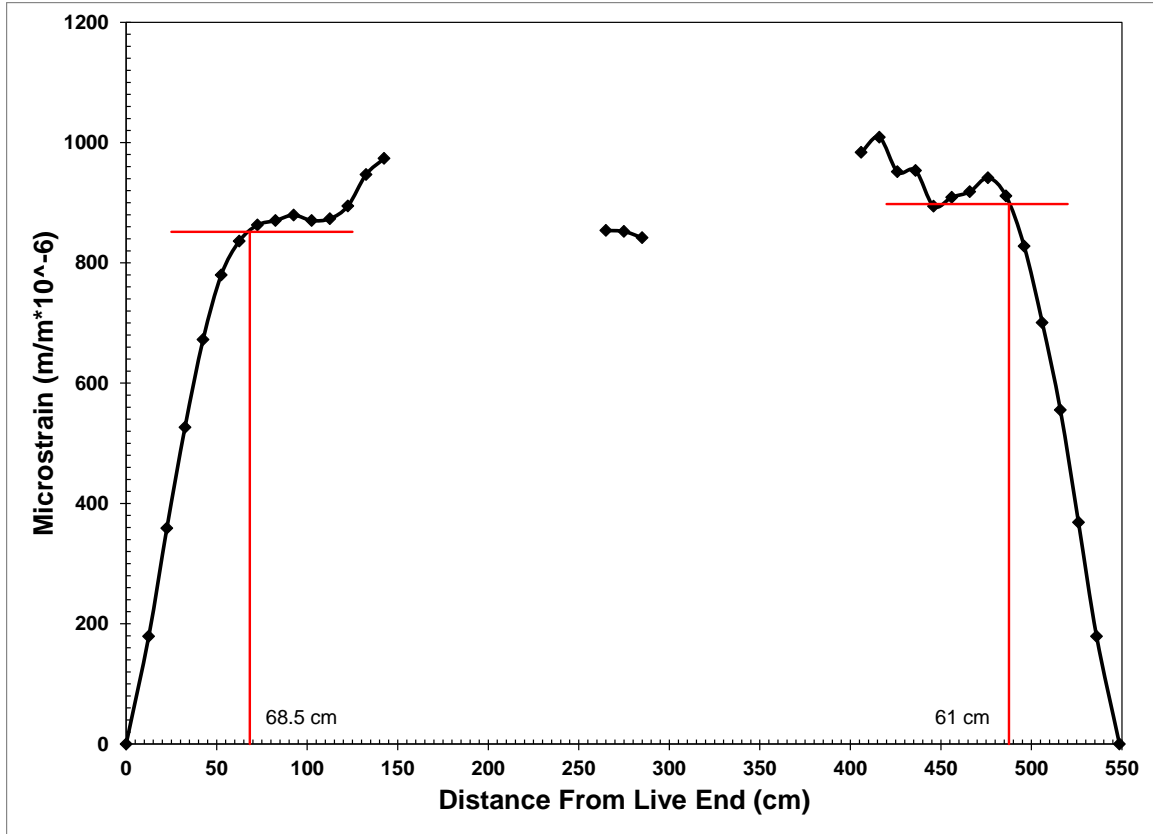


Figure 5.6: 28-Day strain profile with 95% AMS for specimen NSS-2

The transfer lengths measured over time are presented in Table 5.3. The measured live end transfer length varied over time partially due to the fact that the 95% AMS fell above the initial strain plateau at times and the resulting transfer lengths for those instances were overly long. The dead end transfer length measurement were also slightly erratic over time but showed a net increase of 2 in. (50 mm) between prestress release and 28 days. The final transfer length measurements had a difference of 3 in. (76 mm) between the live and dead ends with the live end having the longer transfer length. The predictions and measured values at 28 days are presented in Table 5.4. Even with the inclusion of the points on the second slope of the strain profile in the average maximum strain, the measured 28-day transfer length was less than that produced by all of the prediction equations.

### 5.2.2.3 NSS-3

The strain profiles for specimen NSS-3 exhibited similar irregularities to those of specimen NSS-2. The north side dead end profile and south side live end profile exhibited smooth plateaus whereas the north side live end and south side dead end had a second slope after an initial plateau. At some ages the south side dead end did not reach a fully distinct plateau. These issues contributed to the irregular shape of the 28-day strain profile shown in Figure 5.7.

The measured transfer lengths over time are presented in Table 5.3. The live end values decreased over time while the dead end values increased over time. The magnitude of the changes in live end transfer length over time is difficult to pinpoint due to the irregular shape of the strain profiles which led to irregular results from the 95% AMS method. The dead end strain profiles had a similarly irregular shape but application of the 95% AMS method was more

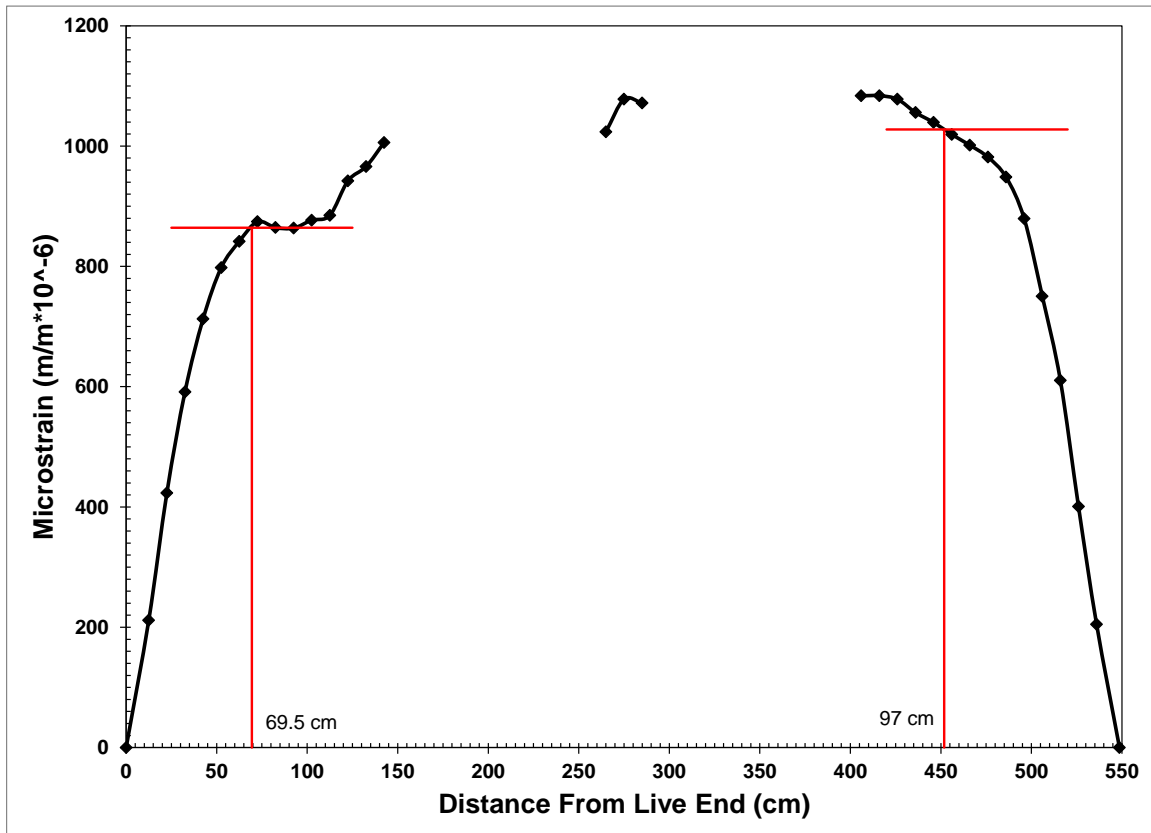


Figure 5.7: 28-Day strain profile with 95% AMS for specimen NSS-3

consistent. The dead end transfer lengths increased by almost 14 in. (355 mm) between prestress release and 28 days. The live end transfer length was nearly 11 in. (280 mm) shorter than the dead end at 28 days and was less than all of the predictions, as presented in Table 5.4. The dead end transfer length at 28 days exceeded all of the predictions except for the very conservative Russell and Burns and Lane equations and the Kose and Burkett equation.

#### 5.2.2.4 NSS-4

The strain profiles for specimen NSS-4 were smoother than those of NSS-2 and NSS-3, but still exhibited some irregularities. The live end strain profiles for both sides had a tendency toward a second slope after the initial plateau and those for the south side dead end did not have a distinct strain plateau after the initial break-over point. These issues led to the shape of the 28-day strain profile shown in Figure 5.8. The measured transfer lengths over time are presented in Table 5.3. Both live and dead end transfer lengths exhibited some variation and a general decrease over time, the live end by over 3 in. (75 mm) and the dead end by 4 in. (100 mm). The measured transfer lengths at 28 days were less than those given by all of the prediction equations, as presented in Table 5.4. This was not the case at all earlier ages. The live end transfer length at 28 days was approximately 5 in. (125 mm) longer than that of the dead end and was very close to the limit given by the ACI prediction equation.

#### 5.2.2.5 NSS-5

The strain profiles for specimen NSS-5 exhibited clear strain plateaus with the exception of that for the north side live end which gradually increased after the break-over from the initial slope. There were some erratic points near the end of the profiles for the dead end as well. The 28-day strain profile shown in Figure 5.9 illustrates the reasonably clear strain plateaus used to determine transfer length. The measured transfer lengths over time are presented in Table 5.3.

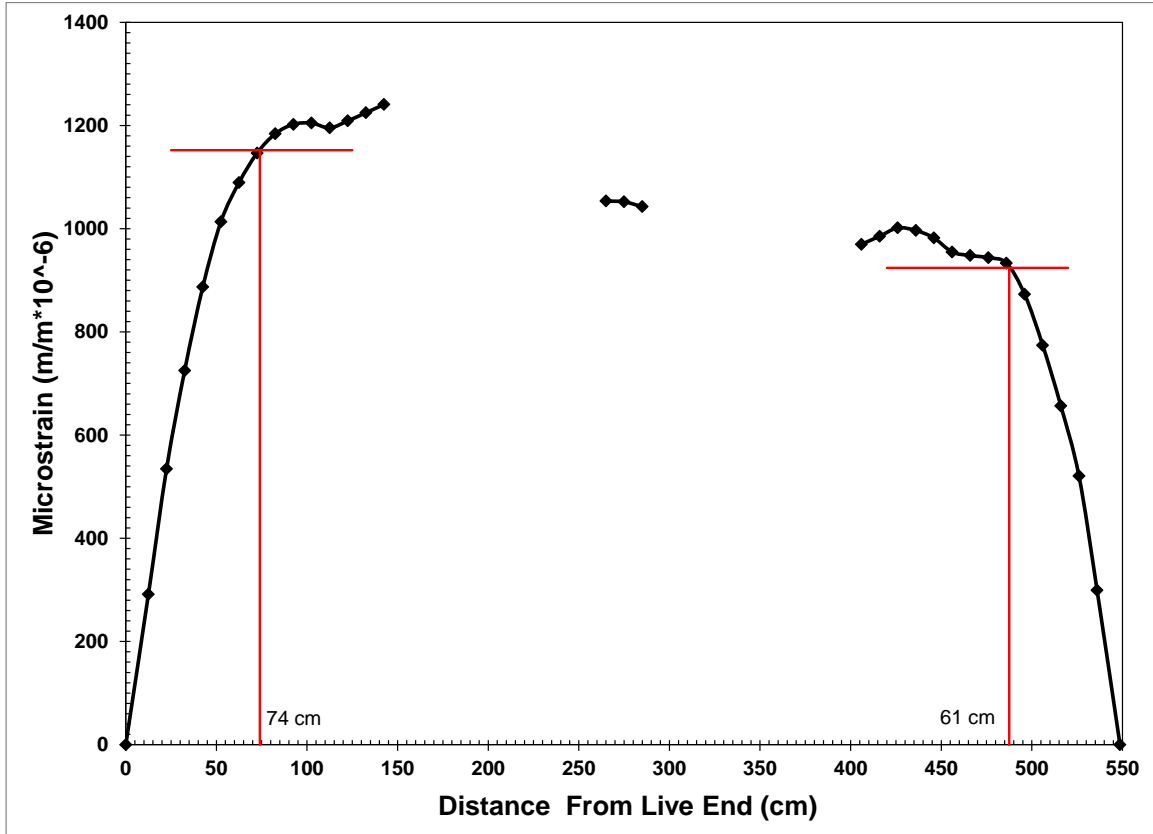


Figure 5.8: 28-Day strain profile with 95% AMS for specimen NSS-4

The live end transfer length decreased over time with a net change of 7 in. (178 mm) between prestress release and 28 days. The dead end transfer length varied slightly over time with a net decrease of less than 0.5 in. (12.5 mm) between prestress release and 28 days. The dead and live end transfer lengths were within 1 in. (25 mm) of each other for this specimen. The measured transfer length was less than that calculated using each of the prediction equations for both the dead and live ends of this specimen.

#### 5.2.2.6 Summary and Discussion

The surface strain data for the normal strength shale (NSS) specimens was more erratic than that for the normal strength clay (NSC) specimens. Cracking of the specimens due to the initial prestress may have contributed to the higher strain measurements and irregular strain profile shapes for these specimens. Due to these irregular strain profiles it was difficult to

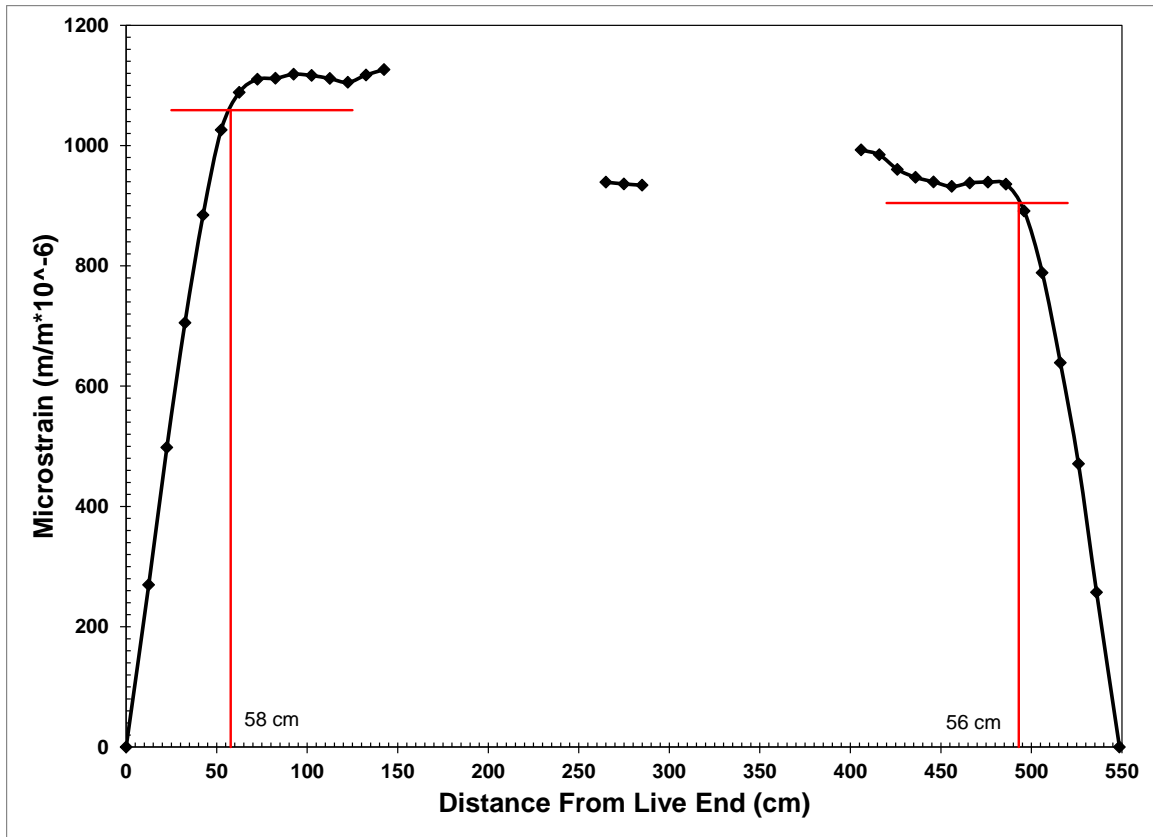


Figure 5.9: 28-Day strain profile with 95% AMS for specimen NSS-5

consistently use the 95% AMS method to determine transfer length. The live end transfer length at 28 days was larger than the dead end transfer length for all specimens except NSS-3 and the live and dead end transfer lengths for specimen NSS-5 were within 1 in. (25 mm) of each other. These two specimens were cast such that the dead end was nearest the abutment opposite the tensioning frame and there may have been some stress retained in the strands after gradual release of the hydraulic pressure. All measured transfer lengths except for the live end of specimen NSS-1 and the dead end of NSS-3 were less than the values produced by each of the prediction equations at 28 days, and the live end of NSS-1 exceeded the prediction by less than 1 in. (25 mm).



### 5.2.3 Normal Strength Limestone (NSL) Beams

Several issues were encountered during transfer length determination for the normal strength limestone (NSL) beams. As this was the second set of beams cast, problems with loose or lost DEMEC gage points persisted into the construction of these specimens. Erratic behavior was observed in several of the strain profiles and several of the profiles did not have an obvious strain plateau. These exhibited the same sort of second slope after the initial break-over point as was observed for the normal strength shale (NSS) beams. Like the normal strength clay (NSC) specimens, these beams were also supported at the third points during the time period measurements were taken.

#### 5.2.3.1 NSL-1

Both the dead and live end north side strain profiles measured for specimen NSL-1 exhibited a second slope after the initial break-over point. The south side strain profiles both reached a peak at the initial break-over and then exhibited a decrease and some erratic behavior. The combination of these profiles led to the peculiar shape of the 28-day average profile shown in Figure 5.10. All data after the initial break-over point were used in calculating the average maximum strain for the live end and the points at and after the second slope change were used for the dead end. The measured transfer lengths over time are presented in Table 5.5. Live and dead end transfer lengths increased approximately 5 in. (125 mm) between prestress release and 28 days. The live end showed a fairly consistent increasing trend while the dead end transfer length was more erratic in its behavior over time. A comparison of the measured transfer length values at 28 days with the values calculated using all of the prediction equations is presented in Table 5.6. The measured transfer lengths for both the live and dead end were less than those calculated using all of the prediction equations.

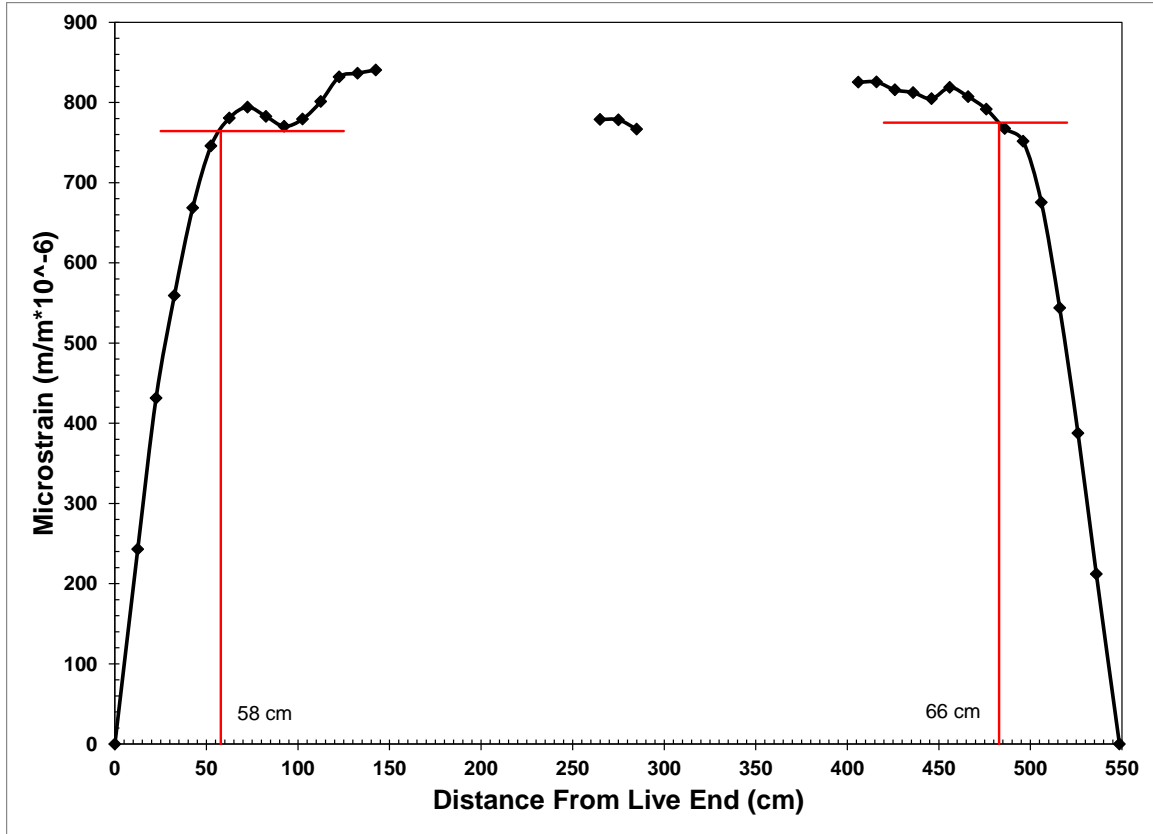


Figure 5.10: 28-Day strain profile with 95% AMS for specimen NSL-1

Table 5.5: NSL Transfer Length Measurements Over Time

End	Live (in.)				Dead (in.)			
	NSL-1	NSL-2	NSL-3	NSL-4	NSL-1	NSL-2	NSL-3	NSL-4
<b>Release</b>	17.7	19.7	19.7	21.7	19.3	18.5	19.7	39.0
<b>3-Day</b>	15.7	20.1	20.9	19.7	26.8	18.9	21.7	40.2
<b>5-Day</b>	16.1	18.1	22.0	21.3	25.6	18.9	23.6	41.3
<b>7-Day</b>	18.5	17.7	23.2	21.7	25.2	20.1	23.6	42.1
<b>14-Day</b>	20.5	19.7	22.4	20.9	25.6	18.1	21.7	40.6
<b>28-Day</b>	22.8	18.5	22.8	20.5	24.4	18.9	23.2	40.6

Note: 1 in. = 25.4 mm

### 5.2.3.2 NSL-2

The live end strain profiles for specimen NSL-2 were somewhat erratic while the dead end profiles had reasonably smooth strain plateaus. The north side live end strain profile exhibited a double slope similar to that of several other specimens. The south side live end profile had a peak at the initial break-over point and then exhibited a decreasing trend. A minor

Table 5.6: Comparison of NSL Transfer Length Predictions

Specimen	NSL-1	NSL-2	NSL-3	NSL-4
Measured (Live) (in.)	22.8	18.5	22.8	20.5
Measured (Dead) (in.)	24.4	18.9	23.2	40.6
ACI 318/AASHTO LRFD (in.)	34.0	34.4	33.3	33.6
ACI (50d <sub>b</sub> ) (in.)	30.0	30.0	30.0	30.0
AASHTO (60d <sub>b</sub> ) (in.)	36.0	36.0	36.0	36.0
Zia and Mostafa (in.)	28.1	26.2	36.2	34.7
Shahawy, Deatherage et al., Buckner (in.)	37.4	37.6	37.2	37.3
Russell and Burns (in.)	51.0	51.6	49.9	50.4
Russell and Burns (80d <sub>b</sub> ) (in.)	48.0	48.0	48.0	48.0
Lane (in.)	67.4	56.0	57.0	56.8
Kose and Burkett (in.)	37.6	34.5	34.8	34.7
Ramirez and Russell (in.)	31.8	30.8	35.6	34.8

Note: 1 in. = 25.4 mm

irregularity was evident on the north side dead end profile at 28 days whereas both dead end profiles were very smooth at all other ages. The effects of these profiles can be seen in the average 28-day profile presented in Figure 5.11. All points past the initial break-over were used to calculate the average maximum strain for the live end while all points past the first point at the same level as the average of the plateau were used for the dead end. The measured transfer lengths over time are presented in Table 5.5. The live end transfer length exhibited somewhat erratic behavior over time and had a net decrease of approximately 1 in. (25 mm) between prestress release and 28 days. The dead end transfer length was very consistent over time with a net increase of less than ½ in. (12.5 mm) between prestress release and 28 days. The measured transfer lengths at 28 days for this specimen were very short and were less than those calculated using all of the prediction equations, as shown in Table 5.6.

#### 5.2.3.4 NSL-3

The strain profiles for specimen NSL-3 exhibited the same dual slope behavior that was observed for several of the other specimens. The measurements at the beam midpoint concurred with the second increase on the north side, but not on the south side of the beam. The south side

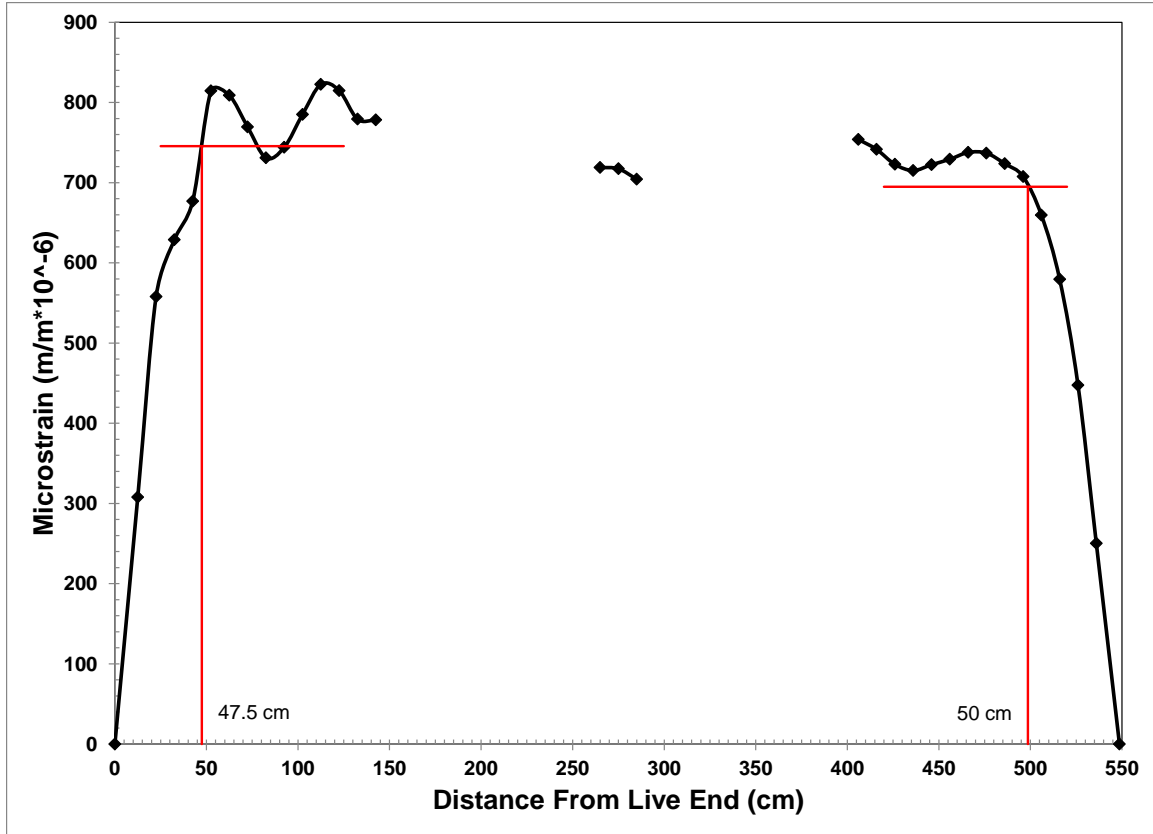


Figure 5.11: 28-Day strain profile with 95% AMS for specimen NSL-2

live end profile exhibited a decrease in magnitude after the initial break-over point and was slightly erratic. The erratic behavior could be traced to irregularities in measurements for two point sets that both included the same individual point. The nature of the moving average used for the 95% AMS method allowed these irregularities to affect a larger portion of the strain profile than just one individual point. Since the cause of this irregularity was unknown, it was not removed from the data set. The resulting average 28-day strain profile is presented in Figure 5.12. All points after the initial break-over were included in the average maximum strain calculation for each end. In this average profile the points at the beam midpoint concur with the trend indicated by the measurements at both ends.

The measured transfer lengths over time are presented in Table 5.5. The live end transfer length increased by approximately 3 in. (75 mm) between prestress release and 28 days, but was

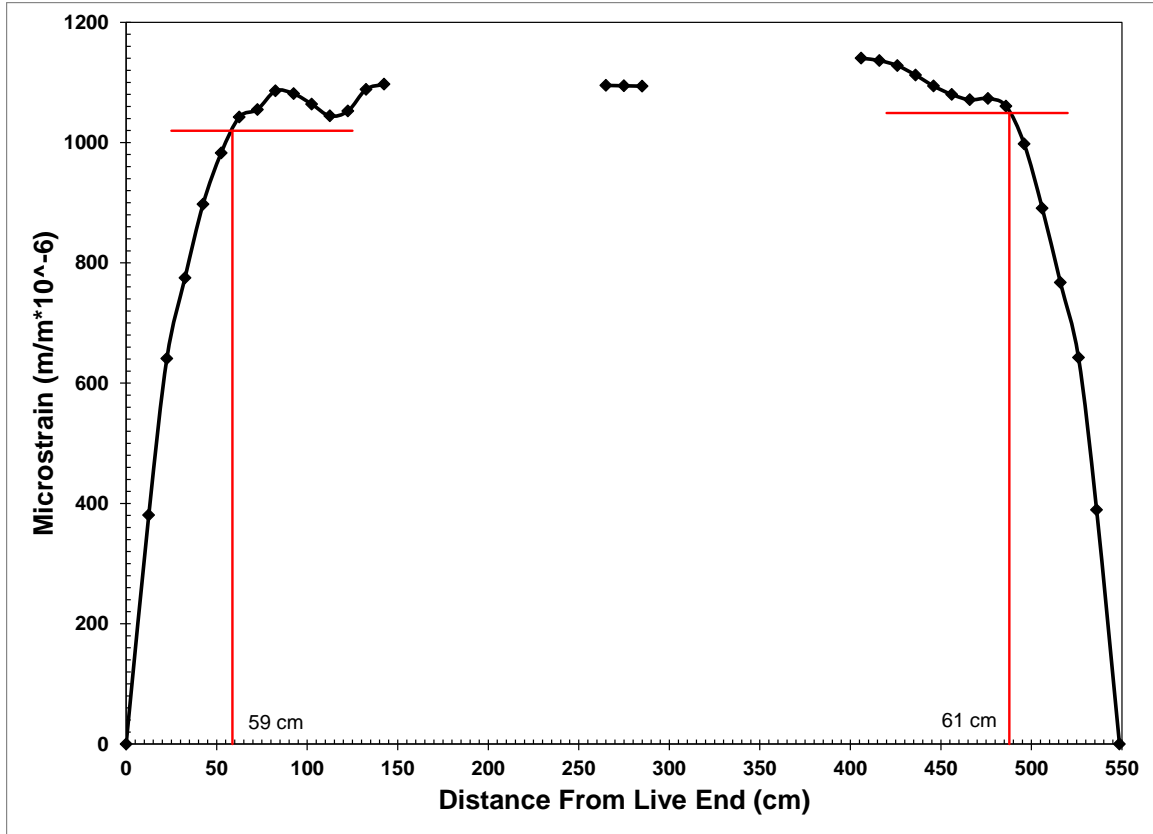


Figure 5.12: 28-Day strain profile with 95% AMS for specimen NSL-3

fairly consistent after 7 days of age. The dead end transfer length increased by 3.5 in. (89 mm) over the 28 day time period. It was fairly consistent after 5 days of age with a slight anomaly at 14 days. The measured transfer lengths at 28 days are shown in Table 5.6 along with the values calculated using the different prediction equations. The measured transfer lengths for both the live and dead ends of the specimen were less than those calculated using each of these equations.

#### 5.2.3.4 NSL-4

The strain plateaus for specimen NSL-4 were reasonably smooth with only some slightly erratic behavior on the south side dead end profile caused by the measurements for a single set of points. The average strain profile at 28 days is presented in Figure 5.13. This strain profile indicates that the transfer length for the dead end of the specimen was significantly longer than those of the other NSL specimens. This was attributed to the very poor consolidation at that end

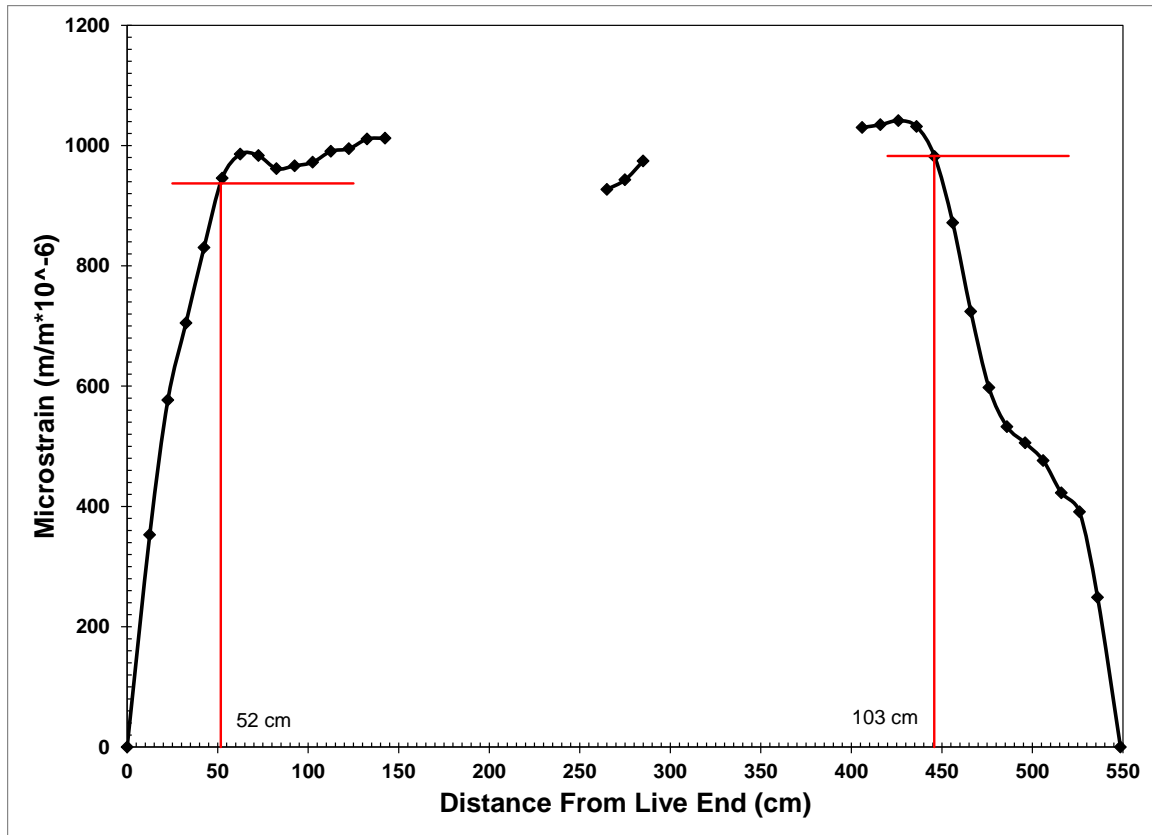


Figure 5.13: 28-Day strain profile with 95% AMS for specimen NSL-4

of the specimen. All points at and past the initial break-over point were used in calculating the average maximum strain for both the live and dead ends. The measured transfer lengths over time are presented in Table 5.5. The live end transfer length exhibited a decrease of just over 1 in. (25 mm) between prestress release and 28 days, but was consistent over time. The dead end transfer length was very large, but only increased by approximately 1.5 in. (38 mm) between prestress release and 28 days. As presented in Table 5.6, the measured live end transfer length at 28 days was less than that calculated using each of the prediction equations while the dead end transfer length exceeded all but the very conservative Russell and Burns and Lane equations.

#### 5.2.3.5 Summary and Discussion

The strain profiles for all of the normal strength limestone (NSL) specimens exhibited some erratic behavior. Some of these issues can be attributed to errors in the DEMEC

measurements and possibly to the placement of the beam specimens during storage. As with the normal strength clay (NSC) specimens, the effect of errors in the measurements was limited by the redundancy of data in the form of measurements on both sides of each specimen. These beams were supported at approximately the third points during storage which may have contributed to additional compressive strains at the level of the prestressing steel. Differences between the strain profiles at release and those at later ages that would confirm this phenomenon were not present, however. The changes in transfer length between prestress release and 28 days were similar to those for the other NS specimens, with most increases over time equal to or greater than those of the other NS specimens. The dead end transfer lengths were greater than the live end for all specimens at 28 days. This is unusual when compared to data from the other NS specimens. The live and dead end transfer lengths were similar at both release and 28 days for all specimens except NSL-4. This anomalous specimen had very poor consolidation near the dead end which caused the excessively large transfer length.

#### **5.2.4 High Strength Clay (HSC) Beams**

The strain profiles of the high strength clay (HSC) specimens had well defined plateaus and exhibited slightly less erratic behavior than the normal strength (NS) specimens. The improved surface finish of these specimens from the use of plastic sheeting to line the formwork also facilitated better DEMEC point placement. A small peak at the initial break-over point was consistently observed in the strain profiles for each specimen. It was unclear what caused this behavior.

##### **5.2.4.1 HSC-1**

Specimen HSC-1 was instrumented with DEMEC points along its entire length in order to gain insight into why the data from the beam midpoints did not always agree with the end

profiles for the earlier specimens. The points were placed in the same arrangement as that used for the other beam specimens with the extra gage points added from each end. A slight gap in data existed since the points from each end and those at the beam midpoint did not overlap exactly. The strain profiles for each side and end displayed some erratic behavior. The south side dead end had the most consistently obvious strain plateau with a slight dip caused by a single measurement just after the initial break-over point. The south side live end profile exhibited a secondary slope after the initial plateau and then decreased to the level of the measurements at the beam midpoint. Both south side profiles concurred with the measurements at the beam midpoint. The north side dead end profile exhibited a sharp decline after the initial strain plateau to a level well below the measurements at the beam centerline. The north side live end profile had a secondary slope after the initial plateau with a decline after the peak to a level less than the midpoint measurements. The shape of the north side live end profile improved substantially over time. The average 28-day strain profile is shown in Figure 5.14. All points between the initial break-over points at each end were included in the average maximum strain calculation. This was done to compensate for the erratic nature of this strain profile since the magnitude of strain for both ends of the specimen was very similar.

The measured transfer lengths over time are presented in Table 5.7. The live end transfer length measured at release was nearly double that measured at 28 days and a steady decrease in magnitude was visible over time. The vast discrepancy in magnitude is partially due to the erratic nature of the strain profile at early ages. The dead end transfer length had an increasing trend over time with a net increase of almost 3 in. (75 mm) between prestress release and 28 days. A comparison between the measured transfer lengths at 28 days and the values calculated using the different prediction equations is presented in Table 5.8. The measured 28-day transfer



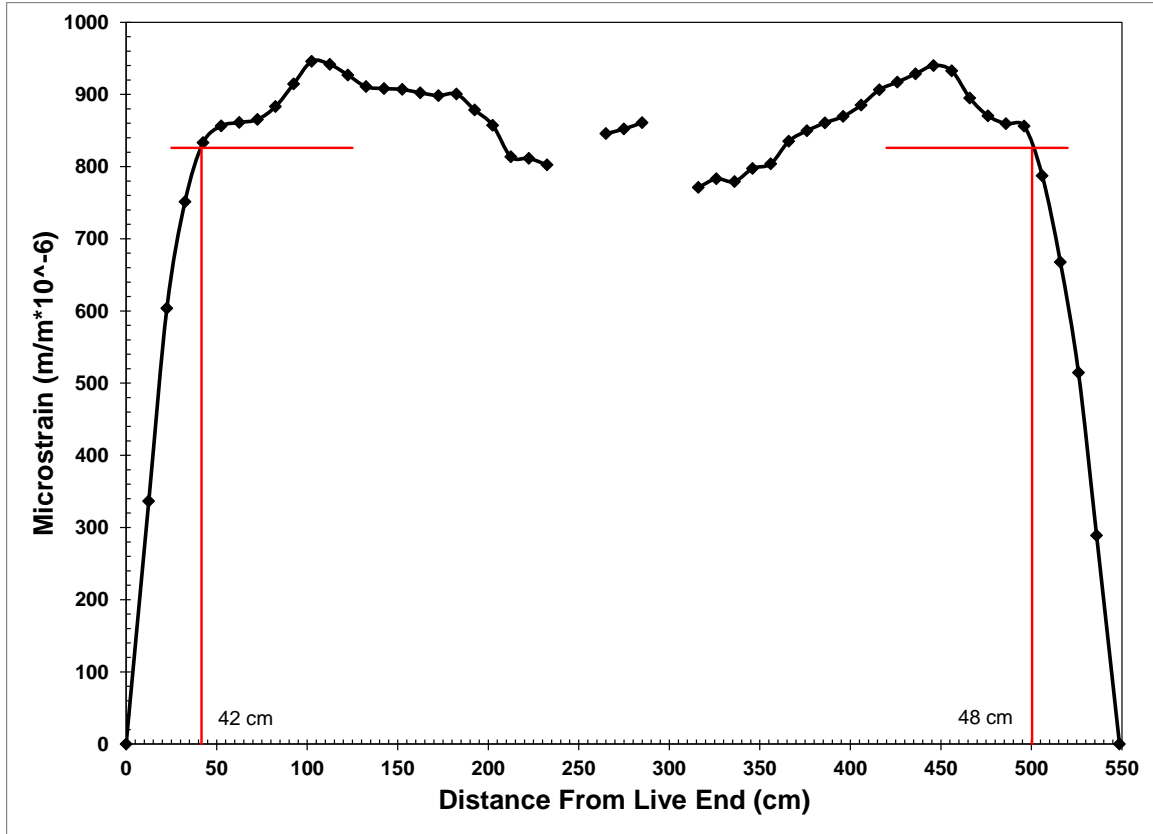


Figure 5.14: 28-Day strain profile with 95% AMS for specimen HSC-1

lengths were very short for this specimen and were less than the values calculated using all of the prediction equations.

#### 5.2.4.2 HSC-2

The south side strain profiles for specimen HSC-2 exhibited obvious plateaus that improved over time. The live end profile reached a peak at the break-over point and had a

Table 5.7: HSC Transfer Length Measurements Over Time

End	Live (in.)				Dead (in.)			
	HSC-1	HSC-2	HSC-3	HSC-4	HSC-1	HSC-2	HSC-3	HSC-4
Release	30.7	18.9	18.5	20.1	16.1	14.2	19.7	15.0
3-Day	30.1	20.3	19.5	20.5	16.5	15.7	21.9	15.9
5-Day	24.2	19.3	19.9	21.7	17.9	15.6	23.6	16.9
7-Day	21.3	19.5	20.1	24.4	18.1	15.4	22.0	16.5
14-Day	19.7	19.5	20.5	22.6	18.1	15.4	21.1	16.9
28-Day	16.5	19.3	20.7	24.0	18.9	15.7	20.5	17.7

Note: 1 in. = 25.4 mm

Table 5.8: Comparison of HSC Transfer Length Predictions

Specimen	HSC-1	HSC-2	HSC-3	HSC-4
Measured (Live) (in.)	16.5	19.3	20.7	24.0
Measured (Dead) (in.)	18.9	15.7	20.5	17.7
ACI 318/AASHTO LRFD (in.)	33.5	33.4	33.6	33.5
ACI (50d <sub>b</sub> ) (in.)	30.0	30.0	30.0	30.0
AASHTO (60d <sub>b</sub> ) (in.)	36.0	36.0	36.0	36.0
Zia and Mostafa (in.)	22.2	23.2	21.3	21.8
Shahawy, Deatherage et al., Buckner (in.)	36.9	36.8	36.9	36.9
Russell and Burns (in.)	50.2	50.0	50.4	50.2
Russell and Burns (80d <sub>b</sub> ) (in.)	48.0	48.0	48.0	48.0
Lane (in.)	62.8	59.5	67.4	63.6
Kose and Burkett (in.)	36.4	35.4	37.6	36.6
Ramirez and Russell (in.)	28.9	29.5	28.4	28.7

Note: 1 in. = 25.4 mm

decrease in magnitude in the direction of the beam midpoint. The dead end profile exhibited an increase toward the end of the measurement length, but both dead and live ends trended toward the values of the measurements at the beam midpoint. The north side live end profile had an irregularity most likely caused by the measurement at a single pair of points and the magnitude of strain was somewhat larger than the measurements taken at the beam midpoint. The north side dead end profile reached a peak at the initial break-over point and trended toward decreasing magnitude, which concurred with the measurements at the beam midpoint. The average strain profile at 28 days is presented in Figure 5.15. The strain plateaus are clear and trend toward the values measured at the beam midpoint. All measurements after the initial break-over point were used in calculating the average maximum strain for each end. The maximum strain magnitude was fairly consistent along the length of the beam except for the peak on the live end profile.

The measured transfer lengths over time are presented in Table 5.7. The live and dead end transfer lengths were very consistent over time. The live end transfer length had a net increase of less than ½ in. (12.5 mm) and the dead end transfer length 1.5 in. (38 mm) between

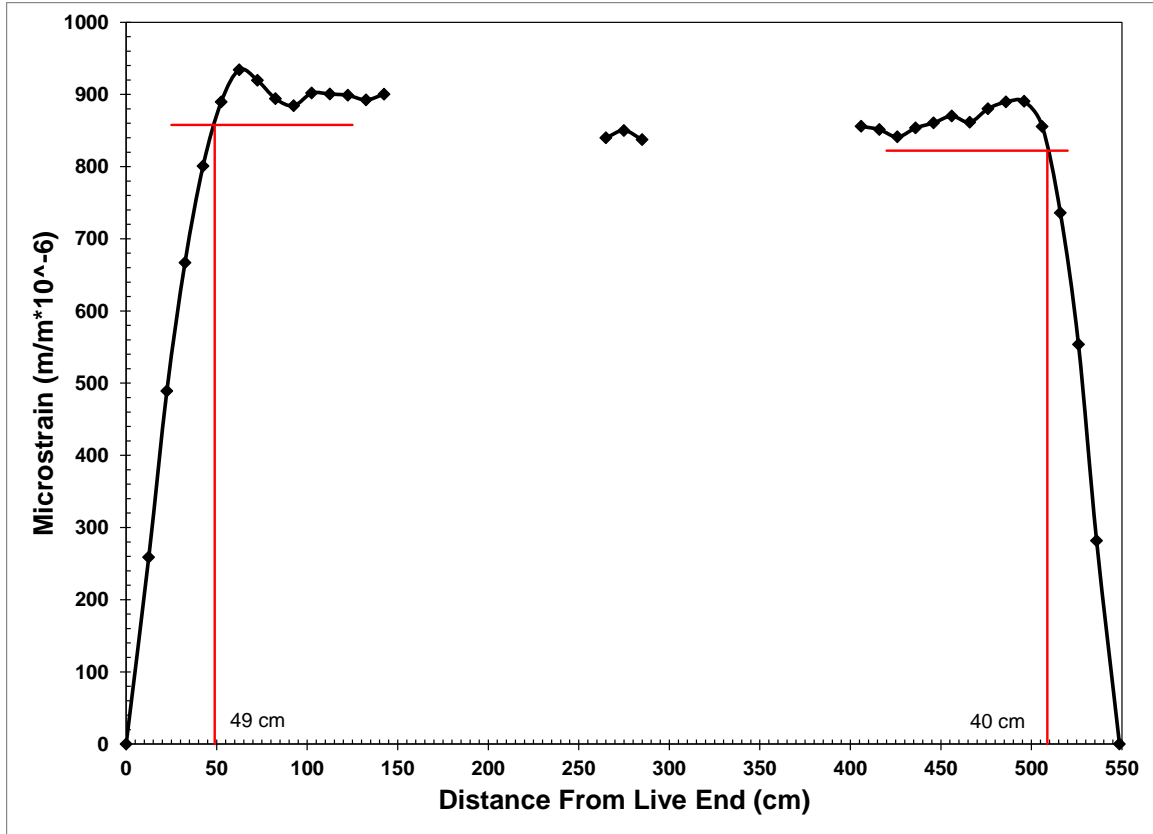


Figure 5.15: 28-Day strain profile with 95% AMS for specimen HSC-2

prestress release and 28 days. The measured 28-day transfer lengths for the live and dead ends were smaller than the values calculated using all of the equations, as shown in Table 5.8.

#### 5.2.4.3 HSC-3

The strain profiles for specimen HSC-3 exhibited clear plateaus with all having a slight downward trend after the initial break-over point except for the south side dead end which had an upward trend. These also trended toward the values measured near the beam centerline except for the south side dead end. The average strain profile at 28 days is presented in Figure 5.16.

The strain plateaus are clearly evident in spite of the decrease in magnitude of strain on the live end and the dip in magnitude on the dead end. All values past the initial break-over point were used for calculating the average maximum strain for each end. The measured transfer lengths over time are presented in Table 5.7. The live end transfer length had an increasing trend with a

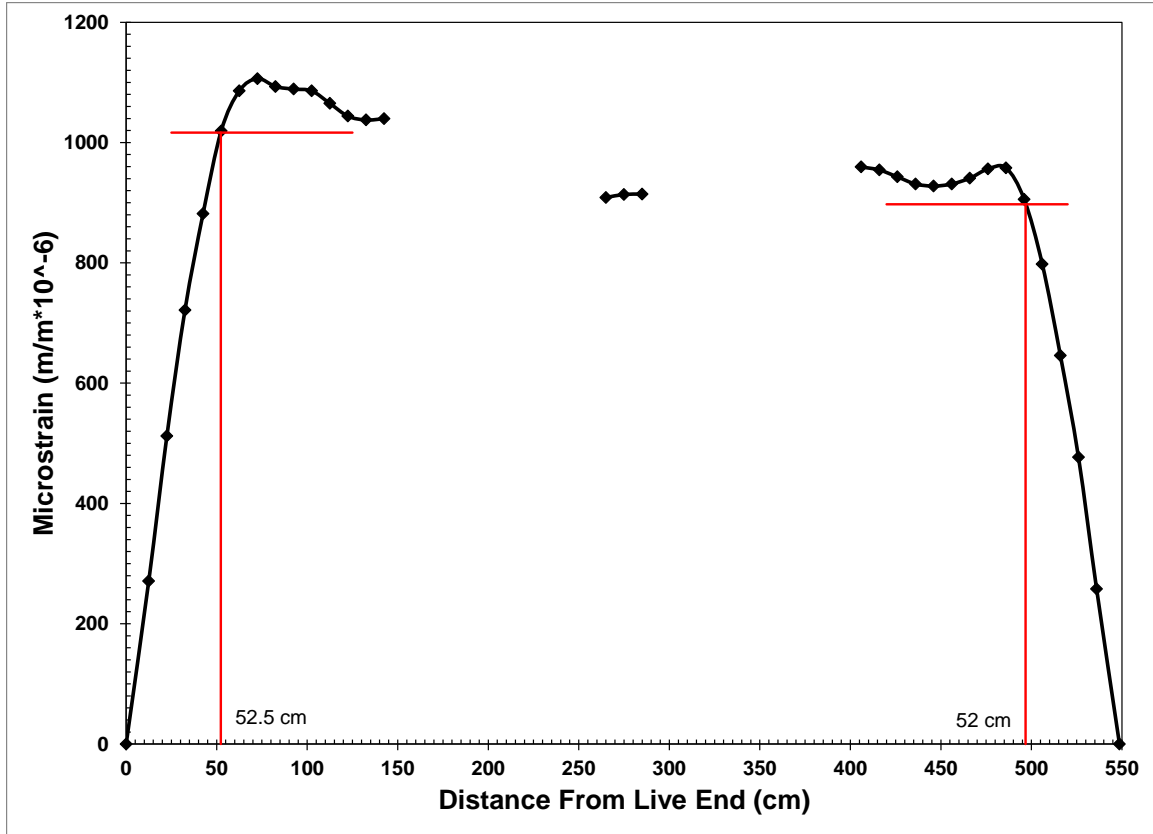


Figure 5.16: 28-Day strain profile with 95% AMS for specimen HSC-3

net increase of just over 2 in. (50 mm) between prestress release and 28 days. The dead end transfer length was erratic over time but had a net increase of almost 1 in. (25 mm) between prestress release and 28 days. The measured transfer lengths at 28 days, presented in Table 5.8, were less than all of the calculated predictions. The Zia and Mostafa prediction was less than 1 in. (25 mm) greater than the measured values, however.

#### 5.2.4.4 HSC-4

The south side strain profiles exhibited clear plateaus with only a small increase at the end of the dead end profile. Both end plateaus had a magnitude less than the measurements at the beam midpoint. The north side profiles had a second slope on the live end and a peak at the break-over point followed by a clear plateau on the dead end. Both end profiles trended toward the measurements at the midpoint. The 28 day average strain profile is presented in Figure 5.17.

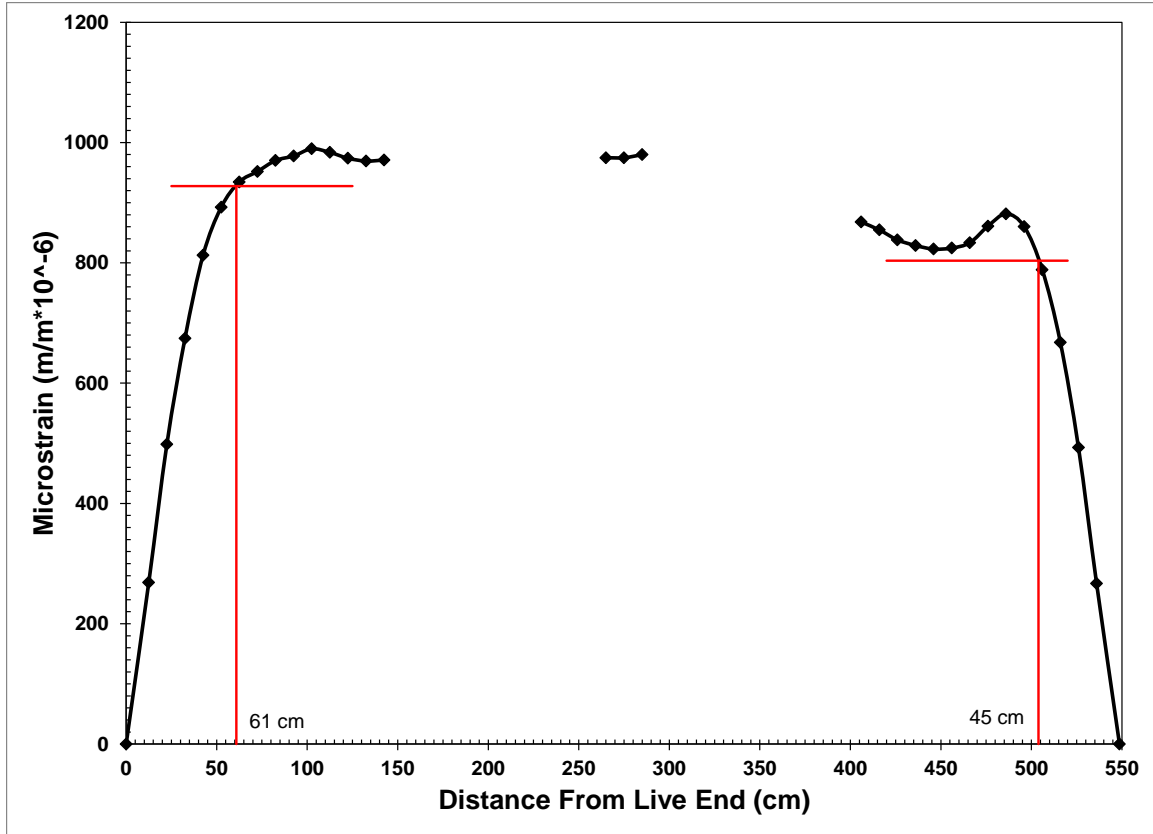


Figure 5.17: 28-Day strain profile with 95% AMS for specimen HSC-4

The influence of the north side measurements on the final values was evident in the shape of the dead end profile and the unclear break-over point on the live end. The magnitude of strain on the live end was also greater than that on the dead end. All values at approximately the same level as the strain plateau were used to calculate the average maximum strain for the live end and all points past the break-over point were used strain for the dead end.

The measured transfer lengths over time are presented in Table 5.7. The live and dead end transfer lengths exhibited an increase over 28 days with the live end increasing by a net of nearly 4 in. (100 mm) and the dead end increasing by almost 3 in. (75 mm). The dead end transfer length was significantly shorter than the live end. This discrepancy was influenced by the difference in the magnitude of strains for each of the beam ends and the lack of a clear break-over point on the live end strain profile. The measured transfer lengths at 28 days along with the

values calculated using the prediction equations are presented in Table 5.8. The dead end transfer length is less than that predicted by all of the equations. The live end transfer length was less than that calculated using the code equations, but was greater than the Zia and Mostafa prediction, which was very small for all of the HSC specimens.

#### 5.2.4.5 Summary and Discussion

The strain profiles for each of the high strength clay (HSC) beams had well defined strain plateaus that allowed for simple calculation of the transfer length using the 95% AMS method. Specimen HSC-1 had the most erratic strain behavior, partially due to issues with DEMEC point placement. The measured transfer lengths were significantly less than the ACI/AASHTO code predictions except that the live end of specimen HSC-1 was greater than the ACI  $50d_b$  requirement at release and 3 days. The measured values were also less than those calculated using the other prediction equations at 28 days except for the live end of HSC-4 which exceeded the value given by the Zia and Mostafa equation. The live end transfer lengths were greater than the dead end transfer lengths at 28 days for all specimens except HSC-1, and the live end was greater for this specimen at all other ages. The live and dead end transfer lengths for specimen HSC-3 were very similar and the dead end value was larger in magnitude at some ages.

#### 5.2.5 High Strength Shale (HSS) Beams

The strain profiles for the high strength shale (HSS) specimens exhibited some erratic behavior but had clearly defined strain plateaus. The most common issue was a second slope showing an increase in strain after the initial break-over point. Some slight irregularities were observed that were most likely caused by measurements between a single pair of points. The effect of these irregularities was tempered by the fact that measurements from both sides of each specimen were averaged for the final strain profiles.

### 5.2.5.1 HSS-1

The strain profiles for specimen HSS-1 were the most erratic of those in this set of specimens. The north side live and dead end profiles exhibited a clear plateau after a peak at the initial break-over point. The dead end profile had a minor dip caused by the measurement at a single set of points. The south side dead and live end profiles had a secondary slope after the initial break-over point with the live end portion reaching a peak and then decreasing in magnitude. These profiles combined to yield the slightly erratic 28-day average profile presented in Figure 5.18. The strain plateau was clear for both ends, however, and all the points past the initial break-over point were used to calculate the average maximum strain for each end. Both ends trended toward the values measured near the beam midpoint and the live end strains had a larger magnitude than those on the dead end.

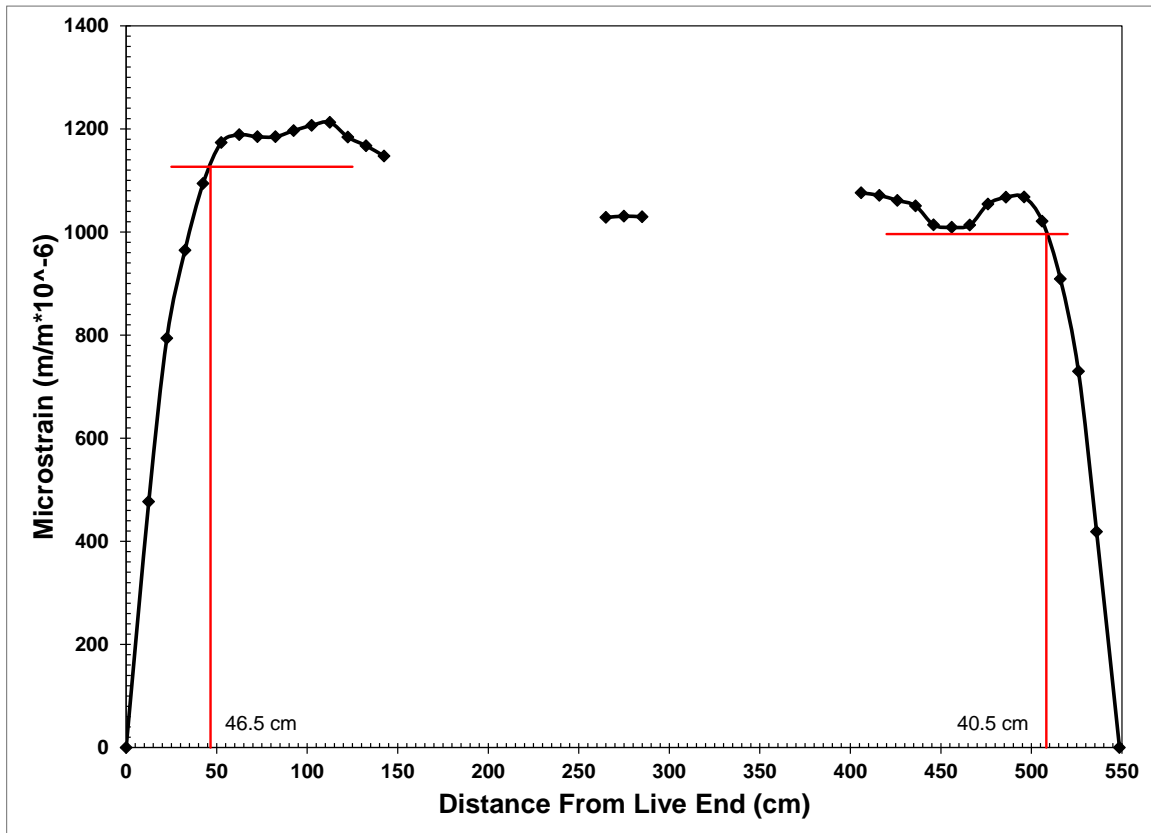


Figure 5.18: 28-Day strain profile with 95% AMS for specimen HSS-1

The measured transfer lengths over time are presented in Table 5.9. Both live and dead end transfer lengths exhibited a decrease in magnitude over time. The live end had a net decrease of 4.5 in. (115 mm) between prestress release and 28 days. The dead end transfer length decreased just over 2.5 in. (64 mm) between prestress release and 28 days, but was very stable after 5 days. The measured transfer lengths at 28 days and values calculated using the various prediction equations are presented in Table 5.10. The measured transfer lengths were less than all of the values calculated using the prediction equations.

Table 5.9: HSS Transfer Length Measurements Over Time

End Specimen	Live (in.)				Dead (in.)			
	HSS-1	HSS-2	HSS-3	HSS-4	HSS-1	HSS-2	HSS-3	HSS-4
<b>Release</b>	22.8	20.5	23.8	26.8	18.5	16.1	19.1	16.3
<b>3-Day</b>	21.1	18.1	24.2	22.0	16.7	18.1	19.7	16.1
<b>5-Day</b>	19.9	18.1	23.2	18.9	15.7	17.3	17.5	15.4
<b>7-Day</b>	19.5	15.9	23.0	17.9	15.4	16.9	16.5	15.0
<b>14-Day</b>	18.9	16.5	22.6	17.7	15.7	17.1	17.3	15.0
<b>28-Day</b>	18.3	15.9	20.5	16.7	15.9	16.3	16.3	14.2

Note: 1 in. = 25.4 mm

Table 5.10: Comparison of HSS Transfer Length Predictions

Specimen	HSS-1	HSS-2	HSS-3	HSS-4
Measured (Live) (in.)	18.3	15.9	20.5	16.7
Measured (Dead) (in.)	15.9	16.3	16.3	14.2
ACI 318/AASHTO LRFD (in.)	33.3	32.9	32.7	34.0
ACI (50d <sub>b</sub> ) (in.)	30.0	30.0	30.0	30.0
AASHTO (60d <sub>b</sub> ) (in.)	36.0	36.0	36.0	36.0
Zia and Mostafa (in.)	22.7	24.9	25.1	19.5
Shahawy, Deatherage et al., Buckner (in.)	36.8	36.6	36.5	37.1
Russell and Burns (in.)	49.9	49.4	49.0	51.1
Russell and Burns (80d <sub>b</sub> ) (in.)	48.0	48.0	48.0	48.0
Lane (in.)	68.7	70.7	55.3	64.4
Kose and Burkett (in.)	37.9	38.4	34.3	36.8
Ramirez and Russell (in.)	29.2	30.5	30.6	27.4

Note: 1 in. = 25.4 mm



### 5.2.5.2 HSS-2

The strain profiles for specimen HSS-2 were the smoothest of those for this set of specimens. Secondary slopes were observed for all ends except the north side dead end, which had a slight decreasing trend after the initial break-over. These issues were fairly minor, as shown in the 28-day strain profile presented in Figure 5.19. The live end exhibited a secondary slope and a small peak was evident at the break-over point for the dead end. The strain plateaus were very distinct and trended toward the values measured at the midpoint of the specimen. The magnitude of the concrete surface strains was also greater for the live end than for the dead end.

The measured transfer lengths over time are presented in Table 5.9. The live end transfer length decreased by approximately 4.5 in. (115 mm) between prestress release and 28 days, but was very consistent after 7 days. The larger magnitude at early ages was caused by the

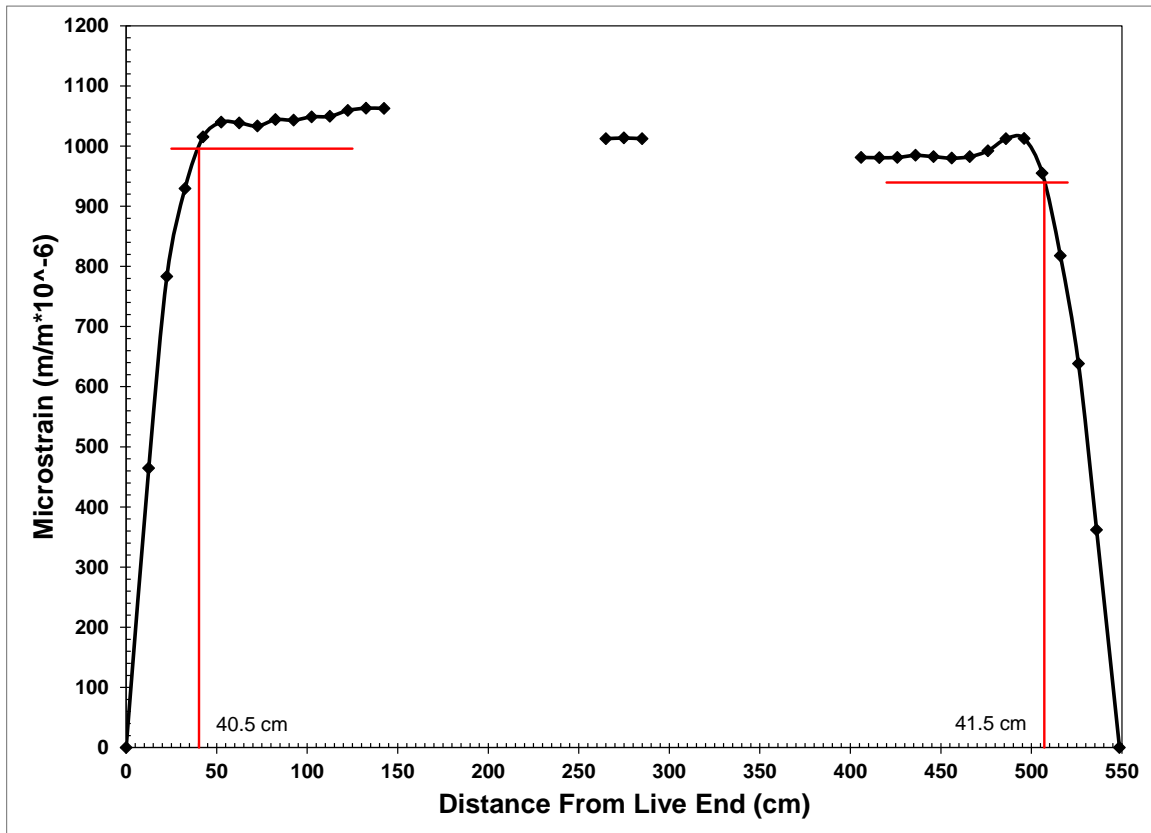


Figure 5.19: 28-Day strain profile with 95% AMS for specimen HSS-2

secondary slope of the strain profile that decreased over time. The dead end transfer length was somewhat erratic over time and did not exhibit an increasing or decreasing trend. The dead end transfer length was slightly larger than the live end at 28 days, but the values were very similar with a difference of less than ½ in. (12.5 mm). The measured transfer lengths at 28 days are presented in Table 5.10 along with the corresponding values produced by the prediction equations. The measured transfer lengths were very short, were approximately half of the code predictions, and were significantly less than the values calculated using every other prediction equation.

### 5.2.5.3 HSS-3

The live end strain profiles for specimen HSS-3 exhibited some erratic behavior. The north side had a secondary slope after an initial plateau and the south side had an irregularity most likely caused by the measurement at a single pair of points. The dead end profiles were very smooth with only a slight secondary slope. There was a significant disparity in the magnitude of strain between the live and dead ends at early ages that decreased over time. The average strain profile at 28 days is presented in Figure 5.20. The end profiles had a greater magnitude of strain than the measurements at the beam midpoint even at 28 days. The measured transfer lengths over time are presented in Table 5.9. The live end transfer length was greater than the dead end at all ages, but exhibited a decrease of over 3 in. (75 mm) between release and 28 days. The dead end transfer length also decreased almost 3 in. (75 mm) over time. As shown in Table 5.10, the measured transfer lengths at 28 days were substantially less than those calculated using all of the prediction equations.

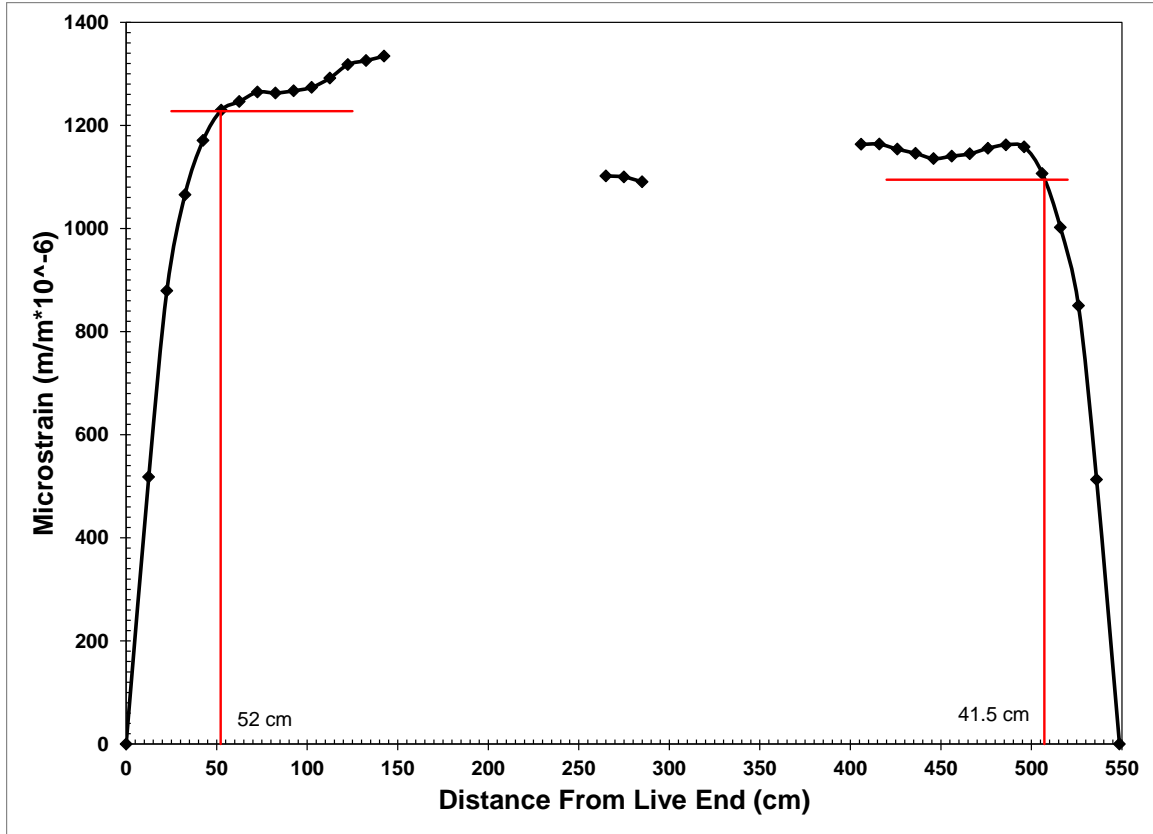


Figure 5.20: 28-Day strain profile with 95% AMS for specimen HSS-3

#### 5.2.5.4 HSS-4

The strain profiles for specimen HSS-4 exhibited clear plateaus with a consistent downward trend after the initial break-over. The south side live end profile also had a small peak at the initial break-over point. The live end profiles were more erratic and had larger magnitudes than the dead end profiles at early ages. These disparities were reconciled over time until only the north side live end was slightly larger in magnitude than the north side dead end and did not concur with the measurements at the beam midpoint. The average strain profile at 28 days is presented in Figure 5.21.

The measured transfer lengths over time are presented in Table 5.9. The live end transfer length was greater than the dead end at all ages and decreased by over 10 in. (250 mm) between prestress release and 28 days. The large values at early ages were due to erratic behavior in the

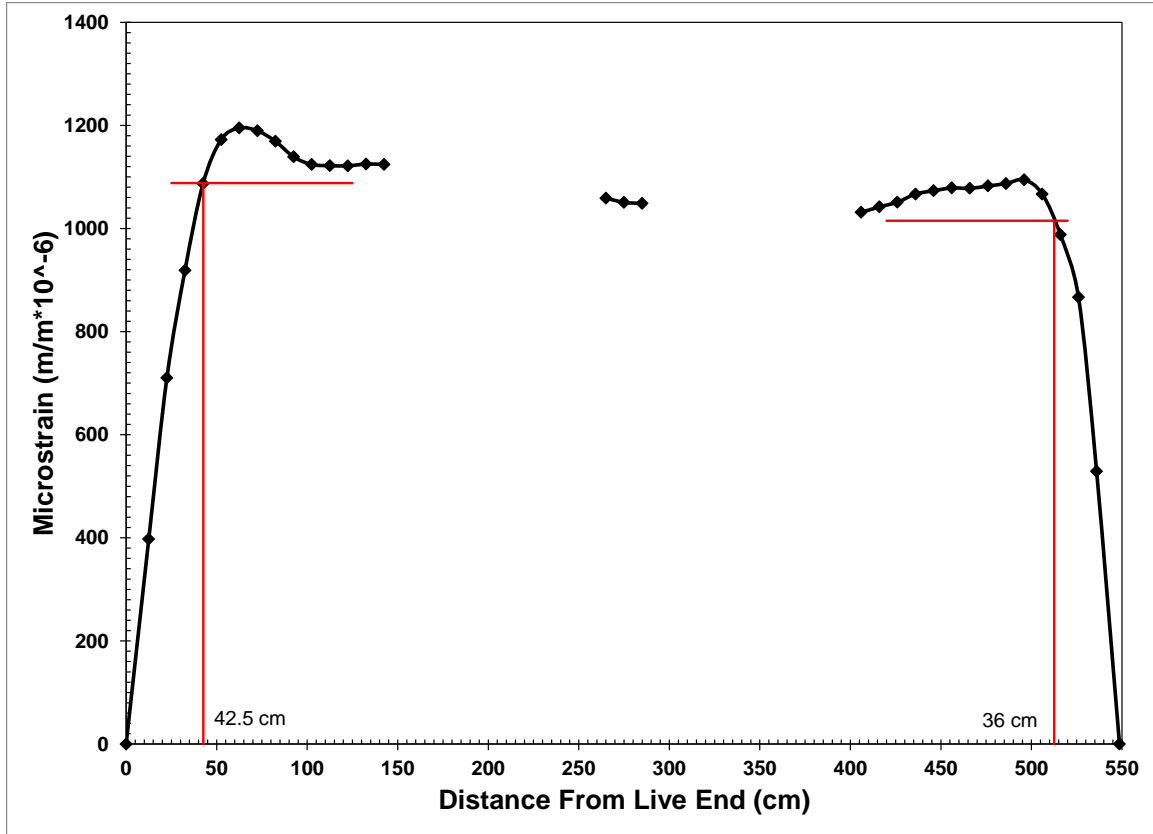


Figure 5.21: 28-Day strain profile with 95% AMS for specimen HSS-4

strain profile that tempered over time. The dead end transfer length had a more moderate decrease of just over 2 in. (50 mm) between prestress release and 28 days. The measured transfer lengths at 28 days presented in Table 5.10 were again very short and were approximately half of the values predicted using the code equations. The other prediction equations all yielded values significantly greater than those measured at 28 days.

#### 5.2.5.5 Summary and Discussion

The strain profiles for the high strength shale (HSS) specimens had clear strain plateaus that allowed for a simple determination of transfer length using the 95% AMS method. The live end transfer length was typically greater than that of the dead end for all specimens at all ages. Specimen HSS-2 had very similar live and dead end transfer lengths with the dead end having a slightly larger magnitude at 28 days. The measured transfer lengths were significantly less than

those predicted by the ACI and AASHTO equations at all ages. The other prediction equations also exceeded the measured transfer lengths at 28 days by a substantial amount. The very short transfer lengths for the HSS specimens may have been influenced by a degree of segregation of the concrete mixture that was discovered during flexural testing. The concrete immediately around the strands tended to have less coarse aggregate than the concrete in the upper reaches of each specimen. The high strength, high quality paste mitigated effects of low aggregate stiffness and interaction between large aggregate particles and the strand. Since any coarse aggregate particles touching the strand would not conform to the shape of the strand and would therefore reduce bond in that area, the entire length of paste was able to bond with the strand.

### **5.2.6 High Strength Limestone (HSL) Beams**

The strain profiles for the high strength limestone (HSL) specimens exhibited well defined strain plateaus with only minor anomalies. The magnitude of the strain measurements was less than that of the other specimens. As was the case for the normal strength clay (NSC) specimens, difficulties with the epoxy used to place DEMEC points caused issues with a small number of points that produced erratic data before those points were eventually lost.

#### **5.2.6.1 HSL-1**

The strain profiles for specimen HSL-1 had very well defined strain plateaus with only minor peaks at the initial break-over point for all profiles except the south side live end. The magnitude of the live end strain measurements was greater than those of the dead end and the beam midpoint, but these differences decreased somewhat over time. The average strain profile at 28 days is presented in Figure 5.22. A peak at the initial break-over point is evident on the dead end, and the live end had a greater strain magnitude than the dead end. The measured transfer lengths over time are presented in Table 5.11. The live end transfer length was greater

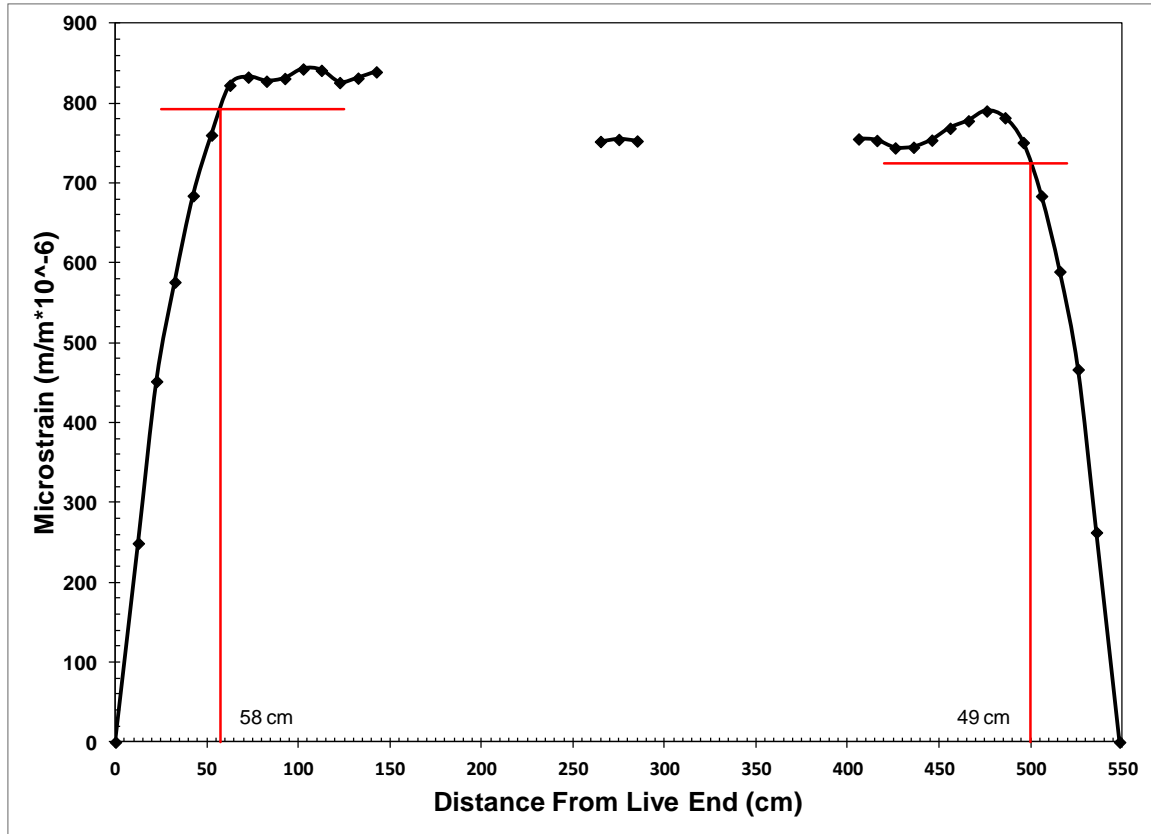


Figure 5.22: 28-Day strain profile with 95% AMS for specimen HSL-1

than that of the dead end at all ages, was fairly consistent over time, and had a net increase of approximately 1 in. (25 mm) between prestress transfer and 28 days. The dead end transfer length was very consistent over time with a slight irregularity at 5 days of age. The measured transfer lengths and calculated predictions at 28 days are presented in Table 5.12. The measured

Table 5.11: HSL Transfer Length Measurements Over Time

End	Live (in.)				Dead (in.)			
	HSL-1	HSL-2	HSL-3	HSL-4	HSL-1	HSL-2	HSL-3	HSL-4
<b>Release</b>	21.7	20.9	18.1	19.7	19.3	20.3	18.9	19.5
<b>3-Day</b>	21.5	18.9	18.9	18.7	18.1	22.4	18.7	19.3
<b>5-Day</b>	20.9	19.7	18.7	18.3	16.7	23.6	18.1	19.5
<b>7-Day</b>	22.2	19.7	18.9	19.3	17.9	23.0	18.7	19.3
<b>14-Day</b>	21.5	19.5	19.5	17.9	17.5	23.6	18.5	19.3
<b>28-Day</b>	22.8	20.9	20.5	19.5	19.3	25.2	19.3	19.7

Note: 1 in. = 25.4 mm

Table 5.12: Comparison of HSL Transfer Length Predictions

Specimen	HSL-1	HSL-2	HSL-3	HSL-4
Measured (Live) (in.)	22.8	20.9	20.5	19.5
Measured (Dead) (in.)	19.3	25.2	19.3	19.7
ACI 318/AASHTO LRFD (in.)	35.2	35.3	35.3	35.2
ACI (50d <sub>b</sub> ) (in.)	30.0	30.0	30.0	30.0
AASHTO (60d <sub>b</sub> ) (in.)	36.0	36.0	36.0	36.0
Zia and Mostafa (in.)	20.2	19.7	20.1	20.4
Shahawy, Deatherage et al., Buckner (in.)	37.9	37.9	37.9	37.9
Russell and Burns (in.)	52.8	52.9	52.9	52.9
Russell and Burns (80d <sub>b</sub> ) (in.)	48.0	48.0	48.0	48.0
Lane (in.)	49.9	48.1	47.3	45.1
Kose and Burkett (in.)	32.7	32.2	31.9	31.3
Ramirez and Russell (in.)	27.5	27.2	27.4	27.6

Note: 1 in. = 25.4 mm

transfer lengths were smaller than the predictions calculated using the code equations and all others except that the live end transfer length exceeded the Zia and Mostafa equation.

#### 5.2.6.2 HSL-2

The strain profiles for specimen HSL-2 exhibited well defined strain plateaus. All profiles except for the north side live end had a downward slope after the initial break-over point. The north side live end profile exhibited an increase at the end of the measured length most likely caused by poor data at a single point. Data from one pair of points on the south side dead end profile was removed from the calculations as these were deemed erroneous. The live end strain measurements again had a larger magnitude than those for the dead end, and the strains at each end had a larger magnitude than those at the beam midpoint for all but the north side dead end. The 28-day average strain profile is presented in Figure 5.23.

The measured transfer lengths over time are presented in Table 5.11. The dead end transfer length was greater than the live end over time and by more than 4 in. (100 mm) at 28 days. It exhibited growth of approximately 5 in. (125 mm) between prestress release and 28 days. The live end transfer length was very consistent over time. The measured transfer lengths

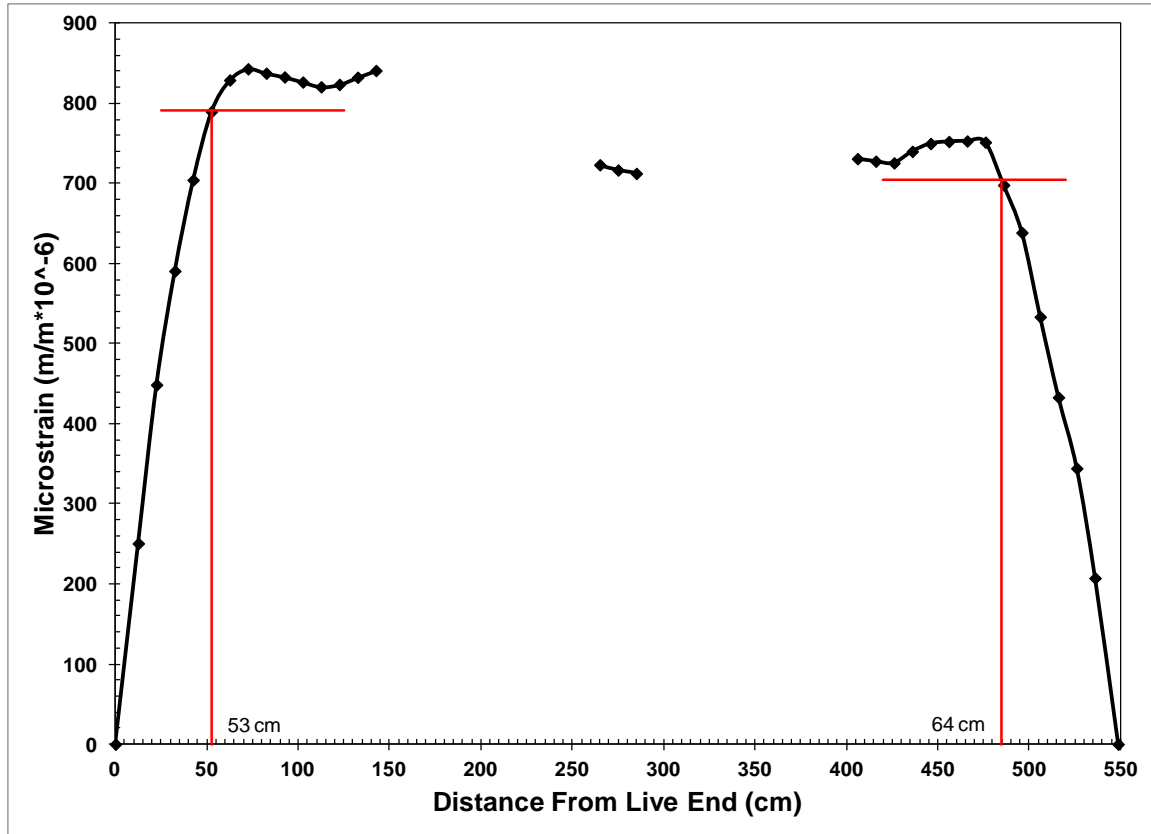


Figure 5.23: 28-Day strain profile with 95% AMS for specimen HSL-2

at 28 days were substantially less than the predictions produced by the code equations, as shown in Table 5.12. The dead and live end transfer lengths were greater than the prediction produced by the Zia and Mostafa equation. It was unusual for the dead end transfer length to exceed the live end transfer length by almost 5 in. (125 mm). The placement of the beam within the prestressing bed, as mentioned in Section 5.2.1.5, may have contributed to this difference.

### 5.2.6.3 HSL-3

The strain profiles for specimen HSL-3 were slightly more irregular than those of the other HSL specimens. The north side live end profile had a very smooth strain plateau while the dead end profile was erratic, did not have an absolutely clear plateau, and trended upward in magnitude after the initial break-over. The profiles of both ends trended toward the midpoint measurements. The south side live end profile had a peak at the initial break-over followed by a



downward trend. The south side dead end also trended toward decreasing magnitude with a slight irregularity caused by a lost DEMEC point. It also had a larger strain magnitude than the live end, which was unusual. Both live and dead end south side profiles had strain magnitudes greater than that of the measurements taken at the beam midpoint. The 28-day average strain profile presented in Figure 5.24 illustrated the erratic behavior of the dead end profiles for this specimen. The strain plateaus are clearly evident and the magnitude of the strains is fairly consistent along the entire length of the beam with only slightly larger values for the live end.

The measured transfer lengths over time are presented in Table 5.11. The transfer lengths for both ends were very close in magnitude with the live end slightly larger after 14 days. The live end transfer length had more pronounced growth over time with a net increase of almost 2.5 in. (64 mm) between prestress release and 28 days. The measured transfer lengths at 28 days

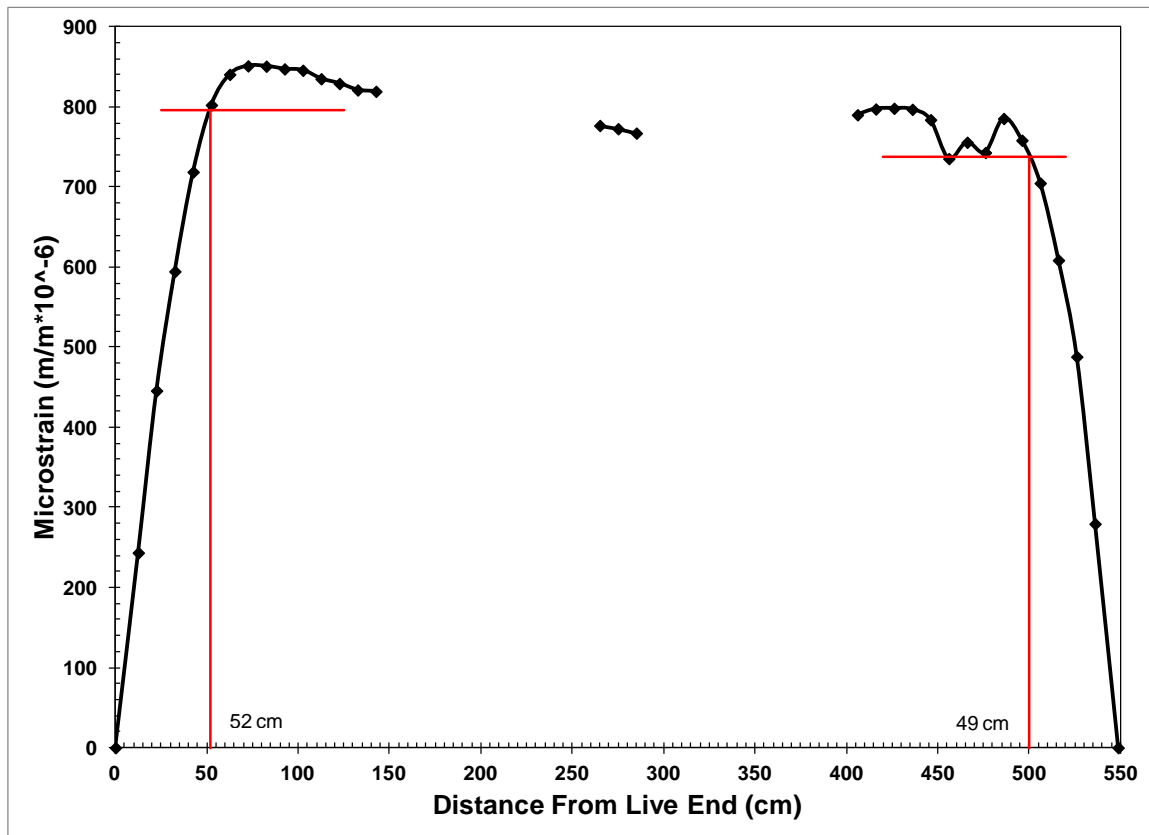


Figure 5.24: 28-Day strain profile with 95% AMS for specimen HSL-3

presented in Table 5.12 were significantly less than those predicted by the code equations and were less than all of the predictions except that the live end transfer length slightly exceeded that calculated using the Zia and Mostafa equation.

#### 5.2.6.4 HSL-4

The strain profiles for specimen HSL-4 were the smoothest of those for the HSL specimens. The dead end profiles for both sides had downward trends after the initial break-over point. The south side live end also had a downward trend along with an irregularity most likely caused by poor data at a single set of points. The live end profiles had a slightly larger strain magnitude than the dead end profiles and the north side dead end exceeded the magnitude of the measurements at the beam midpoint. The 28-day average strain profile is presented in Figure 5.25, which exhibited slightly erratic behavior, and the live end strain profile had a larger

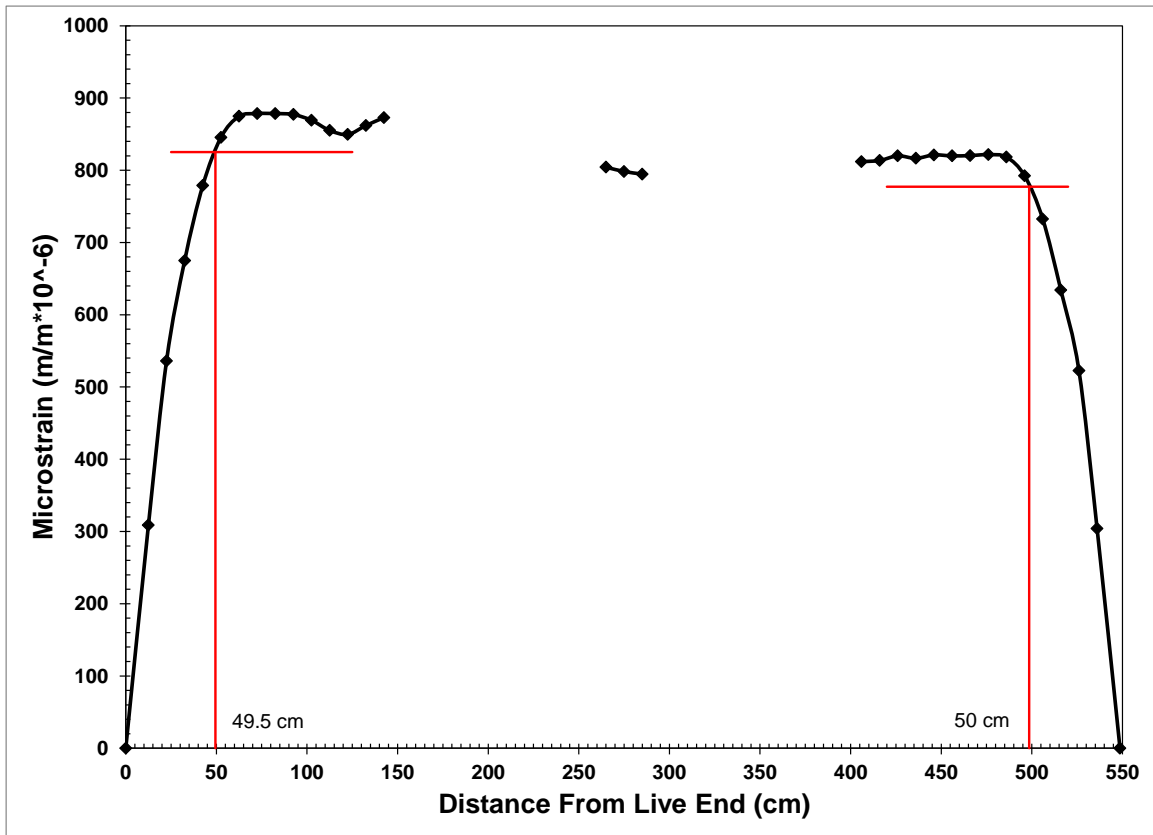


Figure 5.25: 28-Day strain profile with 95% AMS for specimen HSL-4

magnitude than the dead end. The plateaus were very clear. The measured transfer lengths presented in Table 5.11 were very similar for both ends of the specimen and the dead end transfer length was exceptionally consistent over time. The measured values at 28 days shown in Table 5.12 were substantially smaller than all of the predictions except for that calculated using the Zia and Mostafa equation which was greater than, but very close to, the measured values.

#### 5.2.6.5 Summary and Discussion

The strain profiles for the high strength limestone (HSL) specimens were very smooth and exhibited very well defined strain plateaus. The measured transfer lengths were significantly less than the predictions calculated using the ACI and AASHTO code provisions at 28 days. The same was true for all of the other prediction equations except for the Ramirez and Russell equation when compared to the dead end of specimen HSL-2 and the Zia and Mostafa equation. The Ramirez and Russell prediction only exceeded the dead end transfer length of specimen HSL-2 by 2 in. (50 mm) while it exceeded the other measured values by approximately 5 in. (125 mm) or more. The Zia and Mostafa prediction was exceeded by the transfer length of at least one end of all specimens except HSL-4 and was very close to the measured values for all other cases.

#### 5.2.7 Summary of DEMEC Transfer Lengths

Substantial difficulties and irregularities were experienced during the collection of DEMEC data. These were attributed to inexperience using the DEMEC system, problems with the epoxy used to place the DEMEC gage points, the support conditions of the specimens during storage, and inconsistencies caused by the relatively low strengths of the normal strength (NS) concrete mixtures made with lightweight aggregate. The issues associated with using the DEMEC system were quickly corrected over time and most likely were not a problem after the

normal strength clay (NSC) beam series. In most NSC cases effects of any issues were limited by the fact that the final values were based on the average of measurements taken on both sides of each specimen. Issues with the epoxy continued throughout the research project, but were minor and had a reduced impact over time. High temperatures during point placement also contributed to problems with the epoxy. The placement of specimens in the yard was adjusted during the first 28 days of age for the normal strength shale (NSS) beams and so had no impact on any of the high strength (HS) beam series.

Secondary slopes after the initial break-over point were common throughout the different beam series. Slopes tending toward smaller strain values were most likely caused by flexural strain due to the self-weight of the members. The initial prestress put the beam in compression at the location of the prestressing steel whereas the self-weight of the member induced tension stress and in turn strain in this location that would decrease the magnitude of compressive strain shown in the strain profiles. The cause of secondary slopes tending toward increasing values of strain was not as clear. The high release stresses for the small member cross-section pushed the concrete into the range of inelastic behavior. The low tensile strength of the LWSCC mixtures let to cracking of the beam section due to the initial prestress, which in turn reduced the moment of inertia of the section. These two factors were most prevalent outside the transfer length where the prestress reached its full magnitude and combined to produce larger strains in this section of the beams than expected. In the case of the NSC and normal strength limestone (NSL) specimens, which were not supported at the beam ends during storage, the additional compressive strain caused by the flexural behavior of the overhangs may have contributed to these secondary slopes. In all cases, these slopes affected the transfer length determined using the 95% Average Maximum Strain Method, and thus affected the reliability of the method.

The majority of the transfer lengths trended toward an increase over time that varied in magnitude. A decrease in transfer length over time was observed for some cases, especially where the data were very erratic at early ages. These decreases in transfer length were typically attributed to the measurement and calculation methods and not the actual behavior of the specimens. The transfer lengths typically stabilized at between 5 and 14 days of age with very little growth occurring after this point. The live end transfer lengths were typically larger than the dead end for the same specimen, but in many cases both were very similar or the dead end transfer length was larger. The impact of the proximity to the live end was visible in the larger magnitude of concrete strain, and therefore stress, for the live ends of the specimens. The positioning of the beams within the prestressing bed appeared to correlate with the specimens where the dead end transfer length was larger. These usually were beams cast at the end of the prestressing bed opposite the tensioning frame. If the beams did not move properly during the gradual release of prestress, some tension was held between the abutment and the dead end of the specimen that was released suddenly when the strands were cut. Specimens with clear external evidence of poor consolidation also exhibited poor bond performance in the form of long transfer lengths. Specimens where some segregation, but adequate consolidation of the sand cement mortar, was later discovered during beam testing had similar to shorter transfer lengths than properly consolidated specimens.

The average measured transfer lengths are presented in Figure 5.26 along with the limits given by the ACI  $50d_b$  and AASHTO  $60d_b$  predictions. Small sample statistical analysis utilizing a t-distribution was applied to analyze the difference in means, due to the small sample size of only 8 or 10 data points for each concrete type. A hypothesis of equal means was tested and a statistically significant difference in the transfer length behavior was considered if this

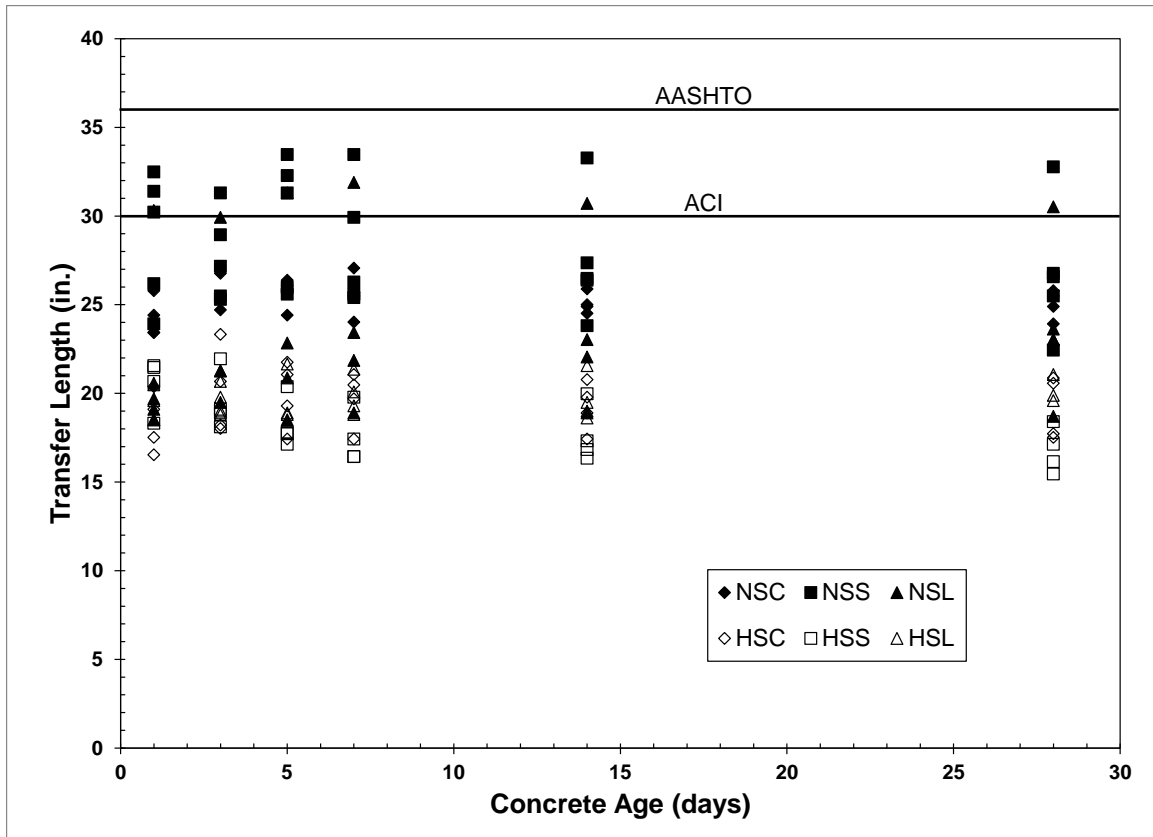


Figure 5.26: Average DEMEC transfer length measurements

hypothesis was rejected using the statistical test. No statistically significant difference was detected between the NSC and NSS transfer lengths. The standard deviation for both of these transfer length series was very high which may have masked differences that appeared evident in Figure 5.26. The statistical analysis did not indicate a significant difference between the means for the high strength clay (HSC) and high strength shale (HSS) series either. The standard deviations for these two sample sets were much more reasonable values in comparison to the means. A summary of the statistical parameters and analyses are presented in Appendix D.2.

Statistical analysis indicated a significant difference between the means of the NSC and HSC average transfer length measurements at 5, 7, 14, and 28 days. A similar difference was indicated between all NSS and HSS transfer length measurements. These results indicated that compressive strength at release is a major variable affecting transfer length for LWSCC. No

statistically significant difference was detected between the means of the NSL and high strength limestone (HSL) series, in spite of the differences in compressive strength. These differences correlate with observations made from the data plotted in Figure 5.26.

The one very large transfer length from the dead end of specimen NSL-4 inflated the mean value and standard deviation for the NSL set of beams. The standard deviations for the dead end and total NSL data set were 9.5 in. and 7.0 in. (241 mm and 178 mm) respectively at 28 days if this data point was included. These values were 2.9 in. and 2.3 in. (74 mm and 58 mm) for dead end and total NSL data set respectively if that point was not included. Based on the observation of very poor consolidation for that specimen, this data point was not included in the set used for comparison with the LWSCC mixtures. The comparison of the NSC and NSL means only indicated a statistically significant difference for the live end at 5 days and the total data set at release and 5 days. The NSC data had the most variability at these early ages. A statistically significant difference was detected between the means of the NSS and NSL series for all live end measurements and the total data sets. Such a difference was only detected for the dead end measurements at release. The comparison of the HSC and high strength limestone (HSL) data sets showed a statistically significant difference between the means for only the dead end at release, and this difference was in favor of the HSC measurements being smaller. A statistically significant difference was detected between the means of the HSS and HSL series for the live and dead ends at one and 28 days, for the dead end at 7 days, and for the total data set at 28 days. These differences were also in favor of the HSS transfer lengths being smaller in magnitude. All of these differences correlated with the results presented in Figure 5.26.

The 95 percent upper-confidence bound for the mean of each transfer length data set was compared to the ACI and AASHTO requirements of  $50d_b$  and  $60d_b$  respectively in order to

determine if the mean was likely greater than the values given by these requirements. The values calculated for each beam series are presented in Tables 5.13 through 5.15. The upper bound for the NSC series live end exceeded the ACI provision at all ages and the AASHTO provision at 3 days. The dead end and average upper bound was very close to the ACI provision, but did not exceed it at any age. The upper bound for the NSS series live end exceeded the ACI provision at all ages, but was very close at 14 and 28 days. The dead end upper bound exceeded the ACI requirement at all ages except release and 3 days, and the average upper bound exceeded the ACI requirement at all ages except 28 days. This value was very nearly equal to the ACI provision. The 95 percent upper-confidence bound for the NSL specimens did not exceed the values given by the ACI and AASHTO provisions if the outlying point from specimen NSL-4 was not included. When this point was included in the data set, the dead end 95 percent upper-

Table 5.13: 95% Upper-Confidence Bound for the Mean of Using a t Distribution

Time	NSC (in.)			NSS (in.)			Prediction (in.)	
	Live	Dead	Average	Live	Dead	Average	ACI	AASHTO
Release	32.2	26.0	26.8	40.2	26.2	33.1	30	36
3-Day	37.7	29.6	29.9	33.2	27.7	30.3	30	36
5-Day	34.0	29.9	29.2	37.7	32.9	33.2	30	36
7-Day	33.8	29.5	28.9	32.0	34.5	31.4	30	36
14-Day	33.8	28.5	28.7	30.4	33.6	30.4	30	36
28-Day	34.0	28.8	28.8	30.2	32.6	29.7	30	36

Note: 1 in. =25.4 mm

Table 5.14: 95% Upper-Confidence Bound for the Mean Using a t Distribution

Time	HSC (in.)			HSS (in.)			Prediction (in.)	
	Live	Dead	Average	Live	Dead	Average	ACI	AASHTO
Release	28.9	19.1	22.6	26.5	19.3	23.0	30	36
3-Day	28.5	20.9	23.2	24.3	19.5	21.4	30	36
5-Day	23.9	22.7	22.0	22.7	17.8	19.9	30	36
7-Day	23.9	21.4	21.6	22.6	17.0	19.3	30	36
14-Day	22.3	20.7	20.8	22.1	17.6	19.2	30	36
28-Day	23.8	20.6	20.9	20.2	16.9	18.0	30	36

Note: 1 in. =25.4 mm



Table 5.15: 95% Upper-Confidence Bound for the Mean Using a t Distribution

Time	NSL (in.)			HSL (in.)			Prediction (in.)	
	Live	Dead	Average	Live	Dead	Average	ACI	AASHTO
Release	21.6	19.9	20.3	21.9	20.2	20.5	30	36
3-Day	21.8	27.1	22.8	21.0	21.9	20.6	30	36
5-Day	22.6	26.8	23.0	20.7	23.0	20.8	30	36
7-Day	23.3	26.0	23.3	21.8	22.4	21.1	30	36
14-Day	22.2	26.2	22.8	21.3	22.9	21.0	30	36
28-Day	23.6	25.6	23.1	22.6	24.3	22.3	30	36

Note: 1 in. =25.4 mm

confidence bound did exceed both provisions, but the average value upper bound did not. The upper bounds for the HSC, HSS, and HSL specimens did not exceed the ACI or AASHTO provisions.

### 5.3 End Slip Transfer Lengths

End slips measured as described in Section 3.8.3 were used to determine the transfer lengths presented in this section using the theoretical relationship

$$L_t = \alpha L_{es} \left[ \frac{E_{ps}}{f_{si}} \right]$$

also described in Section 3.8.3, where  $L_t$  is the transfer length (in.),  $L_{es}$  is the measured end slip (in.),  $E_{ps}$  is the modulus of elasticity of the prestressing strand (ksi),  $f_{si}$  is the initial prestress (ksi), and  $\alpha$  is a factor accounting for the assumed steel stress distribution. The constant  $\alpha$  is taken as 2.0 for a linear steel stress distribution and 3.0 for a parabolic steel stress distribution. The transfer lengths determined using end slip did not always correlate well with those measured using the DEMEC system and the 95% Average Maximum Strain method. The transfer length results, calculated using the equation and each variation of  $\alpha$ , are presented along with a comparison to the DEMEC transfer lengths. Finally the DEMEC data were used to estimate the most likely value of  $\alpha$ , considering the DEMEC transfer lengths to be the correct measurements.

### 5.3.1 Normal Strength Clay (NSC) Specimens

Since Plexiglas plates were not used for the ends of the normal strength clay (NSC) specimens, the end slip measurements for these beams were much more inconsistent than the measurements for the remainder of the beams. The end slip values varied between 0.028 in. and 0.098 in. (0.71 mm and 2.49 mm) at release and between 0.008 in. and 0.092 in. (0.20 mm and 2.34 mm) at 28 days. The average transfer lengths calculated using these end slip measurements are presented in Figure 5.27 and the live and dead end values are presented in tabular form in Appendix D.4. The inconsistency of these values can be partially attributed to the poor end condition of the beams which made obtaining repeatable measurements very difficult. The use of  $\alpha = 3$  gave much better agreement with the DEMEC transfer length measurements than  $\alpha = 2$  for all cases except for the live end of NSC-4. Smaller end slip values typically corresponded to shorter DEMEC transfer lengths except in the case of the dead end of NSC-4.

### 5.3.2 Normal Strength Shale (NSS) Specimens

The addition of the Plexiglas end plates mentioned in Section 3.8.2.5 greatly improved the consistency of the end slip measurements and resulting transfer lengths for the beam sets cast after the NSC series. The normal strength shale (NSS) average transfer lengths calculated from the end slip measurements are presented in Figure 5.28 and the live and dead end values are presented in tabular form in Appendix D.4. The end slips measured for the NSS specimens varied from 0.034 in. to 0.064 in. (0.86 mm to 1.63 mm) at release and from 0.041 in. to 0.088 in. (1.04 mm to 2.23 mm) at 28 days. The use of  $\alpha = 3$  produced much better agreement with the DEMEC transfer lengths than  $\alpha = 2$  for most cases. This was not true for the live end of NSS-1 and some inconsistencies throughout the data set that were most likely caused by erratic strain profiles from the DEMEC measurements. The end slips did not correlate with the large DEMEC

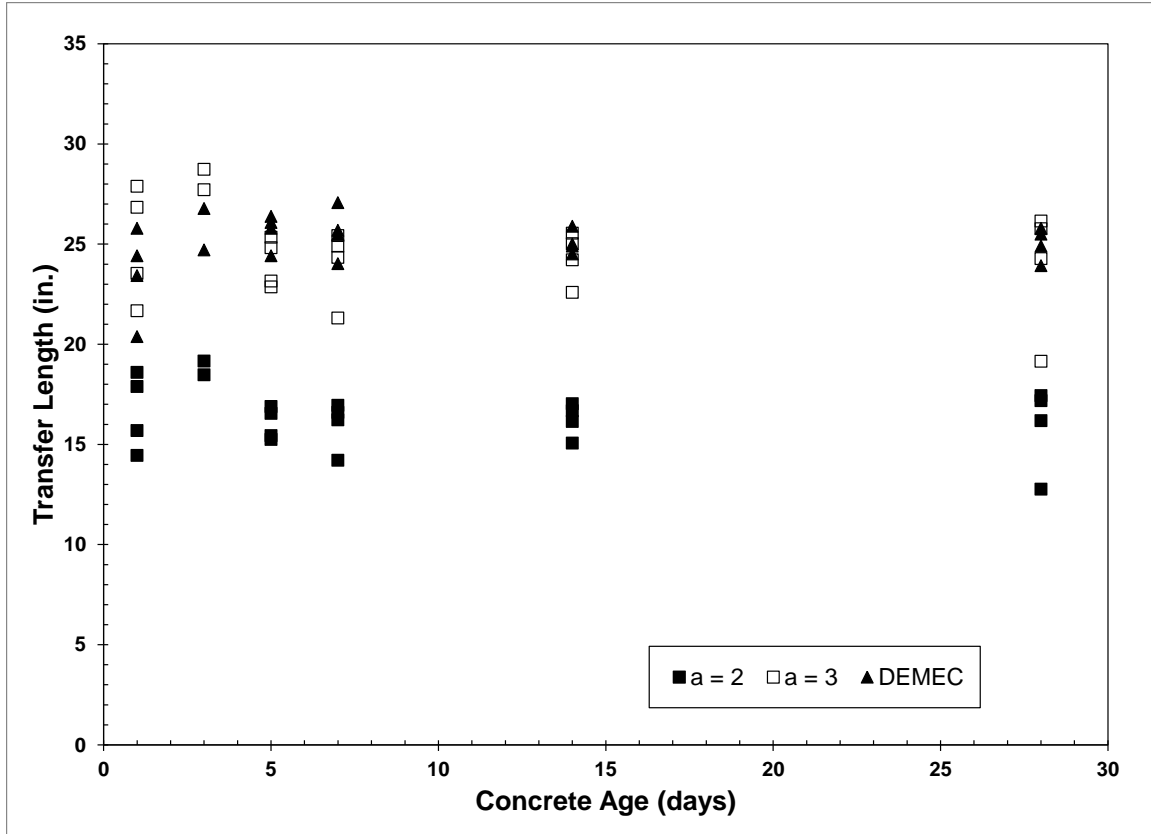


Figure 5.27: Average NSC transfer length measurements

Transfer lengths determined for specimen NSS-3 and the live end of specimen NSS-4. They did not correlate well with the large transfer length measured for the live end of specimen NSS-1.

### 5.3.3 Normal Strength Limestone (NSL) Specimens

The end slips and resulting transfer lengths were very consistent for the normal strength limestone (NSL) specimens. This trend was observed in the average transfer lengths plotted in Figure 5.29 and the live and dead end values presented in tabular form in Appendix D.4. The measured end slips varied from 0.026 in. to 0.144 in. (0.66 mm to 3.66 mm) at release and 0.047 in. to 0.169 in. (1.19 mm to 4.29 mm) at 28 days. The larger end of the spectrum came from the dead end of specimen NSL-4 which was very poorly consolidated. All other measurements were less than 0.050 in. and 0.068 in. (1.27 mm and 1.73 mm) at release and 28 days respectively.

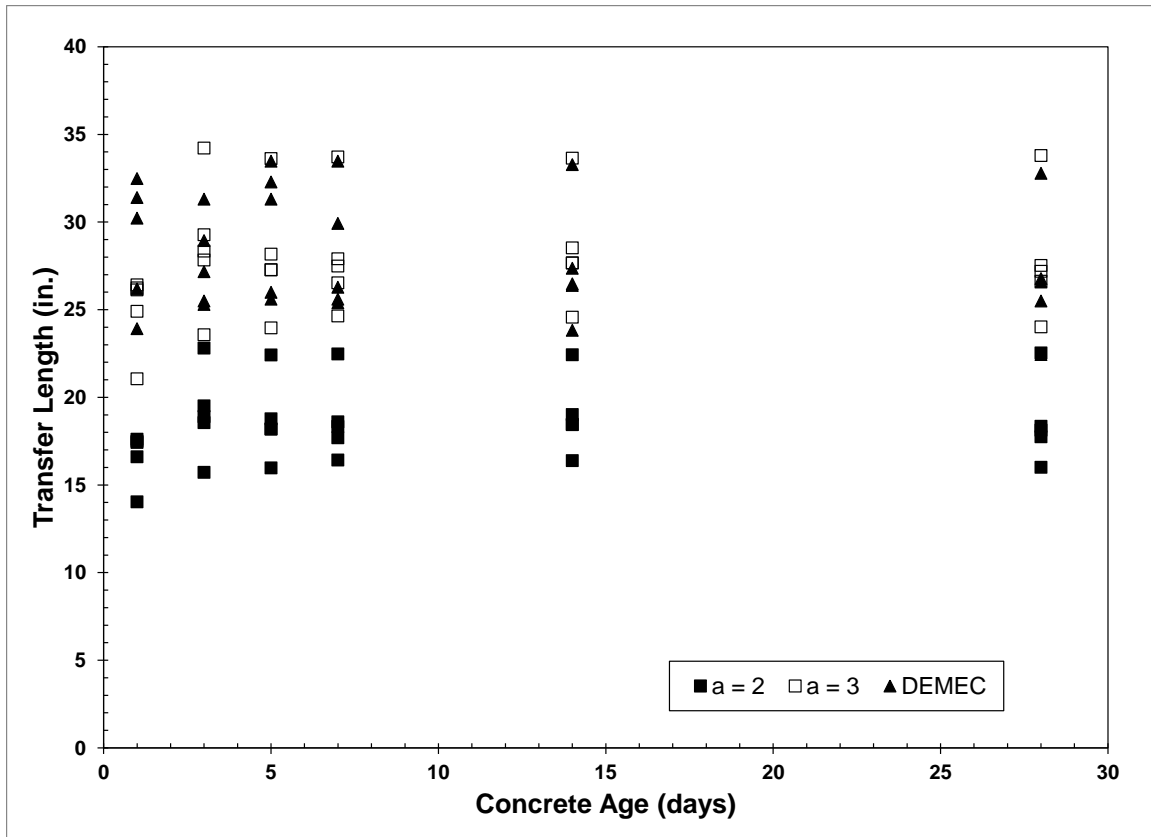


Figure 5.28: Average NSS transfer length measurements

The comparison between the DEMEC transfer lengths and those using the measured end slips and the various values of  $\alpha$  was very inconsistent, but the use of  $\alpha = 2$  produced values closest to the DEMEC measurements. The DEMEC transfer lengths were typically somewhere between the end slip transfer lengths calculated using  $\alpha = 2$  and  $\alpha = 3$ . The greatest disparity was between the values for the poorly consolidated dead end of specimen NSL-4.

### 5.3.4 High Strength Clay (HSC) Specimens

The end slips and resulting transfer lengths measured for the high strength clay (HSC) beams were small in magnitude and very consistent for each specimen. The measured end slips ranged from 0.022 in. to 0.039 in. (0.56 mm to 0.99 mm) at release and 0.028 in. to 0.056 in. (0.71 mm to 1.42 mm) at 28 days of age. All specimens exhibited a trend of increasing end slip

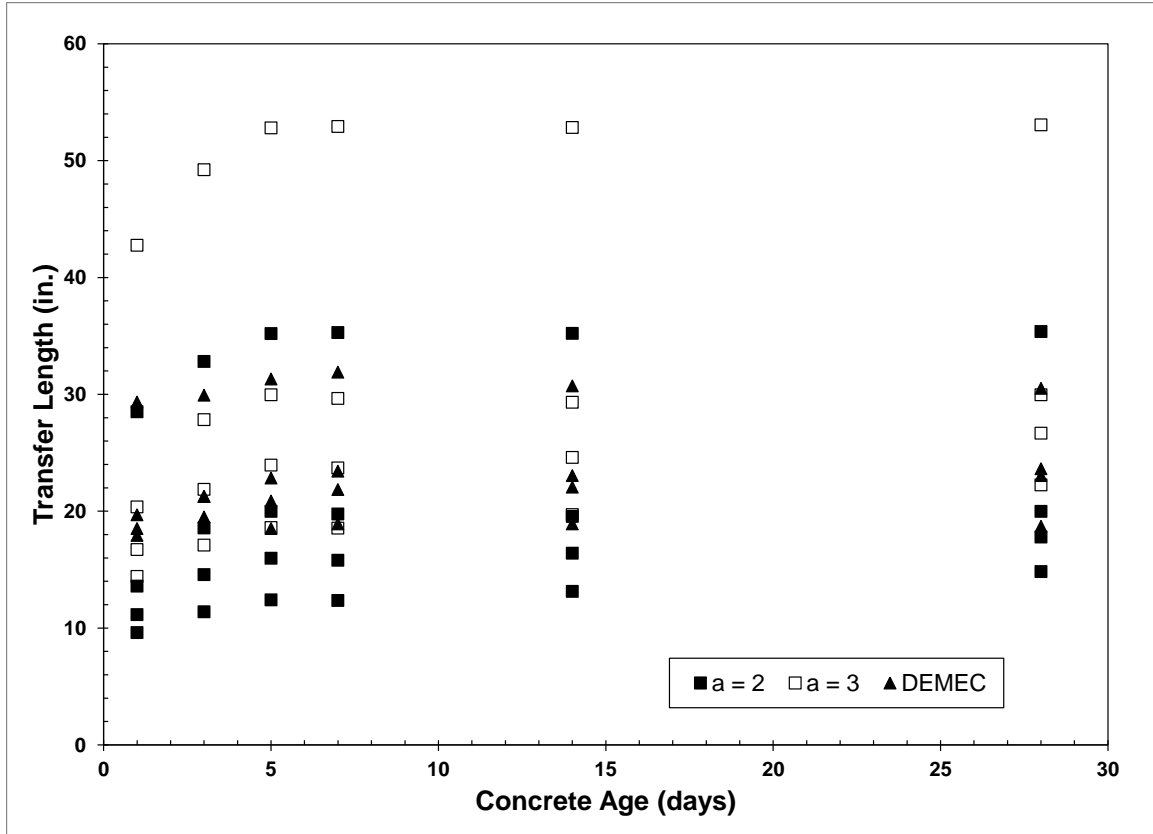


Figure 5.29: Average NSL transfer length measurements

over time for both the live and dead ends. The average transfer lengths are presented in Figure 5.30 and the live and dead end values are presented in Appendix D.4. The dead end transfer lengths measured at 28 days were greater than those of the live end for all specimens except HSC-1. The end slip transfer lengths calculated using  $\alpha = 3$  were very similar to those measured using the DEMEC system in almost all cases. Those calculated using  $\alpha = 2$  were very small.

### 5.3.5 High Strength Shale (HSS) Specimens

The end slips and resulting transfer lengths for the HSS specimens were very small in magnitude and were very consistent for each specimen. The end slip values ranged between 0.019 in. and 0.045 in. (0.48 mm and 1.14 mm) at prestress release and between 0.028 in. and 0.055 in. (0.71 mm and 1.40 mm) at 28 days of age. The average transfer lengths calculated

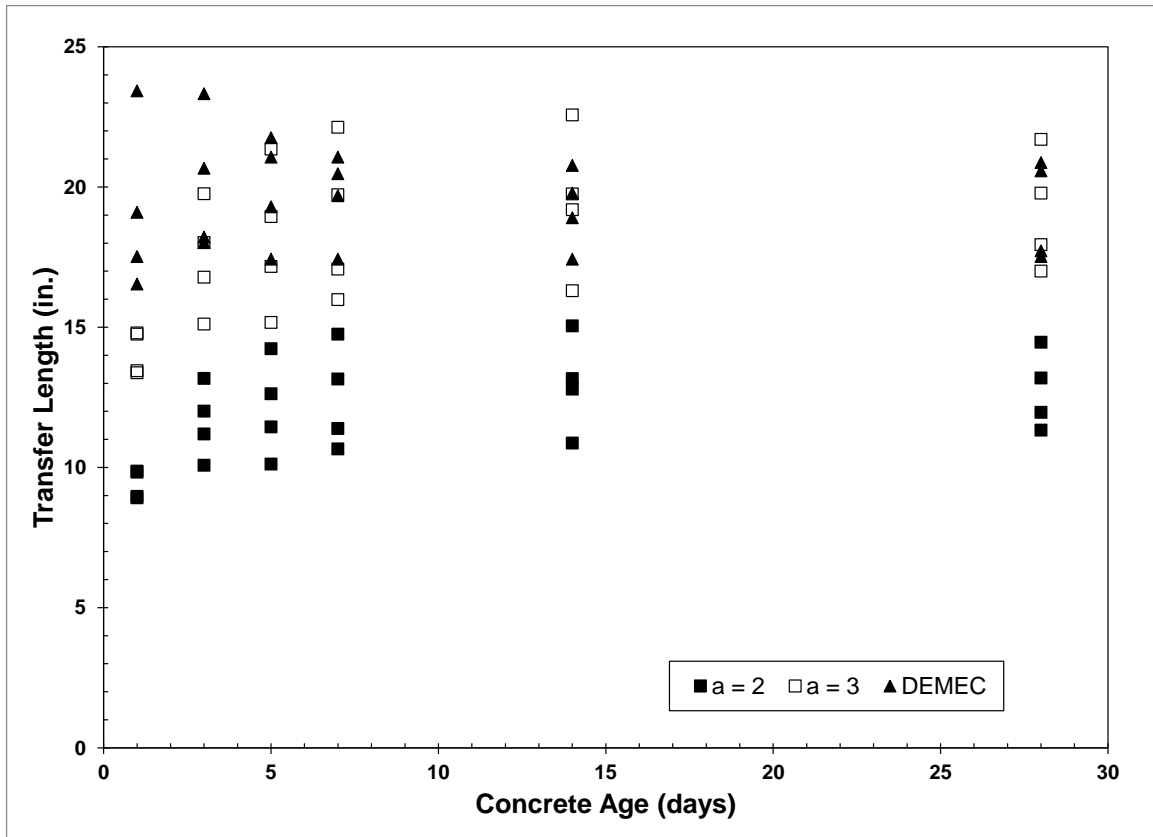


Figure 5.30: Average HSC transfer length measurements

using these end slips are presented in Figure 5.31 and the live and dead end values are presented in Appendix D.4. These values indicated a trend of increasing transfer lengths over time with the greatest increases occurring at early ages. The live end transfer lengths at 28 days were greater than the dead end for all but specimen HSS-2. The comparison of DEMEC transfer lengths to those calculated using the measured end slips was very inconsistent. The DEMEC transfer lengths typically fell into a range between the values calculated using  $\alpha = 2$  and  $\alpha = 3$  with neither providing a decidedly better correlation.

### 5.3.6 High Strength Limestone (HSL) Specimens

The end slip values measured for the high strength limestone (HSL) specimens and the resulting transfer lengths were consistent for each specimen. The average transfer length values

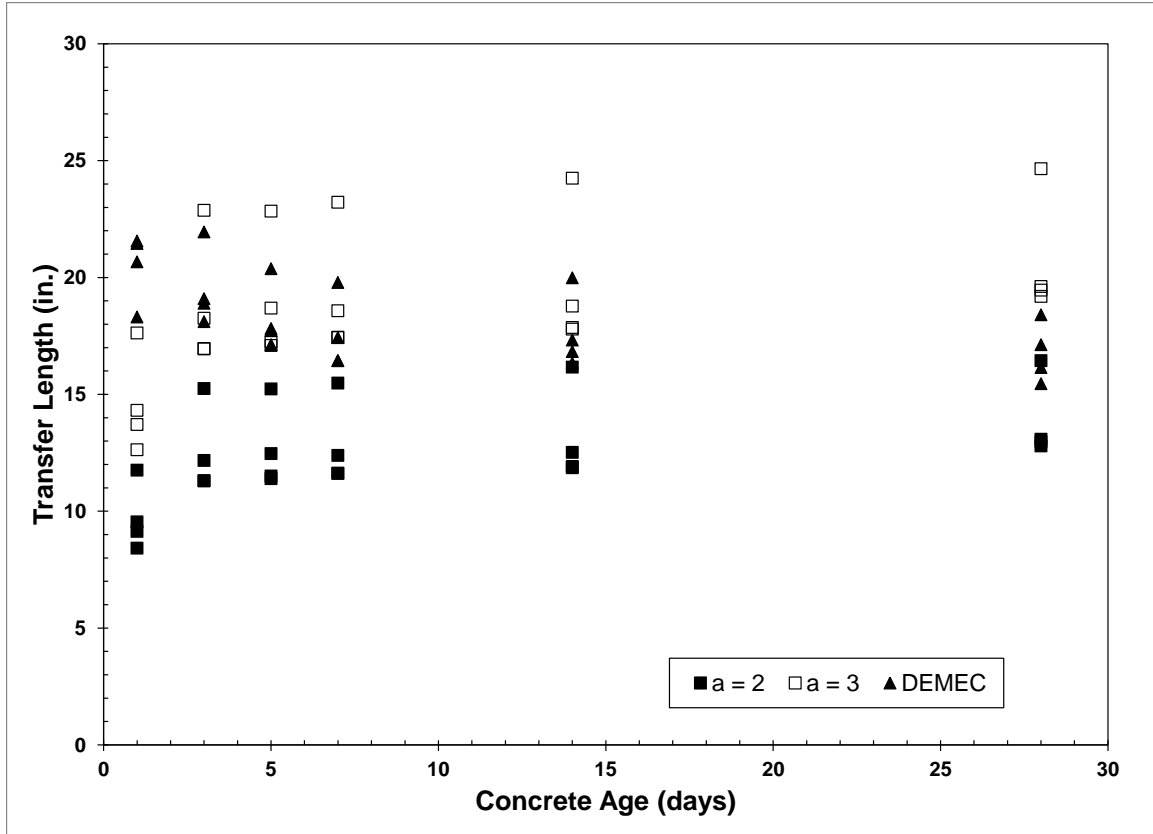


Figure 5.31: Average HSS transfer length measurements

are presented in Figure 5.32 and the live and dead end values are presented in tabular form in Appendix D.4. Some instances of erratic behavior were observed for specimen HSL-4, but all specimens exhibited a trend of increasing transfer length over time with the greatest increases between release and 3 days and between 14 and 28 days. The dead end transfer lengths were greater than those for the live end for all specimens except HSL-4. In most cases, the end slip transfer lengths calculated using  $\alpha = 2$  produced the best agreement with those measured using the concrete surface strains and the DEMEC system. The DEMEC transfer lengths typically fell in the range between the values produced using  $\alpha = 2$  and  $\alpha = 3$ .

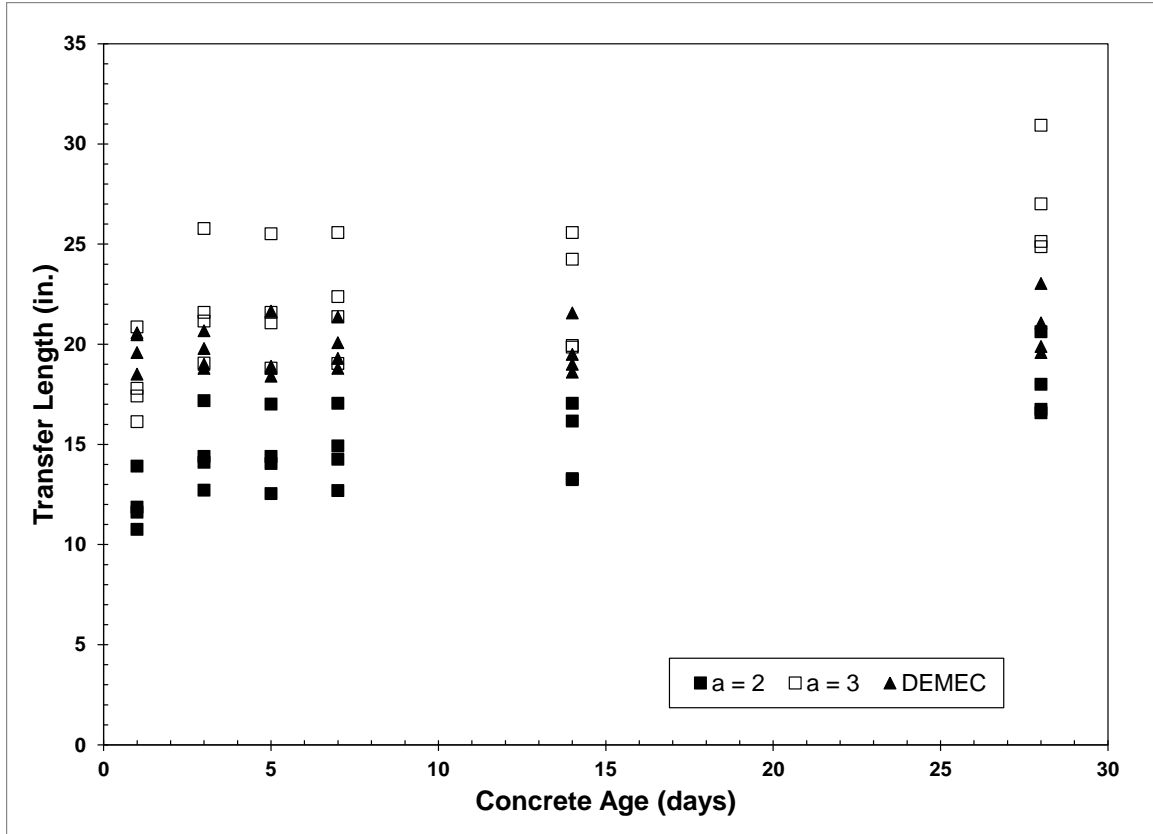


Figure 5.32: Average HSL transfer length measurements

### 5.3.7 Summary of End Slip Transfer Lengths

The use of end slip measurements to determine transfer length typically yielded results that were adequate for assessing the bond performance of the members. In most cases the results were very consistent for a given specimen, and many times more so than the transfer lengths measured using the DEMEC system and the 95% Average Maximum Strain method. There was no clear indication that the magnitude of live or dead end transfer length was consistently greater than the other as was typically the case for the DEMEC measurements.

### 5.4 Comparison of DEMEC and End Slip Transfer Lengths

The difference in calculation method along with the differences in measurements taken at the concrete surface and measurements of strand movement resulted in a disparity between the



end slip and DEMEC transfer lengths. The transfer lengths calculated using the measured end slips and using the typically assumed constant bond stress/linear steel stress distribution resulting in  $\alpha = 2$  were generally less than those measured using the DEMEC system. The values calculated assuming a linear bond stress/quadratic steel stress distribution and the resulting  $\alpha = 3$  were typically larger than those measured using the DEMEC system. Plotting the measured end slip against the DEMEC transfer length did not result in a clear correlation between the two as outlying points made a linear fit impractical. A linear fit was assumed based on the theoretical relationship presented in Section 5.3 and assuming a constant value of  $f_{si}$ . Other trend relationships did not result in a marked improvement. Removing the outlying points caused by the very poorly consolidated dead end of specimen NSL-4 made fitting the curve with a linear relationship more practical. This relationship is shown in Figure 5.33, but was still a poor correlation with the data. The constant from this relationship was used along with an average initial prestress ( $f_{si}$ ) of 183.9 ksi (1268 MPa) to calculate  $\alpha = 2.85$  from the equation presented in Section 5.3. Separating the data into NS and HS points did not produce a marked improvement in the fit of the data and resulted in  $\alpha = 2.87$  and  $\alpha = 2.81$  respectively.

Comparisons of the average 28-day live and dead end transfer lengths using  $\alpha = 2$ ,  $\alpha = 3$ , and  $\alpha = 2.85$  are presented in Appendix D.5. Figure 5.34 shows the comparison of average DEMEC and end slip transfer lengths at 28 days using  $\alpha = 2$  for the end slip calculations. The end slip transfer lengths were significantly less than those measured using the DEMEC system. The average end slip value for the NSL specimens was skewed by the very large end slip measured for the dead end of specimen HSL-4 which led to the close correlation using  $\alpha = 2$ . Figure 5.35 shows the comparison between the DEMEC and end slip transfer lengths calculated using  $\alpha = 3$  at 28 days. These end slip transfer lengths were much closer to the DEMEC values

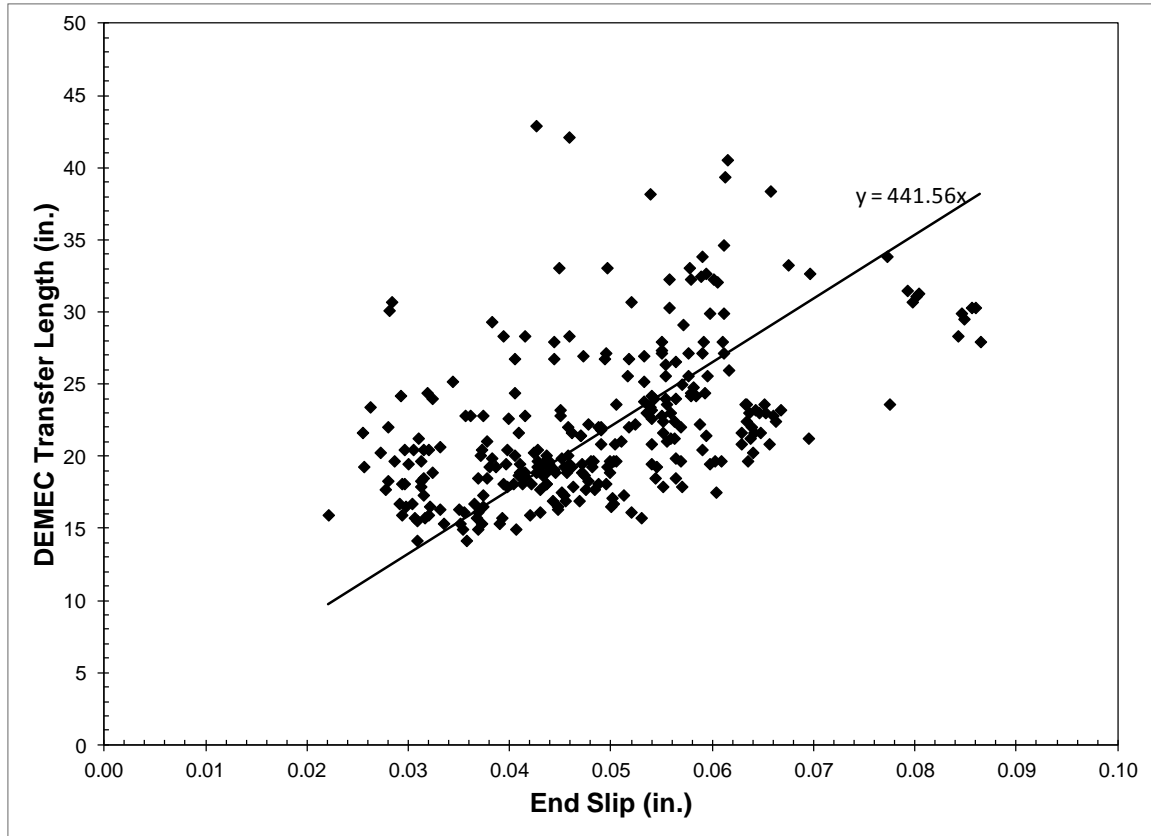


Figure 5.33: Comparison of DEMEC transfer lengths and measured end slip for the NSC, NSS, and HSC specimens. The values for the NSL specimens were skewed by the very large end slip measured for the dead end of specimen NSL-4. When that data point was removed the disparity between the two values was not as substantial. The DEMEC transfer lengths were in a range between the end slip transfer lengths calculated using  $\alpha = 2$  and  $\alpha = 3$  for the NSL, HSS, and HSL specimens. A comparison between the average DEMEC and end slip transfer lengths using  $\alpha = 2.85$  is presented in Figure 5.36. These values improved the correlation between the methods for some of the specimens and worsened it for others. It was not clear that using  $\alpha = 2.85$  was a marked improvement in the end slip transfer length calculation. The data were too scattered and erratic.

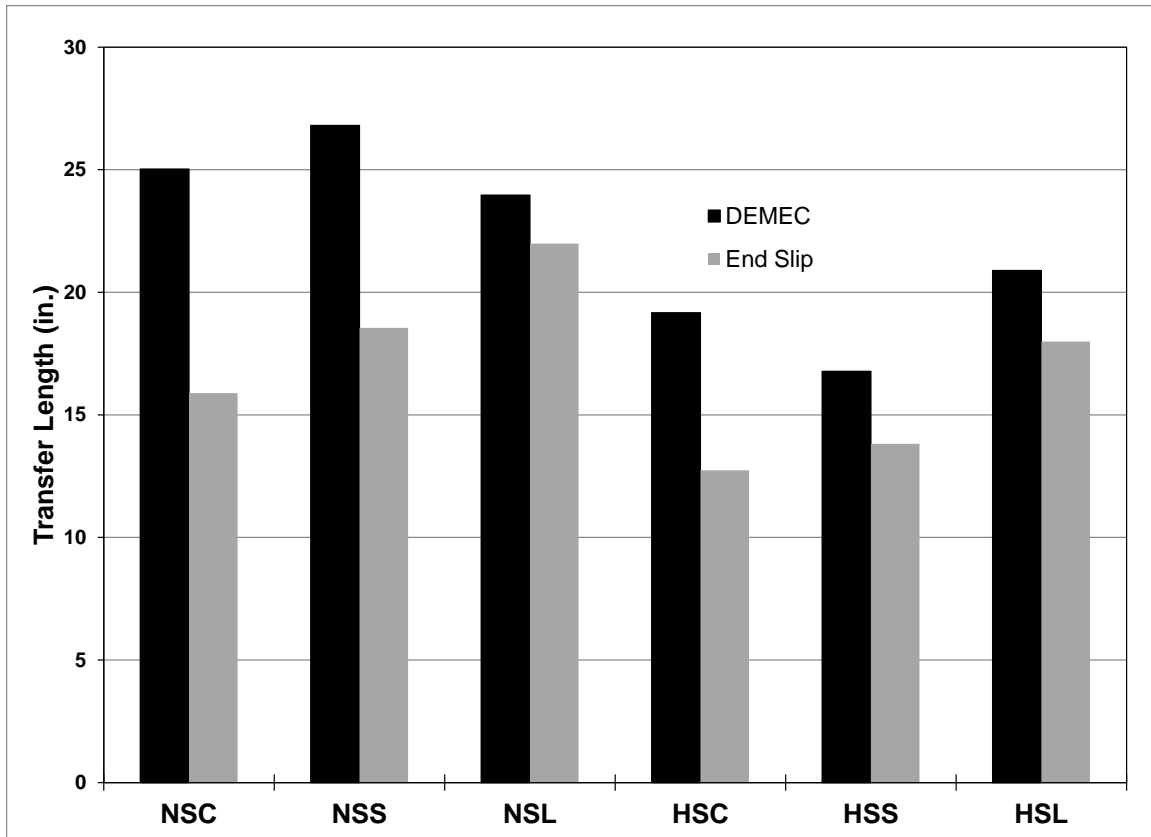


Figure 5.34: Average DEMEC and end slip ( $\alpha = 2$ ) transfer lengths at 28 days

There were too many variables at work to totally isolate the reasons for the disparity between the end slip and DEMEC transfer lengths. However, both methods can be used to produce a valid indication of the transfer bond performance of prestressing strands cast in these concrete types. Issues with strain behavior caused by high release stresses and cracking of the sections with low tensile strength reduced the appeal of using the DEMEC system to determine transfer length. The lack of adequate knowledge of the bond/steel stress distribution in the transfer zone and the lack of established measurement procedures reduced the appeal of using end slip to determine transfer length. Therefore, one method does not really stand out above the other in producing exact values of transfer length, while both produce a valid indication of bond performance.

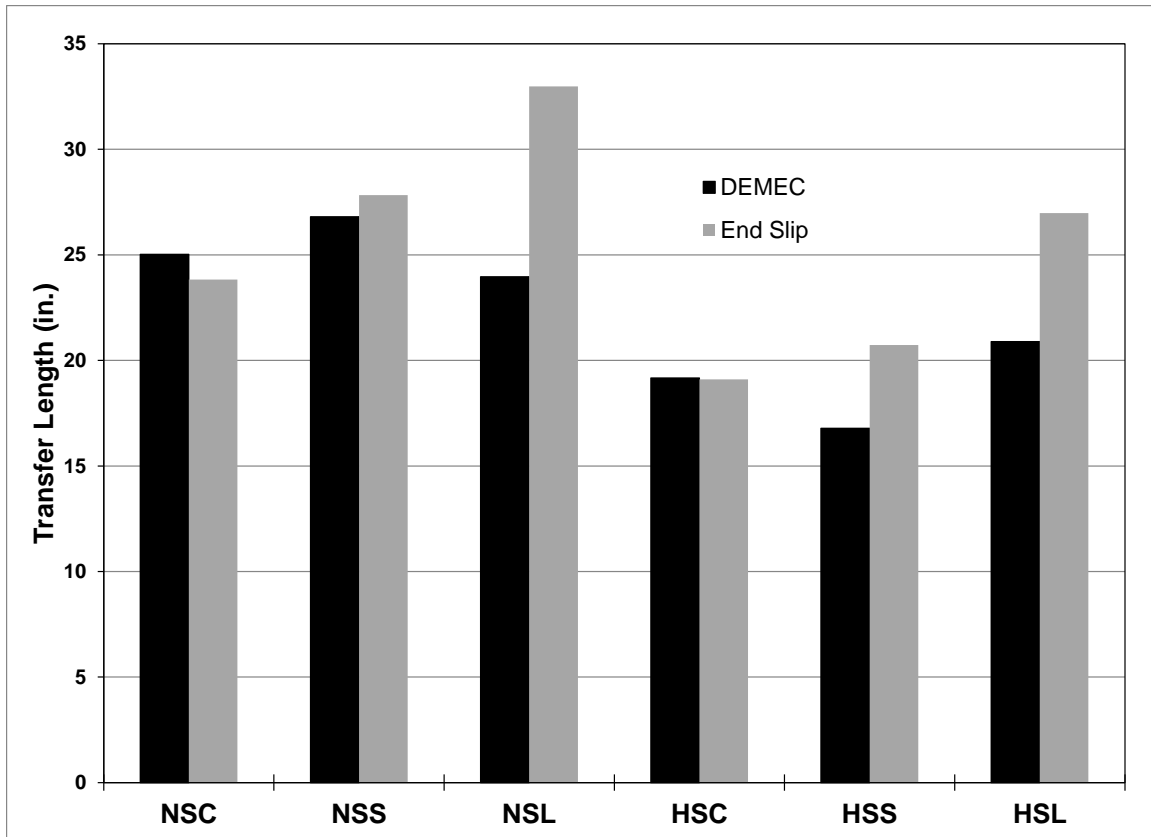


Figure 5.35: Average DEMEC and end slip ( $\alpha = 3$ ) transfer lengths at 28 days

## 5.5 Conclusion

The transfer lengths presented herein were measured using concrete surface strains with the DEMEC system and end slips measured using steel clamps attached to each strand along with a depth micrometer. Numerous difficulties were encountered in measuring the transfer length for these beam specimens due to issues with the epoxy used to attach the DEMEC points, a faulty depth micrometer, and poor end conditions for the normal strength clay (NSC) specimens. The effects of the issues with the epoxy were tempered by using measurements on both sides of each specimen, and these issues were resolved early in beam specimen construction. Issues with end slip measurements were solved for all specimens after the NSC series by purchasing a new depth micrometer and adding Plexiglas plates to the beam ends. No

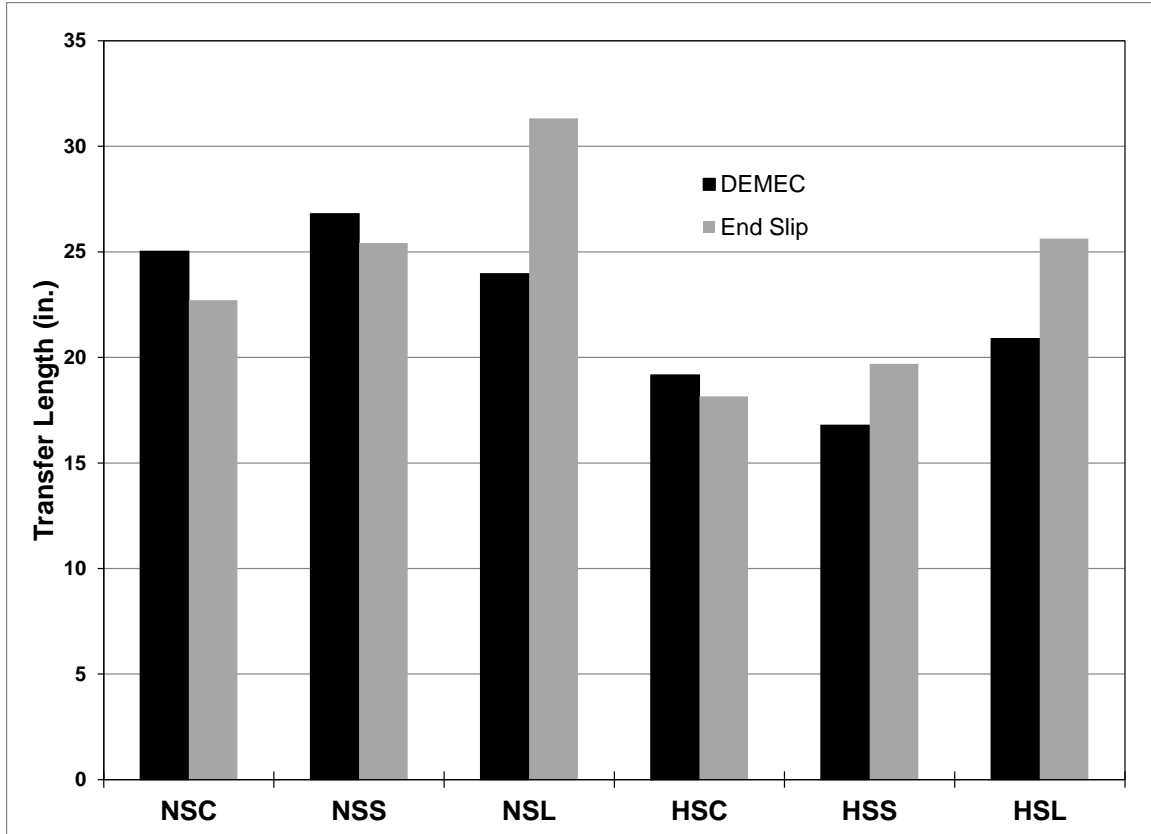


Figure 5.36: Average DEMEC and end slip ( $\alpha = 2.85$ ) transfer lengths at 28 days

significant difference was observed between the transfer lengths measured for each concrete type at a similar strength except for between the normal strength shale (NSS) and normal strength limestone (NSL) specimens. The live end transfer lengths for the NSS and NSC specimens and the average transfer lengths for the NSS specimens indicated consistent potential for exceeding the code predictions. The transfer lengths measured using concrete surface strains and the DEMEC system typically fell into a range bounded by end slip transfer lengths calculated using  $\alpha = 2$  and  $\alpha = 3$  when the values were compared.

## Chapter 6: Development Length Results

### 6.1 Introduction

In addition to the bond behavior in regard to transfer of prestress, this research project also focused on the bond behavior of members under load. The main characteristic used to quantify the bond behavior at the full strength of the member is development length. As defined in Chapter 1, the development length is the distance from the free end of the prestressing strand required to fully bond the strand to the concrete such that the full strength of the strand may be utilized (ACI 2011). This chapter begins with results of the Standard Test for Strand Bond (STSB) utilized to confirm the bonding quality of the 0.6 in. (15.2 mm) prestressing strand used in this project. The results of the flexural tests conducted on each end of the 25 prestressed beam specimens described in Section 3.8 are presented in detail. Beams from each series were typically tested in reverse order of casting, and therefore, numbering. These tests were used to bracket the development length for each concrete type. The ranges determined from these results were then compared to predictions calculated with the equations provided in accepted design codes and previous research. A summary of the full results for each specimen is presented in Appendix E.

### 6.2 Standard Test for Strand Bond (STSB)

The Standard Test for Strand Bond (STSB) was performed in accordance with the procedures described in Section 3.7 to assess the bonding quality of the prestressing strand used to construct the beam specimens. The results from the six specimens that made up the test are presented in Table 6.1. The force required to induce 0.10 in. (2.5 mm) of free end slip for each specimen exceeded the 10,800 lb (48.0 kN) minimum requirement for an individual specimen.

The average load of 19,180 lb (85.3 kN) exceeded the minimum requirement of 12,600 lb (56.0

Table 6.1: STSB Results for the Strand Used to Construct Beam Specimens

Strand Specimen	Load at Slip (lb)		Mortar Flow	Compressive Strength (psi)	
	0.01 in.	0.10 in.		22 hour	23 hour
1	13,560	18,010	112	5070	5270
2	14,600	19,340			
3	11,960	16,170			
4	14,170	18,540	100	5070	5210
5	15,730	21,010			
6	16,930	22,020			
Average	14,490	19,180	106	5070	5240

Note: 1 lbf = 4.448 N, 1 psi = 0.006895 MPa,

kN) for a six specimen set by 52 percent. The compressive strength of the mortar exceeded the upper limit of 5000 psi (34.5 MPa) both before and after pullout testing was performed, which would bias the results toward higher pullout values. The maximum of 270 psi (1.9 MPa) excess in compressive strength (5 percent) most likely would not have had a contribution significant enough to lead to results 50 percent greater than the minimum pullout load. Plots showing load versus ram travel and dead end slip for each test are presented in Appendix F.

### 6.3 Normal Strength Clay (NSC) Development Length

#### 6.3.1 NSC-1

##### 6.3.1.1 Dead End

The dead end of specimen NSC-1 was tested at an embedment length of 50 in. (1270 mm) to confirm the result of the previous test of the dead end of specimen NSC-2 at the same embedment. This embedment was approximately 53 percent of the development length predicted using the ACI/AASHTO equation. Flexural cracking began directly beneath the applied load, as shown in Figure 6.1. These initial flexural cracks grew as the load increased and other cracks appeared further away from the applied load that exhibited flexure/shear behavior as they propagated toward the applied load. The beam exhibited very ductile behavior during a period of yielding that is clearly visible in the plot of applied moment and measured deflection



Figure 6.1: Cracking pattern of specimen NSC-1D

presented in Figure 6.2 before the test concluded with crushing of the top compression fiber.

The maximum load for the test was 35.33 kips (157.2 kN) corresponding to a maximum moment of 939 k-in. (106.1 kN-m) which was approximately equal to the nominal moment of 933 k-in. (105.4 kN-m) calculated using strain compatibility. Combined with no strand slip, this result indicated that the development length for this specimen was less than the 50 in. (1270 mm) embedment.

#### 6.3.1.2 Live End

The live end of specimen NSC-1 was tested at an embedment length of 45 in. (1143 mm), corresponding to 48 percent of the ACI/AASHTO development length, after the purely flexural failure of the dead end of NSC-1. This was the shortest embedment length tested for this series of beams. The first flexural cracks appeared directly under the applied load. These were soon followed by shear cracks beginning near the beam end and propagating toward the load where



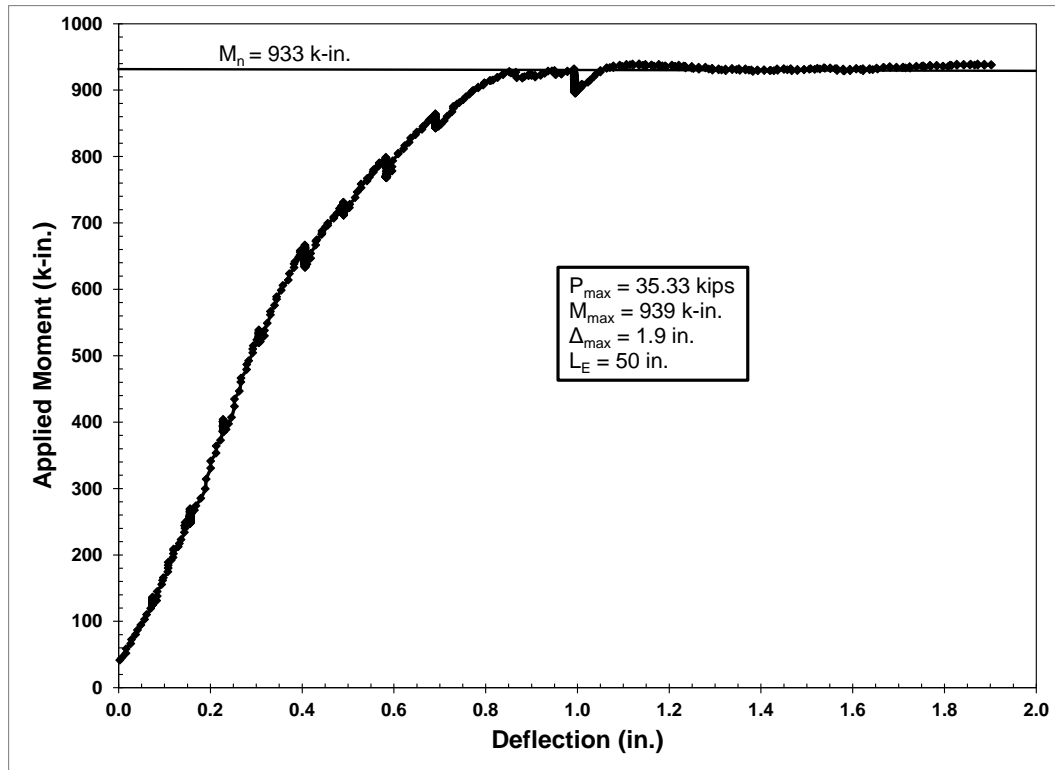


Figure 6.2: Plot of moment vs. deflection for specimen NSC-1D

they became nearly horizontal, as shown in Figure 6.3. The shear and cracking behavior observed in this test was most likely caused by the poor consolidation of this end of the member. The cracks followed the location of the compression steel indicating poor bond between this steel and the concrete. The maximum load carried by this member, 27.48 kips (122.2 kN), corresponded to a maximum moment of 703 k-in. (79.4 kN-m), well below the nominal moment of 933 k-in. (105.4 kN-m). The abrupt release of energy at the time of complete failure is clearly visible in Figure 6.4. The shear cracking at the maximum load was accompanied by significant strand slip that amounted to more than 0.10 in. (2.5 mm) by the end of the test. The shear failure and poor consolidation of this specimen did not indicate a definite conclusion about the development length.



Figure 6.3: Shear cracking and poor consolidation of specimen NSC-1L

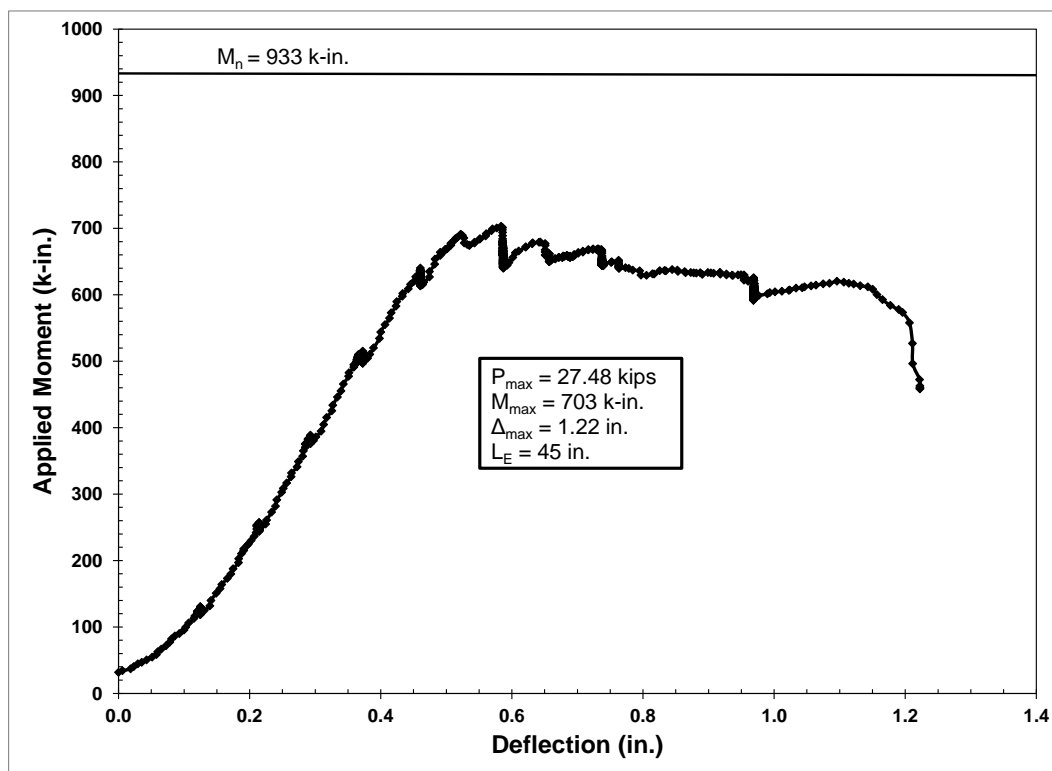


Figure 6.4: Plot of moment vs. deflection for specimen NSC-1L

## 6.3.2 NSC-2

### 6.3.2.1 Dead End

The dead end of specimen NSC-2 was tested at an embedment length of 50 in. (1270 mm) in response to the flexural failure of the live end of NSC-2 at an embedment of 55 in. (1397 mm). This embedment corresponded to 50 percent of the ACI/AASHTO development length. The first attempt to test this end resulted in a fracture of the corner of the beam end due to support placement too near the end of the specimen. The specimen was then reloaded with the support located farther from the end. Flexural cracking first appeared directly beneath the applied load followed by other cracks farther from the load that exhibited flexure/shear behavior as the load increased. The beam did not exhibit substantial yielding, as shown in Figure 6.5, but reached a maximum load and moment of 42.46 kips (188.9 kN) and 1067 k-in. (120.6 kN-m), respectively, before crushing of the top compressive fiber occurred. The beam was loaded

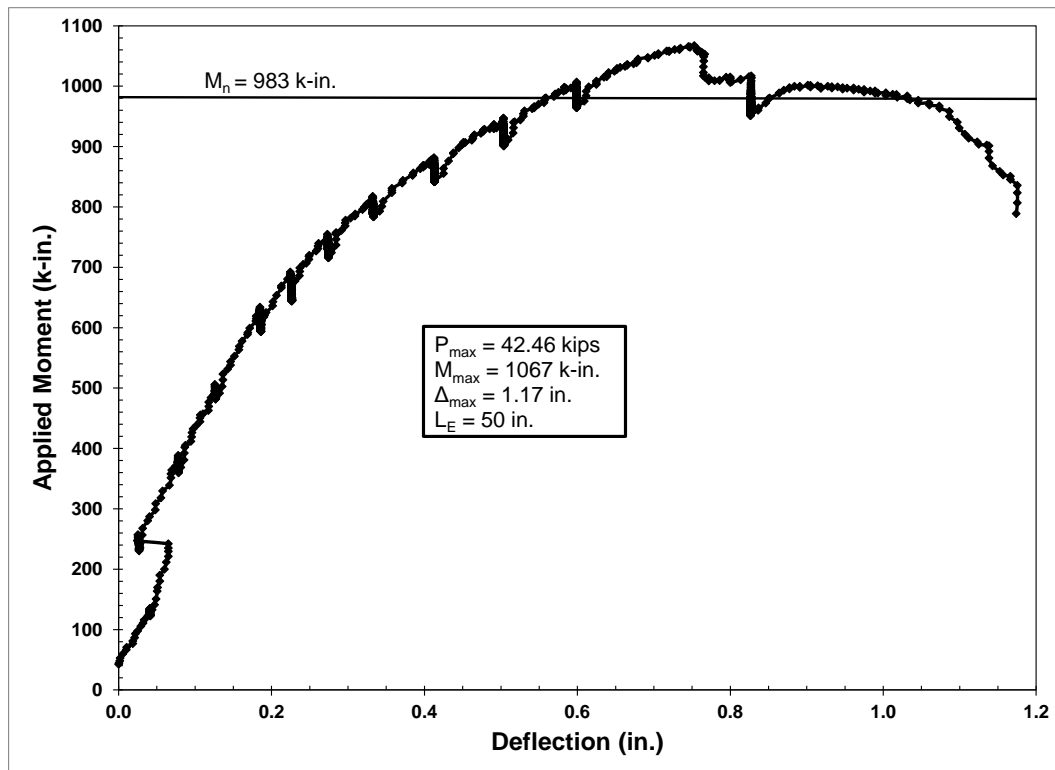


Figure 6.5: Plot of moment vs. deflection for specimen NSC-2D

further leading to a catastrophic shear collapse that also revealed buckling of the compression reinforcement and large particles of unmixed cement, as shown in Figure 6.6. The calculated nominal moment of 983 k-in. (111.1 kN-m) was exceeded by 8.5 percent during the test with no measured end slip, indicating that the development length was less than 50 in. (1270 mm).

#### 6.3.2.2 Live End

The live end of specimen NSC-2 was tested at an embedment length of 55 in. (1397 mm), which corresponded to 55 percent of the ACI/AASHTO development length, in response to the shear failure with end slip of the dead end of NSC-3. Flexural cracking first appeared directly beneath the applied load followed by other cracks farther from the load that exhibited flexure/shear behavior as the load increased. Horizontal cracks formed at approximately the location of the compression reinforcement immediately before failure. The cracking pattern immediately before failure is shown in Figure 6.7. The beam exhibited substantial yielding,



Figure 6.6: Failure of specimen NSC-2D

shown in Figure 6.8, after reaching a maximum load and moment of 40.58 kips (180.5 kN) and 1094 k-in. (123.6 kN-m), respectively, before crushing of the top compressive fiber. The beam was loaded further leading to a catastrophic shear collapse that revealed buckling of the compression reinforcement, which was most likely the cause of the horizontal cracking. The calculated nominal moment of 983 k-in. (111.1 kN-m) was exceeded by approximately 11 percent during the test with no measured end slip, which indicated that the development length was less than 55 in. (1270 mm).

### 6.3.3 NSC-3

#### 6.3.3.1 Dead End

The dead end of specimen NSC-3 was loaded at an embedment length of 52 in. (1321 mm) in response to the shear failure with strand slip of the live end of NSC-3 at an embedment



Figure 6.7: Cracking pattern of specimen NSC-2L

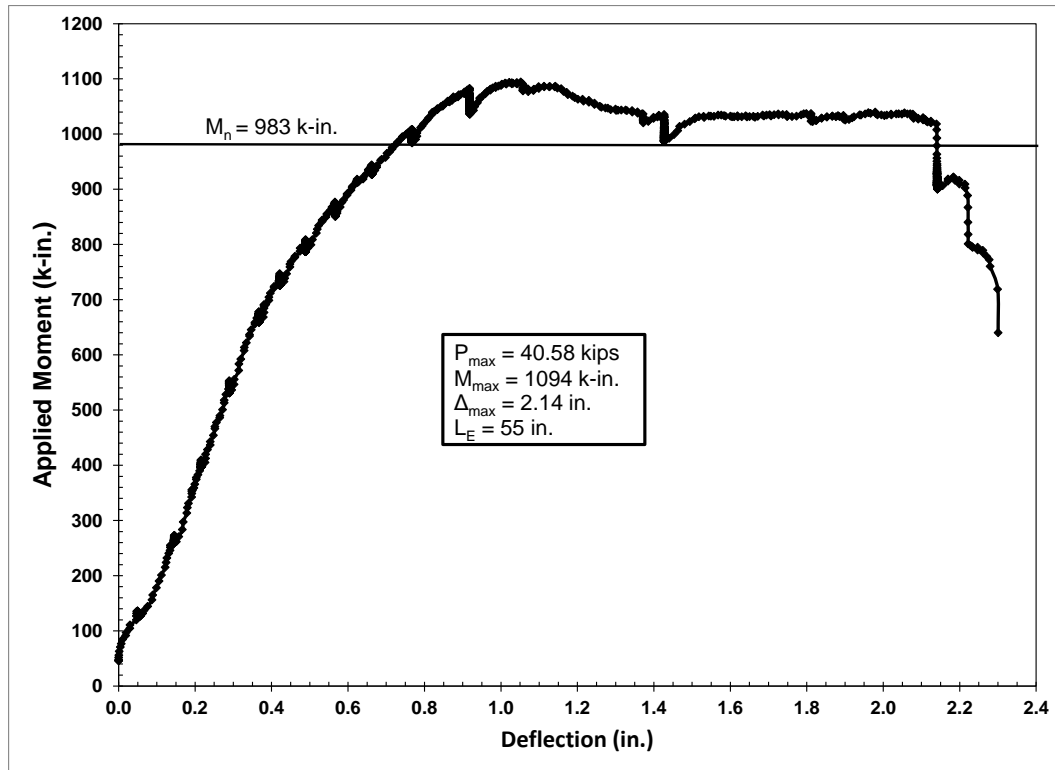


Figure 6.8: Plot of moment vs. deflection for specimen NSC-2L

of 48 in. (1219 mm). The 52 in. (1321 mm) embedment corresponded to 55 percent of the ACI/AASHTO development length calculated for this specimen. Flexural cracking began directly beneath the applied load followed by other cracks exhibiting some flexure/shear behavior. A large shear crack, shown in Figure 6.9, developed at the onset of the shear failure that occurred at the maximum load and moment of 36.20 kips (161 kN) and 969 k-in. (109.5 kN-m), respectively. The sudden failure at maximum load is clearly illustrated in Figure 6.10. Though the beam failed due to shear, the maximum moment exceeded the calculated nominal moment of 935 k-in. (105.6 kN-m) by approximately 3.5 percent with less than 0.10 in. (2.5 mm) strand slip even after the shear failure. These results indicated that the development length was less than the 52 in. (1321 mm) embedment.



Figure 6.9: Shear cracking of specimen NSC-3D

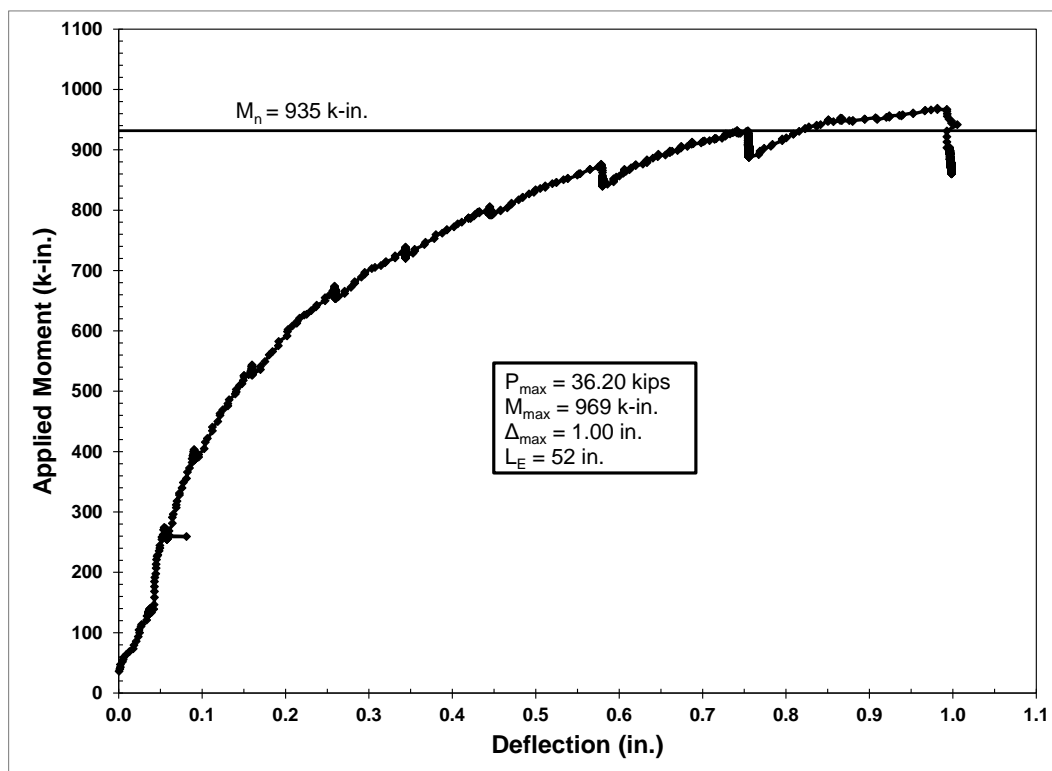


Figure 6.10: Plot of moment vs. deflection for specimen NSC-3D

### 6.3.3.2 Live End

The live end of specimen NSC-3 was tested with an embedment length of 48 in. (1219 mm), corresponding to 51 percent of the calculated ACI/AASHTO development length. This test was used to confirm the results of the test on the dead end of specimen NSC-4 and after the flexural failure of the live end of specimen NSC-4 at an embedment of 60 in. (1524 mm). The first flexural cracking occurred directly under the applied load. These flexural cracks were followed by a shear crack that originated at the near support and propagated at an approximately 45 degree angle to the top of the specimen at the maximum load and moment of 32.40 kips (144.1 kN) and 859 k-in. (97.1 kN-m), respectively, as shown in Figure 6.11. Another shear crack formed approximately 8 in. (200 mm) from the near support and horizontal cracking occurred at the level of the compression steel on the north side of the specimen. End slip was recorded simultaneously with the appearance of the shear cracks. The sudden failure of the



Figure 6.11: Shear cracking of specimen NSC-3L



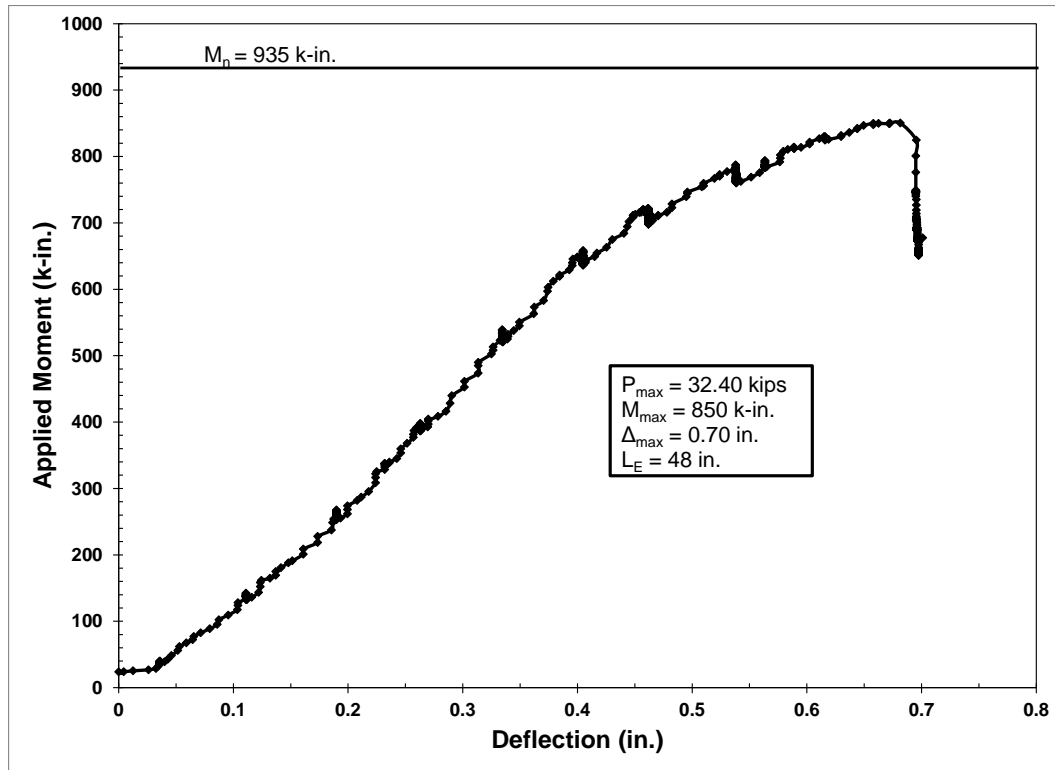


Figure 6.12: Plot of moment vs. deflection for specimen NSC-3L

specimen is illustrated in Figure 6.12. Even though the maximum moment was much less than the calculated nominal moment of 935 k-in. (105.6 kN-m) and greater than 0.1 in. (2.5 mm) of strand slip was recorded, the shear failure of this specimen did not allow for a definite conclusion concerning the development length.

### 6.3.4 NSC-4

#### 6.3.4.1 Dead End

The dead end of specimen NSC-4 was the first specimen tested. It was tested at an embedment length of 48 in. (1219 mm), corresponding to 51 percent of the calculated ACI/AASHTO development length. Initial flexural cracking occurred near the applied load followed by cracks farther from the load that had some flexure/shear behavior, as shown in Figure 6.13. A shear crack formed at a load close to the maximum load and propagated from



Figure 6.13: Cracking behavior of specimen NSC-4D

near the near support to the top of the specimen. The member exhibited substantial ductility, illustrated in Figure 6.14, followed by crushing of the top compression fiber at the maximum load and moment of 39.20 kips (174.4 kN) and 1029 k-in. (116.3 kN-m), respectively. Strand slip of approximately 0.02 in. (0.5 mm) was recorded at the end of the test. The flexural failure with minimal end slip and the fact that the maximum moment exceeded the calculated nominal moment, 960 k-in. (108.5 kN-m), by 7 percent combined to indicate that the development length was less than the 48 in. (1219 mm) embedment used for this test. However, dead ends typically had shorter transfer lengths than the live ends of the specimens, which could limit the applicability of this conclusion to every specimen.

#### 6.3.4.2 Live End

The live end of specimen NSC-4 was tested at an embedment length of 60 in. (1524 mm), which was approximately 60 percent of the calculated ACI/AASHTO development length. The

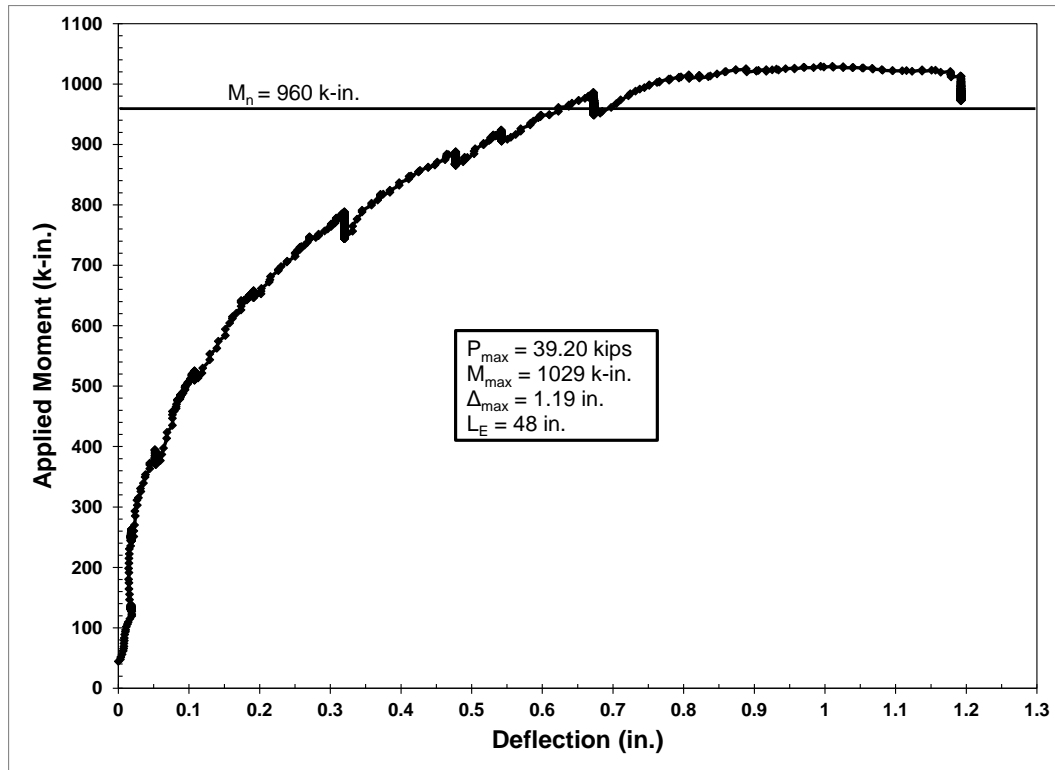


Figure 6.14: Plot of moment vs. deflection for specimen NSC-4D

initial flexural cracks began directly beneath the applied load and were followed by additional cracks along the beam that exhibited flexure/shear behavior, as shown in Figure 6.15. The beam exhibited significant ductility, as shown in Figure 6.16, before crushing of the top compression fiber occurred at a maximum load and moment of 36.52 kips (162.4 kN) and 1093 k-in. (123.5 kN-m), respectively. No strand slip was detected and the maximum moment exceeded the calculated nominal moment of 960 k-in. (108.5 kN-m) by 14 percent indicating that the development length was less than the 60 in. (1524 mm) embedment length.

### 6.3.5 Summary and Discussion

Analysis of the results of the flexural test data summarized in Table 6.2 indicated that the development length for the normal strength clay (NSC) specimens was between 45 in. and 50 in. (1143 mm and 1270 mm). Since live ends were only tested at 55 in. (1397 mm) and 48 in. (1219



Figure 6.15: Cracking behavior of specimen NSC-4L

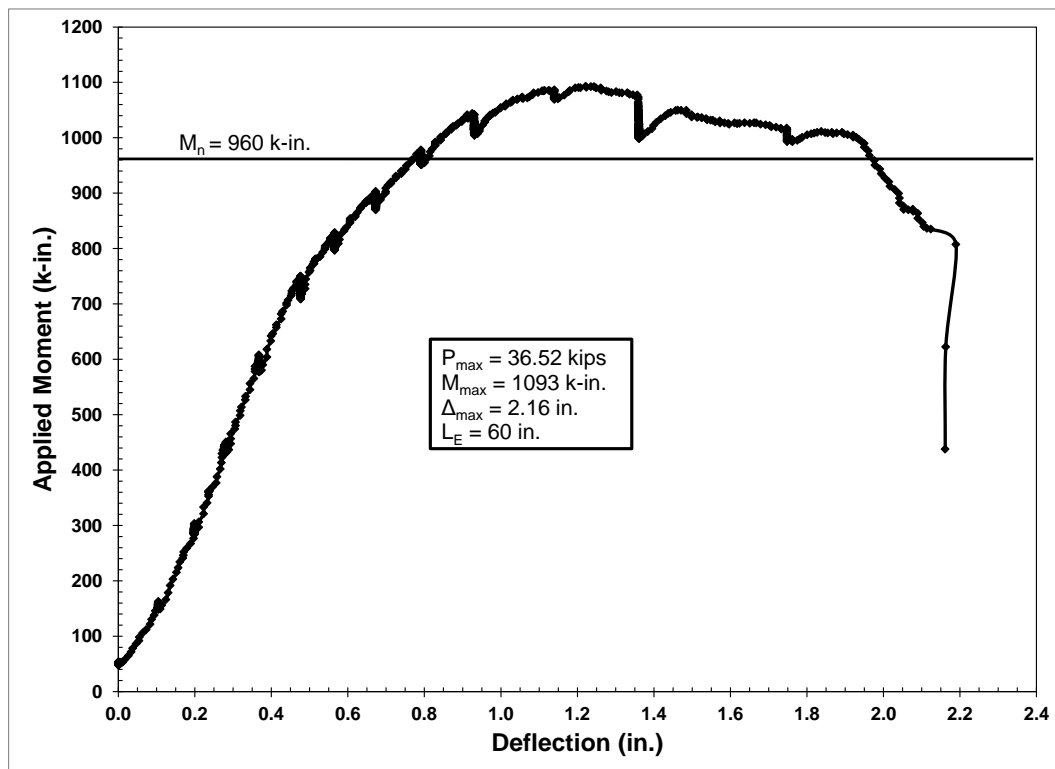


Figure 6.16: Plot of moment vs. deflection for specimen NSC-4L

mm), the development length was certainly less than 55 in. (1397 mm). The values calculated using the various prediction equations mentioned in Chapter 2 are presented in Table 6.3. The measured development length was approximately half that calculated using the ACI/AASHTO equation. It was between 52 and 60 percent of the prediction computed using the Ramirez and Russell equation, between 41 and 53 percent of the predictions given by the Zia and Mostafa, Buckner, and Kose and Burkett equations, between 28 and 35 percent of the very conservative Lane equation, and was approximately 35 percent of the prediction produced by the Deatherage et al. equation.

Table 6.2: Summary of NSC Flexural Test Data

Test	$f_{se}$ (ksi)	$f_{ps}$ (ksi)	$M_n$ (k-in.)	$M_{max}$ (k-in.)	Max Slip (in.)	Failure Type	$L_E$ (in.)
NSC-1D	153.24	259.9	933	939	--	FL	50
NSC-1L				703	>0.10	SH/ES	45
NSC-2D	160.18	262.3	983	1067	--	FL	50
NSC-2L				1094	--	FL/SH	55
NSC-3D	151.96	259.4	935	969	>0.06	SH/ES	52
NSC-3L				850	>0.10	SH/ES	48
NSC-4D	154.93	261.3	960	1029	0.02	FL/ES/SH	48
NSC-4L				1093	--	FL	60

Note: 1 in. = 25.4 mm, 1 lbf = 4.448 N, 1 psi = 0.006895 MPa,

Table 6.3: Development Length Predictions for the NSC Specimens

Specimen	ACI/ AASHTO (in.)	Ramirez/ Russell (in.)	Zia/ Mostafa (in.)	Deatherage et al. (in.)	Buckner (in.)	Lane (in.)	Kose/ Burkett (in.)
NSC-1	94.7	95.4	115.5	131.7	99.7	183.6	111.0
NSC-2	100.7	83.6	121.5	145.2	109.1	140.9	94.9
NSC-3	94.9	95.9	118.1	132.3	100.1	181.5	110.2
NSC-4	94.8	90.5	115.9	131.6	99.7	154.9	102.2

Note: 1 in. = 25.4 mm

## 6.4 Normal Strength Shale (NSS) Development Length

### 6.4.1 NSS-1

#### 6.4.1.1 Dead End

Specimen NSS-1 was the last NSS specimen tested. The dead end was tested with an embedment of 45 in. (1143 mm), corresponding to 47 percent of the calculated ACI/AASHTO development length, after the flexural failure of the dead end at an embedment of 50 in. (1270 mm). Initial flexural cracking began directly beneath the applied load and other flexure and flexure/shear cracks appeared with increasing load. Minor strand slip was recorded on one strand at a load and moment of 39.50 kips (175.7 kN) and 995 k-in. (112.4 kN-m) respectively, which was 2.5 percent greater than the calculated nominal moment capacity of 931 k-in (105.2 kN-m). The beam exhibited extremely ductile behavior, shown in Figure 6.17, culminating with crushing of the top compressive fiber after a maximum load and moment of 40.40 kips (179.7 kN) and 1018 k-in. (115.0 kN-m) respectively. Additional strand slip was measured during yielding of the specimen with a maximum magnitude of 0.03 in. (0.76 mm), well below the 0.10 in. (2.5 mm) threshold considered for bond failure. The cracking patterns and failure of this specimen are visible in Figure 6.18. The maximum applied moment exceeded the calculated nominal moment before strand slip occurred indicating that the development length was near, but less than the 45 in. (1143 mm) embedment. This was in spite of a long transfer length caused by low strength at prestress release.

#### 6.4.1.2 Live End

The live end of specimen NSS-1 was tested at an embedment length of 50 in (1270 mm) which corresponded to 52 percent of the ACI/AASHTO development length. The embedment was chosen based on the results of the flexural tests on the other NSS specimens. Flexural

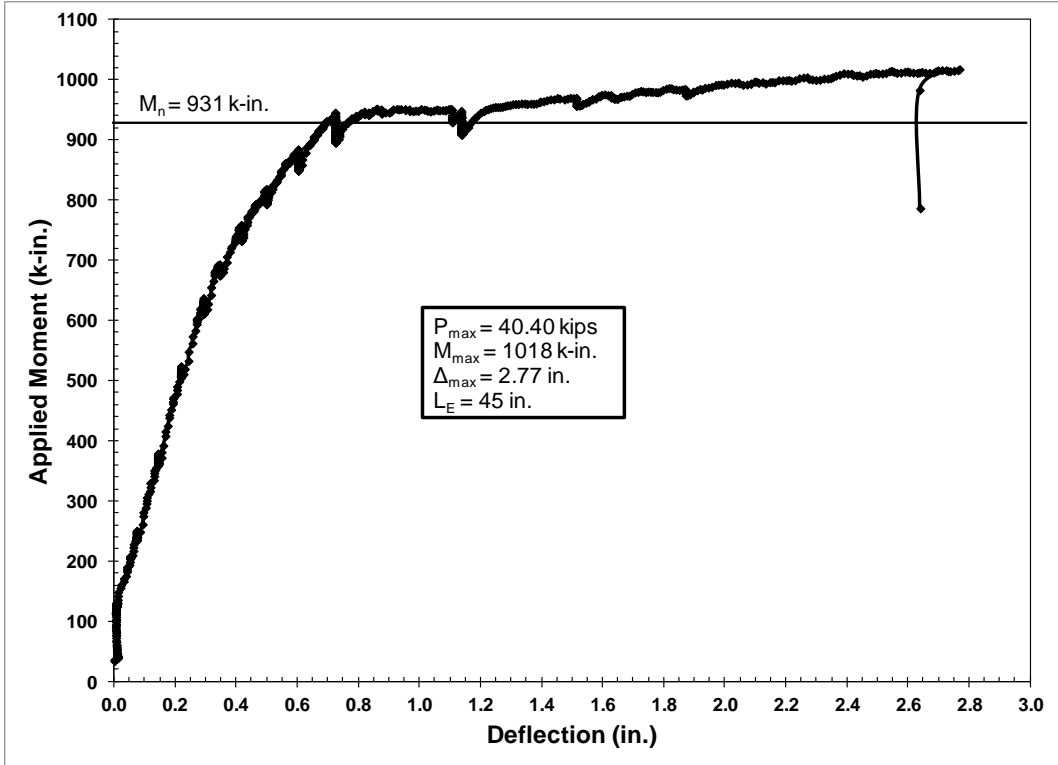


Figure 6.17: Plot of moment vs. deflection for specimen NSS-1D



Figure 6.18: Cracking behavior and failure of specimen NSS-1D

cracking commenced directly beneath the applied load and continued with other flexure and flexure/shear cracks developing along the span length. The first measured strand slip was recorded at a load and moment, 37.40 kips (166.4 kN) and 982 k-in. (111.0 kN-m) respectively, that exceeded the calculated nominal moment of 931 k-in. (105.2 kN-m) by 5.5 percent. The beam exhibited extremely ductile behavior, as indicated by Figure 6.19, with significant deflection measured before crushing occurred in the extreme compression fiber. The maximum load and moment held by this specimen were 38.40 kips (170.8 kN) and 1008 k-in. (113.9 kN-m) respectively and the failure of the specimen is shown in Figure 6.20. The ductile flexure failure of this specimen, even with 0.09 in. (2.3 mm) of strand slip recorded after the nominal moment was exceeded, indicated that the development length was less than 50 in. (1270 mm).

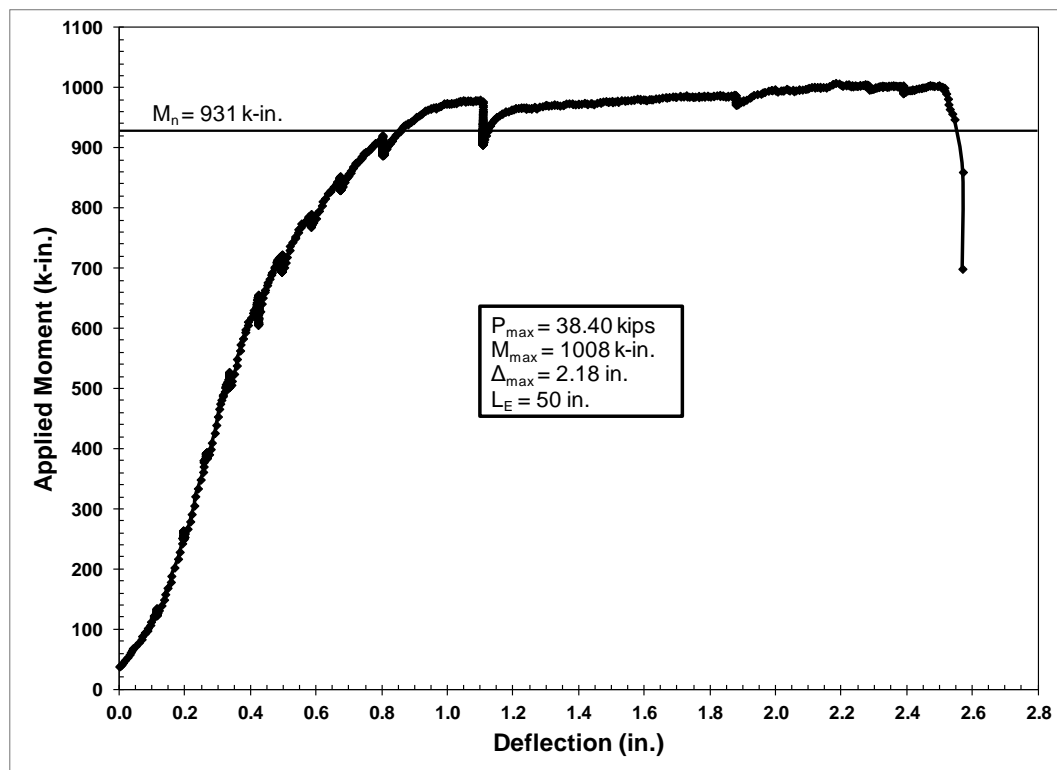


Figure 6.19: Plot of moment vs. deflection for specimen NSS-1L





Figure 6.20: Cracking behavior and failure of specimen NSS-1L

## 6.4.2 NSS-2

### 6.4.2.1 Dead End

Specimen NSS-2 was the first NSS specimen tested. The dead end was loaded at an embedment length of 49 in. (1245 mm), corresponding to 52 percent of the ACI/AASHTO development length, based on the results of the flexural tests on the NSC specimens. Flexural cracking commenced directly beneath the applied load with other flexure/shear cracks developing as the applied load increased, as shown in Figure 6.21. One of these cracks propagated almost horizontally at the level of the compression reinforcement, which led to delamination of the top of the beam specimen when crushing of the concrete occurred. The beam exhibited some ductility, as shown in Figure 6.22, and no strand slip before failing with catastrophic concrete crushing. The maximum load and moment of 38.20 kips (169.9 kN) and



Figure 6.21: Cracking behavior and beginning of failure of specimen NSS-2D

989 k-in. (111.7 kN-m), respectively, exceeded the calculated nominal moment of 968 k-in. (109.4 kN-m) by 2 percent. The flexural failure of this specimen indicated that the development length was less than the 49 in. (1245 mm) embedment length.

#### 6.4.2.2 Live End

The live end of specimen NSS-2 was tested at an embedment length of 40 in. (1016 mm), which corresponded to 43 percent of the ACI/AASHTO development length, after the flexural failure of the dead end. The first flexural cracks appeared directly beneath the applied load and other cracks formed that exhibited greater flexure/shear behavior as the load increased. Strand slip was measured immediately before the maximum load and moment of 40.58 kips (180.5 kN) and 960 k-in. (108.5 kN-m), respectively, were achieved. Significant shear cracking, shown in Figure 6.23, occurred simultaneously with the maximum load and a measured strand slip of

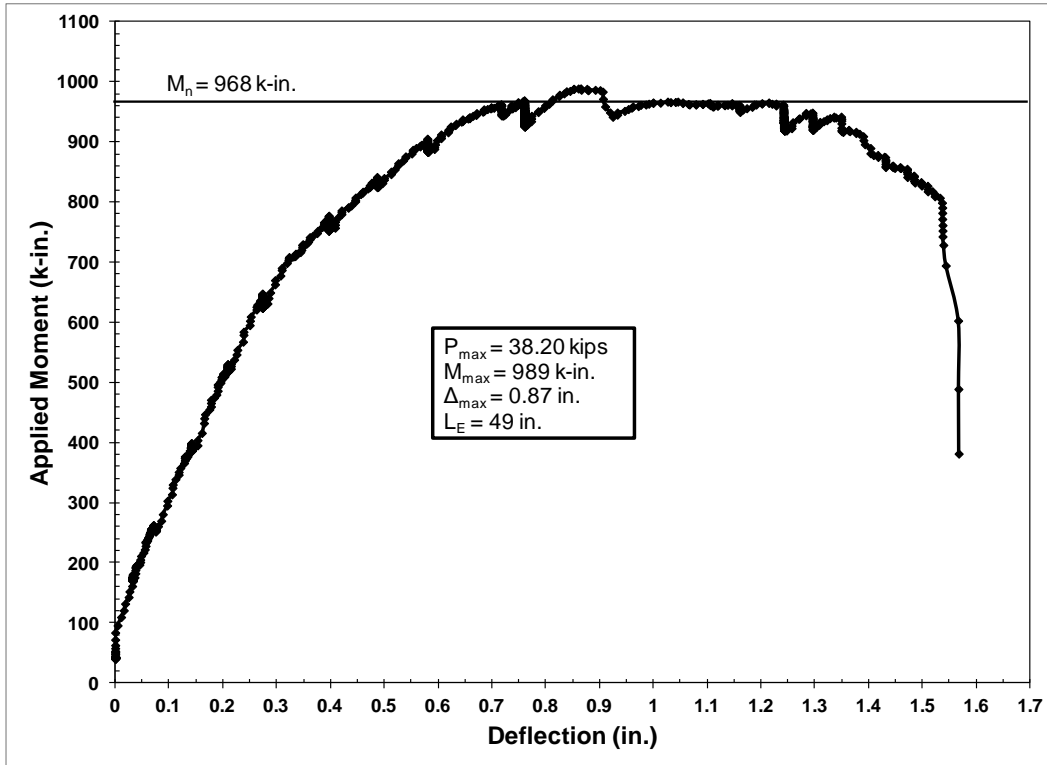


Figure 6.22: Plot of moment vs. deflection for specimen NSS-2D

approximately 0.03 in. (0.76 mm). The sudden failure of the member is illustrated in the plot presented in Figure 6.24. Strand slip increased to greater than 0.10 in. (2.5 mm) after the shear failure. The combination of this shear failure with strand slip at an applied moment near, but less than, the nominal moment indicated that the development was greater than the tested embedment length of 40 in. (1016 mm). Segregation was evident in the concrete below the prestressing strands in the form of only sand/cement mortar present beneath the strands. The concrete and segregated portion were still adequately consolidated with no voids, but mortar surrounds and fills around the strands differently due to the lack of large aggregate particles, which may have contributed to the bond behavior of this specimen.



Figure 6.23: Shear failure of specimen NSS-2L

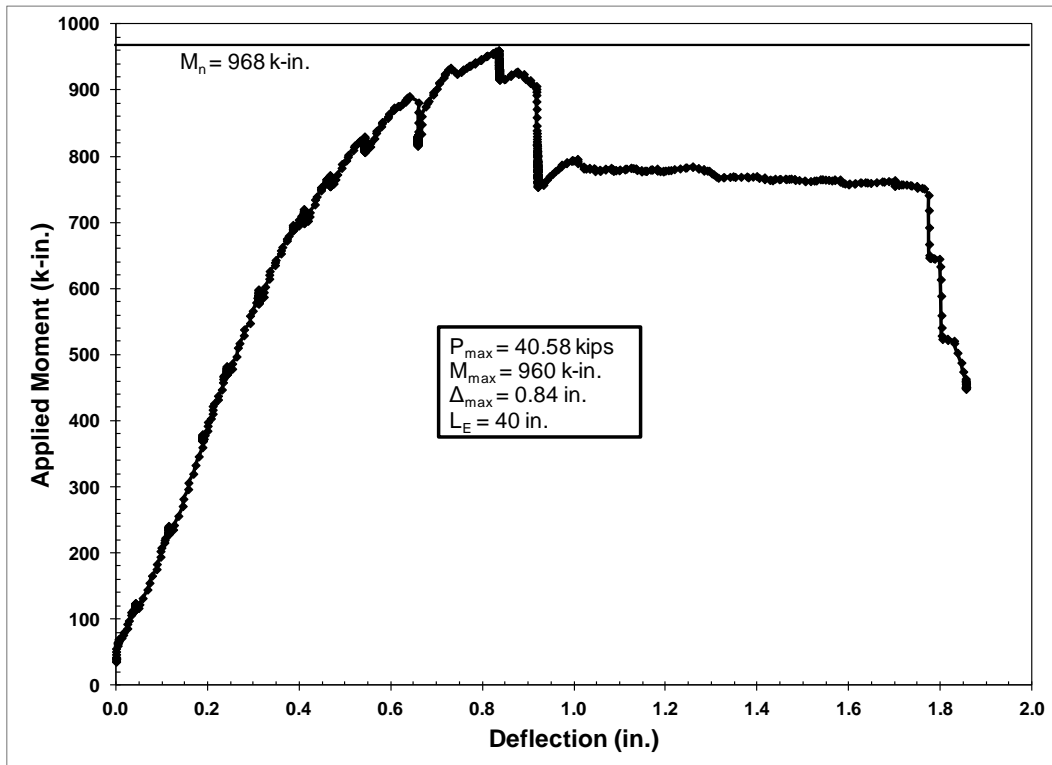


Figure 6.24: Plot of moment vs. deflection for specimen NSS-2L

### 6.4.3 NSS-3

#### 6.4.3.1 Dead End

The dead end of specimen NSS-3 was loaded at an embedment length of 40 in. (1016 mm), corresponding to 43 percent of the ACI/AASHTO development length, due to the flexural failure of the live end of specimen NSS-3. Initial flexural cracking occurred directly beneath the applied load with other flexural cracks developing until the maximum load and moment of 35.07 kips (158.8 kN) and 830 k-in. (93.8 kN-m) were reached. A large shear crack, shown in Figure 6.25, occurred at the maximum load and strand slip was measured immediately following. This shear failure is indicated by the behavior shown in Figure 6.26. The maximum load was well below the calculated nominal moment of 963 k-in. (108.8 kN-m). The combination of a shear failure with end slip exceeding 0.10 in. (2.5 mm) did not produce a definite conclusion concerning the development length, but supported the conclusion that the development length



Figure 6.25: Shear failure of specimen NSS-3D

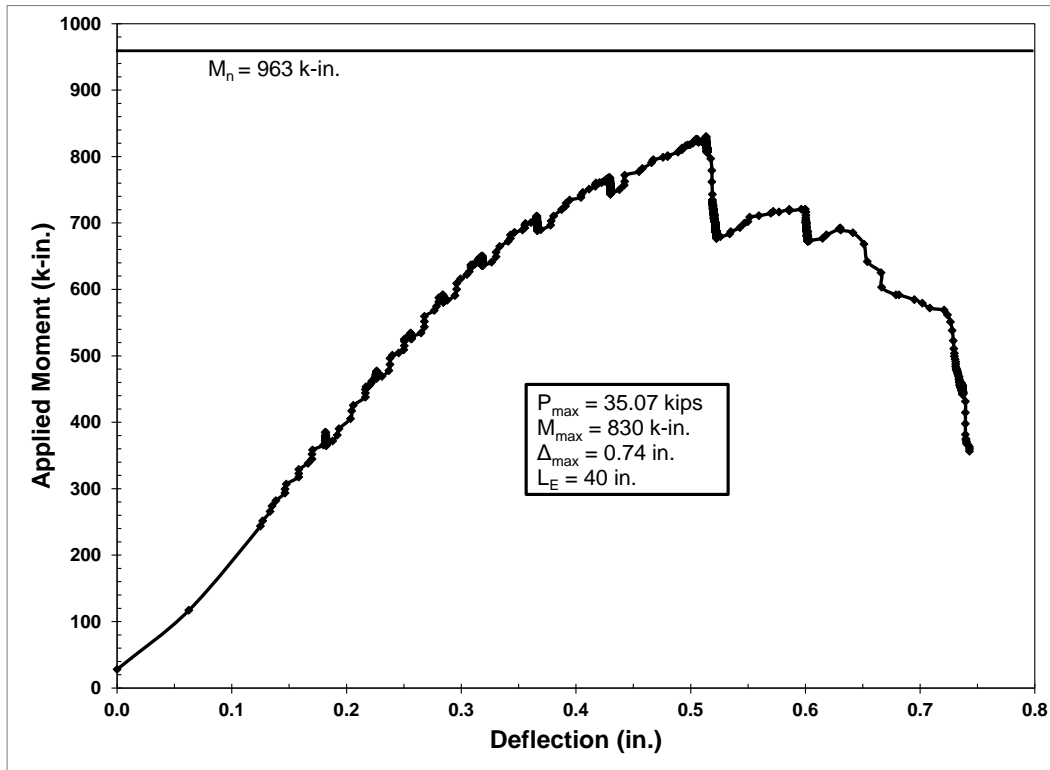


Figure 6.26: Plot of moment vs. deflection for specimen NSS-3D

was greater than the 40 in. (1016 mm) embedment. Segregation similar to that observed in specimen NSS-2 with only sand/cement paste below the prestressing strands was noticeable for specimen NSS-3, as shown in Figure 6.25. This separated portion was still well-consolidated as in specimen NSS-2.

#### 6.4.3.2 Live End

The live end of specimen NSS-3 was tested at an embedment of 45 in. (1143 mm), which corresponded to approximately 48 percent of the calculated ACI/AASHTO development length. This embedment was chosen based on the shear failure of the live end of specimen NSS-2 at an embedment of 40 in. (1016 mm). Flexural cracking began directly beneath the applied load and other flexure/shear cracks formed under increasing load. The beam exhibited significant deflection after the maximum load and moment of 40.81 kips (181.5 kN) and 1028 k-in. (116.1 kN-m), respectively, were reached. The test ended with crushing of the top compression fiber

and fracture of at least one of the prestressing strands. The behavior of this specimen is shown in Figure 6.27 and the failure in Figure 6.28. Measured strand slip coincided with fracture of this prestressing strand. The clear flexural failure of this specimen, at a moment exceeding the calculated nominal moment of 963 k-in. (108.8 kN-m) by 6.7 percent, on a live end indicated that the development length was less than the 45 in. (1143 mm) embedment length.

#### 6.4.4 NSS-4

##### 6.4.4.1 Dead End

The dead end of specimen NSS-4 was tested at an embedment length of 47.5 in. (1207 mm), corresponding to approximately 51 percent of the ACI/AASHTO development length, after the shear failure of the live end of specimen NSS-4 at an embedment of 45 in. (1016 mm). The first flexural cracks occurred directly beneath the applied load followed by additional flexure and

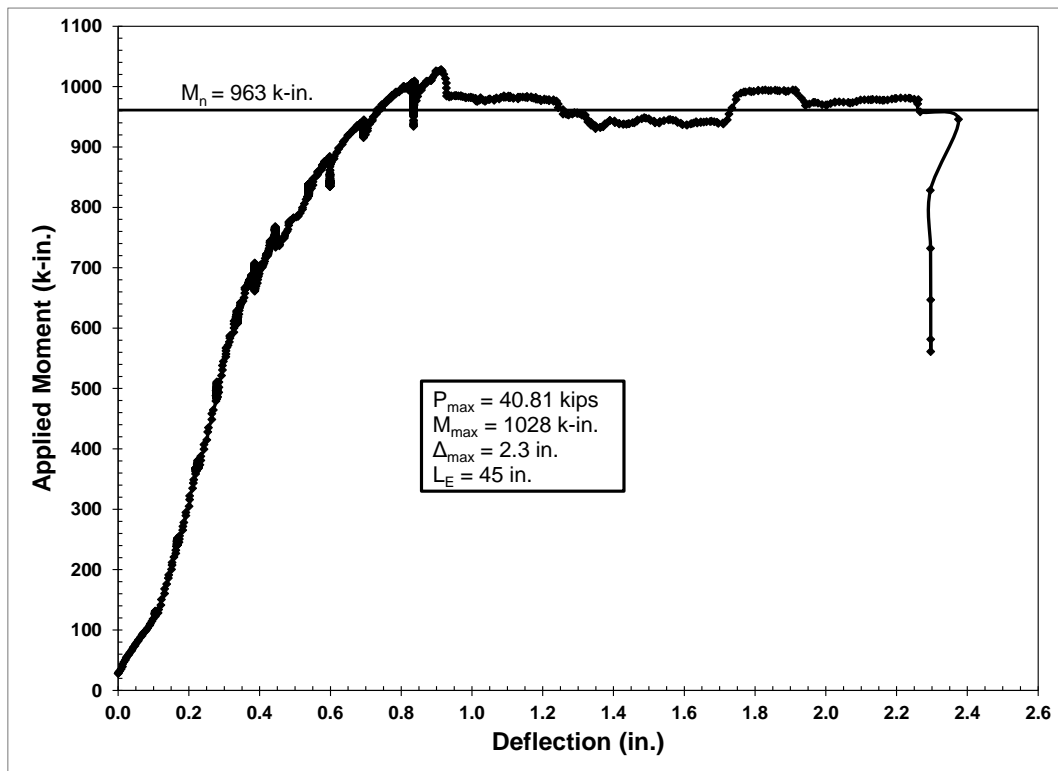


Figure 6.27: Plot of moment vs. deflection for specimen NSS-3L



Figure 6.28: Failure of specimen NSS-3L

flexure/shear cracking along the length of the span. The beam exhibited significant deflection, shown in Figure 6.29, after reaching a maximum load and moment of 38.84 kips (172.8 kN) and 1001 k-in. (113.1 kN-m) and before crushing of the extreme compression fiber, shown in Figure 6.30, occurred. The clear flexural failure with no measured strand slip at a moment 3 percent greater than the nominal moment of 972 k-in. (109.8 kN-m) indicated that the development length was less than the 47.5 in. (1207 mm) embedment length.

#### 6.4.4.2 Live End

The live end of specimen NSS-4 was tested at an embedment length of 45 in. (1143 mm), corresponding to 48 percent of the ACI/AASHTO development length, due to the shear failure of the dead end of specimen NSS-3 at an embedment of 40 in. (1016 mm). Flexure and flexure shear cracks developed with increasing load after beginning directly beneath the applied load.

The beam failed suddenly, as shown in Figure 6.31, at the maximum load and moment of 39.98



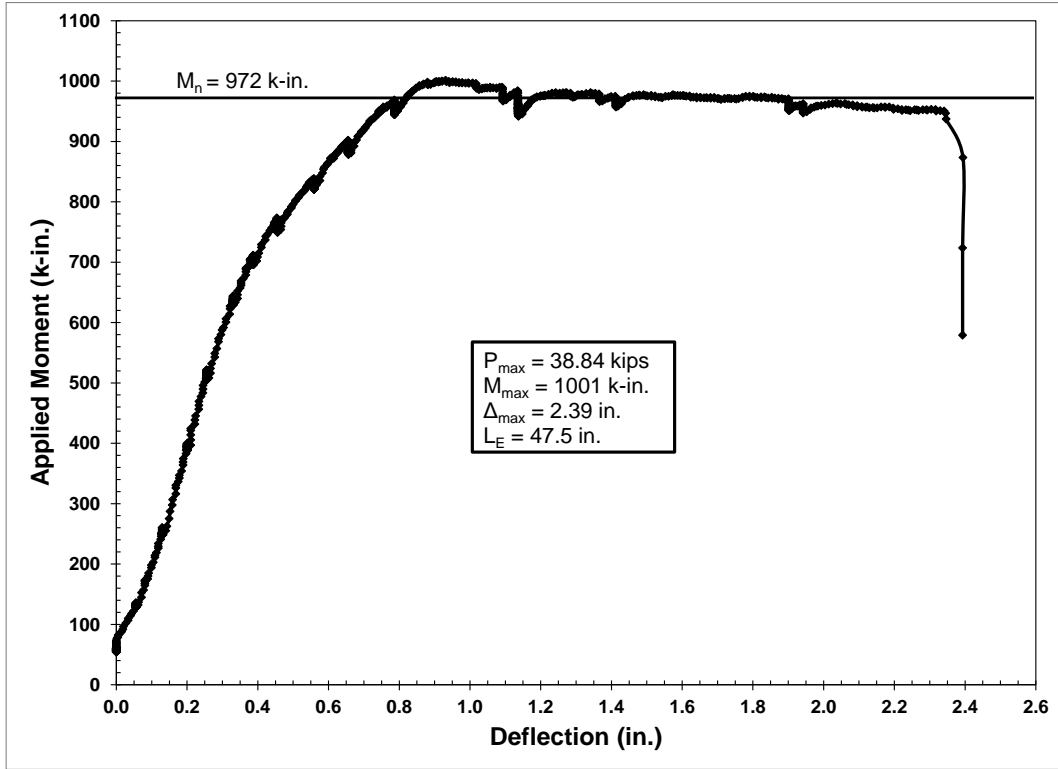


Figure 6.29: Plot of moment vs. deflection for specimen NSS-4D



Figure 6.30: Failure of specimen NSS-4D

kips (177.8 kN) and 1007 k-in (113.8 kN-m) due to the formation of very large shear cracks. These cracks, shown in Figure 6.32 for the south side, commenced at the near support and propagated upward at an approximately 45° angle to the top of the beam on the south side and along the line of the compression reinforcement to the applied load on the north side. End slip was recorded immediately before the shear failure occurred and reached a total of 0.10 in. (2.5 mm). The sudden shear failure at an applied moment 3.6 percent larger than the calculated nominal moment of 972 k-in. (109.8 k-in.) and no strand slip measured until a moment approximately equal to the nominal moment indicated that the development length was most likely near, but less than, the embedment length of 45 in. (1143 mm). The transfer length for this end was also relatively large and greater than that of the corresponding dead end which gave further evidence to a development length shorter than 45 in. (1143). No segregation of the concrete was observed in the pieces recovered after the sudden shear failure.

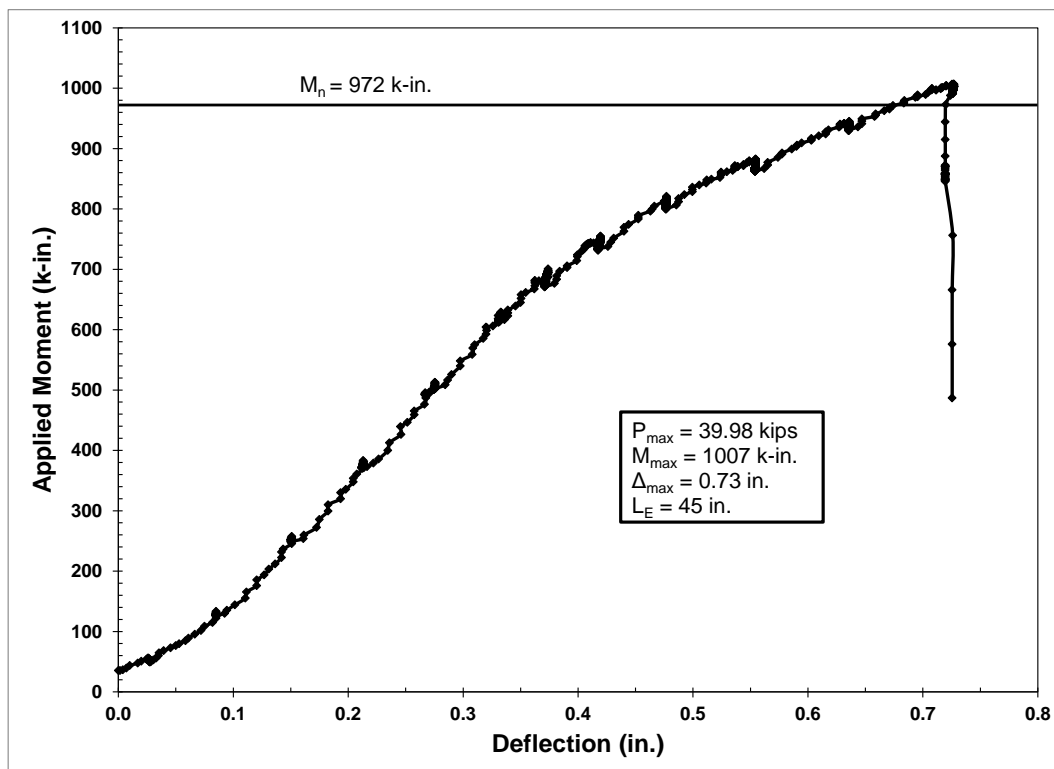


Figure 6.31: Plot of moment vs. deflection for specimen NSS-4L



Figure 6.32: South side shear cracking of specimen NSS-4L

## 6.4.5 NSS-5

### 6.4.5.1 Dead End

The dead end of specimen NSS-5 was tested at an embedment length of 45 in. (1143 mm), corresponding to 48 percent of the ACI/AASHTO development length, due to the flexural failure of the dead end of specimen NSS-4 at an embedment of 47.5 in. (1207 mm). Cracking under loading followed the typical pattern for flexural behavior, as shown in Figure 6.33. Flexural cracks that propagated upward first appeared directly beneath the applied load and were followed by flexure and flexure/shear cracking at other points along the beam with increasing load. The specimen experienced significant deflection after reaching a maximum load and moment of 40.90 kips (181.9 kN) and 1030 k-in. (116.4 kN-m), respectively, and before crushing of the extreme compression fiber. This behavior is shown in Figure 6.34. No strand slip was

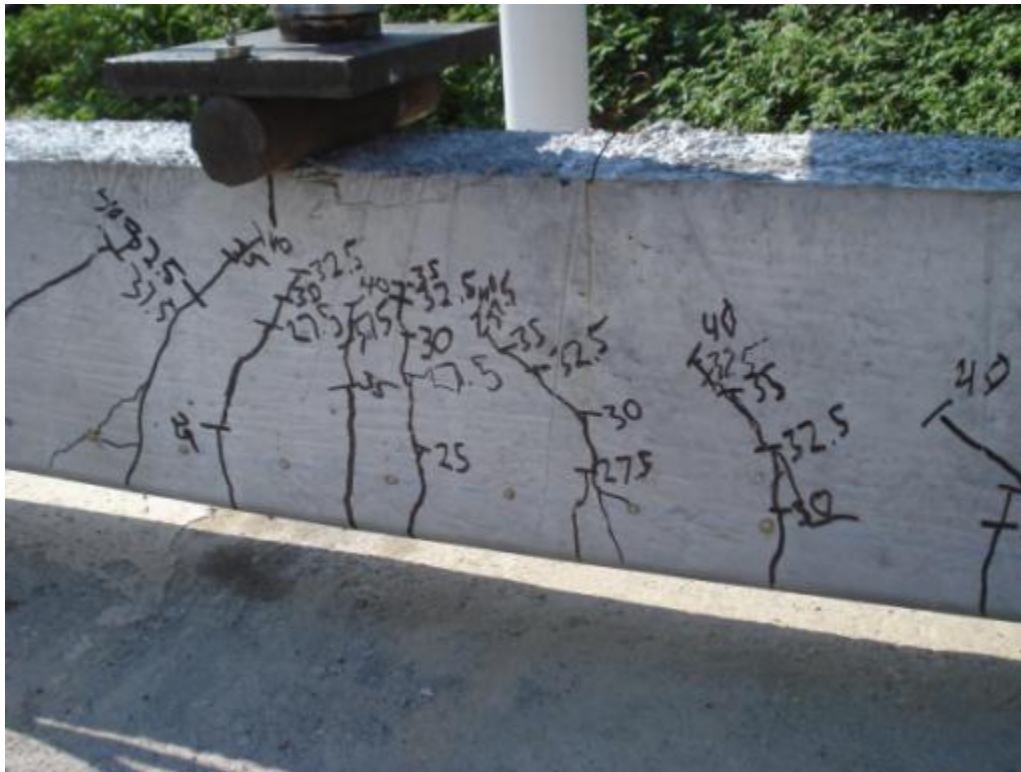


Figure 6.33: Flexural cracking with beginning of concrete crushing for NSS-5D

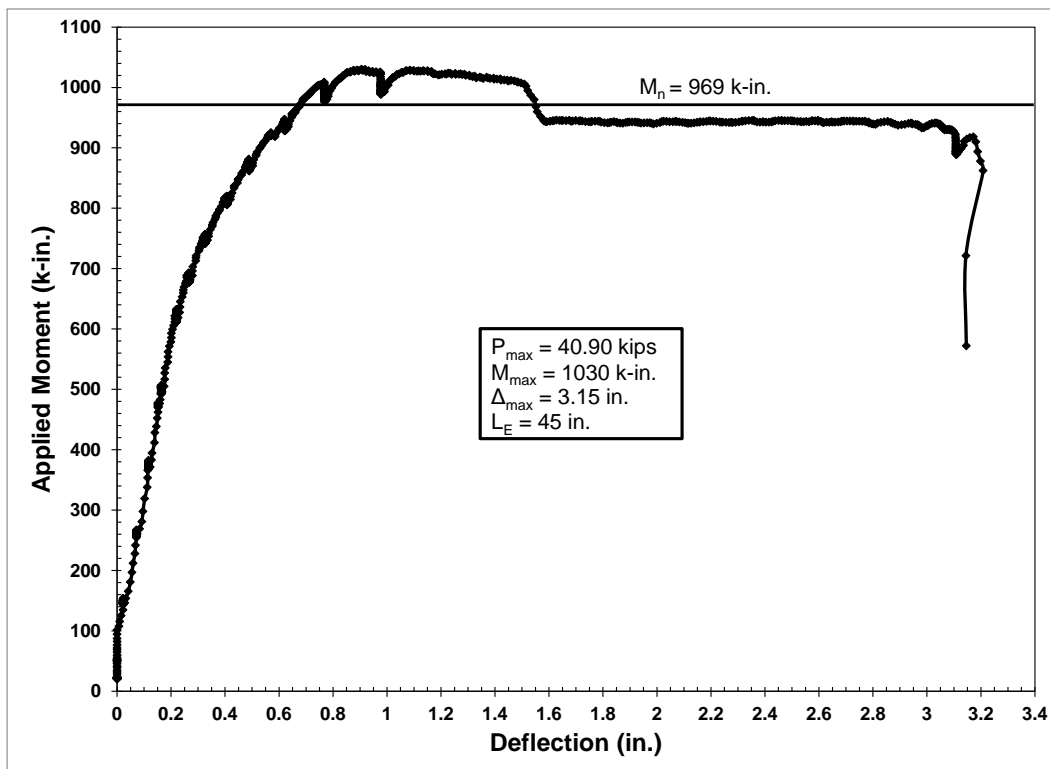


Figure 6.34: Plot of moment vs. deflection for specimen NSS-5D

measured during this test. The maximum load was 6.3 percent greater than that causing the calculated nominal moment of 969 k-in. (109.5 kN-m), indicating that the development length was less than 45 in. (1143 mm).

#### 6.4.5.2 Live End

The live end of specimen NSS-5 was tested at an embedment length of 40 in., corresponding to 42 percent of the ACI/AASHTO development length, due to the flexural failure of the dead end of specimen NSS-5 at an embedment of 45 in. (1143 mm) The beam exhibited typical flexural behavior and cracking before a sudden large shear crack formed at the maximum load and moment of 35.03 kips (155.8 kN) and 773 k-in. (87.3 kN-m) This crack began near the support, propagated at an approximately 45° angle to the top of the beam, as shown in Figure 6.35, and was accompanied by slip measured on both prestressing strands. The sudden failure of this specimen is visible in the load-deflection plot presented in Figure 6.36. The sudden shear



Figure 6.35: Shear cracking of specimen NSS-5L

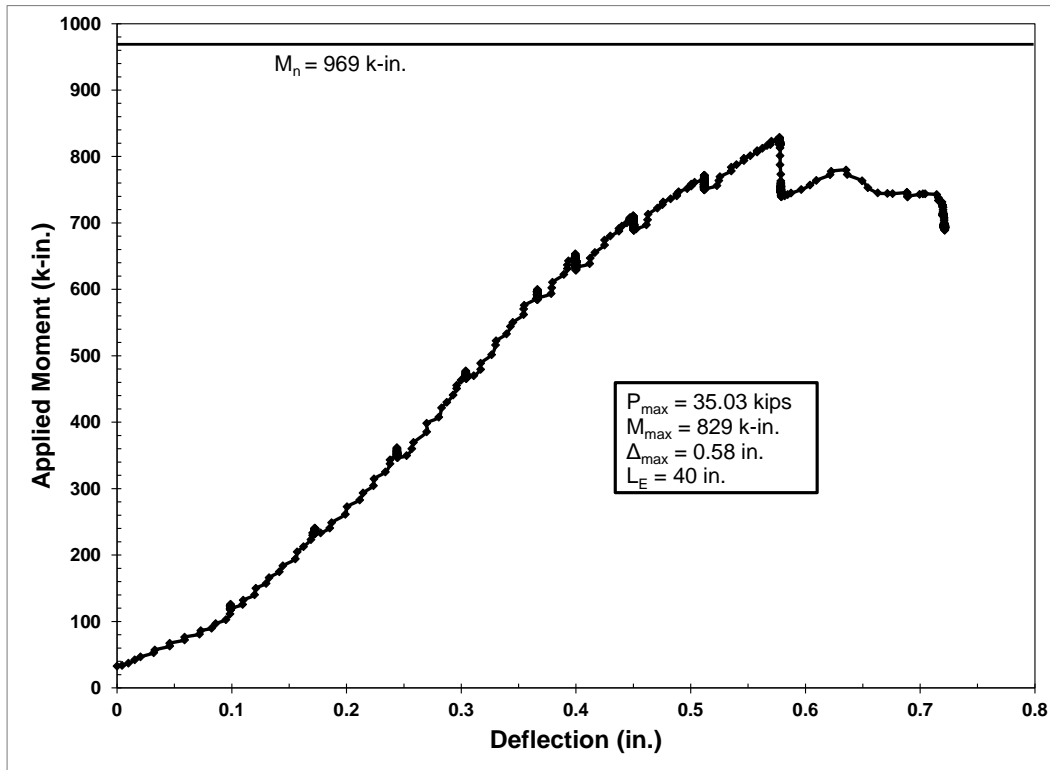


Figure 6.36: Plot of moment vs. deflection for specimen NSS-5L

failure due to the very short embedment length made it impossible to make a distinct conclusion concerning the development length for this specimen. The beam failed at a load significantly smaller than the 969 k-in. (109.5 kN-m) nominal moment and strand slip was not measured until after the occurrence of the shear failure.

#### 6.4.6 Summary and Discussion

Analysis of the flexural test results summarized in Table 6.4 indicated that the development length of the normal strength shale (NSS) specimens was between 40 in. (1016 mm) and 45 in. (1143 mm). All specimens tested at an embedment of 45 in. (1143 mm) exhibited flexural failures with only minor strand slip at a load greater than the nominal moment, or in shear at a load significantly higher than the nominal moment. This was true for both dead ends and live ends that had transfer lengths substantially longer than the dead ends. The

Table 6.4: Summary of NSS Flexural Test Data

Test	$f_{se}$ (ksi)	$f_{ps}$ (ksi)	$M_n$ (k-in.)	$M_{max}$ (k-in.)	Max Slip (in.)	Failure Type	$L_E$ (in.)
NSS-1D	151.0	259.6	931	1018	0.03 <sup>1</sup>	FL/ES	45
NSS-1L				1008	0.09	FL/ES	50
NSS-2D	157.3	261.7	968	989	--	FL	49
NSS-2L				960	>0.10	SH/ES	40
NSS-3D	158.0	261.6	963	830	>0.10	SH/ES	40
NSS-3L				1028	0.04 <sup>1,2</sup>	FL	45
NSS-4D	157.7	261.9	972	1001	--	FL	47.5
NSS-4L				1007	>0.10 <sup>3</sup>	SH/ES	45
NSS-5D	156.1	261.7	969	1030	--	FL	45
NSS-5L				829	>0.10 <sup>3</sup>	SH/ES	40

Note: <sup>1</sup>indicates one strand only, <sup>2</sup>indicates after strand fracture, <sup>3</sup>indicates accompanied shear failure, 1 in. = 25.4 mm, 1 lbf = 4.448 N, 1 psi = 0.006895 MPa,

combination of these factors indicated that the development length was certainly less than 45 in. (1143 mm). The tests conducted at an embedment of 40 in. (1016 mm) all ended with shear failures accompanied by strand slip. The shear failures did not produce a definite conclusion concerning the development length of these specimens, but provided an indication that the development length was most likely greater than 40 in. (1016 mm).

Development length predictions calculated using the equations introduced in Chapter 2 are presented in Table 6.5. The range measured during flexural testing was significantly smaller than the values calculated using all of the prediction equations. The measured development length was approximately 48 percent of that given by the ACI/AASHTO equation, between 45 and 51 percent of that given by the Ramirez and Russell equation, approximately 45 percent of

Table 6.5: Development Length Predictions for the NSS Specimens

Specimen	ACI/ AASHTO (in.)	Ramirez/ Russell (in.)	Zia/ Mostafa (in.)	Deatherage et al. (in.)	Buckner (in.)	Lane (in.)	Kose/ Burkett (in.)
NSS-1	95.4	99.4	124.1	133.5	100.9	190.6	112.6
NSS-2	94.1	88.0	111.7	130.0	98.7	147.3	100.0
NSS-3	93.8	88.2	109.6	129.4	98.3	151.6	101.7
NSS-4	94.0	87.3	112.2	129.9	98.6	142.2	98.4
NSS-5	94.6	88.9	115.5	131.1	99.4	146.1	99.4

Note: 1 in. = 25.4 mm

the prediction given by the Buckner equation, and between 40 and 45 percent of the Kose and Burkett prediction. When compared to the more conservative Zia and Mostafa, Deatherage et al., and Lane predictions, the measured development length was between 36 and 41 percent, approximately 35 percent, and between 24 and 32 percent of the predicted values, respectively.

## **6.5 Normal Strength Limestone (NSL) Development Length**

### **6.5.1 NSL-1**

#### **6.5.1.1 Dead End**

The dead end of specimen NSL-1 was tested at an embedment length of 37 in. (940 mm), corresponding to 41 percent of the ACI/AASHTO development length, after the flexural failure of the dead end of specimen NSL-2 at an embedment of 40 in. (1016 mm). The beam exhibited typical flexural behavior until the sudden appearance of large shear cracks that began near the support and propagated to the top of the specimen at an approximately 45° angle, as shown in Figure 6.37. These cracks occurred at the maximum load and moment of 39.56 kips (176.0 kN) and 946 k-in. (106.9 kN-m), respectively, which was near, but 2.5 percent less than, the nominal moment of 971 k-in. (109.7 kN-m). The shear failure was accompanied by substantial strand slip after the shear cracks appeared. The sudden failure of this specimen is visible in the behavior shown in Figure 6.38. The shear failure at a very short embedment length and an applied moment less than the nominal moment did not give a clear indication regarding the development length for this specimen.

#### **6.5.1.2 Live End**

The live end of specimen NSL-1 was tested at an embedment of 39.5 in. (1003 mm), corresponding to 44 percent of the ACI/AASHTO calculated development length, after the shear failure of the dead end of the specimen at a 37 in. (940 mm) embedment. Cracking followed





Figure 6.37: Shear cracking of specimen NSL-1D

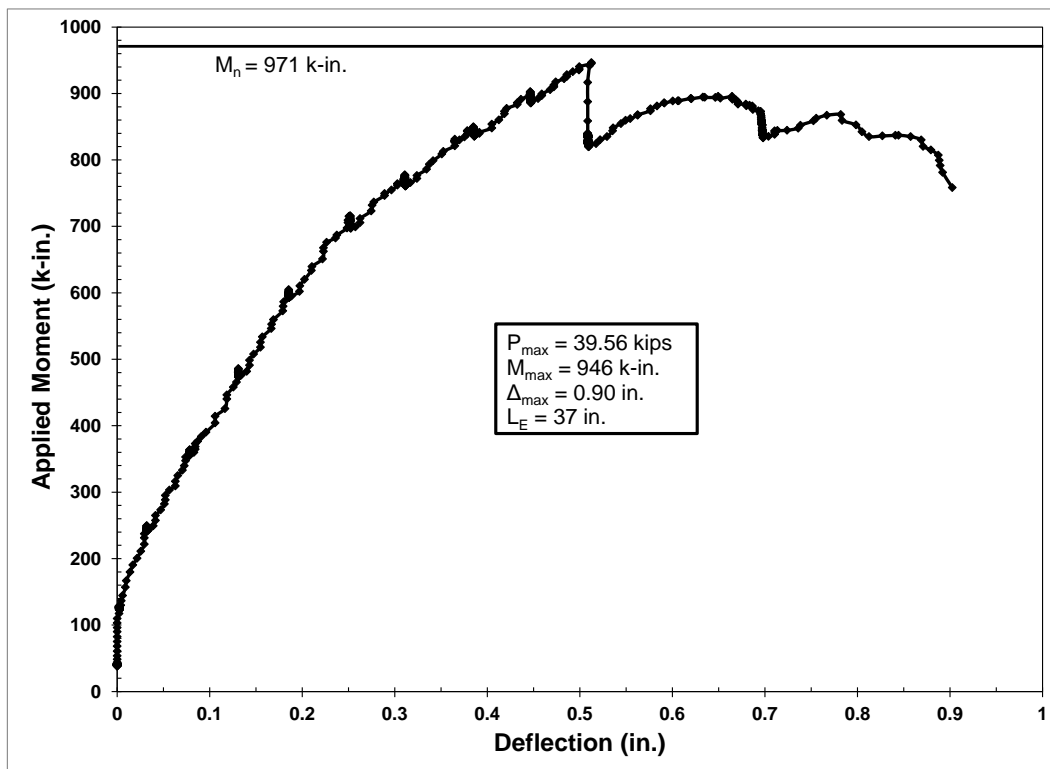


Figure 6.38: Plot of moment vs. deflection for specimen NSL-1D

typical patterns for flexural behavior including flexure cracks appearing directly beneath the applied load followed by flexure/shear cracks at further increments from the applied load, as shown in Figure 6.39. These cracks opened to substantial widths of greater than 0.15 in. (3.8 mm), much greater than the width of flexural cracks observed in most of the other specimens, before crushing of the extreme compression fiber occurred. Strand slip was measured at a load and moment of 40.95 kips (182.2 kN) and 976 k-in. (110.3 kN-m), exceeding the nominal moment of 971 k-in. (109.7 kN-m) by 0.5 percent. The maximum load and moment of 45.03 kips (200.3 kN) and 1073 k-in. (121.2 kN-m) were reached with approximately 0.09 in. (2.3 mm) of strand slip. The beam exhibited significant deflection and the measured strand slip increased to greater than 0.20 in. (5.1 mm) before the beam was considered to be completely failed. The level of deflection at nearly constant load is visible in the load-deflection plot presented in Figure 6.40. The occurrence of significant strand slip at a load exceeding the nominal moment by 10.5



Figure 6.39: Cracking of specimen NSL-1L

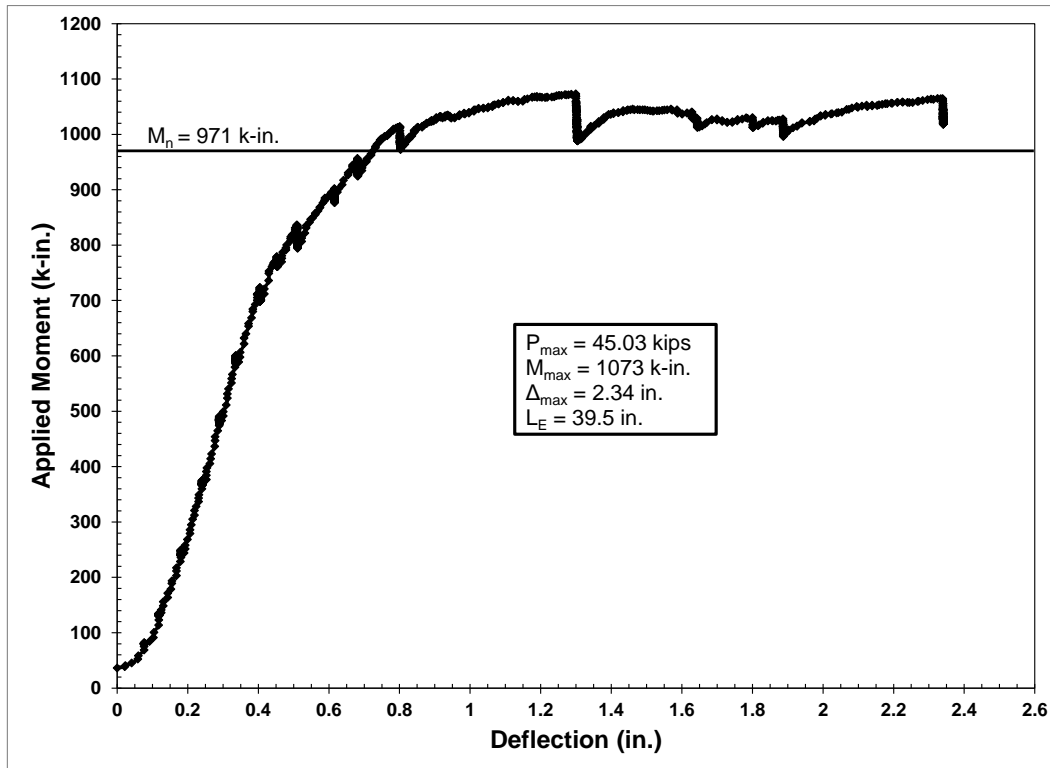


Figure 6.40: Plot of moment vs. deflection for specimen NSL-1L

percent indicated that the 39.5 in. (1003 mm) embedment length was greater than, but close to the development length for this specimen.

## 6.5.2 NSL-2

### 6.5.2.1 Dead End

The dead end of specimen NSL-2 was tested at an embedment of 40 in. (1016 mm), corresponding to 45 percent of the calculated ACI/AASHTO development length, following the flexural failure of the live end at an embedment of 43 in. (1092 mm). The beam exhibited typical flexural behavior with flexural cracks occurring directly beneath the applied load followed by flexure/shear cracks at increments along the beam. These cracks propagated toward the top of the beam before crushing of the extreme compression fiber occurred after the maximum load and corresponding moment of 45.86 kips (204.0 kN) and 1174 k-in. (132.6 kN-

m) were reached. The beam exhibited significant deflection with no increase in load, as shown in Figure 6.41. In addition to crushing of the top compression fiber, significant spalling occurred at the support caused by the proximity of the support to the beam end, shown in Figure 6.42. The flexural failure of this specimen at a load exceeding the nominal moment of 994 k-in. (112.3 kN-m) by 18 percent, with no measured strand slip, indicated that the development length was less than the 40 in. (1016 mm) embedment.

#### 6.5.2.2 Live End

The live end of specimen NSL-2L was tested at an embedment of 43 in. (1092 mm), corresponding to 48 percent of the calculated ACI/AASHTO development length, due to the shear failure of the dead end of specimen NSL-3 at an embedment of 40 in. (1016 mm). The specimen exhibited typical flexural behavior with flexure cracks appearing directly beneath the applied load followed by flexure/shear cracks at other increments along the beam. These cracks

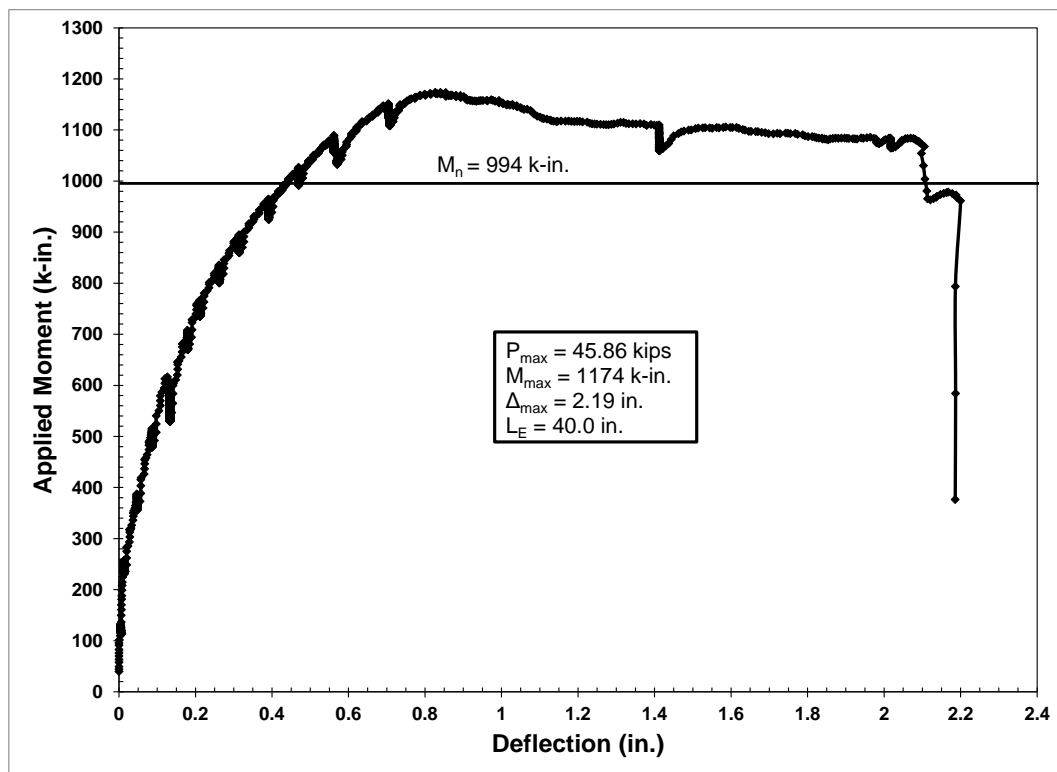


Figure 6.41: Plot of moment vs. deflection for specimen NSL-2D



Figure 6.42: Spalling at support of specimen NSL-2D

propagated with additional load and widened substantially as the beam experienced significant deflection after the maximum load and corresponding moment of 44.63 kips (198.5 kN) and 1124 k-in. (127.0 kN-m) were reached. The test ended with crushing of the top compression fiber. The width of the cracks is shown in Figure 6.43 and the compression failure and the significant yielding of the specimen is visible in Figure 6.44. The flexural failure with no strand slip at a load exceeding the nominal moment of 994 k-in. (112.3 kN-m) by 13 percent indicated that the development length was less than the tested embedment of 43 in. (1092 mm).

### 6.5.3 NSL-3

#### 6.5.3.1 Dead End

The dead end of specimen NSL-3 was tested at an embedment of 40 in. (1016 in.), corresponding to 44 percent of the ACI/AASHTO predicted development length, after the



Figure 6.43: Cracking of specimen NSL-2L

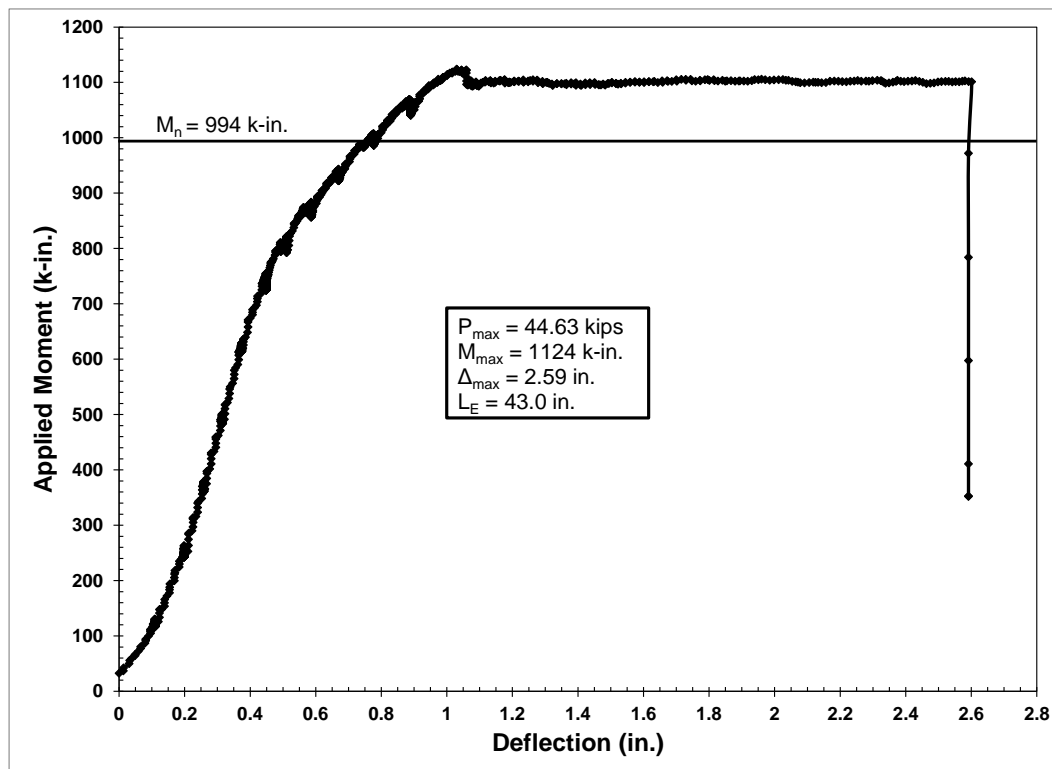


Figure 6.44: Plot of moment vs. deflection for specimen NSL-2L

flexure/bond failure of the live end of the specimen at an embedment of 34 in. (864 mm). Flexural cracking was first observed directly beneath the applied load and then at increments along the beam. These cracks propagated under increasing load until a large shear crack, shown in Figure 6.45, formed at the maximum load and corresponding moment of 42.68 kips (189.9 kN) and 1092 k-in. (123.4 kN-m). This shear crack began approximately halfway between the applied load and the support and propagated at an approximately 45° angle to the top of the specimen. Strand slip was recorded soon after the appearance of the shear crack and reached a magnitude greater than 0.10 in. (2.5 mm) before the end of the test. The beam continued to support load at a magnitude less than the maximum applied load through substantial deflection before crushing of the extreme compression fiber occurred, as shown in Figure 6.46. The beam held a load 9.9 percent greater than that resulting in the nominal moment of 994 k-in. (112.3 kN-m), before the beam failed in shear due to the short embedment length, and before any slip was



Figure 6.45: Shear cracking of specimen NSL-3D

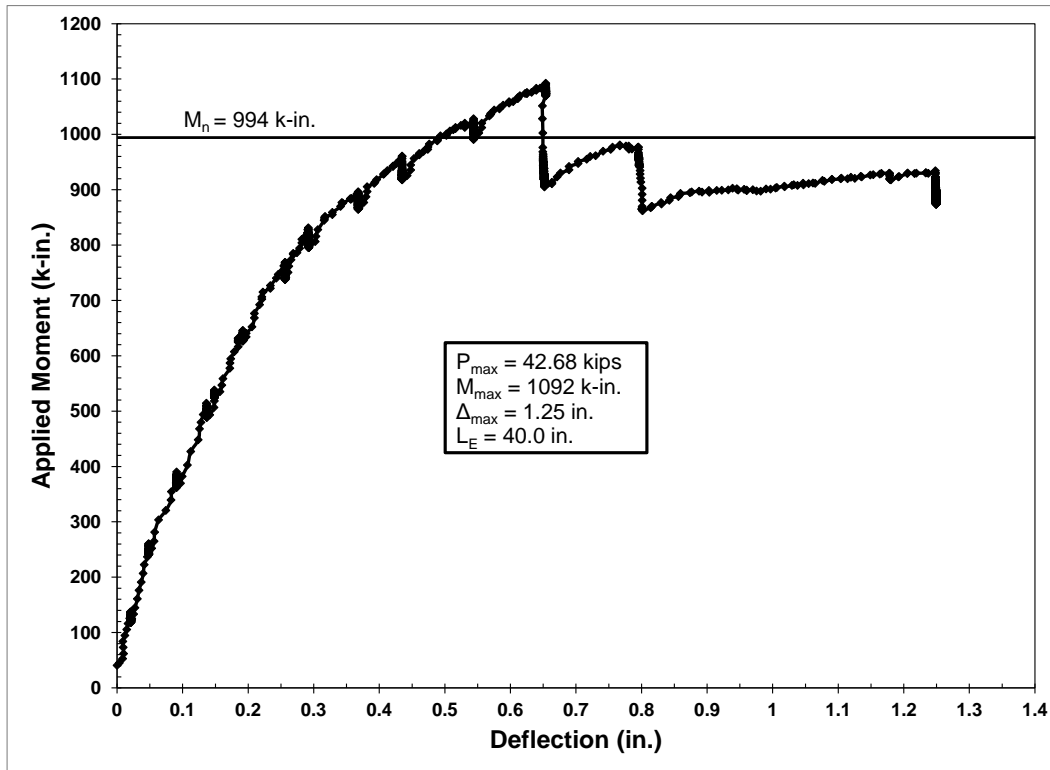


Figure 6.46: Plot of moment vs. deflection for specimen NSL-3D

recorded. It was therefore concluded that the development length was less than the 40 in. (1016 mm) embedment.

#### 6.5.3.2 Live End

The live end of specimen NSL-3 was tested at an embedment of 34 in. (864 mm), corresponding to 37 percent of the ACI/AASHTO calculated development length, due to the flexural failure of the live end of specimen NSL-4 at an embedment of 47 in. (1194 mm). The beam exhibited typical flexural cracking beneath the applied load and very few other cracks along the length of the beam. Strand slip was first measured at a load and corresponding moment of approximately 44.40 kips (197.5 kN) and 982 k-in. (111.0 kN-m), approximately 1.2 percent less than the nominal moment of 994 k-in. (112.3 kN-m). The beam reached a maximum load and moment of 46.20 kips (205.5 kN) and 1022 k-in. (115.5 kN-m) before exhibiting increasing deflection and strand slip until crushing of the extreme compression fiber occurred.



The behavior of the beam under load is shown in Figure 6.47 and the cracking and failure of the beam is shown in Figure 6.48. The maximum recorded strand slip was greater than 0.05 in. (1.3 mm), but did not exceed the 0.10 in. (2.5 mm) considered as the requirement for bond failure. Since the specimen exceeded the nominal moment by 2.8 percent with less than 0.10 in. (2.5 mm) strand slip, it was concluded that the development length was very near, but likely slightly less than the 34 in. (864 mm) embedment.

## 6.5.4 NSL-4

### 6.5.4.1 Dead End

The dead end of specimen NSL-4 was very poorly consolidated and had an extremely long transfer length. It was therefore tested at an embedment of 56 in. (1422 mm), corresponding to 62 percent of the ACI/AASHTO development length, since this was the longest

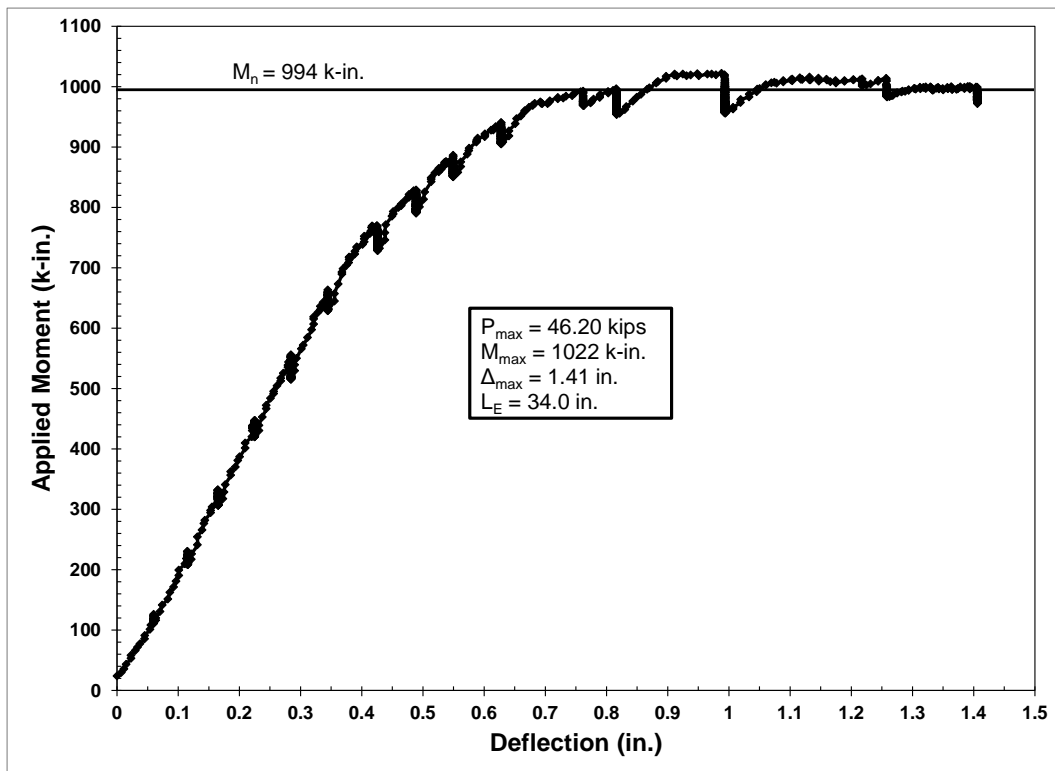


Figure 6.47: Plot of moment vs. deflection for specimen NSL-3L



Figure 6.48: Cracking and failure of specimen NSL-3L

embedment length intended for testing with this set of specimens. Strand slip was first measured at a very low load of 15.70 kips (69.8 kN) and moment of 465 k-in. (52.5 kN-m). A large shear crack soon followed beginning approximately halfway between the support and the applied load. Cracking and spalling also occurred at the near support due to the short overhang used for this specimen. The LVDTs were removed to prevent damage after the end began spalling, and the strands were marked with a permanent marker. Strand slip was visible to the naked eye even after the LVDTs had indicated slip greater than 0.10 in. (2.5 mm) before their removal. The beam exhibited a single flexural crack beneath the applied load that did not propagate very far upward into the beam before failure occurred at a maximum load and corresponding moment of 27.80 kips (123.7 kN) and 823 k-in. (93.0 kN-m), 17.5 percent less than the nominal moment of 998 k-in. (112.8 kN-m). The erratic behavior of this member is shown in Figure 6.49 and the cracking and failure of the beam is shown in Figure 6.50. The failure included widening of the

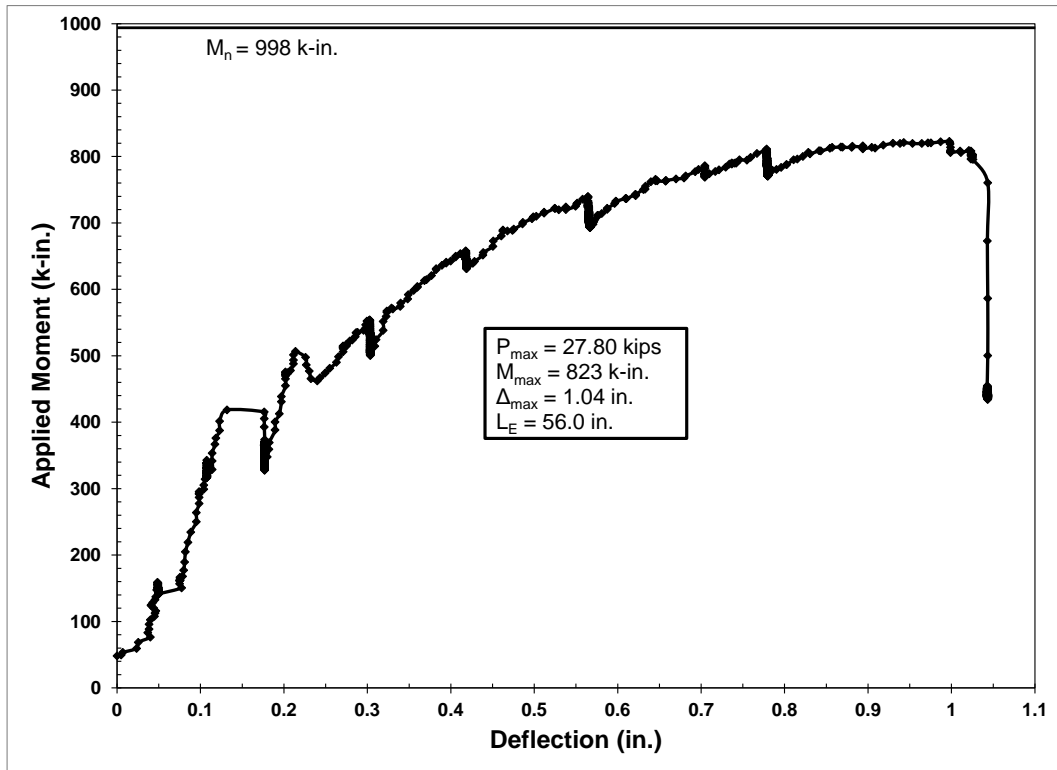


Figure 6.49: Plot of moment vs. deflection for specimen NSL-4D



Figure 6.50: Shear cracking and failure of specimen NSL-4D

shear crack as well as delamination of the top concrete surface at approximately the level of the compression reinforcement. The poor consolidation of this end led to the sudden shear failure that did not provide a clear indication of the development length for this set of specimens.

#### 6.5.4.2 Live End

The live end of specimen NSL-4 was the first NSL specimen tested. An embedment length of 47 in. (1194 mm) was used for the test, corresponding to 52 percent of the ACI/AASHTO development length, based on the results of the NSC flexural tests. The beam exhibited typical flexural cracking beginning directly beneath the applied load followed by additional flexure and flexure/shear cracks at other points along the beam, as shown in Figure 6.51. Additional deflection occurred after the maximum load and corresponding moment of 43.56 kips (193.8 kN) and 1143 k-in. (129.1 kN-m) were reached and before crushing of the extreme compression fiber occurred, as illustrated in Figure 6.52. Since the maximum load



Figure 6.51: Cracking and failure of specimen NSL-4L

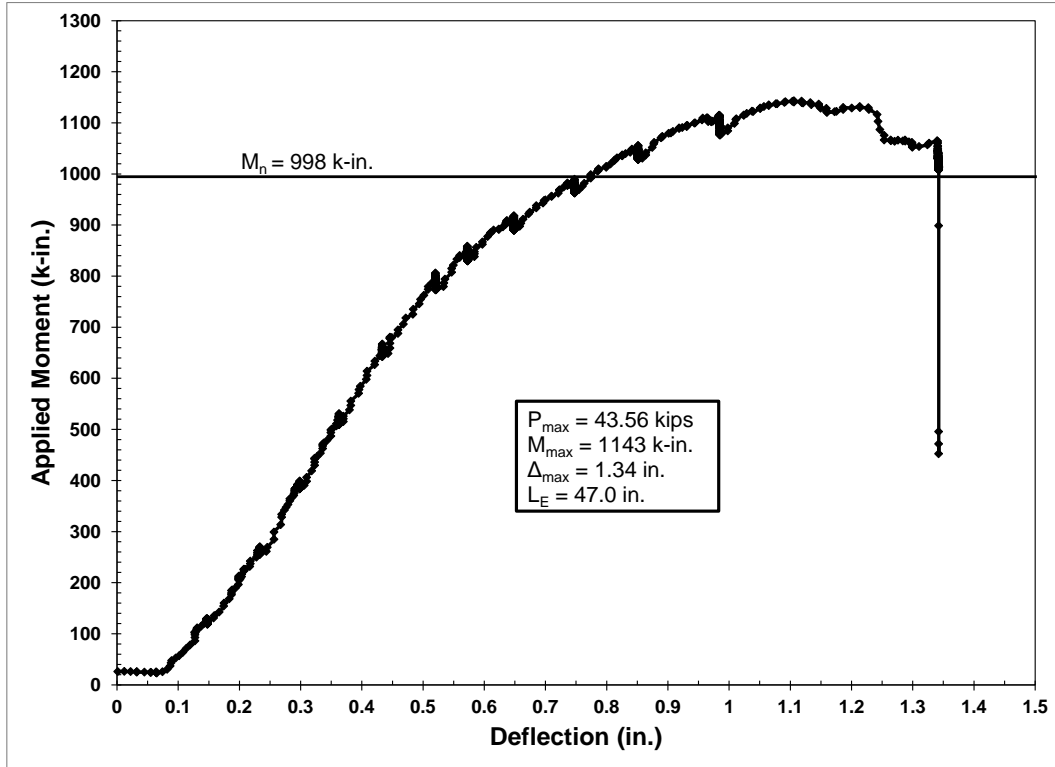


Figure 6.52: Plot of moment vs. deflection for specimen NSL-4L

exceeded the nominal moment of 998 k-in. (112.8 kN-m) by 14.5 percent and the specimen failed in flexure with no measured slip, the development length was less 47 in. (1194 mm).

### 6.5.5 Summary and Discussion

The results of the flexural tests summarized in Table 6.6 indicated that the development length of the normal strength limestone (NSL) specimens was less than 40 in. (1016 mm) and possibly as small as 34 in. (864 mm). The tests at 40 in. (1016 mm) and 39.5 in. (1003 mm) indicated that the development length was less than these values. The shear failure that occurred at the 37 in. (940 mm) embedment complicated the data analysis, but the test at 34 in. (864 mm) indicated that the development length was very close to this value.

Development length predictions for the NSL specimens produced by the various equations mentioned in Chapter 2 are presented in Table 6.7. The 40 in. (1016 mm) bound

Table 6.6: Summary of NSL Flexural Test Data

Test	$f_{se}$ (ksi)	$f_{ps}$ (ksi)	$M_n$ (k-in.)	$M_{max}$ (k-in.)	Max Slip (in.)	Failure Type	$L_E$ (in.)
NSL-1D	169.9	262.2	971	946	$>0.10^1$	SH/ES	37
NSL-1L				1073	$>0.20$	FL/ES	39.5
NSL-2D	171.9	262.9	994	1174	--	FL	40
NSL-2L				1124	--	FL	43
NSL-3D	166.4	262.7	994	1092	$>0.10^1$	SH/ES	40
NSL-3L				1022	$>0.05$	FL/ES	34
NSL-4D	168.1	263.0	998	823	$>0.10^1$	SH/ES	56
NSL-4L				1143	--	FL	47

<sup>1</sup> indicates accompanied shear failure

Note: 1 in. = 25.4 mm, 1 lbf = 4.448 N, 1 psi = 0.006895 MPa,

for development length was approximately 45 percent of the development length calculated using the ACI/AASHTO equation and the 34 in. (864 mm) minimum was approximately 38 percent of the ACI/AASHTO value. The 40 in. (1016 mm) limit was approximately 48 to 50 percent of the Ramirez and Russell prediction, 37 to 42 percent of the Zia and Mostafa prediction, 43 percent of the Buckner prediction, and 41 to 44 percent of the Kose and Burkett prediction. It was approximately 33 percent and 30 to 35 percent of the more conservative Deatherage et al. and Lane equations, respectively. These percentages decreased substantially if the 34 in. (864 mm) minimum was considered instead. These results indicated that the measured development length for these specimens was significantly less than that calculated using all of the prediction equations.

Table 6.7: Development Length Predictions for NSL Specimens

Specimen	ACI/ AASHTO (in.)	Ramirez/ Russell (in.)	Zia/ Mostafa (in.)	Deatherage et al. (in.)	Buckner (in.)	Lane (in.)	Kose/ Burkett (in.)
NSL-1	89.3	83.9	97.3	120.4	92.7	135.2	98.3
NSL-2	89.0	78.6	94.5	119.5	92.2	114.8	90.9
NSL-3	91.1	83.8	108.5	123.9	95.0	119.2	91.6
NSL-4	90.6	83.0	106.0	122.8	94.3	118.2	91.4

Note: 1 in. = 25.4 mm

## 6.6 High Strength Clay (HSC) Development Length

### 6.6.1 HSC-1

#### 6.6.1.1 Dead End

The dead end of specimen HSC-1 was tested at an embedment of 40 in. (1016 mm), corresponding to 44 percent of the ACI/AASHTO calculated development length, after the flexural failure of the live end of specimen HSC-1 at an embedment of 50 in. (1270 mm). The specimen exhibited typical flexural cracking, shown in Figure 6.53, beginning directly beneath the applied load and spreading in both directions as the load increased with those farther from the load exhibiting flexure/shear behavior. A shear crack originating at the support and propagating to the top of the beam was observed at near the maximum load. The beam exhibited some ductile behavior after reaching the maximum load and corresponding moment of 42.60 kips



Figure 6.53: Cracking and failure of specimen HSC-1D

(189.5 kN) and 1008 k-in. (113.9 kN-m) and before crushing of the extreme compression fiber occurred. The beam had an area of poor consolidation directly beneath the applied load that contributed to the sudden compression failure, the results of which are illustrated in Figure 6.54. The flexure failure of this specimen at a load 2.5 percent greater than the nominal moment of 983 k-in. (111.1 kN-m) with less than 0.01 in. (0.3 mm) of strand slip indicated that the development length was less than the 40 in. (1016 mm) embedment.

#### 6.6.1.2 Live End

The live end of specimen HSC-1 was the first HSC specimen tested. An embedment length of 50 in. (1270 mm) was used for the test, corresponding to 55 percent of the ACI/AASHTO calculated development length, and was chosen based on the results of the NS tests. The beam exhibited typical flexure and flexure/shear cracking behavior as shown in Figure 6.55. Significant deflection occurred after the maximum load and corresponding moment of

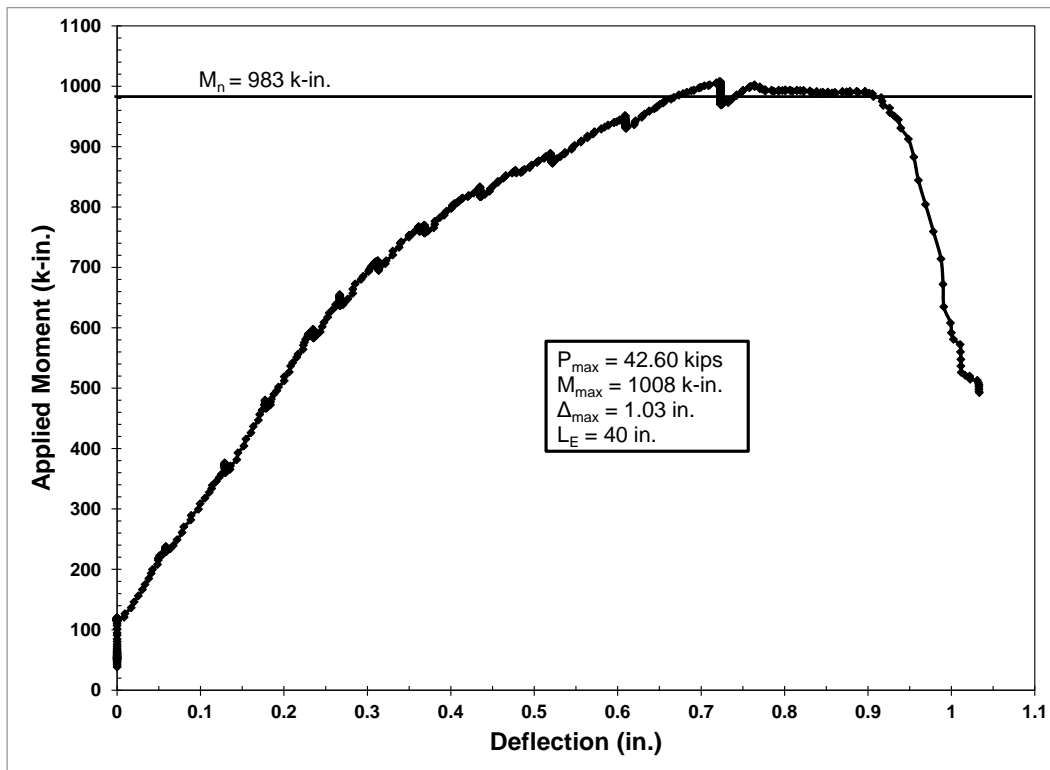


Figure 6.54: Plot of moment vs. deflection for specimen HSC-1D





Figure 6.55: Cracking of specimen HSC-1L

41.96 kips (186.6 kN) and 1101 k-in. (124.4 kN-m) were surpassed followed by crushing of the extreme compression fiber, as shown in Figure 6.56. No strand slip was recorded and the flexural failure at a load 12 percent greater than the 983 k-in. (111.1 kN-m) nominal moment indicated that the development length was less than the 50 in. (1270 mm) embedment.

## 6.6.2 HSC-2

### 6.6.2.1 Dead End

The dead end of specimen HSC-2 was tested at an embedment of 44.25 in. (1124 mm), corresponding to 49 percent of the ACI/AASHTO calculated development length, in order to confirm the results of the test on the live end of the specimen at an embedment of 45 in. (1143 mm). The specimen exhibited typical flexural behavior with cracking commencing directly beneath the applied load and other cracks forming along the length beam that exhibited

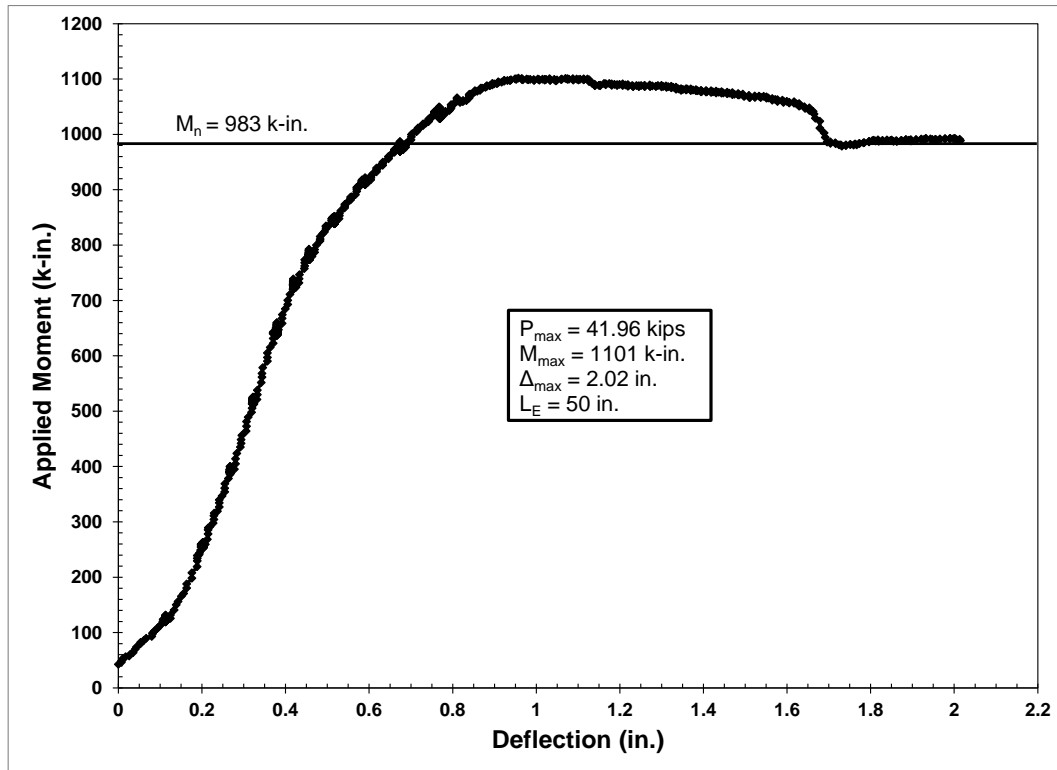


Figure 6.56: Plot of moment vs. deflection for specimen HSC-1L

flexure/shear behavior. Significant deflection, as shown in Figure 6.57, was recorded after reaching a maximum load and corresponding moment of 41.06 kips (182.6 kN) and 1026 k-in. (115.9 kN-m) and before the beam failed due to catastrophic crushing of the concrete in compression. The cracking and failure of the specimen is shown in Figure 6.58. The purely flexural failure of this specimen at an applied load approximately 3.7 percent greater than the 989 k-in. (111.7 kN-m) nominal moment, with no measured strand slip, indicated that the development length was less than the 44.25 in. (1124 mm) embedment.

#### 6.6.2.2 Live End

The live end of specimen HSC-2 was tested at an embedment of 45 in. (1143 mm), corresponding to 50 percent of the ACI/AASHTO development length, after the shear failure of the dead end of specimen HSC-1 at an embedment of 40 in. (1016 mm). The beam exhibited typical flexural behavior with well-defined flexural cracks forming directly beneath the applied

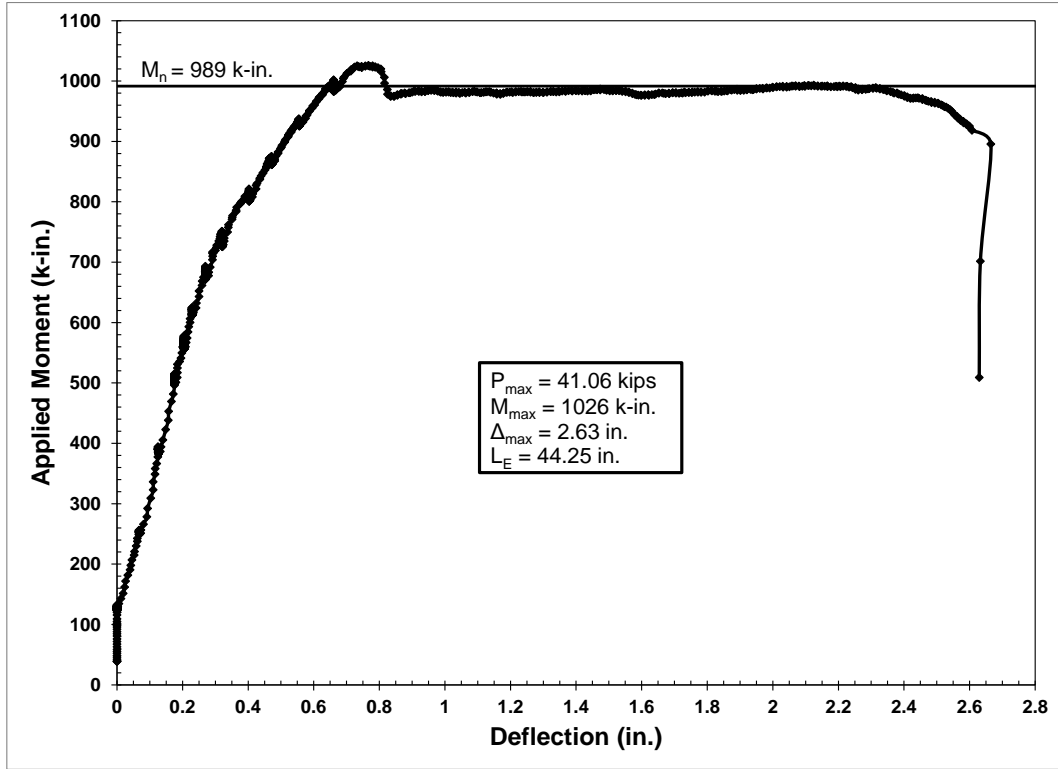


Figure 6.57: Plot of moment vs. deflection for specimen HSC-2D



Figure 6.58: Cracking and failure of specimen HSC-2D

load followed by other flexure and flexure/shear cracks at increments along the beam, as shown in Figure 6.59. Minor strand slip was recorded at a load and moment of 38.65 kips (171.9 kN) and 974 k-in. (110.0 kN-m), 1.5 percent less than the 989 k-in. (111.7 kN-m) nominal moment. This slip was followed by the formation of a shear crack extending from the support to the top of the specimen at the maximum load and corresponding moment of 40.80 kips (181.5 kN) and 1027 k-in. (116.0 kN-m). The beam exhibited some additional deflection before crushing of the concrete in compression occurred, as shown in Figure 6.60, with a measured strand slip of approximately 0.02 in. (0.5 mm). The failure of the beam at a load 3.8 percent greater than the nominal moment with strand slip less than the 0.10 in. (2.5 mm) limit considered for a bond failure, indicated that the development length was less than the 45 in. (1143 mm) embedment.



Figure 6.59: Cracking and failure of specimen HSC-2L

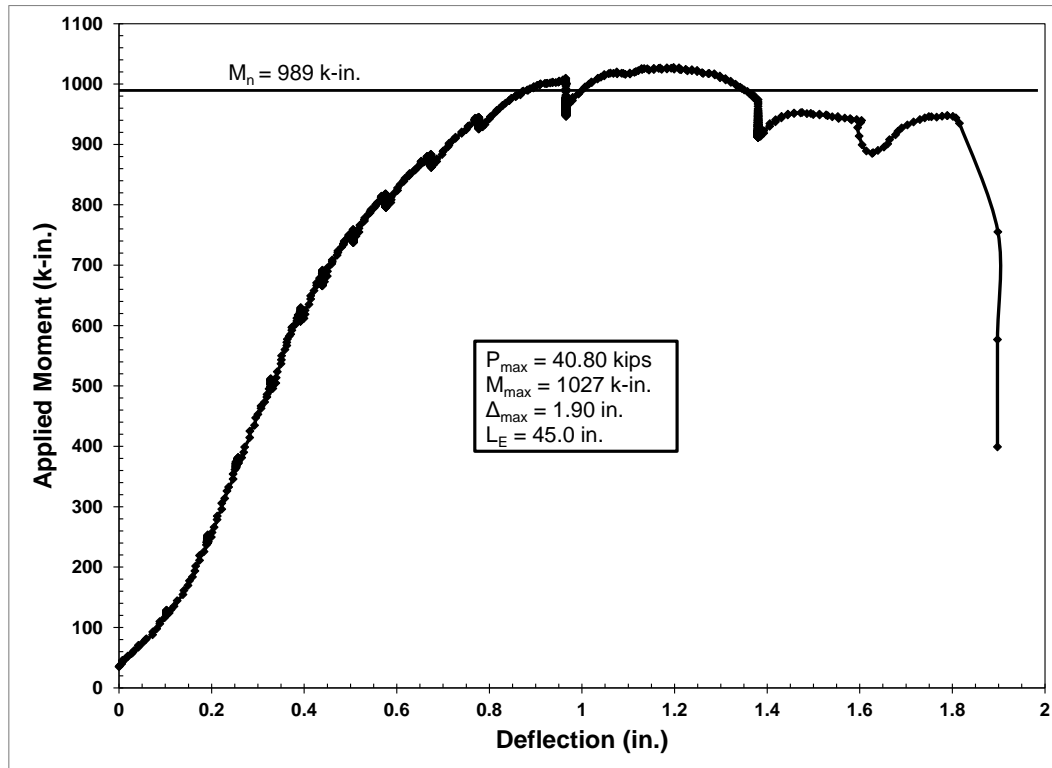


Figure 6.60: Plot of moment vs. deflection for specimen HSC-2L

### 6.6.3 HSC-3

#### 6.6.3.1 Dead End

The dead end of specimen HSC-3 was tested at an embedment of 42.5 in. (1080 mm), corresponding to 47 percent of the ACI/AASHTO development length. This embedment length was chosen after the flexure and shear failures of the live ends of specimens HSC-2 and HSC-3 at embedment lengths of 45 in. (1143 mm) and the flexure failure of the dead end of specimen HSC-2 at a 44.25 in. (1124 mm) embedment. The beam first exhibited typical flexural cracking directly beneath the applied load followed by shear cracking between the applied load and the support. A major shear crack formed beginning at the support and propagating to the top of the beam at an approximately 45° angle at a load and corresponding moment of 32.85 kips (146.1 kN) and 804 k-in. (90.8 kN-m). This crack was accompanied by the beginning of strand slip and

occurred at a moment 17.5 percent less than the 974 k-in. (110.0 kN-m) nominal moment. Other shear cracks formed as the load increased, as shown in Figure 6.61, before the maximum load and corresponding moment of 37.59 kips (167.2 kN) and 920 k-in. (103.9 kN-m) were achieved. The sudden failure of this specimen is illustrated in Figure 6.62. The occurrence of shear cracking was the cause of the greater than 0.10 in. (2.5 mm) of measured strand slip for this specimen, and the shear failure at a load less than the nominal moment did not lead to a definite indication of the development length.

#### 6.6.3.2 Live End

The live end of specimen HSC-3 was tested an embedment of 45 in. (1143 mm), corresponding to 50 percent of the ACI/AASHTO development length, to confirm the results of the tests on specimen HSC-2. The beam exhibited typical flexural behavior before the formation of shear cracks at a load and corresponding moment of 37.20 kips (165.5 kN) and 937 k-in.



Figure 6.61: Cracking and failure of specimen HSC-3D

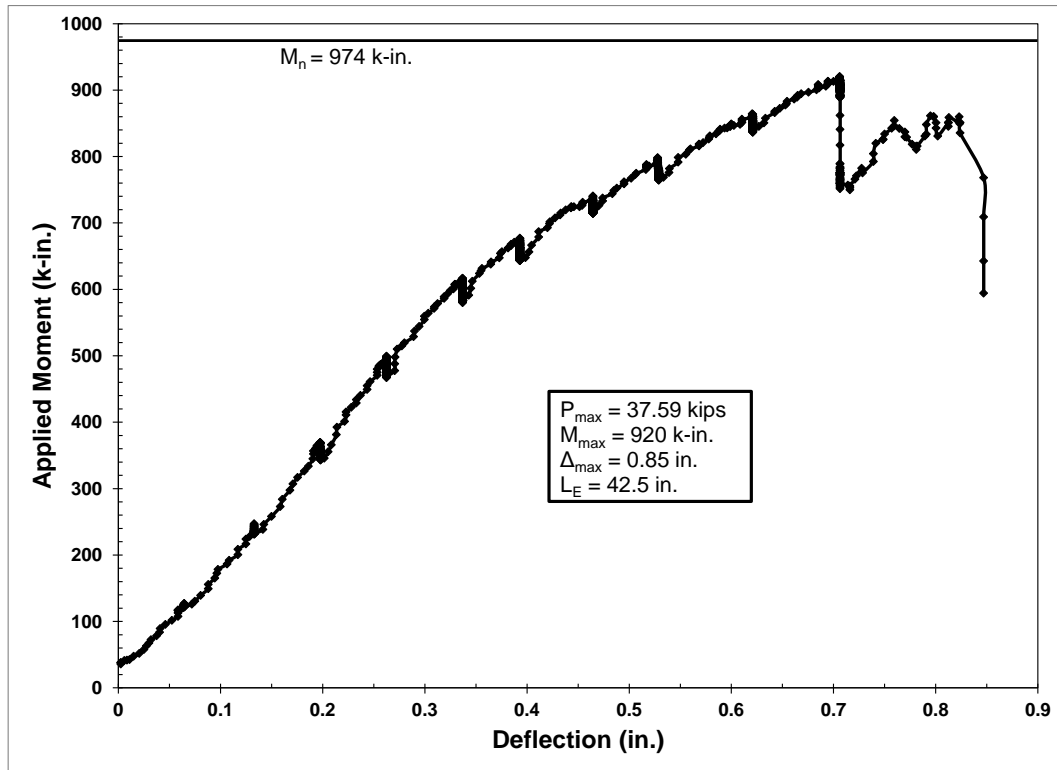


Figure 6.62: Plot of moment vs. deflection for specimen HSC-3D

(105.9 kN-m). These shear cracks were accompanied by initial strand slip. Shear cracking and slip increased with increasing load until the occurrence of an explosive shear failure at the maximum load and corresponding moment of 41.26 kips (183.5 kN) and 1039 k-in. (117.4 kN-m). The result of this explosive failure is shown in Figure 6.63 and the behavior of the specimen is illustrated in Figure 6.64. The occurrence of a major shear failure at a load 6.7 percent greater than the nominal moment of 974 k-in. (110.0 kN-m), combined with measured strand slip caused by shear cracking, did not produce a distinct indication of the development length.

## 6.6.4 HSC-4

### 6.6.4.1 Dead End

The dead end of specimen HSC-4 was tested at an embedment of 37.5 in. (953 mm), corresponding to 41 percent of the ACI/AASHTO development length, in order to extend the



Figure 6.63: Shear failure of specimen HSC-3L

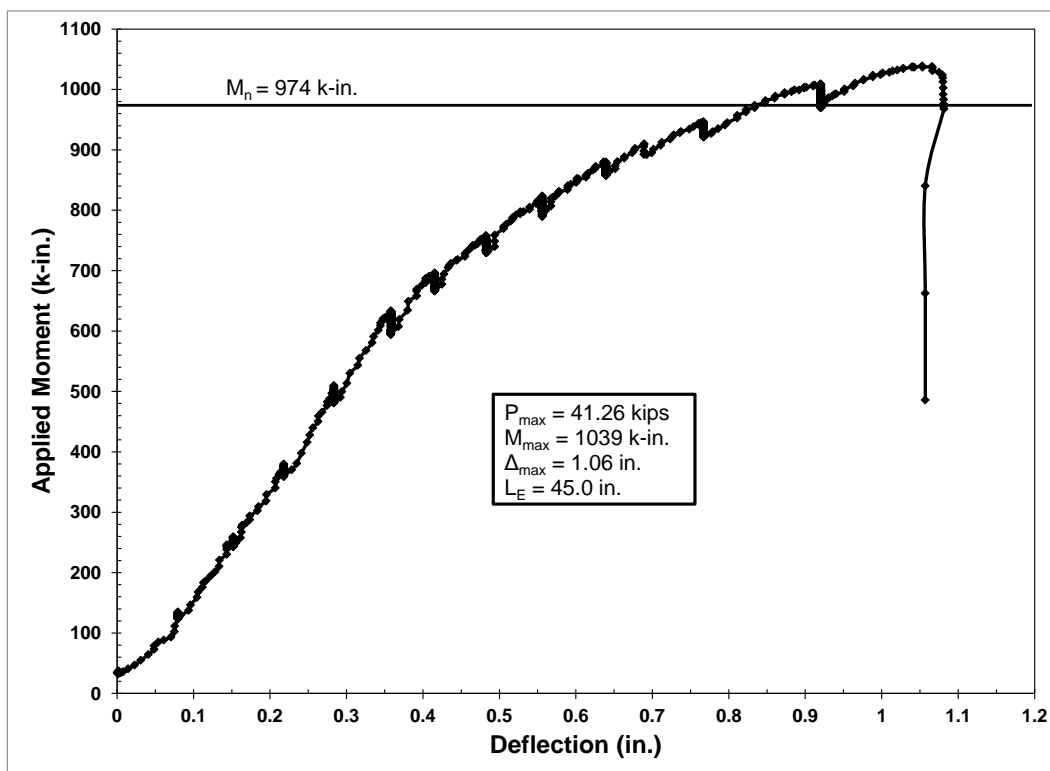


Figure 6.64: Plot of moment vs. deflection for specimen HSC-3L



data range after the previously tested HSC specimens. The beam exhibited typical flexure and flexure/shear cracking before developing shear cracks at a load and corresponding moment of approximately 39.0 kips (173.5 kN) and 886 k-in. (100.1 kN-m) immediately followed by measured strand slip. The severe shear cracking is shown in Figure 6.65. The specimen withstood some additional load and achieved a maximum load and corresponding moment of 42.77 kips (190.3 kN) and 972 k-in. (109.8 kN-m) with additional strand slip up to greater than 0.15 in. (3.8 mm). This maximum load was approximately 1 percent less than the 981 k-in. (110.8 kN-m) nominal moment. The failure behavior of this specimen is illustrated in Figure 6.66. The sudden shear failure of this specimen coupled with strand slip at a load approximately equal to the nominal moment did not provide an absolutely distinct indication of the development length, but the development length was most likely greater than the 37.5 in. (953 mm) embedment.



Figure 6.65: Shear failure of specimen HSC-4D

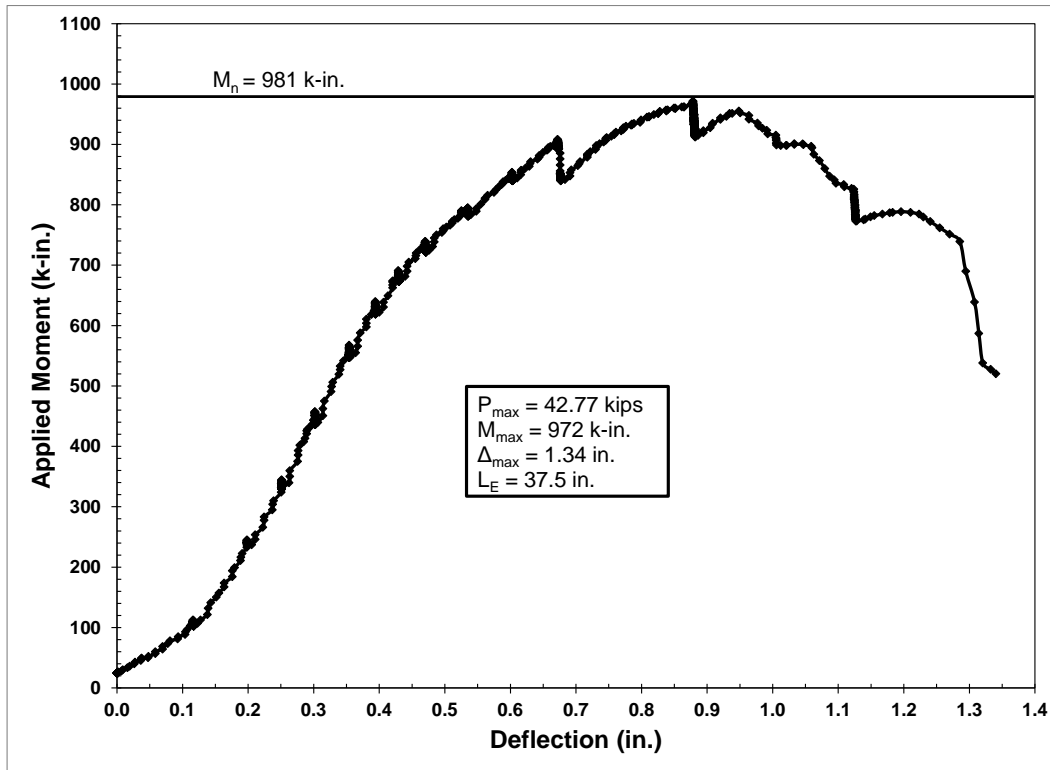


Figure 6.66: Plot of moment vs. deflection for specimen HSC-4D

#### 6.6.4.2 Live End

The live end of specimen HSC-4 was tested at an embedment of 47.5 in. (1207 mm), corresponding to 52 percent of the ACI/AASHTO development length, in order to increase the data range from the previously tested HSC specimens. The beam exhibited typical flexure and flexure/shear cracking up until the point of crushing of the extreme compression fiber, as shown in Figure 6.67. Significant deflection occurred after the maximum load and corresponding moment of 40.15 kips (178.6 kN) and 1035 k-in. (116.9 kN-m) were reached and before crushing of the extreme compression concrete occurred. The yield plateau for this specimen was below the level of the 981 k-in. (110.8 kN-m) nominal moment, as shown in Figure 6.68. However, the purely flexural failure of this specimen at a load 5 percent greater than the nominal moment with no measured strand slip indicated that the development length was less than the 47.5 in. (1207 mm) embedment.



Figure 6.67: Cracking and failure of specimen HSC-4L

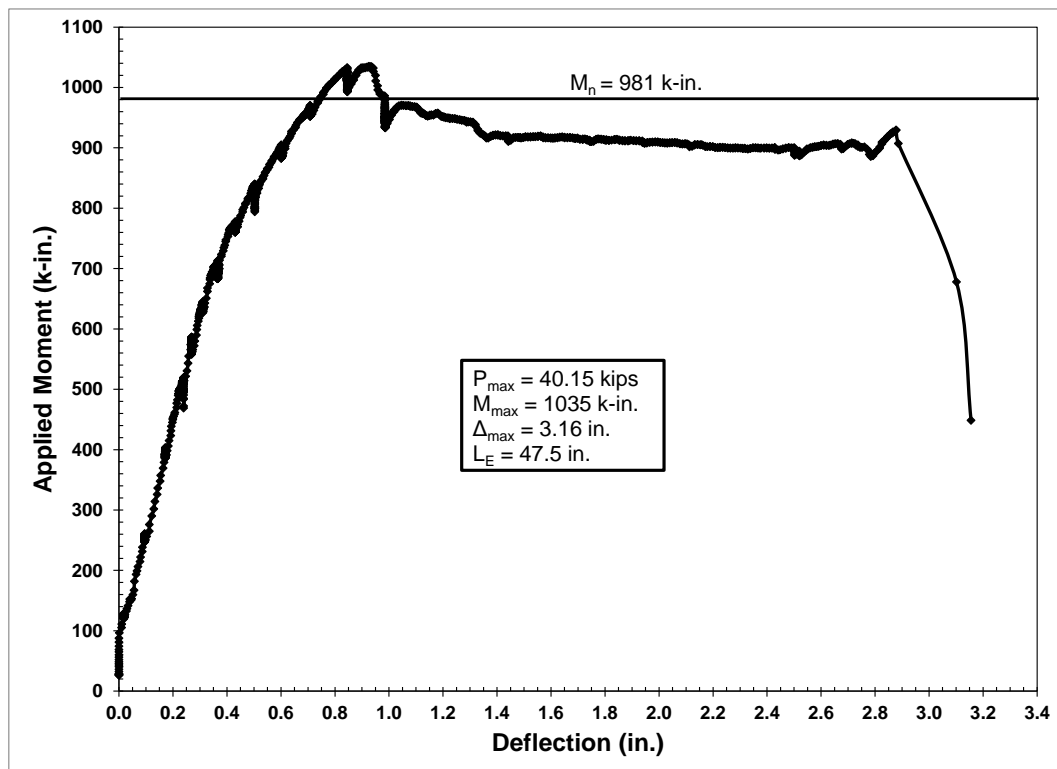


Figure 6.68: Plot of moment vs. deflection for specimen HSC-4L

### 6.6.5 Summary and Discussion

The flexural tests summarized in Table 6.8 indicated that the development length of the high strength clay (HSC) specimens was less than 45 in. (1143 mm) and likely between 37.5 in. (953 mm) and 40 in. (1016 mm). The strand slip measured for the specimens tested at 45 in. (1143 mm) and 42.5 in. (1080 mm) was caused by shear cracks that occurred within the transfer length and not purely based on bond with the concrete. The specimens tested at 45 in. (1143 mm) achieved an applied moment greater than the nominal moment calculated for those specimens. These facts and the purely flexural failure of specimen HSC-2D tested at 44.25 in. (1124 mm) indicated that the development length was less than 45 in. (1143 mm). Specimen HSC-1D tested at 40 in. (1016 mm) reached a moment greater than the nominal moment while specimen HSC-4D tested at 37.5 in. (953 mm) withstood a load very close to the nominal moment before experiencing slip and shear behavior. This indicated that the development length was between 37.5 in. (953 mm) and 40 in. (1016 mm).

The values of development length produced by the various prediction equations described in Chapter 2 are presented in Table 6.9. The 40 in. (1016 mm) limit on the measured development length was approximately 44 percent of the ACI/AASHTO prediction, 43 percent

Table 6.8: Summary of HSC Flexural Test Data

Test	$f_{se}$ (ksi)	$f_{ps}$ (ksi)	$M_n$ (k-in.)	$M_{max}$ (k-in.)	Max Slip (in.)	Failure Type	$L_E$ (in.)
HSC-1D	167.4	262.6	983	1008	<0.01	FL/SH	40.0
HSC-1L				1101	--	FL	50.0
HSC-2D	166.8	262.8	989	1026	--	FL	44.25
HSC-2L				1027	0.02	FL/SH/ES	45.0
HSC-3D	167.9	262.5	974	920	>0.10 <sup>1</sup>	SH/ES	42.5
HSC-3L				1039	>0.15 <sup>1</sup>	SH/ES	45.0
HSC-4D	167.4	262.6	981	972	>0.15 <sup>1</sup>	SH/ES	37.5
HSC-4L				1035	--	FL	47.5

Note: <sup>1</sup> indicates accompanied shear failure, 1 in. = 25.4 mm, 1 lbf = 4.448 N, 1 psi = 0.006895 MPa,

Table 6.9: Development Length Predictions for the HSC Specimens

Specimen	ACI/ AASHTO (in.)	Ramirez/ Russell (in.)	Zia/ Mostafa (in.)	Deatherage et al. (in.)	Buckner (in.)	Lane (in.)	Kose/ Burkett (in.)
HSC-1	90.6	79.3	93.6	122.6	94.0	128.8	95.4
HSC-2	90.9	78.7	95.2	123.2	94.4	123.3	93.2
HSC-3	90.3	80.6	92.2	122.0	93.6	136.5	98.3
HSC-4	90.6	79.5	93.2	122.5	94.0	130.3	95.9

Note: 1 in. = 25.4 mm

of the Zia and Mostafa prediction and the Buckner prediction, and 42 percent of the Kose and Burkett prediction. These four equations provided very similar predictions for development length. The measured development length was approximately 50 percent of the Ramirez and Russell prediction, which provided the closest prediction to the measured values. The measured development length was approximately 32 percent and 29 to 32 percent of the predictions produced by the very conservative Deatherage et al. and Lane equations respectively. Every equation overestimated the measured development length by at least 100 percent.

## 6.7 High Strength Shale (HSS) Development Length

### 6.7.1 HSS-1

#### 6.7.1.1 Dead End

The dead end of specimen HSS-1 was tested at an embedment of 40 in. (1016 mm), corresponding to 44 percent of the calculated ACI/AASHTO development length, following the flexural failure of the live end at a 50 in. (1270 mm) embedment. The beam exhibited typical flexure and flexure/shear cracking behavior before a large shear crack formed at a load of approximately 40.20 kips (178.8 kN) and corresponding moment of 951 k-in. (107.4 kN-m). As shown in Figure 6.69, this crack began at the support and propagated upward at an approximately 45° angle to the level of the compression reinforcement, which it followed to the applied load. This shear crack was accompanied by strand slip that reached a maximum of 0.04



Figure 6.69: Shear cracking of specimen HSS-1D

in. (1.0 mm) before the end of the test. After initial shear cracking, the beam was reloaded to the maximum load of 40.24 kips (179.0 kN) and corresponding moment of 952 k-in. (107.6 kN-m). The beam lost a substantial amount of its load carrying capacity, but exhibited additional deflection, shown in Figure 6.70, before a catastrophic failure of the specimen. The shear failure, with limited strand slip, at a load 2 percent less than the 972 k-in. (109.8 kN-m) nominal moment, did not produce a distinct indication concerning the development length, but did provide evidence to the possibility of a development length less than 40 in. (1016 mm).

#### 6.7.1.2 Live End

The live end of specimen HSS-1 was the first HSS specimen tested. An embedment of 50 in. (1270 mm), corresponding to 55 percent of the ACI/AASHTO development length, was used for the test, which was consistent with the beginning embedment length for the other beam series. The beam exhibited typical flexure and flexure/shear cracking and exhibited significant

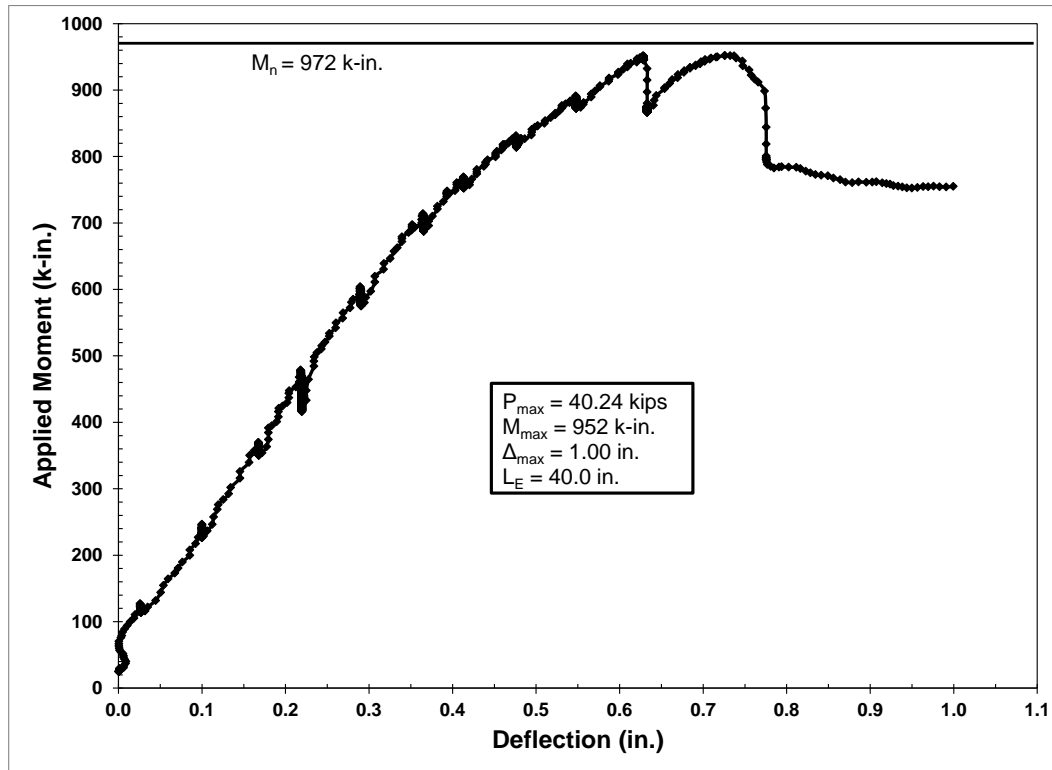


Figure 6.70: Plot of moment vs. deflection for specimen HSS-1D

deflection after the maximum load and corresponding moment of 41.18 kips (183.2 kN) and 1081 k-in. (122.1 kN-m) were achieved, as shown in Figure 6.71. The beam was loaded until explosive crushing of the concrete occurred, the result of which is shown in Figure 6.72. Minor strand slip was recorded at the time of concrete crushing, but was most likely caused by the violent release of energy. The purely flexural failure of this specimen at a load exceeding the 972 k-in. (109.8 kN-m) nominal moment by 11 percent indicated that the development length was less than the 50 in. (1270 mm) embedment.

## 6.7.2 HSS-2

### 6.7.2.1 Dead End

The dead end of specimen HSS-2 was tested at an embedment of 42.5 in. (1080 mm), corresponding to 46 percent of the ACI/AASHTO development length, following the flexural

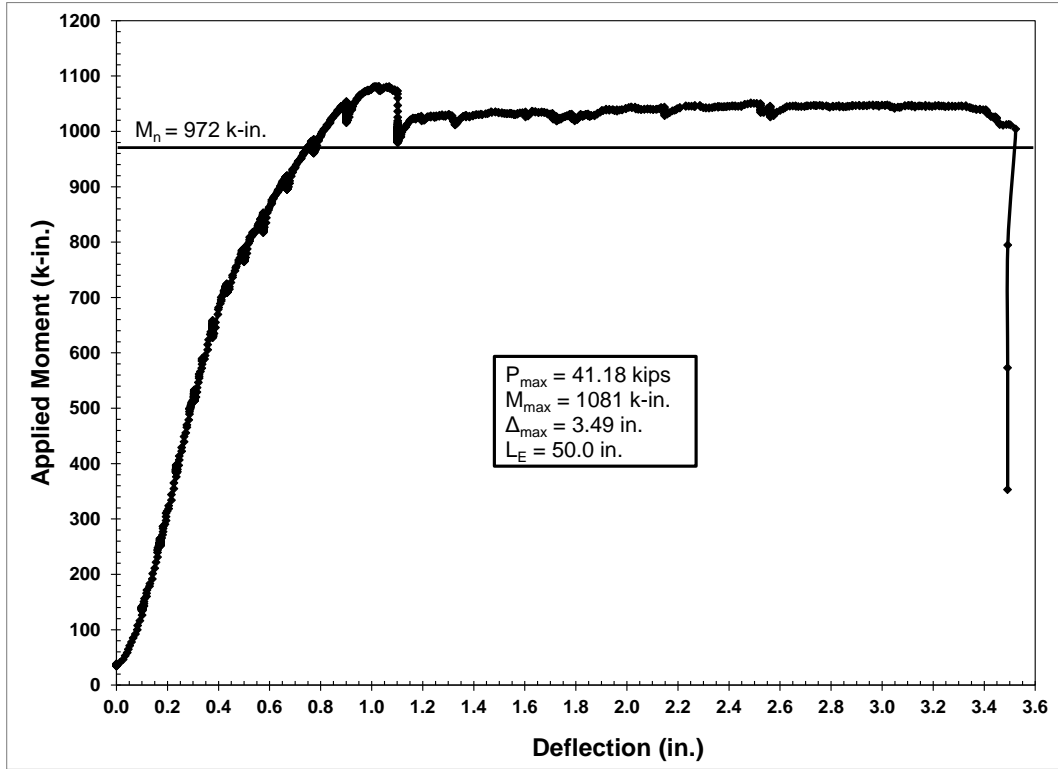


Figure 6.71: Plot of moment vs. deflection for specimen HSS-1L



Figure 6.72: Cracking and failure of specimen HSS-1L



failure of the live end of the specimen at a 45 in. (1143 mm) embedment. The beam exhibited typical flexure and flexure/shear cracking before experiencing an explosive crushing of the concrete in compression that including buckling of the compression reinforcement, as shown in Figure 6.73. Significant deflection was observed after the maximum load and corresponding moment of 44.86 kips (199.5 kN) and 1098 k-in. (124.1 kN-m) were reached. This additional deflection was exhibited while sustaining a load greater than that causing the nominal moment, as shown in Figure 6.74. The purely flexural failure of this specimen at a load 13 percent greater than the 968 k-in. (109.4 kN-m) nominal moment with no recorded strand slip indicated that the development length was less than the 42.5 in. (1080 mm) embedment.

#### 6.7.2.2 Live End

The live end of specimen HSS-2 was tested at an embedment of 45 in. (1143 mm), corresponding to 49 percent of the calculated ACI/AASHTO development length, following the



Figure 6.73: Cracking and failure of specimen HSS-2D

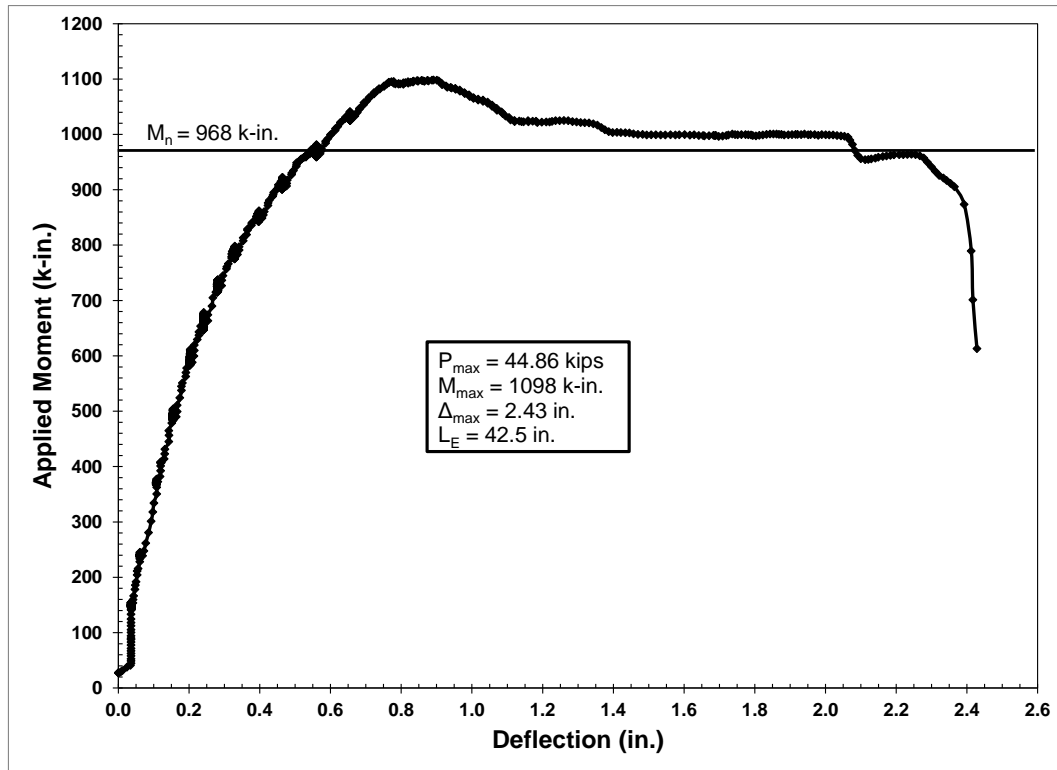


Figure 6.74: Plot of moment vs. deflection for specimen HSS-2D

shear failure of the dead end of specimen HSS-1 at an embedment of 40 in. (1016 mm). The beam exhibited typical flexure and flexure-shear cracking with the flexure cracks directly beneath the applied load reaching a width greater than 1/8 in. (3.2 mm) before crushing of the extreme compression fiber occurred. The width of the cracks is visible in Figure 6.75.

Significant deflection was recorded after the maximum load and corresponding moment of 42.60 kips (189.5 kN) and 1073 k-in. (121.2 kN-m) were reached. This additional deflection, shown in Figure 6.76, occurred while the specimen held a load greater than that corresponding to the 968 k-in. (109.4 kN-m) nominal moment. At least one of the prestressing strands fractured at the same time that the concrete failed in compression and minor strand slip was recorded simultaneously with this fracture. The flexural failure of this specimen at a load 11 percent greater than the nominal moment accompanied by strand fracture and no strand slip indicated that the development length was less than the 45 in. (1143 mm) embedment.



### 6.7.3 HSS-3

#### 6.7.3.1 Dead End

The dead end of specimen HSS-3 was tested at an embedment of 35 in. (889 mm), corresponding to 38 percent of the ACI/AASHTO development length, after the flexural failure of the live end of the specimen at an embedment of 40 in. (1016 mm). This specimen exhibited typical flexure and flexure/shear cracking with some of the flexure/shear cracks closer to the near support reaching a substantial width before completion of the test, as shown in Figure 6.77. The beam exhibited strand slip while under sustained load, immediately after the maximum load and corresponding moment of 42.60 kips (189.5 kN) and 923 k-in. (104.3 kN-m) were reached. The strand slip increased under continued loading; with deflection occurring faster than the beam could be loaded, as shown in Figure 6.78, until strain sufficient to cause crushing of the concrete was achieved in the extreme compression fiber. While it is possible that the flexure/shear cracks



Figure 6.77: Cracking and failure of specimen HSS-3D showing crack width

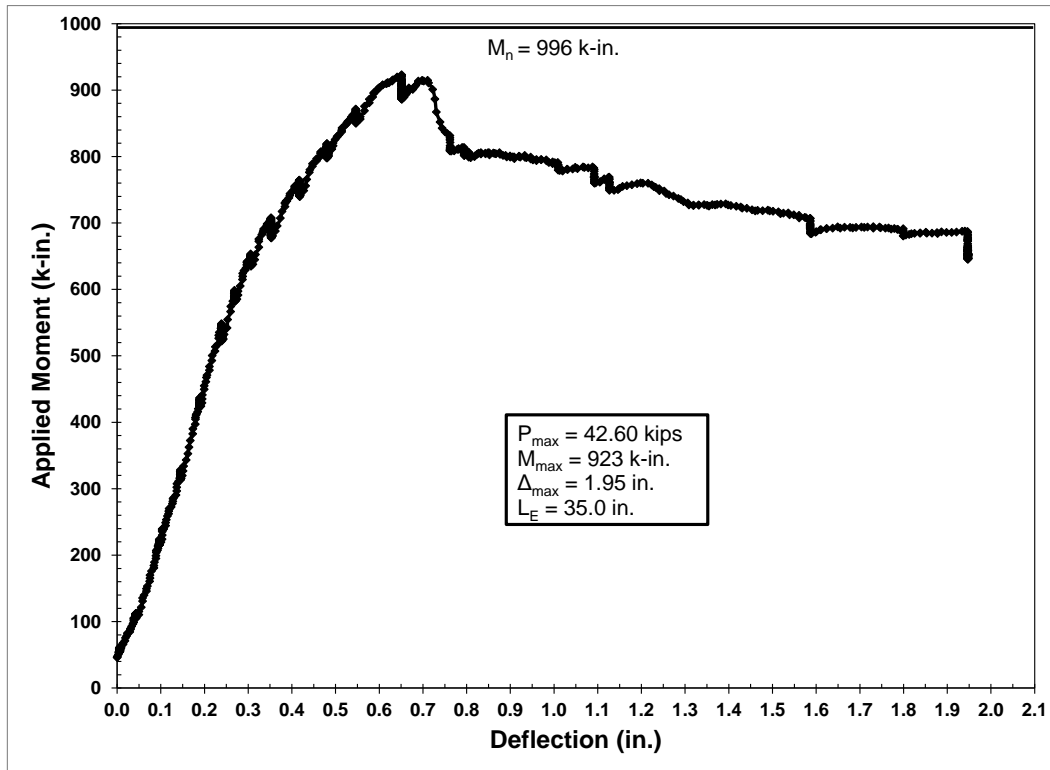


Figure 6.78: Plot of moment vs. deflection for specimen HSS-3D

may have caused some of the strand slip, these cracks were observed well before strand slip was recorded. The bond failure of this specimen at a load 7 percent less than the 996 k-in. (112.5 kN-m) calculated nominal moment indicated that the development length was greater than the 35 in. (889 mm) embedment. Due to the width of the flexural cracks, substantial segregation was noticed at this end of the specimen that was not present in specimens HSS-1 and HSS-2. This reduction of coarse aggregate around the strands may have affected the development length.

#### 6.7.3.2 Live End

The live end of specimen HSS-3 was tested at an embedment of 40 in. (1016 mm), corresponding to 43 percent of the ACI/AASHTO development length, after the flexural failure of the dead end of specimen HSS-2 at an embedment of 42.5 in. (1080 mm). The beam exhibited typical flexure and flexure/shear cracking and a crack running along the level of the compression reinforcement, as shown in Figure 6.79, which led to spalling of concrete from the



Figure 6.79: Cracking and failure of specimen HSS-3L

top of the beam. The beam exhibited significant deflection after achieving a maximum load and corresponding moment of 40.42 kips (179.8 kN) and 956 k-in. (108.0 kN-m). This deflection occurred faster than load could be applied, as shown in Figure 6.80, and eventually concrete crushing occurred at the extreme compression fiber. The maximum load was approximately 4 percent less than the calculated nominal moment of 996 k-in. (112.5 kN-m), but the beam exhibited a flexural failure with no measured strand slip. This result indicated that the development length was less than the 40 in. (1016 mm) embedment. The discrepancy between the maximum applied moment and the calculated nominal moment was most likely due to discrepancies between the material properties used to calculate the nominal moment and the actual properties of the concrete in the beam or due to errors in steel placement within the beam.

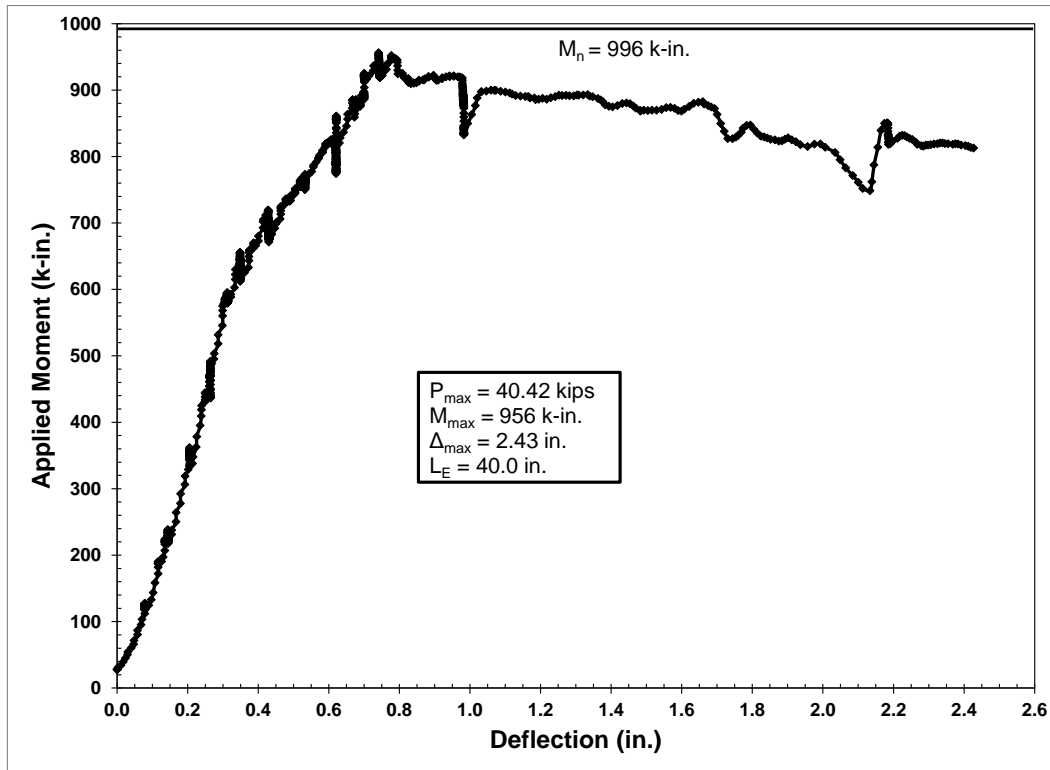


Figure 6.80: Plot of moment vs. deflection for specimen HSS-3L

## 6.7.4 HSS-4

### 6.7.4.1 Dead End

The dead end of specimen HSS-4 was tested at an embedment of 40 in. (1016 mm), corresponding to 45 percent of the ACI/AASHTO development length. This embedment was chosen due to the bond failures of the dead end of specimen HSS-3 and the live end of HSS-4 at embedment lengths of 35 in. (889 mm) and 37.5 in. (953 mm) respectively. The beam exhibited typical flexural behavior with flexure and flexure/shear cracking, as shown in Figure 6.81. Significant deflection was measured after the maximum load and corresponding moment of 44.13 kips (196.3 kN) and 1044 k-in. (118.0 kN-m) were reached. This deflection was experienced at a load greater than that leading to the nominal moment of 980 k-in. (110.7 kN-m), as shown in Figure 6.82. The flexural cracks directly beneath the applied load reached



Figure 6.81: Cracking and failure of specimen HSS-4D

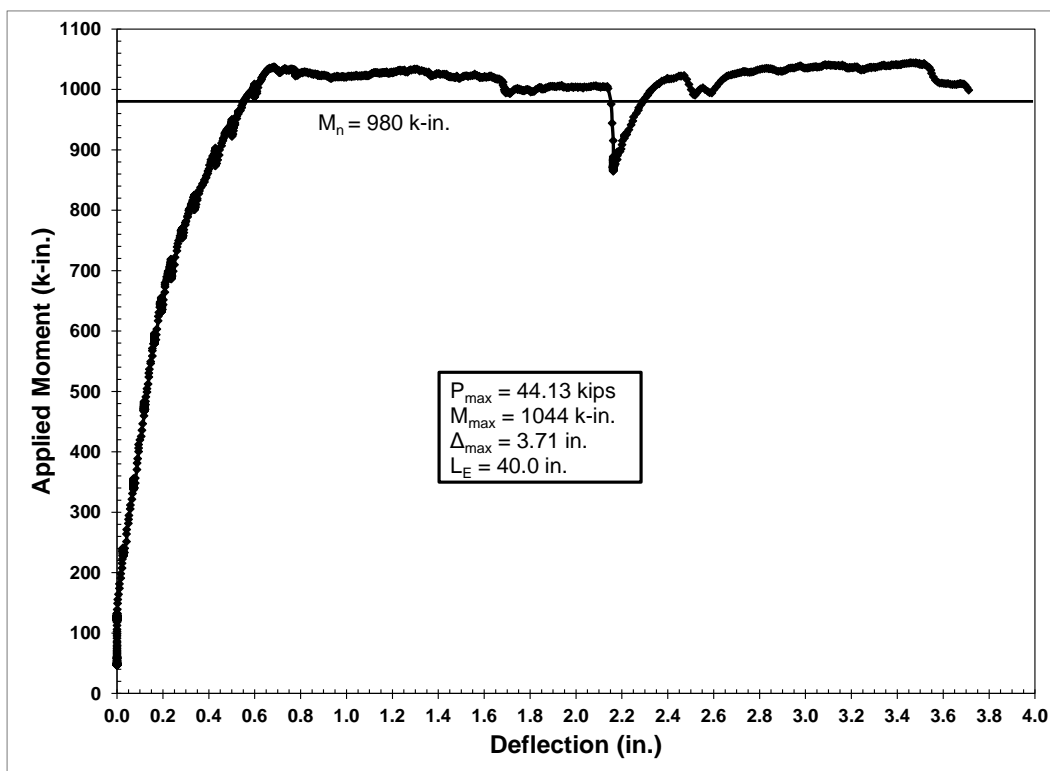


Figure 6.82: Plot of moment vs. deflection for specimen HSS-4D



significant width before the beam completely failed due to crushing of the concrete in compression, as shown in Figure 6.81. Strand slip was measured on one strand immediately before the maximum load was achieved and reached a maximum of 0.05 in. (1.3 mm) at failure. This flexural failure at a moment 7 percent greater than the nominal moment with strand slip recorded after reaching the nominal moment indicated that the development length was less than 40 in. (1016 mm).

#### 6.7.4.2 Live End

The live end of specimen HSS-4 was tested at an embedment of 37.5 in. (953 mm), corresponding to 42 percent of the ACI/AASHTO development length, after the bond failure of the dead end of specimen HSS-3 at an embedment of 35 in. (889 mm). The beam exhibited typical flexural behavior with some shear cracking occurring near the applied load at higher loads, as shown in Figure 6.83. Significant strand slip was measured at and after the maximum



Figure 6.83: Cracking and failure of specimen HSS-4L

load and corresponding moment of 41.29 kips (183.7 kN) and 938 k-in. (106.0 kN-m) with a total measured strand slip of greater than 0.20 in. (5.1 mm). The beam continued to exhibit deflection at a reduced load carrying capacity, as shown in Figure 6.84, until sufficient strain was reached in the extreme compression fiber to cause crushing of the concrete. Some shear failure-type behavior was also exhibited, most likely caused by the excessive strand slip.

Segregation in the form of sand/cement mortar with very little coarse aggregate was visible in the concrete below the prestressing strands, but the concrete and this mortar exhibited no substantial voids or poor consolidation. The difference in how this mortar with no large aggregate particles surrounded the strands may have influenced the bond behavior of this specimen. Failure of the beam due to strand slip at a moment 4 percent less than the nominal moment of 980 k-in. (110.7 kN-m) indicated that the development length was greater than, but likely near, the 37.5 in. (953 mm) embedment.

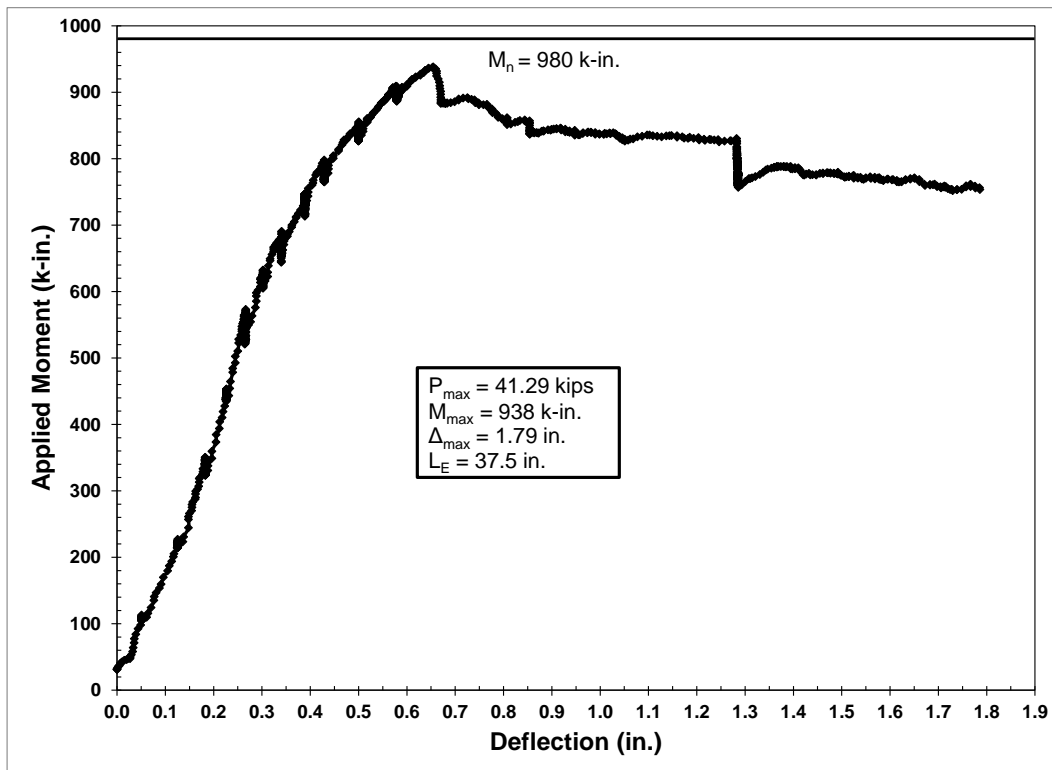


Figure 6.84: Plot of moment vs. deflection for specimen HSS-4L

### 6.7.5 Summary and Discussion

The flexural tests summarized in Table 6.10 indicated that the development length of the high strength shale (HSS) specimens was between 37.5 in. (953 mm) and 40 in. (1016 mm). The flexural failures of tests HSS-3L and HSS-4D with no significant slip indicated that the development length was less than 40 in. (1016 mm). These tests followed flexural failures at the embedment lengths greater than 40 in. (1016 mm), as shown in Table 6.10. The bond failures of tests HSS-3D and HSS-4L at 35 in. (889 mm) and 37.5 in. (953 mm), respectively, indicated that the development length was greater than these values. The shear failure of test HSS-1D at a 40 in. (1016 mm) embedment at a moment within 2 percent of the nominal moment also provided evidence that the development length was near this value. Segregation observed in specimens HSS-3 and HSS-4 may have affected the bond behavior of these specimens, but the performance of specimens HSS-1 and HSS-2, which did not exhibit this segregation, concurred with the tests of HSS-3 and HSS-4. Even though the aggregate separated from the mortar in specimens HSS-3 and HSS-4, the concrete did not exhibit voids or poor consolidation. This fact combined with the high strength of the paste and the similarity in stiffness between the paste and lightweight aggregate explains the lack of detrimental effects on bond behavior.

Table 6.10: Summary of HSS Flexural Test Data

Test	$f_{se}$ (ksi)	$f_{ps}$ (ksi)	$M_n$ (k-in.)	$M_{max}$ (k-in.)	Max Slip (in.)	Failure Type	$L_E$ (in.)
HSS-1D	166.4	262.3	972	952	0.04	SH/ES	40
HSS-1L				1081	<0.01	FL	50
HSS-2D	164.5	262.1	968	1098	--	FL	42.5
HSS-2L				1073	0.01 <sup>1</sup>	FL	45
HSS-3D	163.3	262.8	996	923	>0.20	BD	35
HSS-3L				956	--	FL	40
HSS-4D	170.2	262.7	980	1044	<0.05	FL	40
HSS-4L				938	>0.20	BD	37.5

Note: <sup>1</sup> indicates accompanied strand fracture, 1 in. = 25.4 mm, 1 lbf = 4.448 N, 1 psi = 0.006895 MPa

The development length predictions calculated using the equations described in Chapter 2 are presented in Table 6.11. The 40 in. (1016 mm) development length limit was approximately 44 percent of the ACI/AASHTO development length, between 40 and 45 percent of the Zia and Mostafa prediction, approximately 42 percent of the Buckner prediction, and between 40 and 44 percent of the Kose and Burkett prediction. The Ramirez and Russell equation produced the smallest estimate, but the measured development length was still only 48 to 51 percent of this value. The measured development length was only approximately 32 percent and 28 to 34 percent of the very conservative Deatherage et al. and Lane equations, respectively. All of the prediction equations produced estimates significantly greater in magnitude than the measured development length.

Table 6.11: Development Length Predictions for the HSS Specimens

Specimen	ACI/ AASHTO (in.)	Ramirez/ Russell (in.)	Zia/ Mostafa (in.)	Deatherage et al. (in.)	Buckner (in.)	Lane (in.)	Kose/ Burkett (in.)
HSC-1	90.8	81.8	94.6	123.1	94.3	139.6	99.1
HSC-2	91.5	83.7	98.1	124.5	95.2	144.1	100.3
HSC-3	92.4	78.2	99.8	126.1	96.2	117.7	90.4
HSC-4	89.5	78.4	88.9	120.4	92.6	130.2	96.4

Note: 1 in. = 25.4 mm

## 6.8 High Strength Limestone (HSL) Development Length

### 6.8.1 HSL-1

#### 6.8.1.1 Dead End

The dead end of specimen HSL-1 was tested at an embedment of 40 in. (1016 mm), corresponding to 46 percent of the ACI/AASHTO development length, after the flexural failure of the live end of the specimen at a 50 in. (1270 mm) embedment. The beam exhibited typical flexure and flexure/shear cracking throughout the test, and strand slip was recorded at a load and moment of approximately 39.50 kips (175.7 kN) and 935 k-in. (105.6 kN-m). Slip increased

with increasing load, reaching a value of approximately 0.10 in. at the maximum load and corresponding moment of 45.90 kips (204.2 kN) and 1086 k-in. (122.7 kN-m). Slip continued to increase as the beam continued to deflect at a reduced load carrying capacity before sufficient strain occurred to produce crushing of the extreme compression fiber, at which point the measured slip exceeded 0.5 in. (12.7 mm). The behavior of this specimen is illustrated in Figure 6.85. The flexural cracks reached a significant width and the bottom of the beam was almost touching the strong floor at the end of the test, as shown in Figure 6.86. The bond failure of this specimen at a load 7.5 percent greater than the 1010 k-in. (114.1 kN-m) nominal moment indicated that the development length was near and likely greater than 40 in. (1016 mm).

#### 6.8.1.2 Live End

The live end of specimen HSL-1 was the first test of the HSL specimens. An embedment of 50 in. (1270 mm), corresponding to 57 percent of the ACI/AASHTO development length, was

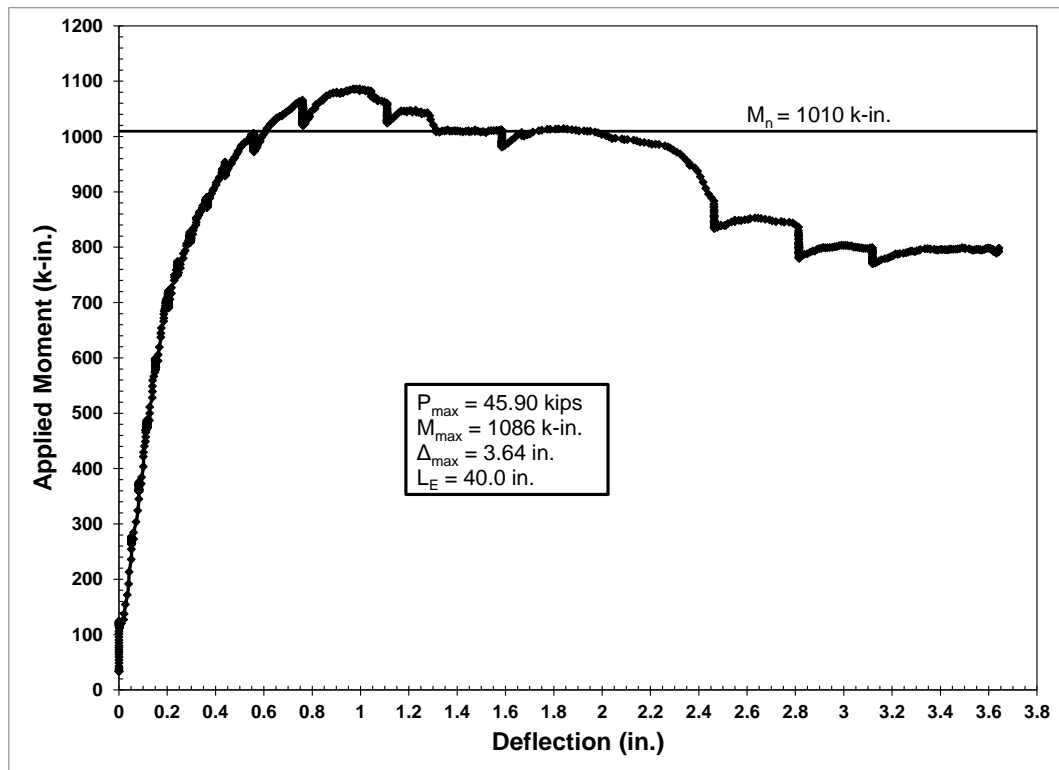


Figure 6.85: Plot of moment vs. deflection for specimen HSL-1D



Figure 6.86: Cracking and failure of specimen HSL-1D

used for the test in accordance with the first test of the other beam series. The beam exhibited typical flexural behavior including flexure and flexure/shear cracking and significant deflection after achieving the maximum load and corresponding moment of 44.09 kips (196.1 kN) and 1157 k-in. (130.7 kN-m), as shown in Figure 6.87. Complete failure of the beam occurred due to crushing of the extreme compression fiber and flexural cracks widened to the point that portions of the concrete between the major flexural cracks fell from the beam, as shown in Figure 6.88. No strand slip was recorded even at a moment 15 percent greater than the 1010 k-in. nominal moment, which indicated that the development length was less than the 50 in. (1270 mm) embedment.

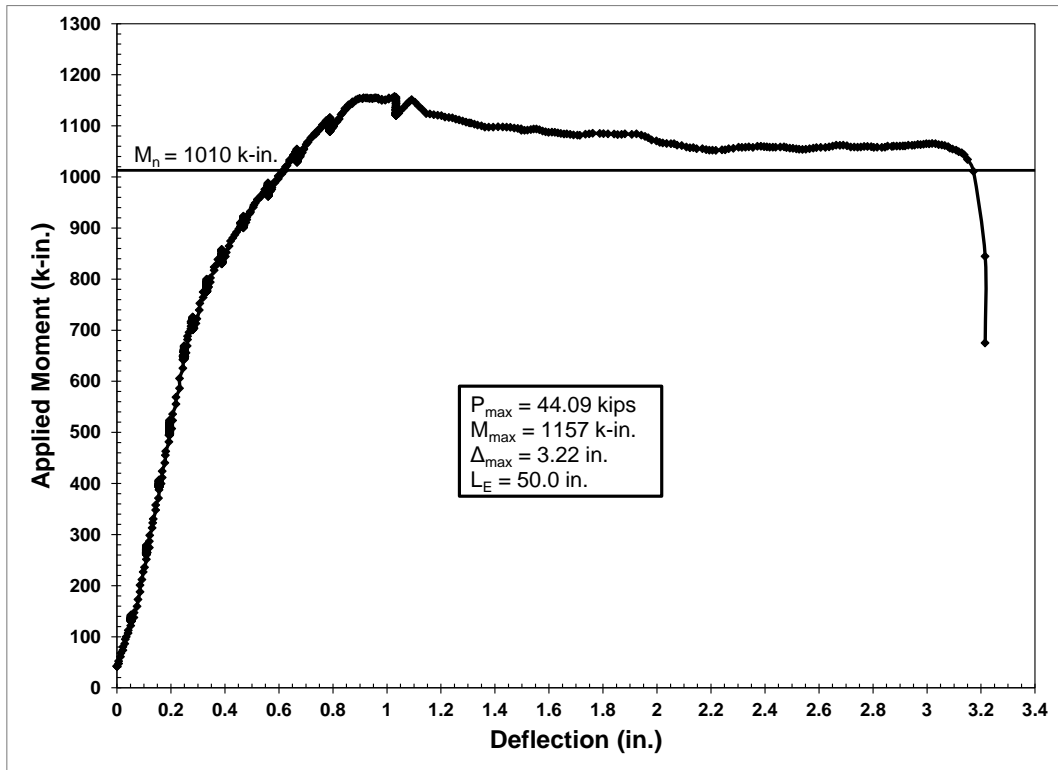


Figure 6.87: Plot of moment vs. deflection for specimen HSL-1L



Figure 6.88: Cracking and failure of specimen HSL-1L

## 6.8.2 HSL-2

### 6.8.2.1 Dead End

The dead end of specimen HSL-2 was tested at an embedment of 47.5 in. (1207 mm), corresponding to 54 percent of the ACI/AASHTO development length, after the flexural failure with strand slip of the live end of the specimen at an embedment of 45 in. (1143 mm). The beam exhibited typical flexural behavior with flexure and flexure/shear cracking occurring directly beneath and near the applied load. Strand slip was recorded at a load close to the maximum applied load and approximately 2.5 percent less than the 1015 k-in. (114.7 kN-m) calculated nominal moment. The beam exhibited significant deflection after achieving the maximum load and corresponding moment of 40.96 kips (182.2 kN) and 1056 k-in. (119.3 kN-m), as shown in Figure 6.89. Strand slip greater than 0.10 in. (2.5 mm) was not recorded until well after the maximum moment was achieved, and reached a value greater than 0.15 in. (3.8 mm). Complete

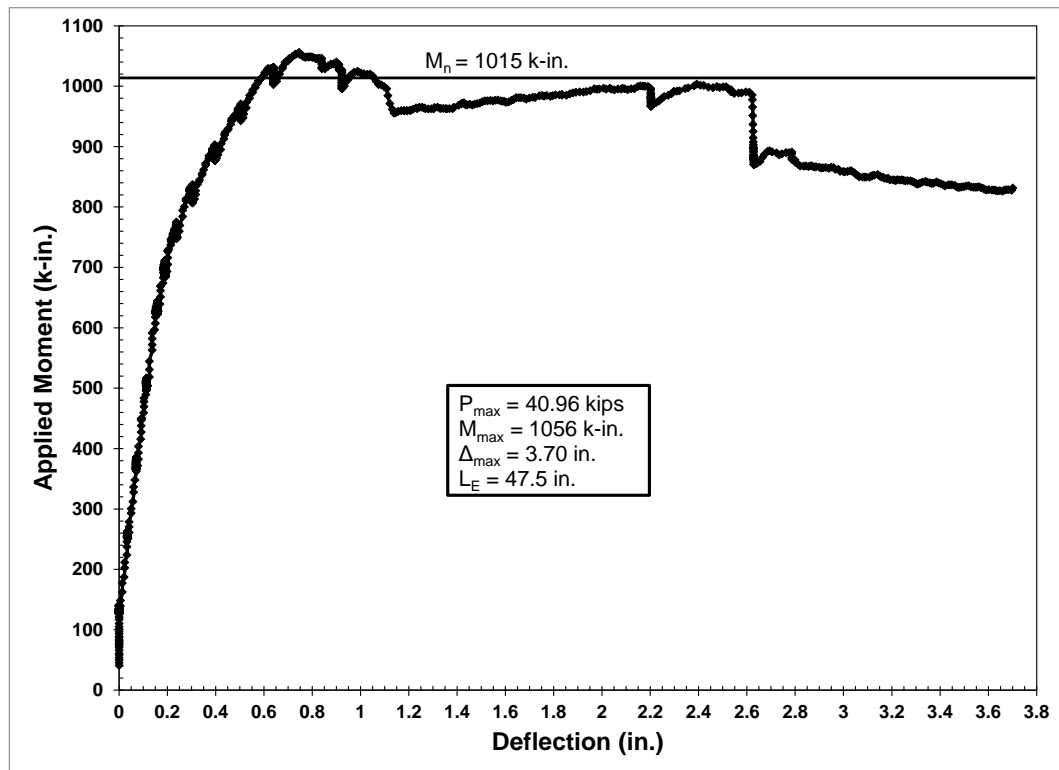


Figure 6.89: Plot of moment vs. deflection for specimen HSL-2D



failure of the specimen included crushing of the concrete in compression and was accompanied by loss of concrete between the major flexural cracks, as shown in Figure 6.90. The flexural/bond failure of this specimen at a load approximately 4 percent greater than the nominal moment indicated that the development length was close to and likely less than the 47.5 in. (1207 mm) embedment. The measured transfer length for the dead end of this specimen was the largest of those measured for the HSL specimens indicating that the development length of this specimen should theoretically be the largest of those for the HSL specimens.

#### 6.8.2.2 Live End

The live end of specimen HSL-2 was tested at an embedment of 45 in. (1143 mm), corresponding to 51 percent of the ACI/AASHTO development length, following the bond failure of the dead end of specimen HSL-1 at an embedment of 40 in. (1016 mm). The beam exhibited typical flexural behavior including flexure and flexure/shear cracking at the point of



Figure 6.90: Cracking and failure of specimen HSL-2D

applied load and along the length of the span. One of these cracks reached a substantial width at failure of the specimen, as shown in Figure 6.91. Strand slip was recorded at a load very near the maximum load and approximately 11 percent greater than the 1015 k-in. (114.7 kN-m) nominal moment. Strand slip was approximately 0.02 in. (0.5 mm) at the maximum load and corresponding moment of 45.21 kips (201.1 kN) and 1139 k-in. (128.7 kN-m). The beam exhibited significant deflection after the maximum moment was reached along with increased strand slip up to a value greater than 0.10 in. (2.5 mm) before crushing of the extreme compression fiber occurred. A significant portion of the deflection occurred at a moment greater than the nominal moment, as shown in Figure 6.92. The flexural failure of this specimen with significant strand slip at a moment 12 percent greater than the calculated nominal moment indicated that the development length was near and less than the 45 in. (1143 mm) embedment.



Figure 6.91: Cracking and failure of specimen HSL-2L

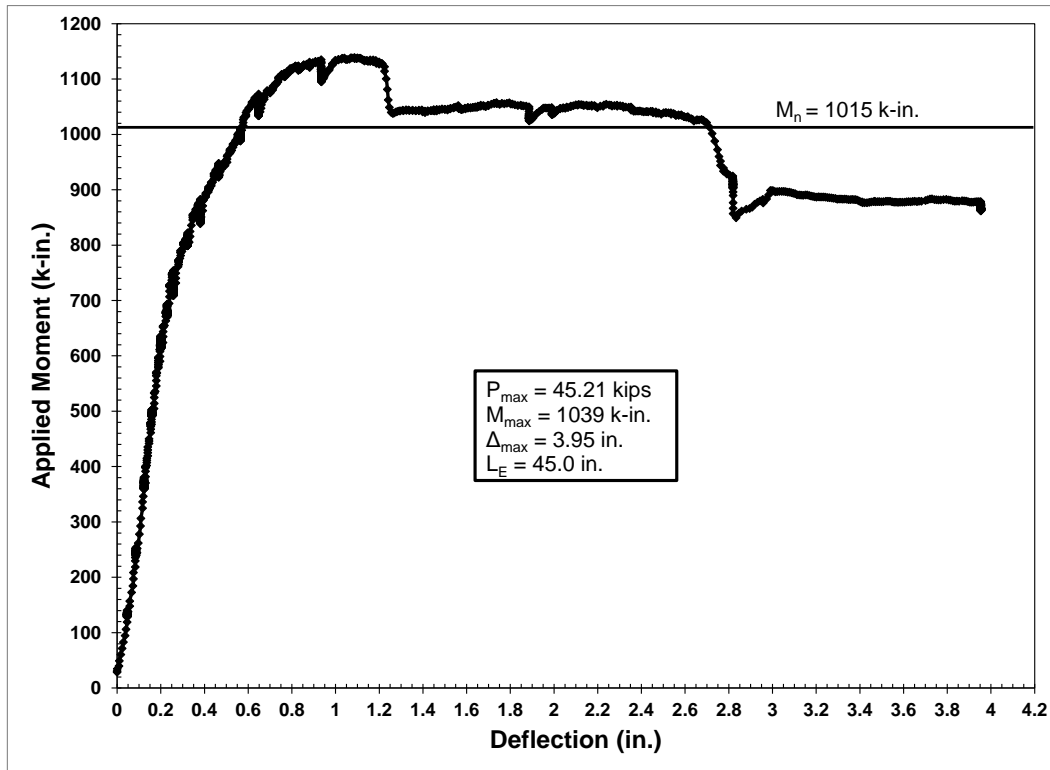


Figure 6.92: Plot of moment vs. deflection for specimen HSL-2L

### 6.8.3 HSL-3

#### 6.8.3.1 Dead End

The dead end of specimen HSL-3 was tested at an embedment of 42.5 in. (1080 mm), corresponding to 48 percent of the ACI/AASHTO development length, following the flexural failures of the live ends of specimens HSL-2 and HSL-3 at embedment lengths of 45 in. (1143 mm) and 47.5 in. (1207mm), respectively. The beam exhibited typical flexural behavior with flexure and flexure/shear cracks near the applied load. Significant deflection was measured after achieving the maximum load and corresponding moment of 42.47 kips (188.9 kN) and 1040 k-in. (117.5 kN-m). Most of this deflection occurred at a load greater than the nominal moment, as shown in Figure 6.93. Minor strand slip was recorded near the end of the test but did not exceed 0.02 in. (0.5 mm) even after fracture of the prestressing strands. The flexural crack directly

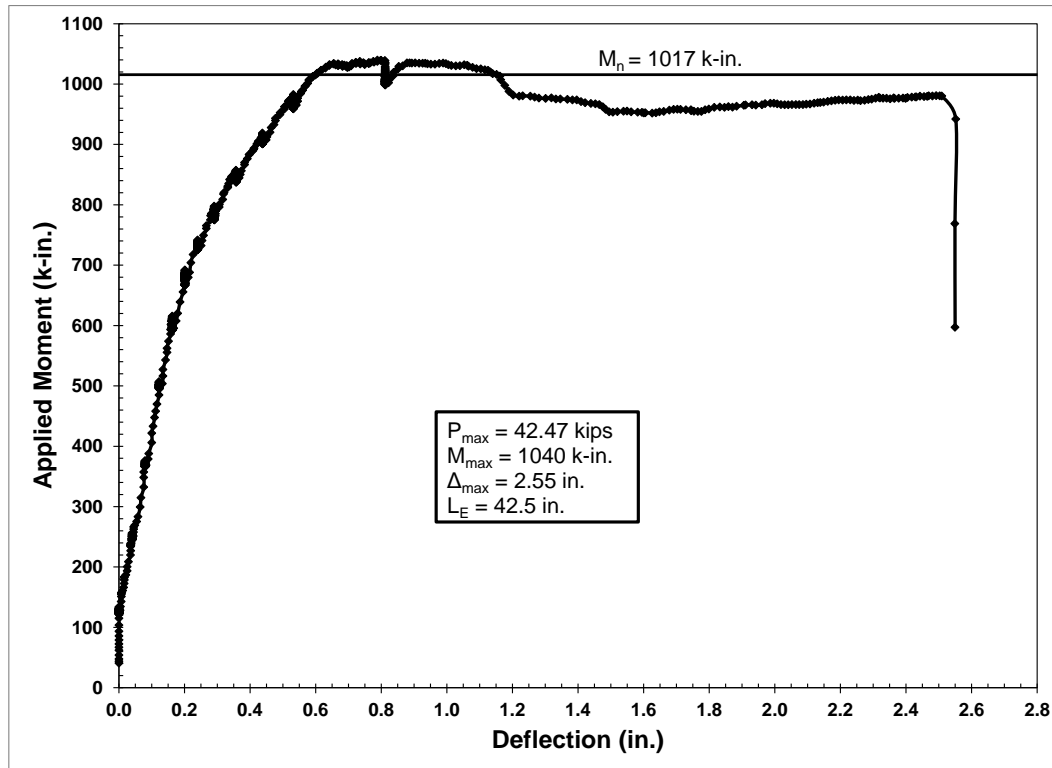


Figure 6.93: Plot of moment vs. deflection for specimen HSL-3D

beneath the applied load reached a width of greater than 0.5 in. (12.7 mm), as shown in Figure 6.94, prior to crushing of the top compression fiber and fracture of the prestressing strands. This flexural failure including strand fracture with minimal strand slip, at an applied moment 2 percent greater than the 1017 k-in. (114.9 kN-m) nominal moment, indicated that the development length was less than the 42.5 in. (1080 mm) embedment.

#### 6.8.3.2 Live End

The live end of specimen HSL-3 was tested at an embedment of 47.5 in. (1207 mm), corresponding to 54 percent of the ACI/AASHTO development length, to confirm the results of the test of the dead end of specimen HSL-2 at the same embedment. The beam exhibited typical flexure and flexure/shear cracking directly beneath and near the applied load. Significant deflection was recorded after the maximum load and corresponding moment of 40.64 kips (180.8 kN) and 1048 k-in. (118.4 kN-m) were reached. The excellent yield plateau observed in this test



Figure 6.94: Cracking and failure of specimen HSL-3D

is shown in Figure 6.95. The extreme compression concrete crushed at failure and both prestressing strands fractured, as shown in Figure 6.96. The flexural failure of this specimen with no measured strand slip at a load 3 percent greater than the 1017 k-in. (114.9 kN-m) nominal moment indicated that the development length was less than 47.5 in. (1207 mm).

#### 6.8.4 HSL-4

##### 6.8.4.1 Dead End

The dead end of specimen HSL-4 was tested at an embedment of 35 in. (889 mm), corresponding to 40 percent of the ACI/AASHTO development length, following the flexural failure of the live end of the specimen at an embedment of 40 in. (1016 mm). The beam exhibited typical flexure and flexure/shear cracking, as shown in Figure 6.97. Strand slip was first recorded at a load and moment of 40.80 kips (181.5 kN) and 884 k-in. (99.9 kN-m) or

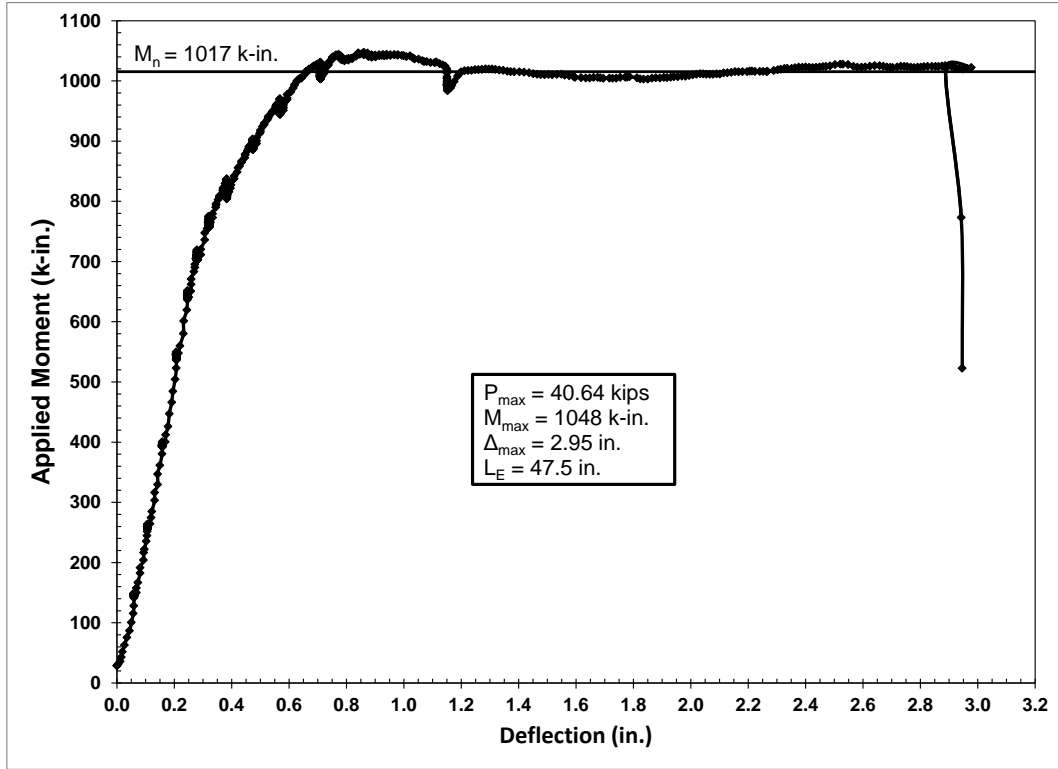


Figure 6.95: Plot of moment vs. deflection for specimen HSL-3L



Figure 6.96: Strand fracture at failure of specimen HSL-3L



Figure 6.97: Cracking and failure of specimen HSL-4D

approximately 16 percent less than the calculated nominal moment. Continued strand slip was measured up to 0.04 in. (1.0 mm) at the maximum load and corresponding moment of 43.53 kips (193.6 kN) and 943 k-in. (106.5 kN-m) with a maximum measured strand slip of greater than 0.25 in. (6.4 mm) before the end of the test. Significant deflection was measured, as shown in Figure 6.98, at a continuously reduced capacity after the maximum load was reached, which produced sufficient strain in the extreme compression fiber to cause crushing of the concrete. The failure of this specimen due to loss of bond of the prestressing strand at a moment 8 percent less than the 1023 k-in. (115.6 kN-m) nominal moment with no evidence of shear failure indicated that the development length was greater than the 35 in. (889 mm) embedment.

#### 6.8.4.2 Live End

The live end of specimen HSL-4 was tested at an embedment of 40 in. (1016 mm), corresponding to 45 percent of the ACI/AASHTO development length, following the flexural

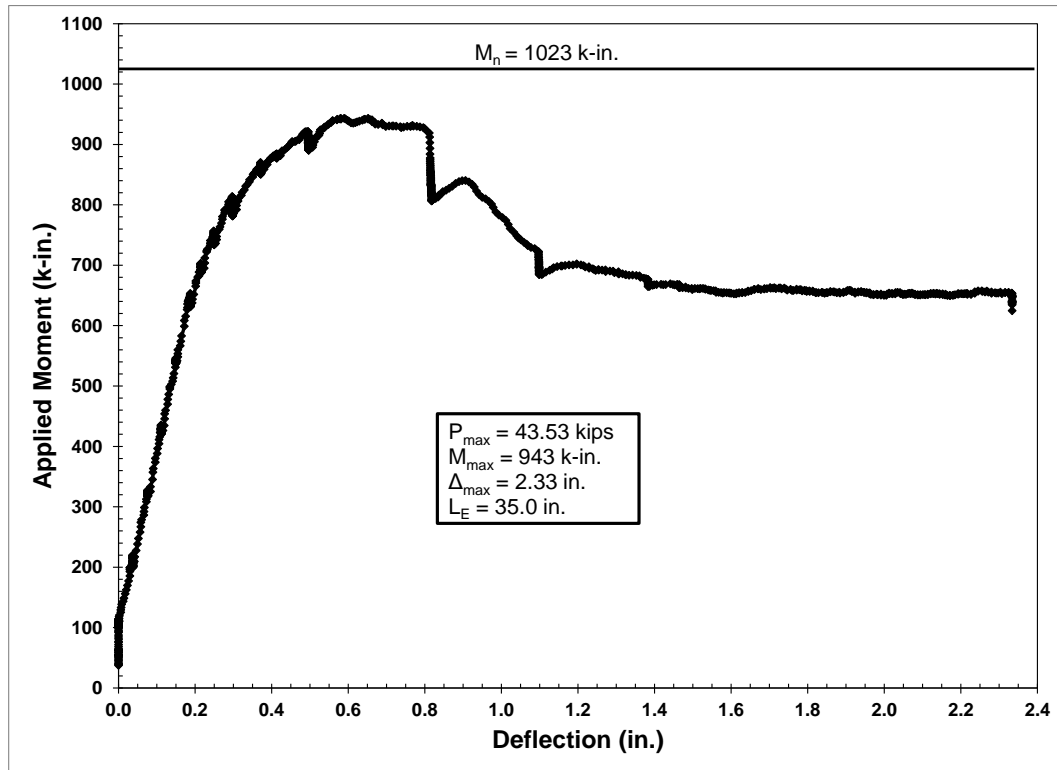


Figure 6.98: Plot of moment vs. deflection for specimen HSL-4D

failure of the live end of specimen HSL-3 at an embedment of 42.5 in. (1080 mm). The beam exhibited typical flexural behavior including flexure and flexure/shear cracking, as shown in Figure 6.99. Strand slip was detected immediately before the maximum load and reached approximately 0.02 in. (0.5 mm) at the maximum load and corresponding moment of 44.45 kips (197.7 kN) and 1051 k-in. (118.7 kN-m). Substantial deflection was recorded after the maximum load was achieved, as shown in Figure 6.100, and before crushing of the extreme compression fiber occurred. Small shear cracks accompanied a major release of energy from the beam and measured strand slip, but these cracks did not grow to a significant width. Additional strand slip was measured up to a magnitude greater than 0.10 in. (2.5 mm) on one strand and greater than 0.05 in. (1.3 mm) on the other. The flexural failure of this specimen with significant strand slip measured beginning at a load approximately 2 percent greater than the 1023 k-in.





Figure 6.99: Cracking and failure of specimen HSL-4L

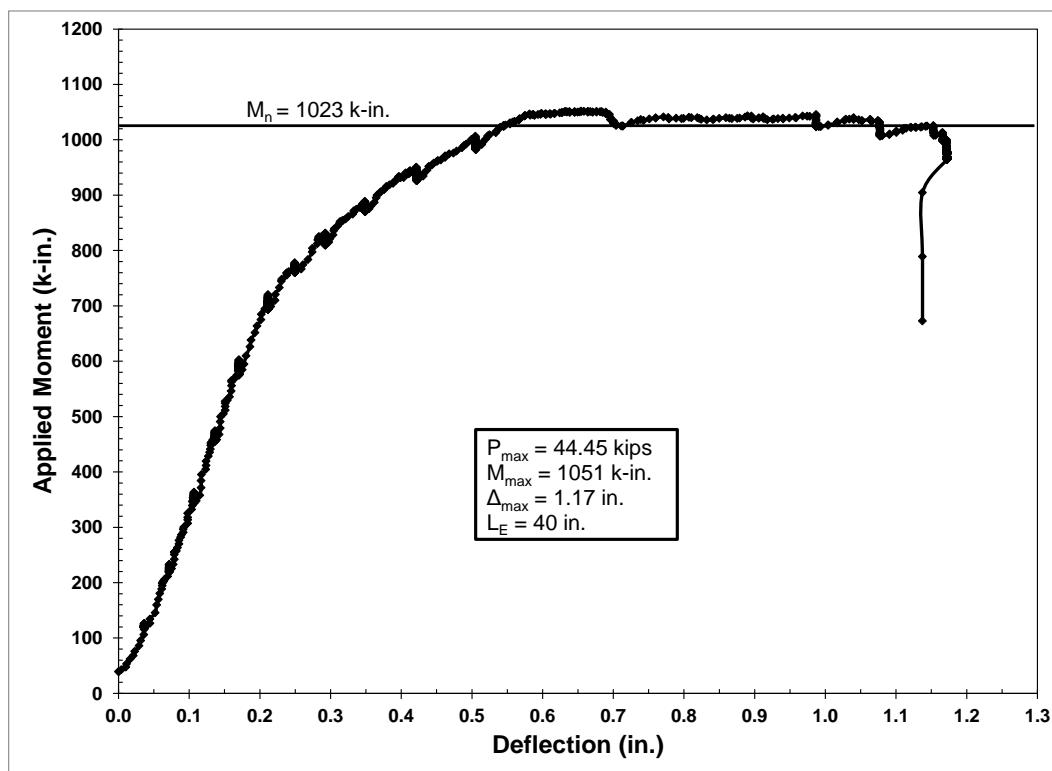


Figure 6.100: Plot of moment vs. deflection for specimen HSL-4L

(115.6 kN-m) nominal moment indicated that the development length was nearly equal to the 40 in. (1016 mm) embedment and was possibly less than this value.

### 6.8.5 Summary and Discussion

The flexural tests described in Sections 6.8.1 to 6.8.4 and summarized in Table 6.12 indicated that the development length of the high strength limestone (HSL) series of beam specimens was between 40 in. (1016 mm) and 42.5 in. (1080 mm). The flexural failures with significant strand slip observed at embedments of 40 in. (1016 mm) indicated that the development length was very likely approximately equal to this embedment length, and did indicate a possibility that the development length was shorter than 40 in. (1016 mm). The flexural test using an embedment of 42.5 in. (1080 mm) resulted in a flexural failure without significant strand slip, providing the upper bound of the development length range. All other embedments greater than 42.5 in. (1080 mm) resulted in flexural failures at loads exceeding the calculated nominal moment, indicating that the development length was less than these embedment lengths. Strand slip recorded during the tests of specimen HSL-2 did not reach significant levels until after the nominal moment had been exceeded.

The development lengths calculated for the HSL specimens using the prediction equations presented in Chapter 2 are presented in Table 6.13. The 40 in. (1016 mm)

Table 6.12: Summary of HSL Flexural Test Data

Test	$f_{se}$ (ksi)	$f_{ps}$ (ksi)	$M_n$ (k-in.)	$M_{max}$ (k-in.)	Max Slip (in.)	Failure Type	$L_E$ (in.)
HSL-1D	176.0	263.8	1010	1086	>0.50	BD	40
HSL-1L				1157	--	FL	50
HSL-2D	176.4	264.0	1015	1056	>0.15	FL/ES	47.5
HSL-2L				1139	>0.10	FL/ES	45
HSL-3D	176.3	264.0	1017	1040	0.02	FL	42.5
HSL-3L				1048	--	FL	47.5
HSL-4D	176.2	264.2	1023	943	>0.25	BD	35
HSL-4L				1051	>0.10	FL/ES	40

Note: 1 in. = 25.4 mm, 1 lbf = 4.448 N, 1 psi = 0.006895 MPa,

Table 6.13: Development Length Predictions for the HSL Specimens

Specimen	ACI/ AASHTO (in.)	Ramirez/ Russell (in.)	Zia/ Mostafa (in.)	Deatherage et al. (in.)	Buckner (in.)	Lane (in.)	Kose/ Burkett (in.)
HSL-1	87.9	72.8	86.0	116.9	90.5	103.0	86.6
HSL-2	87.8	71.8	85.4	116.8	90.5	99.9	85.3
HSL-3	87.9	71.6	85.9	116.9	90.6	98.5	84.7
HSL-4	88.1	70.9	86.4	117.2	90.8	95.0	83.1

Note: 1 in. = 25.4 mm

development length was approximately 45 percent of the prediction calculated using the ACI/AASHTO equation, 46 percent of the Zia and Mostafa prediction, 44 percent of the Buckner prediction, and 46 to 48 percent of the value produced by the Kose and Burkett equation. The measured development length was approximately 34 and 39 to 42 percent of the typically very conservative Deatherage et al. and Lane predictions, respectively. The Lane prediction was tempered somewhat by the high compressive strength of this mixture. The Ramirez and Russell equation produced the closest prediction to the measured values, but the measured development length was still only approximately 55 percent of the prediction. As with the other series of specimens, the development length measured for the HSL specimens was significantly less than that calculated using all prediction equations.

## 6.9 Conclusion

The development lengths presented herein and summarized in Table 6.14 were measured using iterative flexural testing on each end of each specimen for each beam series. The embedment length was chosen based on the failure type of previously tested specimens. A small difference was observed between the measured development lengths of the normal strength clay (NSC) and high strength clay (HSC) and normal strength shale (NSS) and high strength shale (HSS) specimens, with the higher strength specimens having a shorter development length.

When compared to the limestone mixtures, the NSC and NSS mixtures had slightly larger

Table 6.14: Summary of Measured Development Length

Beam Series	Development Length (in.)	ACI/AASHTO (in.)
NSC	45 – 50	96.3
NSS	40 – 45	94.4
NSL	34 – 40	90.0
HSC	37.5 – 40	90.6
HSS	37.5 – 40	91.1
HSL	40 – 42.5	87.9

Note: 1 in. = 25.4 mm

development lengths than the normal strength limestone (NSL) mixture and the HSC and HSS mixtures had development lengths slightly shorter than the high strength limestone (HSL) mixture. The measured development length for each beam series was significantly less than that calculated using each of the prediction equations presented in Chapter 2. The relationship of each embedment length to these predictions is presented in Appendix E. The measured development lengths were typically less than half of the values calculated using the ACI/AASHTO equation. The excellent bonding characteristics of the prestressing strand indicated by high pullout values measured in the STSB contributed to these differences. None of the equations proposed by previous research, or those in the established codes, include a specific quantification of strand quality other than the minimum STSB values recommended by Ramirez and Russell (Ramirez 2008).

The measured development lengths for the normal strength mixtures were slightly shorter than twice their respective average transfer lengths. The HSC and HSL development lengths were approximately equal to twice their average transfer lengths, and the HSS development length was slightly longer than twice the average transfer length. These observations make sense in the context of the force and stress required to be withstood by the transfer and flexural bond length respectively. The transfer length must anchor the entire effective prestress while the flexural bond length is only required to anchor the difference in stress between the effective

prestress and the stress at the nominal strength of the member. This difference in stress is typically significantly less than the effective prestress. Based on these two facts, the transfer length should comprise the larger portion of the development length. Increased transfer lengths caused by sudden release of prestress and larger end forces caused by greater numbers of strands would lead to larger development lengths. The very short transfer length for the HSS specimens, yet development length very similar to the other beam series, indicates that the development length has a relatively constant value in the face of very short transfer lengths. The differences in bonding mechanisms plays a role in the difference in transfer and flexural bond lengths, however, as the Hoyer effect present in the transfer length is not available in the flexural bond length.

## Chapter 7: Conclusions

### 7.1 Introduction

The focus of this research project involved investigating the bond of 0.6 in. (15.2 mm) prestressing strands cast in lightweight self-consolidating concrete (LWSCC). The factors used to characterize this bond behavior included transfer length and development length. Transfer length was determined using both concrete surface strain and strand end slip. Development length was determined using iterative flexural testing with varied embedment lengths. The results presented in the preceding chapters describe these behaviors for the specimens cast using mix designs developed in the first phase of the project. The measured transfer and development lengths of the LWSCC specimens were compared to those measured for the normal weight self-consolidating concrete (NWSCC) specimens as well as to the predictions made by the accepted ACI/AASHTO code equations and equations developed by previous researchers. These comparisons lend themselves to several insights and conclusions presented in this chapter. The lessons learned and conclusions drawn from the mix design phase of the project are presented first followed by those concerning the transfer and development length behavior of the 25 beam specimens cast for this project.

### 7.2 Mix Design Phase

The four LWSCC and two conventional SCC mixtures resulting from the mix design phase of the project met the required specifications within acceptable limits. Mixtures having a compressive strength of 4000 psi (28 MPa) and 6000 psi (41 MPa) at one day that also met the required fresh concrete property specifications were successfully developed using each aggregate. The relatively weak lightweight aggregates did not allow for the 8000 psi (55 MPa) compressive strength at 28 days targeted for the high strength (HS) LWSCC mixtures. The 28-

day compressive strength for these mixtures was on the order of 7000 psi (48 MPa) instead. The following conclusions can be drawn from the trial batching required for the development of these mixtures.

- J-Ring may produce a poor assessment of passing ability for LWSCC. The change in height from inside to outside of the J-Ring produced inconsistent values when compared to the difference between slump flow and J-Ring flow. This may have been due to differences in measurement location between tests.
- Differences in slump flow and J-Ring flow as large as 4 in. (100 mm) resulted in adequate consolidation for the beam specimens. Values of  $T_{20}$  as large as 7 seconds also produced adequate consolidation
- The variables with the greatest effect on fresh concrete properties include cementitious material content and type, total water content, and aggregate type and content. Superplasticizer dosage is also very important, and with experience, can be adjusted to account for changes in ambient temperature. When developing LWSCC mixtures, a relatively high cementitious material content and substantial total water content, even with a low  $w/c$ , are necessary for adequate flow. A small maximum aggregate size is critical to prevent excessive blockage.
- Cementitious material content, aggregate strength and quality, and to a lesser extent, maximum aggregate size are the most important variables affecting the early age strength of concrete that is vital for prestressed concrete applications. The cementitious material content must be high to compensate for the relatively weak lightweight aggregate.
- In order to produce LWSCC with a high early age compressive strength the reaction rate of the cementitious material is critical. High early strength, Type III cement combined

with a partial replacement of fly ash is required to reach the high strength levels required at one day while still retaining the workability of SCC. These mixtures also have a higher strength at 28 days, which is due to the incorporation of fly ash into the mixture combined with the curing water available within the lightweight aggregate particles.

- Presoaking the lightweight aggregate for a consistent time period is necessary to obtain a consistent moisture content. A relationship between bulk density of the presoaked aggregate and the aggregate moisture content is effective for consistently estimating aggregate moisture content. An error typically exists between the estimated moisture content of the aggregate used for mix design adjustments and that measured from the sample used to determine aggregate bulk density. The effects of these errors on workability of the concrete can be accounted for by adjusting the superplasticizer dosage during mixing of each batch.
- The effects of minor moisture content errors on the compressive strength of the concrete were minimal. Mixtures with moisture content errors within a range of  $\pm 3\%$  exhibited adequate compressive strengths. A larger range may be acceptable, but data at larger errors was limited. The lack of sensitivity to these errors was most likely due to the high cement content for all of the mixtures and the limiting effect of the coarse aggregate on the compressive strength of the lightweight concrete.
- The LWSCC moduli of elasticity were approximately 30 percent less than those of the limestone mixtures at one day and approximately 30 to 40 percent less at 28 days. The moduli were similar for the two lightweight aggregates at similar strength levels.
- Measured moduli of elasticity were not representative of the variation in compressive strength observed between the batches used to cast the beam specimens, but were in



adequate agreement with the ACI equation to justify use of these calculated values in prestress loss calculations requiring modulus of elasticity.

- Using dynamic modulus measurement methods appeared to have potential for use in making fast determinations of modulus of elasticity and thereby transfer length behavior, but insufficient data were collected to produce an adequate relationship.
- The combination of strength and workability required for LWSCC usable in prestressed applications is difficult to obtain and requires excellent quality control. Each aggregate presented different challenges and levels of difficulty in producing consistent concrete mixtures. Limestone coarse aggregate resulted in the most consistent and reliable performance followed by the expanded clay, and expanded shale aggregates.

### **7.3 Transfer Length**

Numerous difficulties were encountered during measurement of transfer length using the DEMEC system and the 95% Average Maximum Strain Method and end slip. Despite these difficulties, each method demonstrated its effectiveness in consistently measuring transfer length. The following conclusions can be drawn from the results of these measurements.

#### **7.3.1 DEMEC Measurements**

- Surface strain profiles of the LWSCC specimens were much more erratic than those of the NWSKC specimens. This was most likely due to cracking in the LWSCC members, caused by a smaller tensile strength combined with high release stresses, and a smaller stiffness for the LWSCC.
- The effects of any issues in DEMEC measurements were mitigated by using measurements from the opposite side of specimens in areas where DEMEC points were

lost. DEMEC transfer length results were confirmed by end slip measurements and by similar development lengths for each concrete type.

- Transfer length measurements typically exhibited some change over time with the majority of the change occurring during the first 14 days. Therefore measurements at 28 days of age should be adequate for an assessment of behavior during the service life of a member.
- Live end transfer lengths were typically longer than corresponding dead end transfer lengths, which indicates that longer transfer lengths would occur in beams with a sudden release of prestress. The disparity between live and dead end would most likely be more pronounced with a sudden release, if the strands were not cut at both ends simultaneously.
- No significant difference was detected between the transfer lengths measured for beams cast using the different lightweight aggregates at the same strength level.
- Significant differences were detected between the transfer lengths of the normal strength (NS) and high strength (HS) specimens for both the expanded clay and expanded shale mixtures, but not the limestone mixtures. This indicates that compressive strength at release is an important variable affecting transfer length of LWSCC members. This relationship is partially due to the larger effect of paste quality on the stiffness of these concrete mixtures than in mixtures with stiff coarse aggregates.
- A significant difference was observed between the normal strength shale (NSS) and normal strength limestone (NSL) live end and average transfer lengths, but only between the normal strength clay (NSC) and NSL transfer lengths at a limited number of live end and average measurements. The behavior of the lightweight and conventional NS

mixtures was similar, but the differences observed in this testing would most likely be more pronounced in members with greater numbers of prestressing strands and constructed using a sudden release of prestress.

- A limited number of transfer length measurements indicated significant differences between the high strength limestone (HSL) and both high strength clay (HSC) and high strength shale (HSS) specimens, but all differences were in favor of the lightweight mixtures having shorter transfer lengths. The mixtures using lightweight aggregates with a high compressive strength at one day of age exhibited no negative consequences on the transfer length of the specimens.
- Segregation noticed during beam testing for some of the NS and HS members utilizing expanded shale aggregate produced some skew in the results for these beam series. The lack of coarse aggregate, but still adequate consolidation, around the strands in these members led to better bonding and shorter transfer lengths, but poor aggregate distribution has the potential to adversely affect other properties of the members.
- On an average basis the ACI/AASHTO equations appeared to be adequate for all NS mixtures. When compared using further statistical analysis, the ACI  $50d_b$  prediction was less than the limit considered to hold the mean with 95% confidence for the live end of the NSC specimens and for most cases of the NSS specimens. The AASHTO  $60d_b$  prediction was greater than that value for these specimens. The ACI and AASHTO equations were greater than the statistical limits for the NSL specimens.
- The ACI/AASHTO equation and the ACI  $50d_b$  predictions produced the best actual estimates of the measured transfer lengths for the NSC, NSS, and NSL specimens at 28 days. Of all the prediction equations, these values were the closest to individual

measured values as well as to the average values, but no significant conservatism was evident for the NSC and NSS specimens. The AASHTO  $60d_b$ ; Zia and Mostafa; Shahawy, Deatherage et al., and Buckner; and Ramirez and Russell equations all produced similar predictions that exceeded the high 95% upper-confidence bounds for the mean for the NSC and NSS specimens at 28 days.

- The ACI/AASHTO equations were adequate on both an average basis and when examined using further statistical analysis for the HSC and HSS specimens, as well as for the HSL specimens.
- The Zia and Mostafa equation produced the closest prediction to the actual measured transfer length for the HSC, HSS, and HSL specimens at 28 days. When compared to the 95% upper-confidence bounds, the Zia and Mostafa equation was less than the live end HSC value, was greater than the HSS values, and was less than the HSL values. The Ramirez and Russell and ACI  $50d_b$  predictions exceeded the 95% upper-confidence bounds for the HSC and HSL specimens, with the Ramirez and Russell equation yielding a slightly better prediction.
- The inclusion of compressive strength at release in the Zia and Mostafa and Ramirez and Russell equations improved these predictions for the HS specimens.
- Concrete compressive strength in excess of 4000 psi (28 MPa) at release of prestress produces adequate conformance with the code predicted transfer length, but 6000 psi (41 MPa) is a more conservative value and would better handle sudden release and larger numbers of strands.

### 7.3.2 End Slip Measurements

- End slip measurements produced a consistent measure of transfer length and bond performance. While most likely not as accurate as the DEMEC measurements due to needs for standardization of measurement and calculation method, these measurements have the potential for a quick and reliable method of assessing bond performance.
- Transfer lengths measured using DEMEC measurements and end slip did not match up exactly due to the difference in measurements at the concrete surface and at the prestressing strand and the assumptions of stress variation in the prestressing strand used to calculate the transfer length from the measured end slip.
- The values of  $\alpha$  corresponding to a linear steel stress distribution and a parabolic steel stress distribution bounded the values of transfer length calculated using the DEMEC measurements and 95% Average Maximum Strain Method. An  $\alpha$  of 2.85 was determined from a best fit of the end slip and DEMEC transfer length data, which does agree with previous research findings of 2.86 (FIP 1982), but the fit of the data was very poor due to substantial scatter in the data.
- More research is necessary to resolve the discrepancy between the two transfer length methods and to determine the actual bond/steel stress distribution used in the theoretical relationship connecting end slip and transfer length.

### 7.4 Development Length

- The bonding capacity of the prestressing strand was very good, as shown by the standard test for strand bond (STSB), and application of any of the following conclusions requires similar strand quality.

- The measured development lengths were similar in magnitude for all concrete types. They were approximately 50 percent or less of the ACI/AASHTO development length prediction, thereby demonstrating the adequacy of these predictions for these LWSCC mixtures with margin to account for increases resulting from field conditions.
- Segregation in the form of only sand/cement mortar present below the prestressing strands did not adversely affect the measured development length as long as the mortar and remainder of the concrete were adequately consolidated. However, this segregation would cause issues in other areas of beam behavior.
- The measured development lengths were approximately twice the measured transfer lengths and would increase with increased transfer lengths caused by sudden prestress release and large end stresses resulting from large numbers of prestressing strands.
- Shear failures at very short embedment lengths complicated determination of development length, leaving open the possibility of shorter development lengths for the NSC, NSS, and HSC specimens. Shear cracking in the transfer zone resulting from the reduced shear capacity of lightweight concrete led to strand slip.
- The Ramirez and Russell development length prediction provided more reasonable development length predictions than any of the other equations, but these still significantly exceeded the measured values. No other prediction equation exhibited a marked improvement over the ACI/AASHTO equation and barring full-scale testing of LWSCC members, the development length predictions should not be decreased.
- Concrete compressive strength does not appear to be a significant variable in the measured development lengths, but its inclusion in the Ramirez and Russell prediction equation did produce better results.

## 7.5 Recommendations

- The limit of difference between J-Ring and slump flow should be increased to 4 in. (100 mm) for LWSCC. An upper limit of 7 seconds should be used for  $T_{20}$ .
- The use of lightweight self-consolidating concrete in prestressed applications should not be hindered due to concerns of bond behavior as long as the concrete meets requirements for SCC behavior. The ACI/AASHTO transfer length equations produced an accurate prediction and the measured development lengths were significantly less than those produced by the equation for this material.
- Compressive strength in excess of 6000 psi (41 MPa) at prestress release should be considered for LWSCC in prestressed applications to ensure adequate bond performance.
- Care should be taken to account for the reduced shear capacity of lightweight concrete when designing LWSCC members for shear, as shear cracking in the transfer zone leads to strand slip.
- Honeycombing and voids caused by concrete with inadequate flow characteristics resulted in definite negative effects on bond performance while some segregation led to better bond performance. Care should be taken to ensure that concrete meets the required specifications for SCC, with any error made on the side of larger flow values.
- The ACI and AASHTO equations should continue to be used for LWSCC. The more conservative values of the AASHTO  $60d_b$ ; Zia and Mostafa; Shahawy, Deatherage et al., and Buckner; and Ramirez and Russell transfer length equations should be considered for LWSCC when compressive strength at release is less than 6000 psi (41 MPa) at prestress release.

- The incorporation of the STSB value for a particular prestressing strand into the transfer and development length equations has potential for including the bond quality of the strand and should be investigated.
- Since this research considered ideal condition of gradual prestress release and only two prestressing strands in rectangular specimens, testing should be extended to full-size LWSCC members to determine the effects of sudden release and the interaction of large numbers of strands. A numerical model should also be investigated as a method to scale the results presented herein to full-size specimens. These results are need to ensure accuracy of the development length used for debonding and draped strand arrangements.

## **7.6 Contribution to the Body of Knowledge**

Numerous research projects have been conducted concerning prestressing strand bond in the form of transfer and development length since the 1950s. Very little bond research has focused on members cast with lightweight self-consolidating concrete (LWSCC), a concrete type with properties varying significantly from those of the concrete used in the development of the equations used to predict transfer and development length. This dissertation presents data concerning transfer and development length in members cast using LWSCC that fills gaps in the available data. The current ACI and AASHTO (ACI 2011, AASHTO 2007) code predictions were shown to produce accurate predictions for transfer length and the measured development lengths were significantly less than those produced by the code equation. Adjustments to accepted fresh SCC properties in the form of a  $T_{20}$  as high as 7 seconds and difference between slump flow and J-Ring flow of up to 4 in. (100 mm) were also recommended for LWSCC used for bridge girders.



## References

ACI Committee 211, "Standard Practice for Selecting Proportions for Structural Lightweight Concrete (ACI 211.2-98), American Concrete Institute, 1998.

ACI Committee 213, *Guide for Structural Lightweight-Aggregate Concrete (ACI 213R-03)*, American Concrete Institute, Farmington Hills, Michigan, 2003, 38 pp.

ACI Committee 318, *Building Code Requirements for Structural Concrete (ACI 318-11) and Commentary (ACI 318R-11)*, American Concrete Institute, Farmington Hills, Michigan, 2011.

American Association of State Highway and Transportation Officials (AASHTO).LRFD Bridge Design Specifications. Customary U.S. Units. 4th Edition. Washington D.C. 2007.

Andrawes, B., Shin, M., Pozolo, A. *Transfer and Development Length of Prestressing Tendons in Full-Scale AASHTO Prestressed Concrete Girders Using Self-Consolidating Concrete*, ICT-09-038, Illinois Center for Transportation, Urbana, IL, March 2009 pp. 1-53.

ASTM C29/C29M, 2009, "Standard Test Method for Bulk Density ("Unit Weight") and Voids in Aggregate," ASTM International, West Conshohocken, PA, 2009.

ASTM C39/C39M, 2011a, "Standard Test Method for Compressive Strength of Cylindrical Concrete Specimens," ASTM International, West Conshohocken, PA, 2011.

ASTM C127, 2007, "Standard Test Method for Density, Relative Density (Specific Gravity), and Absorption of Coarse Aggregate," ASTM International, West Conshohocken, PA, 2007.

ASTM C136, 2006, "Standard Test Method for Sieve Analysis of Fine and Coarse Aggregates," ASTM International, West Conshohocken, PA, 2006.

ASTM C138/C138M, 2010b, "Standard Test Method for Density (Unit Weight), Yield, and Air Content (Gravimetric) of Concrete," ASTM International, West Conshohocken, PA, 2010.

ASTM C173/C173M, 2010b, "Standard Test Method for Air Content of Freshly Mixed Concrete by the Volumetric Method," ASTM International, West Conshohocken, PA, 2010.

ASTM C215, 2008, "Standard Test Method for Fundamental Transverse, Longitudinal, and Torsional Frequencies of Concrete Specimens," ASTM International, West Conshohocken, PA, 2008.

ASTM C231/C231M, 2010, "Standard Test Method for Air Content of Freshly Mixed Concrete by the Pressure Method," ASTM International, West Conshohocken, PA, 2010.

- ASTM C469/C469JM, 2010, “Standard Test Method for Static Modulus of Elasticity and Poisson’s Ratio of Concrete in Compression,” ASTM International, West Conshohocken, PA, 2010.
- ASTM C1231/C1231M, 2010a, “Standard Practice for Use of Unbonded Caps in Determination of Compressive Strength of Hardened Concrete Cylinders,” ASTM International, West Conshohocken, PA, 2010.
- ASTM C1611/C1611M, 2009be1, “Standard Test Method for Slump Flow of Self-Consolidating Concrete,” ASTM International, West Conshohocken, PA, 2009.
- ASTM C1621/C1621M, 2009b, “Standard Test Method for Passing Ability of Self-Consolidating Concrete by J-Ring,” ASTM International, West Conshohocken, PA, 2009.
- Balázs, G. L., “Transfer Length of Prestressing Strand as a Function of Draw-In and Initial Prestress,” *PCI Journal*, Vol. 38, No. 2, March-April 1993, pp. 86-93.
- Bender, B. F., “Economics and Use of Lightweight Concrete in Prestressed Structures,” *PCI Journal*, Vol. 25, No. 6, November-December 1980, pp. 62-67.
- Bonen, D. and Shah, S. P., “Fresh and Hardened Properties of Self-Consolidating Concrete,” *Progress of Structural Engineering Materials*, 7, 2005, pp14-26.
- Buckner, C. D. “A Review of Strand Development Length for Pretensioned Concrete Members,” *PCI Journal*, Vol. 40, No. 2, March-April 1995, pp. 84-105.
- Burgueno, R. and Haq M. “Development Length of Prestressing Strands in Precast/Prestressed Girders using Self Compacting Concrete,” *Proceedings of the Structures Congress and Exposition, Metropolis and Beyond-Proceedings of the 2005 Structures Congress and the 2005 Forensic Engineering Symposium*, 2005, pp. 1673-1680.
- Castrodale, R. W., Harmon, K. S., “Durability of Lightweight Concrete Bridges,” *Proceedings PCI-FHWA National Bridge Conference*, Paper No. 48, Orlando, 2008, pp 1-35.
- Colleparidi, M., Borsoi, A., Colleparidi, S., and Troli, R., “Recent Developments of Special Self-Compacting Concretes,” *ACI Special Publication SP222-01*, Vol. 222, May 2004, pp. 1-17.
- Cousins, T. E., Badeaux, M. H., and Moustafa, S. “Proposed Test for Determining Bond Characteristics of Prestressing Strand,” *PCI Journal*, Vol. 37, No. 1, January-February 1992, pp. 66-73.
- Deatherage, J. H., Burdette, E. G., Chew, C. K. “Development Length and Lateral Spacing Requirements of Prestressing Strand for Prestressed Concrete Bridge Girders,” *PCI Journal*, Vol. 39, No. 1, January-February 1994, pp. 70-83.
- Do, N. H. *Developing High Strength Self-Consolidating Concrete Mixtures for use in Bridge Girders*, MS Thesis, University of Arkansas, Fayetteville, AR, 2007, 112 pp.

Fédération International de la Précontrainte (FIP), “Test for the Determination of Tendon Transmission Length Under Static Conditions,” *Report of Prestressing Steel: 7*, FIP, Wexham Springs, U.K., 1982.

Ferhadi, R. and Badie, S. “Examining Various Options to Extend Span Range of Precast Prestressed Concrete Bridge Girders,” *Proceedings 2010 Concrete Bridge Conference Paper No. 64*, Phoenix, AZ, Portland Cement Association, February 24-26, 2010, pp. 1-25.

Floyd, R. W., Ruiz, E. D., Do, N. H., Staton, B. W., and Hale, W. M., “Transfer and Development Length of High Strength SCC Beams,” *Proceedings PCI-FHWA National Bridge Conference*, Paper No. 25, Orlando, 2008, pp 1-13.

Floyd, R., Ruiz, E., Do, N., Staton, B., and Hale, W., “Development Lengths of High Strength Self-Consolidating Concrete Beams”, *PCI Journal*, Winter Issue 2011, pp. 36-53.

Girgis, A. F. M., Tuan, C. Y. “Bond Strength and Transfer Length of Pretensioned Bridge Girders Cast With Self-Consolidating Concrete,” *PCI Journal*, Vol. 50, No. 6, November-December 2005, pp 72-87.

Greene Jr., G. G. and Graybeal, B., “FHWA Research Program on Lightweight High-Performance Concrete — Development Length of Prestressing Strand,” *Proceedings 2010 Concrete Bridge Conference Paper No. 49*, Phoenix, AZ, Portland Cement Association, February 24-26, 2010, pp. 1-8.

Grotheer, S. J., *Evaluation of Lightweight Concrete Mixtures for Bridge Deck and Prestressed Bridge Girder Applications*, MS Thesis, Kansas State University, Manhattan, Kansas, 2008, 158 pp.

Hamilton III, H. R., Labonte, T., and Ansley, M. H. “Behavior of Pretensioned Type II AASHTO Girders Constructed with Self-Consolidating Concrete,” *ACI Special Publication SP231-15*. 2005 pp. 253-270.

Hanson, N.W. and Kaar, P.H. “Flexural Bond Tests of Pretensioned Prestressed Beams,” *Journal of the American Concrete Institute*, Proceedings Vol. 55, Issue 7, January 1959. pp. 783-802.

Hanson, N. W. “Influence of Surface Roughness of Prestressing Strand on Bond Performance,” *PCI Journal*, Vol. 14, No. 1, February 1969, pp. 32-45.

Hegger, J., Bülte, S., Kommer, B. “Structural Behavior of Prestressed Beams Made With Self-consolidating Concrete,” *PCI Journal*, Vol. 52, No. 4, July-August 2007, pp. 34-42

Janney, J.R., “Nature of Bond in Pretensioned Prestressed Concrete,” *Journal of American Concrete Institute*, Proceedings Vol. 50, No. 9, May 1954, pp. 717-736.

Kaszynska, M., "Lightweight Self-Consolidating Concrete for Bridge Applications," *Proceedings 2010 Concrete Bridge Conference Paper No. 84*, Phoenix, AZ, Portland Cement Association, February 24-26, 2010, pp. 1-11.

Khan, F. R. "Lightweight Concrete for Total Design of One Shell Plaza," *ACI Special Publication SP29-01*, American Concrete Institute, Farmington Hills, Michigan, 1971, pp. 1-14.

Khan, F. R., Stockbridge, G., and Brown, E. J. "Quality Concrete of High Strength Lightweight Concrete for One Shell Plaza," *ACI Special Publication SP29-02*, American Concrete Institute, Farmington Hills, Michigan, 1971, pp. 15-34.

Khayat, K. H. and Mitchell, D., "Self-Consolidating Concrete for Precast, Prestressed Concrete Bridge Elements," *NCHRP Report 628*, Transportation Research Board, 2009, 99 pp.

Kose, M. M. and Burkett, W. R., "Evaluation of Code Requirement for 0.6 in. (15 mm) Prestressing Strand," *ACI Structural Journal*, Vol. 102, No. 3, May-June 2005, pp. 422-428.

Kose, M. M. and Burkett, W. R. "Formulation of New Development Length Equation for 0.6 in. Prestressing Strand," *PCI Journal*, Vol. 50, No. 5, September-October 2005, pp. 96-105.

Lachemi, M., Bae, S., Hossain, K. M. A., and Sahmaran, M. "Steel-Concrete Bond Strength of Lightweight Self-Consolidating Concrete," *Materials and Structures*, Vol. 42, No. 7, 2009, pp. 1015-1023.

Lane, S. N., "Transfer Lengths in Rectangular Prestressed Concrete Concentric Specimens," *Public Roads*, Vol. 56, No. 2, September 1992, pp. 67-71.

Lane, S. N., "A New Development Length Equation for Pretensioned Strands in Bridge Beams and Piles," *Research Report FHWA-RD-98-116*, Structures Division, Federal Highway Administration, McLean, VA, 1998, 134 pp.

Larson, K. H., Peterman, R. J., Esmaily, A. "Bond Characteristics of Self-consolidating Concrete for Prestressed Bridge Girders," *PCI Journal*, Vol. 52, No. 4, July-August 2007, pp. 44-57.

Logan, D.R. "Acceptance Criteria for Bond Quality of Strand for Pretensioned Prestressed Concrete Applications," *PCI Journal*, Vol. 42, No. 2, March-April 1997, pp. 52-90.

Lopez, M., Kahn, L. F., and Kurtis, K. E., "Creep and Shrinkage of High-Performance Lightweight Concrete," *ACI Materials Journal*, Vol. 101, No. 5, September-October 2004, pp. 391-399.

Lutz, B. A., Russell, B. W., and Burns, N. H., "Measurement of Development Length of 0.5-inch and 0.6-inch Diameter Prestressing Strand in Fully Bonded Concrete Beams," *FHWA Report No. FHWA/TX-92+1210-3*, Center for Transportation Research, The University of Texas at Austin, Austin, Texas, February 1992, 110 pp.

Makarichev, V. V. "Prestressed Lightweight and Cellular Concrete," *PCI Journal*, Vol. 9, No. 3, June 1964, pp. 60-65.

Marti-Vargas, J. R., Arbelaez, C. A., Serna-Ros, P., Fernandez-Prada, M. A., and Miguel-Sosa, P. F., "Transfer and Development Lengths of Concentrically Prestressed Concrete", *PCI Journal*, Vol. 51, No. 5, September-October 2006, pp. 74-85.

Meyer, K. F. and Kahn, L. F. "Lightweight Concrete Reduces Weight and Increases Span Length of Pretensioned Concrete Bridge Girders," *PCI Journal*, Vol. 47, No. 1, January-February 2002, pp. 68-75.

Meyer, K. F., Kahn, L. F., "Transfer and Development Length of 0.6 inch Strand in High Strength Lightweight Concrete," *High-Performance Structural Lightweight Concrete (SP-218)*, American Concrete Institute, Farmington Hills Michigan, 2004, pp. 9-28.

Meyer, K. F., "Design Issues Involving Lightweight Concrete: A Current Perspective," *Proceedings 2010 Concrete Bridge Conference Paper No. 67*, Phoenix, AZ, Portland Cement Association, February 24-26, 2010, pp. 1-11.

Mitchell, D. W., Marzouk, H. "Bond Characteristics of High-Strength Lightweight Concrete," *ACI Structural Journal*, Vol. 104, No. 1, January-February 2007, pp. 22-29.

Mor, A., "Steel-Concrete Bond in High-Strength Lightweight Concrete," *ACI Materials Journal*, Vol. 89, No. 1, January-February 1992, pp. 76-82.

Naito, C. J., Brunn, G., Parent, G., and Tate, T. *Comparative Performance of High Early Strength and Self-Consolidating Concrete for Use in Precast Bridge Beam Construction*, ATLSS Report #05-03, Advanced Technology for Large Structural Systems, Bethlehem, PA, May 2005, 102 pp.

Naito, C. J., Parent, G., and Brunn, G., "Performance of Bulb-Tee Girders Made with Self-Consolidating Concrete," *PCI Journal*, Vol. 51, No. 6, November-December 2006, pp. 72-85.

Nassar, A. J., "Investigation of Transfer Length, Development Length, Flexural Strength and Prestress Loss Trend in Fully Bonded High Strength Lightweight Prestressed Girders," 2002, Thesis, Virginia Polytechnic Institute and State University.

Nichols, G. W. and Ledbetter, W. B., "Bond and Tensile Capacity of Lightweight Aggregates," *ACI Journal Proceedings*, Vol. 67, No. 12, December 1970, pp. 959-962.

Nordby, G. M. and Venuti, W. J., "Fatigue and Static Tests of Steel Strand Prestressed Beams of Expanded Shale Concrete and Conventional Concrete," *ACI Journal Proceedings*, Vol. 54, No. 8, August 1957, pp. 141-160.

Okamura, H., Ouchi, M. "Self-Compacting Concrete," *Journal of Advanced Concrete Technology*, Vol. 1, No. 1, April 2003, pp. 5-15.

Osborn, A. E. N., Lawler, J. S., and Connolly, J. D., *Acceptance Tests for Surface Characteristics of Steel Strands in Prestressed Concrete*, NCHRP Report 621, National Cooperative Highway Research Program, Transportation Research Board, Washington, D.C., 2008, 141 pp.

PCI Industry Handbook Committee, *PCI Design Handbook: Precast and Prestressed Concrete 7<sup>th</sup> Edition*, Precast/Prestressed Concrete Institute, Chicago, IL, 2010.

Persson, B., "A Comparison Between Mechanical Properties of Self-Compacting Concrete and the Corresponding Properties of Normal Concrete," *Cement and Concrete Research*, 2001 193-198.

Peterman, R. J., Ramirez, J. A., Olek, J. "Design of Semi-lightweight Bridge Girders: Development Length Considerations," *Transportation Research Record* No. 1696, Fifth International Bridge Engineering Conference, Tampa, 2000, pp 41-47.

Peterman, R. J., "The effects of As-Cast Depth and Concrete Fluidity on Strand Bond," *PCI Journal*, Vol. 52, No. 3, May-June 2007, pp. 72-101.

Ramirez, J. A. and Russell, B. W., *Transfer, Development, and Splice Length for Strand/Reinforcement in High-Strength Concrete*, NCHRP Report 603, National Cooperative Highway Research Program, Transportation Research Board, Washington, D.C., 2008, 131 pp.

"Report of the FIP Commission on Prestressed Lightweight Concrete", *PCI Journal*, Vol. 12, No. 3, June 1967, pp. 68-93.

Rose, D. R. and Russell, B. W. "Investigation of Standardized Tests to Measure the Bond Performance of Prestressing Strand," *PCI Journal*, Vol. 42, No. 4, July-August 1997, pp. 56-80.

Ruiz, E. D., Staton, B. W., Do, N. H., and Hale, W. M. "Estimating Transfer Lengths of Precast/Prestressed Beams Cast with Self-Consolidating Concrete," TRB 2007 Annual Meeting, 2006.

Russell, B. W., and Burns, N. H., "Measured Transfer Lengths of 0.5 and 0.6 in. Strands in Pretensioned Concrete," *PCI Journal*, Vol. 41, No. 5, September-October 1996, pp. 44-65.

Shahawy, M. "A Critical Evaluation of the AASHTO Provisions for Strand Development Length of Prestressed Concrete Members," *PCI Journal*, Vol. 46, No. 4, July-August 2001, pp. 94-117.

Shahawy, M., Moussa, I., Batchelor, B. "Strand Transfer Lengths in Full Scale AASHTO Prestressed Concrete Girders," *PCI Journal*, Vol. 37, No. 3, May-June 1992, pp. 84-96.

Shi, C. and Wu, Yanzhong, "Mixture Proportioning and Properties of Self-Consolidating Lightweight Concrete Containing Glass Powder," *ACI Materials Journal*, Vol. 102, No. 5, September-October 2005, pp. 355-363.

Slate, F. O., Nilson, A. H., and Martinez, S. "Mechanical Properties of High-Strength Lightweight Concrete," *ACI Journal Proceedings*, Vol. 83, No. 4, July 1986, pp. 606-613.

Smith, J., Floyd, R., Bymaster, J., and Hale, W., "From the Lab to the Field: Batching SCC", *Proceedings of the PCI Annual Convention and National Bridge Conference*, Paper No. 104, Salt Lake City, UT, October 22-26, 2011.

Sobin, N. T., *Evaluation of Strand Bond Assurance Tests for Pretensioned Applications*, MS Thesis, University of Arkansas, Fayetteville, AR, 2005, 112 pp.

Staton, B. W., Do, N. H., Ruiz, E. D., and Hale, W. M., "Transfer Lengths of Prestressed Beams Cast with Self-Consolidating Concrete," *PCI Journal*, Vol. 54, No. 2, Spring 2009, pp. 64-83.

Thatcher, D. B., Heffington, J. A., Kolozs, R. T., Sylva III, G. S., Breen, J. E., and Burns, N. H., "Structural Lightweight Concrete Prestressed Girders and Panels," Report No. FHWA/TX/1852-1, Center for Transportation Research, Austin, TX, 2002.

Thorsen, N., "Use of Large Tendons in Pre-Tensioned Concrete," *ACI Journal Proceedings*, Vol. 52, No. 2, February 1956, pp. 649-659.

Trent, J. D. *Transfer Length, Development Length, Flexural Strength, and Prestress Loss Evaluation in Pretensioned Self-Consolidating Concrete Members*, MS Dissertation, Virginia Polytechnic Institute and State University, Blacksburg, VA, 2007, pp. 1-152.

Wall, J. R., "Non-Traditional Lightweight Concrete for Bridges, A Lightweight Aggregate Manufacturers Review of Current Practice," *Proceedings 2010 Concrete Bridge Conference Paper No. 74*, Phoenix, AZ, Portland Cement Association, February 24-26, 2010, pp. 1-12.

Ward, D. B., Floyd, R. W., and Hale, W. M., "Bond of 0.5 in. Diameter Strands Cast in Lightweight SCC," *Proceedings PCI-FHWA National Bridge Conference*, San Antonio, TX, 2009, pp 1-11.

Zhang, M. H. and Gjovrov, O. E. "Mechanical Properties of High-Strength Lightweight Concrete," *ACI Materials Journal*, Vol. 88, No. 3, May 1991, pp. 240-247.

Zhu, W., Bartos, P. J. M., "Permeation Properties of Self-Compacting Concrete," *Cement and Concrete Research*, 33, 2003, pp. 921-926.

Zia, P. and Mostafa, T. "Development Length of Prestressing Strands," *PCI Journal*, Vol. 22, No. 5, September-October 1977, pp. 54-65.

## Appendix A: Testing Procedures

### A.1 Strand Tensioning

The following procedure was used to tension each set of prestressing strands used for beam construction, based on the work of Staton (Staton et al. 2009):

1. Plastic sheeting was laid out between the ERC door and the east abutment.
2. Each strand was pulled past the abutment and marked at a length of 55 ft (16.8 m).
3. Each strand was cut with a chop saw and pulled through the abutments, formwork, rebar cages, and reaction block.
4. The dead end was chucked with approximately 6 in. (150 mm) of free strand past the end of the chucks.
5. The hydraulic rams were advanced to  $1\frac{1}{8}$  in. (28.6 mm) by measuring between the reaction block and the face of the hydraulic rams with a set of steel calipers. When one ram reached the required extension it was disconnected to allow the other to advance independently.
6. The strands were pulled as tight as possible by hand and chucks were placed on the strands against the reaction block.
7. The rams were advanced until the pressure in the system reached 50 psi (0.34 MPa) to ensure all slack was out of the strands.
8. The strands were marked approximately 1 in. (25 mm) from the back of the chucks. This distance was measured with the calipers and recorded.
9. The hydraulic rams were advanced until the extension past the face of the ram was exactly 6 in. (152 mm). This included the original  $1\frac{1}{8}$  in (28.6 mm) spacing,  $\frac{1}{8}$  in. (3.2



- mm) for removing any slack in the strands,  $\frac{1}{8}$  in. (3.2 mm) for seating of each chuck, and 4.5 in. of strand elongation required to reach the initial prestress of 202.5 ksi (1396 MPa).
10. Steel blocks with a width of exactly 6 in. (152 mm) were placed between the face of the rams and the reaction block to hold the prestress and the pressure was released from the hydraulic system.
  11. The distance between the back of the chuck and the previously mentioned mark was measured and recorded to confirm the assumed chuck seating.
  12. At the time of prestress release the rams were advanced slightly to allow for removal of the steel blocks and the pressure was released from the system to gradually release the prestress.
  13. The de-tensioned strands were cut using an angle grinder and cutting disk.

## **A.2 Standard Test for Strand Bond (STSB)**

The following procedure was used to test all STSB specimens based on the procedures outlined by Sobin (Sobin 2005):

- “1. The MTS computer was turned on and data acquisition software was loaded.
2. The hydraulic pump was turned on and run for 30 minutes prior to testing to bleed any air from the system and to heat the hydraulic oil.
3. Three 2 in. (50 mm) mortar cubes were broken at the beginning of each test. If the average strength of the initial cubes did not meet the minimum strength criteria of 4500 psi (31 MPa), the strengths were not included in the strength average and time was given for the specimens to strengthen. If the mortar cubes did meet the minimum strength criteria they were used in the strength average and the testing procedure progressed.
4. The specimen was placed in the load frame apparatus with the bearing plate and neoprene pad. The chuck was then attached to the free end of the strand. The bottom frame section was then raised and the chuck was pushed against the bearing plate in the bottom frame until an approximate distance of 6 in. (150 mm) from the bottom of the specimen to the middle of the chuck was reached. The bridge measurement system was attached to the specimen and leveled with the aid of a common bubble level.
5. The MTS software was initiated with the naming of the sample.

6. The specimen was loaded at a rate of 0.10 in. (2.5 mm) per minute as measured from the travel of the ram. The load rate was maintained until 0.70 in. (17.8 mm) of ram travel was reached.
7. The load at 0.01 and 0.10 in. (0.25 to 2.5 mm) of dead end slip was measured separately in a notebook along with any notes about the test.
8. The program was stopped after 0.70 in. (17.8 mm) of ram travel was measured. The load was then released as the bottom frame was raised towards the top test frame.
9. The specimen was removed from the test frame and the chuck, bearing plates, and neoprene pad were removed.
10. The next specimen was tested and these procedures were followed until all three specimens were tested and recorded.
11. After testing all specimens, the remaining three mortar cubes were then tested so that an average mortar strength before and after the test was recorded” (Sobin 2005).

### **A.3 Flexural Testing**

The following procedures were used for each flexural test based on the work of Floyd (Floyd et al. 2011):

1. The beam was placed on rollers on the strong floor outside of the load frame and the support and load locations were marked.
2. The beam was rolled into place under the load frame and lifted using a tractor loader.
3. The supports were put in place, the beam was lowered onto them, and final location adjustments were made.
4. The load application roller and top plate were placed at the load point and the ram was advanced to hold them in place.
5. The LVDTs were attached to the free strand ends and the linear encoder was attached to the top plate.
6. The data acquisition software was initialized by naming the test.
7. The ram was advanced until the double channel reached the top of the frame. The load at this point was typically about 1000 lb (4.45 kN).

8. The LVDTs and cable encoder were tested and zeroed and an initial manual deflection measurement was taken with a steel rule between the top plate and strong floor.
9. Load was applied in 5000 lb (22.2 kN) increments until the first cracks were observed and 2500 lb (11.1 kN) increments after cracking.
10. Manual deflection measurements were taken after each load increment and the beam was examined for cracks.
11. Each crack was traced with a permanent marker and labeled with the load.
12. Strand slip (if any) was recorded after each load increment and if the measured slip was about to exceed the range of the LVDTs, they were removed, or reset and zeroed to record additional slip.
13. After the maximum load was reached, photos were taken of the cracking pattern.
14. The beam was loaded to complete failure, and photos were taken of the failure.
15. The data acquisition program was stopped and the file saved.
16. The pressure was released from the hydraulic system and the LVDTs, linear encoder, and load application plate were removed.
17. The beam was placed on rollers and either aligned to test the other end or removed.
18. The failure type was examined and used to select the embedment length for the next test.

## Appendix B: Beam Analysis Calculations

### B.1 Cross-Section Properties

Beam dimensions varied slightly due to imperfections and slight modifications to the wood forms. The gross cross-section properties presented in Table B.1 were calculated using the relationships

$$A_g = bh, I_g = \frac{bh^3}{12}, \text{ and } y_{bot} = \frac{h}{2}$$

where  $A_g$  is the gross cross-sectional area (in<sup>2</sup>),  $b$  is the width of the cross-section (in.),  $h$  is the total depth of the cross-section (in.),  $I_g$  is the moment of inertia of the gross cross-section (in<sup>4</sup>), and  $y_{bot}$  is the distance from the base to the centroid of the cross-section (in.).

Transformed section properties are presented in Tables B.2 and B.3. The transformed cross-sectional area,  $A_{tr}$ , was calculated using the relationship

$$A_{tr} = A_g + (n_{ps} - 1)A_{ps} + (n' - 1)A'_s$$

where,  $n_{ps}$  is the ratio of the prestressing steel and concrete elastic moduli ( $E_{ps}/E_c$ ),  $A_{ps}$  is the area of prestressing steel (in<sup>2</sup>),  $n'$  is the ratio of the compression reinforcement and concrete moduli of elasticity ( $E_s/E_c$ ), and  $A'_s$  is the area of compression reinforcement (in<sup>2</sup>). The modulus of elasticity of the prestressing steel was taken as 28,500 ksi (197 GPa) and that of the compression reinforcement as 29,000 ksi (200 GPa). The distance from the base of the cross section to the transformed section centroid,  $y_{tr}$ , was determined using the first moment of area in the form of

$$y_{tr} = \frac{A_g y_{bot} + (n_{ps} - 1)A_{ps} y_{ps} + (n' - 1)A'_s y'_s}{A_{tr}}$$

where  $y_{ps}$  is the distance from the base of the cross-section to the centroid of the prestressing steel (in.),  $y'_s$  is the distance from the base of the cross-section to the centroid of the compression reinforcement (in.), and the other variables are as defined previously. The moment of inertia of

Table B.1: Beam Gross-Section Properties

Beam	<i>b</i> (in.)	<i>h</i> (in.)	<i>A<sub>g</sub></i> (in <sup>2</sup> )	<i>I<sub>g</sub></i> (in <sup>4</sup> )	<i>y<sub>bot</sub></i> (in.)	Beam	<i>b</i> (in.)	<i>h</i> (in.)	<i>A<sub>g</sub></i> (in <sup>2</sup> )	<i>I<sub>g</sub></i> (in <sup>4</sup> )	<i>y<sub>bot</sub></i> (in.)
NSC-1	6.60	12.0	79.2	950.4	6.0	HSC-1	6.75	12.0	81.0	972.0	6.0
NSC-2	6.75	12.0	81.0	972.0	6.0	HSC-2	6.75	12.0	81.0	972.0	6.0
NSC-3	6.60	11.8	77.6	892.2	5.9	HSC-3	6.75	12.0	81.0	972.0	6.0
NSC-4	6.70	12.0	80.4	964.8	6.0	HSC-4	6.75	12.0	81.0	972.0	6.0
NSS-1	6.75	12.0	81.0	972.0	6.0	HSS-1	6.75	12.0	81.0	972.0	6.0
NSS-2	6.75	12.0	81.0	972.0	6.0	HSS-2	6.75	12.0	81.0	972.0	6.0
NSS-3	6.75	12.0	81.0	972.0	6.0	HSS-3	6.75	12.0	81.0	972.0	6.0
NSS-4	6.75	12.0	81.0	972.0	6.0	HSS-4	6.75	12.0	81.0	972.0	6.0
NSS-5	6.75	12.0	81.0	972.0	6.0	HSL-1	6.75	12.0	81.0	972.0	6.0
NSL-1	6.60	12.0	79.2	950.4	6.0	HSL-2	6.75	12.0	81.0	972.0	6.0
NSL-2	6.70	12.0	80.4	964.8	6.0	HSL-3	6.75	12.0	81.0	972.0	6.0
NSL-3	6.80	12.0	81.6	979.2	6.0	HSL-4	6.75	12.0	81.0	972.0	6.0
NSL-4	7.0	12.0	84.0	1008.0	6.0						

Note: 1 in. = 25.4 mm

the transformed section,  $I_{tr}$ , was calculated using the parallel axis theorem in the form of the relationship

$$I_{tr} = I_g + A_g(\Delta y_1)^2 + (n_{ps} - 1)A_{ps}(\Delta y_2)^2 + (n' - 1)A'_s(\Delta y_3)^2$$

where  $\Delta y_1$  is the distance between the transformed section centroid and the gross section centroid (in.),  $\Delta y_2$  is the distance between the transformed section centroid and the centroid of the prestressing steel (in.), and  $\Delta y_3$  is the distance between the transformed section centroid and the centroid of the compression reinforcement (in.). Transformed section properties were calculated at release and 28 days and also for an assumed cracked section with the only difference being that the gross concrete area included only the uncracked portion of the section. Transformed section properties at release were designated with an additional  $i$  subscript.

Table B.2: Normal Strength (NS) Beam Transformed-Section Properties

Beam	$A_{tri}$ (in <sup>2</sup> )	$I_{tri}$ (in <sup>4</sup> )	$y_{tri}$ (in.)	$\Delta y_{1i}$ (in.)	$\Delta y_{2i}$ (in.)	$\Delta y_{3i}$ (in.)	$A_{tr}$ (in <sup>2</sup> )	$I_{tr}$ (in <sup>4</sup> )	$y_{tr}$ (in.)	$\Delta y_1$ (in.)	$\Delta y_2$ (in.)	$\Delta y_3$ (in.)
NSC-1	92.6	1129	6.2	0.2	4.2	3.3	90.8	1106	6.1	0.1	4.1	3.4
NSC-2	92.6	1127	6.1	0.1	4.1	3.4	90.0	1092	6.1	0.1	4.1	3.4
NSC-3	91.0	1060	6.0	0.1	4.0	3.2	88.9	1033	6.0	0.1	4.0	3.2
NSC-4	93.3	1137	6.1	0.1	4.1	3.4	90.5	1099	6.1	0.1	4.1	3.4
NSS-1	94.8	1156	6.2	0.2	4.2	3.3	92.2	1121	6.1	0.1	4.1	3.4
NSS-2	93.4	1137	6.1	0.1	4.1	3.4	90.8	1103	6.1	0.1	4.1	3.4
NSS-3	93.3	1136	6.1	0.1	4.1	3.4	91.2	1108	6.1	0.1	4.1	3.4
NSS-4	93.2	1134	6.1	0.1	4.1	3.4	90.4	1097	6.1	0.1	4.1	3.4
NSS-5	93.6	1139	6.1	0.1	4.1	3.4	90.5	1099	6.1	0.1	4.1	3.4
NSL-1	87.1	1056	6.1	0.1	4.1	3.4	85.9	1041	6.1	0.1	4.1	3.4
NSL-2	87.9	1065	6.1	0.1	4.1	3.4	86.4	1045	6.1	0.1	4.1	3.4
NSL-3	90.4	1097	6.1	0.1	4.1	3.4	87.6	1060	6.1	0.1	4.1	3.4
NSL-4	92.7	1124	6.1	0.1	4.1	3.4	90.0	1089	6.1	0.1	4.1	3.4

Note: 1 in. = 25.4 mm

Table B.3: High Strength (HS) Beam Transformed-Section Properties

Beam	$A_{tri}$ (in <sup>2</sup> )	$I_{tri}$ (in <sup>4</sup> )	$y_{tri}$ (in.)	$\Delta y_{1i}$ (in.)	$\Delta y_{2i}$ (in.)	$\Delta y_{3i}$ (in.)	$A_{tr}$ (in <sup>2</sup> )	$I_{tr}$ (in <sup>4</sup> )	$y_{tr}$ (in.)	$\Delta y_1$ (in.)	$\Delta y_2$ (in.)	$\Delta y_3$ (in.)
HSC-1	90.7	1101	6.1	0.1	4.1	3.4	89.9	1091	6.1	0.1	4.1	3.4
HSC-2	90.8	1103	6.1	0.1	4.1	3.4	89.6	1087	6.1	0.1	4.1	3.4
HSC-3	90.5	1099	6.1	0.1	4.1	3.4	90.3	1096	6.1	0.1	4.1	3.4
HSC-4	90.7	1101	6.1	0.1	4.1	3.4	90.0	1093	6.1	0.1	4.1	3.4
HSS-1	91.0	1105	6.1	0.1	4.1	3.4	90.5	1099	6.1	0.1	4.1	3.4
HSS-2	91.5	1113	6.1	0.1	4.1	3.4	90.7	1102	6.1	0.1	4.1	3.4
HSS-3	92.0	1119	6.1	0.1	4.1	3.4	89.9	1091	6.1	0.1	4.1	3.4
HSS-4	89.8	1090	6.1	0.1	4.1	3.4	89.7	1089	6.1	0.1	4.1	3.4
HSL-1	87.5	1058	6.1	0.1	4.1	3.4	86.5	1046	6.1	0.1	4.1	3.4
HSL-2	87.4	1057	6.1	0.1	4.1	3.4	86.4	1044	6.1	0.1	4.1	3.4
HSL-3	87.4	1057	6.1	0.1	4.1	3.4	86.3	1043	6.1	0.1	4.1	3.4
HSL-4	87.4	1057	6.1	0.1	4.1	3.4	86.1	1041	6.1	0.1	4.1	3.4

Note: 1 in. = 25.4 mm

## B.2 Moment Capacity Using Strain Compatibility

The nominal moment for each beam specimen was determined using the equation

$$M_n = 0.85f'_c b \frac{a}{2} \left( c - \frac{a}{2} \right) + A'_s f'_s (c - d') + A_{ps} f_{ps} (d_p - c)$$

where  $M_n$  is the nominal moment capacity (k-in.),  $f'_c$  is the concrete compressive strength at 28 days (ksi),  $b$  is the width of the beam cross-section (in.),  $c$  is the distance from the compression

face of the beam to the neutral axis (in.),  $a$  is the depth of the simplified Whitney compression stress block determined using the coefficient  $\beta_1$  obtained from the ACI code (in.) ( $a = \beta_1 c$ ) (ACI 2011),  $f'_s$  is the stress in compression reinforcement (ksi),  $d'$  is the distance from the compression face to the compression reinforcement (in.),  $f_{ps}$  is the stress in the prestressing steel at nominal moment (ksi),  $d_p$  is the distance from the compression face to the prestressing steel (in.), and the other variables are as defined previously. The value of each parameter used in the calculations and the resulting nominal moment capacities are presented in Table B.4.

The steel stress at nominal moment,  $f_{ps}$ , was determined by calculating the strain in the prestressing steel and then using the stress strain relationship for the strand to obtain the corresponding stress as described in the PCI Design Handbook (PCI 2010). This calculation was broken into three parts. First

$$\varepsilon_1 = \frac{f_{se}}{E_{ps}}$$

where  $\varepsilon_1$  is the strain caused by the effective prestress after all losses (in./in.),  $f_{se}$  is the effective prestress after all losses calculated as described in Section B.4 (ksi), and  $E_{ps}$  is the modulus of elasticity of the prestressing steel (ksi). Second

$$\varepsilon_2 = \frac{\frac{f_{se} A_{ps}}{A_g} + \frac{f_{se} A_{ps} e^2}{I_g}}{E_c}$$

where  $\varepsilon_2$  is the strain in the concrete required to reach zero compressive stress (in./in.),  $e$  is the eccentricity of prestressing strands at mid-span (in.),  $E_c$  is the modulus of elasticity of the concrete (ksi), and the other terms are as defined previously. Third

$$\varepsilon_3 = \frac{0.003(d_p - c)}{c}$$

Table B.4: Moment Capacity Calculations

Beam	$a$ (in.)	$c$ (in.)	$\varepsilon_1$ (in./in.)	$\varepsilon_2$ (in./in.)	$\varepsilon_3$ (in./in.)	$\varepsilon'_s$ (in./in.)	$f_{ps}$ (ksi)	$f'_s$ (ksi)	$M_n$ (k-in.)
NSC-1	3.00	3.79	0.00538	0.00067	0.00492	0.00102	259.9	29.6	933
NSC-2	2.28	3.32	0.00562	0.00055	0.00604	0.00074	262.3	21.5	983
NSC-3	2.96	3.76	0.00533	0.00065	0.00479	0.00100	259.4	29.1	905
NSC-4	2.60	3.51	0.00544	0.00059	0.00555	0.00086	261.3	25.0	960
NSS-1	3.02	3.78	0.00530	0.00062	0.00494	0.00102	259.6	29.5	931
NSS-2	2.50	3.44	0.00552	0.00058	0.00572	0.00082	261.7	23.8	968
NSS-3	2.57	3.48	0.00554	0.00060	0.00562	0.00085	261.6	24.5	963
NSS-4	2.43	3.40	0.00553	0.00056	0.00583	0.00079	261.9	23.0	972
NSS-5	2.47	3.42	0.00548	0.00056	0.00577	0.00081	261.7	23.5	969
NSL-1	2.46	3.45	0.00596	0.00046	0.00570	0.00082	262.2	23.9	971
NSL-2	2.12	3.26	0.00603	0.00042	0.00621	0.00070	262.9	20.2	994
NSL-3	2.13	3.24	0.00584	0.00040	0.00626	0.00068	262.7	19.8	994
NSL-4	2.09	3.18	0.00590	0.00039	0.00643	0.00064	263.0	18.6	998
HSC-1	2.31	3.33	0.00587	0.00056	0.00600	0.00075	262.6	21.8	983
HSC-2	2.21	3.29	0.00585	0.00054	0.00613	0.00072	262.8	20.8	989
HSC-3	2.43	3.40	0.00589	0.00059	0.00582	0.00080	262.5	23.1	974
HSC-4	2.33	3.35	0.00587	0.00057	0.00596	0.00076	262.6	22.0	981
HSS-1	2.47	3.42	0.00584	0.00060	0.00577	0.00081	262.3	23.4	972
HSS-2	2.52	3.45	0.00577	0.00060	0.00569	0.00083	262.1	24.0	968
HSS-3	2.10	3.22	0.00573	0.00055	0.00631	0.00067	262.8	19.5	996
HSS-4	2.35	3.36	0.00597	0.00056	0.00593	0.00077	262.7	22.3	980
HSL-1	1.98	3.05	0.00618	0.00040	0.00684	0.00054	263.8	15.7	1010
HSL-2	1.94	2.99	0.00619	0.00039	0.00703	0.00049	264.0	14.3	1015
HSL-3	1.92	2.96	0.00619	0.00038	0.00713	0.00047	264.0	13.5	1017
HSL-4	1.88	2.89	0.00618	0.00038	0.00739	0.00040	264.2	11.7	1023

Note: 1 in. = 25.4 mm, 1 psi = 0.006895 MPa

where  $\varepsilon_3$  is the strain in the steel at failure (in./in.) and the other variables are as defined previously. The total strain used to calculate  $f_{ps}$  was calculated by summing these three portions.

$$\varepsilon_{ps} = \varepsilon_1 + \varepsilon_2 + \varepsilon_3$$

This value of strain was then used to calculate  $f_{ps}$  using the relationship

$$f_{ps} = 28,500\varepsilon_{ps}$$

for  $\varepsilon_{ps} \leq 0.0085$  and the relationship

$$f_{ps} = 270 - \frac{0.04}{\varepsilon_{ps} - 0.007}$$



for  $\varepsilon_{ps} > 0.0085$ . The determination of  $f_{ps}$  required an iterative process, and Microsoft Excel was used to change the value of  $a$  until the internal forces were balanced as per the equation

$$A_{ps}f_{ps} = 0.85f'_c b a + A'_s f'_s$$

where  $f'_s$  was determined based on the strain in the compression steel,  $\varepsilon'_s$ . If  $\varepsilon'_s \geq 0.00207$ ,  $f'_s$  was taken as 60 ksi. If  $\varepsilon'_s < 0.00207$ ,  $f'_s = \varepsilon'_s E_s$ , where  $E_s$  is the modulus of elasticity of the reinforcing steel and  $\varepsilon'_s$  was determined using the relationship

$$\varepsilon'_s = \frac{(c - d')0.003}{c}$$

where  $c$  was included in the iterations mentioned previously.

### B.3 Shear Capacity

Shear capacity calculations and design of shear reinforcement were initially based on a nominal moment of  $M_n = 90$  k-ft = 1080 k-in. (122.0 kN-m) with the beam simply supported on 6 in. (150 mm) neoprene bearings with a span length of 18 feet (5.5 m). The required point load was then determined for various configurations using the relationship

$$M_{max} = \frac{Pab}{l} \rightarrow P = \frac{M_{max}l}{ab}$$

where  $M_{max}$  is the maximum applied moment (k-ft),  $P$  is the applied point load (kips),  $a$  is the distance from the near support to the point load (ft),  $b$  is the distance from the far support to the point load (ft), and  $l$  is the span length (ft). The point load was then used to determine the support reactions and the resulting shear and bending moment diagrams. The beam arrangement and free body diagram are shown in Figure B.1. The equations of statics were used to determine the reactions resulting in the relationships

$$R_B = \frac{Pa}{l} \text{ and } R_A = P - R_B$$

which in turn led to the shear and bending moment diagrams shown in Figure B.2. The design shear and corresponding moment are allowed to be determined at a distance  $h/2$  from the support, but since the maximum moment and shear occurred in the same location, these values were used for calculation of the concrete shear capacity,  $V_c$ .



Figure B.1: Beam support conditions and free body diagram for initial shear calculations

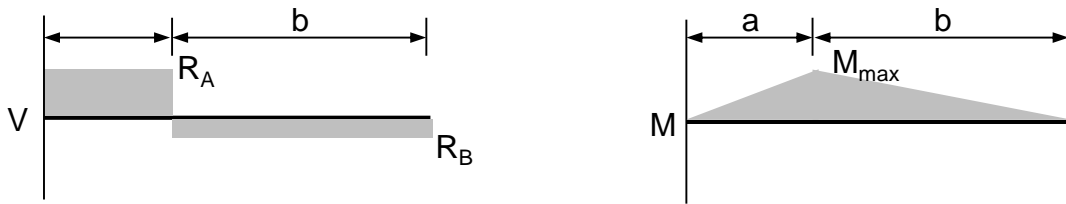


Figure B.2: Beam support conditions and free body diagram for initial shear calculations

The shear capacity contribution of the concrete was determined using the provisions of the ACI 318 Building Code Requirements for Structural Concrete (ACI 2011). The first possibility considered was the relationship

$$V_c = \left( 0.6\lambda\sqrt{f'_c} + 700\frac{V_u d_p}{M_u} \right) b_w d$$

$$2\lambda\sqrt{f'_c} b_w d \leq V_c \leq 5\lambda\sqrt{f'_c} b_w d$$

where  $\lambda$  is the factor accounting for lightweight concrete equal to 0.85 for sand lightweight concrete,  $f'_c$  is the concrete compressive strength at 28 days (psi),  $V_u$  is the design shear force (kips),  $d_p$  is the distance from the extreme compression fiber to the prestressing steel (in.),  $M_u$  is the design moment at the same location as  $V_u$  (k-in.),  $b_w$  is the width of the concrete cross-section (in.), and  $d$  is the effective depth of the cross-section equal to  $d_p$  in this case (in.).

The second possibility was the relationship

$$V_{ci} = 0.6\lambda\sqrt{f'_c}b_wd_p + V_d + \frac{V_iM_{cre}}{M_{max}}$$

where  $V_d$  is the shear force due to the dead load at the section under consideration (lb),  $V_i$  is the shear force at the section due to externally applied loads occurring simultaneously with  $M_{max}$  (lb),  $M_{max}$  is the maximum moment at the section due to externally applied loads (lb-in.),  $M_{cre}$  is the moment causing cracking at the section due to externally applied loads (lb-in.), and the other variables are as defined previously. The value of  $M_{cre}$  was calculated using the relationship

$$M_{cre} = \frac{I}{y_t} (6\lambda\sqrt{f'_c} + f_{pe} - f_d)$$

where  $I$  is the moment of inertia of the cross-section (in<sup>4</sup>),  $y_t$  is the distance from the neutral axis to the extreme section where tensile stress is caused under loading (in.),  $f_{pe}$  is the compressive stress caused by the effective prestress after all losses at the extreme section where tensile stress is caused under loading (psi),  $f_d$  is stress due to dead load at the extreme fiber of section where tensile stress is caused under loading (psi), and the other variables are as described previously.

An assumption of effective prestress was made considering  $f_{se} = 175$  ksi (1207 MPa). The value of  $f_{pe}$  was then calculated using the relationship

$$f_{pe} = -\frac{f_{se}A_{ps}}{A_g} - \frac{f_{se}A_{ps}ec_2}{I_g}$$

where  $c_2$  is the distance between the neutral axis and the extreme section where tensile stress is caused under loading, and the other variables are as defined previously. The value  $f_d$  was calculated using the relationship

$$f_d = \frac{M_d y_t}{I_g}$$

where  $M_d$  is the moment due to only the dead load of the member (lb-in.), and the other variables are as defined previously. The value of  $M_d$  was calculated using the relationship

$$M_d = \frac{w_d x}{2} (l - x)$$

where  $w_d$  is the dead load of the member (lb/ft),  $x$  is the distance to the applied load from the near support (ft), and  $l$  is the span length (ft).

The final possibility was the relationship

$$V_{cw} = (3.5\lambda\sqrt{f'_c} + 0.3f_{pc})b_w d_p + V_p$$

where  $f_{pc}$  is the compressive stress in the concrete after allowing for all losses at the centroid of the cross-section (psi),  $V_p$  is the vertical component of the effective prestress force at section (lb), and the other variables are as defined previously. A reduced prestress was used in the calculation of  $f_{pc}$  when the section was within the predicted  $50d_b$  (30 in.) transfer length using the relationship

$$f_{pc} = \frac{f_{se} A_{ps}}{A_g} \frac{x}{30}$$

where  $x$  is the distance from the support to the section considered (in.) and

$$\frac{x}{30} \leq 1.0.$$

The smallest value of the preceding possibilities was taken as the concrete contribution to shear strength. After examining the first set of assumed conditions it was determined that the original  $V_c$  calculation was the simplest and most conservative and this equation was used for the remainder of the calculations.

The spacing of shear reinforcement,  $s$  (in.), was determined using the relationships

$$V_n = V_c + V_s$$

and

$$V_s = \frac{A_v f_{yt} d}{s}$$

where  $V_n$  is the nominal shear capacity (lb),  $V_s$  is the contribution of steel reinforcement to the shear capacity (lb),  $A_v$  is the area of shear reinforcement at a section (in<sup>2</sup>), taken as 0.0982 in<sup>2</sup> for the reinforcement used,  $f_{yt}$  is the yield stress of the shear reinforcement (psi),  $d$  is the distance from the compression face to the primary reinforcement (in.), and  $s$  is the center-to-center spacing of the shear reinforcement (in.). Calculated values of each parameter using the 18 ft (5.5 m) span length for each set of considered conditions are shown in Table B.5. These resulted in the original shear design of stirrups spaced at 3 in. (75 mm) for the first 4 ft (1.2 m) from each end and 5 in. (125 mm) for the remainder of the beam.

Revised calculations were made for beams cast after the NSC and NSL specimens using a 9 ft (2.7 m) span length with an overhang at the far end. The effects of this overhang were deemed negligible and design shear calculations were based on the applied load on a 9 ft (2.7 m) simple span. The same procedures mentioned previously were used for determination of shear capacity based on established spacing, and the comparison to estimated loadings is presented in Table B.6. These calculations resulting in extending the 3 in. (75 mm) spacing to the first 5 ft (1.5 m) from each end.

Table B.5: Initial Shear Capacity Parameters

$f'_c$ (psi)	$a$ (ft)	$b$ (ft)	$l$ (ft)	$M_{max}$ (k-ft)	$V_u$ (kips)	$V_c$ (kips)	$V_{ci}$ (kips)	$V_{cw}$ (kips)	$V_s$ (kips)	$s$ (in.)
6000	2.0	16.0	18.0	90.0	45.0	21.4	24.0	30.2	23.6	2.5
6000	2.5	15.5	18.0	107.6	43.1	17.7	--	--	25.4	2.3
6000	4.0	14.0	18.0	98.0	24.5	12.0	--	--	12.5	4.7
6000	6.0	12.0	18.0	90.0	15.0	8.89	--	--	6.1	9.6
6000	4.0	14.0	18.0	90.0	22.48	12.04	--	--	10.4	5.6
6000	2.5	15.5	18.0	90.0	36.0	17.7	--	--	18.3	3.2

Note: 1 ft = 0.3048 m, 1 kip = 4.448 kN

Table B.6: Initial Shear Capacity Parameters

$f'_c$ (psi)	$a$ (ft)	$b$ (ft)	$l$ (ft)	$M_{max}$ (k-ft)	$V_u$ (kips)	$V_c$ (kips)	$V_s$ (kips)	$s$ (in.)	Result
7000	4.0	5.0	9.0	90.0	22.5	12.3	19.6	3.0	G
7000	4.0	5.0	9.0	90.0	18.0	10.3	11.8	5.0	G
7000	2.5	6.5	9.0	90.0	30.8	15.7	19.6	3.0	G
7000	2.5	6.5	9.0	90.0	19.2	10.9	11.8	5.0	G
7000	2.0	7.0	9.0	90.0	45.0	21.7	19.6	3.0	NG
6000	4.0	5.0	9.0	87.2	21.8	12.0	19.6	3.0	G
6000	4.0	5.0	9.0	87.2	17.4	10.1	11.8	5.0	G

Note: 1 ft = 0.3048 m, 1 kip = 4.448 kN, G indicates adequate, NG indicates inadequate

## B.4 Prestress Losses

Prestress losses used to determine  $f_{se}$  required for nominal moment calculations and transfer and development length predictions were calculated using the AASHTO refined method (AASHTO 2007). Total prestress losses were divided into the immediate elastic shortening losses and the time dependent creep, shrinkage, and relaxation losses. Only the equations considering losses between the time of prestress release and deck placement were considered since no deck was placed on the test specimens. The calculations of each particular prestress loss are described in Sections B.4.1 to B.4.4.

### B.4.1 Elastic Shortening

Elastic shortening losses were calculated using the equation

$$\Delta f_{pES} = \frac{E_{ps}}{E_{ci}} f_{cgp}$$

where  $\Delta f_{pES}$  is the elastic shortening loss (ksi),  $E_{ci}$  is the modulus of elasticity of the concrete at prestress transfer (ksi),  $E_{ps}$  is the modulus of elasticity of the prestressing steel (ksi), and  $f_{cgp}$  is the concrete stress at the center of gravity of the prestressing steel due to the prestress force and self-weight of the member at the section of maximum moment at prestress transfer. The relationship used to calculate this stress was

$$f_{cgp} = f_{pi} A_{ps} \left( \frac{1}{A_{tri}} + \frac{e_{trms}^2}{I_{tri}} \right) - \frac{M_0 e_{trms}}{I_{tri}}$$

where  $f_{pi}$  is the stress in the strands immediately prior to transfer (ksi), taken as 202.5 ksi,  $A_{ps}$  is the area of prestressing steel ( $\text{in}^2$ ),  $A_{tri}$  is the transformed cross-sectional area at prestress release ( $\text{in}^2$ ),  $e_{trms}$  is the eccentricity of the prestressing force based on the transformed section at mid-span at release (in.),  $I_{tri}$  is the transformed section moment of inertia at release ( $\text{in}^4$ ), and  $M_0$  is the moment at the point of maximum moment caused by the self-weight of the member (k-in.).

Required parameters and the resulting elastic shortening losses are presented in Table B.7.

Table B.7: Elastic Shortening Parameters

Beam	$e_g$ (in.)	$e_{tr}$ (in.)	$E_{ci}$ (ksi)	$E_c$ (ksi)	$f_{cgp}$ (ksi)	$M_0$ (k-in.)	$\Delta f_{pES}$ (ksi)
NSC-1	4.00	4.15	2577	2923	2.17	32.0	24.04
NSC-2	4.00	4.13	2933	3671	2.16	34.1	20.95
NSC-3	3.88	4.02	2558	3000	2.19	31.8	24.38
NSC-4	4.00	4.15	2665	3327	2.15	33.4	22.98
NSS-1	4.00	4.15	2504	3037	2.12	34.0	24.09
NSS-2	4.00	4.14	2761	3395	2.14	33.6	22.12
NSS-3	4.00	4.14	2779	3291	2.15	33.2	22.01
NSS-4	4.00	4.14	2808	3546	2.15	34.2	21.77
NSS-5	4.00	4.14	2730	3511	2.14	34.2	22.32
NSL-1	4.00	4.10	4114	4700	2.25	40.0	15.59
NSL-2	4.00	4.09	4318	5208	2.22	41.0	14.67
NSL-3	4.00	4.10	3735	5165	2.16	41.6	16.52
NSL-4	4.00	4.10	3796	5151	2.11	42.7	15.81
HSC-1	4.00	4.11	3450	3710	2.19	34.4	18.10
HSC-2	4.00	4.11	3408	3833	2.19	34.6	18.30
HSC-3	4.00	4.11	3495	3576	2.19	34.3	17.89
HSC-4	4.00	4.11	3446	3659	2.19	34.2	18.12
HSS-1	4.00	4.12	3350	3491	2.19	34.0	18.60
HSS-2	4.00	4.12	3199	3428	2.18	33.8	19.39
HSS-3	4.00	4.13	3078	3716	2.17	33.1	20.10
HSS-4	4.00	4.10	3747	3766	2.21	35.0	16.77
HSL-1	4.00	4.08	4875	5533	2.23	41.5	13.01
HSL-2	4.00	4.08	4938	5637	2.23	41.6	12.86
HSL-3	4.00	4.08	4943	5730	2.23	41.9	12.84
HSL-4	4.00	4.08	4925	5870	2.23	41.9	12.88

Note: 1 in. = 25.4 mm, 1 psi = 0.006895 MPa, 1 kip = 4.448 kN

### B.4.2 Shrinkage

The portion of time dependent losses due to shrinkage of the girder concrete was calculated using the relationship

$$\Delta f_{pSR} = \varepsilon_{bid} E_{ps} K_{id}$$

where  $\Delta f_{pSR}$  is the component of the time dependent prestress losses due to shrinkage of the concrete (ksi),  $\varepsilon_{bid}$  is the concrete shrinkage strain of the girder at the time losses are considered (in./in.),  $E_{ps}$  is the modulus of elasticity of the prestressing steel (ksi),  $K_{id}$  is the transformed section coefficient that accounts for time-dependent interaction between concrete and bonded steel during the time between prestress transfer and time losses are considered.

The coefficient  $\varepsilon_{bid}$  was calculated using the relationship

$$\varepsilon_{bid} = k_s k_{hs} k_f k_{td} 0.48 \times 10^{-3}$$

where  $k_s$  is the factor accounting for volume-to-surface ratio of the member,  $k_{hs}$  is a factor accounting for the effects of humidity,  $k_f$  is a factor accounting for the effect of concrete compressive strength, and  $k_{td}$  is the time development factor. These factors were calculated as follows:

$$k_s = 1.45 - 0.13 \left( \frac{V}{S} \right) \geq 1.0$$

where  $V/S$  is the volume to surface ratio of the member (in.),

$$k_{hs} = 2.00 - 0.014H$$

where  $H$  is the annual average ambient relative humidity (%) taken as 70%, resulting in a  $k_{hs}$  of 1.02,

$$k_f = \frac{5}{1 + f'_{ci}}$$

where  $f'_{ci}$  is the concrete compressive strength at prestress release (ksi), and



$$k_{td} = \frac{t}{61 - 4f'_{ci} + t}$$

where  $t$  is the time between the time of loading for creep or the end of curing for shrinkage and the time losses are considered (days).

The coefficient  $K_{id}$  was calculated using the relationship

$$K_{id} = \frac{1}{1 + \frac{E_p A_{ps}}{E_{ci} A_g} \left[ 1 + \frac{A_g e_{pg}^2}{I_g} \right] [1 + 0.7 \Psi_b(t_f, t_i)]}$$

where  $e_{pg}$  is the eccentricity of the prestressing force based on the gross cross-section (in.),  $\Psi_b(t_f, t_i)$  is the girder creep coefficient at the time shrinkage losses are considered based on the loading at prestress transfer,  $t_f$  is the concrete age at the time shrinkage losses are considered (days) taken as 28 days,  $t_i$  is the concrete age at prestress transfer (days) taken as 1 day, and the other terms are as defined previously. The coefficient  $\Psi_b(t_f, t_i)$  is calculated using the relationship

$$\Psi_b(t_f, t_i) = 1.9 k_s k_{hc} k_f k_{td} t_i^{-0.118}$$

where  $k_{hc}$  is the humidity factor for creep and is calculated using the relationship

$$k_{hc} = 1.56 - 0.008H$$

where  $H$  is the annual average ambient relative humidity (%) taken as 70%, resulting in a  $k_{hc}$  of 1.00. All required parameters and the resulting shrinkage losses are presented in Table B.8.

### B.4.3 Creep

The portion of the time dependent losses due to creep of the girder concrete was calculated using the relationship

$$\Delta f_{pCR} = \frac{E_{ps}}{E_{ci}} f_{cgp} \Psi_b(t_d, t_i) K_{id}$$

where  $\Delta f_{pCR}$  is the portion of the time dependent prestress losses due to creep of the girder concrete (ksi),  $\Psi_b(t_d, t_i)$  is the girder creep coefficient at the time of deck placement (taken as the

Table B.8: Concrete Shrinkage Loss Parameters

Beam	$\varepsilon_{bid}$	$K_{id}$	$k_s$	$k_f$	$k_{id}$	V/S (in.)	$\Psi_b(t_f, t_i)$	$\Delta f_{pSR}$ (ksi)
NSC-1	0.00022	0.816	1.173	1.000	0.384	2.13	0.854	5.11
NSC-2	0.00020	0.842	1.169	0.888	0.397	2.16	0.784	4.84
NSC-3	0.00023	0.811	1.175	1.040	0.380	2.11	0.881	5.25
NSC-4	0.00022	0.823	1.171	1.008	0.383	2.15	0.858	5.18
NSS-1	0.00024	0.809	1.169	1.136	0.371	2.16	0.937	5.57
NSS-2	0.00021	0.831	1.169	0.949	0.389	2.16	0.821	5.01
NSS-3	0.00021	0.833	1.169	0.917	0.393	2.16	0.801	4.90
NSS-4	0.00021	0.833	1.169	0.962	0.388	2.16	0.828	5.07
NSS-5	0.00022	0.827	1.169	1.008	0.383	2.16	0.857	5.21
NSL-1	0.00019	0.881	1.173	0.814	0.409	2.13	0.743	4.81
NSL-2	0.00019	0.889	1.171	0.772	0.417	2.15	0.716	4.68
NSL-3	0.00022	0.869	1.168	0.980	0.386	2.17	0.839	5.36
NSL-4	0.00021	0.876	1.163	0.949	0.389	2.21	0.816	5.25
HSC-1	0.00017	0.868	1.169	0.694	0.436	2.16	0.673	4.29
HSC-2	0.00018	0.866	1.169	0.718	0.430	2.16	0.686	4.36
HSC-3	0.00017	0.870	1.169	0.675	0.442	2.16	0.662	4.23
HSC-4	0.00017	0.868	1.169	0.687	0.438	2.16	0.669	4.26
HSS-1	0.00018	0.864	1.169	0.707	0.433	2.16	0.680	4.31
HSS-2	0.00018	0.857	1.169	0.759	0.420	2.16	0.708	4.46
HSS-3	0.00018	0.852	1.169	0.766	0.419	2.16	0.712	4.46
HSS-4	0.00017	0.879	1.169	0.631	0.457	2.16	0.640	4.13
HSL-1	0.00017	0.904	1.169	0.635	0.455	2.16	0.642	4.27
HSL-2	0.00016	0.906	1.169	0.623	0.460	2.16	0.637	4.23
HSL-3	0.00017	0.905	1.169	0.631	0.457	2.16	0.640	4.26
HSL-4	0.00017	0.905	1.169	0.639	0.454	2.16	0.644	4.28

Note: 1 in. = 25.4 mm, 1 psi = 0.006895 MPa

time creep losses were considered) due to the loading at prestress transfer ,  $t_d$  is the concrete age at deck placement (taken as the time creep losses were considered, 28 days in this case) (days), and the other terms are as described previously. All factors were calculated using the relationships described previously. Required parameters and the resulting creep losses are presented in Table B.9.

#### B.4.4 Relaxation

The portion of the time dependent prestress losses due to relaxation of the prestressing steel were calculated using the relationship

$$\Delta f_{pR1} = \frac{f_{pt}}{K_L} \left( \frac{f_{pt}}{f_{py}} - 0.55 \right) \text{ or } 1.2$$

where  $\Delta f_{pR1}$  is the portion of the time dependent prestress losses due to relaxation of the prestressing steel (ksi),  $f_{pt}$  is the stress in the strands immediately after prestress transfer (ksi),  $f_{py}$  is the yield stress of the prestressing steel, taken as  $0.90f_{pu}$  (243 ksi (1675 MPa)) for low relaxation strand, and  $K_L$  is a factor of 30 for low relaxation strands. Relaxation losses were taken as 1.2 ksi (8.3 MPa) for all specimens as allowed by the AASHTO LRFD specifications (AASHTO 2007). The total prestress losses are presented in Table B.9.

Table B.9: Concrete Creep, Relaxation, and Total Losses

Beam	$f_{cgp}$ (ksi)	$\Psi_b(t_d, t_i)$	$K_{id}$	$f_{pt}$ (ksi)	$\Delta f_{pCR}$ (ksi)	$\Delta f_{pR1}$ (ksi)	$\Delta f_{pTOT}$ (ksi)
NSC-1	2.45	0.854	0.816	178.46	18.90	1.20	49.26
NSC-2	2.39	0.784	0.842	181.55	15.33	1.20	42.32
NSC-3	2.47	0.881	0.811	178.12	19.71	1.20	50.54
NSC-4	2.41	0.858	0.823	179.52	18.21	1.20	47.57
NSS-1	2.39	0.937	0.809	178.41	20.65	1.20	51.51
NSS-2	2.39	0.821	0.831	180.38	16.85	1.20	45.18
NSS-3	2.40	0.801	0.833	180.49	16.40	1.20	44.51
NSS-4	2.39	0.828	0.833	180.73	16.75	1.20	44.79
NSS-5	2.39	0.857	0.827	180.18	17.70	1.20	46.43
NSL-1	2.42	0.743	0.881	186.91	10.98	1.20	32.57
NSL-2	2.38	0.716	0.889	187.83	10.00	1.20	30.56
NSL-3	2.34	0.839	0.869	186.98	13.04	1.20	36.11
NSL-4	2.27	0.816	0.876	186.69	12.18	1.20	34.44
HSC-1	2.39	0.673	0.868	184.40	11.53	1.20	35.12
HSC-2	2.39	0.686	0.866	184.20	11.87	1.20	35.72
HSC-3	2.39	0.662	0.870	184.61	11.24	1.20	34.56
HSC-4	2.39	0.669	0.868	184.38	11.48	1.20	35.06
HSS-1	2.39	0.680	0.864	183.90	11.95	1.20	36.07
HSS-2	2.39	0.708	0.857	183.11	12.94	1.20	37.99
HSS-3	2.40	0.712	0.852	182.40	13.46	1.20	39.21
HSS-4	2.39	0.640	0.879	185.73	10.22	1.20	32.32
HSL-1	2.36	0.642	0.904	189.49	8.02	1.20	26.49
HSL-2	2.36	0.637	0.906	189.64	7.85	1.20	26.14
HSL-3	2.36	0.640	0.905	189.66	7.89	1.20	26.19
HSL-4	2.36	0.644	0.905	189.62	7.96	1.20	26.32

Note: 1 psi = 0.006895 MPa

## B.5 Concrete Elastic Moduli at Seven Days

Table B.10: Measured Modulus of Elasticity at Seven Days of Age

Batch	Static (ksi)	Dynamic (ksi)		ACI (ksi)
		Longitudinal	Transverse	
NSCa	3050 <sup>1</sup>	3330		3070
NSCb	3430	3900	3790	3160
NSSa	4050	4540	4380	4030
NSSb	3820	4540	4210	3730
NSL	5760	5910	5650	5150
HSC	3950	4170	3890	3910
HSS	3130	4000	3660	3250
HSL	5330	6270	5900	6030

Note: 1 psi = 0.006895 MPa, <sup>1</sup> indicates measurement taken at 12 days of age

## Appendix C: Moisture Content Errors

### C.1 Normal Strength Clay (NSC) Trial Batches

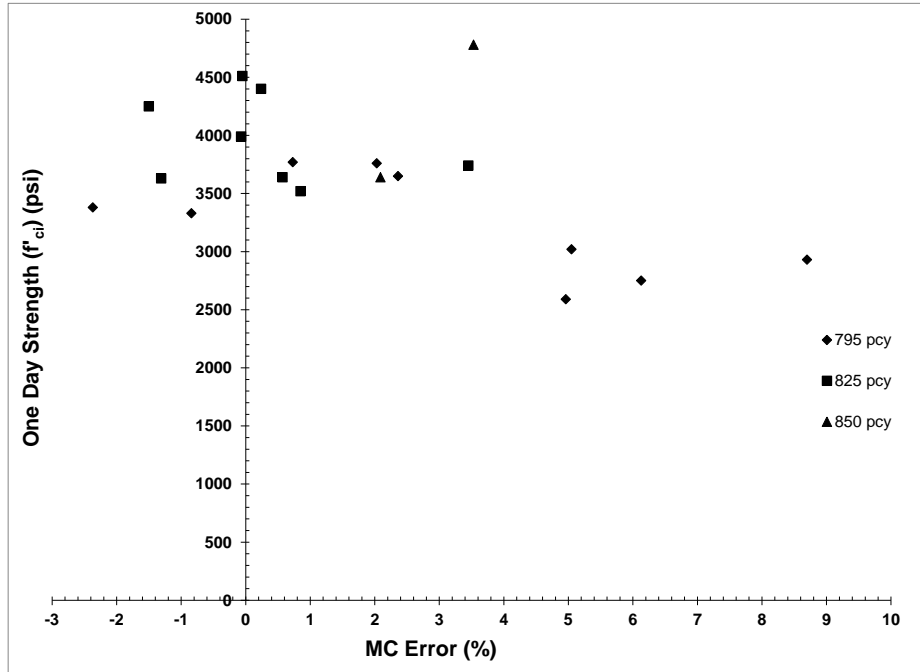


Figure C.1: Effect of aggregate moisture content error on NSC  $f'_{ci}$  by cement content

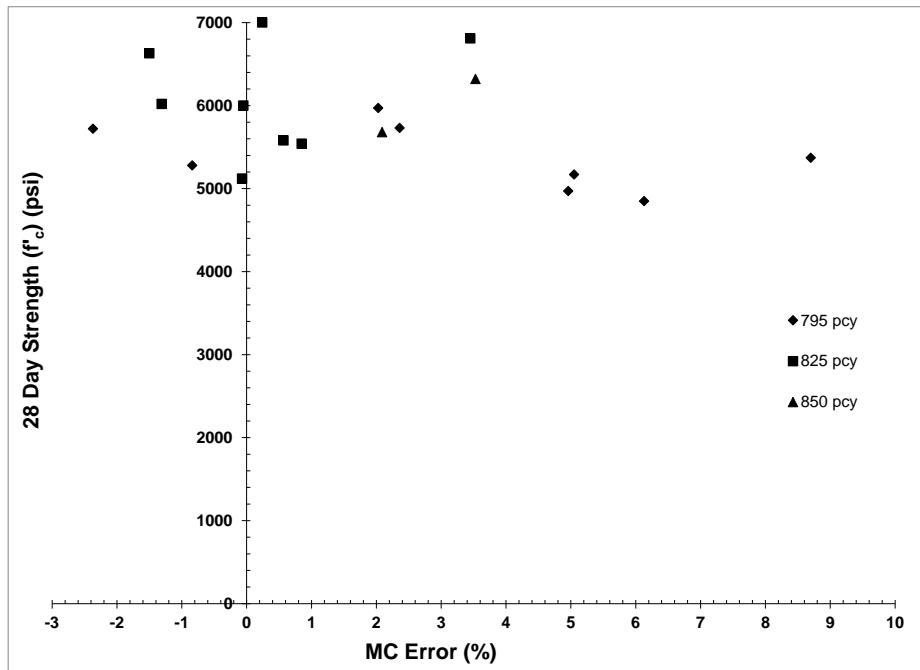


Figure C.2: Effect of aggregate moisture content error on NSC  $f'_c$  by cement content

## C.2 Normal Strength Shale (NSS) Trial Batches

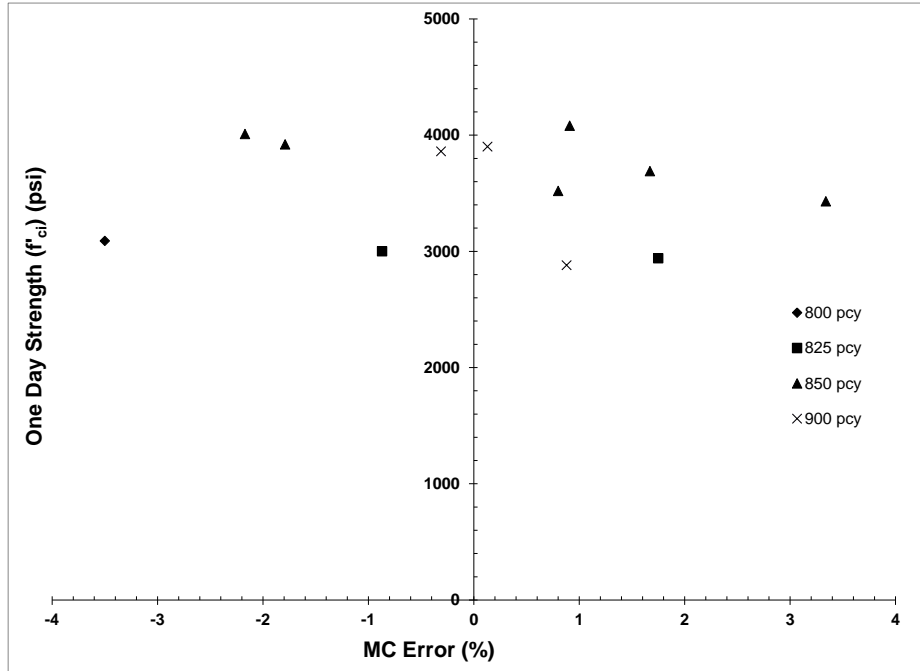


Figure C.3: Effect of aggregate moisture content error on NSS  $f'_{ci}$  by cement content

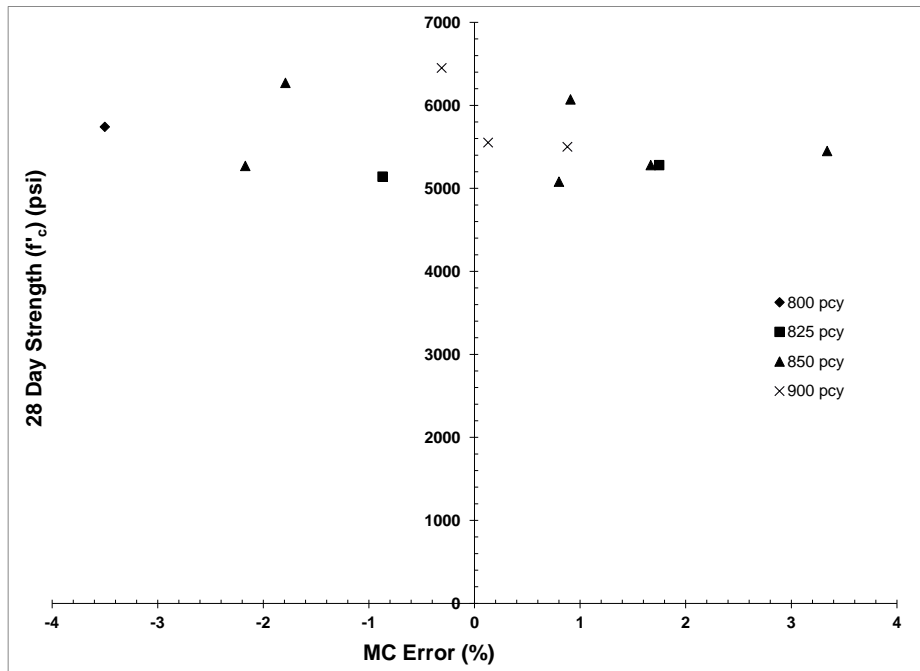


Figure C.4: Effect of aggregate moisture content error on NSS  $f'_c$  by cement content

### C.3 High Strength Clay (HSC) Trial Batches

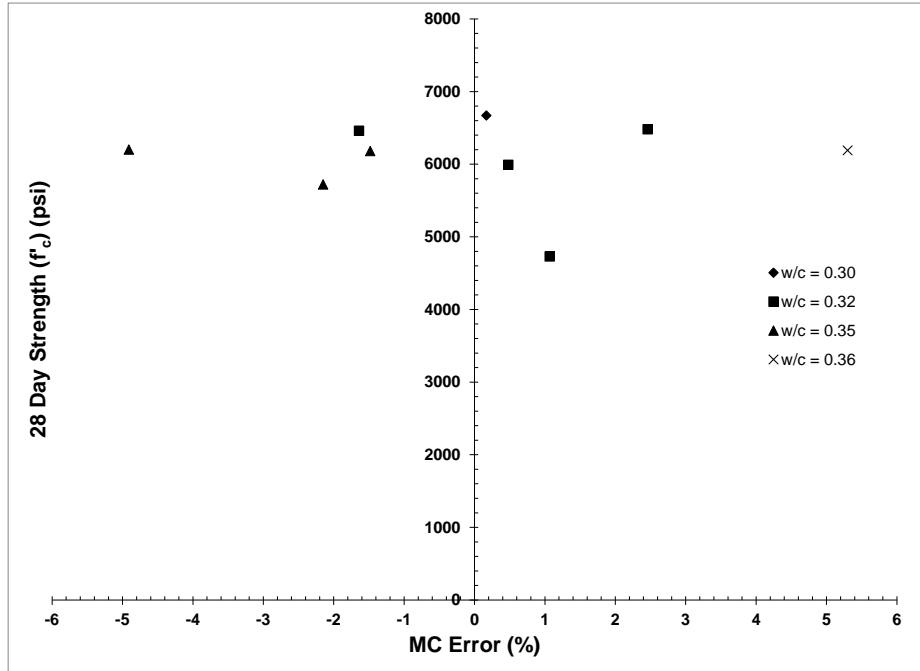


Figure C.5: Effect of aggregate moisture content error on Type I cement HSC  $f'_c$

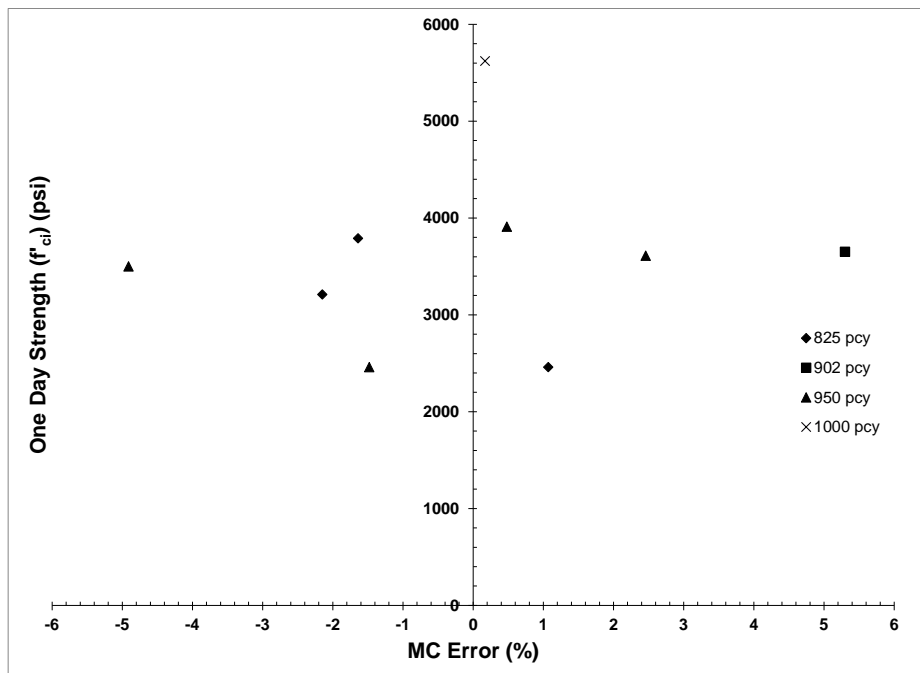


Figure C.6: Effect of aggregate moisture content error on Type I cement HSC  $f'_{ci}$  by cement content

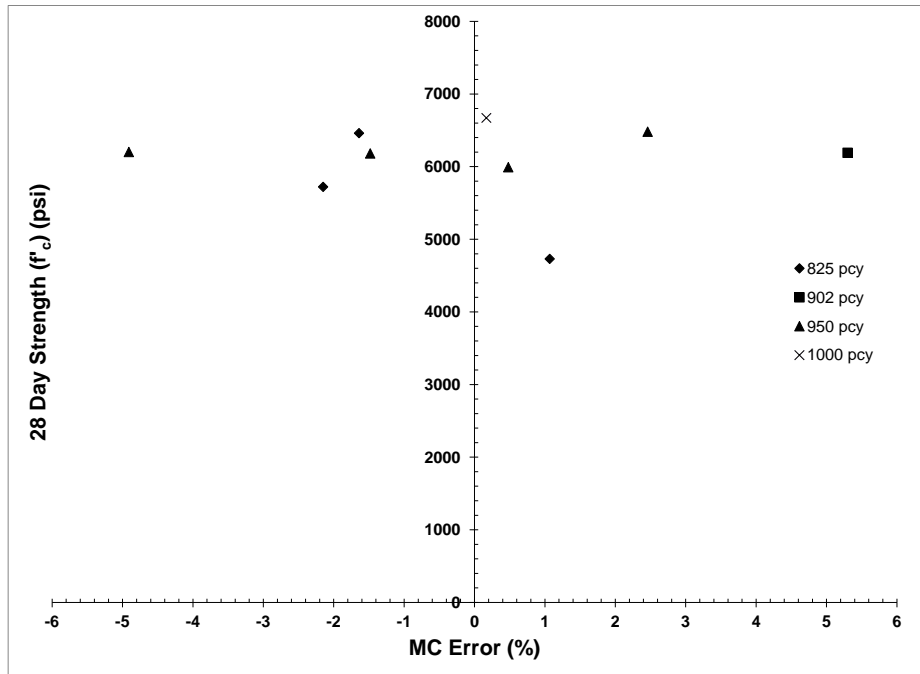


Figure C.7: Effect of aggregate moisture content error on Type I cement HSC  $f'_c$  by cement content

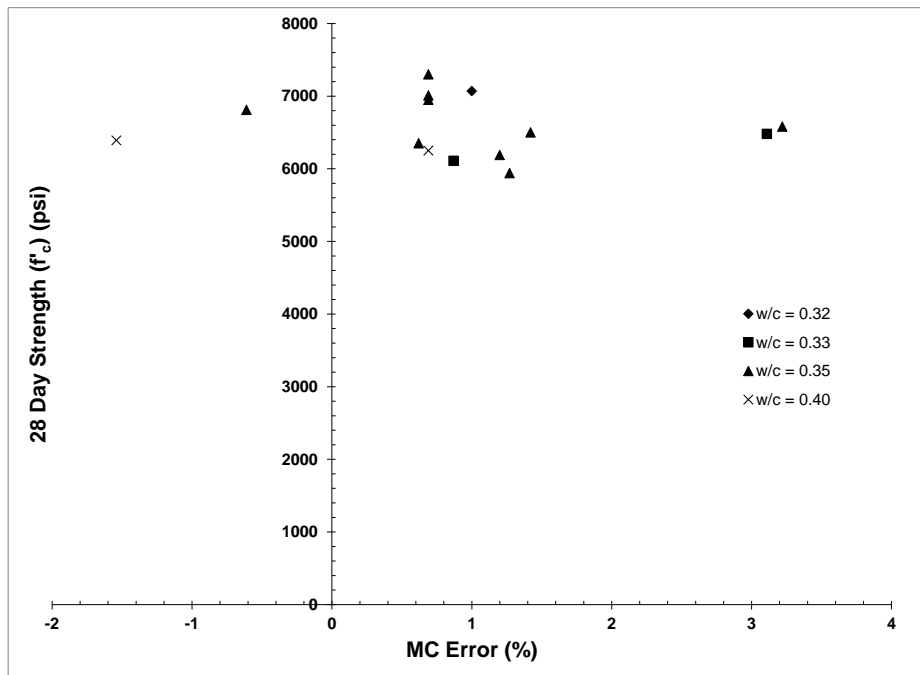


Figure C.8: Effect of aggregate moisture content error on  $f'_c$  of silica fume HSC



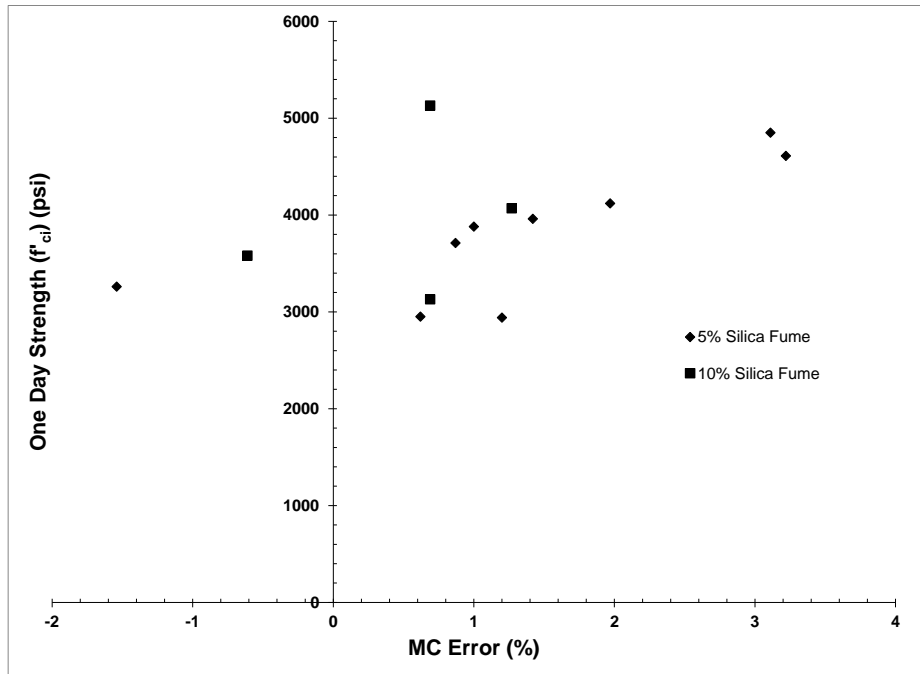


Figure C.9: Effect of aggregate moisture content error on silica fume HSC  $f'_{ci}$  by percent silica fume

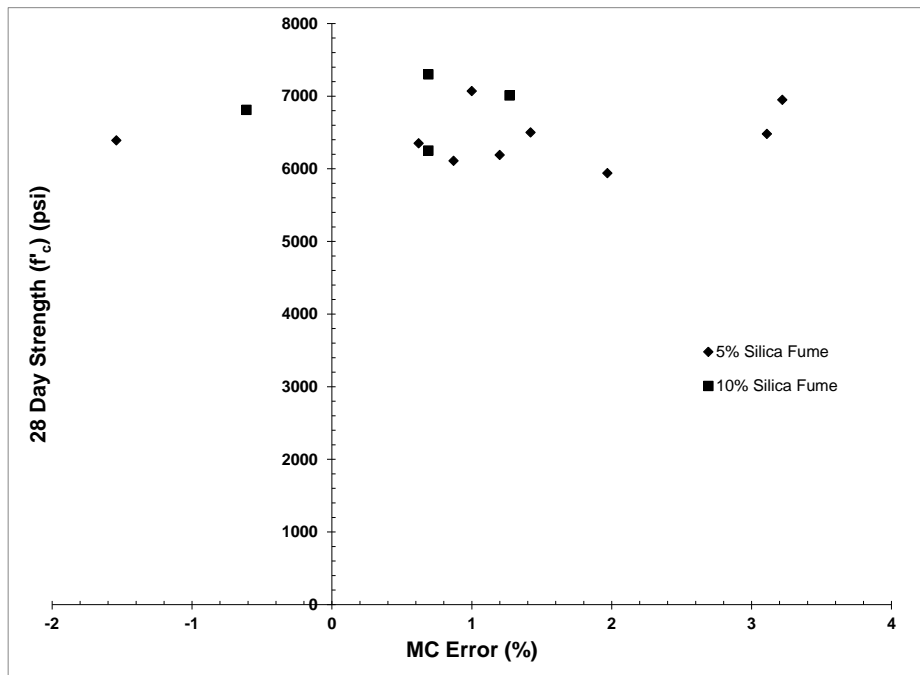


Figure C.10: Effect of aggregate moisture content error on silica fume HSC  $f'_c$  by percent silica fume

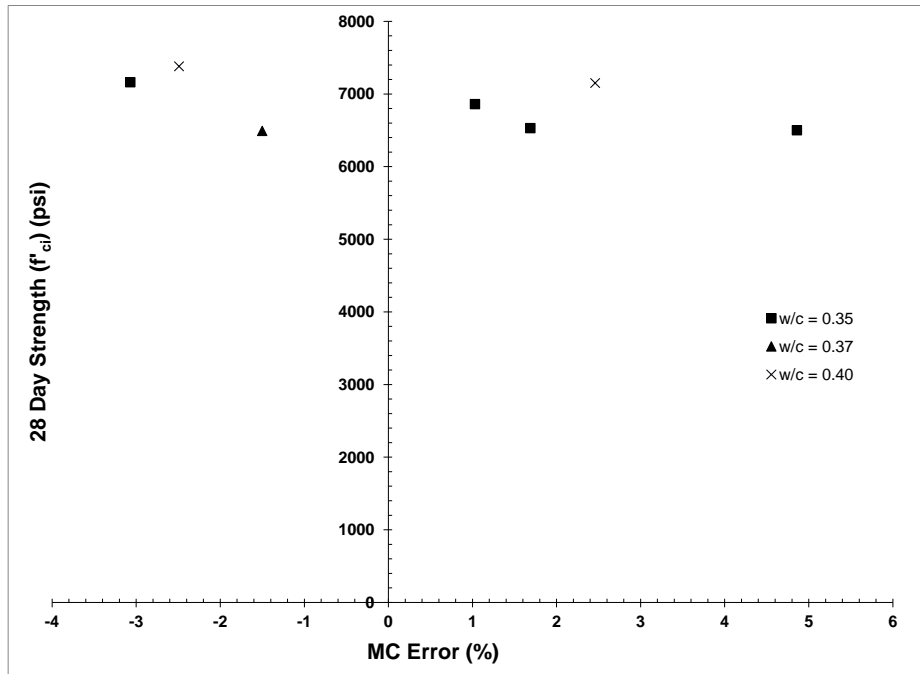


Figure C.11: Effect of aggregate moisture content error on  $f'_{ci}$  of HSC with limestone

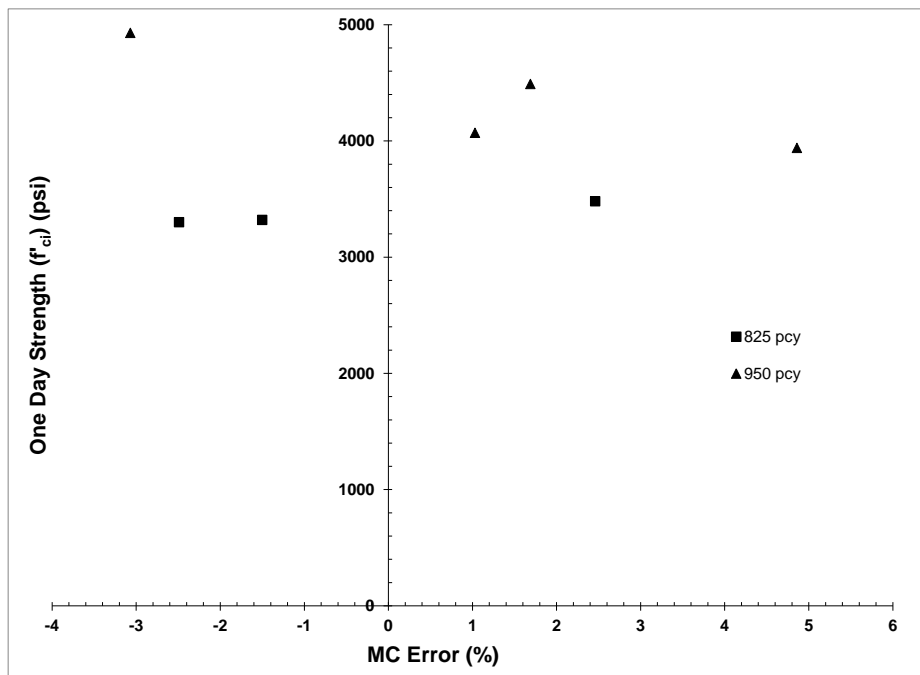


Figure C.12: Effect of aggregate moisture content error on  $f'_{ci}$  of HSC with limestone by cement content

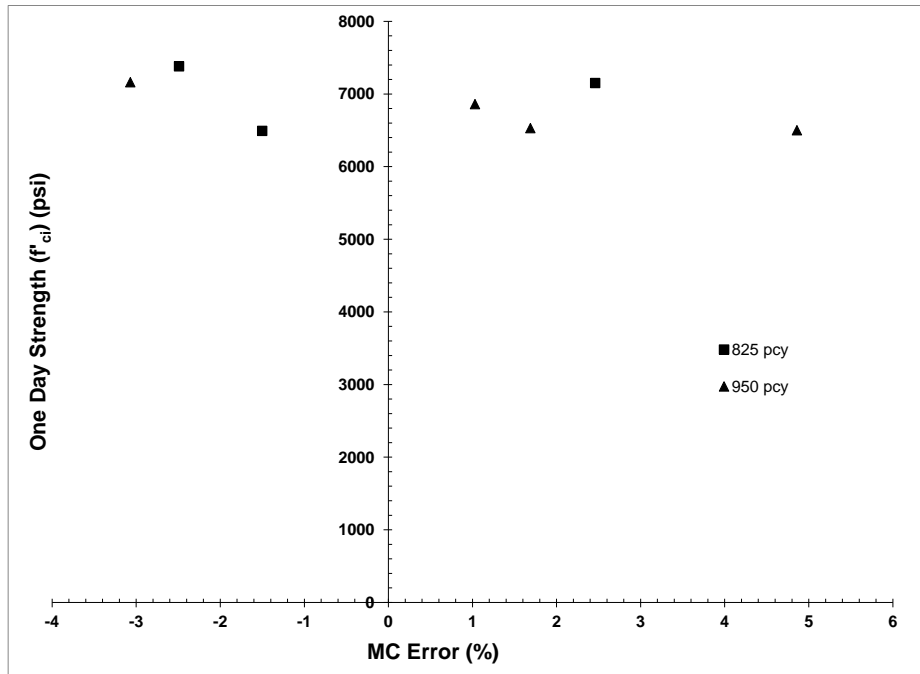


Figure C.13: Effect of aggregate moisture content error on  $f'_{ci}$  of HSC with limestone by cement content

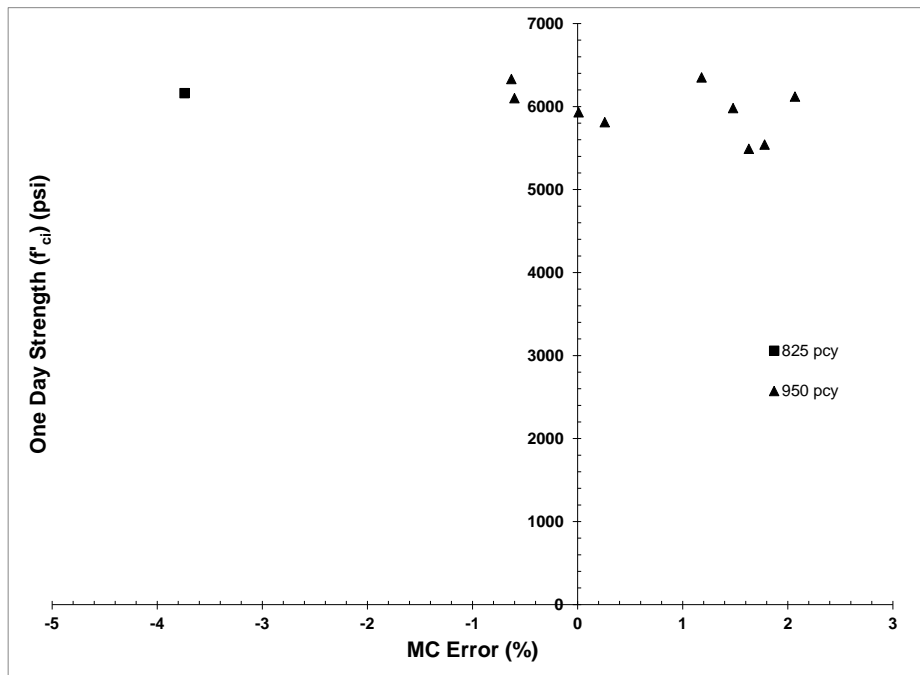


Figure C.14: Effect of aggregate moisture content error on  $f'_{ci}$  of Type III cement HSC by cementitious material content

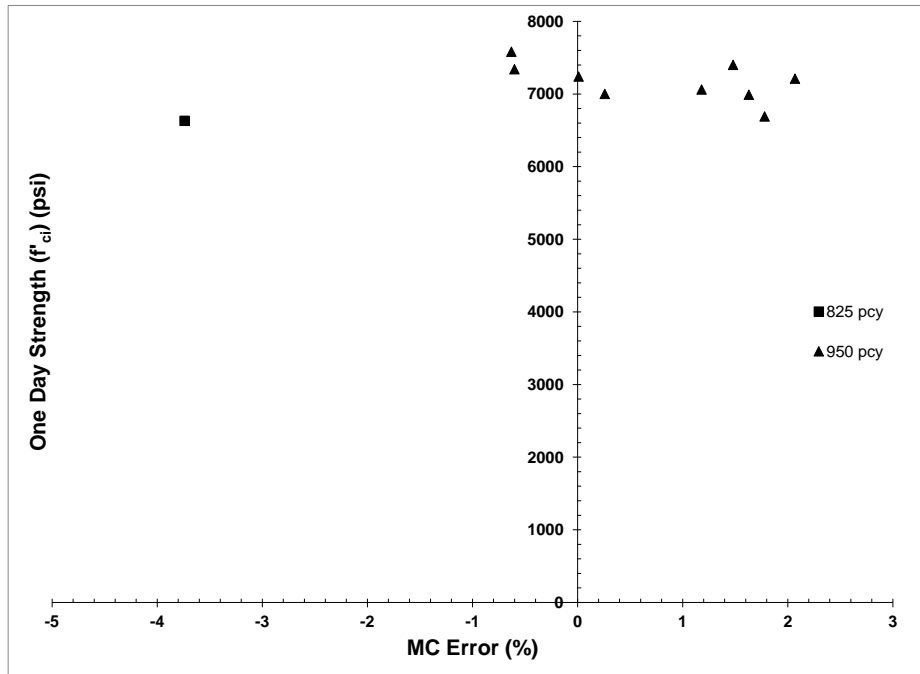


Figure C.15: Effect of aggregate moisture content error on  $f'_c$  of Type III cement HSC by cementitious material content

#### C.4 High Strength Shale (HSS) Trial Batches

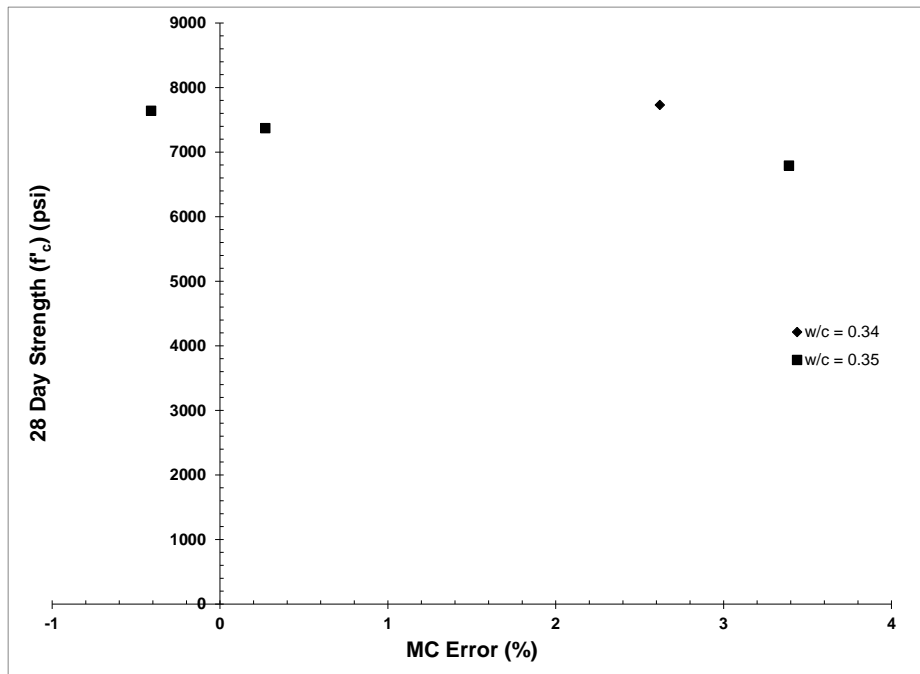


Figure C.16: Effect of aggregate moisture content error on HSS  $f'_c$

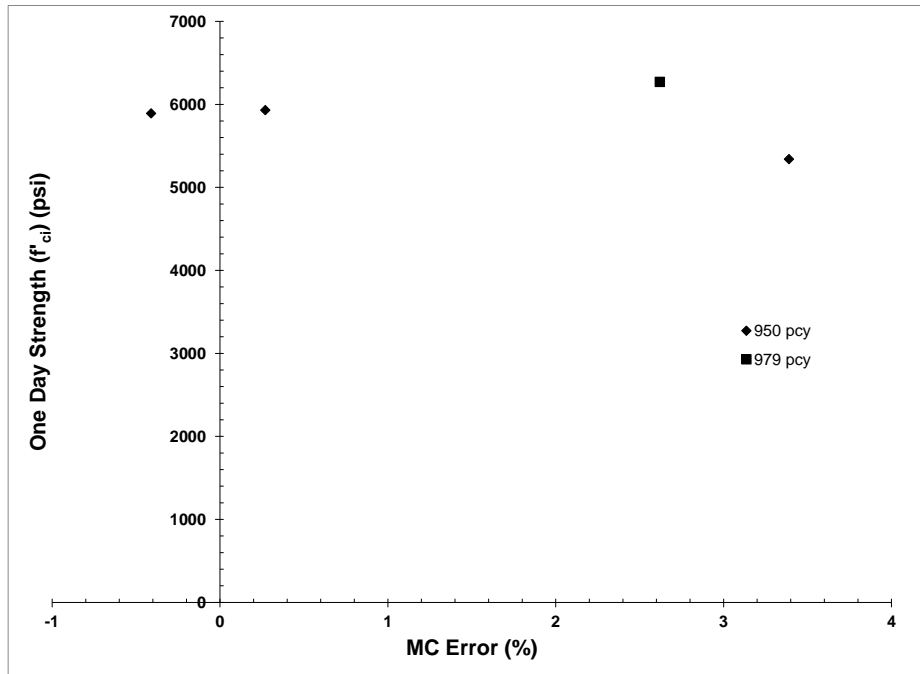


Figure C.17: Effect of aggregate moisture content error on HSS  $f'_{ci}$  by cementitious material content

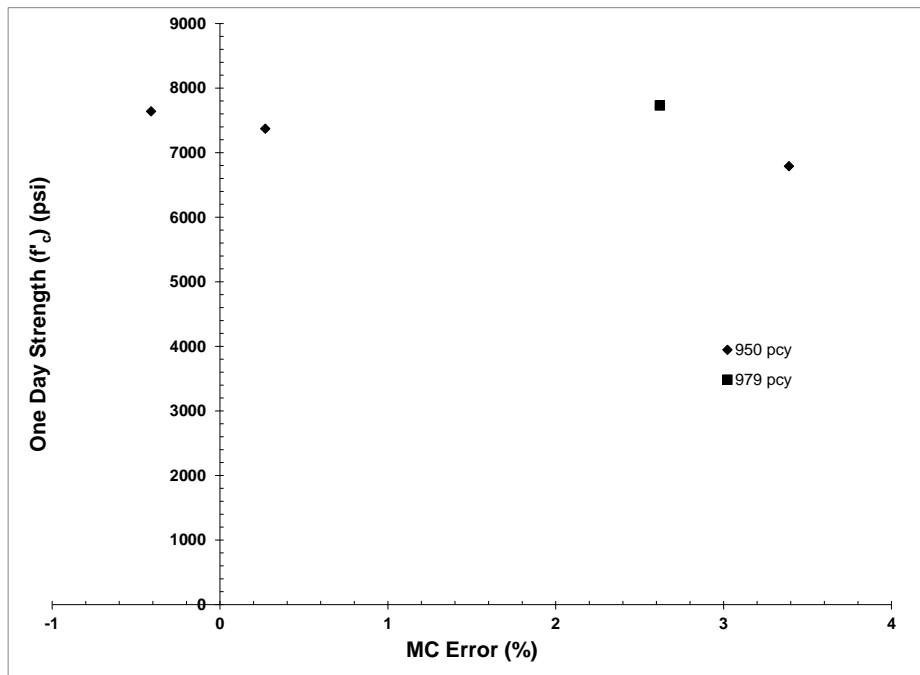


Figure C.18: Effect of aggregate moisture content error on HSS  $f'_c$  by cementitious material content

## Appendix D: Transfer Length Data

### D.1 DEMEC Strain Plots

#### D.1.1 NSC-1

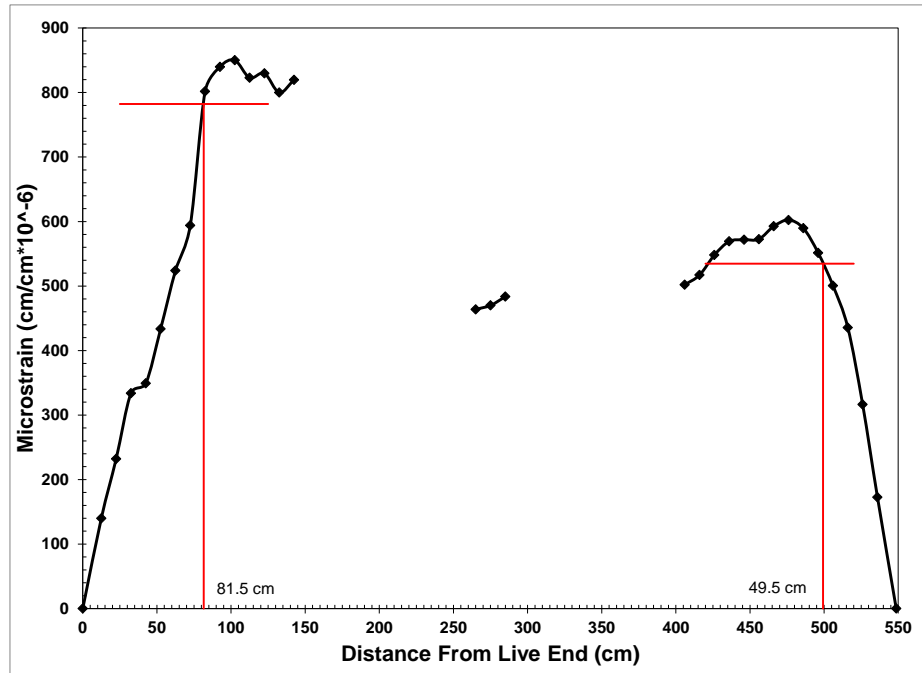


Figure D.1: Release strain profile with 95% AMS for specimen NSC-1

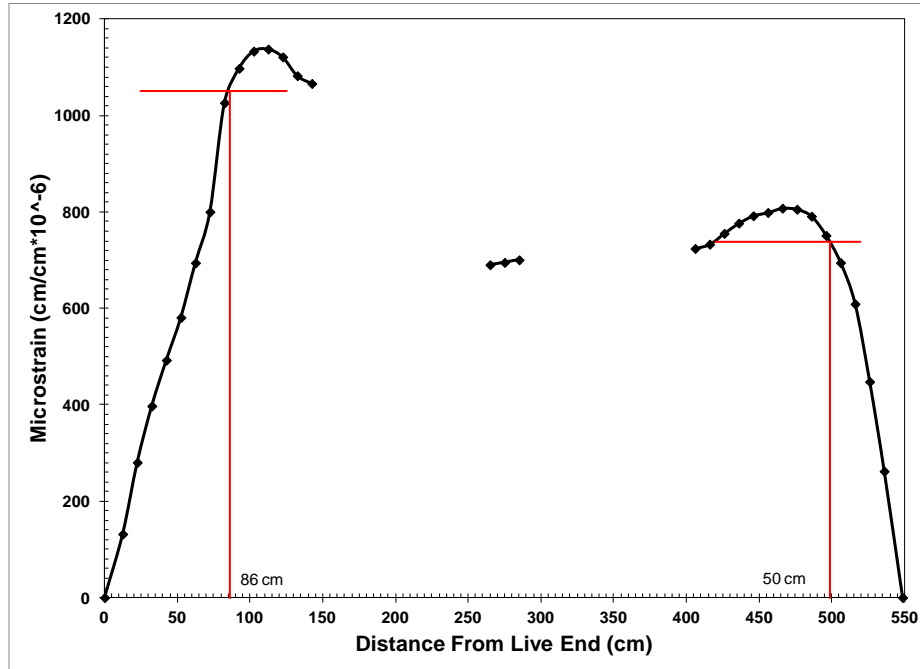


Figure D.2: 3-Day strain profile with 95% AMS for specimen NSC-1

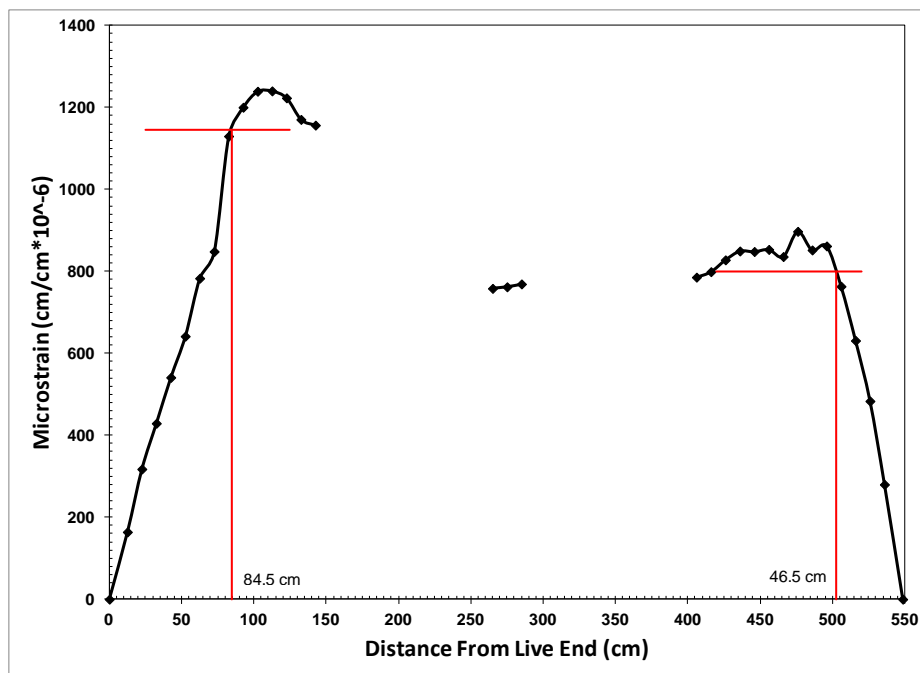


Figure D.3: 5-Day strain profile with 95% AMS for specimen NSC-1

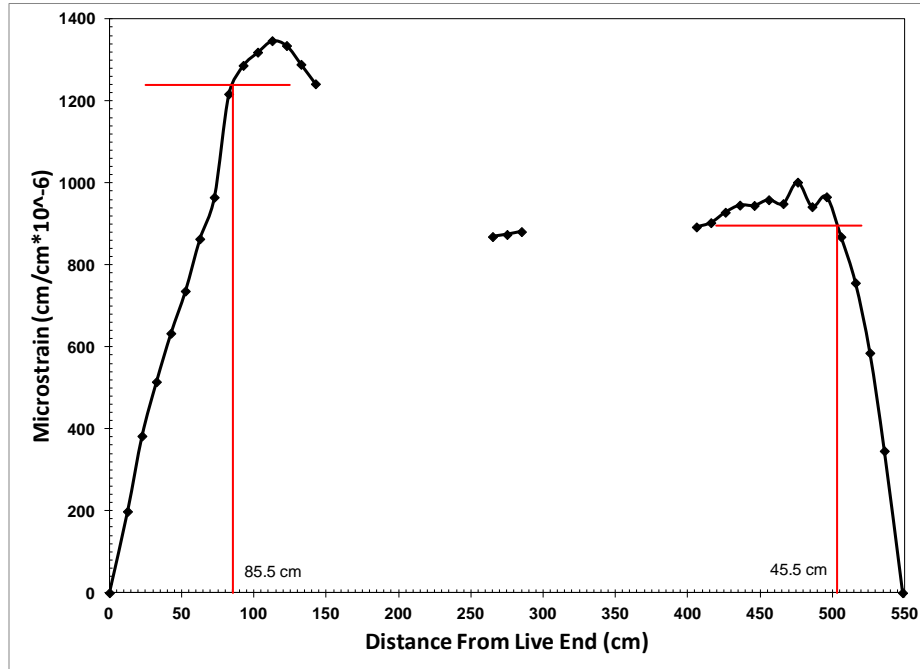


Figure D.4: 7-Day strain profile with 95% AMS for specimen NSC-1

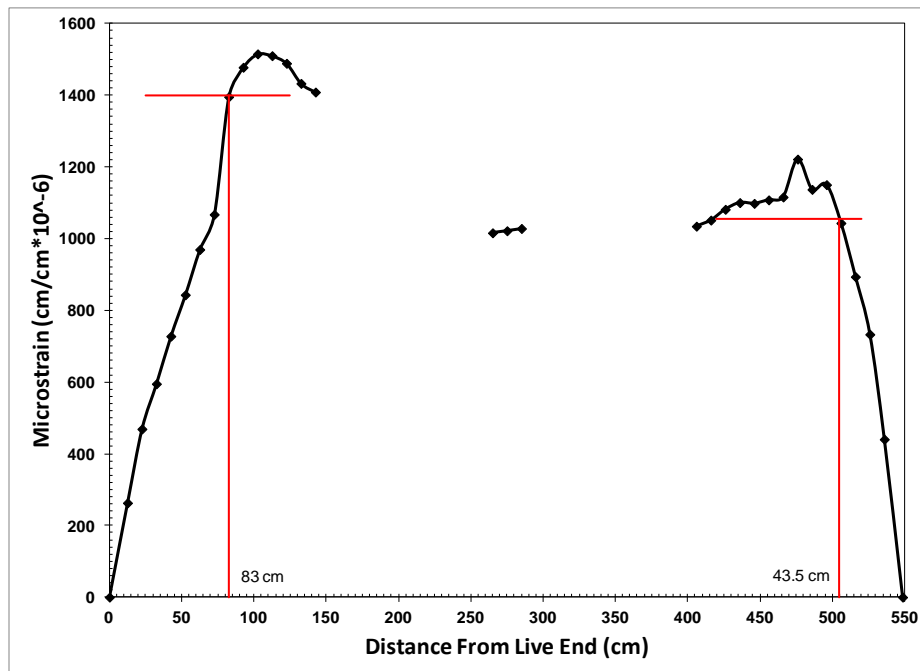


Figure D.5: 14-Day strain profile with 95% AMS for specimen NSC-1



### D.1.2 NSC-2

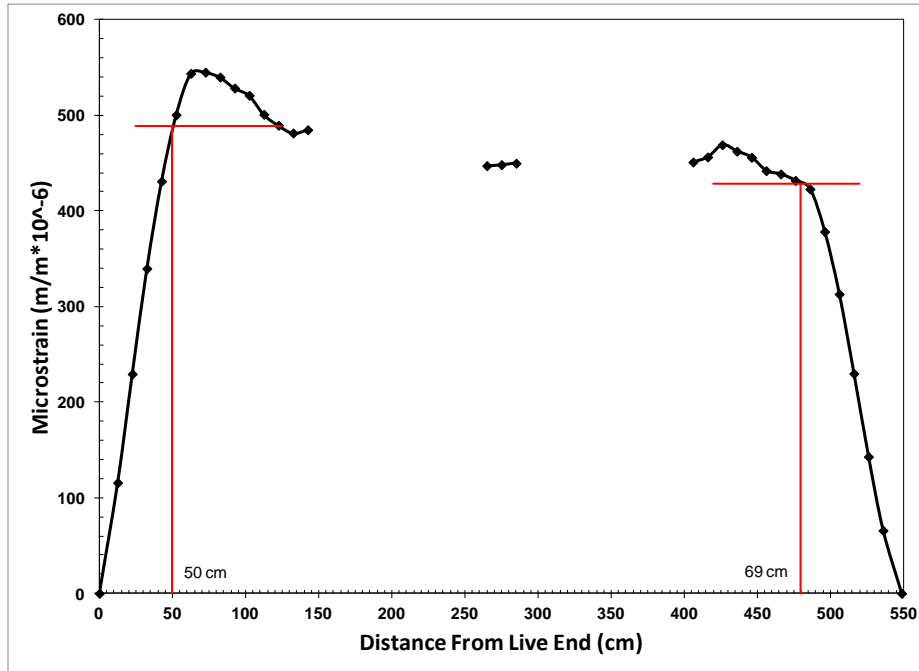


Figure D.6: Release strain profile with 95% AMS for specimen NSC-2

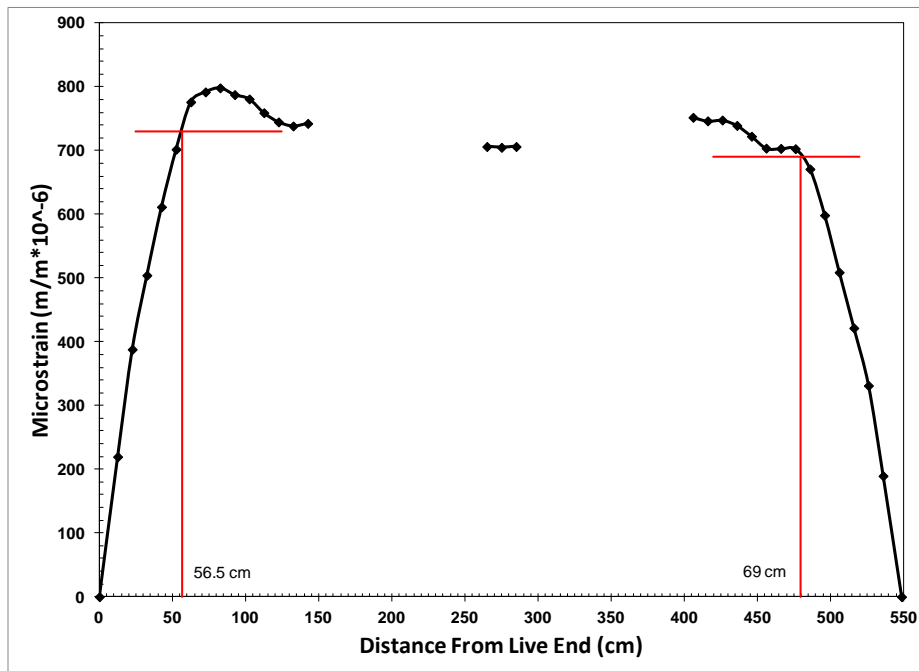


Figure D.7: 3-Day strain profile with 95% AMS for specimen NSC-2

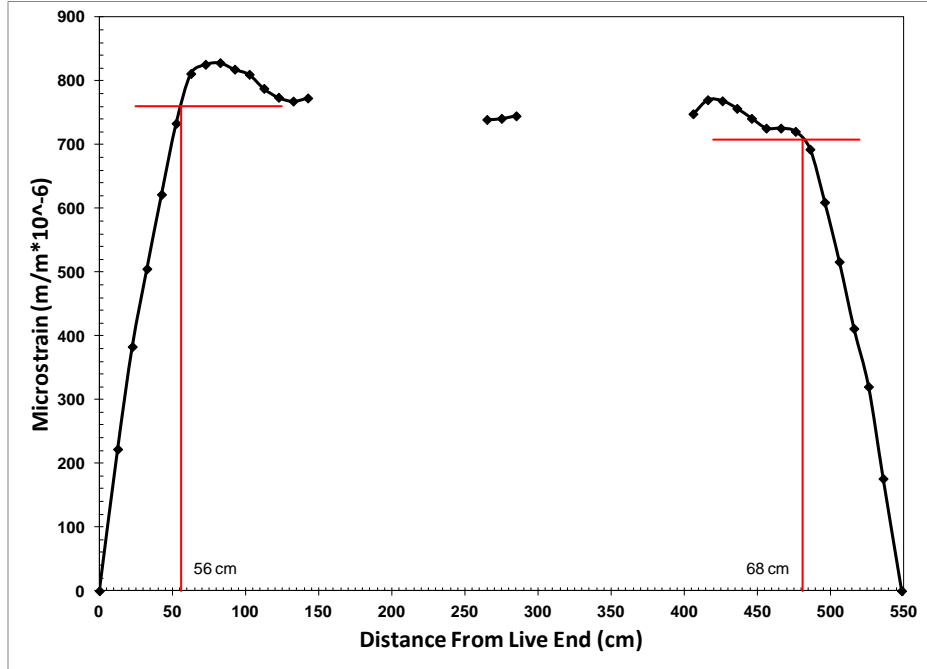


Figure D.8: 5-Day strain profile with 95% AMS for specimen NSC-2

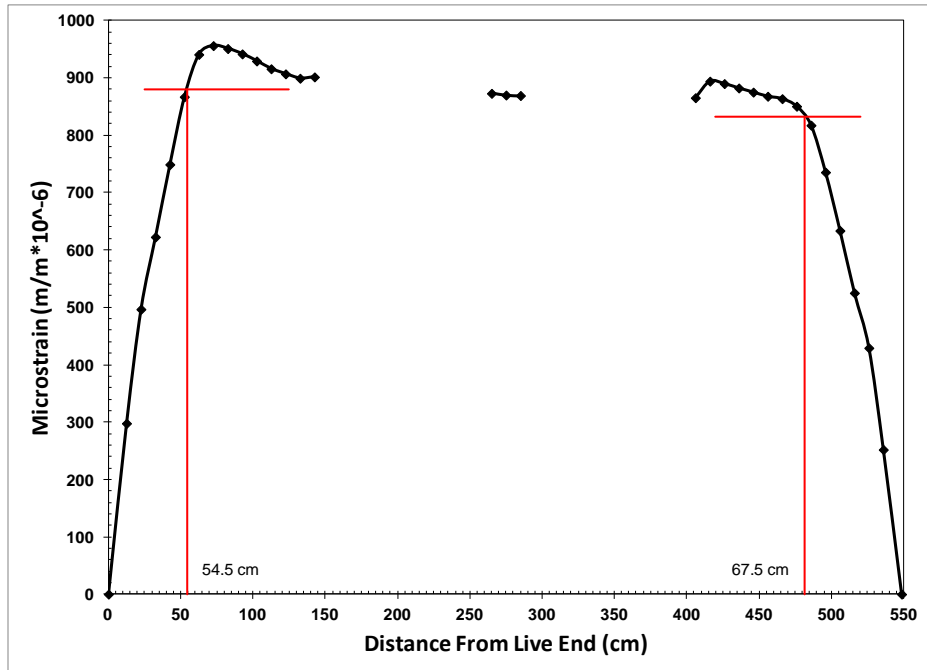


Figure D.9: 7-Day strain profile with 95% AMS for specimen NSC-2

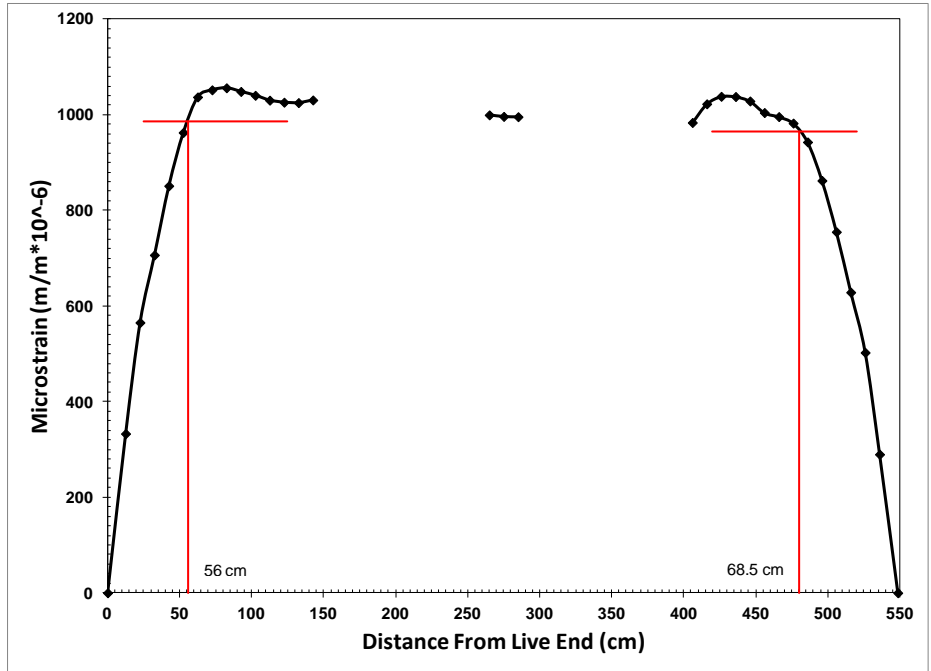


Figure D.10: 14-Day strain profile with 95% AMS for specimen NSC-2

### D.1.3 NSC-3

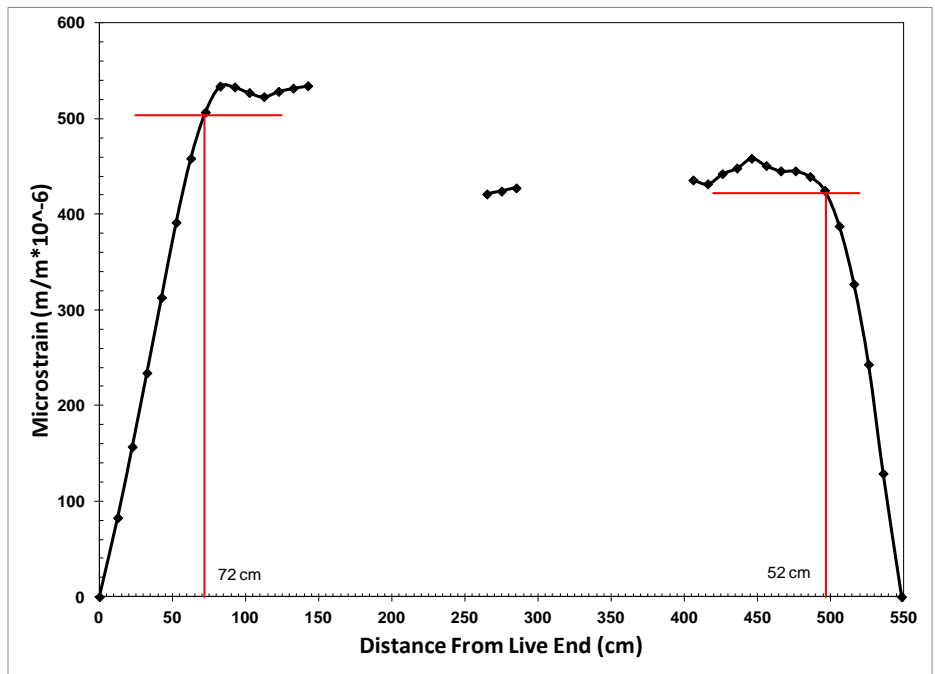


Figure D.11: Release strain profile with 95% AMS for specimen NSC-3

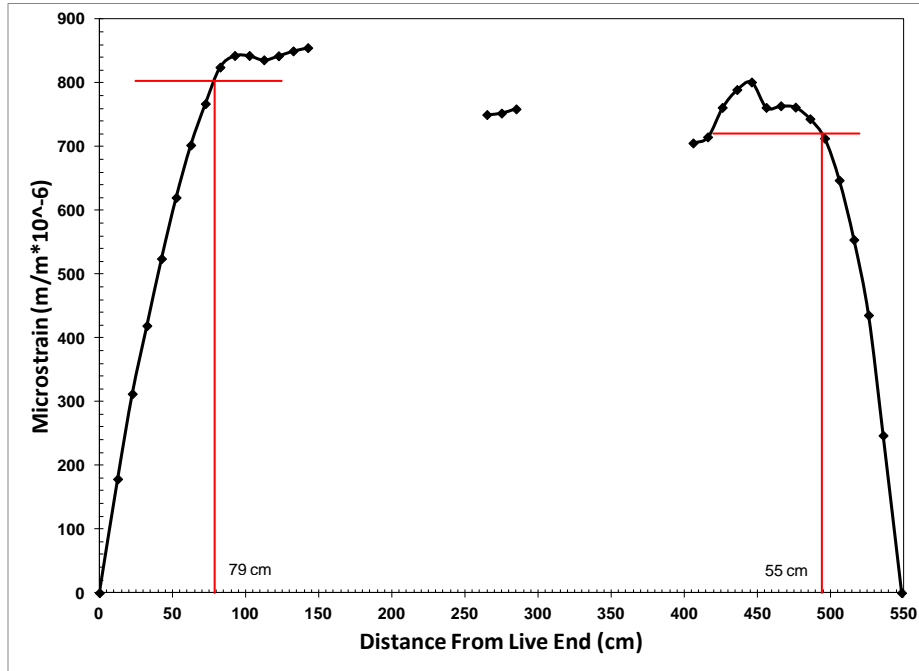


Figure D.12: 5-Day strain profile with 95% AMS for specimen NSC-3

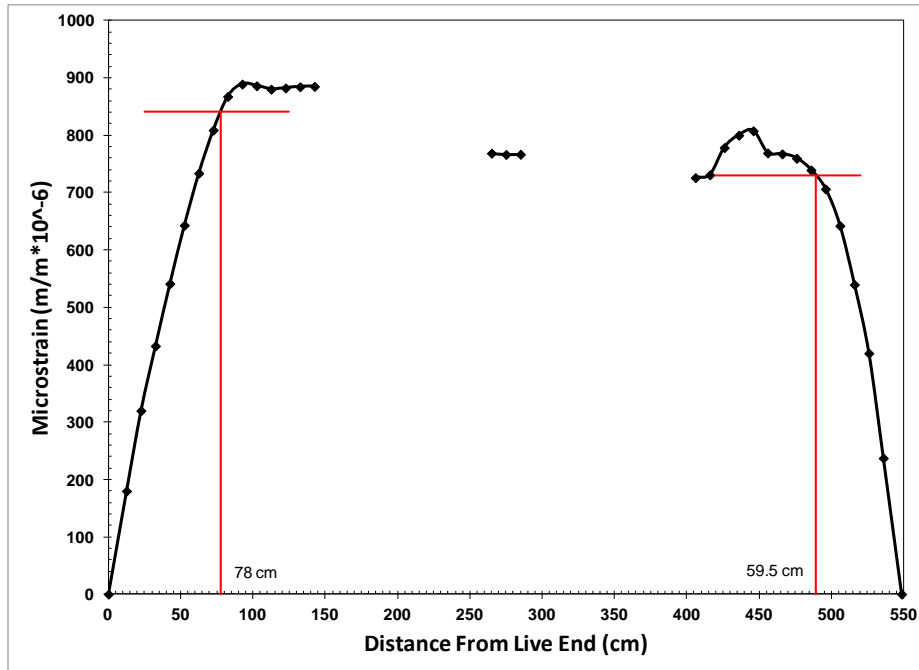


Figure D.13: 7-Day strain profile with 95% AMS for specimen NSC-3

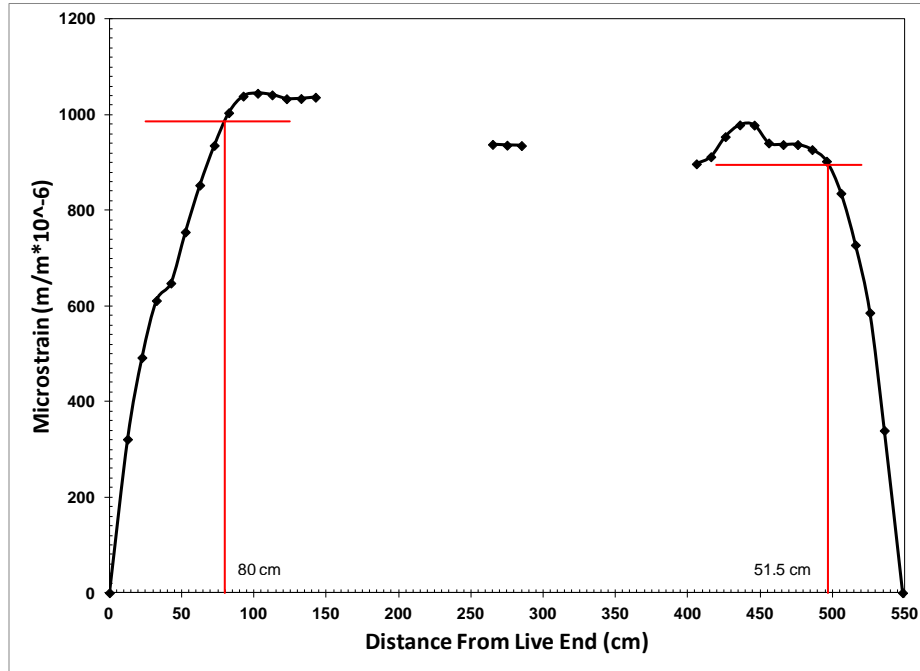


Figure D.14: 14-Day strain profile with 95% AMS for specimen NSC-3

#### D.1.4 NSC-4

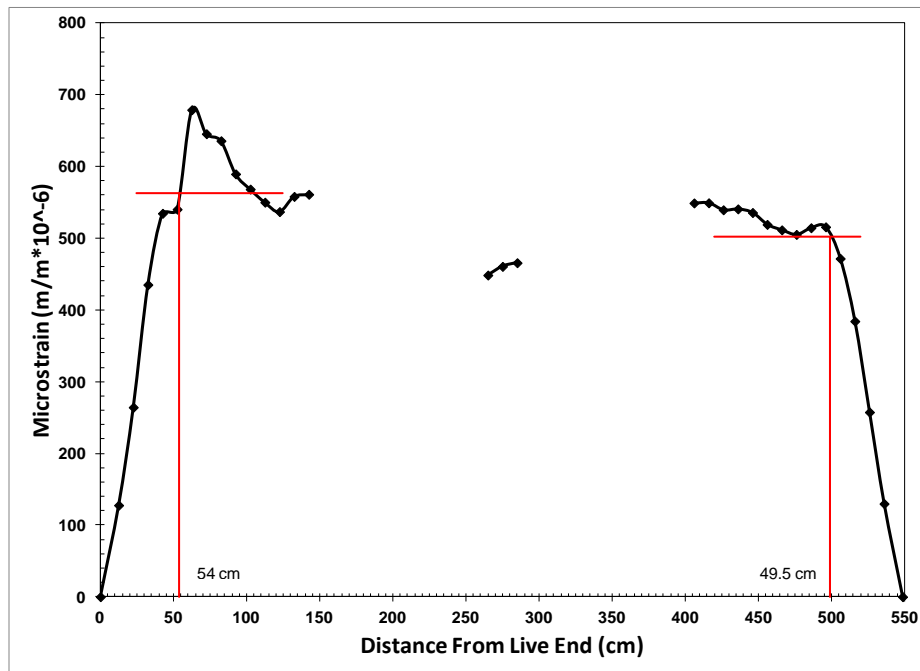


Figure D.15: Release strain profile with 95% AMS for specimen NSC-4

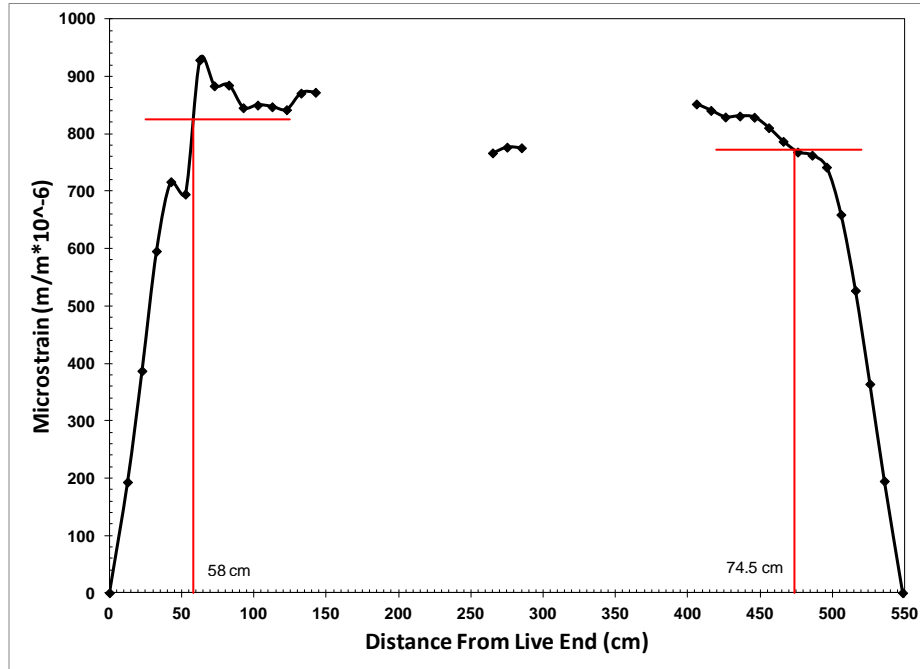


Figure D.16: 5-Day strain profile with 95% AMS for specimen NSC-4

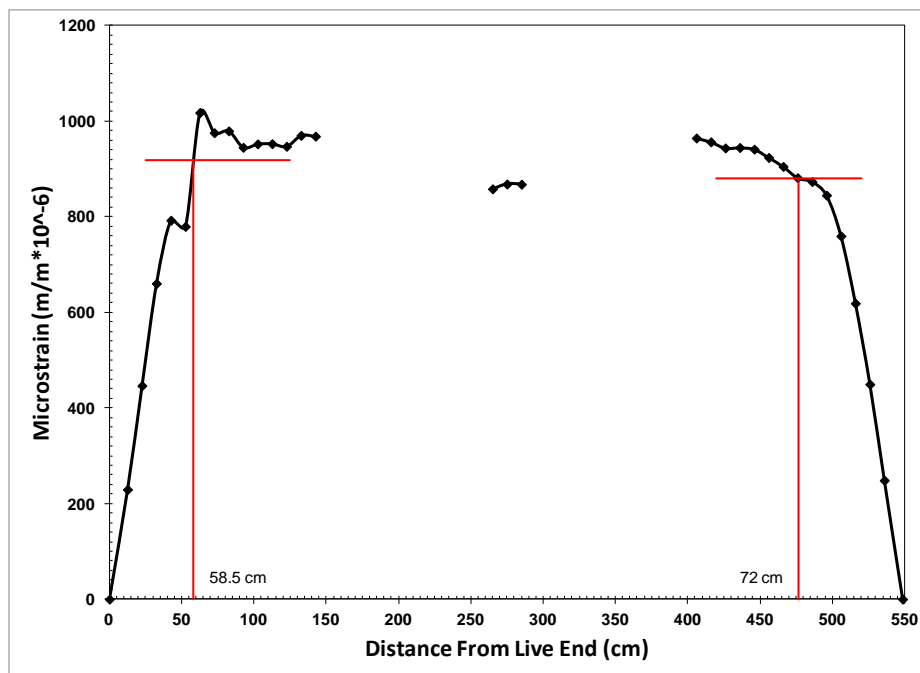


Figure D.17: 7-Day strain profile with 95% AMS for specimen NSC-4

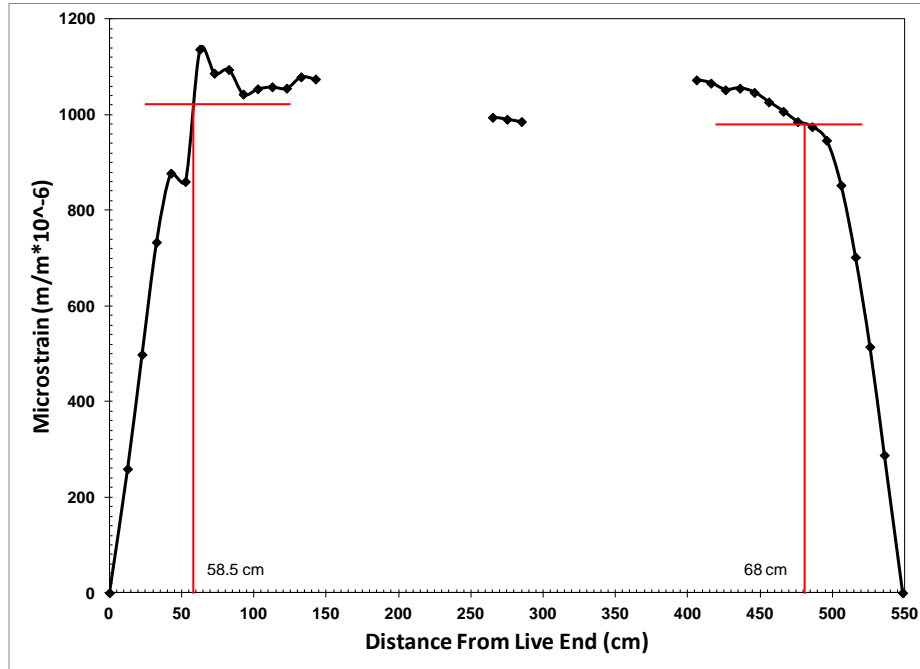


Figure D.18: 14-Day strain profile with 95% AMS for specimen NSC-4

### D.1.5 NSS-1

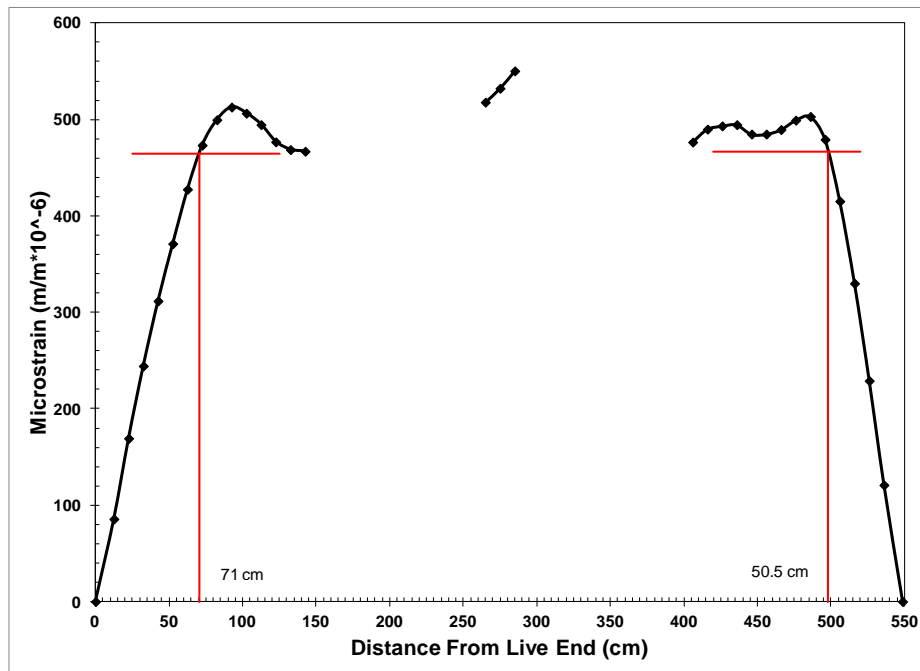


Figure D.19: Release strain profile with 95% AMS for specimen NSS-1

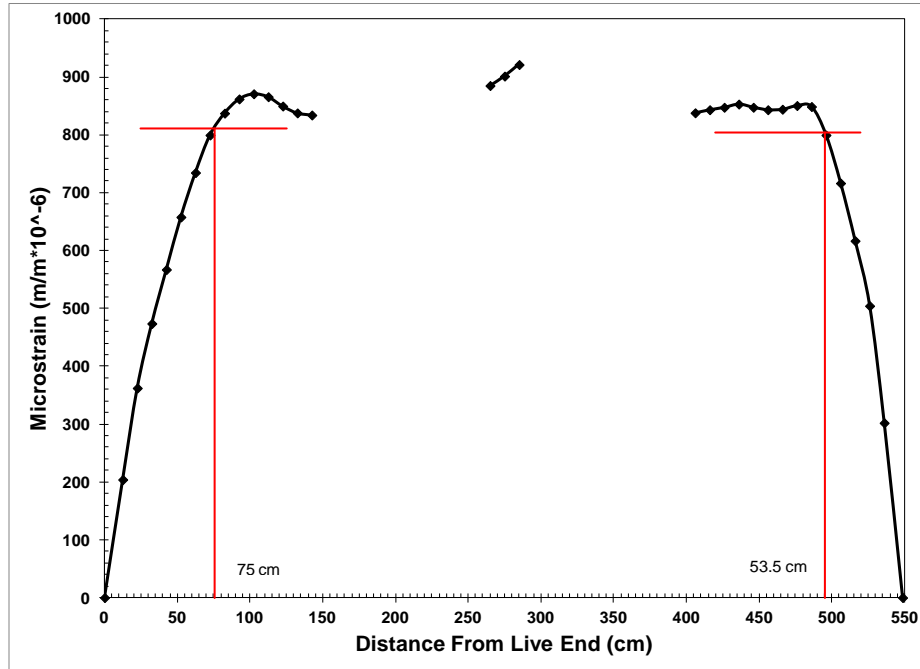


Figure D.20: 3-Day strain profile with 95% AMS for specimen NSS-1

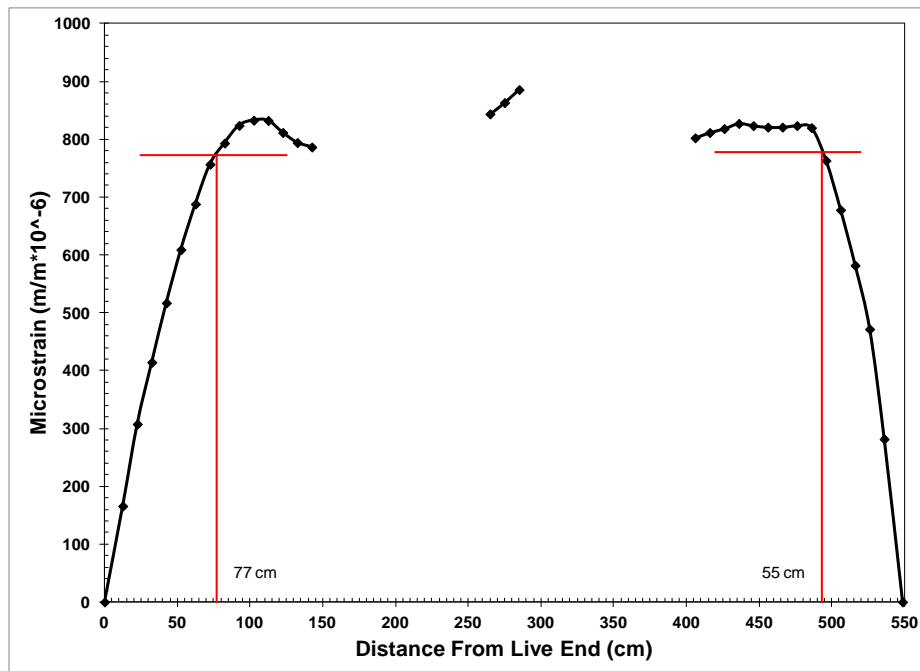


Figure D.21: 5-Day strain profile with 95% AMS for specimen NSS-1



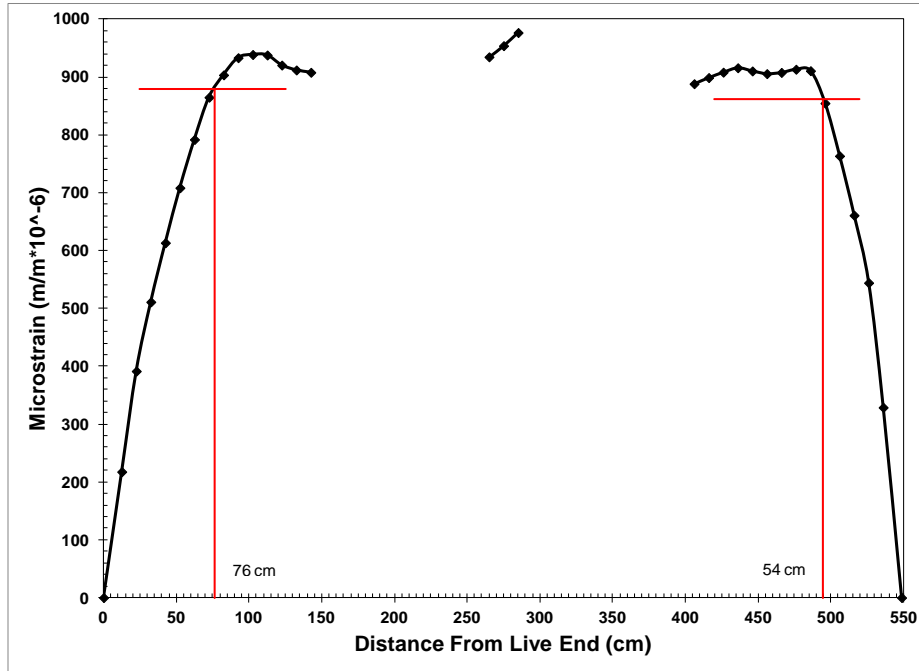


Figure D.22: 7-Day strain profile with 95% AMS for specimen NSS-1

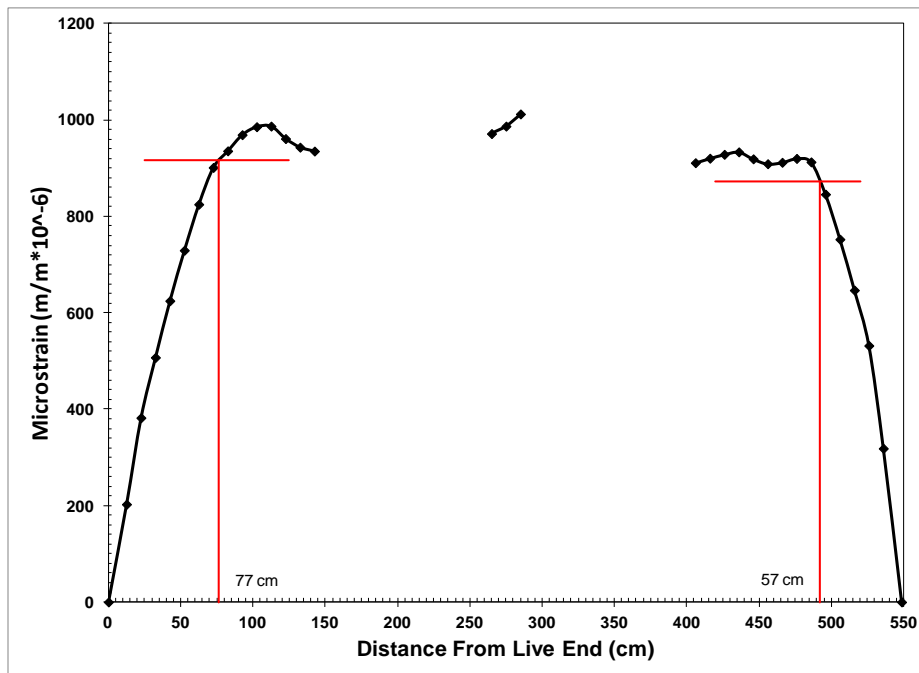


Figure D.23: 14-Day strain profile with 95% AMS for specimen NSS-1

### D.1.6 NSS-2

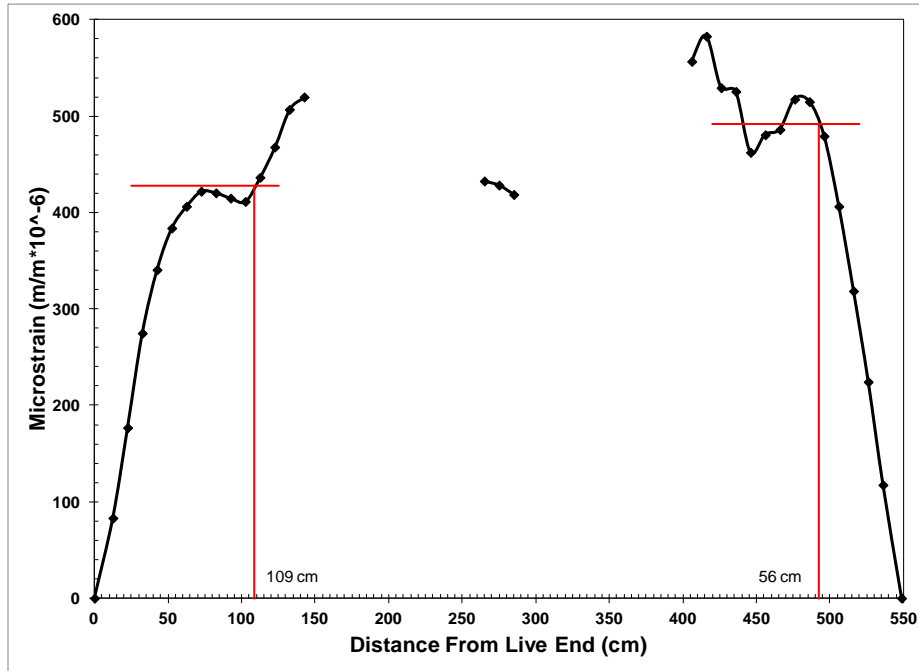


Figure D.24: Release strain profile with 95% AMS for specimen NSS-2

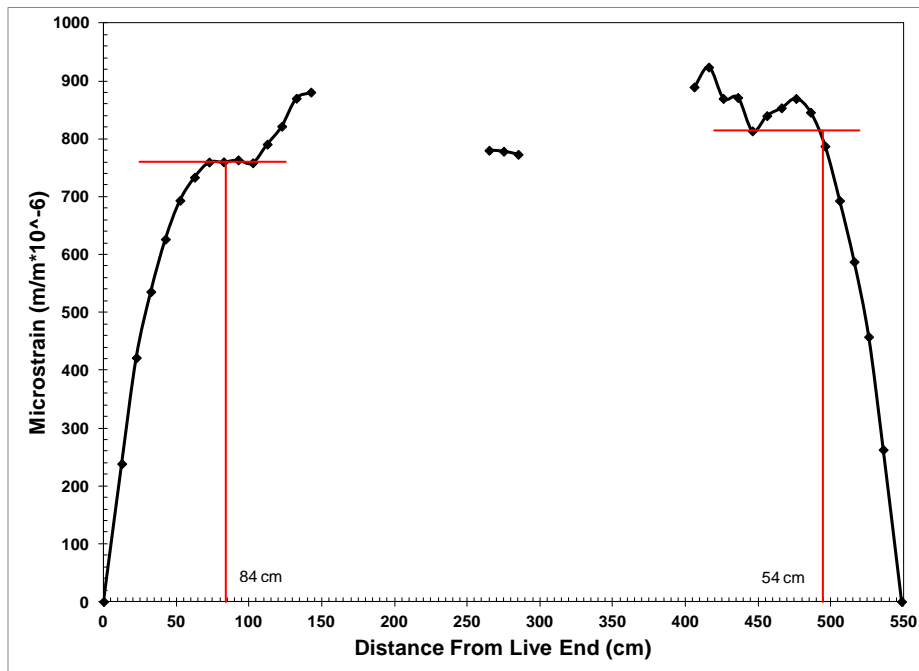


Figure D.25: 3-Day strain profile with 95% AMS for specimen NSS-2

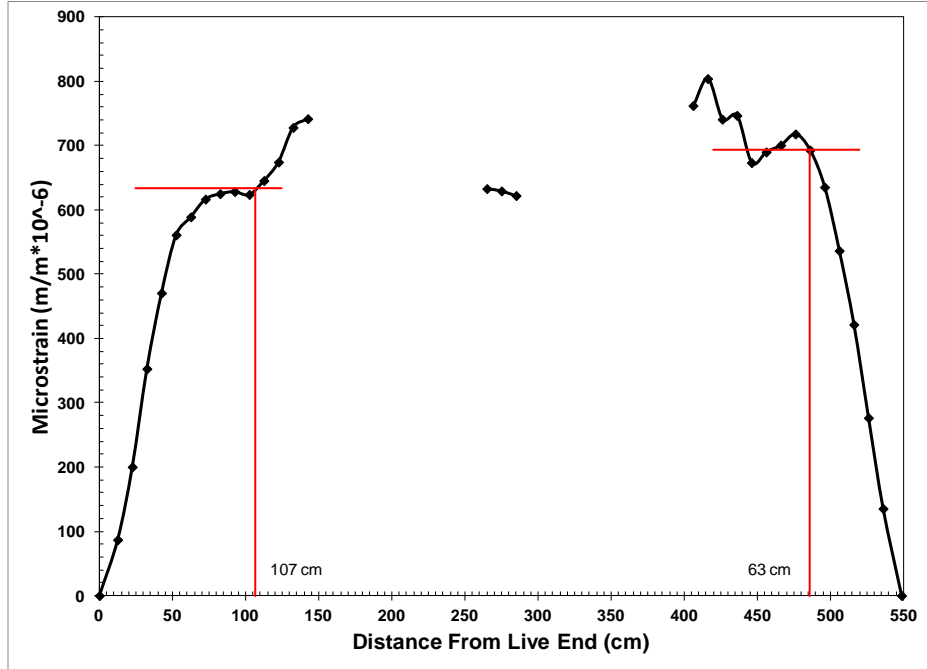


Figure D.26: 5-Day strain profile with 95% AMS for specimen NSS-2

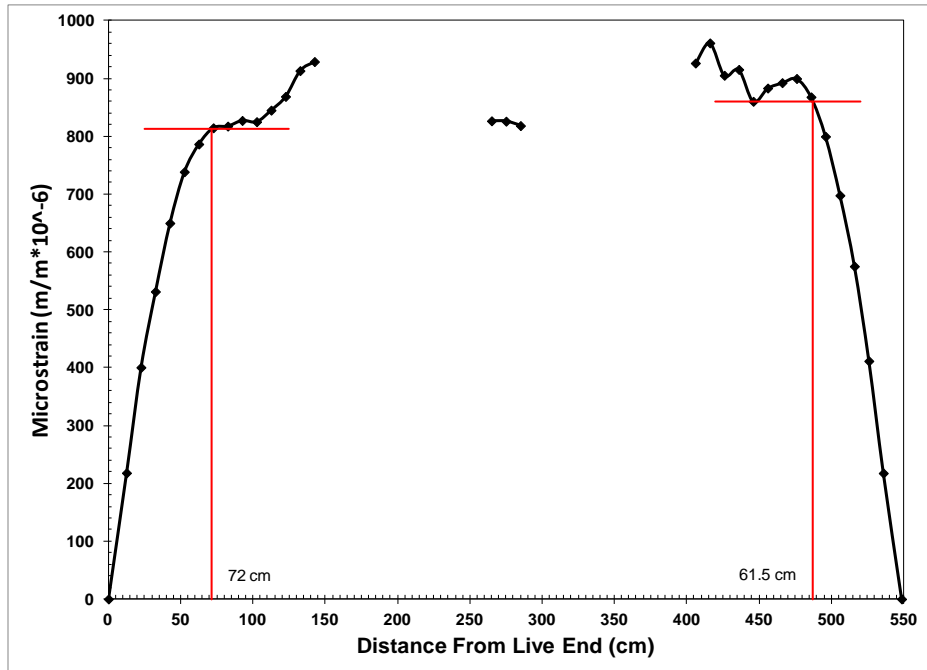


Figure D.27: 7-Day strain profile with 95% AMS for specimen NSS-2

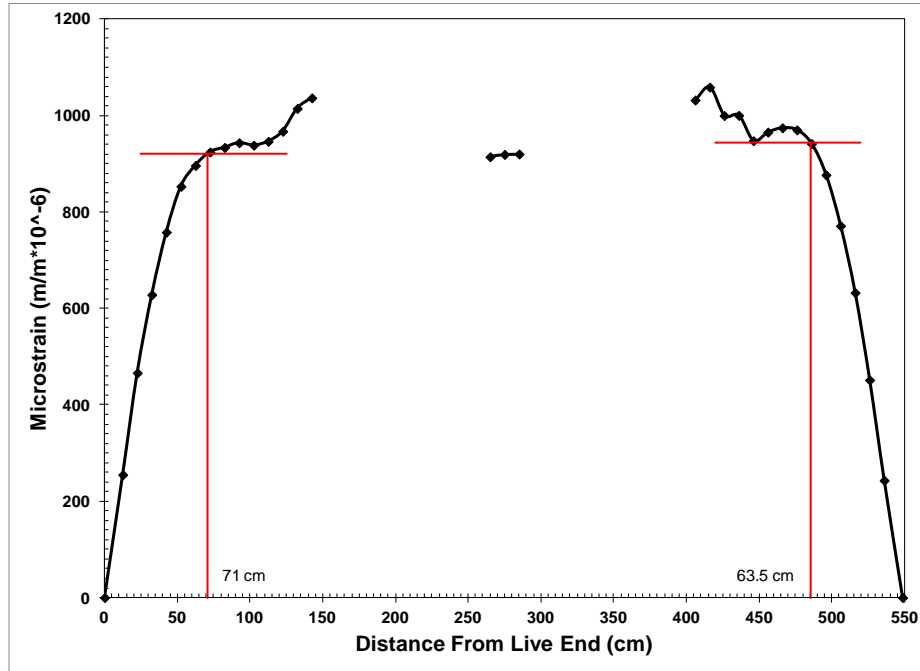


Figure D.28: 14-Day strain profile with 95% AMS for specimen NSS-2

### D.1.7 NSS-3

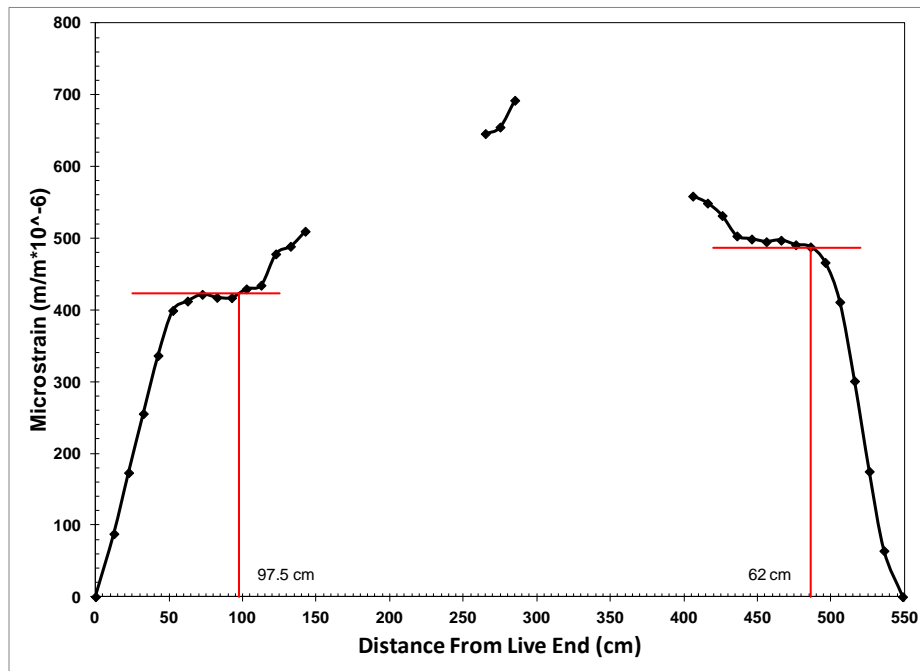


Figure D.29: Release strain profile with 95% AMS for specimen NSS-3

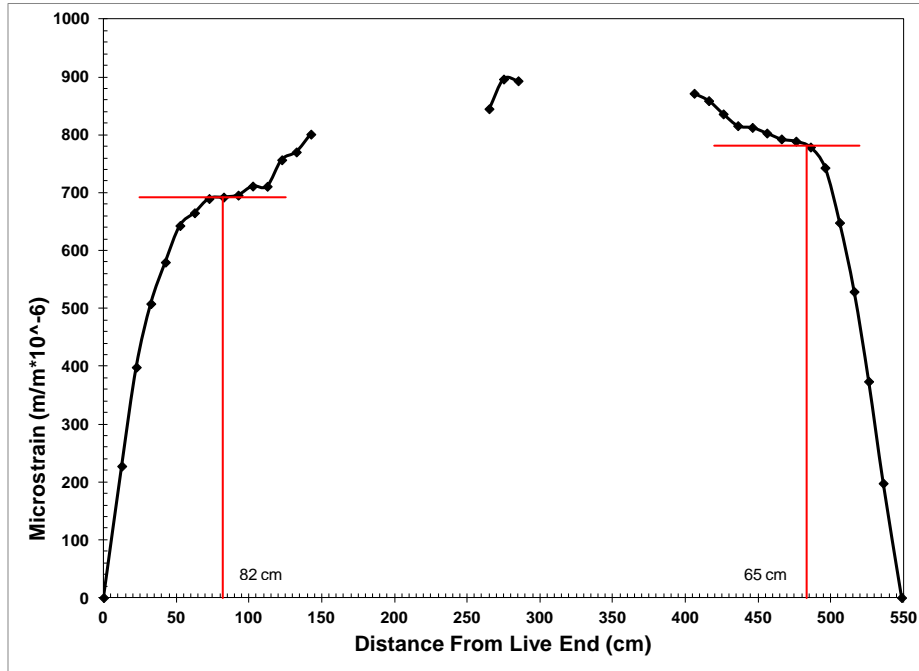


Figure D.30: 3-Day strain profile with 95% AMS for specimen NSS-3

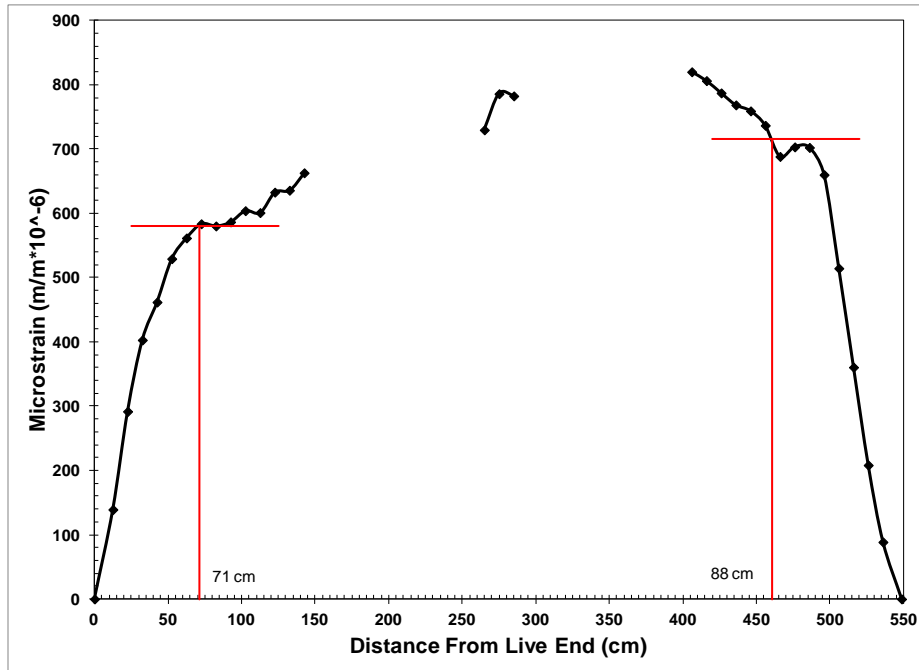


Figure D.31: 5-Day strain profile with 95% AMS for specimen NSS-3

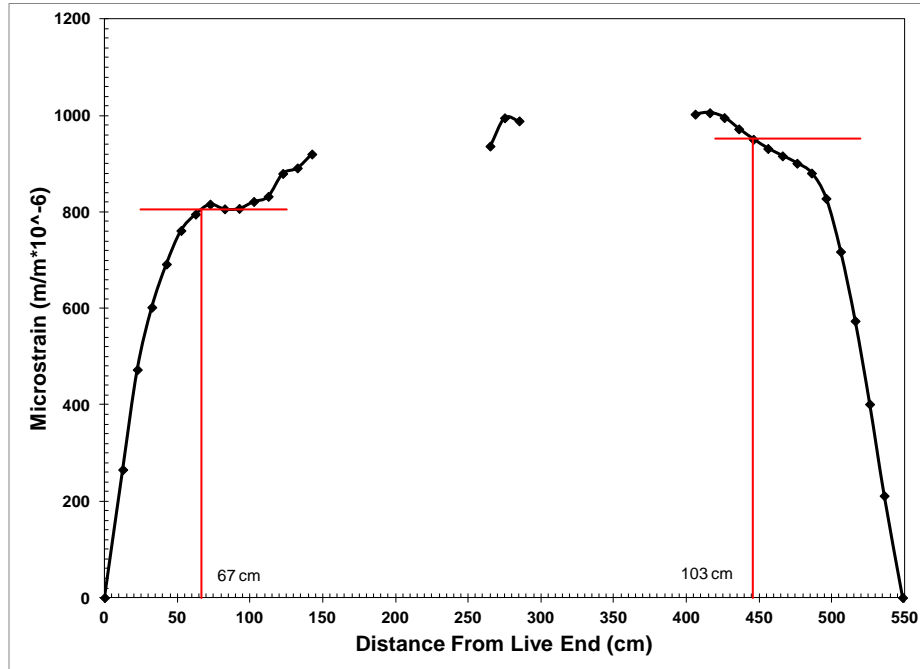


Figure D.32: 7-Day strain profile with 95% AMS for specimen NSS-3

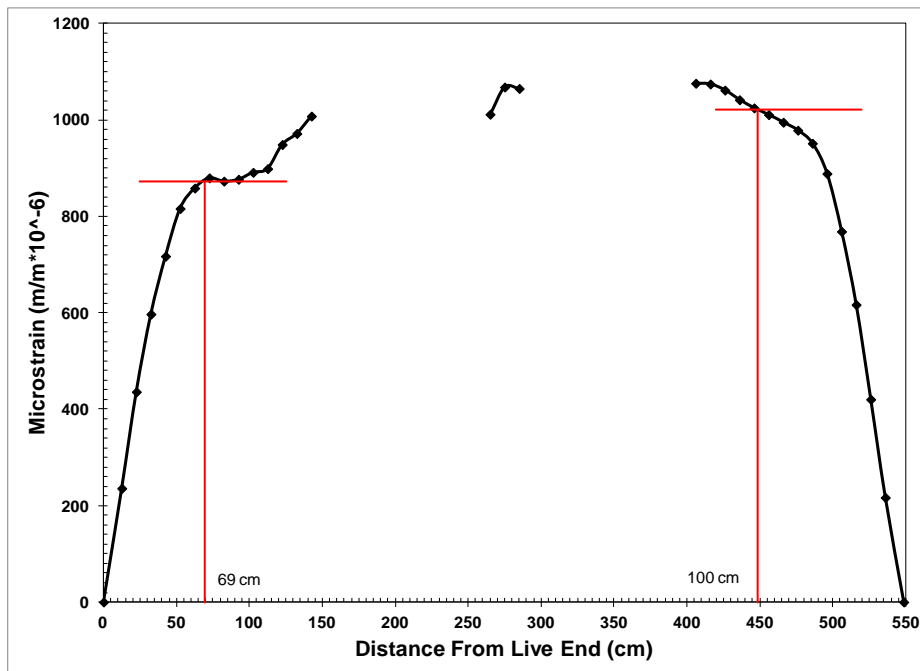


Figure D.33: 14-Day strain profile with 95% AMS for specimen NSS-3

### D.1.8 NSS-4

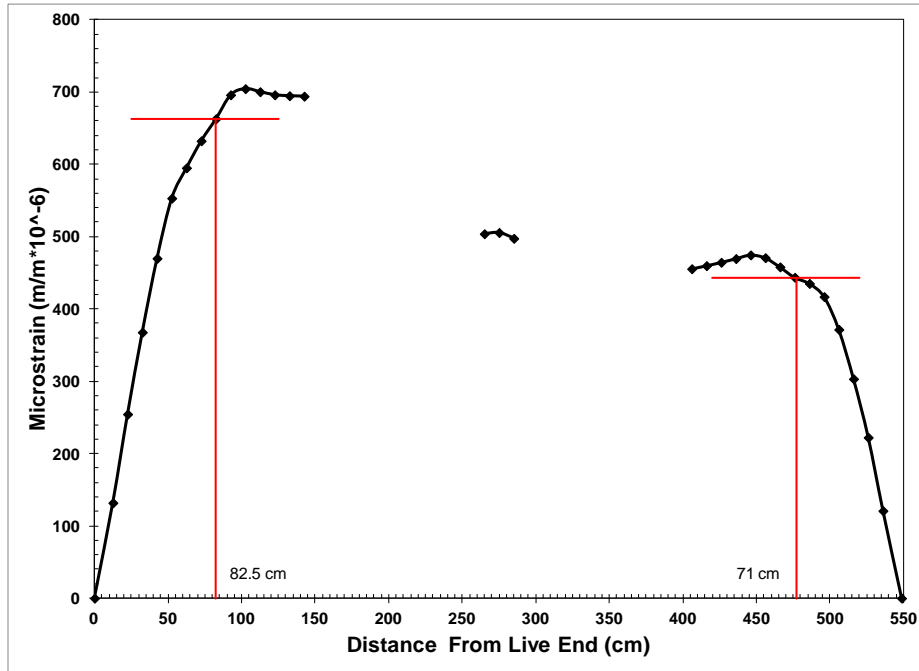


Figure D.34: Release strain profile with 95% AMS for specimen NSS-4

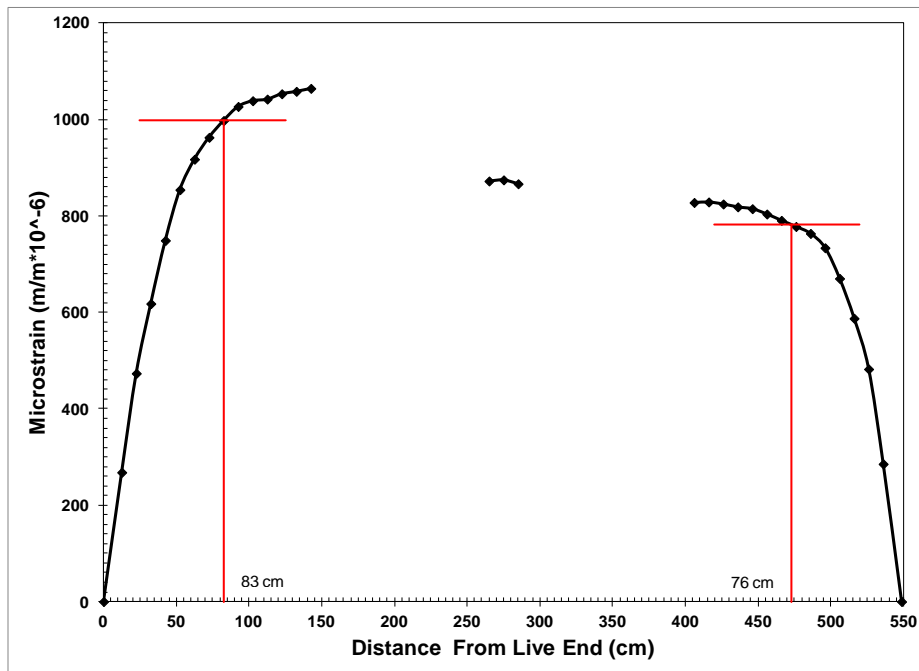


Figure D.35: 3-Day strain profile with 95% AMS for specimen NSS-4

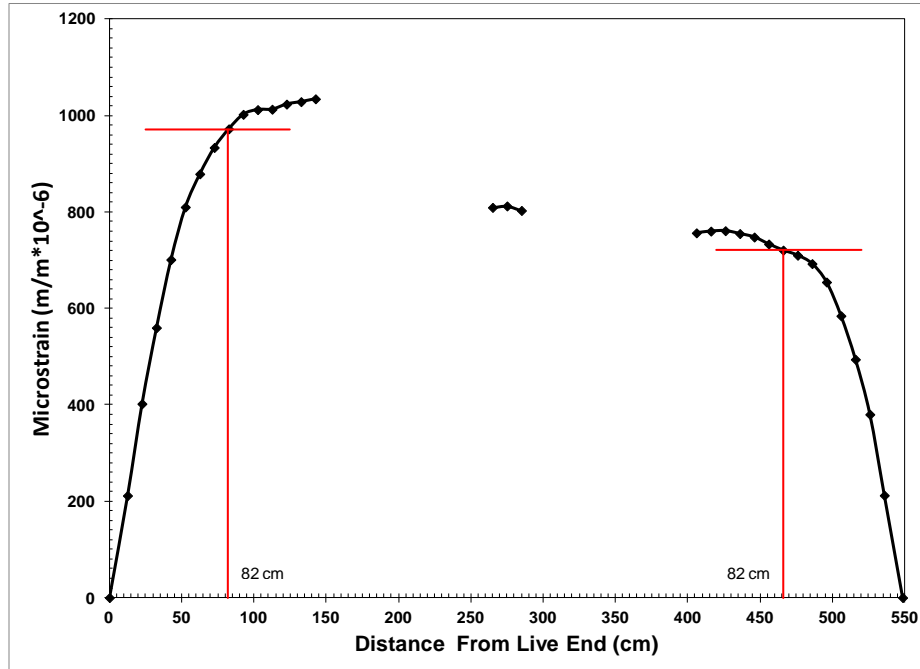


Figure D.36: 5-Day strain profile with 95% AMS for specimen NSS-4

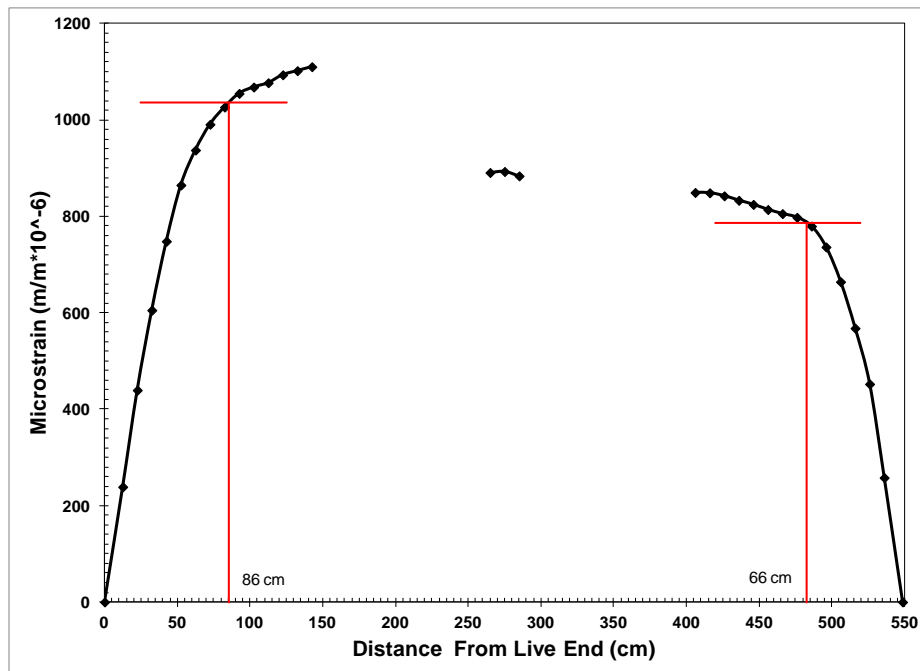


Figure D.37: 7-Day strain profile with 95% AMS for specimen NSS-4



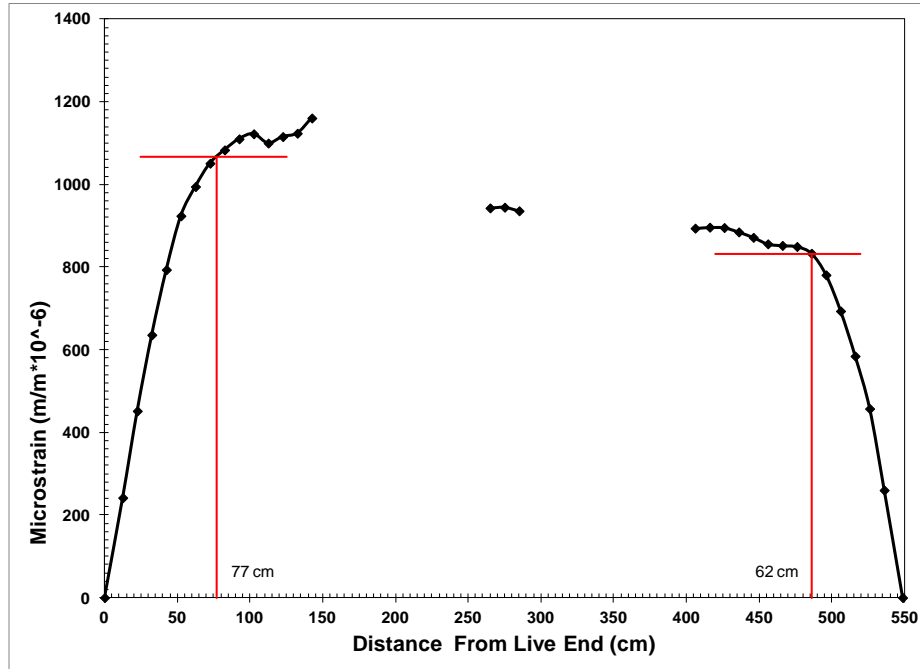


Figure D.38: 14-Day strain profile with 95% AMS for specimen NSS-4

#### D.1.9 NSS-5

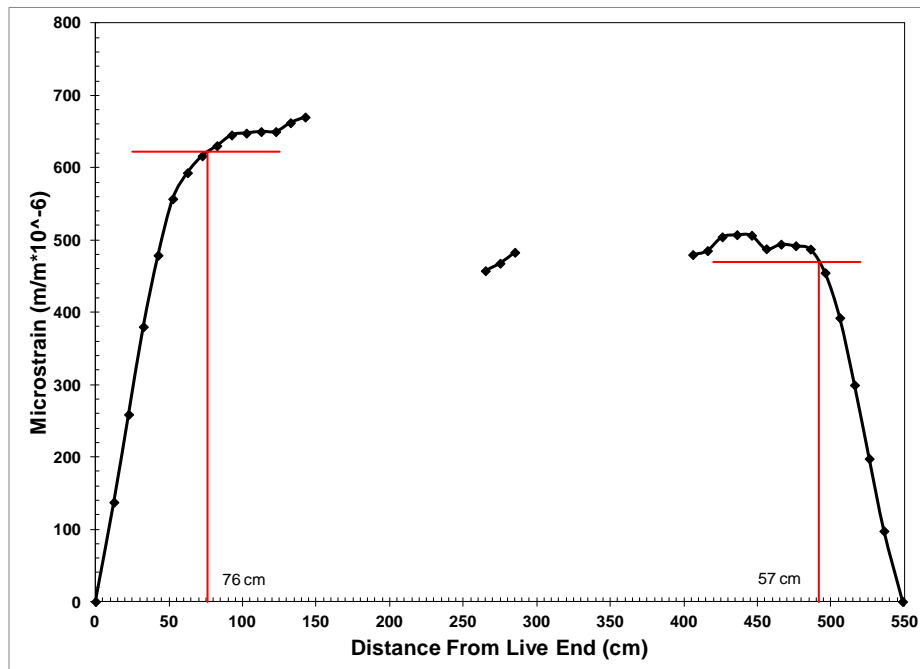


Figure D.39: Release strain profile with 95% AMS for specimen NSS-5

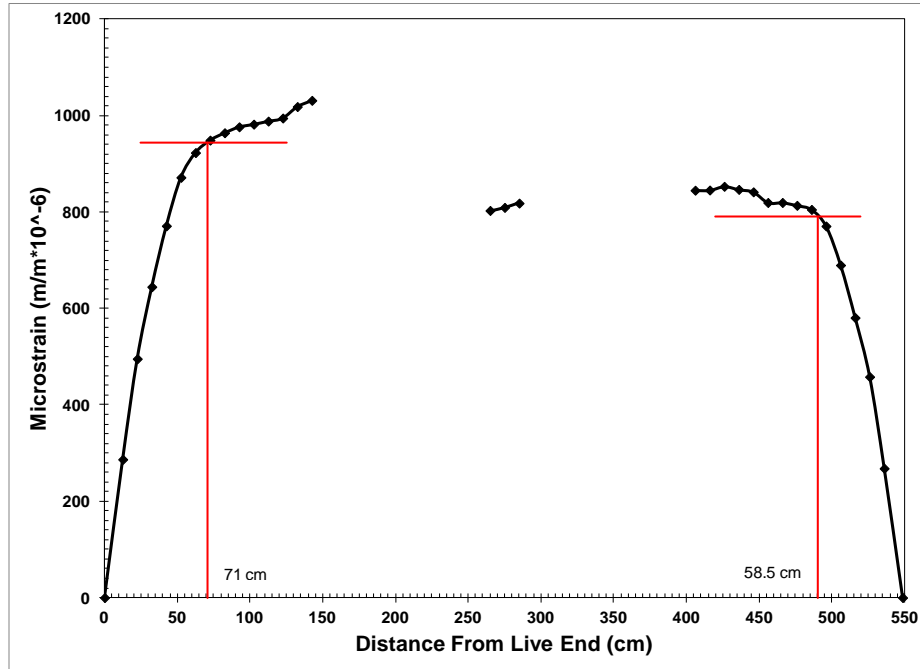


Figure D.40: 3-Day strain profile with 95% AMS for specimen NSS-5

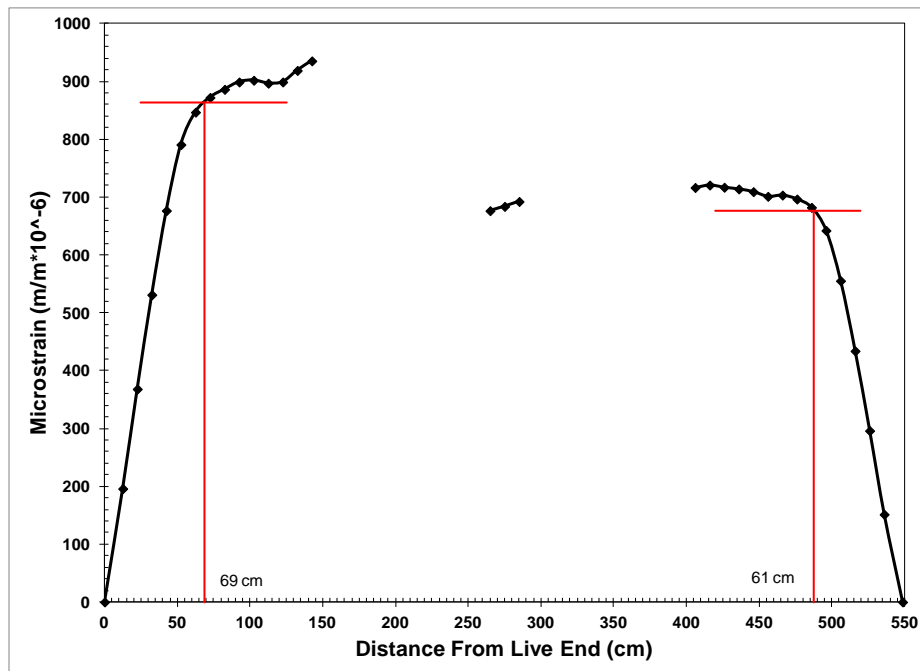


Figure D.41: 5-Day strain profile with 95% AMS for specimen NSS-5

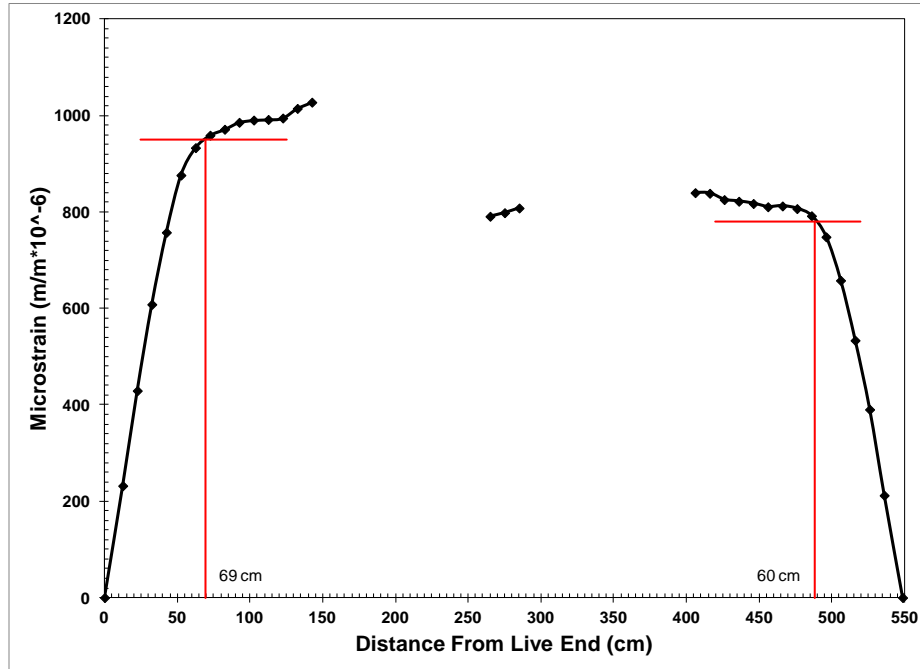


Figure D.42: 7-Day strain profile with 95% AMS for specimen NSS-5

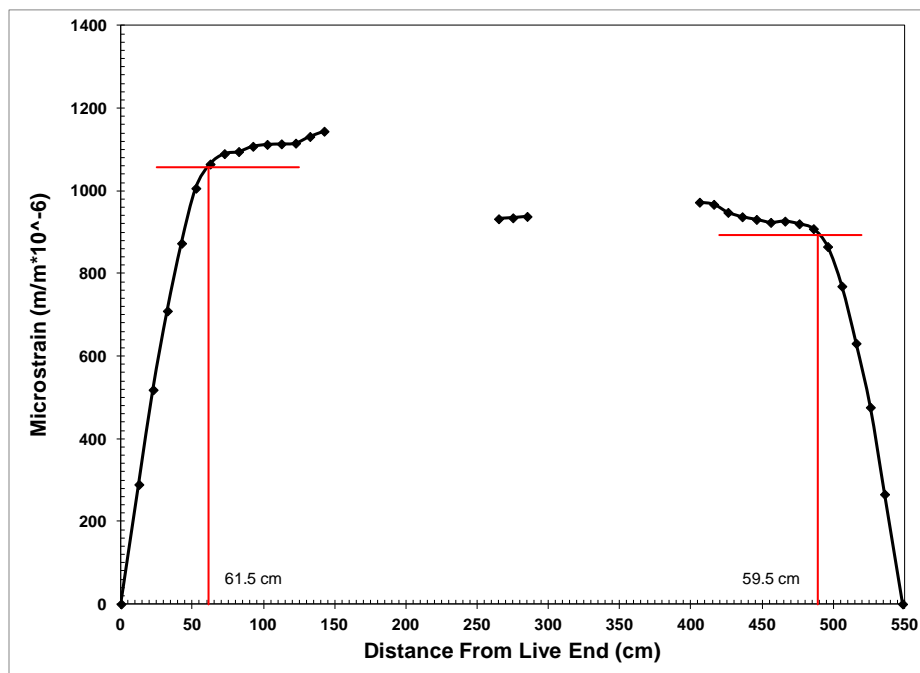


Figure D.43: 14-Day strain profile with 95% AMS for specimen NSS-5

### D.1.10 NSL-1

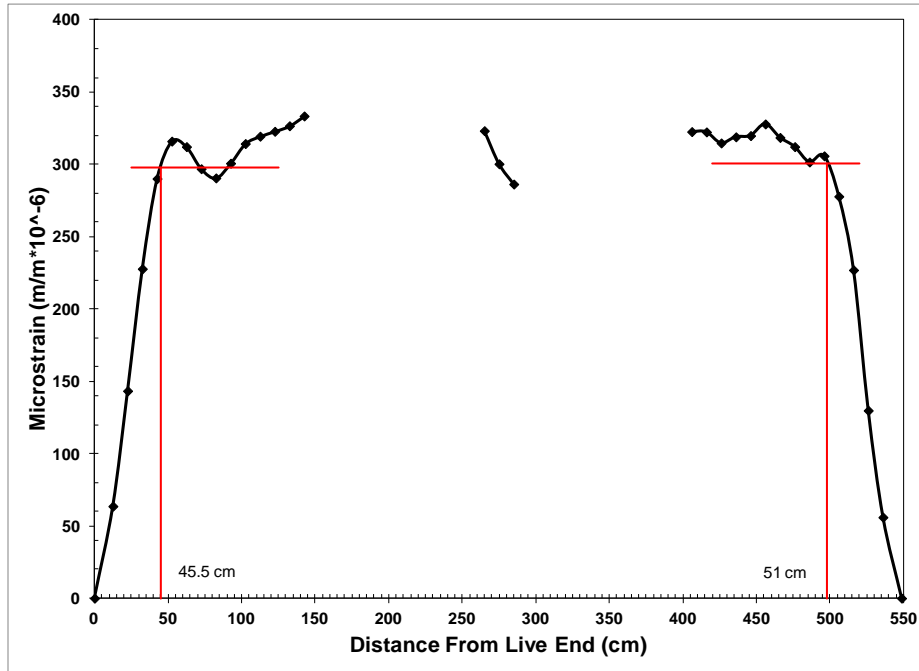


Figure D.44: Release strain profile with 95% AMS for specimen NSL-1

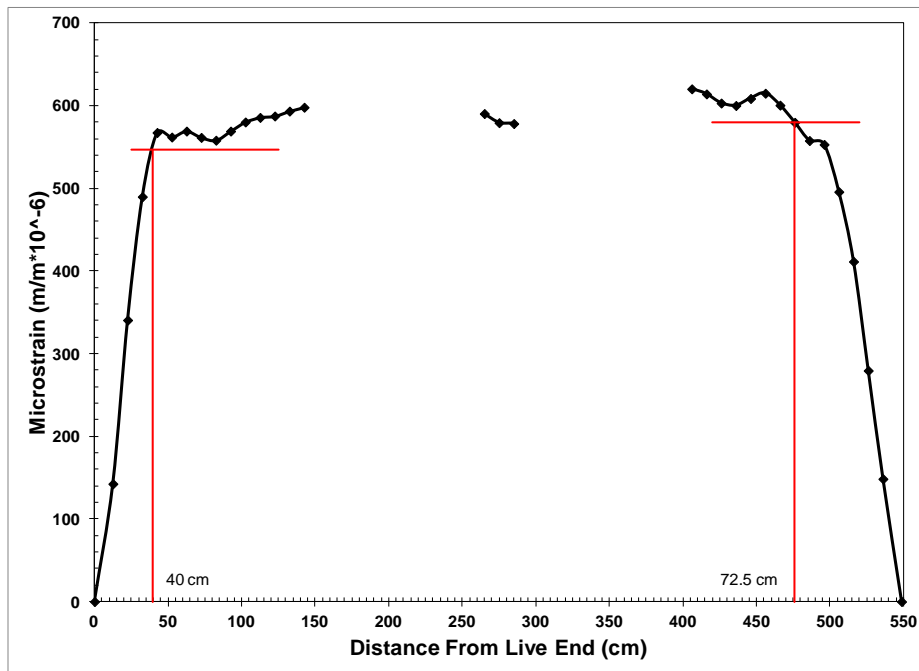


Figure D.45: 3-Day strain profile with 95% AMS for specimen NSL-1

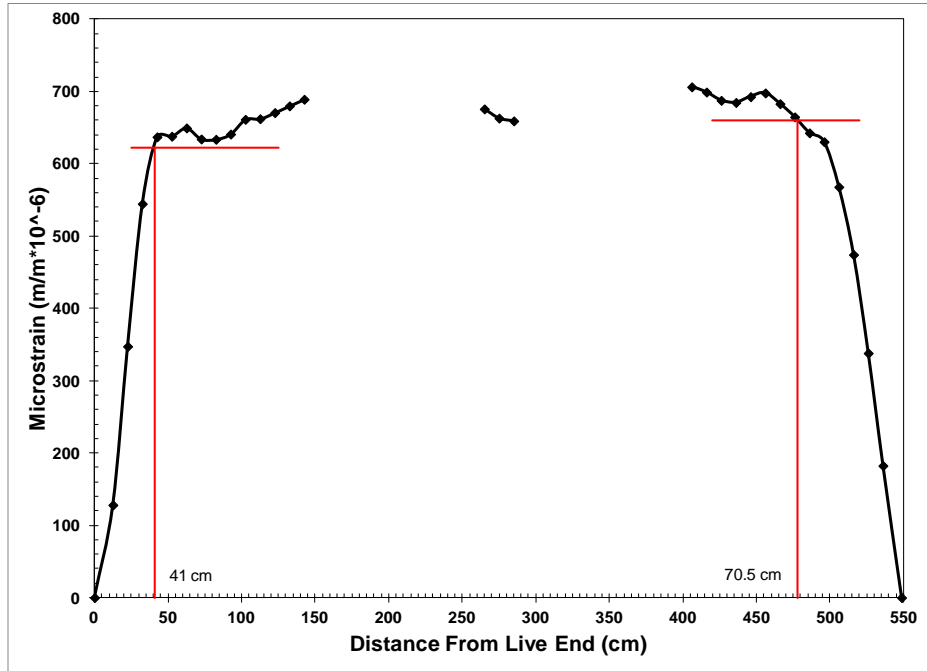


Figure D.46: 5-Day strain profile with 95% AMS for specimen NSL-1

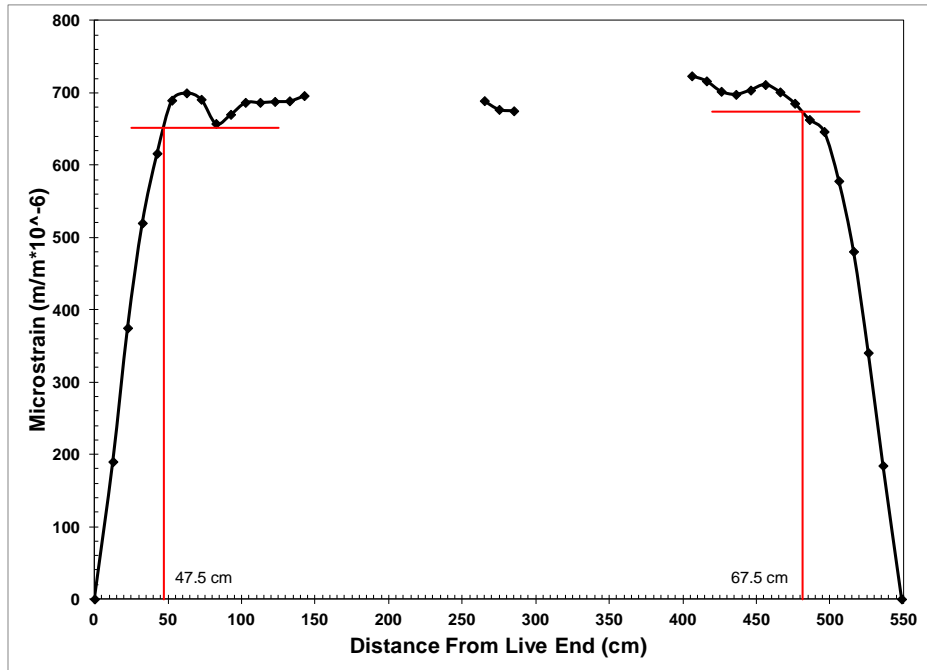


Figure D.47: 7-Day strain profile with 95% AMS for specimen NSL-1

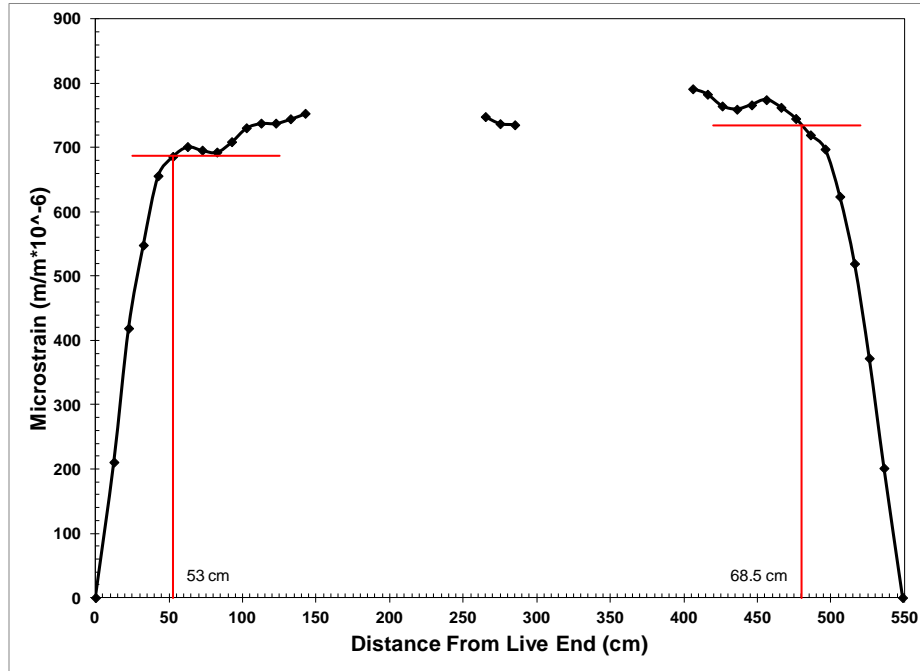


Figure D.48: 14-Day strain profile with 95% AMS for specimen NSL-1

#### D.1.11 NSL-2

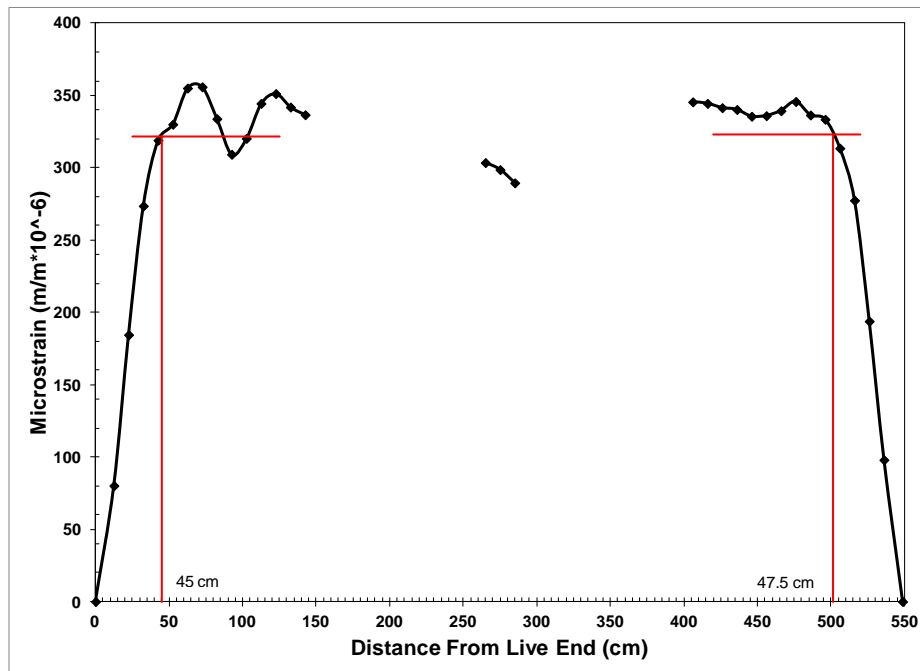


Figure D.49: Release strain profile with 95% AMS for specimen NSL-2

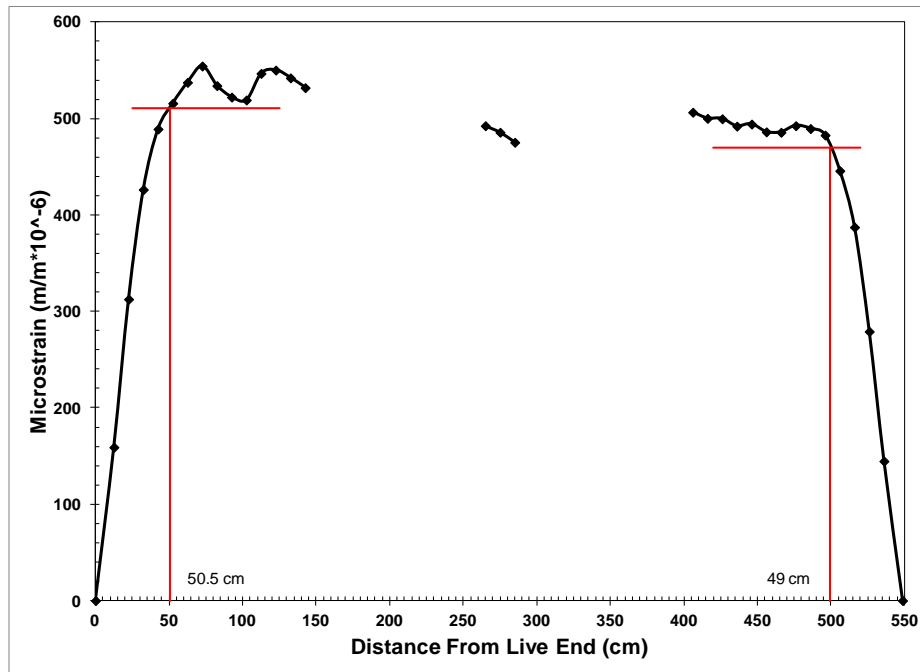


Figure D.50: 3-Day strain profile with 95% AMS for specimen NSL-2

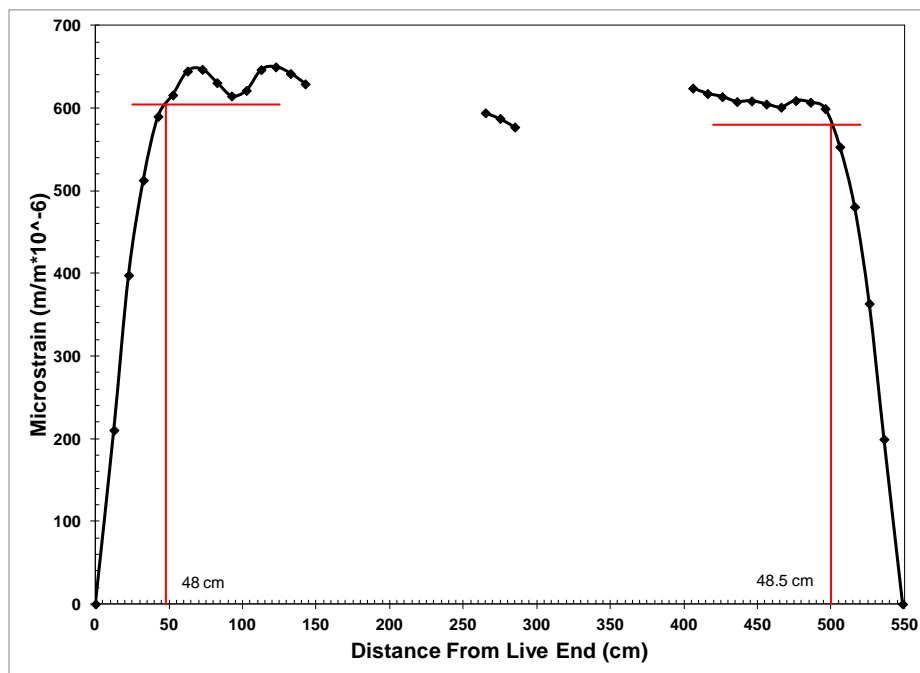


Figure D.51: 5-Day strain profile with 95% AMS for specimen NSL-2

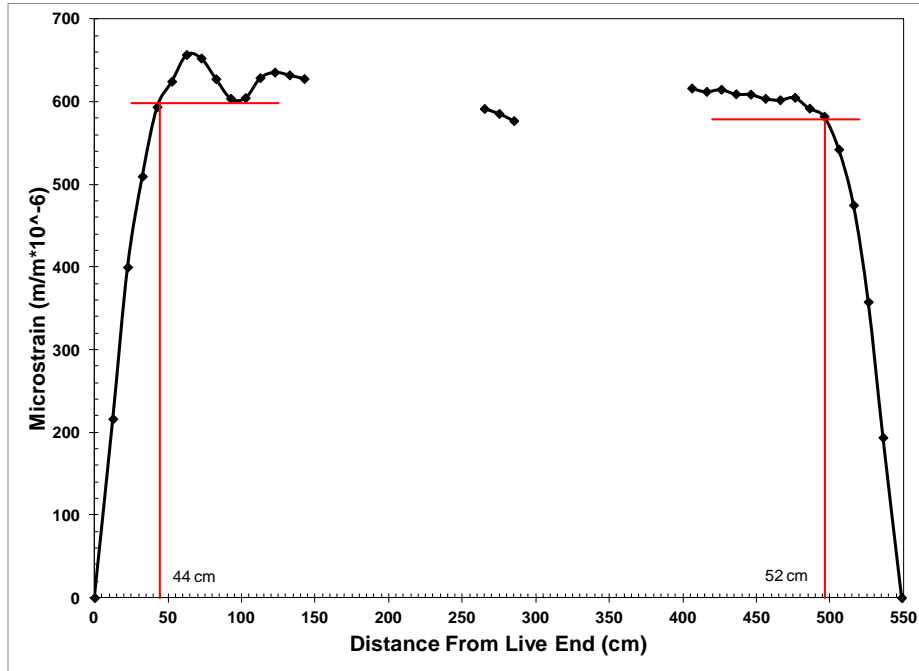


Figure D.52: 7-Day strain profile with 95% AMS for specimen NSL-2

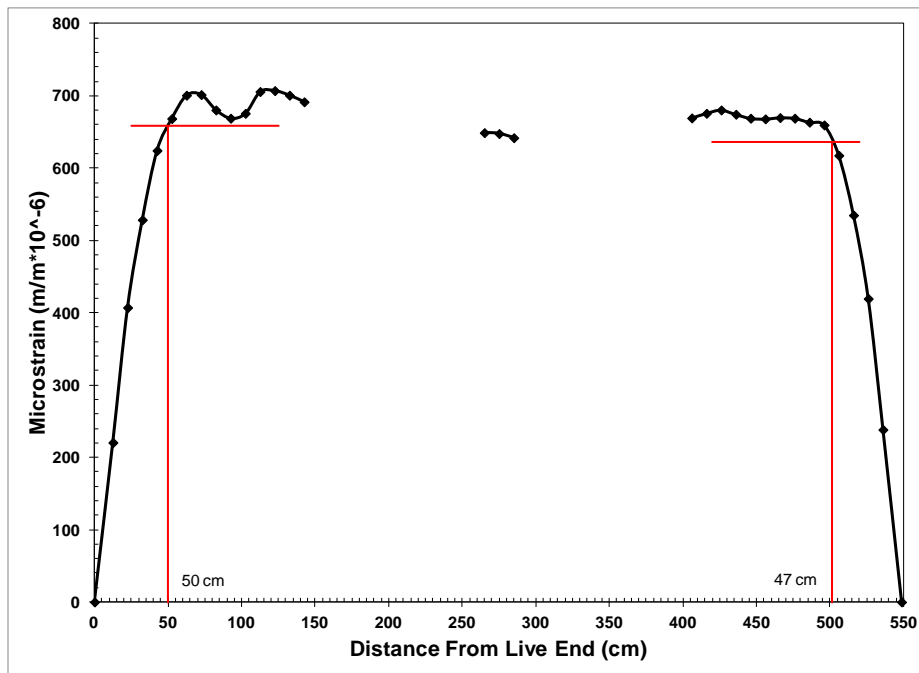


Figure D.53: 14-Day strain profile with 95% AMS for specimen NSL-2



### D.1.12 NSL-3

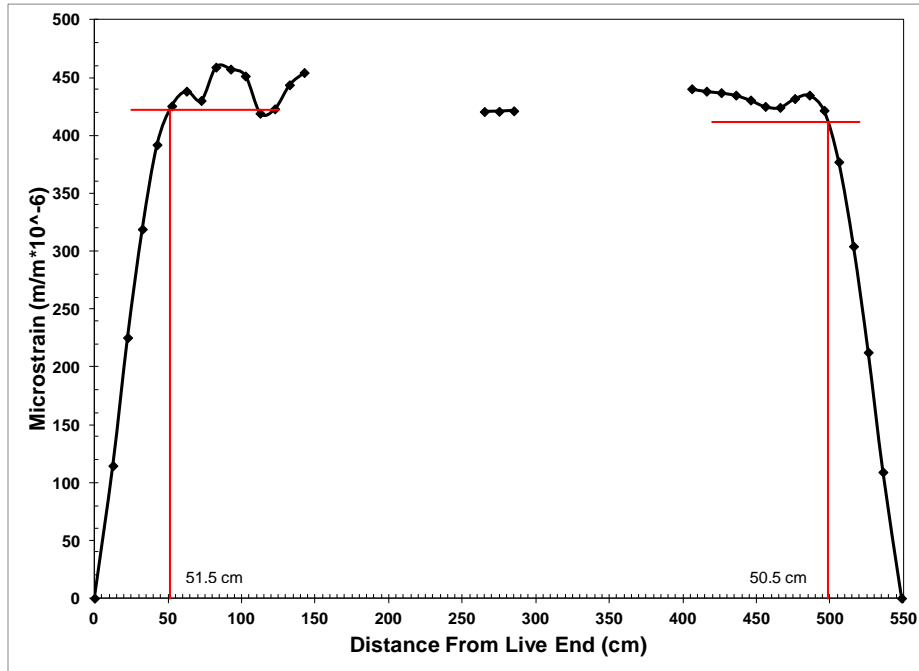


Figure D.54: Release strain profile with 95% AMS for specimen NSL-3

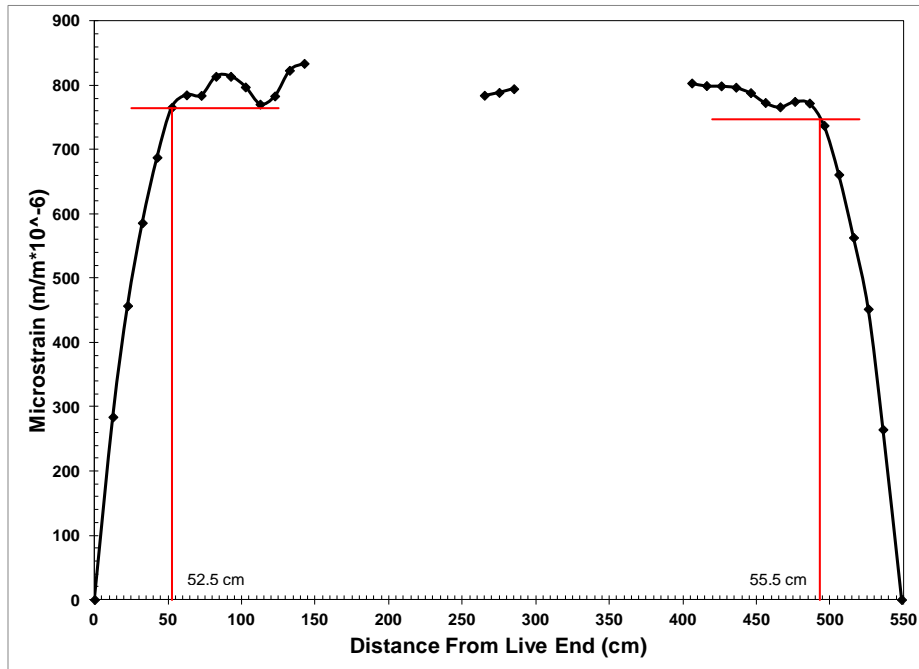


Figure D.55: 3-Day strain profile with 95% AMS for specimen NSL-3

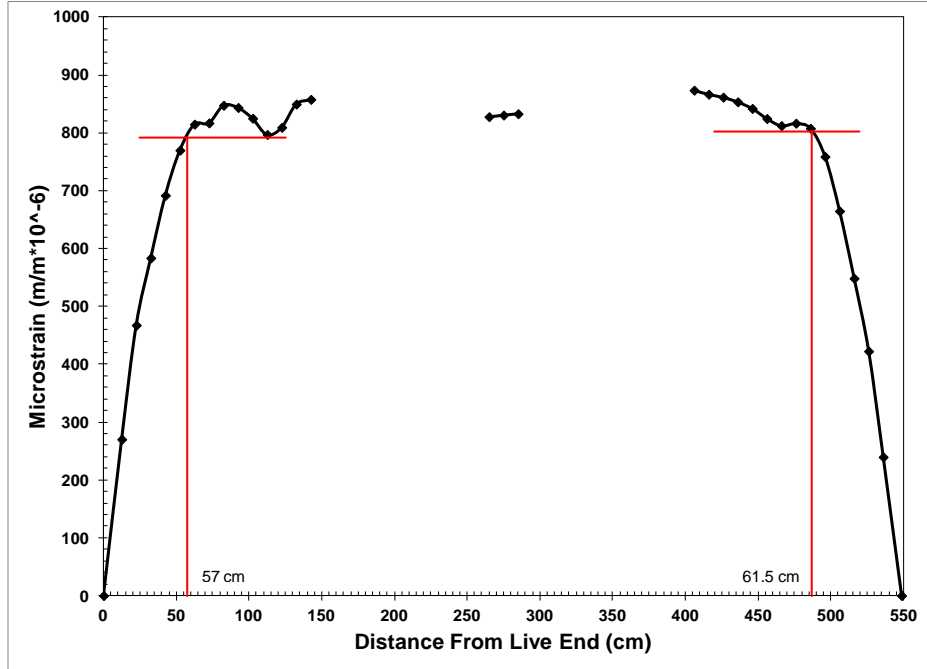


Figure D.56: 5-Day strain profile with 95% AMS for specimen NSL-3

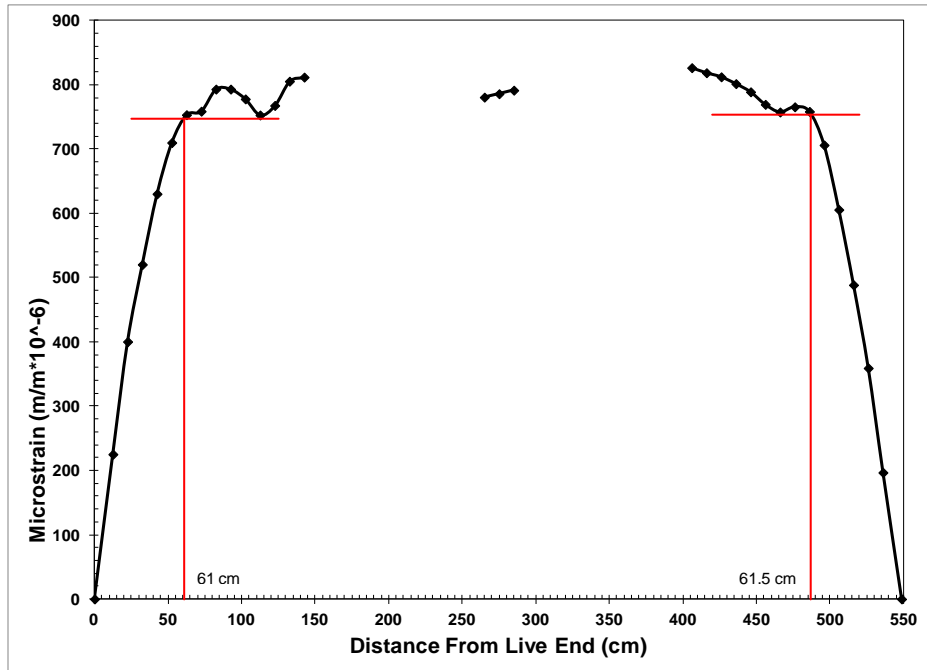


Figure D.57: 7-Day strain profile with 95% AMS for specimen NSL-3

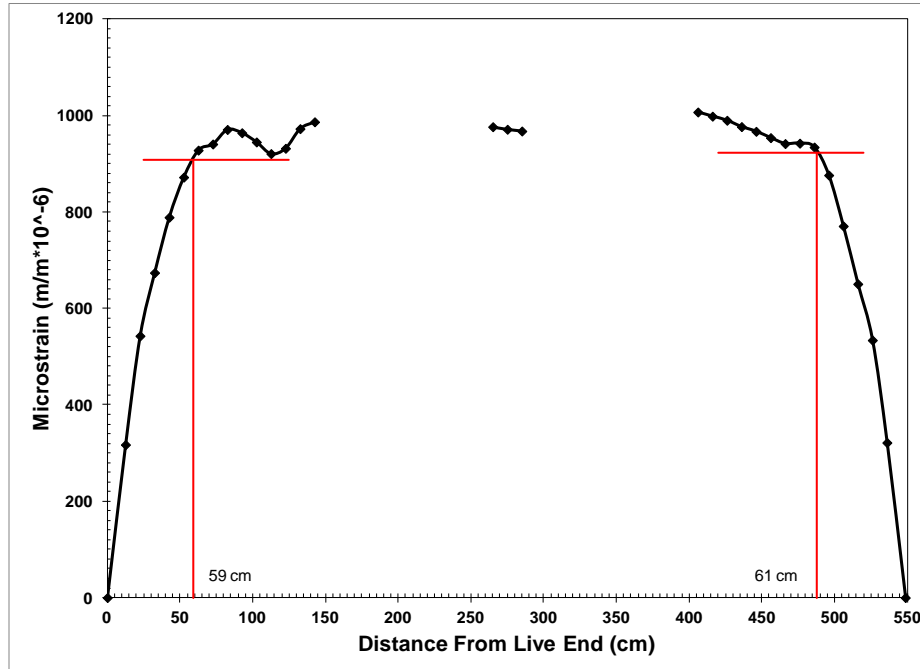


Figure D.58: 14-Day strain profile with 95% AMS for specimen NSL-3

#### D.1.13 NSL-4

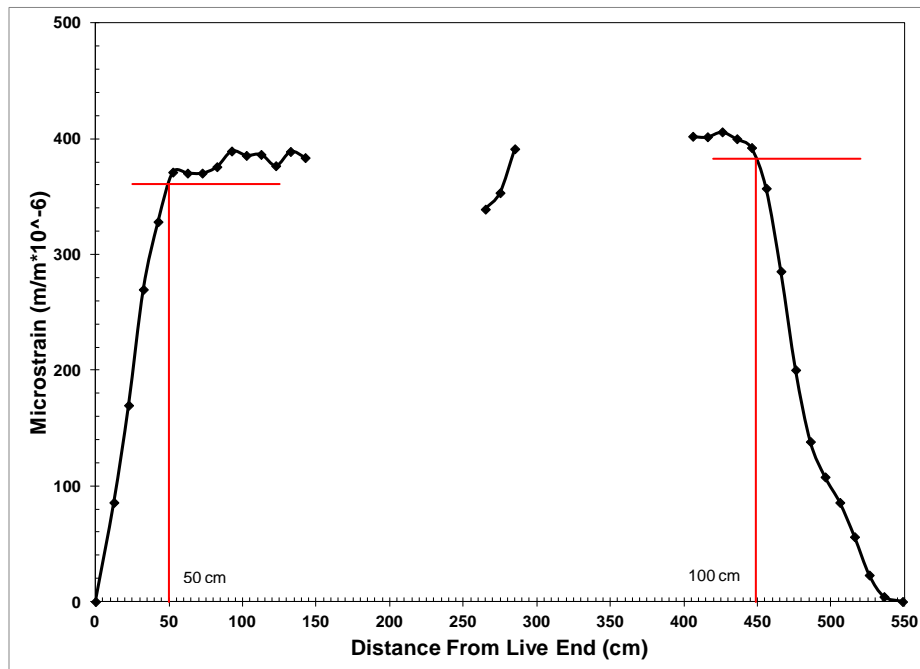


Figure D.59: Release strain profile with 95% AMS for specimen NSL-4

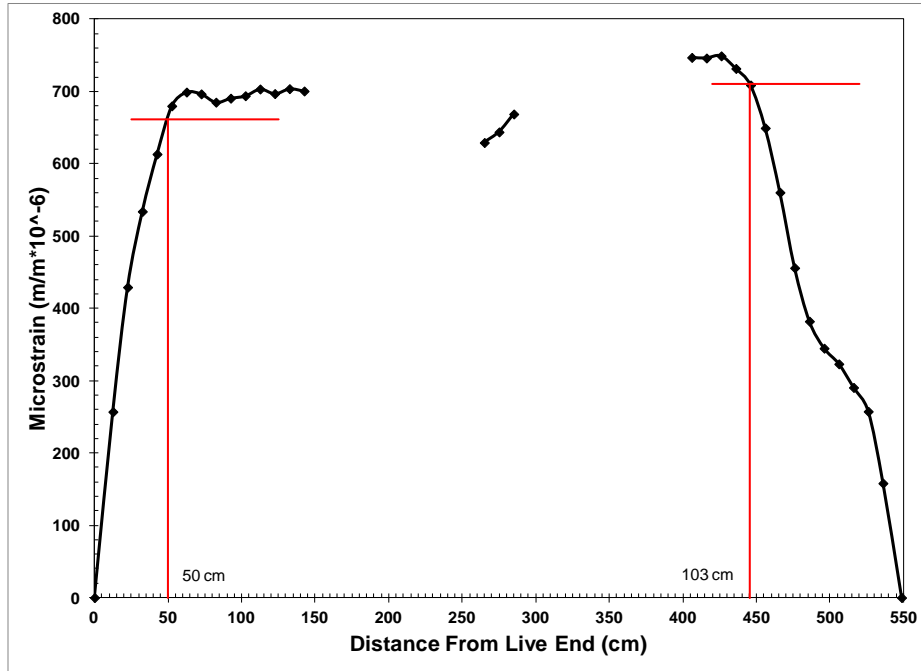


Figure D.60: 3-Day strain profile with 95% AMS for specimen NSL-4

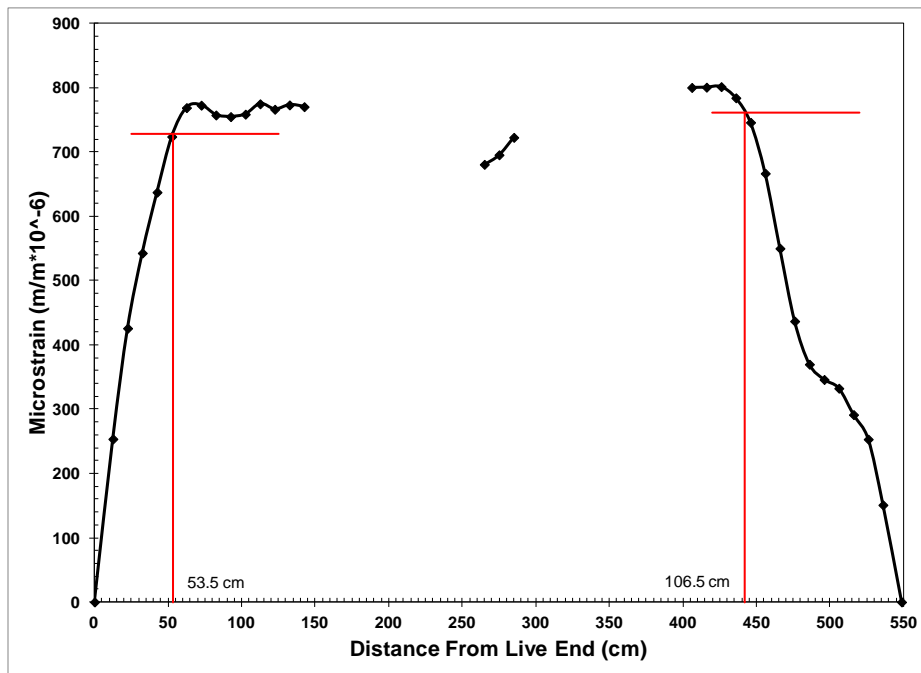


Figure D.61: 5-Day strain profile with 95% AMS for specimen NSL-4

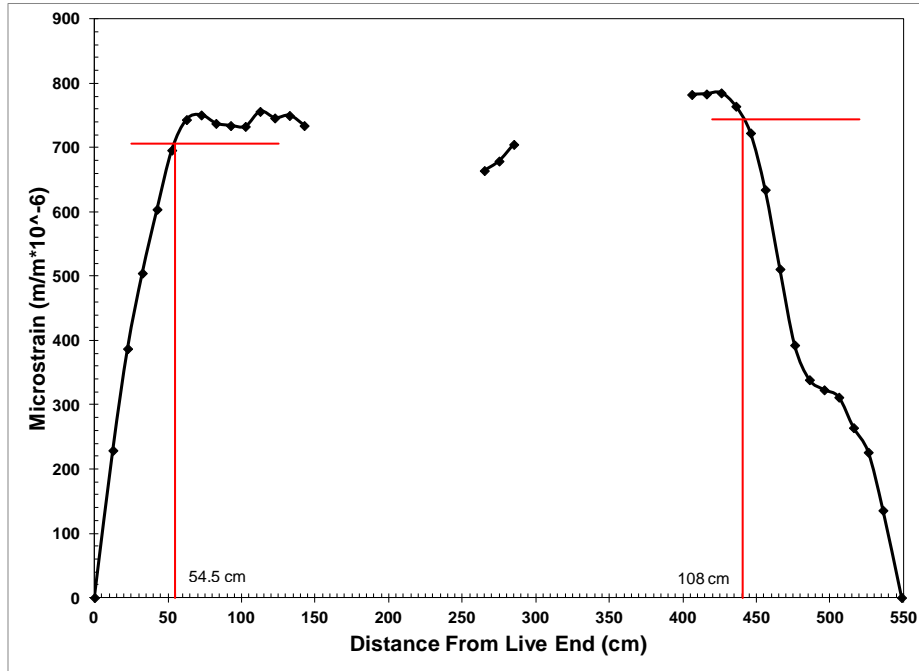


Figure D.62: 7-Day strain profile with 95% AMS for specimen NSL-4

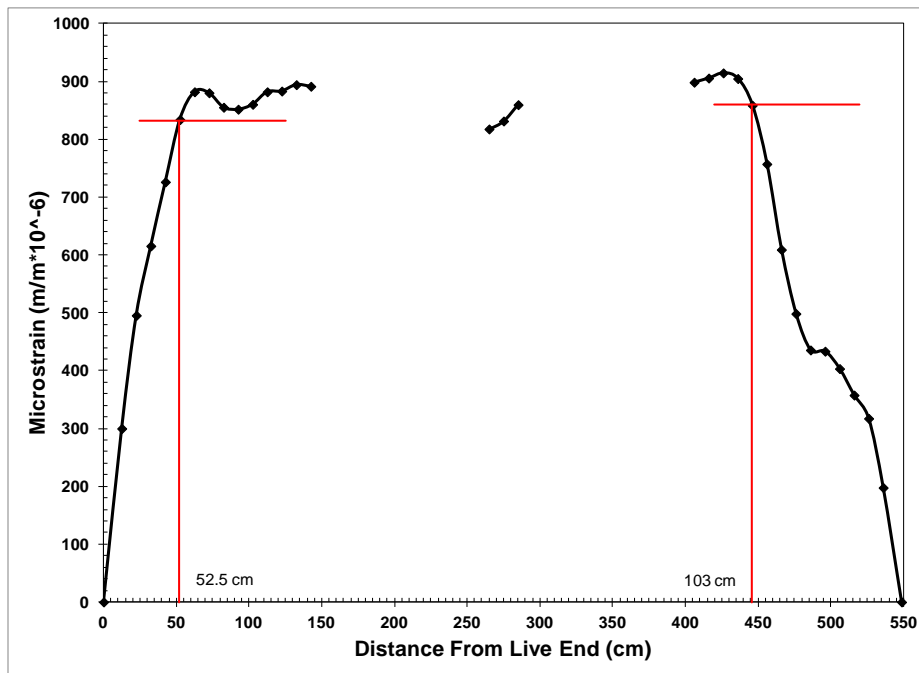


Figure D.63: 14-Day strain profile with 95% AMS for specimen NSL-4

### D.1.14 HSC-1

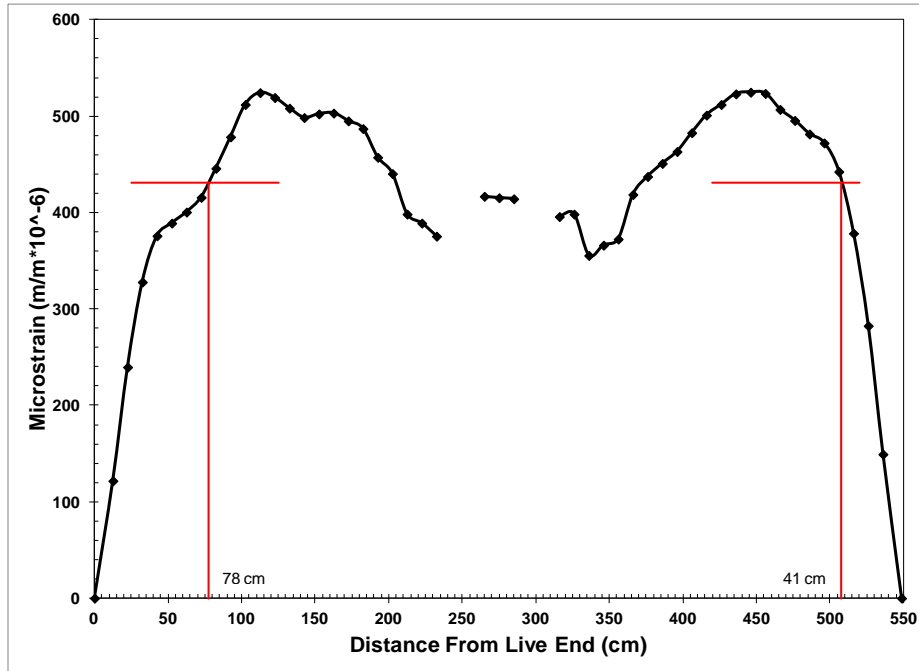


Figure D.64: Release strain profile with 95% AMS for specimen HSC-1

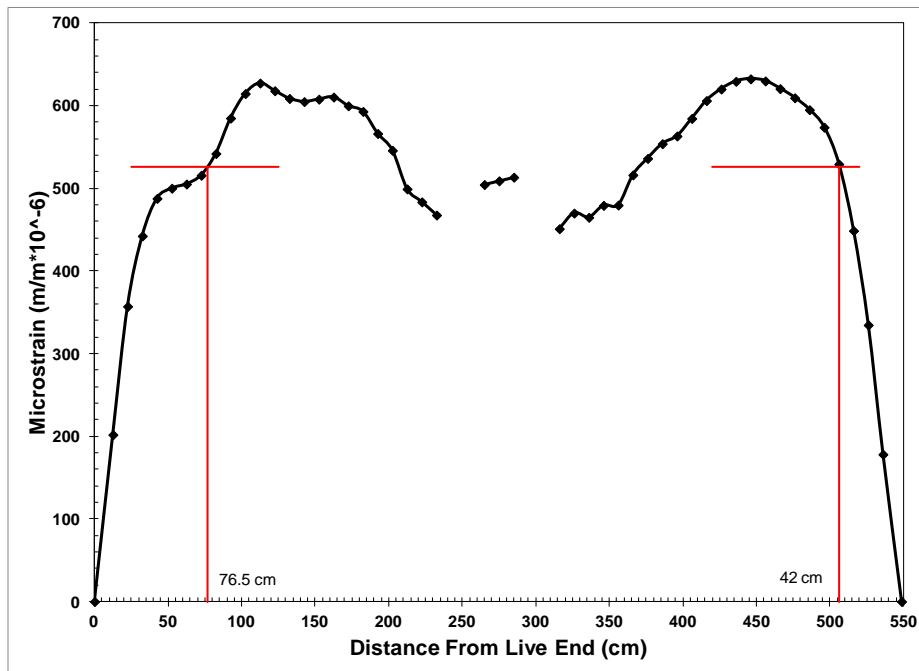


Figure D.65: 3-Day strain profile with 95% AMS for specimen HSC-1

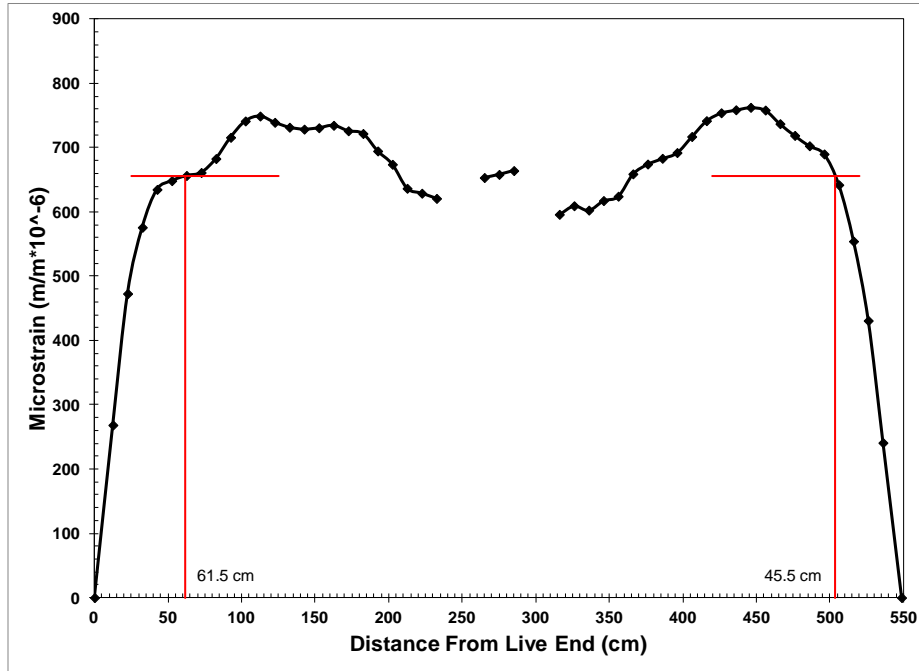


Figure D.66: 5-Day strain profile with 95% AMS for specimen HSC-1

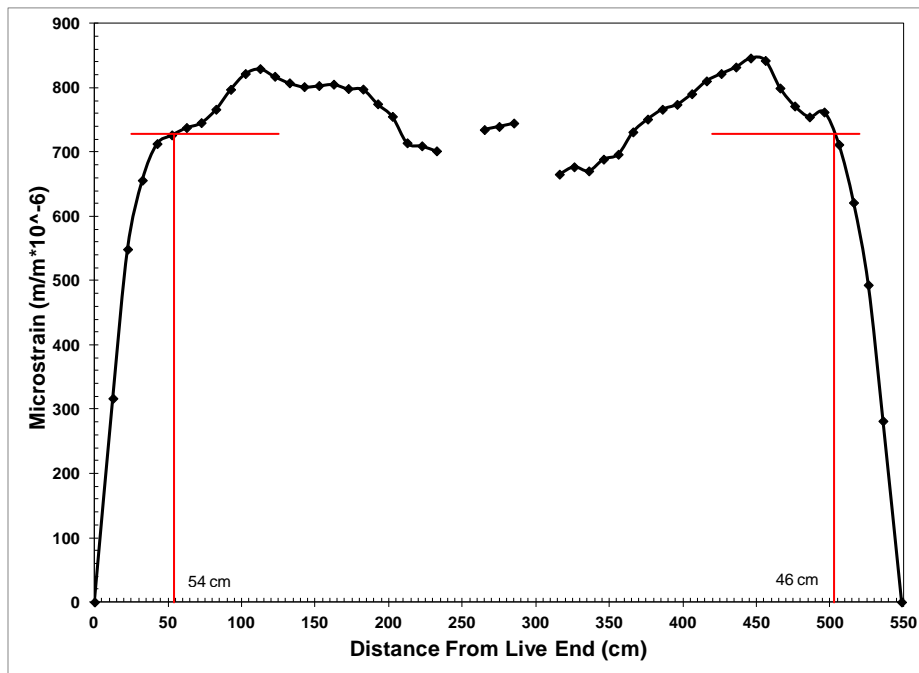


Figure D.67: 7-Day strain profile with 95% AMS for specimen HSC-1

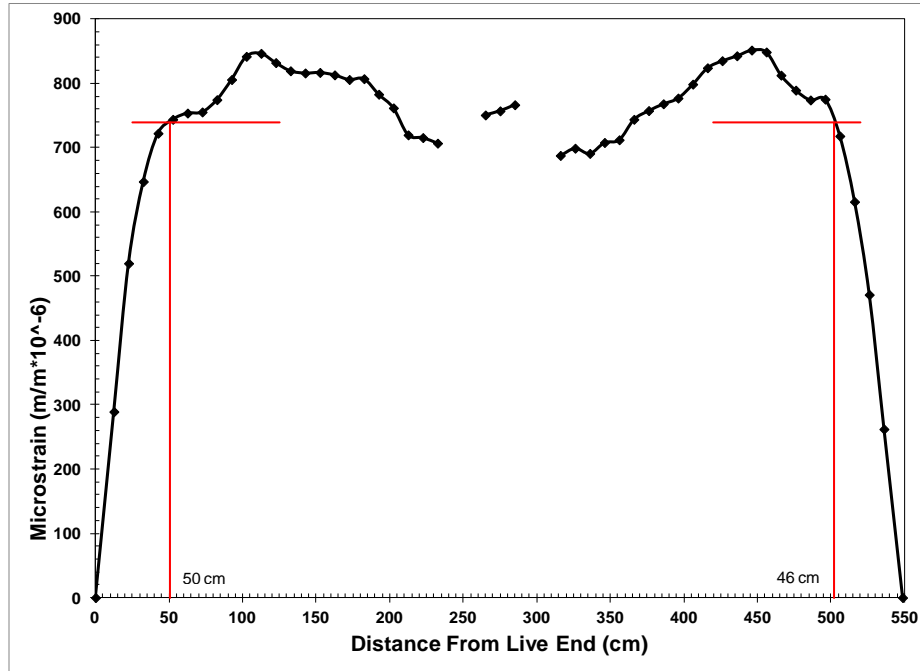


Figure D.68: 14-Day strain profile with 95% AMS for specimen HSC-1

#### D.1.15 HSC-2

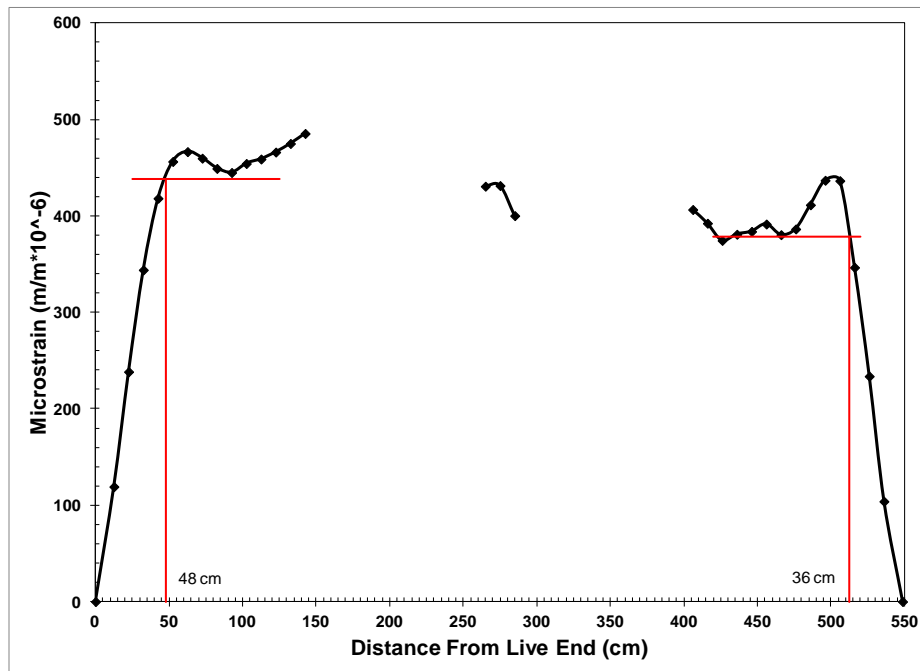


Figure D.69: Release strain profile with 95% AMS for specimen HSC-2



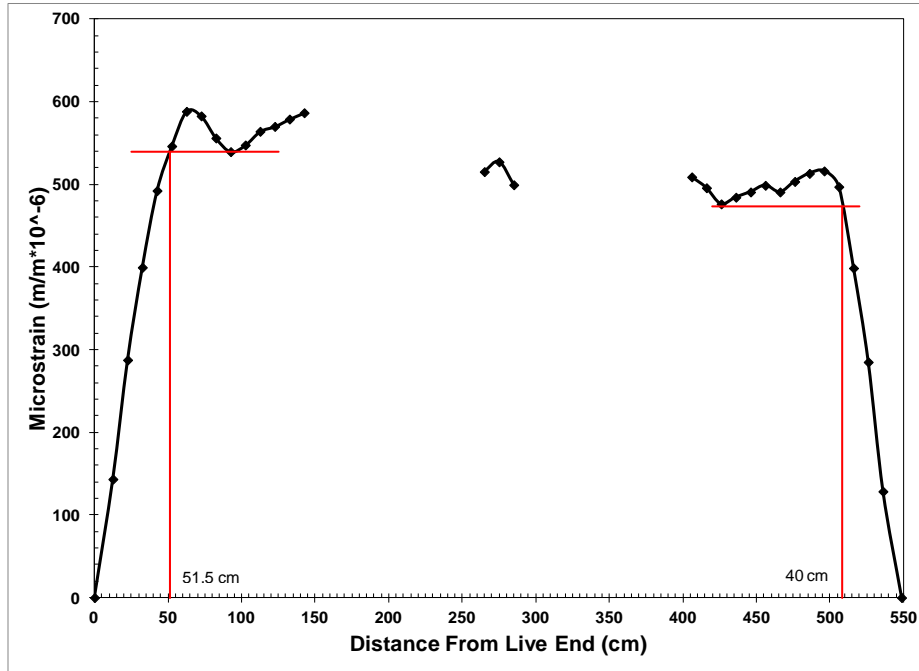


Figure D.70: 3-Day strain profile with 95% AMS for specimen HSC-2

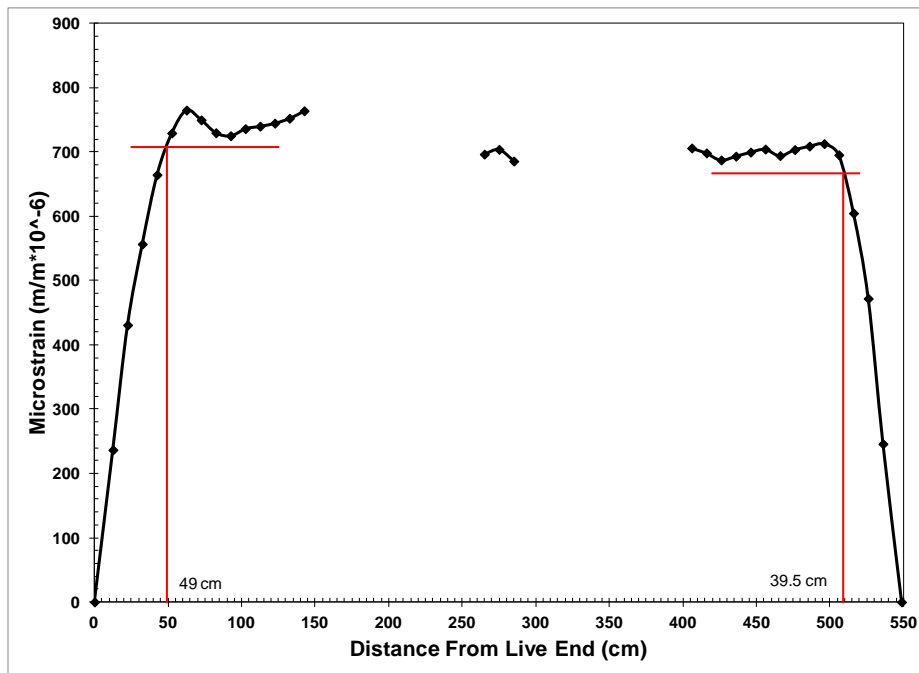


Figure D.71: 5-Day strain profile with 95% AMS for specimen HSC-2

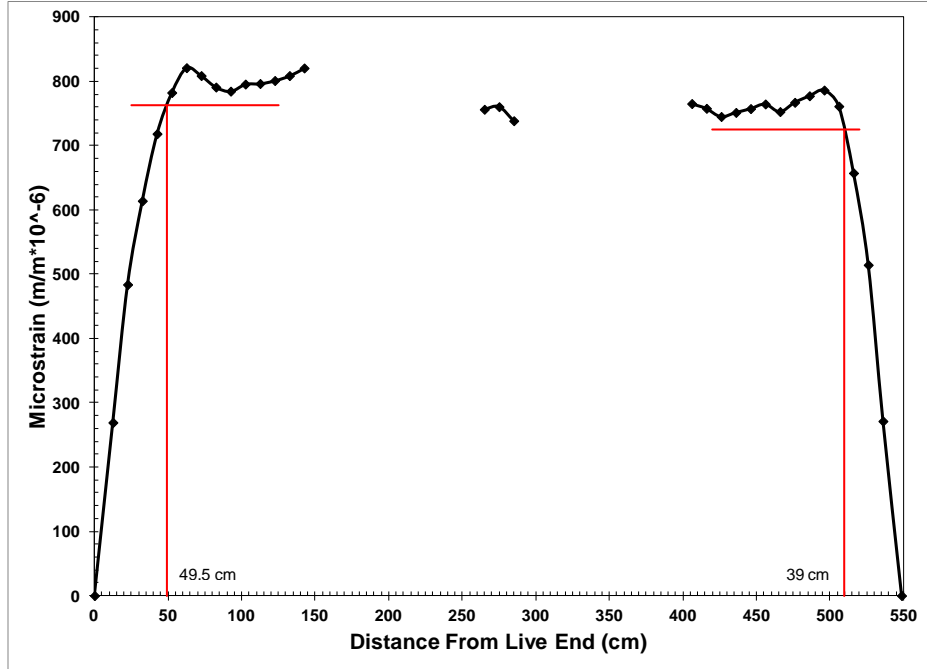


Figure D.72: 7-Day strain profile with 95% AMS for specimen HSC-2

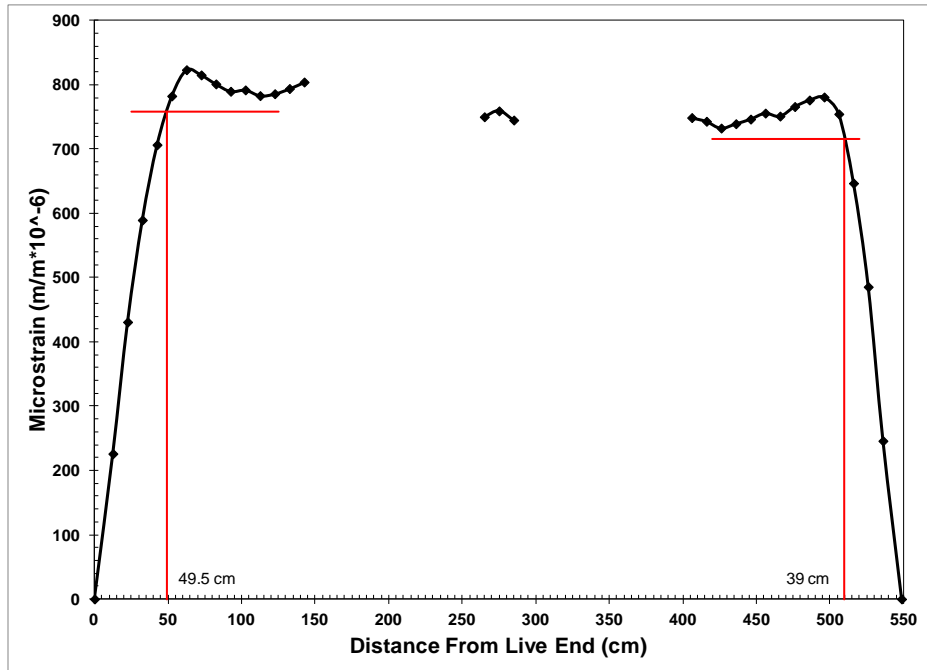


Figure D.73: 14-Day strain profile with 95% AMS for specimen HSC-2

### D.1.16 HSC-3

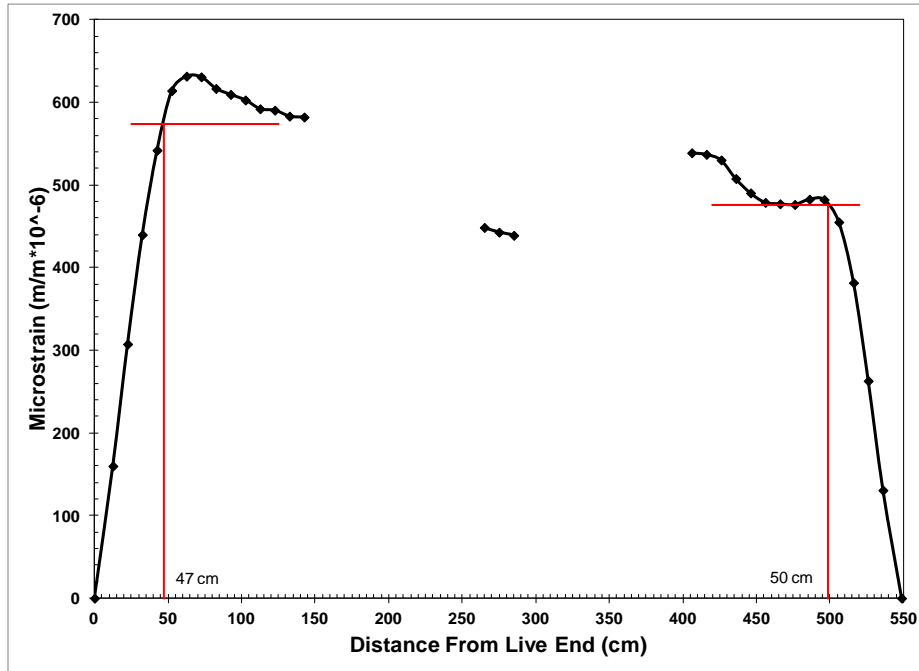


Figure D.74: Release strain profile with 95% AMS for specimen HSC-3

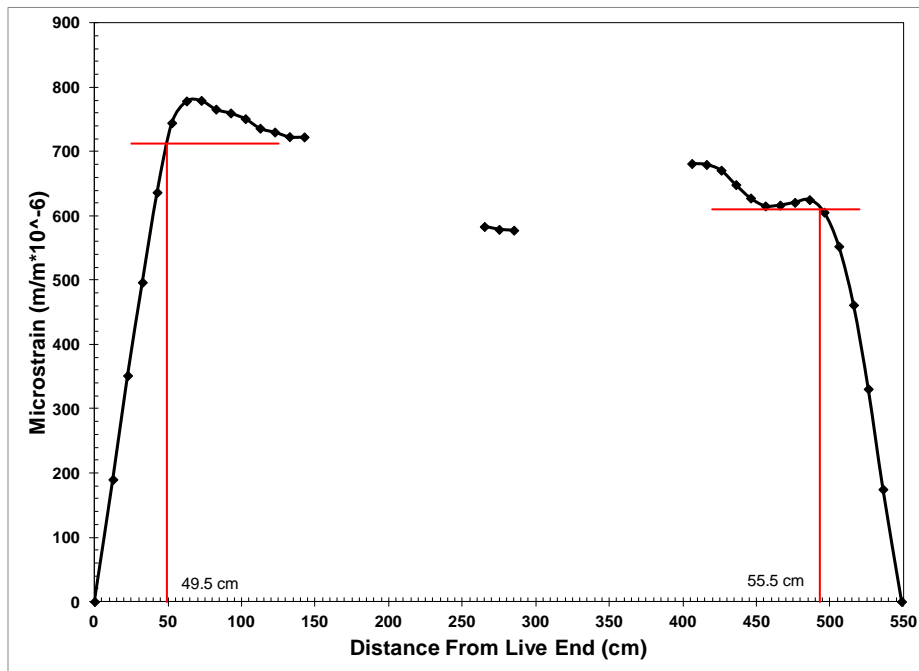


Figure D.75: 3-Day strain profile with 95% AMS for specimen HSC-3

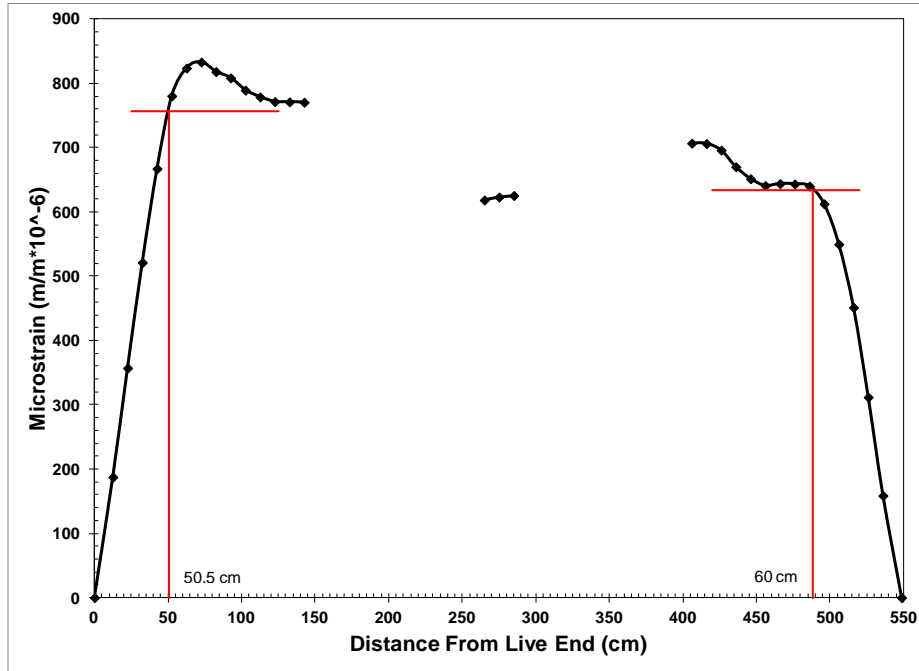


Figure D.76: 5-Day strain profile with 95% AMS for specimen HSC-3

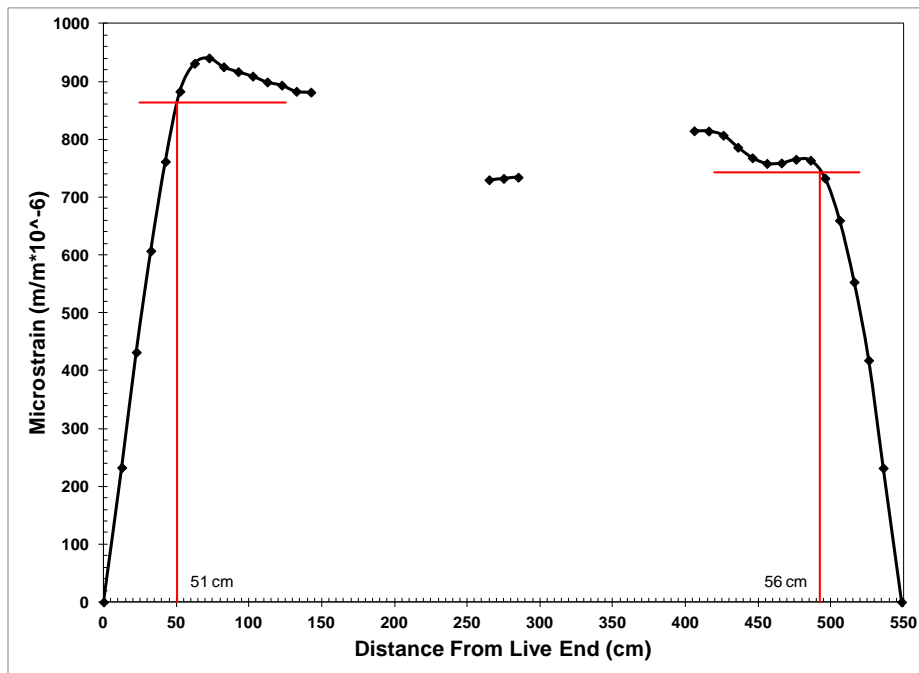


Figure D.77: 7-Day strain profile with 95% AMS for specimen HSC-3

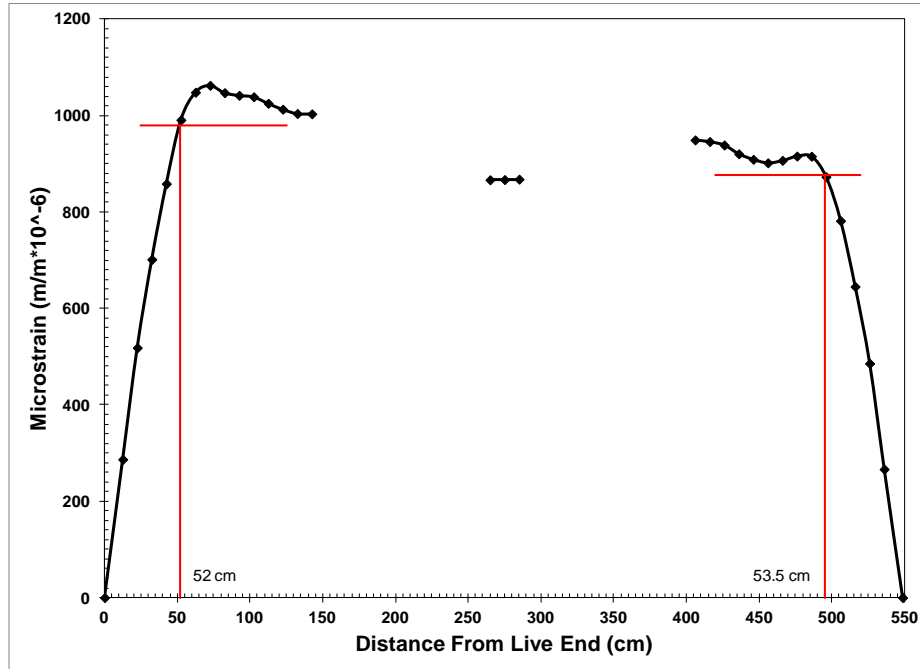


Figure D.78: 14-Day strain profile with 95% AMS for specimen HSC-3

#### D.1.17 HSC-4

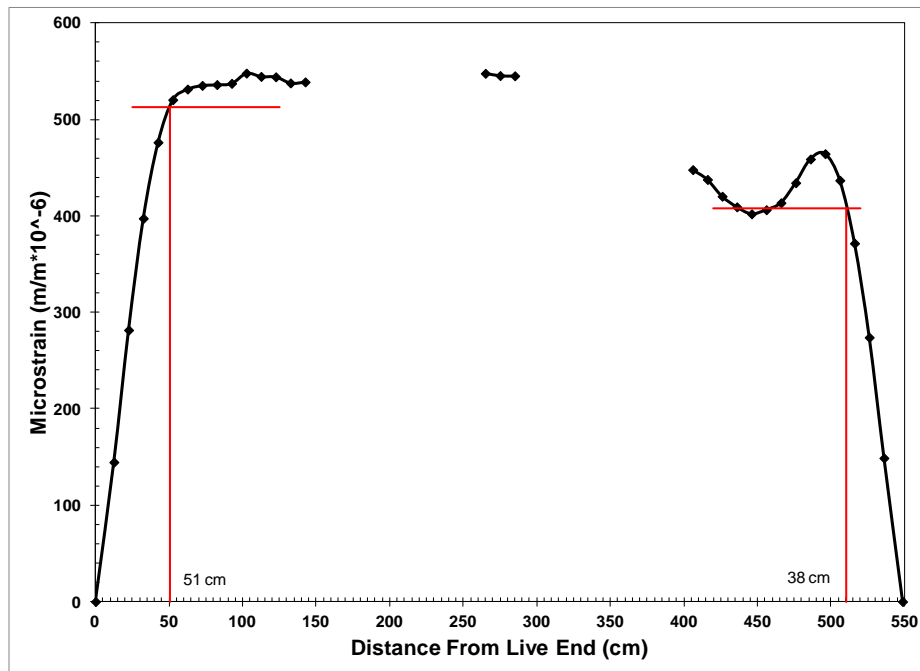


Figure D.79: Release strain profile with 95% AMS for specimen HSC-4

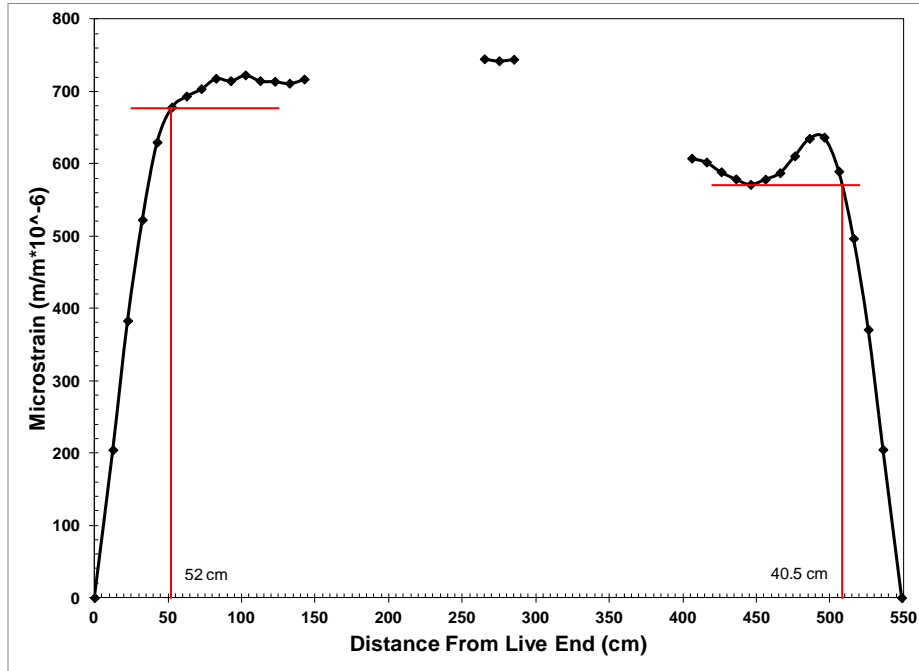


Figure D.80: 3-Day strain profile with 95% AMS for specimen HSC-4

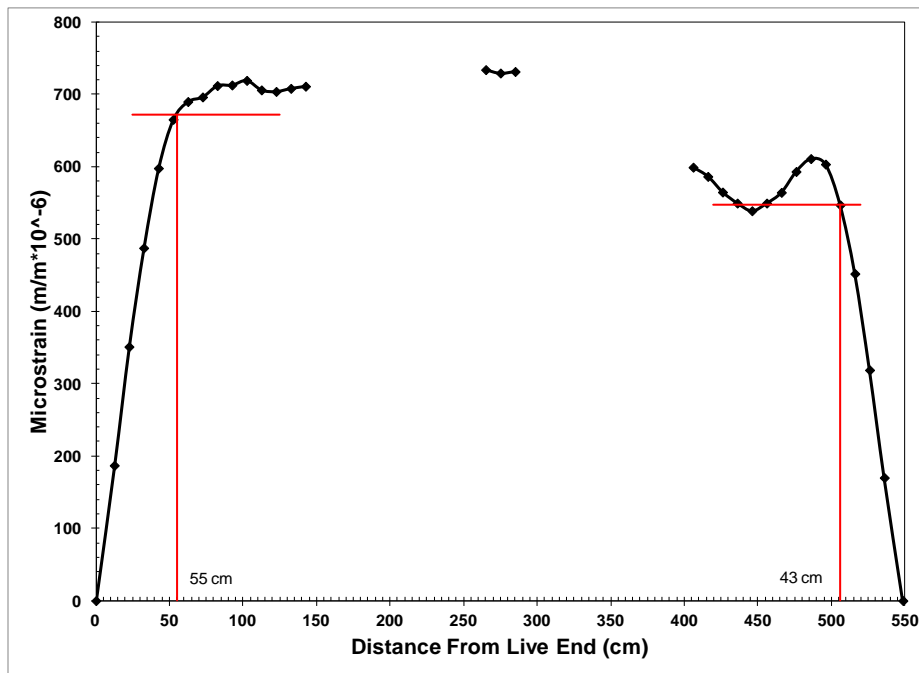


Figure D.81: 5-Day strain profile with 95% AMS for specimen HSC-4

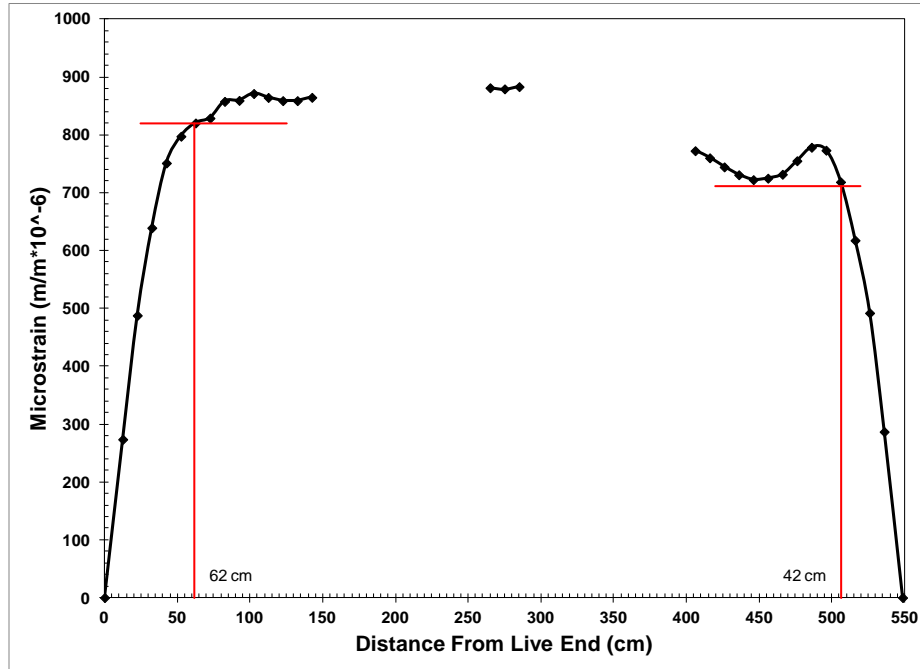


Figure D.82: 7-Day strain profile with 95% AMS for specimen HSC-4

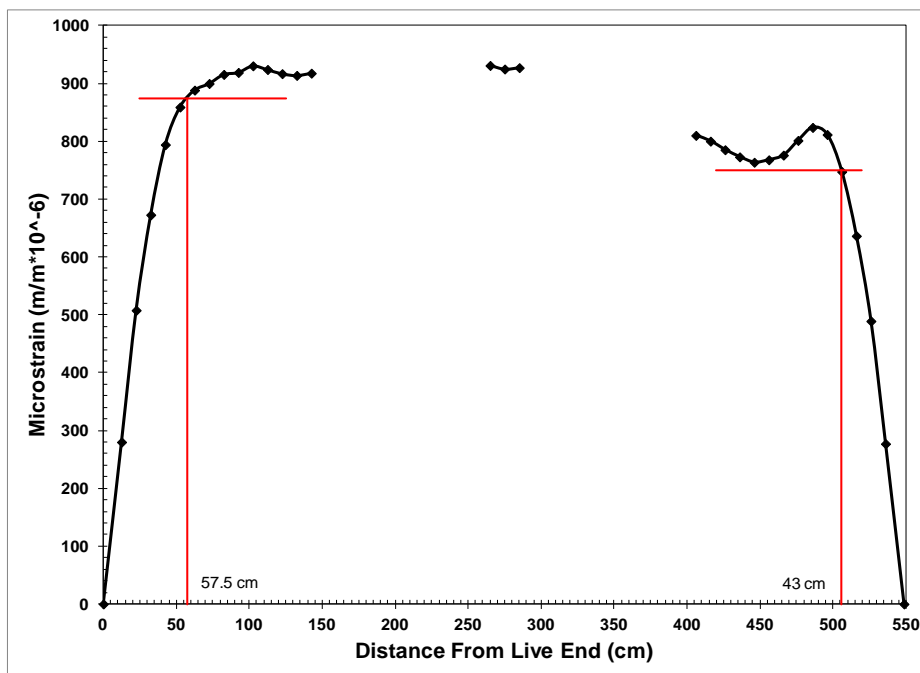


Figure D.83: 14-Day strain profile with 95% AMS for specimen HSC-4

### D.1.18 HSS-1

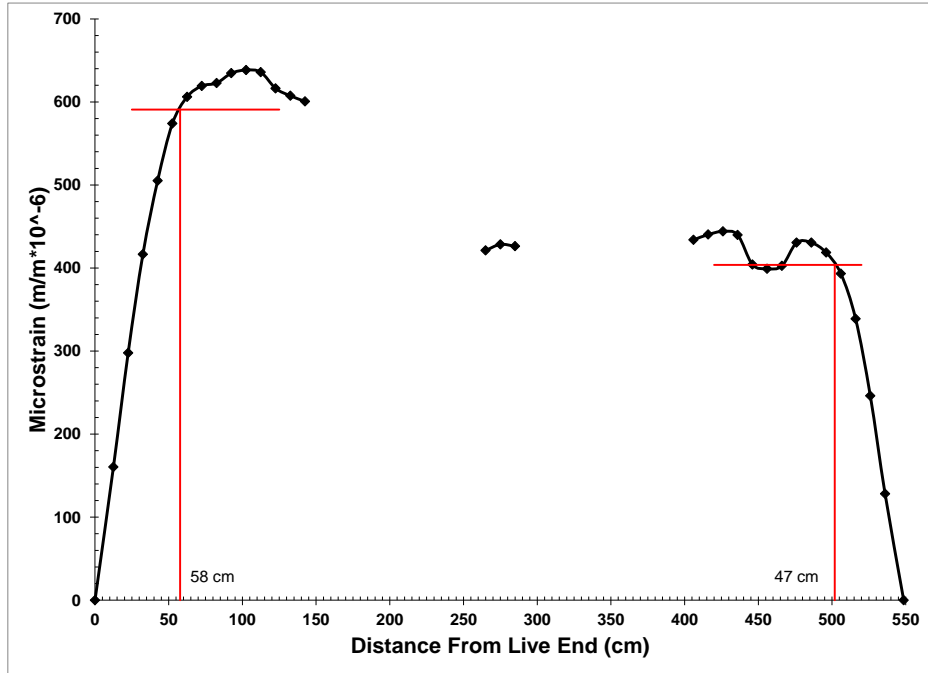


Figure D.84: Release strain profile with 95% AMS for specimen HSS-1

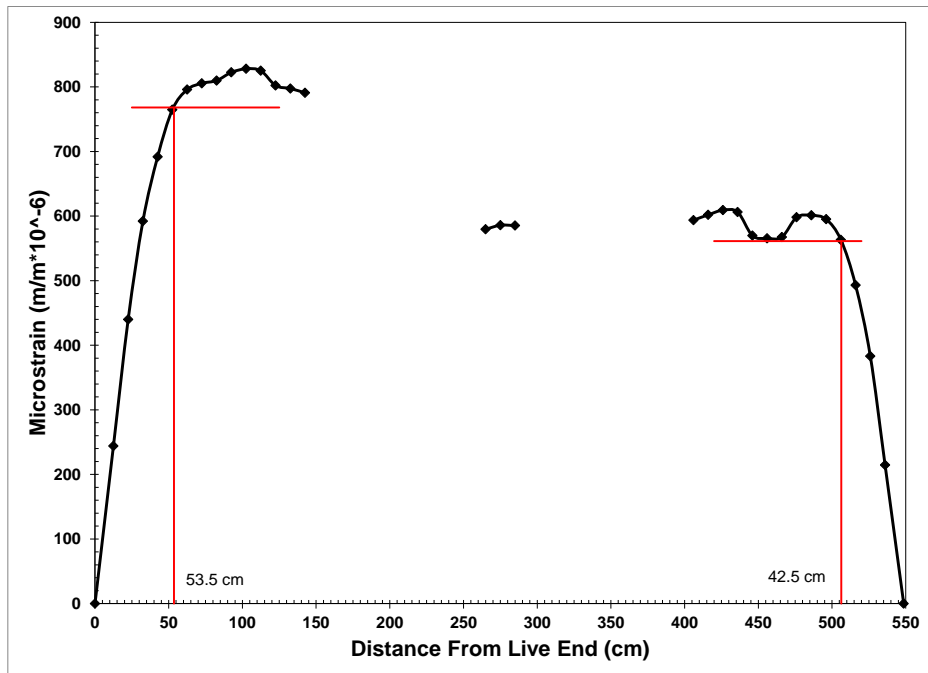


Figure D.85: 3-Day strain profile with 95% AMS for specimen HSS-1



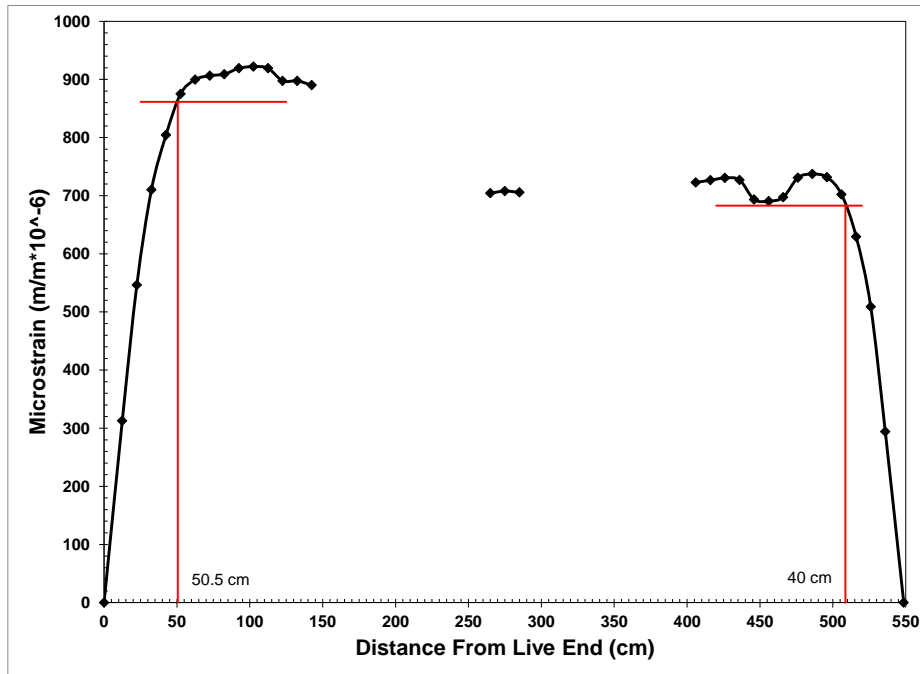


Figure D.86: 5-Day strain profile with 95% AMS for specimen HSS-1

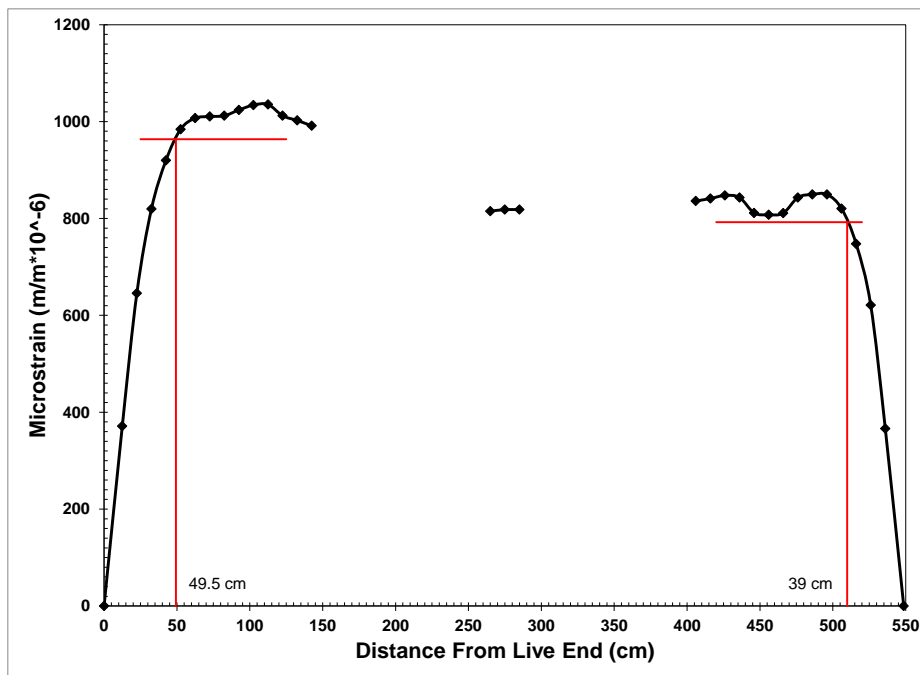


Figure D.87: 7-Day strain profile with 95% AMS for specimen HSS-1

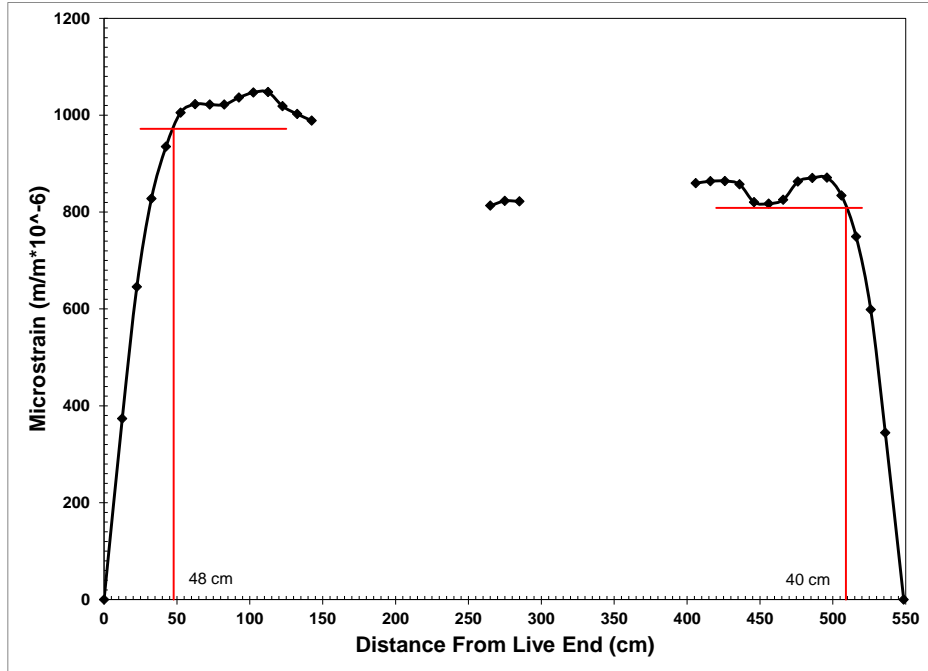


Figure D.88: 14-Day strain profile with 95% AMS for specimen HSS-1

#### D.1.19 HSS-2

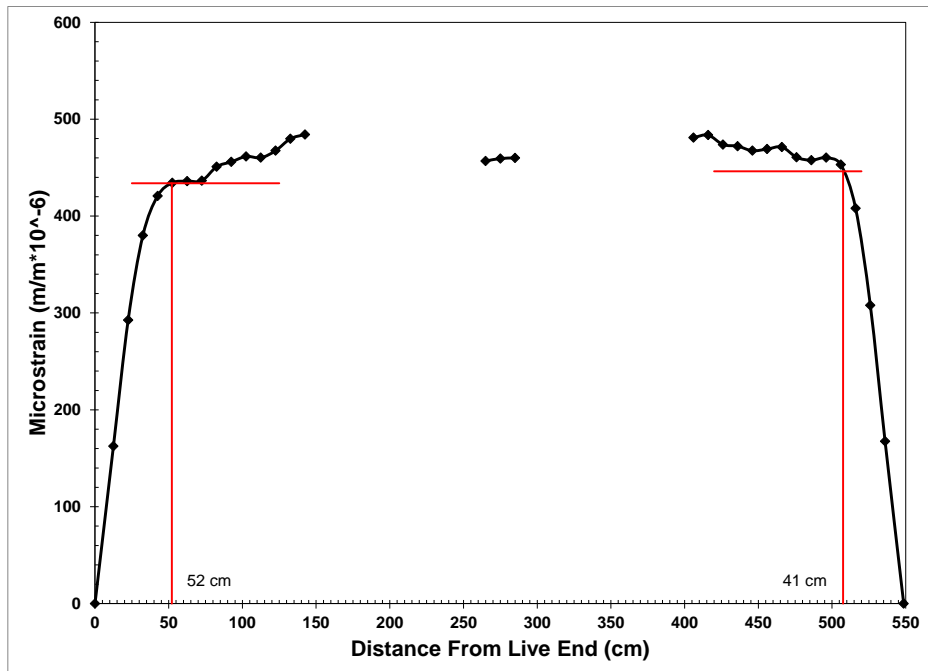


Figure D.89: Release strain profile with 95% AMS for specimen HSS-2

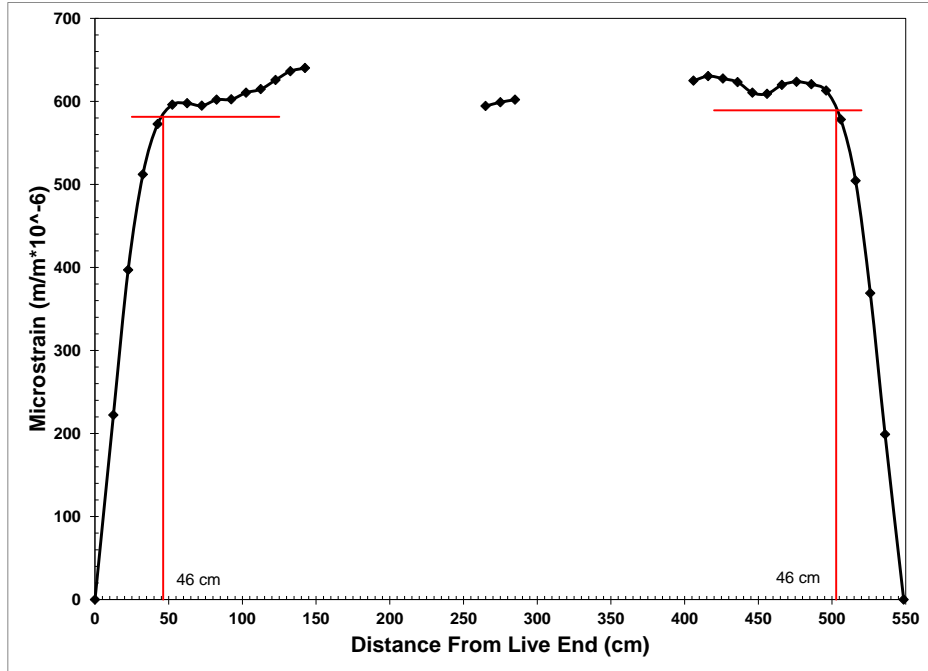


Figure D.90: 3-Day strain profile with 95% AMS for specimen HSS-2

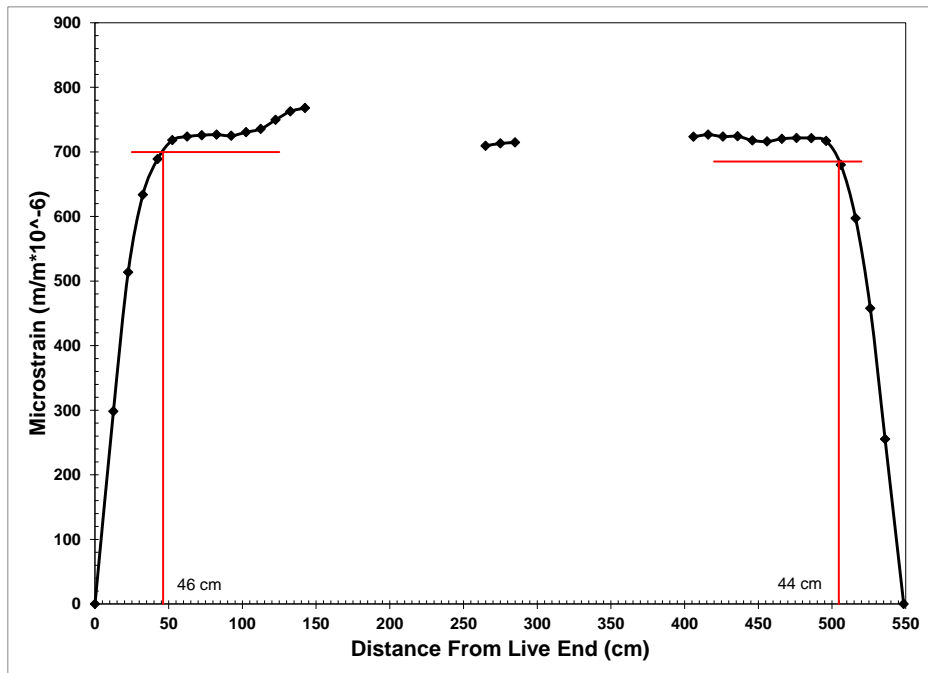


Figure D.91: 5-Day strain profile with 95% AMS for specimen HSS-2

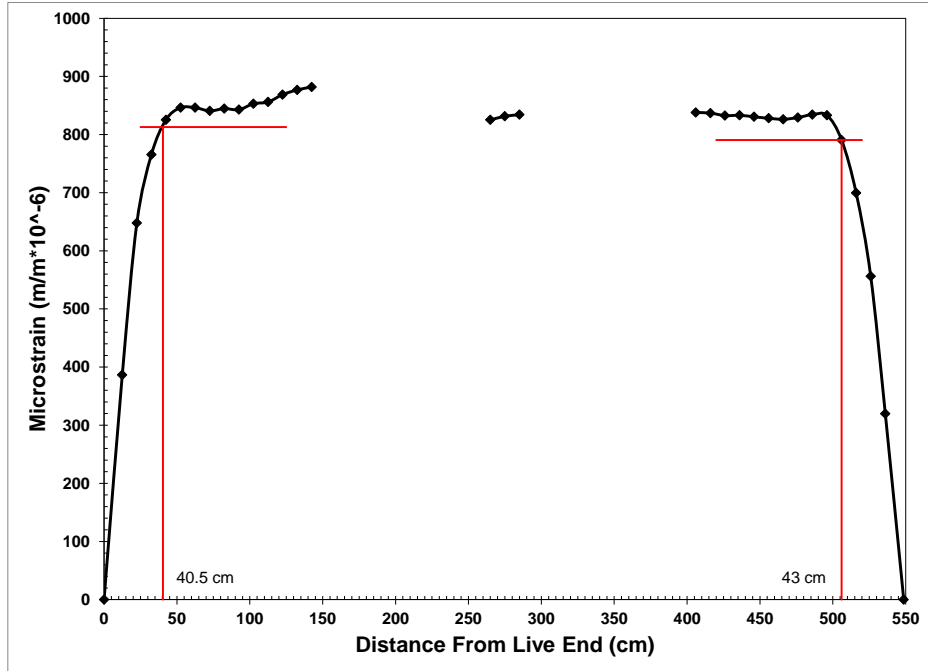


Figure D.92: 7-Day strain profile with 95% AMS for specimen HSS-2

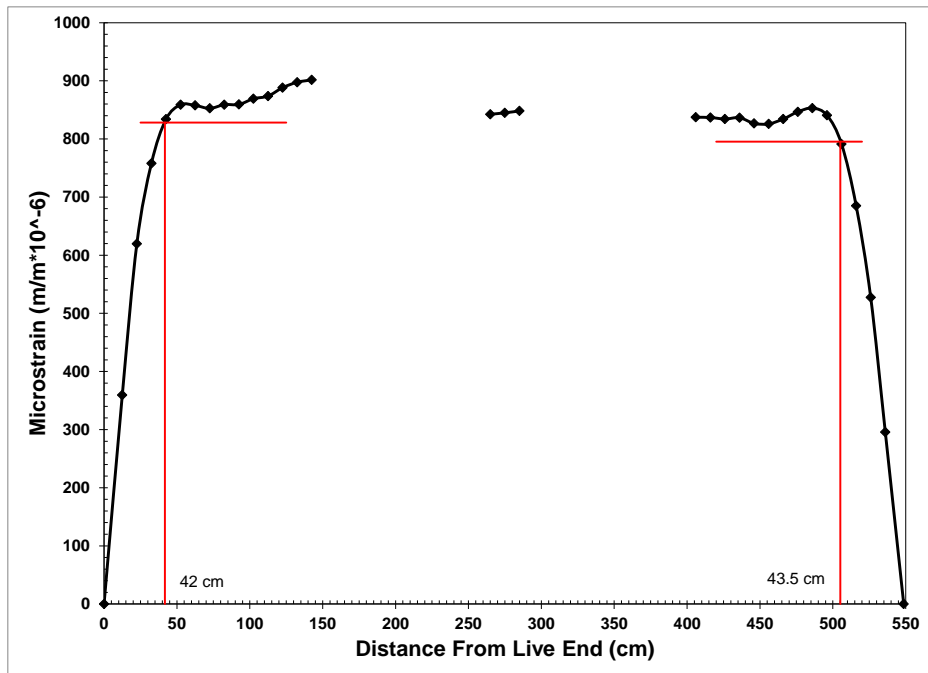


Figure D.93: 14-Day strain profile with 95% AMS for specimen HSS-2

### D.1.20 HSS-3

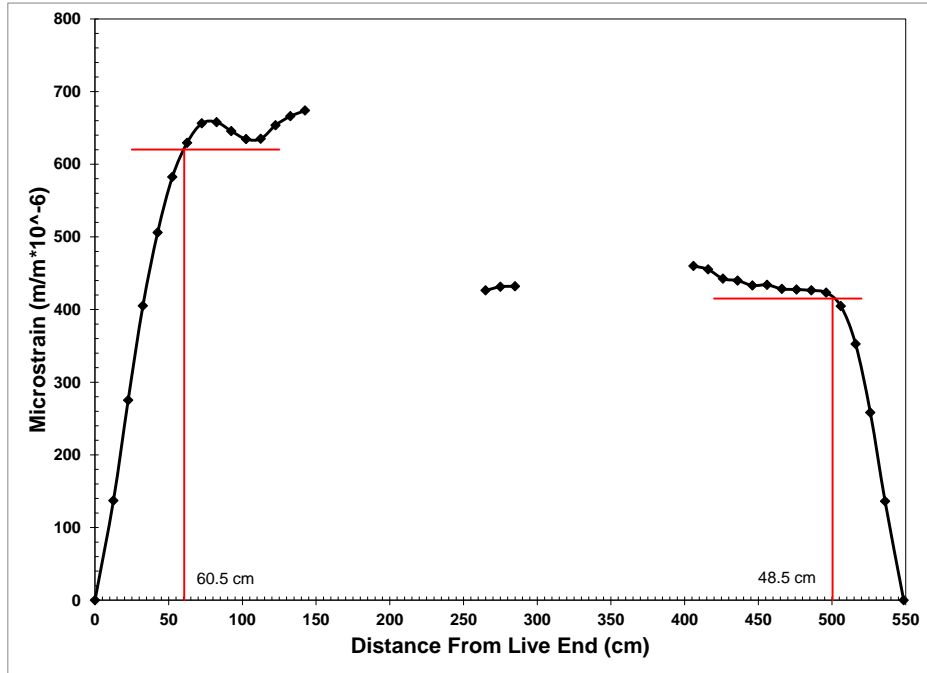


Figure D.94: Release strain profile with 95% AMS for specimen HSS-3

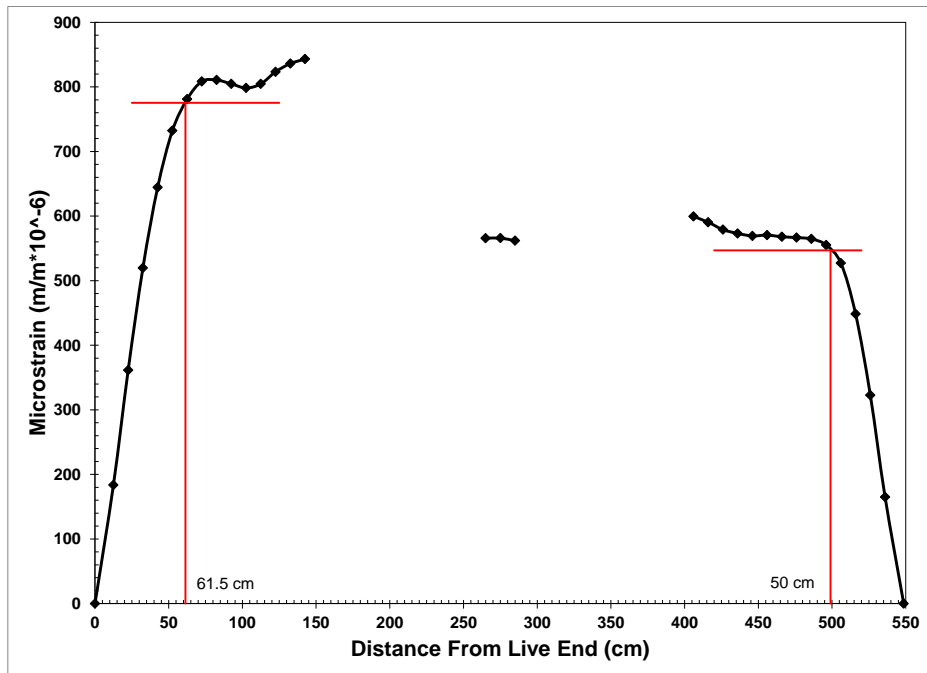


Figure D.95: 3-Day strain profile with 95% AMS for specimen HSS-3

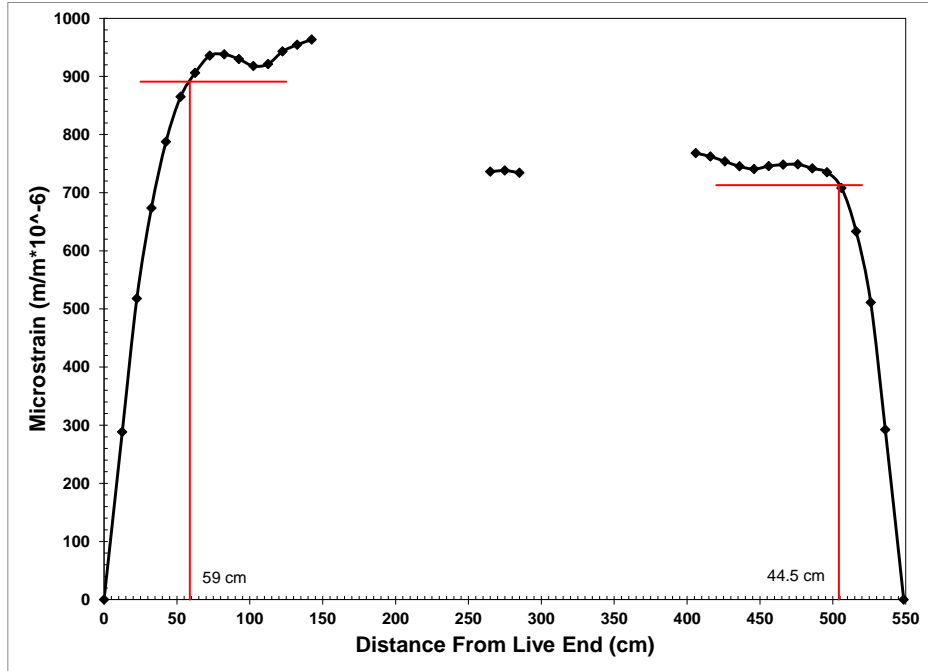


Figure D.96: 5-Day strain profile with 95% AMS for specimen HSS-3

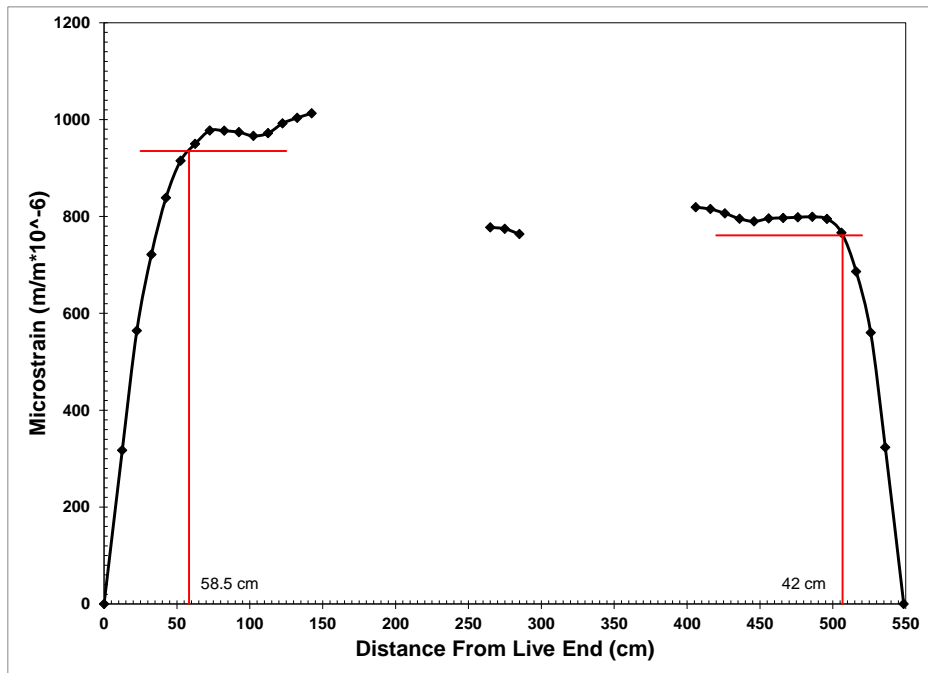


Figure D.97: 7-Day strain profile with 95% AMS for specimen HSS-3

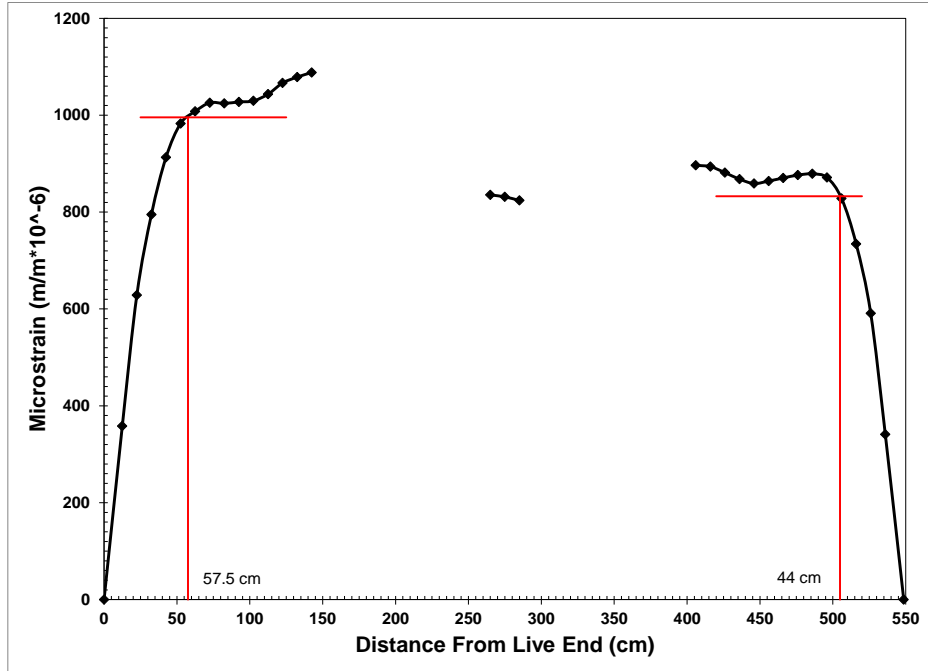


Figure D.98: 14-Day strain profile with 95% AMS for specimen HSS-3

#### D.1.21 HSS-4

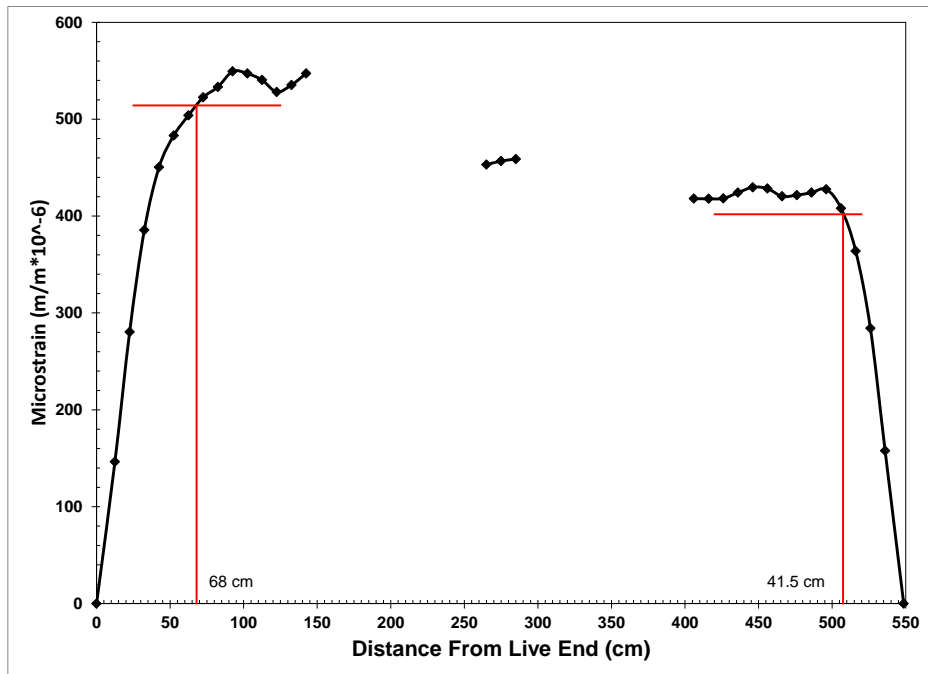


Figure D.99: Release strain profile with 95% AMS for specimen HSS-4

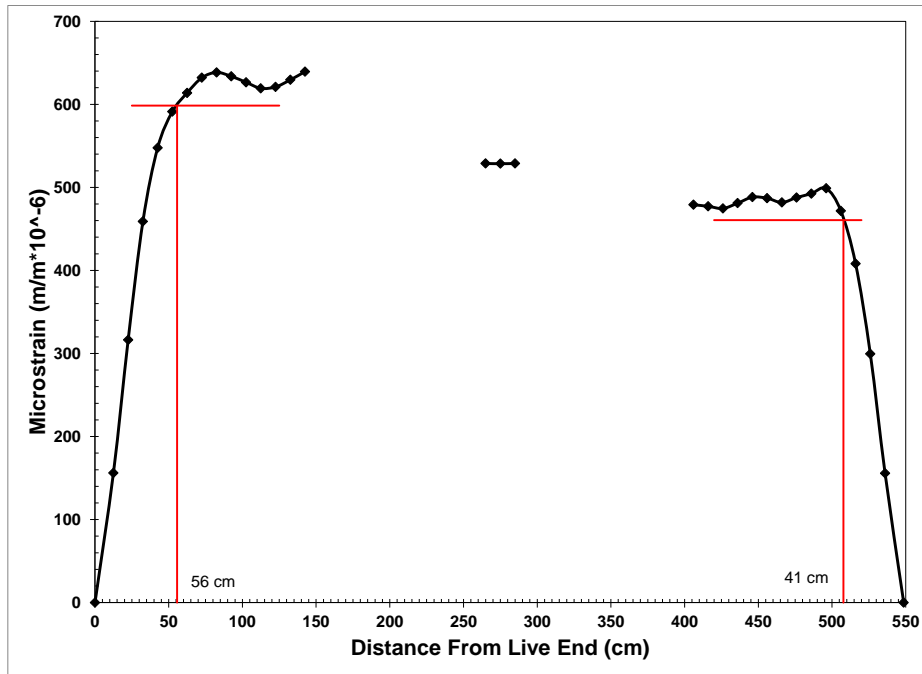


Figure D.100: 3-Day strain profile with 95% AMS for specimen HSS-4

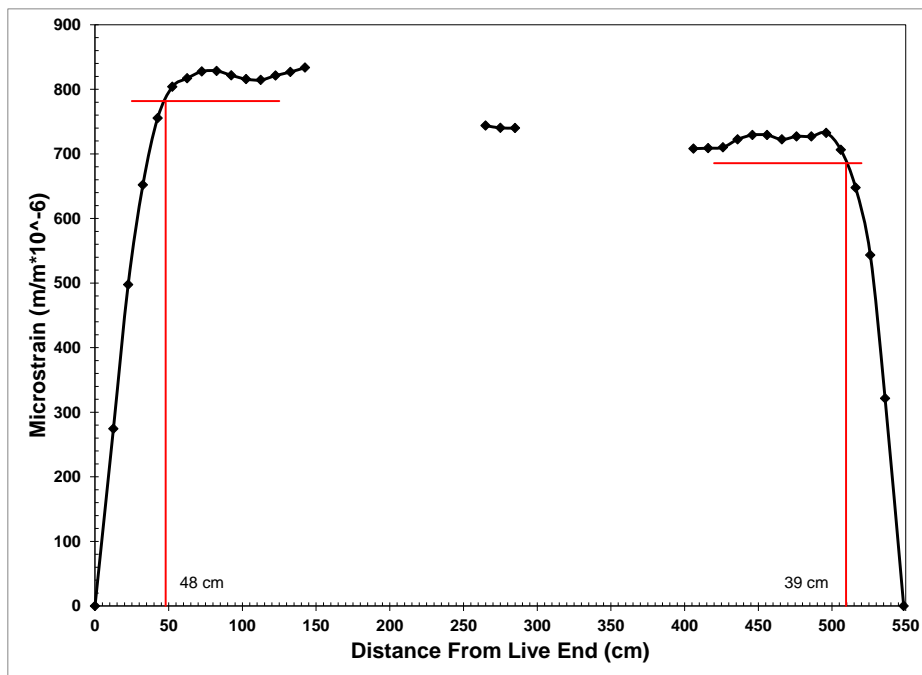


Figure D.101: 5-Day strain profile with 95% AMS for specimen HSS-4



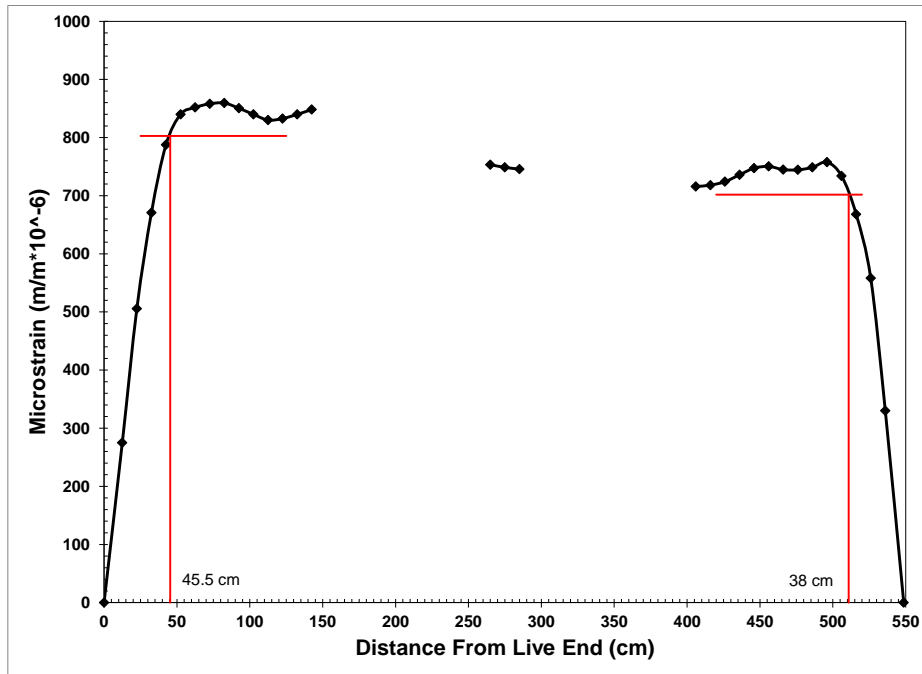


Figure D.102: 7-Day strain profile with 95% AMS for specimen HSS-4

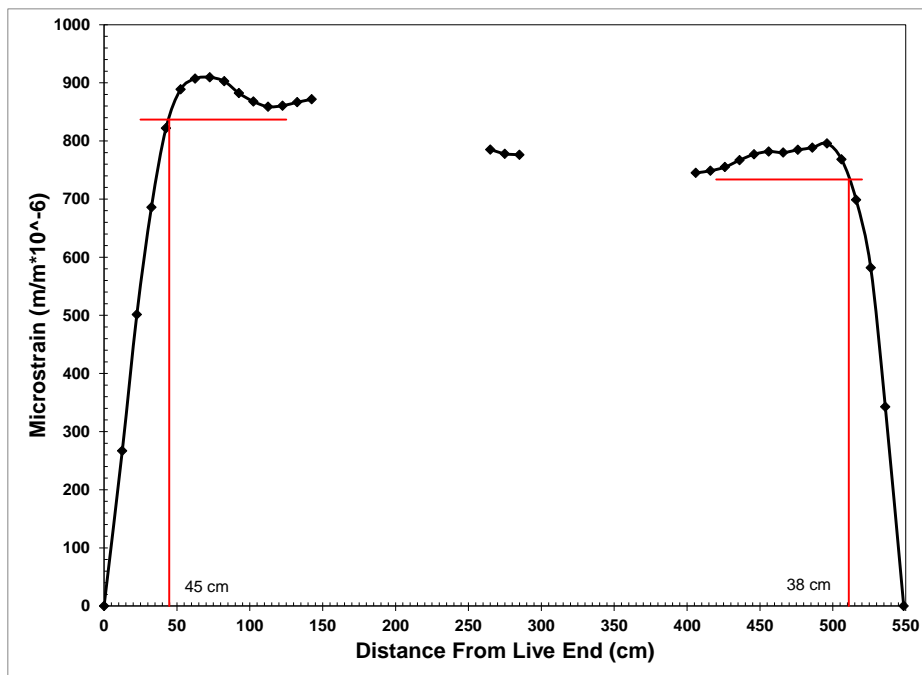


Figure D.103: 14-Day strain profile with 95% AMS for specimen HSS-4

### D.1.22 HSL-1

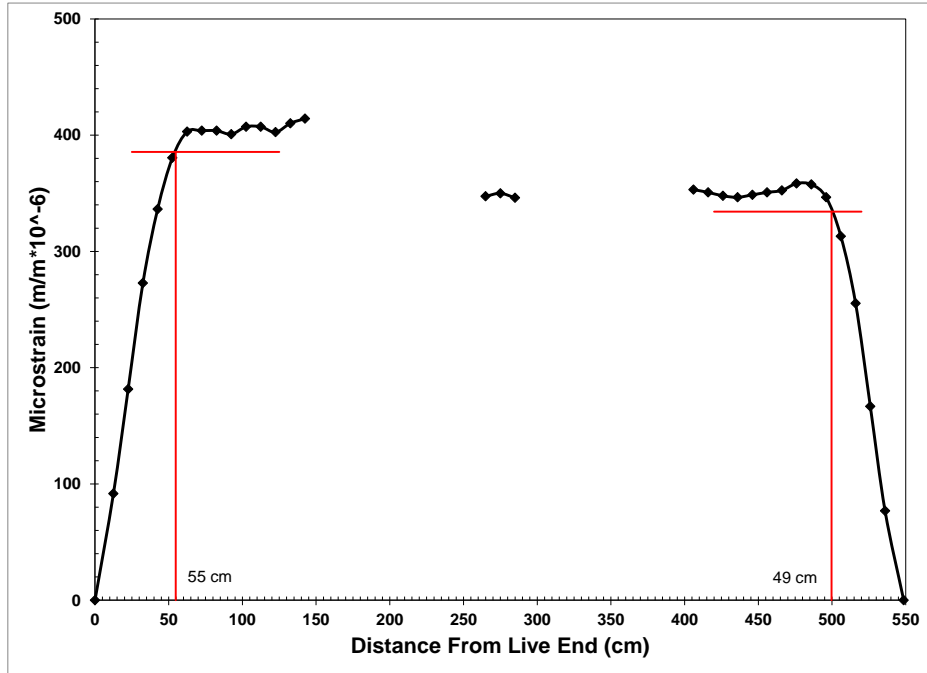


Figure D.104: Release strain profile with 95% AMS for specimen HSL-1

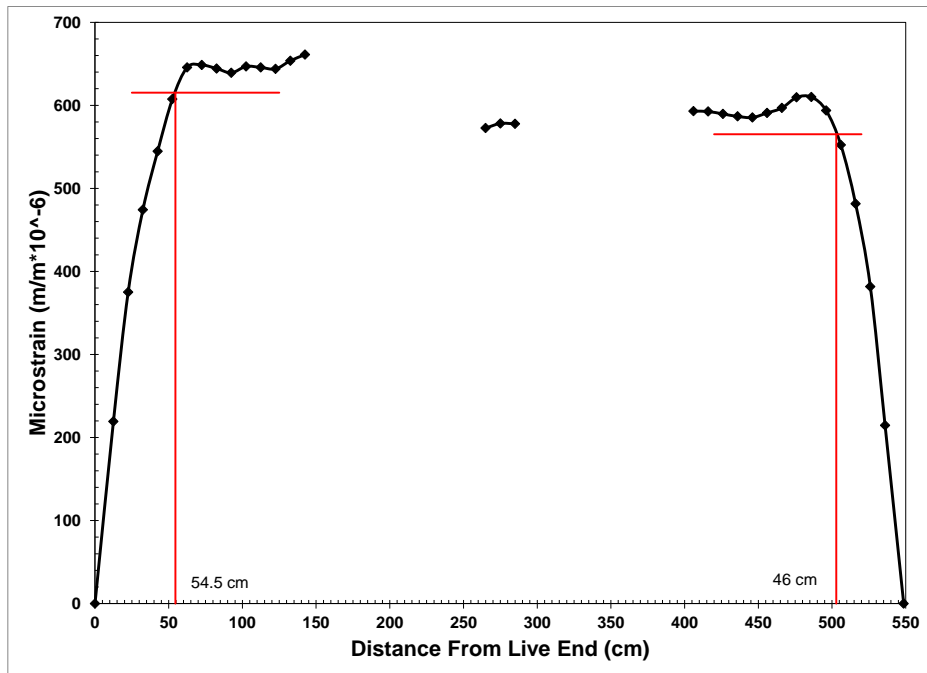


Figure D.105: 3-Day strain profile with 95% AMS for specimen HSL-1

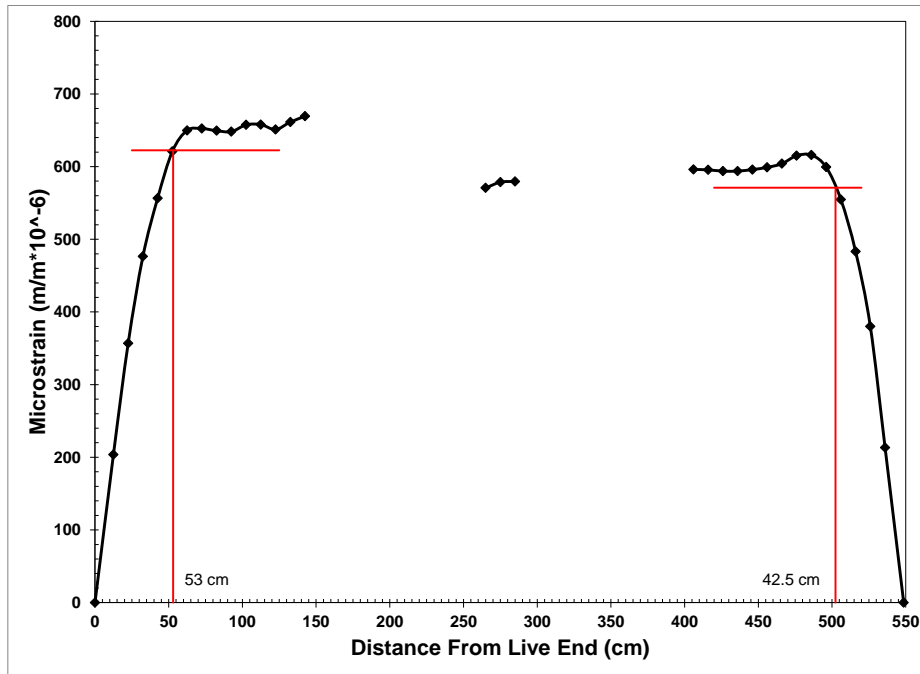


Figure D.106: 5-Day strain profile with 95% AMS for specimen HSL-1

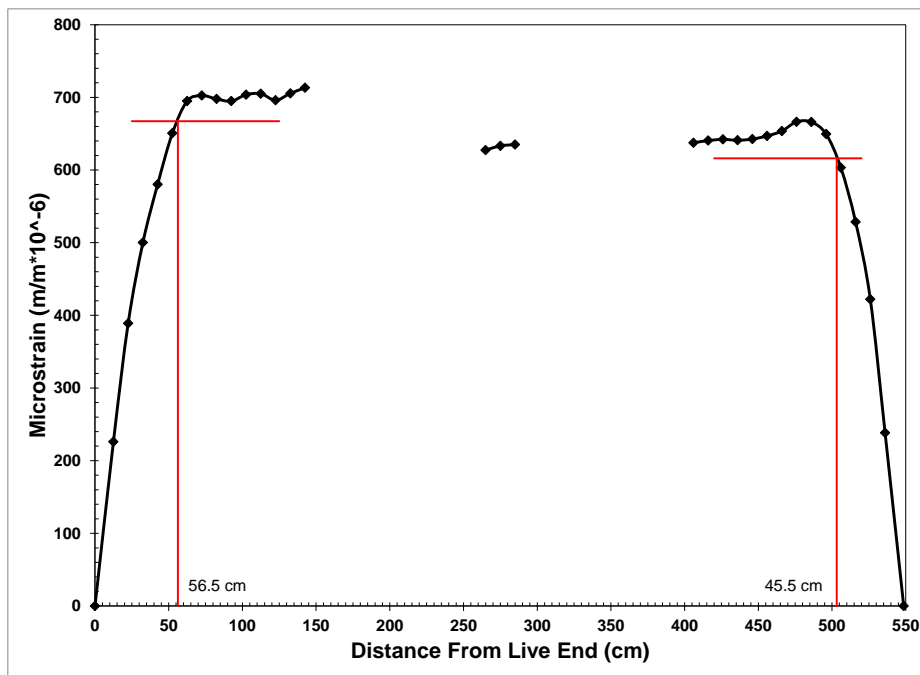


Figure D.107: 7-Day strain profile with 95% AMS for specimen HSL-1

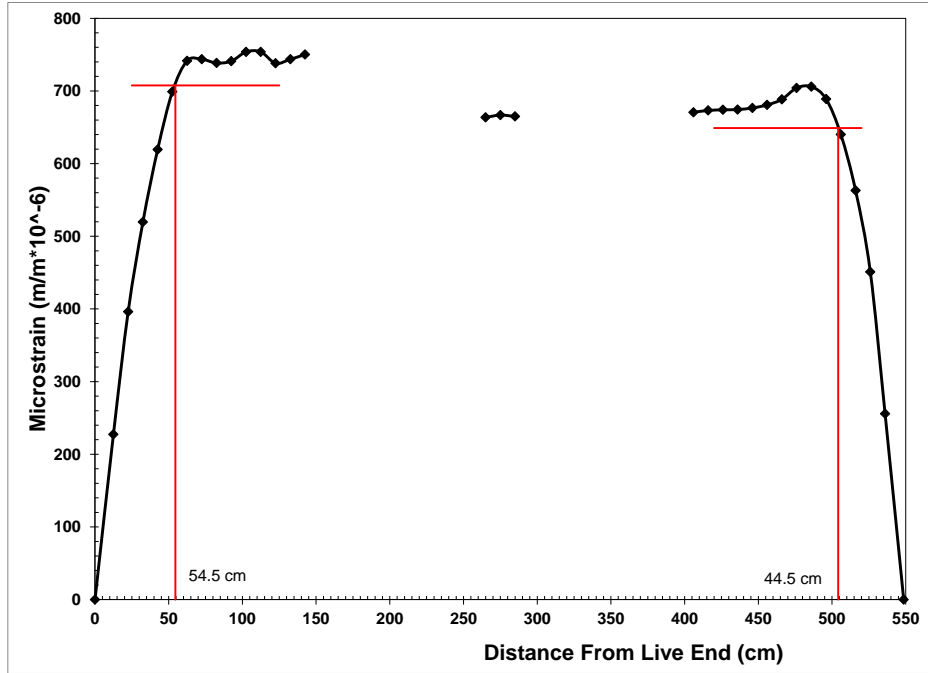


Figure D.108: 14-Day strain profile with 95% AMS for specimen HSL-1

### D.1.23 HSL-2

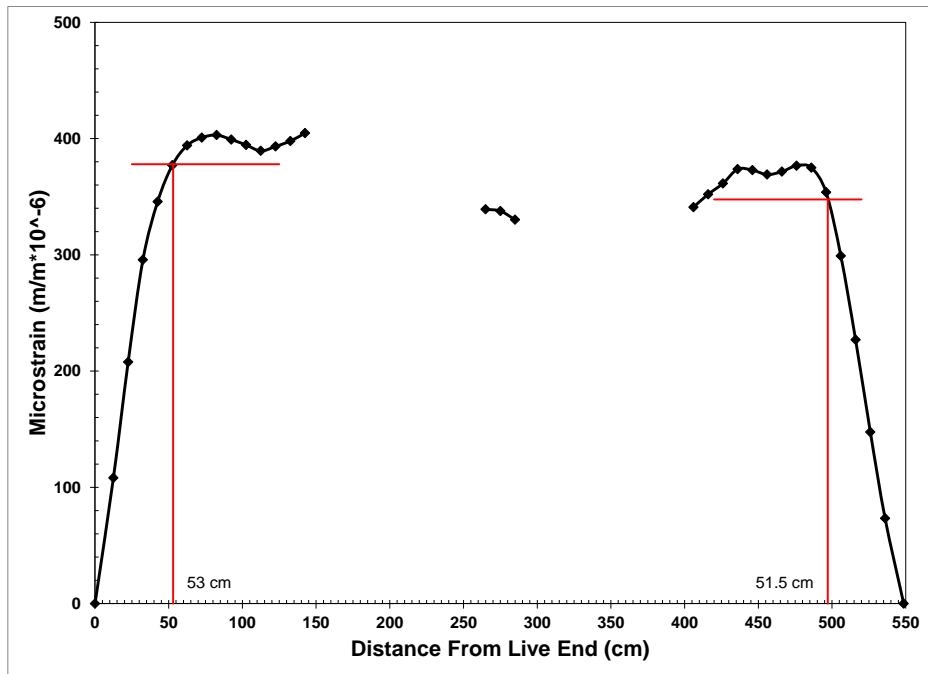


Figure D.109: Release strain profile with 95% AMS for specimen HSL-2

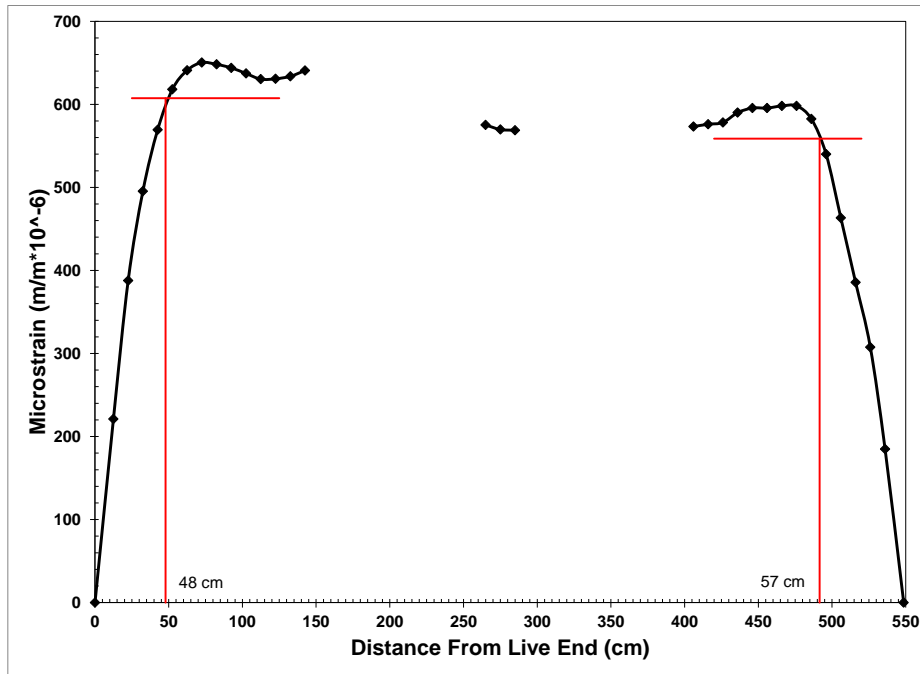


Figure D.110: 3-Day strain profile with 95% AMS for specimen HSL-2

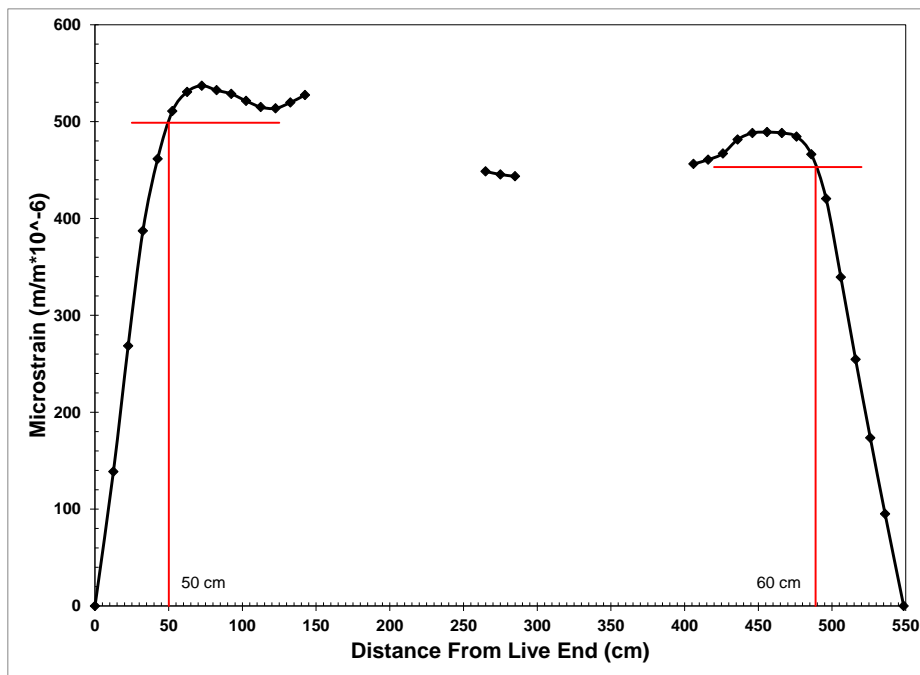


Figure D.111: 5-Day strain profile with 95% AMS for specimen HSL-2

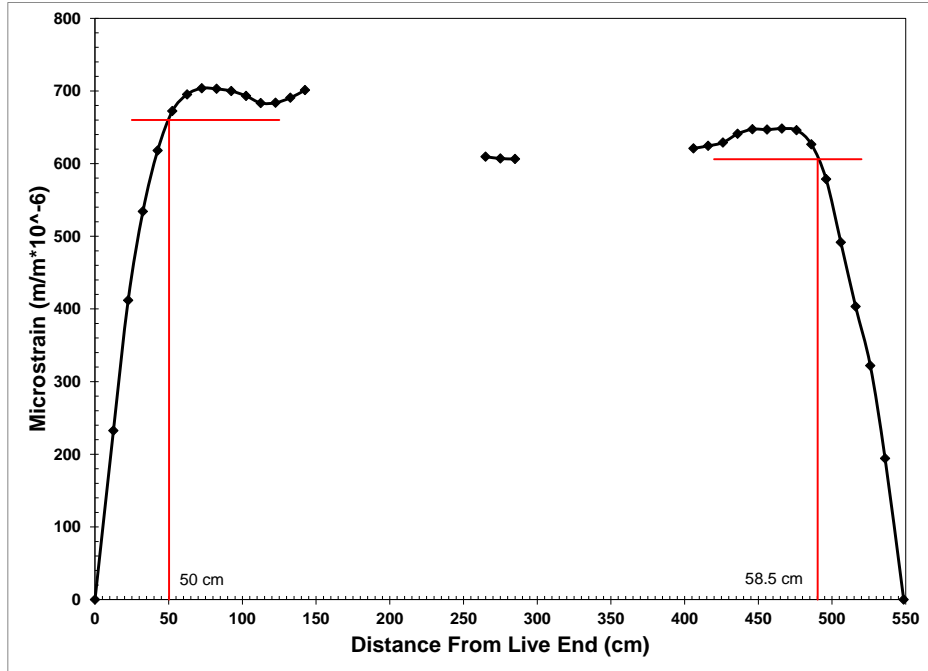


Figure D.112: 7-Day strain profile with 95% AMS for specimen HSL-2

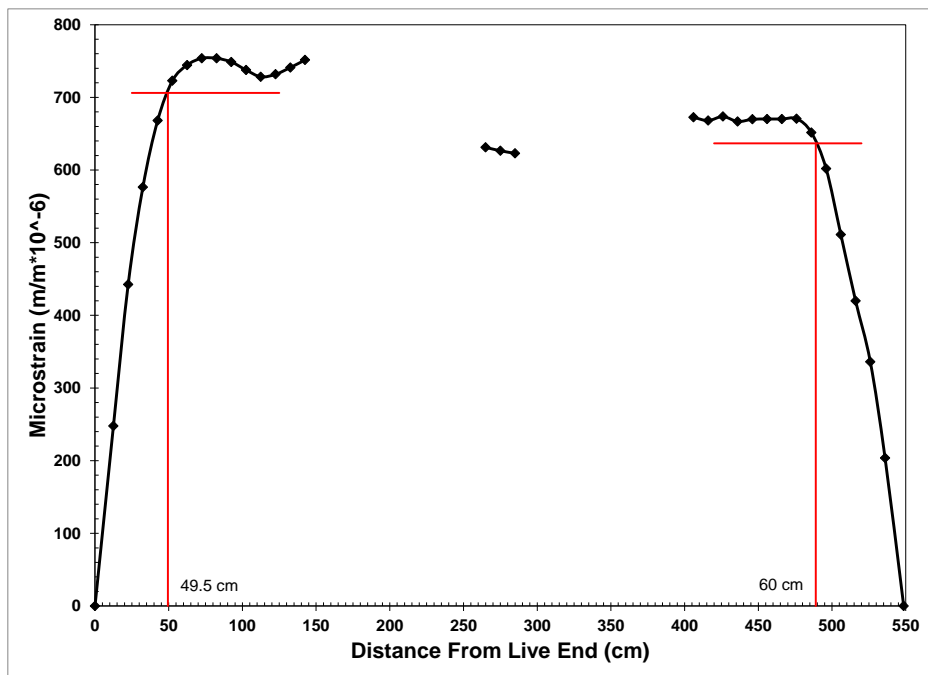


Figure D.113: 14-Day strain profile with 95% AMS for specimen HSL-2

### D.1.24 HSL-3

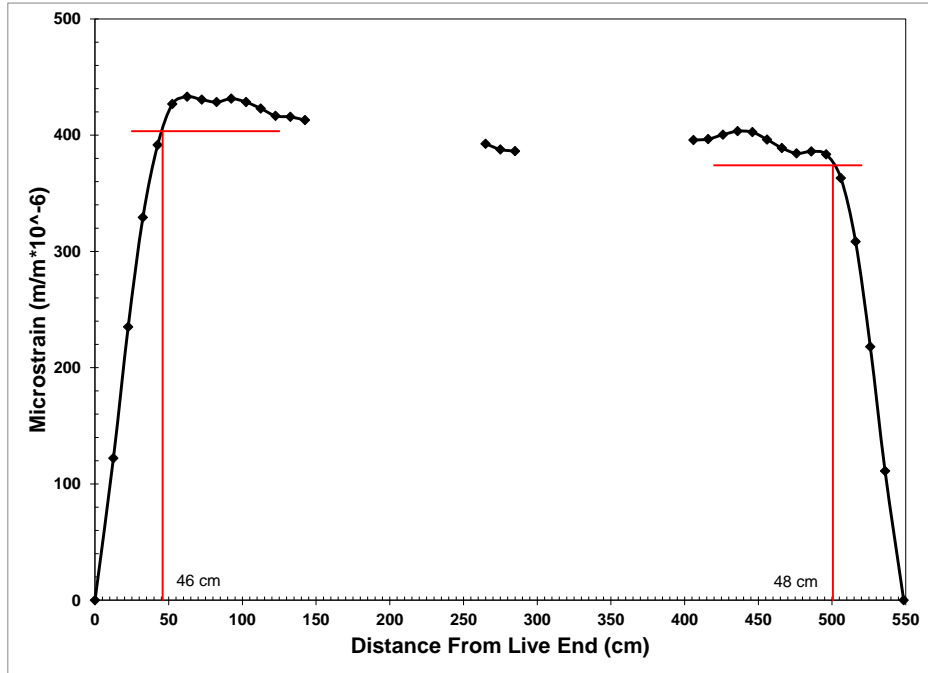


Figure D.114: Release strain profile with 95% AMS for specimen HSL-3

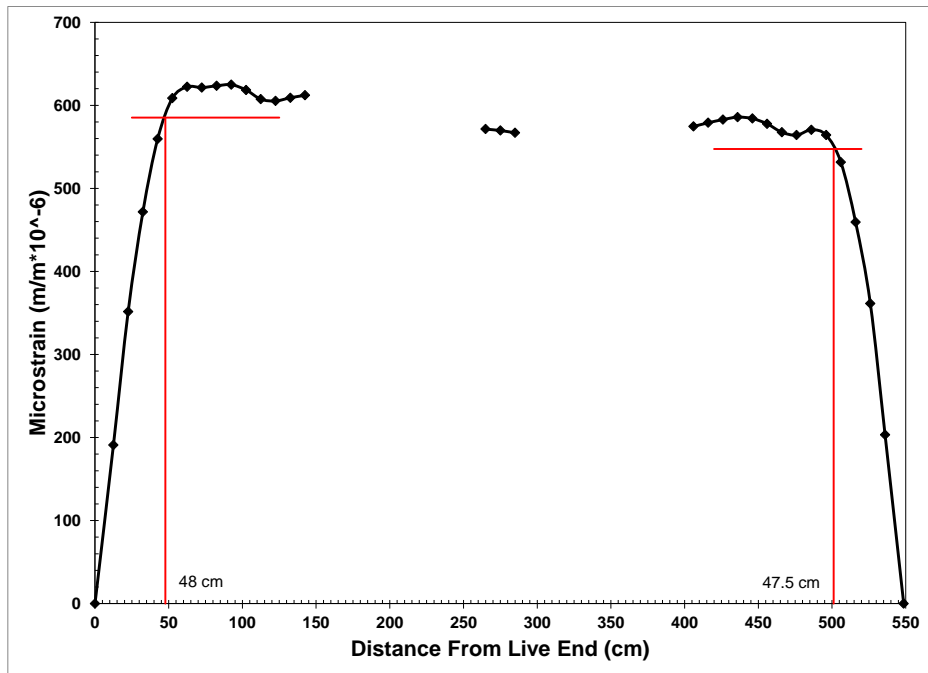


Figure D.115: 3-Day strain profile with 95% AMS for specimen HSL-3

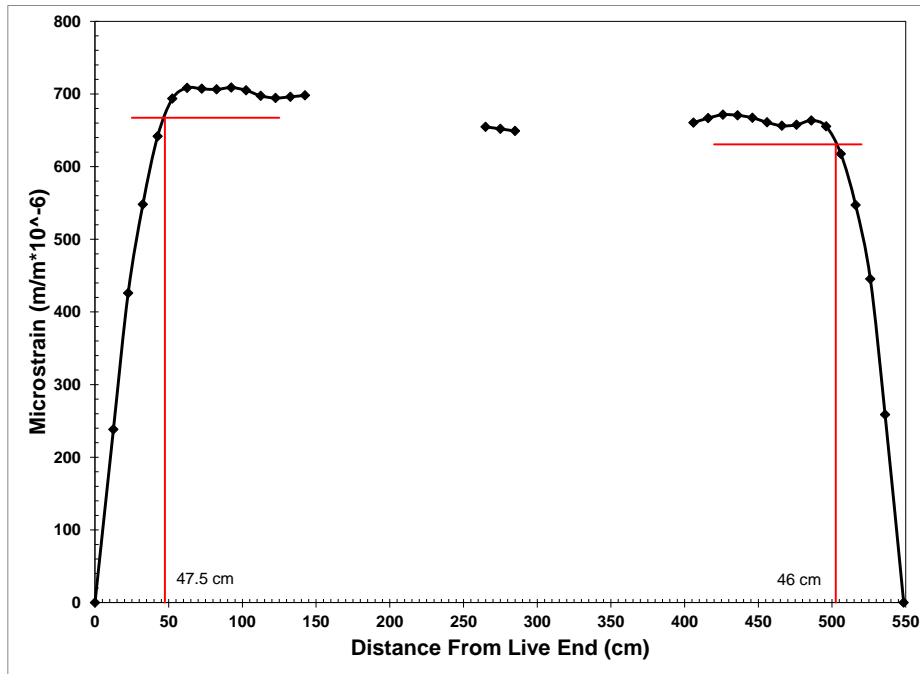


Figure D.116: 5-Day strain profile with 95% AMS for specimen HSL-3

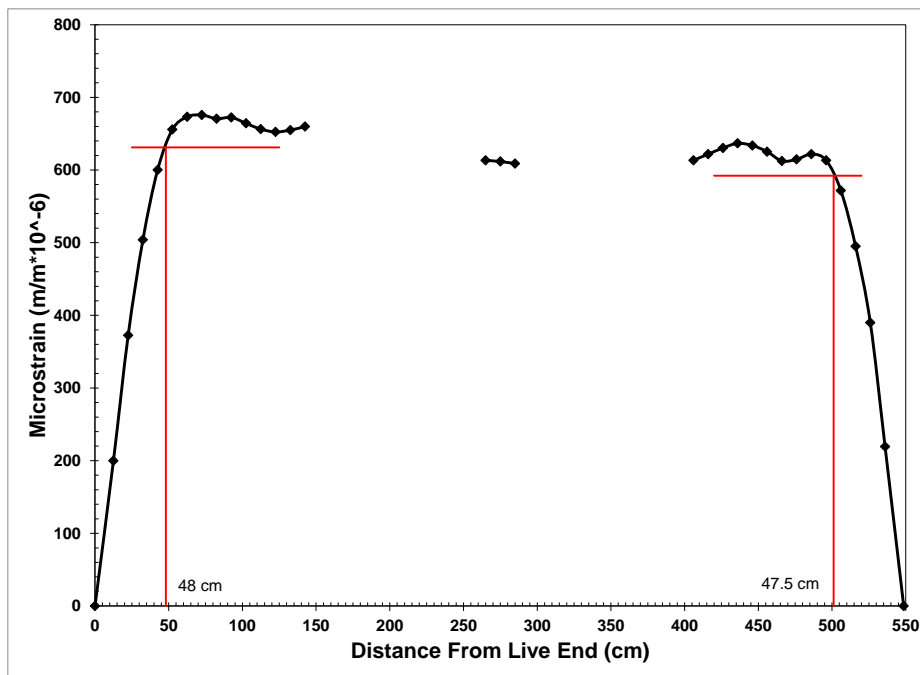


Figure D.117: 7-Day strain profile with 95% AMS for specimen HSL-3



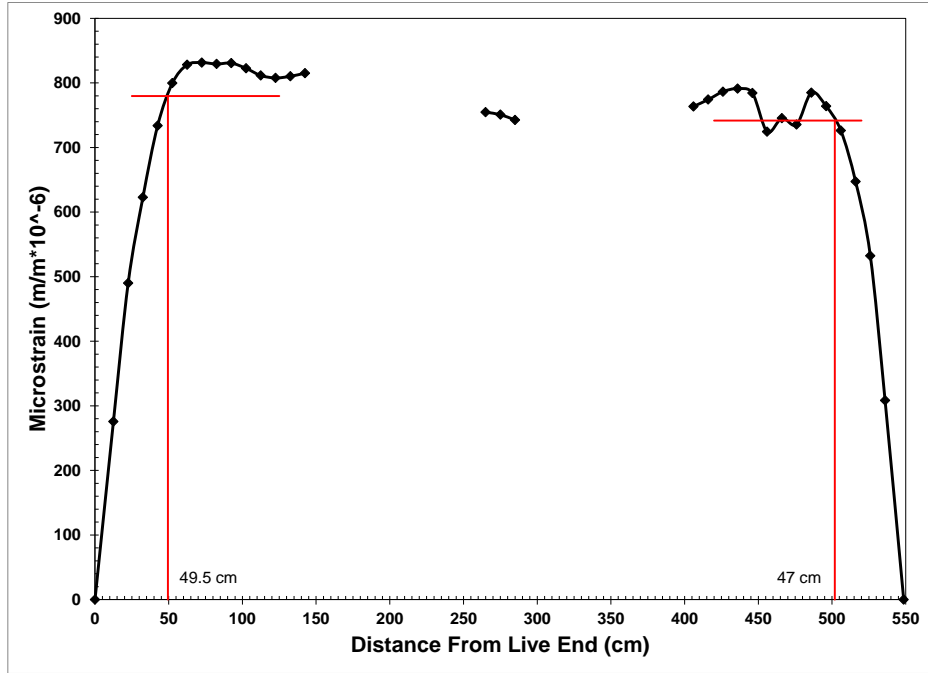


Figure D.118: 14-Day strain profile with 95% AMS for specimen HSL-3

#### D.1.25 HSL-4

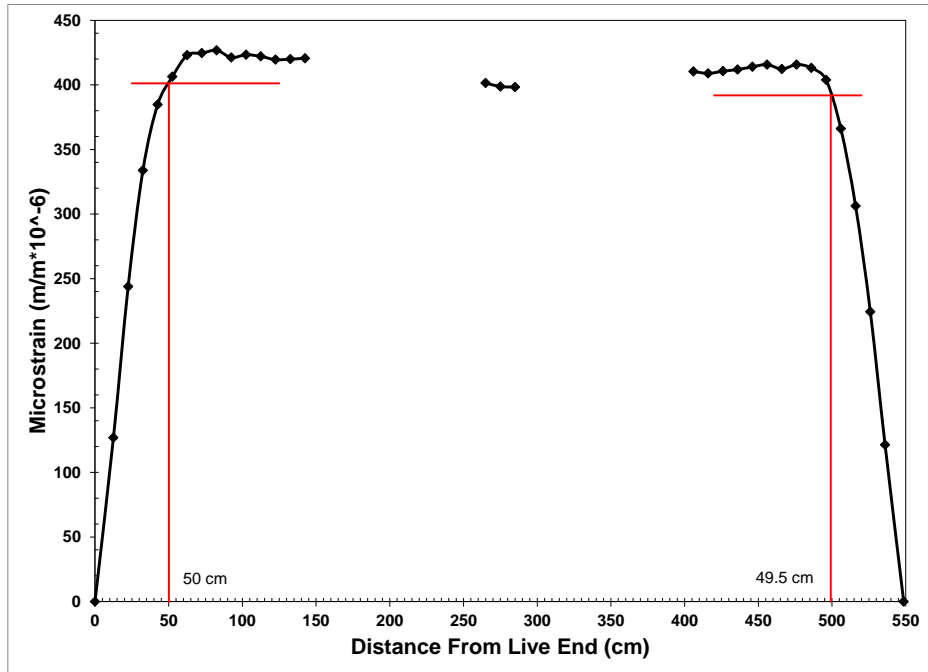


Figure D.119: Release strain profile with 95% AMS for specimen HSL-4

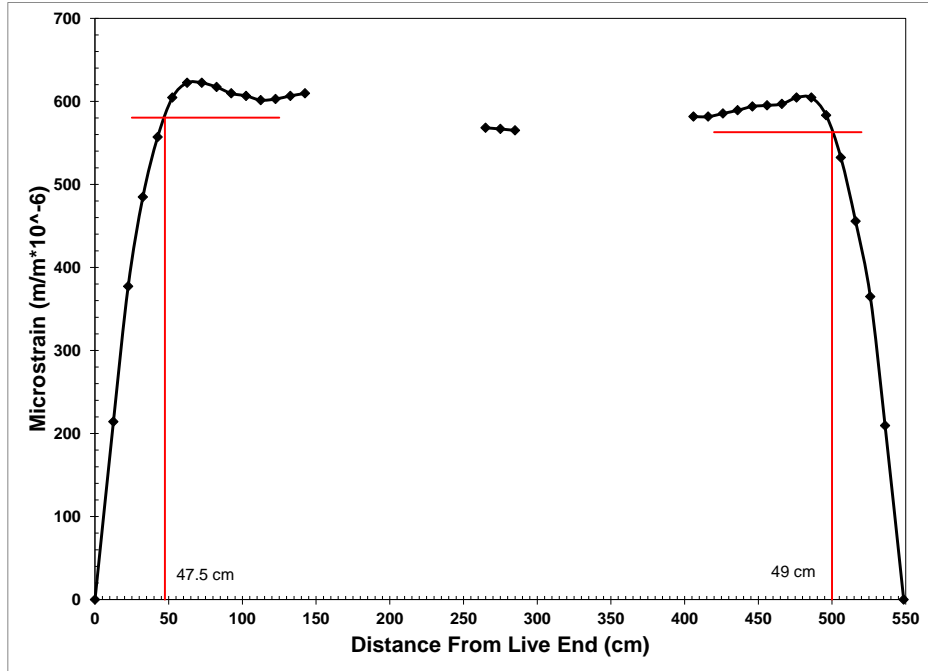


Figure D.120: 3-Day strain profile with 95% AMS for specimen HSL-4

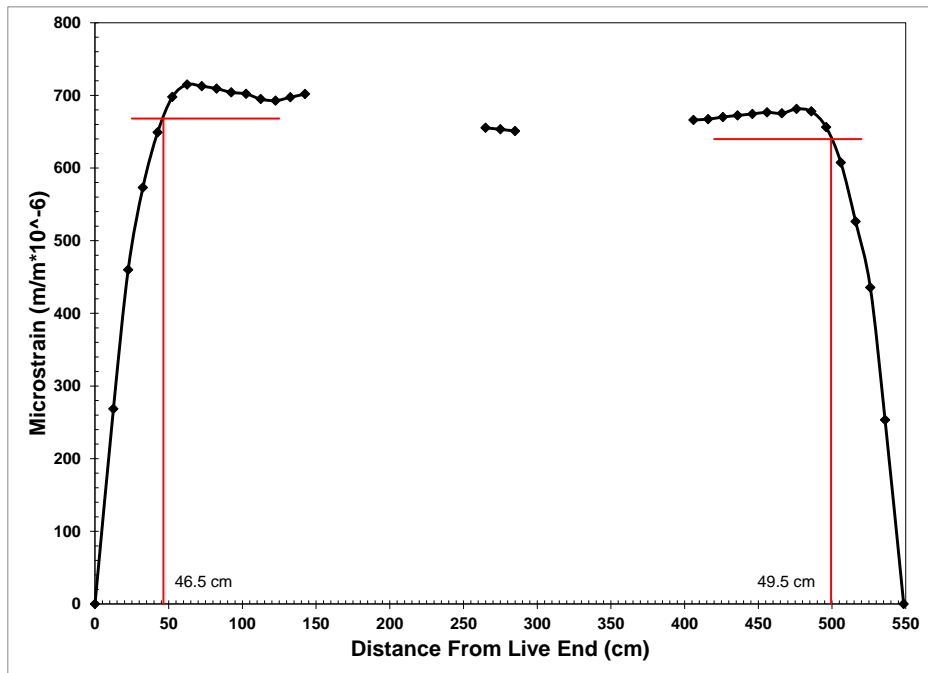


Figure D.121: 5-Day strain profile with 95% AMS for specimen HSL-4

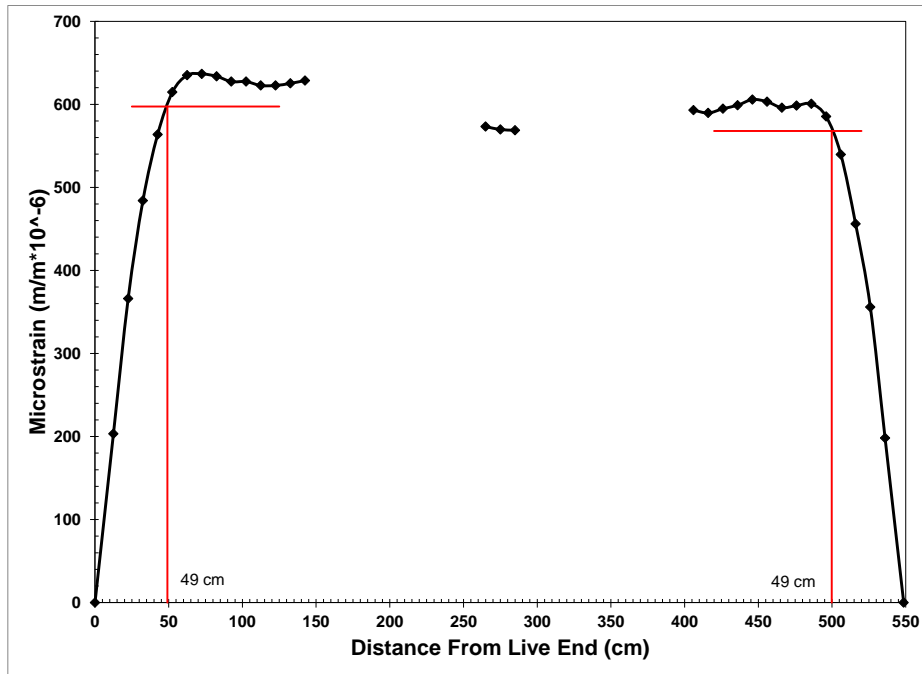


Figure D.122: 7-Day strain profile with 95% AMS for specimen HSL-4

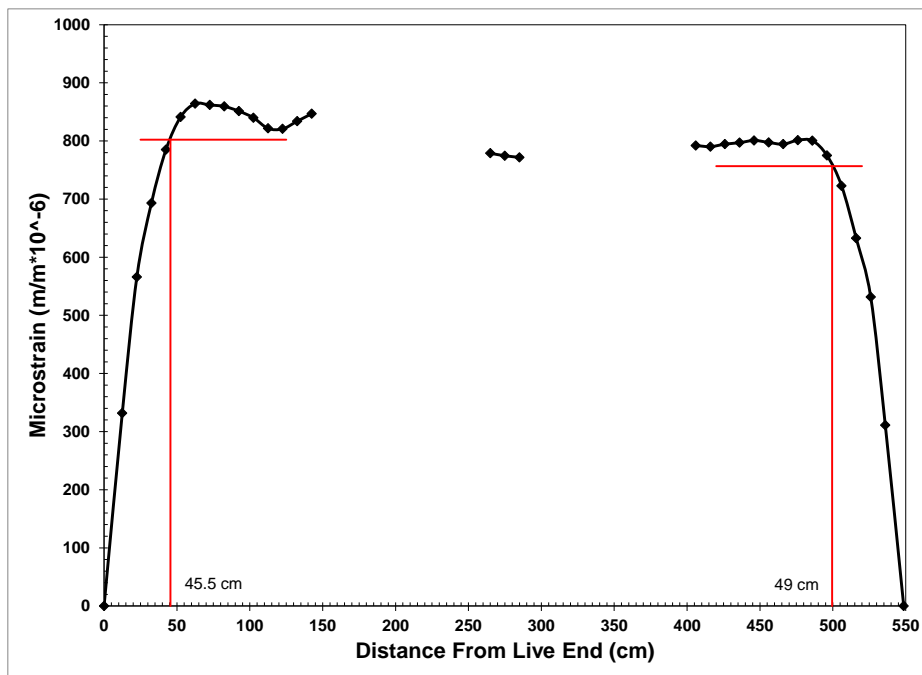


Figure D.123: 14-Day strain profile with 95% AMS for specimen HSL-4

## D.2 DEMEC Transfer Length Statistics

### D.2.1 Sample Statistical Parameters

Table D.1: NSC Series Statistical Parameters

<b>End</b>	<b>Live (in.)</b>		<b>Dead (in.)</b>		<b>Total (in.)</b>	
<b>Parameter</b>	<b>Mean</b>	<b>Std. Dev.</b>	<b>Mean</b>	<b>Std. Dev.</b>	<b>Mean</b>	<b>Std. Dev.</b>
<b>Release</b>	25.3	5.86	21.7	3.70	23.5	4.95
<b>3-Day</b>	28.1	8.21	23.4	5.29	25.7	6.24
<b>5-Day</b>	27.3	5.70	24.0	4.97	25.7	5.26
<b>7-Day</b>	27.1	5.69	24.1	4.58	25.6	5.04
<b>14-Day</b>	27.3	5.55	22.8	4.81	25.1	5.37
<b>28-Day</b>	27.5	5.52	22.6	5.32	25.0	5.65

Note: 1 in. = 25.4 mm

Table D.2: NSS Series Statistical Parameters

<b>End</b>	<b>Live (in.)</b>		<b>Dead (in.)</b>		<b>Total (in.)</b>	
<b>Parameter</b>	<b>Mean</b>	<b>Std. Dev.</b>	<b>Mean</b>	<b>Std. Dev.</b>	<b>Mean</b>	<b>Std. Dev.</b>
<b>Release</b>	34.3	6.20	23.3	3.04	28.8	7.39
<b>3-Day</b>	31.1	2.24	24.2	3.69	27.6	4.65
<b>5-Day</b>	32.0	6.03	27.5	5.65	29.7	5.99
<b>7-Day</b>	29.1	2.96	27.1	7.69	28.1	5.60
<b>14-Day</b>	28.0	2.54	26.9	7.02	27.5	5.01
<b>28-Day</b>	27.4	2.96	26.2	6.74	26.8	4.95

Note: 1 in. = 25.4 mm

Table D.3: NSL Series Statistical Parameters

<b>End</b>	<b>Live (in.)</b>		<b>Dead (in.)</b>		<b>Total (in.)</b>	
<b>Parameter</b>	<b>Mean</b>	<b>Std. Dev.</b>	<b>Mean</b>	<b>Std. Dev.</b>	<b>Mean</b>	<b>Std. Dev.</b>
<b>Release</b>	34.3	6.20	23.3	3.04	28.8	7.39
<b>3-Day</b>	31.1	2.24	24.2	3.69	27.6	4.65
<b>5-Day</b>	32.0	6.03	27.5	5.65	29.7	5.99
<b>7-Day</b>	29.1	2.96	27.1	7.69	28.1	5.60
<b>14-Day</b>	28.0	2.54	26.9	7.02	27.5	5.01
<b>28-Day</b>	27.4	2.96	26.2	6.74	26.8	4.95

Note: 1 in. = 25.4 mm

Table D.4: HSC Series Statistical Parameters

<b>End</b>	<b>Live (in.)</b>		<b>Dead (in.)</b>		<b>Total (in.)</b>	
<b>Parameter</b>	<b>Mean</b>	<b>Std. Dev.</b>	<b>Mean</b>	<b>Std. Dev.</b>	<b>Mean</b>	<b>Std. Dev.</b>
<b>Release</b>	22.0	5.81	16.2	2.43	19.1	5.16
<b>3-Day</b>	22.6	5.04	17.5	2.91	20.1	4.67
<b>5-Day</b>	21.3	2.21	18.5	3.55	19.9	3.11
<b>7-Day</b>	21.3	2.19	18.0	2.92	19.7	2.97
<b>14-Day</b>	20.6	1.44	17.9	2.41	19.2	2.34
<b>28-Day</b>	20.1	3.11	18.2	1.99	19.2	2.63

Note: 1 in. = 25.4 mm

Table D.5: HSS Series Statistical Parameters

<b>End</b>	<b>Live (in.)</b>		<b>Dead (in.)</b>		<b>Total (in.)</b>	
<b>Parameter</b>	<b>Mean</b>	<b>Std. Dev.</b>	<b>Mean</b>	<b>Std. Dev.</b>	<b>Mean</b>	<b>Std. Dev.</b>
<b>Release</b>	23.5	2.61	17.5	1.50	20.5	3.74
<b>3-Day</b>	21.4	2.53	17.7	1.58	19.5	2.78
<b>5-Day</b>	20.0	2.25	16.5	1.09	18.3	2.50
<b>7-Day</b>	19.1	3.00	15.9	0.94	17.5	2.66
<b>14-Day</b>	18.9	2.64	16.3	1.13	17.6	2.36
<b>28-Day</b>	17.9	2.00	15.7	1.03	16.8	1.87

Note: 1 in. = 25.4 mm

Table D.6: HSL Series Statistical Parameters

<b>End</b>	<b>Live (in.)</b>		<b>Dead (in.)</b>		<b>Total (in.)</b>	
<b>Parameter</b>	<b>Mean</b>	<b>Std. Dev.</b>	<b>Mean</b>	<b>Std. Dev.</b>	<b>Mean</b>	<b>Std. Dev.</b>
<b>Release</b>	20.1	1.54	19.5	0.58	19.8	1.12
<b>3-Day</b>	19.5	1.32	19.6	1.93	19.6	1.53
<b>5-Day</b>	19.4	1.14	19.5	2.98	19.4	2.09
<b>7-Day</b>	20.0	1.51	19.7	2.27	19.9	1.79
<b>14-Day</b>	19.6	1.45	19.7	2.69	19.7	2.00
<b>28-Day</b>	20.9	1.40	20.9	2.89	20.9	2.11

Note: 1 in. = 25.4 mm

## D.2.2 95% Confidence Intervals Using a *t* Distribution

Table D.7: NSC Series 95% Confidence Intervals

End	Live (in.)		Dead (in.)		Total (in.)	
	Lower	Upper	Lower	Upper	Lower	Upper
Release	16.0	34.7	15.8	27.5	19.4	27.6
3-Day	15.0	41.1	15.0	31.8	20.5	31.0
5-Day	18.2	36.4	16.1	31.9	21.3	30.1
7-Day	18.0	36.1	16.8	31.3	21.3	29.8
14-Day	18.5	36.1	15.2	30.5	20.6	29.6
28-Day	18.7	36.2	14.1	31.1	20.3	29.8

Note: 1 in. = 25.4 mm

Table D.8: NSS Series 95% Confidence Intervals

End	Live (in.)		Dead (in.)		Total (in.)	
	Lower	Upper	Lower	Upper	Lower	Upper
Release	26.6	42.0	19.6	27.1	23.5	34.1
3-Day	28.3	33.9	19.6	28.8	24.3	31.0
5-Day	24.5	39.4	20.5	34.5	25.4	34.0
7-Day	25.5	32.8	17.6	36.7	24.1	32.1
14-Day	24.8	31.1	18.2	35.6	23.9	31.0
28-Day	23.7	31.1	17.8	34.6	23.3	30.4

Note: 1 in. = 25.4 mm

Table D.9: NSL Series 95% Confidence Intervals

End	Live (in.)		Dead (in.)		Total (in.)	
	Lower	Upper	Lower	Upper	Lower	Upper
Release	17.1	22.2	18.2	20.1	18.4	20.5
3-Day	15.5	22.7	16.1	28.8	17.7	23.3
5-Day	15.0	23.8	17.2	28.2	18.1	23.6
7-Day	16.1	24.4	18.8	27.1	19.1	23.8
14-Day	19.0	22.7	15.8	27.7	19.3	23.2
28-Day	17.8	24.5	17.6	26.8	19.7	23.5

Note: 1 in. = 25.4 mm, excluded data from dead end of NSL-4

Table D.10: HSC Series 95% Confidence Intervals

End	Live (in.)		Dead (in.)		Total (in.)	
	Lower	Upper	Lower	Upper	Lower	Upper
Release	12.8	31.3	12.4	20.1	14.8	23.5
3-Day	14.6	30.6	12.9	22.1	16.1	24.0
5-Day	17.7	24.8	12.9	24.1	17.3	22.5
7-Day	17.8	24.8	13.4	22.7	17.2	22.1
14-Day	18.3	22.9	14.0	21.7	17.3	21.2
28-Day	15.2	25.1	15.0	21.4	17.0	21.4

Note: 1 in. = 25.4 mm

Table D.11: HSS Series 95% Confidence Intervals

<b>End Limit</b>	<b>Live (in.)</b>		<b>Dead (in.)</b>		<b>Total (in.)</b>	
	<b>Lower</b>	<b>Upper</b>	<b>Lower</b>	<b>Upper</b>	<b>Lower</b>	<b>Upper</b>
<b>Release</b>	19.3	27.6	15.1	19.9	17.4	23.6
<b>3-Day</b>	17.3	25.4	15.2	20.2	17.2	21.8
<b>5-Day</b>	16.4	23.6	14.7	18.2	16.2	20.4
<b>7-Day</b>	14.3	23.9	14.5	17.4	15.3	19.7
<b>14-Day</b>	14.7	23.2	14.5	18.1	15.6	19.6
<b>28-Day</b>	14.7	21.0	14.1	17.3	15.2	18.3

Note: 1 in. = 25.4 mm

Table D.12: HSL Series 95% Confidence Intervals

<b>End Limit</b>	<b>Live (in.)</b>		<b>Dead (in.)</b>		<b>Total (in.)</b>	
	<b>Lower</b>	<b>Upper</b>	<b>Lower</b>	<b>Upper</b>	<b>Lower</b>	<b>Upper</b>
<b>Release</b>	17.6	22.5	18.6	20.4	18.8	20.7
<b>3-Day</b>	17.4	21.6	16.6	22.7	18.3	20.8
<b>5-Day</b>	17.6	21.2	14.8	24.2	17.7	21.2
<b>7-Day</b>	17.6	22.4	16.1	23.3	18.4	21.4
<b>14-Day</b>	17.3	21.9	15.5	24.0	18.0	21.3
<b>28-Day</b>	18.7	23.2	16.3	25.5	19.1	22.7

Note: 1 in. = 25.4 mm

### D.2.3 Hypothesis Testing

Hypothesis tests were conducted on the means between the various populations using the assumption of equal variance for both populations and a  $t$  distribution with  $\alpha = 0.05$ . In this analysis  $S_p^2$  is the pooled estimator of the equal population variance,  $\sigma^2$ , calculated using the relationship

$$S_p^2 = \frac{(n_1 - 1)S_1^2 + (n_2 - 1)S_2^2}{n_1 + n_2 - 2}$$

where  $S_1^2$  and  $S_2^2$  are the sample variances and  $n_1$  and  $n_2$  are the corresponding sample sizes.

The null hypothesis was  $\mu_1 = \mu_2$  and the alternate hypothesis was  $\mu_1 \neq \mu_2$ , where  $\mu_1$  and  $\mu_2$  are the population means. The test statistic,  $T_0$ , was calculated using the relationship

$$T_0 = \frac{X_1 - X_2 - (0)}{S_p \sqrt{\frac{1}{n_1} + \frac{1}{n_2}}}$$

where  $X_1$  and  $X_2$  are the sample means. This value was then compared to the  $t$  statistic with degrees of freedom  $v = n_1 + n_2 - 2$  and  $\alpha = 0.05$ . The hypothesis was rejected if  $T_0 > t_{\alpha/2, v}$  or  $T_0 < -t_{\alpha/2, v}$ . In the following tables R indicates rejection of the null hypothesis while FTR indicates failure to reject the hypothesis.



Table D.13: Test for Difference in the Means of the NSC and NSS Series

End	Live				Dead				Total			
Parameter	$S_p$	$T_0$	$t_{0.025,v}$	Conclusion	$S_p$	$T_0$	$t_{0.025,v}$	Conclusion	$S_p$	$T_0$	$t_{0.025,v}$	Conclusion
Release	6.057	-2.212	2.365	FTR	3.338	-0.756	2.365	FTR	6.441	-1.748	2.120	FTR
3-Day	5.638	-0.807	2.365	FTR	4.447	-0.251	2.365	FTR	5.404	-0.741	2.120	FTR
5-Day	5.890	-1.178	2.365	FTR	5.366	-0.963	2.365	FTR	5.681	-1.507	2.120	FTR
7-Day	4.344	-0.709	2.365	FTR	6.542	-0.697	2.365	FTR	5.361	-1.008	2.120	FTR
14-Day	4.107	-0.246	2.365	FTR	6.174	-0.989	2.365	FTR	5.171	-0.973	2.120	FTR
28-Day	4.248	0.021	2.365	FTR	6.173	-0.877	2.365	FTR	5.268	-0.715	2.120	FTR

Table D.14: Test for Difference in the Means of the NSC and NSL Series

End	Live				Dead				Total			
Parameter	$S_p$	$T_0$	$t_{0.025,v}$	Conclusion	$S_p$	$T_0$	$t_{0.025,v}$	Conclusion	$S_p$	$T_0$	$t_{0.025,v}$	Conclusion
Release	4.300	1.861	2.447	FTR	2.653	1.329	2.447	FTR	3.606	2.240	2.145	R
3-Day	6.028	2.101	2.447	FTR	4.687	0.297	2.447	FTR	5.004	2.082	2.145	FTR
5-Day	4.479	2.502	2.447	R	4.272	0.434	2.447	FTR	4.387	2.213	2.145	R
7-Day	4.423	2.172	2.447	FTR	3.730	0.417	2.447	FTR	4.072	2.032	2.145	FTR
14-Day	4.008	2.275	2.447	FTR	4.311	0.344	2.447	FTR	4.149	1.838	2.145	FTR
28-Day	4.173	2.135	2.447	FTR	4.285	0.135	2.447	FTR	4.316	1.588	2.145	FTR

Table D.15: Test for Difference in the Means of the NSS and NSL Series

End	Live				Dead				Total			
Parameter	$S_p$	$T_0$	$t_{0.025,v}$	Conclusion	$S_p$	$T_0$	$t_{0.025,v}$	Conclusion	$S_p$	$T_0$	$t_{0.025,v}$	Conclusion
Release	4.802	4.547	2.365	R	2.328	2.680	2.365	R	5.605	3.528	2.120	R
3-Day	2.262	7.915	2.365	R	3.825	0.675	2.365	FTR	4.128	3.631	2.120	R
5-Day	4.898	3.828	2.365	R	4.826	1.476	2.365	FTR	4.995	3.762	2.120	R
7-Day	2.812	4.697	2.365	R	6.063	1.023	2.365	FTR	4.583	3.083	2.120	R
14-Day	2.063	5.149	2.365	R	5.847	1.312	2.365	FTR	4.069	3.213	2.120	R
28-Day	2.622	3.548	2.365	R	5.439	1.108	2.365	FTR	4.011	2.741	2.120	R

Table D.16: Test for Difference in the Means of the HSC and HSS Series

End	Live				Dead				Total			
Parameter	$S_p$	$T_0$	$t_{0.025,v}$	Conclusion	$S_p$	$T_0$	$t_{0.025,v}$	Conclusion	$S_p$	$T_0$	$t_{0.025,v}$	Conclusion
Release	4.505	-0.448	2.447	FTR	2.022	-0.895	2.447	FTR	4.509	-0.600	2.145	FTR
3-Day	3.987	0.436	2.447	FTR	2.339	-0.089	2.447	FTR	3.844	0.282	2.145	FTR
5-Day	2.231	0.780	2.447	FTR	2.625	1.087	2.447	FTR	2.822	1.151	2.145	FTR
7-Day	2.627	1.192	2.447	FTR	2.167	1.349	2.447	FTR	2.818	1.519	2.145	FTR
14-Day	2.129	1.079	2.447	FTR	1.884	1.182	2.447	FTR	2.349	1.362	2.145	FTR
28-Day	2.613	1.225	2.447	FTR	1.587	2.237	2.447	FTR	2.281	2.093	2.145	FTR

Table D.17: Test for Difference in the Means of the HSC and HSL Series

End	Live				Dead				Total			
Parameter	$S_p$	$T_0$	$t_{0.025,v}$	Conclusion	$S_p$	$T_0$	$t_{0.025,v}$	Conclusion	$S_p$	$T_0$	$t_{0.025,v}$	Conclusion
Release	4.252	0.655	2.447	FTR	1.770	-2.595	2.447	R	3.736	-0.342	2.145	FTR
3-Day	3.682	1.191	2.447	FTR	2.468	-1.213	2.447	FTR	3.477	0.283	2.145	FTR
5-Day	1.759	1.504	2.447	FTR	3.274	-0.425	2.447	FTR	2.647	0.335	2.145	FTR
7-Day	1.884	0.961	2.447	FTR	2.614	-0.932	2.447	FTR	2.452	-0.181	2.145	FTR
14-Day	1.447	0.962	2.447	FTR	2.556	-1.035	2.447	FTR	2.179	-0.407	2.145	FTR
28-Day	2.413	-0.461	2.447	FTR	2.483	-1.513	2.447	FTR	2.380	-1.447	2.145	FTR

Table D.18: Test for Difference in the Means of the HSS and HSL Series

End	Live				Dead				Total			
Parameter	$S_p$	$T_0$	$t_{0.025,v}$	Conclusion	$S_p$	$T_0$	$t_{0.025,v}$	Conclusion	$S_p$	$T_0$	$t_{0.025,v}$	Conclusion
Release	2.142	2.631	2.447	R	1.137	-2.449	2.447	R	2.763	0.516	2.145	FTR
3-Day	2.019	1.207	2.447	FTR	1.763	-1.579	2.447	FTR	2.242	-0.044	2.145	FTR
5-Day	1.786	0.429	2.447	FTR	2.243	-1.893	2.447	FTR	2.306	-1.024	2.145	FTR
7-Day	2.374	-0.381	2.447	FTR	1.736	-3.087	2.447	R	2.267	-2.084	2.145	FTR
14-Day	2.132	-0.522	2.447	FTR	2.064	-2.361	2.447	FTR	2.188	-1.867	2.145	FTR
28-Day	1.726	-2.459	2.447	R	2.172	-3.364	2.447	R	1.993	-4.125	2.145	R

Table D.19: Test for Difference in the Means of the NSC and HSC Series

End	Live				Dead				Total			
Parameter	$S_p$	$T_0$	$t_{0.025,v}$	Conclusion	$S_p$	$T_0$	$t_{0.025,v}$	Conclusion	$S_p$	$T_0$	$t_{0.025,v}$	Conclusion
Release	5.839	0.799	2.447	FTR	3.134	2.443	2.447	FTR	5.058	1.722	2.145	FTR
3-Day	6.813	1.134	2.447	FTR	4.268	1.957	2.447	FTR	5.513	2.062	2.145	FTR
5-Day	4.325	1.979	2.447	FTR	4.316	1.806	2.447	FTR	4.317	2.679	2.145	R
7-Day	4.311	1.889	2.447	FTR	3.839	2.230	2.447	FTR	4.138	2.854	2.145	R
14-Day	4.053	2.352	2.447	FTR	3.808	1.846	2.447	FTR	4.143	2.827	2.145	R
28-Day	4.479	2.315	2.447	FTR	4.016	1.542	2.447	FTR	4.408	2.657	2.145	R

Table D.20: Test for Difference in the Means of the NSS and HSS Series

End	Live				Dead				Total			
Parameter	$S_p$	$T_0$	$t_{0.025,v}$	Conclusion	$S_p$	$T_0$	$t_{0.025,v}$	Conclusion	$S_p$	$T_0$	$t_{0.025,v}$	Conclusion
Release	4.987	3.079	2.365	R	2.496	3.302	2.365	R	6.074	2.895	2.120	R
3-Day	2.373	5.808	2.365	R	2.976	3.092	2.365	R	3.942	4.345	2.120	R
5-Day	4.787	3.527	2.365	R	4.328	3.592	2.365	R	4.789	5.047	2.120	R
7-Day	2.976	4.771	2.365	R	5.847	2.704	2.365	R	4.550	4.916	2.120	R
14-Day	2.583	4.952	2.365	R	5.360	2.807	2.365	R	4.068	5.101	2.120	R
28-Day	2.590	5.208	2.365	R	5.142	2.894	2.365	R	3.912	5.405	2.120	R

Table D.21: Test for Difference in the Means of the NSL and HSL Series

End	Live				Dead				Total			
Parameter	$S_p$	$T_0$	$t_{0.025,v}$	Conclusion	$S_p$	$T_0$	$t_{0.025,v}$	Conclusion	$S_p$	$T_0$	$t_{0.025,v}$	Conclusion
Release	1.575	-0.354	2.447	FTR	0.591	-0.786	2.447	FTR	1.173	-0.551	2.145	FTR
3-Day	1.864	-0.299	2.447	FTR	3.138	1.264	2.447	FTR	2.596	0.745	2.145	FTR
5-Day	2.108	0.000	2.447	FTR	3.217	1.414	2.447	FTR	2.760	0.994	2.145	FTR
7-Day	2.127	0.164	2.447	FTR	2.452	1.864	2.447	FTR	2.340	1.322	2.145	FTR
14-Day	1.313	1.378	2.447	FTR	3.259	0.890	2.447	FTR	2.190	1.461	2.145	FTR
28-Day	1.782	0.195	2.447	FTR	2.898	0.641	2.447	FTR	2.205	0.641	2.145	FTR

### D.3 End Slip Data

Table D.22: NSC End Slip Over Time

End	Live (in.)				Dead (in.)			
Specimen	NSC-1	NSC-2	NSC-3	NSC-4	NSC-1	NSC-2	NSC-3	NSC-4
Release	0.060	0.050	0.084	0.069	0.030	0.049	0.032	0.043
3-Day	0.077	0.059	--	--	0.043	0.059	--	--
5-Day	0.067	0.049	0.080	0.066	0.028	0.049	0.025	0.038
7-Day	0.058	0.047	0.080	0.065	0.031	0.056	0.026	0.039
14-Day	0.070	0.049	0.079	0.065	0.031	0.047	0.027	0.040
28-Day	0.050	0.048	0.080	0.067	0.030	0.055	0.029	0.041

Note: 1 in. = 25.4 mm, -- indicates no measurement

Table D.23: NSS End Slip Over Time

End	Live (in.)					Dead (in.)				
Specimen	NSS-1	NSS-2	NSS-3	NSS-4	NSS-5	NSS-1	NSS-2	NSS-3	NSS-4	NSS-5
Release	--	0.036	0.055	0.054	0.056	0.052	0.053	0.055	0.057	0.055
3-Day	0.086	0.043	0.066	0.059	0.061	0.056	0.057	0.058	0.061	0.056
5-Day	0.085	0.045	0.056	0.059	0.059	0.055	0.056	0.059	0.060	0.056
7-Day	0.086	0.046	0.055	0.058	0.058	0.055	0.058	0.061	0.060	0.054
14-Day	0.085	0.046	0.055	0.059	0.061	0.056	0.058	0.061	0.062	0.055
28-Day	0.086	0.044	0.055	0.056	0.058	0.055	0.057	0.061	0.059	0.054

Note: 1 in. = 25.4 mm, -- indicates erroneous measurement

Table D.24: NSL End Slip Over Time

End	Live (in.)				Dead (in.)			
Specimen	NSL-1	NSL-2	NSL-3	NSL-4	NSL-1	NSL-2	NSL-3	NSL-4
Release	0.036	0.032	0.044	0.045	0.037	0.031	0.045	0.142
3-Day	0.047	0.037	0.060	0.057	0.048	0.038	0.061	0.158
5-Day	0.053	0.040	0.066	0.063	0.052	0.041	0.065	0.167
7-Day	0.052	0.040	0.064	0.064	0.052	0.041	0.065	0.167
14-Day	0.054	0.043	0.064	0.063	0.053	0.044	0.063	0.168
28-Day	0.059	0.048	0.066	0.063	0.058	0.049	0.064	0.169

Note: 1 in. = 25.4 mm

Table D.25: HSC End Slip Over Time

End	Live (in.)				Dead (in.)			
Specimen	HSC-1	HSC-2	HSC-3	HSC-4	HSC-1	HSC-2	HSC-3	HSC-4
Release	0.028	0.032	0.031	0.031	0.030	0.026	0.033	0.032
3-Day	0.028	0.041	0.041	0.037	0.037	0.031	0.044	0.041
5-Day	0.028	0.042	0.043	0.040	0.037	0.032	0.049	0.042
7-Day	0.029	0.043	0.045	0.041	0.040	0.031	0.050	0.044
14-Day	0.031	0.044	0.046	0.040	0.039	0.039	0.052	0.045
28-Day	0.031	0.044	0.043	0.040	0.042	0.033	0.051	0.045

Note: 1 in. = 25.4 mm

Table D.26: HSS End Slip Over Time

End	Live (in.)				Dead (in.)			
Specimen	HSS-1	HSS-2	HSS-3	HSS-4	HSS-1	HSS-2	HSS-3	HSS-4
Release	0.028	0.022	0.045	0.033	0.031	0.032	0.030	0.029
3-Day	0.036	0.030	0.053	0.044	0.037	0.043	0.044	0.035
5-Day	0.038	0.030	0.054	0.046	0.036	0.044	0.043	0.035
7-Day	0.038	0.029	0.054	0.046	0.037	0.045	0.045	0.035
14-Day	0.040	0.029	0.053	0.046	0.037	0.047	0.050	0.035
28-Day	0.044	0.032	0.054	0.048	0.039	0.050	0.051	0.037

Note: 1 in. = 25.4 mm

Table D.27: HSL End Slip Over Time

End	Live (in.)				Dead (in.)			
Specimen	HSL-1	HSL-2	HSL-3	HSL-4	HSL-1	HSL-2	HSL-3	HSL-4
Release	0.036	0.039	0.034	0.038	0.041	0.054	0.037	0.041
3-Day	0.046	0.050	0.044	0.048	0.050	0.064	0.041	0.046
5-Day	0.047	0.050	0.043	0.047	0.049	0.063	0.041	0.046
7-Day	0.049	0.050	0.043	0.048	0.050	0.063	0.041	0.047
14-Day	0.052	0.050	0.047	0.043	0.055	0.064	0.041	0.045
28-Day	0.059	0.060	0.054	0.057	0.060	0.077	0.056	0.054

Note: 1 in. = 25.4 mm

## D.4 End Slip Transfer Lengths

Table D.28: NSC End Slip Transfer Lengths Over Time

	End	Live (in.)				Dead (in.)			
	Specimen	NSC-1	NSC-2	NSC-3	NSC-4	NSC-1	NSC-2	NSC-3	NSC-4
$\alpha = 2$	Release	19.3	15.8	27.0	22.1	9.6	15.5	10.2	13.7
	3-Day	24.7	18.4	--	--	13.6	18.5	--	--
	5-Day	21.6	15.4	25.6	20.9	8.9	15.5	8.2	12.1
	7-Day	18.4	14.7	25.5	20.7	10.0	17.7	8.4	12.5
	14-Day	22.2	15.3	25.4	20.5	10.1	14.8	8.7	12.9
	28-Day	15.8	15.0	25.7	21.2	9.7	17.4	9.2	13.2
$\alpha = 3$	Release	29.0	23.8	40.4	33.1	14.4	23.3	15.3	20.6
	3-Day	37.0	27.7	--	--	20.5	27.8	--	--
	5-Day	32.3	23.1	38.4	31.4	13.4	23.2	12.2	18.2
	7-Day	27.7	22.1	38.3	31.1	15.0	26.5	12.6	18.7
	14-Day	33.3	22.9	38.0	30.8	15.1	22.2	13.1	19.3
	28-Day	23.8	22.5	38.6	31.8	14.5	26.1	13.7	19.8

Note: 1 in. = 25.4 mm, -- indicates no measurement

Table D.29: NSS End Slip Transfer Lengths Over Time

	End	Live (in.)					Dead (in.)				
	Specimen	NSS-1	NSS-2	NSS-3	NSS-4	NSS-5	NSS-1	NSS-2	NSS-3	NSS-4	NSS-5
$\alpha = 2$	Release	--	11.2	17.5	17.0	17.8	16.6	16.8	17.4	18.0	17.4
	3-Day	27.6	13.5	20.8	18.6	19.3	18.0	18.0	18.3	19.2	17.8
	5-Day	27.1	14.2	17.6	18.7	18.7	17.7	17.8	18.8	18.8	17.7
	7-Day	27.3	14.5	17.4	18.2	18.2	17.6	18.4	19.3	19.0	17.2
	14-Day	27.0	14.5	17.5	18.6	19.3	17.8	18.3	19.4	19.4	17.5
	28-Day	27.5	14.0	17.4	17.6	34.9	17.6	18.0	19.3	18.7	53.9
$\alpha = 3$	Release	--	16.9	26.2	25.5	26.7	24.9	25.2	26.0	27.0	26.1
	3-Day	41.4	20.2	31.1	27.8	29.0	27.0	26.9	27.4	28.8	26.7
	5-Day	40.6	21.3	26.4	28.1	28.0	26.6	26.6	28.2	28.3	26.5
	7-Day	41.0	21.7	26.0	27.4	27.3	26.4	27.5	28.9	28.4	25.7
	14-Day	40.5	21.7	26.2	27.9	29.0	26.8	27.4	29.1	29.1	26.3
	28-Day	41.2	21.0	26.0	26.4	52.4	26.4	27.0	29.0	28.0	80.9

Note: 1 in. = 25.4 mm, -- indicates erroneous measurement

Table D.30: NSL End Slip Transfer Lengths Over Time

	End	Live (in.)				Dead (in.)			
	Specimen	NSL-1	NSL-2	NSL-3	NSL-4	NSL-1	NSL-2	NSL-3	NSL-4
$\alpha = 2$	Release	10.9	9.7	13.4	13.7	11.4	9.6	13.8	43.3
	3-Day	14.5	11.3	18.5	17.4	14.7	11.4	18.6	48.3
	5-Day	16.2	12.3	20.1	19.4	15.8	12.5	19.8	51.0
	7-Day	15.8	12.2	19.6	19.5	15.7	12.5	20.0	51.1
	14-Day	16.6	13.0	19.7	19.2	16.2	13.2	19.4	51.2
	28-Day	18.0	14.6	20.3	19.2	17.6	15.0	19.6	51.6
$\alpha = 3$	Release	16.3	14.5	20.0	20.6	17.1	14.3	20.7	64.9
	3-Day	21.7	17.0	27.7	26.0	22.0	17.2	28.0	72.4
	5-Day	24.2	18.4	30.2	29.1	23.7	18.8	29.8	76.5
	7-Day	23.8	18.4	29.4	29.2	23.6	18.7	29.9	76.6
	14-Day	24.9	19.6	29.5	28.8	24.3	19.8	29.1	76.9
	28-Day	27.0	22.0	30.4	28.8	26.3	22.5	29.5	77.3

Note: 1 in. = 25.4 mm

Table D.31: HSC End Slip Transfer Lengths Over Time

	End	Live (in.)				Dead (in.)			
	Specimen	HSC-1	HSC-2	HSC-3	HSC-4	HSC-1	HSC-2	HSC-3	HSC-4
$\alpha = 2$	Release	8.6	10.0	9.4	9.7	9.2	7.9	10.2	10.0
	3-Day	8.8	12.8	12.8	11.5	11.4	9.5	13.5	12.6
	5-Day	8.7	13.1	13.3	12.3	11.5	9.8	15.1	13.0
	7-Day	9.0	13.2	13.9	12.6	12.3	9.5	15.6	13.7
	14-Day	9.6	13.5	14.1	12.5	12.2	12.1	16.0	13.8
	28-Day	9.7	13.6	13.2	12.3	13.0	10.4	15.7	14.1
$\alpha = 3$	Release	13.0	15.0	14.2	14.6	13.8	11.9	15.3	15.0
	3-Day	13.1	19.3	19.2	17.2	17.1	14.3	20.3	18.8
	5-Day	13.0	19.7	20.0	18.4	17.3	14.7	22.7	19.5
	7-Day	13.5	19.8	20.9	18.9	18.4	14.3	23.4	20.5
	14-Day	14.4	20.3	21.2	18.8	18.2	18.1	24.0	20.7
	28-Day	14.5	20.4	19.8	18.5	19.5	15.5	23.6	21.1

Note: 1 in. = 25.4 mm

Table D.32: HSS End Slip Transfer Lengths Over Time

	End	Live (in.)				Dead (in.)			
	Specimen	HSS-1	HSS-2	HSS-3	HSS-4	HSS-1	HSS-2	HSS-3	HSS-4
$\alpha = 2$	Release	8.6	6.9	14.0	10.2	9.7	10.0	9.5	8.9
	3-Day	11.2	9.2	16.6	13.6	11.4	13.4	13.9	10.7
	5-Day	11.7	9.2	16.9	14.0	11.3	13.6	13.6	10.9
	7-Day	11.8	9.1	16.9	14.0	11.4	14.1	14.1	10.8
	14-Day	12.3	9.1	16.7	14.2	11.5	14.6	15.6	10.8
	28-Day	13.8	10.0	16.9	14.8	12.2	15.6	16.0	11.3
$\alpha = 3$	Release	12.9	10.3	21.0	15.2	14.5	14.9	14.3	13.4
	3-Day	16.8	13.8	24.9	20.4	17.1	20.1	20.8	16.1
	5-Day	17.5	13.8	25.3	21.0	17.0	20.4	20.4	16.3
	7-Day	17.8	13.7	25.3	21.0	17.1	21.2	21.1	16.2
	14-Day	18.4	13.7	25.1	21.3	17.3	21.9	23.4	16.3
	28-Day	20.7	15.0	25.3	22.3	18.2	23.4	24.0	17.0

Note: 1 in. = 25.4 mm

Table D.33: HSL End Slip Transfer Lengths Over Time

	End	Live (in.)				Dead (in.)			
	Specimen	HSL-1	HSL-2	HSL-3	HSL-4	HSL-1	HSL-2	HSL-3	HSL-4
$\alpha = 2$	Release	10.7	11.6	10.3	11.4	12.5	16.2	11.2	12.3
	3-Day	13.9	15.1	13.1	14.4	14.9	19.2	12.3	13.8
	5-Day	14.1	15.0	12.8	14.2	14.7	19.0	12.3	13.9
	7-Day	14.7	15.1	13.0	14.3	15.1	19.0	12.4	14.2
	14-Day	15.7	15.0	14.2	12.8	16.6	19.1	12.4	13.6
	28-Day	17.9	18.0	16.2	17.1	18.2	23.3	16.9	16.4
$\alpha = 3$	Release	16.1	17.4	15.5	17.1	18.7	24.3	16.8	18.5
	3-Day	20.8	22.7	19.7	21.6	22.4	28.8	18.5	20.7
	5-Day	21.2	22.5	19.2	21.3	22.0	28.6	18.4	20.8
	7-Day	22.1	22.6	19.5	21.5	22.7	28.5	18.6	21.2
	14-Day	23.6	22.5	21.2	19.3	24.9	28.7	18.6	20.4
	28-Day	26.8	26.9	24.3	25.7	27.2	34.9	25.4	24.6

Note: 1 in. = 25.4 mm



## D.5 Comparisons of Average End Slip and DEMEC Transfer Lengths

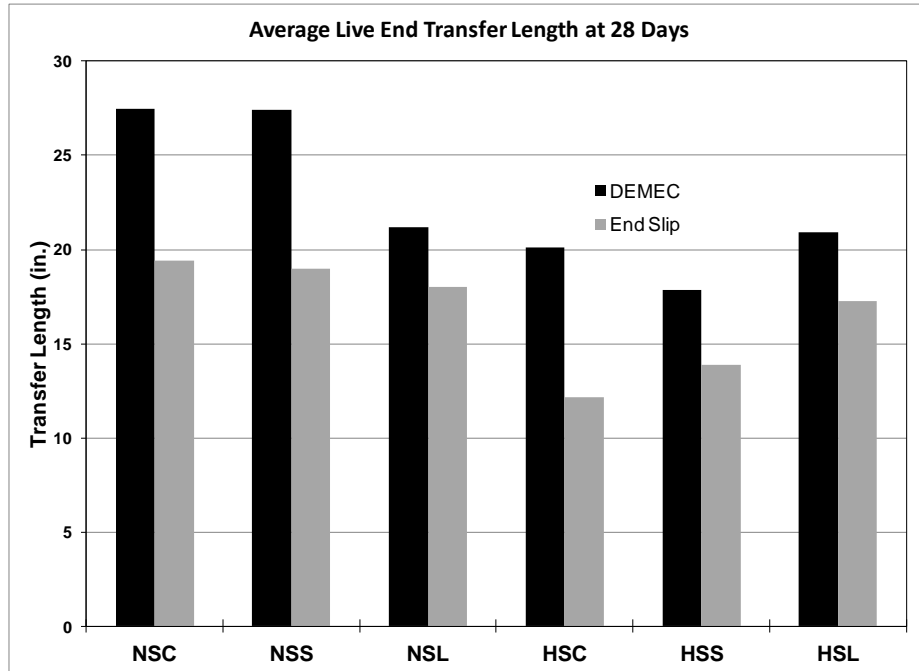


Figure D.124: Live end DEMEC and end slip ( $\alpha = 2$ ) transfer lengths at 28 days

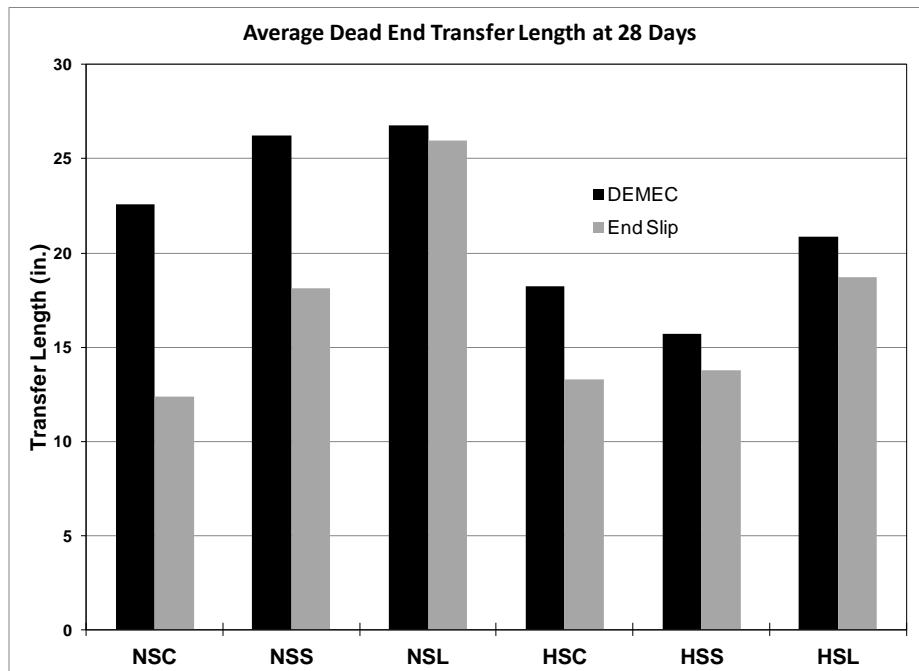


Figure D.125: Dead end DEMEC and end slip ( $\alpha = 2$ ) transfer lengths at 28 days

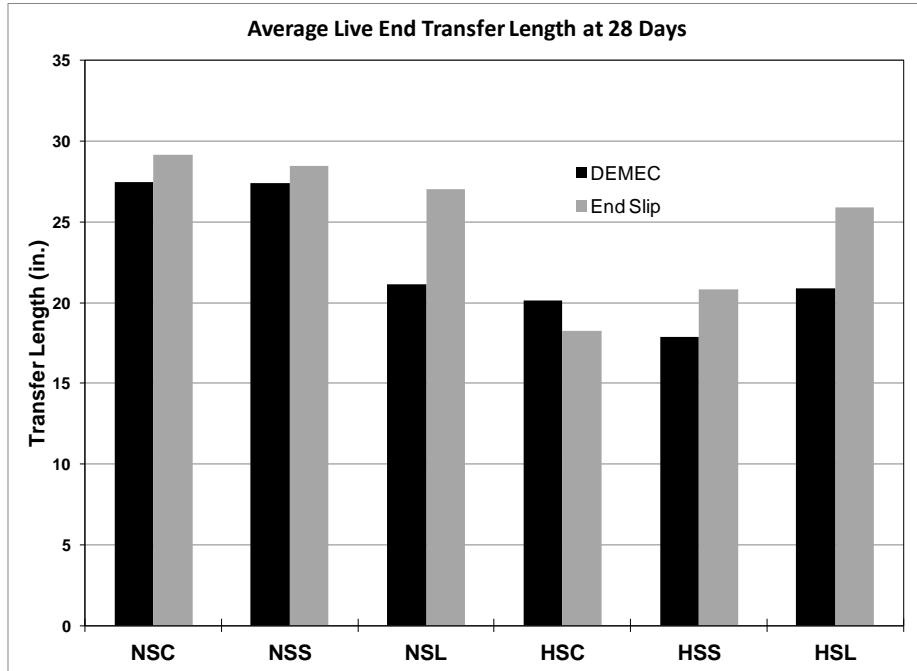


Figure D.126: Live end DEMEC and end slip ( $\alpha = 3$ ) transfer lengths at 28 days

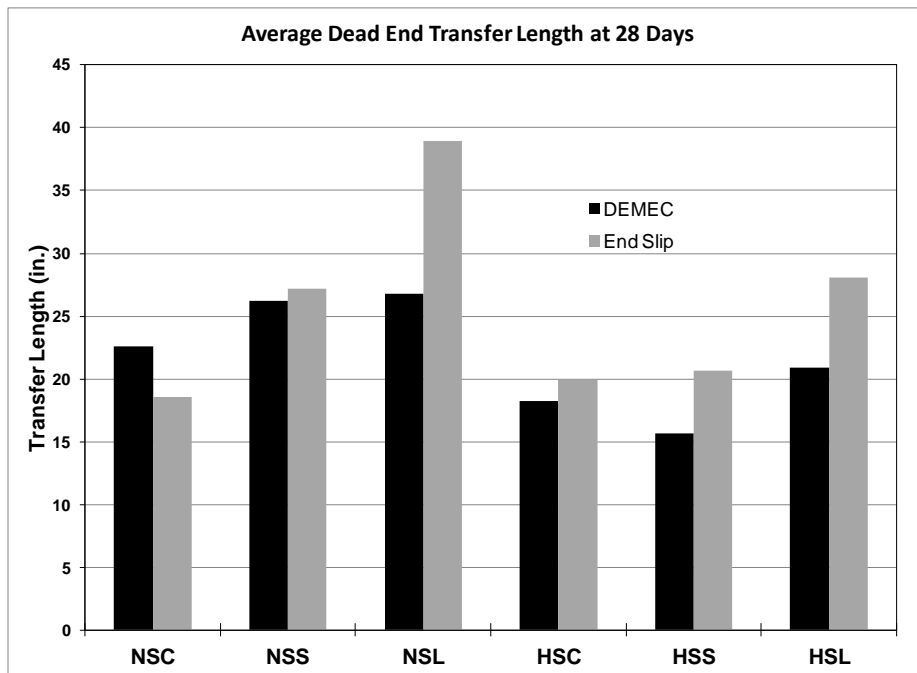


Figure D.127: Dead end DEMEC and end slip ( $\alpha = 3$ ) transfer lengths at 28 days

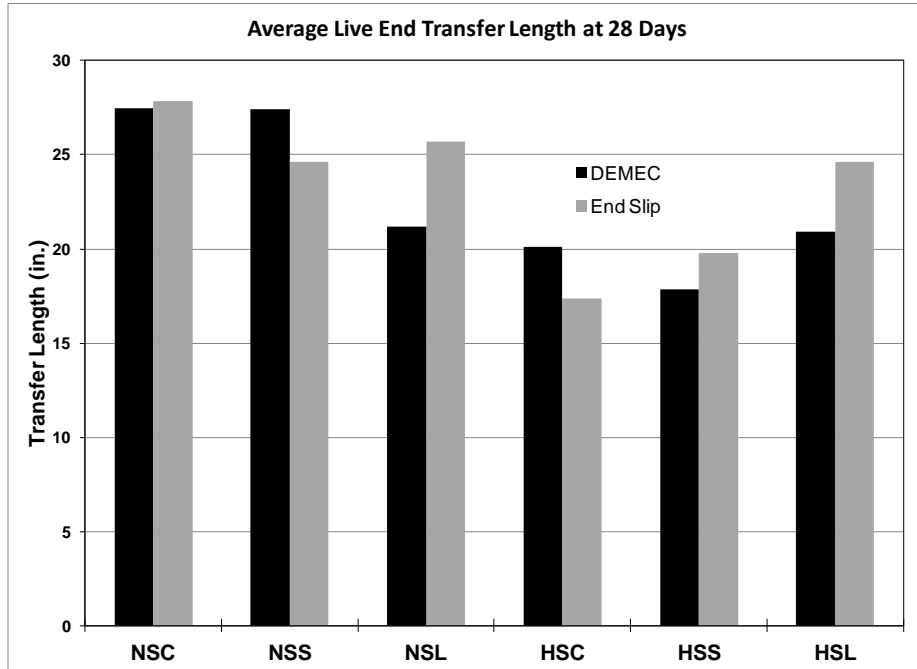


Figure D.128: Live end DEMEC and end slip ( $\alpha = 2.85$ ) transfer lengths at 28 days

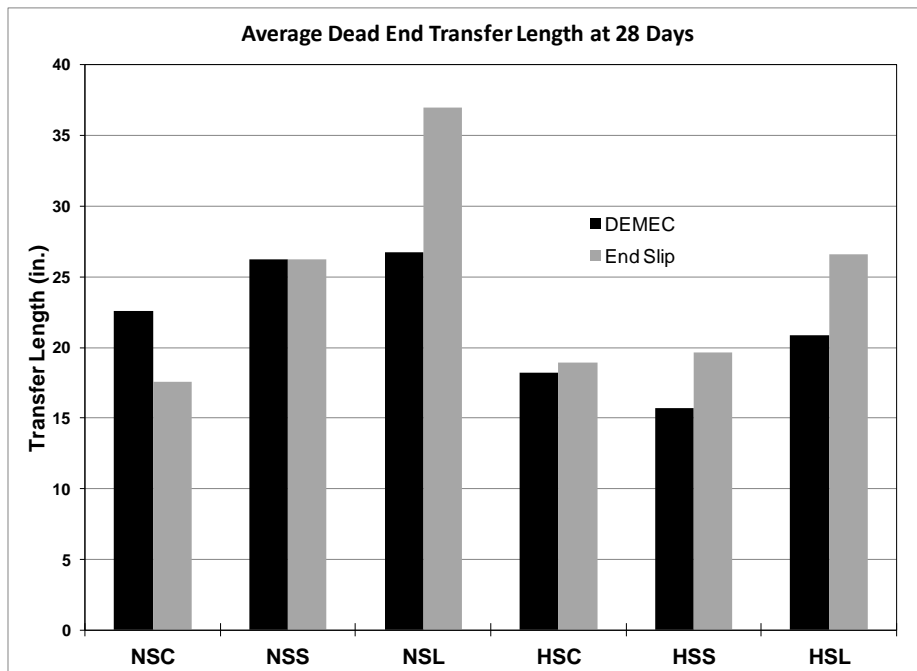


Figure D.129: Dead end DEMEC and end slip ( $\alpha = 2.85$ ) transfer lengths at 28 days

## Appendix E: Development Length Data

### E.1 Normal Strength Clay (NSC) Specimens

Table E.1: Results of Flexural Tests on NSC Specimens

Specimen	1D	1L	2D	2L	3D	3L	4D	4L
$L_E$ (in.)	50	45	50	55	52	48	48	60
$M_n$ (k-in.)	933	933	983	983	935	935	960	960
$M_{cr}$ (k-in.)	493	493	528	528	476	476	502	502
At Cracking								
$\Delta$ (in.)	0.36	0.41	0.18	0.37	0.17	0.41	0.19	0.48
P (kips)	23.00	22.00	25.00	25.00	20.00	25.00	25.00	25.00
M (k-in.)	611	565	629	674	535	657	656	749
At 0.01 in. Strand Slip								
$\Delta$ (in.)	--	0.58	--	--	0.58	0.54	0.67	--
P (kips)	--	27.40	--	--	32.30	29.80	36.20	--
M (k-in.)	--	701	--	--	865	782	950	--
At Maximum Load								
$\Delta$ (in.)	1.13	0.58	0.75	1.05	0.98	0.68	0.99	1.22
P (kips)	35.33	27.48	42.46	40.58	36.20	32.40	39.20	36.52
M (k-in.)	939	703	1067	1094	969	850	1029	1093
At End of Test								
Slip (in.)	--	>0.10	--	--	>0.06	>0.10	0.02	--
$\Delta$ (in.)	1.90	1.22	1.17	2.14	1.00	0.70	1.19	2.16
Crushing	YES	NO	YES	YES	NO	NO	YES	YES
Failure	FL	SH/ES	FL	FL/SH	SH/ES	SH/ES	FL/ES/SH	FL

Note: 1 in. = 25.4 mm, 1 lbf = 4.448 N

Table E.2: NSC Embedment Lengths Divided by Predicted Development Lengths

Specimen	$L_E$ (in.)	ACI	Ramirez/ Russell	Zia/ Mostafa	Deatherage et al	Buckner	Lane	Kose/ Burkett
NSC-1D	50	0.53	0.52	0.43	0.38	0.50	0.27	0.45
NSC-1L	45	0.48	0.47	0.39	0.34	0.45	0.25	0.41
NSC-2D	50	0.50	0.60	0.41	0.34	0.46	0.35	0.53
NSC-2L	55	0.55	0.66	0.45	0.38	0.50	0.39	0.58
NSC-3D	52	0.55	0.54	0.44	0.39	0.52	0.29	0.47
NSC-3L	48	0.51	0.50	0.41	0.36	0.48	0.26	0.44
NSC-4D	48	0.51	0.53	0.41	0.36	0.48	0.31	0.47
NSC-4L	60	0.63	0.66	0.52	0.46	0.60	0.39	0.59

Note: 1 in. = 25.4 mm

## E.2 Normal Strength Shale (NSS) Specimens

Table E.3: Results of Flexural Tests on NSS Specimens

Specimen	1D	1L	2D	2L	3D	3L	4D	4L	5D	5L
$L_E$ (in.)	45	50	49	40	40	45	47.5	45	45	40
$M_n$ (k-in.)	931	931	968	968	963	963	972	972	969	969
$M_{cr}$ (k-in.)	488	488	512	512	513	513	515	515	508	508
<b>At Cracking</b>										
$\Delta$ (in.)	0.29	0.42	0.27	0.31	0.23	0.34	0.33	0.33	0.22	0.37
P (kips)	25.00	25.00	25.00	25.00	20.00	25.00	25.00	25.00	25.00	25.00
M (k-in.)	630	656	647	591	473	630	644	629	630	591
<b>At 0.01 in. Strand Slip</b>										
$\Delta$ (in.)	2.10	1.63	--	0.75	0.52	1.82	--	0.72	--	0.58
P (kips)	$39.50_1$	37.40	--	39.20	33.70	$39.45_2^{1,}$	--	$38.62_3$	--	$32.67_3$
M (k-in.)	995	982	--	928	797	994	--	973	--	773
<b>At Maximum Load</b>										
$\Delta$ (in.)	2.77	2.18	0.87	0.84	0.51	0.91	0.93	0.73	0.91	0.58
P (kips)	40.40	38.40	38.20	40.58	35.07	40.81	38.84	39.98	40.90	35.03
M (k-in.)	1018	1008	989	960	830	1028	1001	1007	1030	829
<b>At End of Test</b>										
Slip (in.)	$0.03^1$	0.09	--	>0.10	>0.10	$0.04^{1,2}$	--	$0.10^3$	--	$>0.10_3$
$\Delta$ (in.)	2.77	2.57	1.57	1.86	0.74	2.30	2.39	0.73	3.15	0.72
Crushing	YES	YES	YES	YES	NO	YES	YES	NO	YES	NO
Failure	FL/ ES	FL/ ES	FL	SH/ ES	SH/ ES	FL	FL	SH/ ES	FL	SH/ ES

Note: 1 in. = 25.4 mm, 1 lbf = 4.448 N, <sup>1</sup>slip on one strand only, <sup>2</sup>slip after strand fracture, <sup>3</sup>slip accompanied shear failure

Table E.4: NSS Embedment Lengths Divided by Predicted Development Lengths

Specimen	$L_E$ (in.)	ACI	Ramirez/ Russell	Zia/ Mostafa	Deatherage et al	Buckner	Lane	Kose/ Burkett
NSS-1D	45	0.47	0.45	0.36	0.34	0.45	0.24	0.40
NSS-1L	50	0.52	0.50	0.40	0.37	0.50	0.26	0.44
NSS-2D	49	0.52	0.56	0.44	0.38	0.50	0.33	0.49
NSS-2L	40	0.43	0.45	0.36	0.31	0.41	0.27	0.40
NSS-3D	40	0.43	0.45	0.36	0.31	0.41	0.26	0.39
NSS-3L	45	0.48	0.51	0.41	0.35	0.46	0.30	0.44
NSS-4D	47.5	0.51	0.54	0.42	0.37	0.48	0.33	0.48
NSS-4L	45	0.48	0.52	0.40	0.35	0.46	0.32	0.46
NSS-5D	45	0.48	0.51	0.39	0.34	0.45	0.31	0.45
NSS-5L	40	0.42	0.45	0.35	0.31	0.40	0.27	0.40

Note: 1 in. = 25.4 mm

### E.3 Normal Strength Limestone (NSL) Specimens

Table E.5: Results of Flexural Tests on NSL Specimens

Specimen	1D	1L	2D	2L	3D	3L	4D	4L
$L_E$ (in.)	37	39.5	40	43	40	34	56	47
$M_n$ (k-in.)	971	971	994	994	994	994	998	998
$M_{cr}$ (k-in.)	556	556	573	573	557	557	568	568
At Cracking								
$\Delta$ (in.)	0.25	0.40	0.20	0.42	0.22	0.39	0.21	0.51
P (kips)	29.00	30.00	27.00	28.00	28.00	33.00	17.00	26.00
M (k-in.)	694	716	691	705	716	729	503	682
At 0.01 in. Strand Slip								
$\Delta$ (in.)	0.51	0.8	--	--	0.65	0.72	0.23	--
P (kips)	35.90 <sup>1</sup>	40.95	--	--	40.20 <sup>1</sup>	44.40	15.70 <sup>1</sup>	--
M (k-in.)	859	976	--	--	1029	982	465	--
At Maximum Load								
$\Delta$ (in.)	0.51	1.3	0.83	1.03	0.65	0.99	1.00	1.11
P (kips)	39.56	45.03	45.86	44.63	42.68	46.20	27.80	43.56
M (k-in.)	946	1073	1174	1124	1092	1022	823	1143
At End of Test								
Slip (in.)	>0.10 <sup>1</sup>	>0.20	--	--	>0.10 <sup>1</sup>	>0.05	>0.10 <sup>1</sup>	--
$\Delta$ (in.)	0.90	2.34	2.19	2.59	1.25	1.41	1.04	1.34
Crushing	NO	YES	YES	YES	YES	YES	NO	YES
Failure	SH/ES	FL/ES	FL	FL	SH/ES	FL/ES	SH/ES	FL

Note: 1 in. = 25.4 mm, 1 lbf = 4.448 N, <sup>1</sup>slip accompanied shear failure

Table E.6: NSL Embedment Lengths Divided by Predicted Development Lengths

Specimen	$L_E$ (in.)	ACI	Ramirez/ Russell	Zia/ Mostafa	Deatherage et al	Buckner	Lane	Kose/ Burkett
NSL-1D	37	0.41	0.44	0.38	0.31	0.40	0.27	0.38
NSL-1L	39.5	0.44	0.47	0.41	0.33	0.43	0.29	0.40
NSL-2D	40	0.45	0.51	0.42	0.33	0.43	0.35	0.44
NSL-2L	43	0.48	0.55	0.46	0.36	0.47	0.37	0.47
NSL-3D	40	0.44	0.48	0.37	0.32	0.42	0.34	0.44
NSL-3L	34	0.37	0.41	0.31	0.27	0.36	0.29	0.37
NSL-4D	56	0.62	0.67	0.53	0.46	0.59	0.47	0.61
NSL-4L	47	0.52	0.57	0.44	0.38	0.50	0.40	0.51

Note: 1 in. = 25.4 mm

## E.4 High Strength Clay (HSC) Specimens

Table E.7: Results of Flexural Tests on HSC Specimens

Specimen	1D	1L	2D	2L	3D	3L	4D	4L
$L_E$ (in.)	40	50	44.25	45	42.5	45	37.5	47.5
$M_n$ (k-in.)	983	983	989	989	974	974	981	981
$M_{cr}$ (k-in.)	544	544	543	543	542	542	543	543
At Cracking								
$\Delta$ (in.)	0.23	0.38	0.18	0.38	0.29	0.33	0.35	0.27
P (kips)	25.00	25.00	21.00	24.00	22.00	25.00	25.00	22.00
M (k-in.)	591	656	525	604	539	630	568	567
At 0.01 in. Strand Slip								
$\Delta$ (in.)	--	--	--	0.97	0.74	0.77	0.72	--
P (kips)	--	--	--	38.65	32.85 <sup>1</sup>	37.20	38.90	--
M (k-in.)	--	--	--	974	804	937	884	--
At Maximum Load								
$\Delta$ (in.)	0.72	0.96	0.77	1.2	0.71	1.05	0.88	0.93
P (kips)	42.60	41.96	41.06	40.80	37.59	41.26	42.77	40.15
M (k-in.)	1008	1101	1026	1027	920	1039	972	1035
At End of Test								
Slip (in.)	<0.01	--	--	0.02	>0.1 <sup>1</sup>	>0.15 <sup>1</sup>	>0.15 <sup>1</sup>	--
$\Delta$ (in.)	1.03	2.02	2.63	1.9	0.85	1.06	1.34	3.16
Crushing	YES	YES	YES	YES	NO	NO	NO	YES
Failure	FL/SH	FL	FL	FL/SH/ES	SH/ES	SH/ES	SH/ES	FL

Note: 1 in. = 25.4 mm, 1 lbf = 4.448 N, <sup>1</sup>slip accompanied shear failure

Table E.8: HSC Embedment Lengths Divided by Predicted Development Lengths

Specimen	$L_E$ (in.)	ACI	Ramirez/ Russell	Zia/ Mostafa	Deatherage et al	Buckner	Lane	Kose/ Burkett
HSC-1D	40	0.44	0.50	0.43	0.33	0.43	0.31	0.42
HSC-1L	50	0.55	0.63	0.53	0.41	0.53	0.39	0.52
HSC-2D	44.25	0.49	0.56	0.46	0.36	0.47	0.36	0.47
HSC-2L	45	0.50	0.57	0.47	0.37	0.48	0.36	0.48
HSC-3D	42.5	0.47	0.53	0.46	0.35	0.45	0.31	0.43
HSC-3L	45	0.50	0.56	0.49	0.37	0.48	0.33	0.46
HSC-4D	37.5	0.41	0.47	0.40	0.31	0.40	0.29	0.39
HSC-4L	47.5	0.52	0.60	0.51	0.39	0.51	0.36	0.50

Note: 1 in. = 25.4 mm

## E.5 High Strength Shale (HSS) Specimens

Table E.9: Results of Flexural Tests on HSS Specimens

Specimen	1D	1L	2D	2L	3D	3L	4D	4L
$L_E$ (in.)	40	50	42.5	45	35	40	40	37.5
$M_n$ (k-in.)	972	972	968	968	996	996	980	980
$M_{cr}$ (k-in.)	538	538	531	531	537	537	547	547
<b>At Cracking</b>								
$\Delta$ (in.)	0.25	0.34	0.19	0.41	0.24	0.31	0.16	0.27
P (kips)	22.00	22.00	23.00	23.00	25.00	25.00	25.00	25.00
M (k-in.)	520	577	563	579	542	591	591	568
<b>At 0.01 in. Strand Slip</b>								
$\Delta$ (in.)	0.63	--	--	3.25	0.69	--	2.49	0.66
P (kips)	37.90 <sup>3</sup>	--	--	27.15 <sup>2</sup>	42.10	--	42.60 <sup>1</sup>	40.70
M (k-in.)	897	--	--	684	912	--	1008	925
<b>At Maximum Load</b>								
$\Delta$ (in.)	0.73	1.03	0.89	1.1	0.65	0.74	3.48	0.65
P (kips)	40.24	41.18	44.86	42.60	42.60	40.42	44.13	41.29
M (k-in.)	952	1081	1098	1073	923	956	1044	938
<b>At End of Test</b>								
Slip (in.)	0.04 <sup>3</sup>	<0.01	--	0.01 <sup>2</sup>	>0.20	--	<0.05 <sup>1</sup>	>0.20
$\Delta$ (in.)	1.00	3.49	2.43	3.25	1.95	2.43	3.71	1.79
Crushing	YES	YES	YES	YES	YES	YES	YES	YES
Failure	SH/ES	FL	FL	FL	BD	FL	FL	BD

Note: 1 in. = 25.4 mm, 1 lbf = 4.448 N, <sup>1</sup>slip on one strand only, <sup>2</sup>slip after strand fracture, <sup>3</sup>slip accompanied shear failure, #indicates slip after strand fracture

Table E.10: HSS Embedment Lengths Divided by Predicted Development Lengths

Specimen	$L_E$ (in.)	ACI	Ramirez/ Russell	Zia/ Mostafa	Deatherage et al	Buckner	Lane	Kose/ Burkett
HSS-1D	40	0.44	0.49	0.42	0.32	0.42	0.29	0.40
HSS-1L	50	0.55	0.61	0.53	0.41	0.53	0.36	0.50
HSS-2D	42.5	0.46	0.51	0.43	0.34	0.45	0.29	0.42
HSS-2L	45	0.49	0.54	0.46	0.36	0.47	0.31	0.45
HSS-3D	35	0.38	0.45	0.35	0.28	0.36	0.30	0.39
HSS-3L	40	0.43	0.51	0.40	0.32	0.42	0.34	0.44
HSS-4D	40	0.45	0.51	0.45	0.33	0.43	0.31	0.41
HSS-4L	37.5	0.42	0.48	0.42	0.31	0.40	0.29	0.39

Note: 1 in. = 25.4 mm



## E.6 High Strength Limestone (NSL) Specimens

Table E.11: Results of Flexural Tests on HSL Specimens

Specimen	1D	1L	2D	2L	3D	3L	4D	4L
$L_E$ (in.)	40	50	47.5	45	42.5	47.5	35	40
$M_n$ (k-in.)	1010	1010	1015	1015	1017	1017	1023	1023
$M_{cr}$ (k-in.)	590	590	592	592	593	593	593	593
<b>At Cracking</b>								
$\Delta$ (in.)	0.20	0.25	0.16	0.2	0.16	0.25	0.19	0.21
P (kips)	30.00	25.00	25.00	25.00	25.00	25.00	30.00	30.00
M (k-in.)	710	656	644	630	612	644	650	710
<b>At 0.01 in. Strand Slip</b>								
$\Delta$ (in.)	0.44	--	0.69	0.88	1.79	--	0.41	0.62
P (kips)	39.50	--	40.40	44.80	39.10 <sup>1</sup>	--	40.80	44.30
M (k-in.)	935	--	1041	1128	957	--	884	1048
<b>At Maximum Load</b>								
$\Delta$ (in.)	1.00	1.03	0.75	1.09	0.79	0.86	0.59	0.65
P (kips)	45.90	44.09	40.96	45.21	42.47	40.64	43.53	44.45
M (k-in.)	1086	1157	1056	1139	1040	1048	943	1051
<b>At End of Test</b>								
Slip (in.)	>0.50	--	>0.15	>0.10	0.02	--	>0.25	>0.10
$\Delta$ (in.)	3.64	3.22	3.70	3.95	2.55	2.95	2.33	1.17
Crushing	YES	YES	YES	YES	YES	YES	YES	YES
Failure	BD	FL	FL/ES	FL/ES	FL	FL	BD	FL/ES

Note: 1 in. = 25.4 mm, 1 lbf = 4.448 N, <sup>1</sup> indicates slip on one strand only

Table E.12: HSL Embedment Lengths Divided by Predicted Development Lengths

Specimen	$L_E$ (in.)	ACI	Ramirez/ Russell	Zia/ Mostafa	Deatherage et al	Buckner	Lane	Kose/ Burkett
HSL-1D	40	0.46	0.55	0.47	0.34	0.44	0.39	0.46
HSL-1L	50	0.57	0.69	0.58	0.43	0.55	0.49	0.58
HSL-2D	47.5	0.54	0.66	0.56	0.41	0.52	0.48	0.56
HSL-2L	45	0.51	0.63	0.53	0.39	0.50	0.45	0.53
HSL-3D	42.5	0.48	0.59	0.49	0.36	0.47	0.43	0.50
HSL-3L	47.5	0.54	0.66	0.55	0.41	0.52	0.48	0.56
HSL-4D	35	0.40	0.49	0.41	0.30	0.39	0.37	0.42
HSL-4L	40	0.45	0.56	0.46	0.34	0.44	0.42	0.48

Note: 1 in. = 25.4 mm

## Appendix F: STSB Curves

### F.1 Batch 1

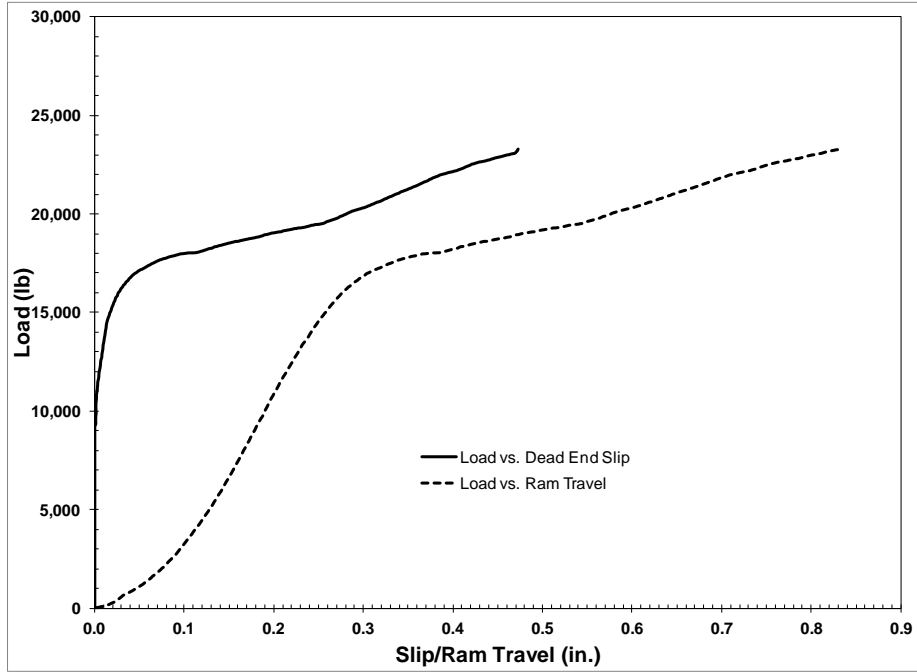


Figure F.1: Load vs. dead end slip and ram travel for strand specimen 1

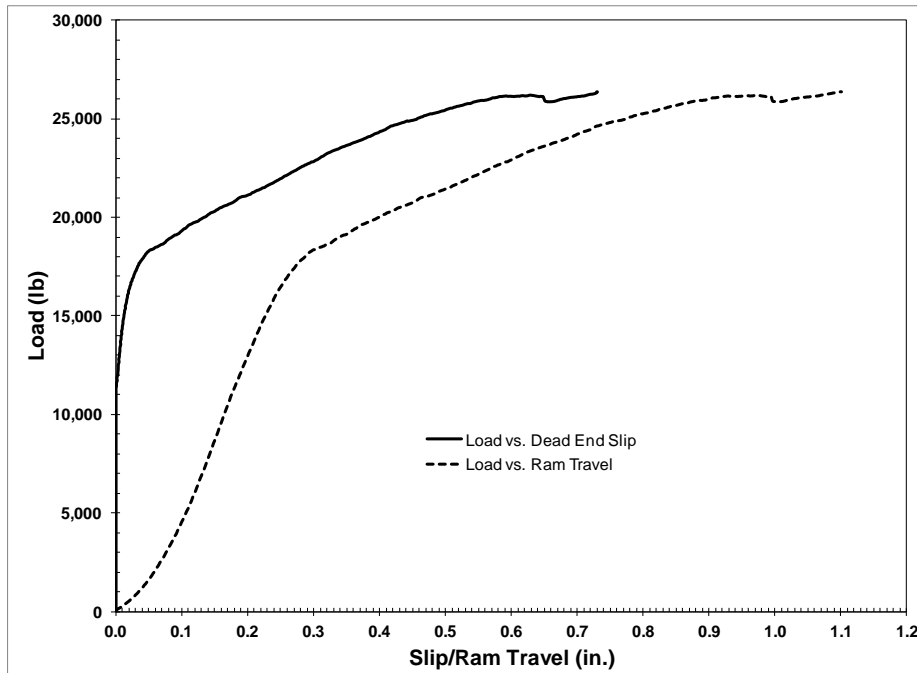


Figure F.2: Load vs. dead end slip and ram travel for strand specimen 2

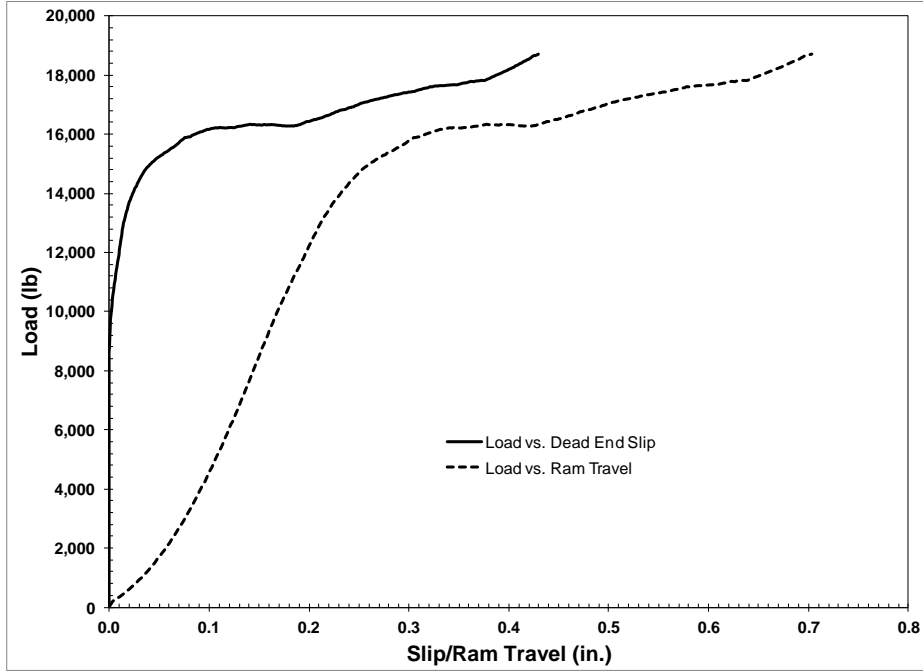


Figure F.3: Load vs. dead end slip and ram travel for strand specimen 3

**F.2 Batch 2**

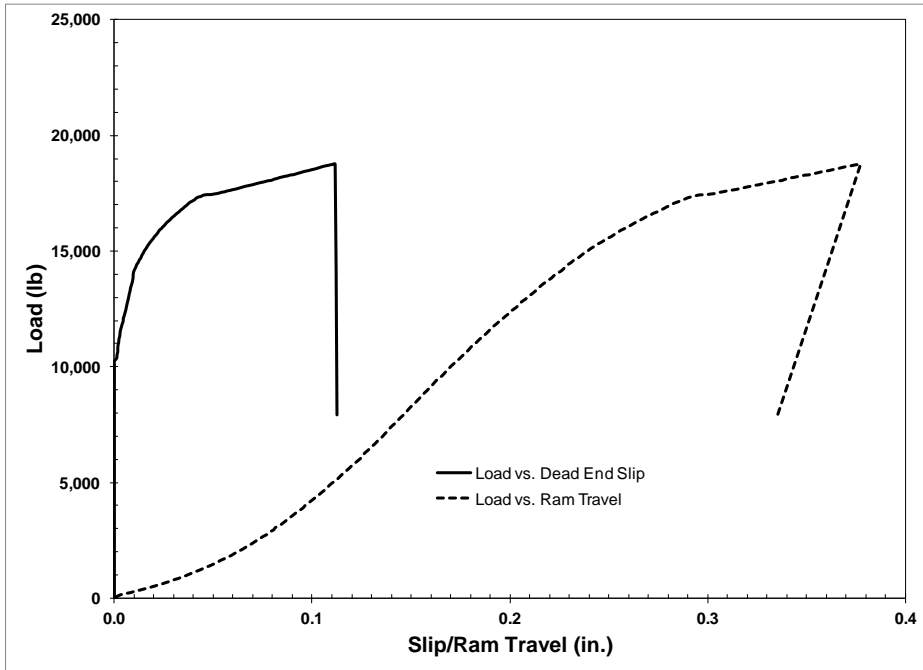


Figure F.4: Load vs. dead end slip and ram travel for strand specimen 4

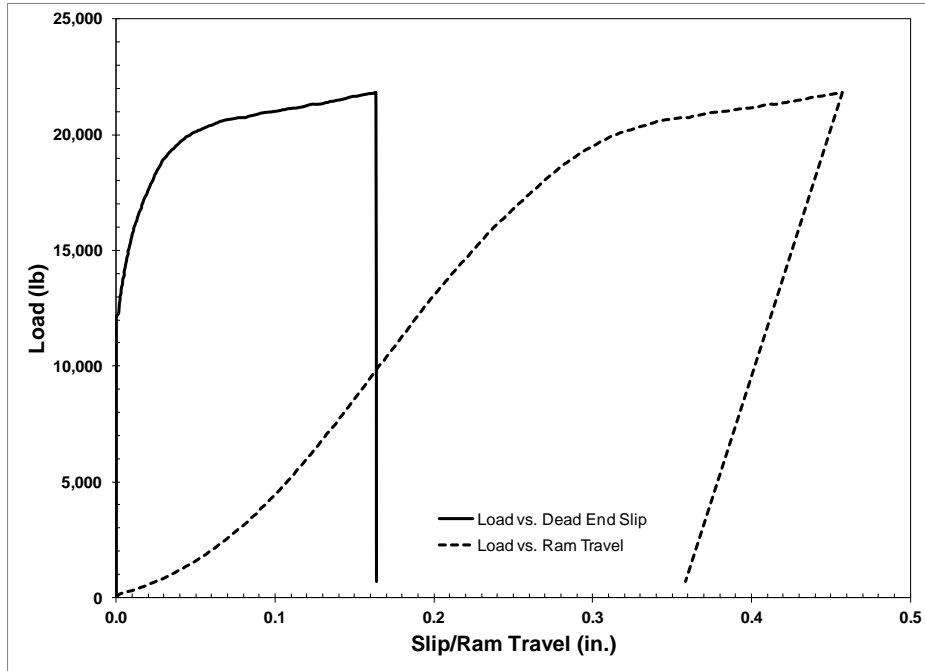


Figure F.5: Load vs. dead end slip and ram travel for strand specimen 5

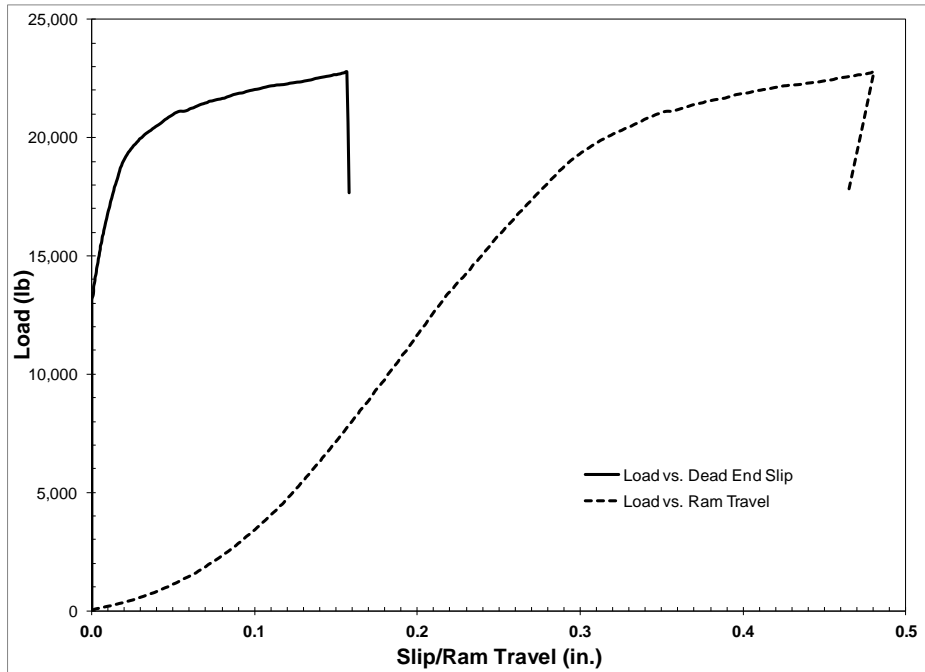


Figure F.6: Load vs. dead end slip and ram travel for strand specimen 6

